

The Development of Portable Chemosensors  
for Atmospheric Radicals

Andrew James Grantham

Doctor of Philosophy

University of York

Chemistry

September 2017

## Abstract

The complex photochemical oxidation cycles involved in the degradative removal of anthropogenic and biogenic hydrocarbons from the atmosphere are mediated by a range of radical intermediates (e.g. peroxy radicals). Thus these radicals are of particular interest in relation to air quality and human health. Speciated measurements of atmospheric radicals pose considerable challenges to analytical chemists. Owing to their low concentrations, high reactivity and short lifetimes, free radical species cannot be easily sampled; therefore direct offline analysis is extremely difficult. Issues such as selectivity, full structure determination, portability and cost (logistics, power, expertise) remain challenging obstacles to atmospheric radical analysis.

Within this thesis, the synthesis and development of a series of novel chemosensors is presented. These are organic trapping compounds that can efficiently and selectively react with a range of radical species. The chemosensor is designed with the aim of radical addition to a double bond, resulting in the loss of a stable radical leaving group. The trapped radical structure is maintained in the reaction products, which are sufficiently stable for offline mass spectrometry. This approach allows for accurate determination of the radical structures and is different to traditional spin trapping, with the captured radical now converted to a stable non radical form.

The developed chemosensors have been tested and evaluated in laboratory and chamber experiments by application to a range of atmospherically relevant systems (e.g. alkene ozonolysis and reactions of  $\cdot\text{OH}$  with alkanes), giving key insights into radical selectivity and reaction mechanisms. They have also been applied to measurements of indoor and outdoor air, providing evidence for the function of this system at atmospheric radical concentrations.

# List of Contents

<b>Abstract.....</b>	<b>2</b>
<b>List of Contents.....</b>	<b>3</b>
<b>List of Figures .....</b>	<b>13</b>
<b>Acknowledgements .....</b>	<b>27</b>
<b>Declaration.....</b>	<b>28</b>
<b>1. Introduction.....</b>	<b>29</b>
1.1 Radical Classification and Stability .....	29
1.2. The Role of Radical Chemistry Within the Atmosphere.....	30
1.2.1. The Hydroxyl Radical in the Atmosphere.....	31
1.2.2. Organic Peroxyl Radicals in the Atmosphere .....	32
1.2.3. The NO <sub>3</sub> Radical in the Atmosphere .....	33
1.3. Current Methods of Atmospheric Radical Detection .....	34
1.3.1. Laser Induced Fluorescence/ Fluorescence Assay by Gas Expansion .....	34
1.3.2. Chemical Ionisation Mass Spectrometry .....	35
1.3.3. Chemiluminescence and Cavity Ring Down Spectroscopy .....	37
1.3.4. Differential Optical Absorption Spectroscopy .....	39
1.3.5. Matrix Isolation EPR .....	40
1.3.6. Other Methods for Radical Detection.....	40
1.3.7. Capture of Criegee Intermediates from Alkene Ozonolysis Systems .....	42
1.3.8. General Disadvantages of Current Techniques .....	43
1.4. Spin Trapping.....	44
1.4.1. Common Spin Traps and Their Use .....	44
1.4.2. Spin Trapping Radicals from the Gas Phase.....	46
1.4.3. Limitations of Spin Trapping .....	47

1.5. Project Aims.....	47
<b>2. Trap Synthesis.....</b>	<b>48</b>
2.1. Introduction.....	48
2.1.1. Design Principles for a Trapping Molecule .....	48
2.1.2. Alkoxyamine Synthesis .....	50
2.1.3. Aims .....	52
2.2. Initial Synthetic Plan .....	52
2.2.1. Reaction Between TEMPO and 3-Methyl-1,4-pentadiene, Using a Cobalt Catalyst Under Oxygen. ....	54
2.2.2. Other Methods of Forming 2.01 Through Hydrogen Abstraction Reactions. ....	57
2.2.3. Reactions in the Presence of an Antioxidant.....	58
2.3. Hydrogen Abstraction Reactions with 3-Methyl-but-1-ene.....	60
2.4. Substitution Reactions to form a Halogen Containing Alkene.....	61
2.5. Reactions via Aldehyde Functionality .....	62
2.5.1. Reaction Between TEMPO and 2-Phenyl propanal, Using a Cobalt Catalyst Under Oxygen. ....	64
2.5.2. Oxidation of a TEMPO Functionalised Alcohol .....	65
2.6. McMillan Chemistry: Use of a Single Electron Transfer Agent .....	67
2.7. Wittig reaction of 2.08.....	70
2.8. Stability of 2.09: Rearrangement to 2.09' .....	71
2.9. Synthesis of Trapping Molecule Derivatives .....	80
2.9.1. A Less Volatile Trapping Agent .....	82
2.10. Future Work .....	87
2.11. Conclusion .....	88
<b>3. Solution Phase Radical Trapping.....</b>	<b>90</b>
3.1. Introduction.....	90

3.1.1. Solution Phase Spin Trapping .....	90
3.1.2. Methods of Radical Generation.....	90
3.1.3. Aims .....	91
3.2. Trapping the <sup>t</sup> BuOO radical .....	92
3.3. Trapping a Methyl Radical.....	93
3.4. Experiments with a Nitrogen Centred Radical .....	95
3.4.1. Trapping a Nitrogen Centred Radical .....	95
3.4.2. Utilisation of Isotopic Labelling .....	98
3.4.3. Fragmentation Experiments on Captured Nitrogen Radicals.....	98
3.4.4. Reactions with 2-Naphthylamine .....	101
3.4.5. Test Reaction with a Surrogate Trapping Molecule .....	102
3.4.6. Fenton Based Amine Radical Generation .....	104
3.5. Experiments with a Sulfur Centred Radical.....	104
3.5.1. Capture of a Sulfur Centred Radical .....	104
3.5.2. Detection of Other Radicals from the Sulfur System .....	105
3.5.3. AIBN Based Thiyl Radical Generation .....	107
3.5.4. Trapping a Deuterated Sulfur Species .....	109
3.6. Future Work.....	111
3.7. Conclusions.....	112
<b>4. Gas Phase Trapping: Alkene Ozonolysis .....</b>	<b>113</b>
4.1. Introduction:.....	113
4.1.1. Ozonolysis: Criegee Intermediates Chemistry and Atmospherically Relevant Species .....	113
4.1.2. Aims .....	118
4.2. Trapping System and Experimental Design.....	118

4.3. Detection of Radical Intermediates from Ozonolysis Reactions.....	122
4.4. Detection of Products from ·OH Attack.....	127
4.5. Detection of Further Radical Species .....	129
4.5.1. Hydroperoxyl Radical Capture .....	129
4.5.2. Capture of Further Oxidation Products .....	130
4.6. Experiments in a Quartz Tube Flow System.....	133
4.6.1. Confirmation of Radicals: Traditional Spin Trapping.....	135
4.6.2. Trapping Products from α-Pinene Ozonolysis Using Adapted Apparatus.....	136
4.6.3. Reactions to Assist Product Identification.....	139
4.6.4. Reactions Investigating the Trapping Process .....	140
4.7. Application of Trapping System to Other Alkenes .....	142
4.7.1. Limonene Ozonolysis .....	142
4.7.2. β-Pinene Ozonolysis.....	145
4.7.3. 2,3-Dimethylbut-2-ene Ozonolysis .....	148
4.8. Future Work.....	150
4.9. Conclusions.....	151
<b>5. Gas Phase Trapping Development and Scoping.....</b>	<b>153</b>
5.1. Introduction.....	153
5.1.1. Gas Phase Trapping: Radicals and Aerosol Composition.....	153
5.1.2. Aims .....	154
5.2. Gas Phase Trapping Method Development .....	155
5.2.1. Scoping a Sample Support .....	155
5.2.2. Scoping the Impact of Sample Loading.....	158
5.2.3. Optimising Sample Packing.....	160
5.3. Variation of Sampling Time .....	163

5.3.1. Optimisation of Sampling Time .....	163
5.3.2. Minimum Sampling Time .....	164
5.4. Radical Capture from a Low Temperature Plasma.....	166
5.4.1. Plasma Overview .....	166
5.4.2. System Design for Capture of Radicals from Plasma.....	167
5.4.3. Detection of NO <sub>x</sub> Adducts.....	168
5.4.4. Detection of HO <sub>2</sub> <sup>·</sup> and H <sup>·</sup> Radicals from a Room Temperature Plasma .....	172
5.5. Conclusions.....	174
<b>6. Detecting Products from Reaction between Alkanes and the Hydroxyl Radical .....</b>	<b>175</b>
6.1. Introduction.....	175
6.1.1. Atmospheric Hydrocarbons .....	175
6.1.2. Aims .....	177
6.2. Reactions with Long Chain Alkanes .....	178
6.2.1. Radical Generation system .....	179
6.2.2. Initial Peroxyl Radical Detection .....	180
6.2.3. Detection of Further Peroxyl Radicals .....	183
6.2.4. Attempted Detection of Alkoxy Radicals.....	190
6.2.5. Time Profiles of Captured Radical Species .....	191
6.3. Comparison between Modelled and Experimental Kinetics.....	192
6.3.1. Use of Chemical Models .....	192
6.3.2. Model Simulations Using the Master Chemical Mechanism.....	193
6.3.3. Evaluation Relative to Experimental Results .....	198
6.4. Calibration of Trapping Methodology .....	201
6.4.1. Methyl Peroxyl Calibration .....	204
6.4.2. Nonane Peroxyl Calibration .....	206

6.4.3. Calibrating to Lower Concentrations.....	207
6.5. Future Work.....	210
6.6. Conclusion .....	211
<b>7. Real World Sampling - Indoor and Outdoor Air.....</b>	<b>212</b>
7.1. Introduction.....	212
7.1.1. Indoor Air .....	212
7.1.2. Outdoor Air .....	215
7.1.3. Aims .....	216
7.2. Indoor Sampling Site details.....	216
7.3. Indoor Air Sampling Results .....	219
7.3.1. A Peroxyl Radical Product from Ozonolysis: Office .....	219
7.3.2. A Peroxyl Radical from $\cdot\text{OH}$ + Limonene Reaction: Office .....	222
7.3.3. Peroxyl Radical Products: Meeting Room .....	224
7.3.4. Alkoxy Radical Products.....	227
7.3.5. Results from Experiments with Bleach.....	228
7.3.6. Other Radicals Captured from Indoor Air.....	229
7.3.7. Experiments with Increased Temporal Resolution.....	235
7.3.8. Air Fragrance Experiments.....	237
7.4. Outdoor Air Sampling .....	238
7.4.1. Products Detected from Ground Level Outdoor Sampling .....	239
7.4.2. Products Detected from Rooftop Outdoor Sampling.....	241
7.4.3. Sampling Time Variation for Outdoor Sampling.....	242
7.5. Future work .....	243
7.6. Conclusions.....	245
<b>8. Conclusions and Future Work.....</b>	<b>246</b>

<b>9. Experimental</b> .....	<b>249</b>
9.1. Experimental Details for Chapter 2: .....	249
9.1.01. Cobalt catalysed reaction between 3-methyl-1,4-pentadiene and TEMPO under an oxygen atmosphere.....	249
9.1.02. Reaction between 3-methyl-1,4-pentadiene and TEMPO under an oxygen atmosphere.....	250
9.1.03. Reaction between 3-methyl-1,4-pentadiene and TEMPO under an oxygen atmosphere with an antioxidant .....	251
9.1.04. Reaction between 3-methyl-1,4-pentadiene and TEMPO using Fenton based radical generation.....	252
9.1.05. Reaction of 3-methyl-1,4-pentadiene and TEMPO under air.....	253
9.1.06. Reaction of 3-methyl-1,4-pentadiene and TEMPO with AlCl <sub>3</sub> .....	253
9.1.07. Reaction of 3-methyl-1,4-pentadiene and TEMPO with FeCl <sub>3</sub> .....	253
9.1.08. Reaction between 3-methyl-but-1-en-3-ol and HBr .....	254
9.1.09. Reaction between 3-methyl-but-1-en-3-ol and PBr <sub>3</sub> .....	254
9.1.10. Reaction between 3-methyl-but-1-en-3-ol and HCl .....	255
9.1.11. Reaction between 3-methyl-but-1-en-3-ol and thionyl chloride .....	255
9.1.12. Reaction of 3-methyl-but-1-ene and TEMPO under Fenton conditions .....	256
9.1.13. Reaction between $\alpha$ -methylstyrene and TEMPO <sup>141</sup> .....	257
9.1.14. Reaction of 2.06 with pyridinium chlorochromate .....	258
9.1.15. Reaction of 2.06 with Dess-Martin Periodinane .....	258
9.1.16. Reaction of 2.06 using the Swern oxidation procedure. ....	259
9.1.17. Reaction between 2-phenylpropanal and TEMPO .....	259
9.1.18. Attempted preparation of 2.08 .....	260
9.1.19. Preparation of 2.07:.....	260
9.1.20. Preparation of 2.10:.....	261

9.1.21. Preparation of 2.12:.....	262
9.1.22. Preparation of 2.09:.....	263
9.1.23. Preparation of 2.11:.....	264
9.1.24. Preparation of 2.13:.....	265
9.1.25. Rearrangement of 2.09 to form 2.09': .....	266
9.1.26. Rearrangement of 2.11 to form 2.11'.....	267
9.1.27. Rearrangement of 2.13 to form 2.13'.....	268
9.1.28. Probing rearrangement by addition of another nitroxide .....	269
9.1.29. Reaction between trans-1,4-cyclohexanedicarboxylic acid and oxalyl chloride .....	269
9.1.30. Reaction between 2.17 and dimethylamine. ....	270
9.1.31. Hydrogenation of 2.18.....	270
9.1.32. Reaction between 2.19 and TEMPO.....	271
9.1.33. Wittig reaction of 2.20.....	272
9.1.34. Rearrangement of 2.16 to form 2.16'.....	273
9.2. Experimental Details for Chapter 3.....	274
9.2.01. Trapping a <sup>t</sup> BuOO· radical .....	274
9.2.02. Trapping a methyl radical .....	274
9.2.03. Trapping an aminyl radical from n-butylamine with PbO <sub>2</sub> radical generation .....	275
9.2.04. Trapping an aminyl radical from isopropylamine with PbO <sub>2</sub> radical generation .....	275
9.2.05. Trapping an aminyl radical from t-butylamine with PbO <sub>2</sub> radical generation .....	276
9.2.06. Trapping an aminyl radical with 2.11 and PbO <sub>2</sub> radical generation.....	276
9.2.07. MSMS Fragmentation experiments.....	277

9.2.08. Trapping an aminyl radical from 2-naphthylamine with PbO <sub>2</sub> radical generation .....	277
9.2.09. Trapping a Deuterated aminyl radical .....	277
9.2.10. Trapping an aminyl radical with Fenton based radical generation .....	278
9.2.11. Attempted Rearrangement of 3.10 .....	278
9.2.12. Trapping a thio radical with PbO <sub>2</sub> radical generation.....	279
9.2.13. Generation and trapping a thio radical with AIBN radical generation .....	279
9.2.14. Trapping radicals from deuterated thiol 3.16 .....	280
9.3. Experimental details for Chapter 4 .....	280
9.3.01. Radical Trapping from an Aerosol Bag System .....	280
9.3.02. Model for Prediction of 4.14 .....	286
9.3.03. General Procedure for Radical Trapping via an Quartz Flow Tube .....	287
9.3.04. Trapping with both 2.09 and 2.13 .....	288
9.3.05. Reaction in the presence of an ·OH scavenger .....	288
9.3.06. A D <sub>2</sub> O Shake Reaction .....	289
9.3.07. Spin Trapping Radicals Produced from the Quartz Flow Tube.....	289
9.3.08. Application of 2.09' to Radical Trapping.....	290
9.3.09. Trapping Radicals from Limonene Ozonolysis .....	290
9.3.10. Trapping Radicals from the Ozonolysis of β-pinene.....	291
9.3.11. Trapping Radicals From the Ozonolysis of Tetramethylethene .....	292
9.4. Experimental details for Chapter 5 .....	292
9.4.01. Optimisation of Sample Support .....	292
9.4.02. Optimisation of Sample Packing.....	293
9.4.03. Signal Variation with Sample Depth .....	294
9.4.04. Optimisation of Sampling Time .....	294

9.4.05. Representative Procedure for Trapping Radicals from a Low Temperature Plasma.....	294
9.4.06. Trapping of NO.....	295
9.4.07. Attempted Trapping of NO <sub>2</sub> .....	296
9.5. Experimental Details for Chapter 6 .....	297
9.5.01. Generation and Trapping of Radicals from dodecane + ·OH reaction.....	297
9.5.02. Generation and Trapping of Radicals from decane + ·OH reaction.....	298
9.5.03. Generation and Trapping of Radicals from Nonane + ·OH reaction.....	298
9.5.04. Application of 2.13 to the nonane + ·OH reaction.....	299
9.5.05. Modelling the Nonane + ·OH reaction with Kintecus .....	300
9.5.06. Testing variations in the model .....	301
9.5.07. Experimental Kinetic Information for Nonane + ·OH reaction .....	302
9.5.08. Calibration of Methane + ·OH reaction for the MeO <sub>2</sub> radical.....	303
9.5.09. Calibration of Nonane + ·OH reaction for the nonane-O <sub>2</sub> radical .....	304
9.6. Experimental Details for Chapter 7 .....	306
9.6.01. Indoor Air Experiments.....	306
9.6.02. Indoor Air Trapping: Small Office .....	307
9.6.03. Modelling the Limonene Ozonolysis system .....	309
9.6.04. Indoor Air Trapping: Meeting room .....	309
9.6.04. Modelling the α-pinene and limonene ozonolysis system.....	311
9.6.05. Outdoor Air Sampling .....	312
<b>List of Abbreviations:.....</b>	<b>313</b>
<b>Key Structures Discussed Throughout this Thesis .....</b>	<b>319</b>
<b>References .....</b>	<b>320</b>

## List of Figures

Figure 1: Resonance Stabilisation of Coppinger's radical <sup>4</sup> .....	29
Figure 2: Cycle of key reactions for ·OH initiated atmospheric oxidation reactions .....	31
Figure 3: An example of ·OH formation following NO <sub>3</sub> addition to a double bond.....	32
Figure 4: Reaction of luminol with NO <sub>2</sub> , to form an excited species. Fluorescence from relaxation of this species is then monitored for NO <sub>2</sub> measurement.....	38
Figure 5: Capture of ·OH by salicylic acid .....	41
Figure 6: Dominant compounds formed from salicylic acid reactions with ·OH .....	41
Figure 7: Structure of a captured Criegee intermediate from Giorio et al. <sup>77</sup> .....	43
Figure 8: Structures of common spin traps.....	45
Figure 9: Traditional spin trapping of a radical species using DMPO .....	45
Figure 10: Target mechanism for trapping reaction (LG = leaving group).....	48
Figure 11: Resonance stabilisation of the TEMPO radical .....	49
Figure 12: Structural template for a radical trapping molecule .....	49
Figure 13: Literature examples of alkoxyamines <sup>106,108</sup> .....	50
Figure 14: Formation of alkoxyamines using Cu(I), as suggested by Matyjaszewski <sup>110</sup> .....	50
Figure 15: Example scheme showing peroxide decay, and subsequent hydrogen abstraction by the hydroxyl radical.....	51
Figure 16: RSA for the formation of a radical trapping compound .....	53
Figure 17: Target reaction between TEMPO and 3-methylbut-1-ene or 3-methyl-1,4-pentadiene .....	53
Figure 18: Hydrogen abstraction with a cobalt catalyst to form <b>2.01</b> .....	54
Figure 19: Alkene region of a <sup>1</sup> H NMR of a mixture of <b>2.01</b> and <b>2.01'</b> .....	55
Figure 20: Resonance forms of the 3-methyl-1,4-pentadiene radical.....	56
Figure 21: Unwanted trapping reaction by primary TEMPO compound <b>2.01'</b> .....	57
Figure 22: Formation of anthracene from 9,10-dihydroanthracene <sup>129</sup> .....	57
Figure 23: Fenton Reaction to generate hydroxyl radicals .....	58
Figure 24: Formation of β-scission product .....	58
Figure 25: Route to formation of 9,11 or 13 hydroperoxy linoleic acid predicted by Brash <sup>135</sup> .....	59

Figure 26: Formation of new target compound <b>2.02</b> .....	60
Figure 27: Alkene region of a <sup>1</sup> H NMR of <b>2.02'</b> .....	61
Figure 28: Bromination of 3-methyl-but-1-en-3-ol forming <b>2.03</b> and <b>2.03'</b> .....	62
Figure 29: RSA for protecting the alkene prior to TEMPO addition .....	63
Figure 30: New target molecule <b>2.05</b> .....	63
Figure 31: Proposed reaction to form <b>2.05</b> .....	64
Figure 32: Formation of <b>2.06</b> via methodology from Prechter et al. <sup>141</sup> .....	65
Figure 33: Oxidation of <b>2.06</b> to form <b>2.05</b> .....	65
Figure 34: Addition of TEMPO via an enamine intermediate .....	67
Figure 35: Attempted formation of <b>2.05</b> by McMillan Chemistry .....	67
Figure 36: Formation of <b>2.07</b> , showing the aldehyde proton H <sub>A</sub> .....	68
Figure 37: Zoomed in section of <sup>1</sup> H NMR for <b>2.07</b> showing singlet aldehyde signal .....	68
Figure 38: HMBC of <b>2.07</b> , showing interaction between the highlighted atoms in <b>2.07</b> ..	69
Figure 39: Target reaction for the formation of <b>2.08</b> .....	69
Figure 40: Formation of <b>2.09</b> through a Wittig reaction of <b>2.07</b> .....	70
Figure 41: <sup>1</sup> H NMR Alkene region of <b>2.09</b> .....	71
Figure 42: Alkene region of a solution of <b>2.09</b> after several hours. New signals are present at 5.3 and 4.3 ppm. ....	72
Figure 43: Structure of rearrangement product, <b>2.09'</b> .....	72
Figure 44: Signals from <b>2.09</b> and <b>2.09'</b> in <sup>13</sup> C and DEPT-135 experiments .....	73
Figure 45: Degradation of <b>2.09</b> to form <b>2.09'</b> .....	74
Figure 46: <b>2.09</b> trapping TEMPO to form <b>2.09'</b> .....	75
Figure 47: Homolysis of <b>2.09</b> , rearrangement and subsequent trapping to form <b>2.09'</b> ....	76
Figure 48: Trend in alkoxyamine C-O bond strength for different nitroxides .....	77
Figure 49: Variation in C-N distance causing changes to C-O BDE, from Moad et al. <sup>155</sup> ....	78
Figure 50: Suprafacial and antarafacial comparison for [1,3] rearrangement .....	78
Figure 51: [1,3] shift from Majumdar et al. <sup>167</sup> .....	79
Figure 52: Di-radical rearrangement from Berson et al. <sup>168</sup> .....	80
Figure 53: Formation of <b>2.10</b> and <b>2.12</b> .....	81
Figure 54: Formation of <b>2.11</b> and <b>2.13</b> .....	81
Figure 55: Structure of decay compounds <b>2.11'</b> and <b>2.13'</b> .....	81

Figure 56: Anticipated boiling points of the expected adducts from H radical capture by <b>2.09</b> and <b>2.11</b> <sup>169,170</sup> .....	82
Figure 57: Structure of new target molecule .....	83
Figure 58: Reaction route to form <b>2.19</b> , precursor to <b>2.16</b> .....	83
Figure 59: Structures of mono and di amides <b>2.18</b> and <b>2.18'</b> .....	84
Figure 60: Formation of <b>2.20</b> . .....	84
Figure 61: Formation of <b>2.16</b> from <b>2.20</b> .....	85
Figure 62: <sup>1</sup> H NMR of <b>2.16</b> .....	86
Figure 63: Rearrangement of <b>2.16</b> to form <b>2.16'</b> .....	86
Figure 64: Different aldehydes that may be suitable precursors for trapping compounds .....	87
Figure 65: An example of a potentially water soluble trapping compound .....	88
Figure 66: Structures of synthesised trapping molecules .....	89
Figure 67: Trapping of <sup>t</sup> BuOO radical by <b>2.09</b> to form <b>3.01</b> .....	92
Figure 68: Signal corresponding to <b>3.01</b> .....	92
Figure 69: MS produced by fragmentation of <b>3.01</b> .....	93
Figure 70: Fragmentation of <b>3.01</b> <sup>192</sup> .....	93
Figure 71: Generation and capture of the methyl radical to form <b>3.02</b> .....	94
Figure 72: Mass Spectrum showing the formation of <b>3.02</b> .....	94
Figure 73: Formation of <b>3.03</b> by capture of a nitrogen centred radical .....	95
Figure 74: MS from <b>3.03'</b> , with a possible structure matching an [M+H-2] <sup>+</sup> ion of <b>3.03</b> ...	95
Figure 75: Expected capture of a nitrogen centred radical from isopropylamine .....	96
Figure 76: '[M+H-2] <sup>+</sup> ' product <b>3.04'</b> .....	96
Figure 77: Possible imine formation from amines .....	97
Figure 78: Reaction to form <b>3.05</b> .....	97
Figure 79: MS for <b>3.05'</b> .....	97
Figure 80: Structure of the deuterated species <b>3.06</b> .....	98
Figure 81: MS of <b>3.07</b> .....	98
Figure 82: Fragmentation of m/z 180 from <b>3.03'</b> , with key fragmentations indicated .....	99
Figure 83: Fragmentation of m/z 180 from <b>3.05'</b> , with key fragmentation indicated .....	99
Figure 84: Anticipated structures corresponding to ions 109 and 107 m/z respectively.	100

Figure 85: n-Butylamine trapping with <b>2.11</b> to form <b>3.08</b> .....	100
Figure 86: Fragmentation of m/z 166 from <b>3.08'</b> , showing fragments at 95 and 93 m/z. .....	101
Figure 87: Anticipated structures for fragments at 95 and 93 /z respectively .....	101
Figure 88: Reaction to form <b>3.09</b> from 2-naphthylamine.....	102
Figure 89: MS of <b>3.09'</b> from naphthylamine radical capture.....	102
Figure 90: Possible scheme for formation of <b>3.10</b> through allylcyclohexylamine.....	103
Figure 91: Post reaction allylcyclohexylamine with no indication of <b>3.10</b> .....	103
Figure 92: Expected formation of <b>3.01</b> via Fenton Reaction .....	104
Figure 93: Expected trapping of a thiyl radical .....	104
Figure 94: MS of thiol reaction products including <b>3.11'</b> .....	105
Figure 95: <b>3.12</b> and <b>3.13</b> , formed following thiyl radicals reacting with oxygen .....	106
Figure 96: Species <b>3.14</b> , giving signal at 358 m/z.....	107
Figure 97: Capture of a thiyl radical, using AIBN as an initiator .....	107
Figure 98: Partial MS of AIBN initiated thiyl radical capture .....	108
Figure 99: Formation of <b>3.17</b> from <b>3.15</b> .....	109
Figure 100: Signal from captured deuterated dodecanethiol radical .....	110
Figure 101: Fragmentation of signal at 334 m/z.....	110
Figure 102: Fragmentations to form 226 m/z. The double bond is arbitrarily positioned on the trap segment of the starting species. ....	110
Figure 103: Signals from <b>3.18</b> and <b>3.19</b> .....	111
Figure 104: General gas phase ozonolysis mechanism.....	113
Figure 105: Resonance forms of a simple Criegee intermediate.....	114
Figure 106: Mechanism for the formation of peroxy radicals from a Criegee intermediate .....	114
Figure 107: Route showing ·OH and a peroxy radical formation from α-pinene ozonolysis .....	115
Figure 108: Formation of pinonic acid from α-pinene ozonolysis <sup>224</sup> .....	116
Figure 109: Proposed mechanism for norpinonic acid formation from Ma et al. <sup>225</sup> .....	117
Figure 110: Schematic for trapping system utilising an aerosol chamber.....	119
Figure 111: Trapping system utilising an aerosol chamber .....	119

Figure 112: Overall MS from $\alpha$ -pinene ozonolysis in an aerosol bag .....	120
Figure 113: Structures of TEMPO based fragments at 158 m/z and 142 m/z .....	121
Figure 114: Detected non-radical products of $\alpha$ -pinene ozonolysis.....	121
Figure 115: Formation of peroxy radicals <b>4.01a</b> and <b>4.01b</b> following $\alpha$ -pinene ozonolysis <sup>229,230</sup> .....	122
Figure 116: <b>4.02a</b> and <b>4.02b</b> , products formed upon trapping <b>4.01a</b> and <b>4.01b</b> with <b>2.09</b> . .....	123
Figure 117: Signal observed for <b>4.02</b> .....	123
Figure 118: MS showing lack of signal for <b>2.02</b> in blank experiment .....	123
Figure 119: Formation of <b>4.03</b> through $\alpha$ -pinene ozonolysis and loss of CO + OH. <sup>229,230</sup>	124
Figure 120: <b>4.04</b> , formed by capture of <b>4.03</b> with <b>2.09</b> .....	124
Figure 121: Signal observed corresponding to <b>4.04</b> .....	125
Figure 122: MS showing lack of signal for <b>4.04</b> from blank experiment .....	125
Figure 123: Compounds formed by capture of <b>4.01</b> and <b>4.03</b> with <b>2.11</b> and <b>2.13</b> .....	126
Figure 124: Radicals formed from $\cdot$ OH attack on $\alpha$ -pinene, in the presence of oxygen <sup>229,230</sup> .....	127
Figure 125: <b>4.10</b> formed by capture of <b>4.09</b> by <b>2.09</b> .....	128
Figure 126: Signal corresponding to <b>4.10</b> .....	128
Figure 127: A route to formation of HO <sub>2</sub> $\cdot$ and pinonaldehyde from $\alpha$ -pinene <sup>229,230</sup> .....	129
Figure 128: Compounds formed by capture of the hydroperoxyl radical by <b>2.09</b> , <b>2.11</b> and <b>2.13</b> respectively. ....	129
Figure 129: Signal corresponding to <b>4.11</b> .....	130
Figure 130: Formation of <b>4.14</b> via <b>4.01b</b> . <sup>245</sup> .....	130
Figure 131: Lack of signal corresponding to trapped <b>4.14</b> .....	131
Figure 132: Formation of bridged peroxides <b>4.15</b> , as suggested by Berndt et al. <sup>242</sup> .....	132
Figure 133: <b>4.16</b> formed by capture of <b>4.15</b> by <b>2.09</b> .....	132
Figure 134: Signal corresponding to <b>4.16</b> .....	133
Figure 135: Schematic of quartz tube sampling system .....	134
Figure 136: Quartz tube sampling system .....	135
Figure 137: EPR from spin trapping of products from the $\alpha$ -pinene ozonolysis gas flow	135
Figure 138: Overall MS of products from $\alpha$ -pinene quartz tube ozonolysis .....	136

Figure 139: Signals detected in quartz tube system, corresponding to <b>4.02</b> , <b>4.10</b> , <b>4.11</b> and lack of signal for <b>4.15</b> .	137
Figure 140: Formation of <b>4.17</b> and <b>4.18</b> <sup>229,230</sup>	138
Figure 141: Compounds from trapped alkoxy radicals	138
Figure 142: MS signals corresponding to <b>4.19</b> and <b>4.20</b>	139
Figure 143: Lack of signal for <b>4.10</b> in the presence of an ·OH scavenger, while <b>4.02</b> can still be observed	139
Figure 145: OH-OD exchange with <b>4.10</b>	140
Figure 144: Change in signal upon D <sub>2</sub> O shake	140
Figure 146: Signal from <b>4.13</b> and <b>4.11</b> detected with a mix of <b>2.13</b> and <b>2.09</b>	141
Figure 147: Application of <b>2.09'</b> to trapping system	141
Figure 148: Formation of peroxy radicals <b>4.21a</b> and <b>4.21b</b> from limonene ozonolysis <sup>229,230</sup>	142
Figure 149: Expected structures of captured ozonolysis products	143
Figure 150: Product <b>4.22</b> , detected from ozonolysis of limonene	143
Figure 151: Formation of RO <sub>2</sub> radicals from ·OH attack on limonene <sup>229,230</sup>	144
Figure 152: MS of <b>4.24</b> , captured from ·OH attack on limonene	144
Figure 153: Expected structure of ·OH attack products from limonene	145
Figure 154: Formation of radicals via Criegee intermediates from β-pinene ozonolysis <sup>229,230</sup>	146
Figure 155: MS of <b>4.26</b>	146
Figure 156: Compound formed by the trapping of <b>4.25</b>	147
Figure 157: Isomers <b>4.27</b> formed from ·OH attack on β-pinene in the presence of oxygen <sup>229,230</sup>	147
Figure 158: Compounds formed on trapping <b>4.27</b>	148
Figure 159: MS for <b>4.28</b>	148
Figure 160: Formation of <b>4.29</b> from TME ozonolysis <sup>229,230</sup>	149
Figure 161: Compound from trapped <b>4.29</b>	149
Figure 162: MS signal from <b>4.30</b>	149
Figure 163: Formation and trapping of <b>4.31</b> from ·OH attack on TME <sup>229,230</sup>	150
Figure 164: MS signal from <b>4.32</b>	150

Figure 165: Simple trapping scheme.....	155
Figure 166: Glass wool loaded inside a sample tube.....	156
Figure 167: Signal change on variation of sample support.....	157
Figure 168: Change of signal for <b>4.11</b> with mass of trap applied .....	158
Figure 169: Comparison of different ratios of silica to trapping material for <b>4.11</b> .....	159
Figure 170: Different methods of silica loading, 'tapped', 'sandwiched' and 'squashed' respectively .....	160
Figure 171: Variation in <b>4.11</b> signal with different packing method. T = Tapped, S = Sandwiched, Sq= Squashed.....	161
Figure 172: Image of tube with a larger silica trap layer .....	162
Figure 173: Variation in signal for <b>4.11</b> with silica depth .....	162
Figure 174: Change in signal for <b>4.11</b> as sampling time is modified from 4-90 minutes .	164
Figure 175: Change in signal for <b>4.11</b> as sampling time is modified between 20-120 seconds .....	165
Figure 176: Scheme for radical trapping from plasma .....	168
Figure 177: <b>5.01</b> and <b>5.02</b> , from <b>2.09</b> capturing NO and NO <sub>2</sub> respectively .....	168
Figure 178: Detection of <b>5.01</b> from various plasma experiments .....	169
Figure 179: Formation of <b>5.03</b> through trapping of NO with <b>2.11</b> .....	170
Figure 180: Comparison of signal for captured NO from <b>2.09</b> and <b>2.11</b> .....	171
Figure 181: Variation in signal for <b>5.01</b> with exposure time.....	172
Figure 182: Variation in signal for <b>4.11</b> as exposure time changes .....	172
Figure 183: Expected product from hydrogen radical capture with <b>2.09</b> .....	173
Figure 184: Possible cations from fragmentations of <b>5.04</b> .....	173
Figure 185: Fragmentation of <b>5.04</b> .....	174
Figure 186: Structures of PFBHA and BSTFA used by Yu et al. for carbonyl and alcohol functionalisation respectively. <sup>303</sup> .....	177
Figure 187: Expected mechanism for the formation of a peroxy radical via hydrogen abstraction from n-nonane (most likely RO <sub>2</sub> species is shown) <sup>229,230</sup> .....	178
Figure 188: Scheme of the alkane reaction and trapping system .....	179
Figure 189: Photo of alkane reaction and trapping system.....	180
Figure 190: MS for <b>6.02</b> from n-decane.....	181

Figure 191: Structure of <b>6.02</b> .....	181
Figure 192: MS signal for <b>6.03</b> , captured <b>6.01</b> .....	182
Figure 193: Structure of adduct <b>6.03</b> .....	182
Figure 194: Different possible isomers of <b>6.03</b> .....	183
Figure 195: Percentage of attack at each carbon environment for hydrogen abstraction from n-nonane using structure activity relationships from Kwok et al. <sup>315</sup> .....	183
Figure 196: 1,5- hydrogen shift to form RO <sub>2</sub> radical <b>6.05</b> .....	184
Figure 197: MS of <b>6.06</b> , trapped <b>6.05</b> .....	184
Figure 198: Structure of <b>6.06</b> , captured <b>6.05</b> .....	185
Figure 199: Example of intramolecular hydrogen abstraction from Jenner et al. <sup>318</sup> .....	185
Figure 200: Routes to form <b>6.09</b> from <b>6.05</b> <sup>229,230</sup> .....	185
Figure 201: MS for <b>4.11</b> , captured hydroperoxyl radical .....	186
Figure 202: Formation of methyl alkoxy radicals via a tetraoxide intermediate .....	186
Figure 203: Formation of <b>6.10</b> and <b>6.11</b> from <b>6.09</b> <sup>229,230</sup> .....	187
Figure 204: TEMPO M+1 signal obscuring any signal for <b>6.09</b> .....	187
Figure 205: MS for <b>6.11</b> , captured <b>6.10</b> .....	188
Figure 206: Formation of <b>6.12</b> , from <b>6.01</b> <sup>229,230</sup> .....	188
Figure 207: MS for <b>6.13</b> , captured <b>6.12</b> .....	189
Figure 208: Structure of <b>6.13</b> .....	189
Figure 209: Structures of <b>6.14</b> and <b>6.15</b> , trapped <b>6.01</b> and <b>6.05</b> respectively .....	189
Figure 210: MS signal for <b>6.14</b> .....	190
Figure 211: MS signal for <b>6.15</b> .....	190
Figure 212: Lack of signal for trapped <b>6.04</b> or <b>6.16</b> .....	191
Figure 213: Structures of alkoxy radicals predicted to be present but not clearly identifiable as captured. ....	191
Figure 214: Variation in signal with experimental time for radicals from by the n-nonane + ·OH reaction .....	192
Figure 215: Impact on <b>6.05</b> concentration by varying RO <sub>2</sub> + RO <sub>2</sub> reaction rates .....	194
Figure 216: Impact on <b>6.05</b> of increasing/decreasing [·OH] in the model .....	195
Figure 217: Variation for <b>6.05</b> with changing wall loss .....	196
Figure 218: Modelled concentrations for initial species RO <sub>2</sub> <b>6.01</b> and RO <b>6.04</b> .....	197

Figure 219: Results of modelling the kinetics of <b>6.01</b> , <b>6.05</b> , <b>6.10</b> , <b>6.12</b> and the hydroperoxy radical from the nonane + $\cdot\text{OH}$ reaction .....	198
Figure 220: Experimental results compared to modelled kinetics for <b>6.01</b> , <b>6.05</b> , the hydroperoxy radical, <b>6.10</b> and <b>6.12</b> .....	199
Figure 221: Set-up for calibration of trapping procedure.....	203
Figure 222: Capture of the methyl peroxide radical, <b>6.17</b> .....	204
Figure 223: MS signal from <b>6.18</b> , captured <b>6.17</b> .....	205
Figure 224: Calibration results for radical <b>6.17</b> .....	205
Figure 225: Calibration results for radical <b>6.01</b> .....	206
Figure 226: Applying dilutions to the methyl peroxy ( <b>6.17</b> ) calibration.....	208
Figure 227: Applying dilutions to <b>6.01</b> calibration.....	208
Figure 228: Room layout for office sampling, showing positions of $\text{O}_3$ monitor, MS, and radical trapping equipment .....	217
Figure 229: Room layout for meeting room sampling, showing positions of $\text{O}_3$ , NO and PM monitors, MS and the radical trapping equipment. ....	217
Figure 230: Plot showing changes in intensity of ozonolysis product <b>4.22</b> during indoor air office experiments .....	220
Figure 231: Limonene decay measured by PTR during experiment 5 (Table 1).....	221
Figure 232: Kintecus plot on the effect of changing [limonene] and [ $\text{O}_3$ ] on [ <b>4.21</b> ] <sup>323</sup> ...222	222
Figure 233: Plot showing changes in intensity of product <b>4.24</b> during office experiments .....	223
Figure 234: Kintecus plot showing the effect of changing [limonene] and [ $\text{O}_3$ ] on [ <b>4.23</b> ] <sup>323</sup> .....	223
Figure 235: Signal variation for <b>4.24</b> and <b>4.22</b> respectively.....	224
Figure 236: Model results for varying meeting room ozone and terpene concentrations <sup>323</sup> .....	225
Figure 237: Change in NO and $\text{NO}_2$ levels upon ozone addition .....	226
Figure 238: Impact on <b>4.21</b> from incorporating NO measurements into the model <sup>323</sup> ...226	226
Figure 239: Alkoxy radicals <b>7.01a</b> and <b>7.02a</b> expected to form in oxidation of limonene .....	227

Figure 240: Modelled concentrations of peroxy species <b>4.21</b> and <b>4.23</b> and alkoxy species <b>7.01</b> and <b>7.02</b> from the indoor air system <sup>323</sup> .....	228
Figure 241: Signals for <b>4.22</b> and <b>4.24</b> respectively in meeting room experiments .....	229
Figure 242: Variation in <b>4.11</b> during indoor air experiments .....	230
Figure 243: PAN formation from the CH <sub>3</sub> C(O)O <sub>2</sub> radical .....	230
Figure 244: A route to form <b>7.03</b> <sup>229,230</sup> .....	231
Figure 245: MS signal for <b>7.04</b> , the captured CH <sub>3</sub> C(O)O <sub>2</sub> radical.....	231
Figure 246: A mechanism for limonaldehyde formation via .OH attack <sup>229,230</sup> .....	232
Figure 247: A mechanism for limonaldehyde formation via ozonolysis <sup>229,230</sup> .....	232
Figure 248: Formation of radical products from limonaldehyde <sup>229,230</sup> .....	233
Figure 249: Model comparing expected formation of radicals <b>7.05</b> with <b>4.21</b> and <b>4.23</b> from ozonolysis and .OH attack on limonene. <sup>323</sup> .....	233
Figure 250: Variation in signal for adduct <b>7.07</b> in VOC+O <sub>3</sub> experiment, and elevated O <sub>3</sub> without VOC experiment respectively. ....	234
Figure 251: Structure for captured <b>7.07</b> .....	234
Figure 252: Variation in signal for adduct <b>4.22</b> during indoor air (meeting room) experiments .....	235
Figure 253: GC-MS data showing limonene decay .....	236
Figure 254: Variation in signal for <b>4.24</b> and <b>4.02</b> respectively during indoor air (meeting room) experiments .....	236
Figure 255: Comparison of signals for <b>4.22</b> from indoor air meeting room.....	237
Figure 256: GC-MS data for limonene from canister samples of air freshener experiment .....	238
Figure 257: Images of indoor and outdoor sampling sites .....	239
Figure 258: Signals detected from ground level outdoor sampling, corresponding <b>4.11</b> , <b>7.08</b> , <b>4.04</b> and <b>6.18</b> clockwise. ....	240
Figure 259: Results showing the capture of radicals from rooftop sampling.....	241
Figure 260: Change in <b>6.18</b> signal strength as sampling time changes in outdoor sampling. ....	242
Figure 261: Lack of signal in night experiments for <b>7.08</b> and <b>4.11</b> .....	243
Figure 262: Formation of <b>2.01</b> by reaction with TEMPO and a Co catalyst.....	249

Figure 263: Formation of <b>2.01</b> and <b>2.01'</b> by reaction with TEMPO .....	250
Figure 264: Formation of <b>2.01</b> and <b>2.01'</b> by reaction with TEMPO in the presence of BHT .....	251
Figure 265: Formation of <b>2.01</b> and <b>2.01'</b> utilising Fenton chemistry .....	252
Figure 266: Formation of <b>2.01</b> and <b>2.01'</b> .....	253
Figure 267: Attempted formation of <b>2.01</b> using AlCl <sub>3</sub> .....	253
Figure 268: Attempted formation of <b>2.01</b> using FeCl <sub>3</sub> .....	253
Figure 269: Formation of <b>2.03</b> and <b>2.03'</b> through reaction with HBr .....	254
Figure 270: Formation of <b>2.03</b> and <b>2.03'</b> through reaction with PBr <sub>3</sub> .....	254
Figure 271: Formation of <b>2.04</b> and <b>2.04'</b> through reaction with HCl .....	255
Figure 272: Formation of <b>2.04</b> and <b>2.04'</b> through reaction with thionyl chloride.....	255
Figure 273: Attempted formation of <b>2.02</b> and <b>2.02'</b> through Fenton reaction.....	256
Figure 274: Formation of <b>2.06</b> , following method of Prechter et al. <sup>141</sup> .....	257
Figure 275: Formation of acetophenone through PCC oxidation.....	258
Figure 276: Attempted oxidation of <b>2.06</b> with DMP.....	258
Figure 277: Attempted Swern oxidation of <b>2.06</b> .....	259
Figure 278: Attempted formation of <b>2.05</b> .....	259
Figure 279: Attempted formation of <b>2.08</b> .....	260
Figure 280: Formation of <b>2.07</b> .....	260
Figure 281: Formation of <b>2.10</b> .....	261
Figure 282: Formation of <b>2.12</b> .....	262
Figure 283: Formation of <b>2.09</b> .....	263
Figure 284: Formation of <b>2.11</b> .....	264
Figure 285: Formation of <b>2.13</b> .....	265
Figure 286: Formation of <b>2.09'</b> .....	266
Figure 287: Degradation of <b>2.09</b> .....	266
Figure 288: Formation of <b>2.11'</b> .....	267
Figure 289: Degradation of <b>2.11</b> .....	267
Figure 290: Formation of <b>2.13'</b> .....	268
Figure 291: Degradation of <b>2.13</b> .....	268
Figure 292: Formation of <b>2.17</b> .....	269

Figure 293: Formation of <b>2.18</b> .....	270
Figure 294: Formation of <b>2.19</b> .....	270
Figure 295: Formation of <b>2.20</b> .....	271
Figure 296: Formation of <b>2.16</b> .....	272
Figure 297: COSY of <b>2.16</b> .....	273
Figure 298: Formation of <b>2.16'</b> .....	273
Figure 299: Trapping of the <sup>t</sup> BuOO· radical by <b>2.09</b> .....	274
Figure 300: Capture of a methyl radical by <b>2.09</b> .....	274
Figure 301: Anticipated reaction for the formation of <b>3.03</b> .....	275
Figure 302: Anticipated reaction for the formation of <b>2.09</b> .....	275
Figure 303: Anticipated reaction for the capture of a nitrogen based radical by <b>2.09</b> ....	276
Figure 304: Anticipated reaction for trapping of an amine radical with <b>2.11</b> .....	276
Figure 305: Anticipated reaction for trapping of an amine radical with <b>2.09</b> .....	277
Figure 306: Capture of a deuterated amine radical.....	277
Figure 307: Anticipated reaction for amine radical trapping with <b>2.09</b> via Fenton chemistry .....	278
Figure 308: Reaction of surrogate trapping molecule <b>3.10</b> .....	278
Figure 309: Anticipated reaction for the capture of a thio based radical by <b>2.09</b> .....	279
Figure 310: Generation and capture of a thio radical using AIBN initiator .....	279
Figure 311: Trapping a thieryl radical from a deuterated thiol .....	280
Figure 312: Schematic representation of aerosol bag system .....	281
Figure 313: MS of products captured from aerosol bag experiment with <b>2.09</b> . The positions of key captured radicals discussed in <b>Chapter 4</b> are indicated .....	281
Figure 314: Capture of <b>4.01</b> to form <b>4.05</b> .....	282
Figure 315: Capture of <b>4.03</b> to form <b>4.06</b> .....	282
Figure 316: Capture of <b>4.09</b> to form <b>4.33</b> .....	283
Figure 317: Capture of HOO·, to form <b>4.12</b> .....	283
Figure 318: Capture of <b>4.01</b> to form <b>4.07</b> .....	284
Figure 319: Capture of <b>4.03</b> to form <b>4.08</b> .....	284
Figure 320: Capture of <b>4.09</b> to form <b>4.34</b> .....	284
Figure 321: Capture of HOO·, to form <b>4.13</b> .....	285

Figure 322: Structures of <b>4.33</b> and <b>4.34</b> .....	285
Figure 323: Lack of <b>4.02</b> from blank experiment.....	285
Figure 324: Lack of <b>4.04</b> from blank experiment.....	286
Figure 325: Modelled formation of <b>4.14</b> compared to <b>4.01</b> .....	287
Figure 326: Schematic for trapping within a quartz flow tube.....	287
Figure 327: MS of products captured from quartz flow tube experiment with <b>2.09</b> . The positions of key captured radicals discussed in <b>Chapter 4</b> are indicated.....	288
Figure 328: <b>4.13</b> and <b>4.11</b> produced from trapping with a mixture of <b>2.09</b> and <b>2.13</b> .....	288
Figure 329: No <b>4.10</b> , but presence of <b>4.02</b> following reaction with an $\cdot\text{OH}$ scavenger....	289
Figure 330: Change in signal for <b>3.10</b> upon $\text{D}_2\text{O}$ shake.....	289
Figure 331: EPR from capture of radicals from $\alpha$ -pinene ozonolysis.....	290
Figure 332: Lack for signal for trapping with <b>2.09'</b> .....	290
Figure 333: Capture of radical products from Limonene, using <b>2.09</b> .....	290
Figure 334: Overall MS from trapping of radicals from limonene.....	291
Figure 335: Capture of radical products from $\beta$ -pinene, using <b>2.09</b> .....	291
Figure 336: Overall MS from trapping products from $\beta$ -pinene.....	291
Figure 337: Capture of Radical Products from TME, using <b>2.09</b> .....	292
Figure 338: MS showing products captured from TME.....	292
Figure 339: Signal for <b>4.11</b> from radical trapping.....	293
Figure 340: MS from exposure of <b>2.09</b> to plasma (with air and water).....	295
Figure 341: Capture of the NO radical.....	295
Figure 342: Target reaction for the capture of $\text{NO}_2$ .....	296
Figure 343: Lack of signal for <b>5.02</b> .....	297
Figure 344: Capture of radical products from dodecane's reaction with $\cdot\text{OH}$ , using <b>2.09</b> .....	297
Figure 345: Capture of radical products from decane's reaction with $\cdot\text{OH}$ , using <b>2.09</b> .....	298
Figure 346: Overall MS for decane reaction.....	298
Figure 347: Capture of radical products from nonane's reaction with $\cdot\text{OH}$ , using <b>2.09</b> .....	298
Figure 348: Overall MS for nonane experiments with <b>2.09</b> .....	299
Figure 349: Capture of radical products from nonane's reaction with $\cdot\text{OH}$ , using <b>2.13</b> .....	299
Figure 350: Overall MS for nonane experiments with <b>2.13</b> .....	300
Figure 351: Model for investigated radical species formed in nonane + $\cdot\text{OH}$ reaction. ....	300

Figure 352: Variation in signal on changing RO <sub>2</sub> reaction rate .....	301
Figure 353: Variation in signal on changing [OH].....	301
Figure 354: Variation in signal on changing wall loss rates .....	302
Figure 355: Experimental kinetic information for Nonane + ·OH reaction.....	303
Figure 356: Trapping the MeO <sub>2</sub> radical to form <b>6.17</b> .....	303
Figure 357: Calibration plot for <b>6.17</b> .....	304
Figure 358: Calibration between lamp current and [HO <sub>x</sub> ].....	304
Figure 359: Trapping the nonane peroxy radical to form <b>6.03</b> .....	304
Figure 360: Calibration plot for <b>6.03</b> .....	305
Figure 361: Relationship between current and [HO <sub>x</sub> ].....	305
Figure 362: Room layout for office sampling, showing positions of O <sub>3</sub> monitor, MS, and radical trapping equipment .....	307
Figure 363: Temperature and O <sub>3</sub> Variation during office experiments.....	308
Figure 364: <b>6.17</b> from indoor air experiments.....	308
Figure 365: Modelled data for office experiments .....	309
Figure 366: Meeting room layout .....	309
Figure 367: Conditions for Meeting room experiments .....	310
Figure 368: Canister data for Air Freshener experiments .....	311
Figure 369: Model variation in meeting room experiments.....	311

## Acknowledgements

During the process of creating this thesis, I have benefitted from the help of many people, which I would like to acknowledge here. Firstly, my supervisors Victor Chechik and Andrew Rickard for their invaluable input throughout the course of my PhD. I would also like to thank members of the Chechik group including Phil Groves, Zhou Lu, Sindhu Suravarum, Brendan Garrett, Rodolfo Estrada Tun, Joe Atkin and Chris Unsworth for creating a supportive lab atmosphere, as well as enduring my presentations at group meetings. In addition to this, I would like to thank Valentin Dru and Martine Ballinger for their work on areas related to this project.

Many of the experiments detailed within this PhD would not have been possible without the help of various people. I would like to thank Heather Fish for help with NMR, as well as Ed Bergstrom and Karl Heaton for help with MS experiments, and also Yury Gorbanev for assistance with plasma experiments. For the calibration experiments conducted at The University of Leeds I would like to thank Lavinia Onel, Paul Seakins and Dwayne Heard for allowing me to use their lab, and enduring my presence in Leeds for a few days. The  $\alpha$ -pinene ozonolysis experiments in an aerosol bag would also not have been possible without the input of Kelly Pereira and Jacqui Hamilton. For the indoor air experiments I would like to thank Terry Dillon, Jacob Shaw, Josh Boothroyd and Marvin Shaw, who conducted other measurements including canister sampling and PTR-MS that have been used here to support the evidence from radical capture. Also thanks to members of WACL for allowing these measurements to take place.

With regard to keeping me sane, I would like to thank many members of York Dancesport, especially Katie Peeling, Katherine Jackson, Lou Lambton, Nicola Haydon, Lydia Teale and Anna Hughes. Also, partners at Waitrose York: in particular Andy Reed, Rob McDermott and Simon Ratcliff. Finally, I would like to thank my family for their support (and proof reading) during the course of this PhD.

## Declaration

I declare that this thesis is a presentation of original work and I am the sole author. This work has not previously been presented for an award at this, or any other, university. All sources are acknowledged as references.

Initial synthesis of precursors **2.10** and **2.12**, as well as traps **2.11** and **2.13** and stability measurements of these latter species, were taken by Valentin Dru, a visiting student working under my supervision. These syntheses were later improved by myself, while all uses of these compounds for radical trapping were also conducted by me.

Measurements taken from the  $\alpha$ -pinene SOA chamber were conducted using a set-up developed by Kelly Pereira and Jacqui Hamilton from the Wolfson Atmospheric Chemistry Laboratories, University of York.

Radical generation using a low temperature plasma was conducted using equipment developed and operated by Yury Gorbanev.

Measurements for the calibrations with n-nonane and methane were collected from a system designed and operated by Lavinia Onel, Dwayne Heard and Paul Seakins from The University of Leeds.

Indoor air experiments were conducted in collaboration with Terry Dillon, Jacob Shaw, Joshua Boothroyd and Marvin Shaw from the Wolfson Atmospheric Chemistry Laboratories, University of York. They took measurements including canister samples, online MS, temperature, O<sub>3</sub> and NO<sub>x</sub>. All radical trapping measurements were taken by myself.

# 1. Introduction

## 1.1 Radical Classification and Stability

In chemistry, radicals can be defined as molecules with an unpaired electron.<sup>1</sup> These species will often be highly reactive, and consequently will be present in low concentrations and exhibit short lifetimes. For example, a lifetime of ca. 5  $\mu\text{s}$  has previously been found for the hydroperoxyl radical ( $\text{HO}_2\cdot$ ) in solution.<sup>2</sup> However, more stable radicals can have considerably longer lifetimes. As an example, 2,2,6,6 – tetramethylpiperidine 1-oxyl (TEMPO) is sufficiently stable to be commercially available. Radical stability is significantly influenced by both mesomeric and steric effects. A radical will be more stable if the unpaired electron can be delocalised, for example around an aromatic system as for the triphenylmethyl radical first described by Gomberg.<sup>3</sup> Other compounds, for example Coppinger's radical, are also highly stable. Indeed, Coppinger's radical is sufficiently stable that it can be isolated in solid form and is effectively inert to reaction with oxygen.<sup>4</sup> This resonance stabilisation is shown in Figure 1.

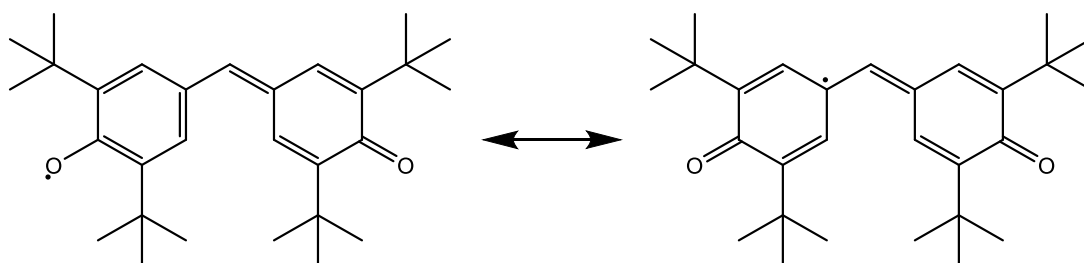


Figure 1: Resonance Stabilisation of Coppinger's radical<sup>4</sup>

This stabilisation is also impacted by steric effects – if access to the radical centre is hindered, the radical will be considerably more stable than a non-hindered equivalent. In Coppinger's radical above the <sup>t</sup>butyl groups provide a large degree of steric bulk to hinder any approach to the radical centre.<sup>4</sup>

Owing to the unpaired electron, radical species will also be paramagnetic. This paramagnetism is the basis for the Electron Paramagnetic Resonance (EPR) based study of radicals. The EPR process works by the application of a magnetic field, whereby the electron spin of the radical will result in two non-degenerate energy levels ( $M_s = +\frac{1}{2}$  and  $M_s = -\frac{1}{2}$ ), analogous to Nuclear Magnetic Resonance (NMR) for nuclear spin. Application of an electromagnetic field, perpendicular to the static magnetic field, can then be used to induce transition from  $M_s = +\frac{1}{2}$  to  $M_s = -\frac{1}{2}$ .<sup>5</sup> The energy gap from between these spin states can be found by use of the below equation, with energy gap ( $\Delta E$ ) between  $M_s = +\frac{1}{2}$  and  $M_s = -\frac{1}{2}$ , where  $g_e$  = g-factor (2.0023 for a free electron),  $\beta_e$  = Bohr magneton and  $B_0$  = external magnetic field.

$$\Delta E = g_e \beta_e B_0 \quad (1)$$

While this technique is more sensitive than NMR, owing to the magnetic moment of an electron being much larger than that of a nucleus (e.g.  $^1\text{H}$ ), its use is much less widespread, largely due to the difficulty in analysing radicals with very short lifetimes. However, the application of spin traps made analysis of short lived radicals significantly easier.

## 1.2. The Role of Radical Chemistry Within the Atmosphere

Radicals form an essential component of atmospheric chemistry, both in the ambient and indoor environments, and as such are of immense interest to atmospheric chemists because of the impact of this chemistry on climate, air quality and human health. The primary example of this would be the role that atmospheric radicals play in the cleaning process of the atmosphere, initiating the oxidative removal of most atmospheric pollutants, such as methane.<sup>6,7</sup> This is shown in a generic scheme in Figure 2. The radical species shown here also play a key role in the formation of 'secondary' pollutants, for example ozone or secondary organic aerosol (SOA).

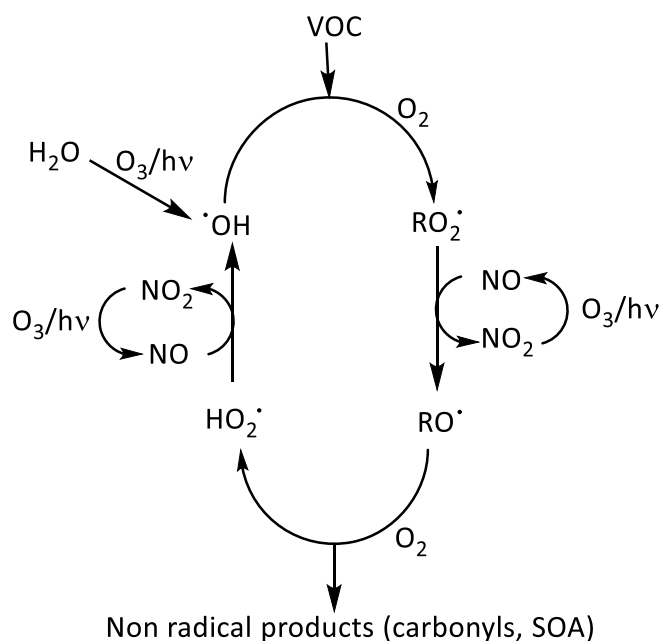
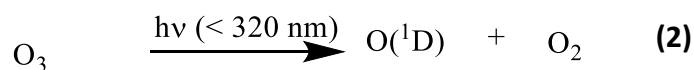


Figure 2: Cycle of key reactions for  $\cdot\text{OH}$  initiated atmospheric oxidation reactions

Atmospheric radicals are present at relatively low concentration: typical  $\cdot\text{OH}$  and  $\text{HO}_2\cdot$  concentrations are  $10^6$  and  $10^8$  molecule  $\text{cm}^{-3}$  respectively during the day.<sup>8</sup> These species will also have short lifetimes, of ca. 1 and 100 s respectively.<sup>9,10</sup> Concentrations of radical species would be expected to vary over time as the Earth's atmosphere changes, however some changes almost cancel one another out. For example, Naik et al. modelled variations in the concentrations of the hydroxyl radical over the last 150 years, and found that these appear to have been reasonably constant over this time.<sup>11</sup> This is because several changes that would increase this concentration (e.g.  $\text{NO}_x$  emissions) have been balanced by those that would decrease it (i.e. CO abundance).

### 1.2.1. The Hydroxyl Radical in the Atmosphere

The hydroxyl radical is one of the most important atmospheric radical species, as it initiates much of the radical chemistry that controls the atmospheric oxidative capacity and composition.<sup>6,12</sup> One of the main mechanisms for  $\cdot\text{OH}$  formation is the photolysis of ozone, as is shown in equations 2 and 3 via the first excited state of oxygen  $\text{O}(^1\text{D})$ .<sup>13,14</sup>



However, there are other important sources of OH radicals, which are responsible for  $\cdot\text{OH}$  generation during the day and night. Photolytic routes such as HONO photolysis, or the photolysis of carbonyls can lead to  $\cdot\text{OH}$  production.<sup>15,16</sup> Another route is from the ozonolysis of alkenes (particularly important at night), which form Criegee intermediates, that can decompose forming HO<sub>x</sub> radicals.<sup>17</sup> The addition of NO<sub>3</sub> to double bonds can, among other reactions, result in nitroxyalkyl radicals which can decompose to form  $\cdot\text{OH}$ , peroxy radicals and organic nitrates.<sup>18,19</sup> One such example of this is given in Figure 3. These processes do not result in as much hydroxyl radical production as the route given in equations 2 and 3. Indeed, night time atmospheric measurements by Emmerson et al. suggested concentrations of  $\cdot\text{OH}$  and HO<sub>2</sub> $\cdot$  at 10<sup>5</sup> and 10<sup>7</sup> molecule cm<sup>-3</sup>.<sup>20</sup>

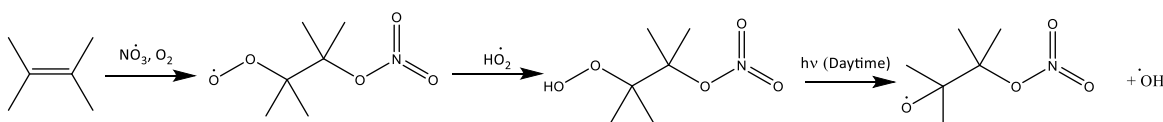


Figure 3: An example of  $\cdot\text{OH}$  formation following NO<sub>3</sub> addition to a double bond

The OH radical will generally react in one of two ways within the atmosphere: hydrogen abstraction, or addition to a double bond. This will subsequently lead to the formation of organic peroxy radicals (as carbon centred radicals will quickly react with oxygen in the atmosphere), which are discussed below.

### 1.2.2. Organic Peroxyl Radicals in the Atmosphere

Organic peroxy radicals (RO<sub>2</sub> radicals) can be formed following oxidation of volatile organic compounds (VOCs) (see Figure 2) via a number of processes – reactions of alkanes with  $\cdot\text{OH}$  and biogenic monoterpenes with  $\cdot\text{OH}$ , Cl or O<sub>3</sub>.<sup>21</sup> The reactivity of this species will vary according to NO<sub>x</sub> levels. At sufficient NO levels, RO<sub>2</sub> radicals can oxidise NO to NO<sub>2</sub>, which can cause photochemical ozone formation. Also, at high NO<sub>x</sub>, (i.e. polluted

environments/night-time) RO<sub>2</sub> radicals can lead to formation of organic nitrates, key compounds in the formation of photochemical smog.<sup>22</sup> The lifetimes of peroxy radicals under these conditions have been modelled to be ca. 5 min, significantly longer than the hydroxyl radical previously discussed.<sup>23</sup> Meanwhile, low NO<sub>x</sub> levels in 'clean' environments will promote reaction with other RO<sub>2</sub> species or HO<sub>2</sub>· in 'RO<sub>2</sub> + RO<sub>2</sub>' reactions. These which will produce alkoxy radicals (RO) and O<sub>2</sub>, and result in the formation of a range of oxygenated species such as alcohols and carbonyls.<sup>24,25</sup>

Whether under high or low NO<sub>x</sub> conditions, reactions of RO<sub>2</sub> species can result in the formation of non-radical products, e.g. formaldehyde formation from isoprene.<sup>26,27</sup> These products will be more oxidised species, so will often be less volatile, hence leading to SOA being formed within the atmosphere (for example from the reaction of monoterpenes with O<sub>3</sub> or ·OH).<sup>28</sup> As such, peroxy radicals are a key step between the degradation of atmospheric species and the formation of SOA.<sup>29</sup>

### 1.2.3. The NO<sub>3</sub> Radical in the Atmosphere

Another important atmospheric radical is NO<sub>3</sub>. The predominant method for formation of this species is shown in equation 4.



The NO<sub>3</sub> radical plays a particularly important role in night-time chemistry, when ·OH concentrations are reduced, and NO<sub>3</sub> is not removed by photolysis. Typical photolytic removal of this species is shown in equations 5 and 6.



Measurements of this species have detected night-time concentrations of 1.5 x 10<sup>10</sup> molecules cm<sup>-3</sup>.<sup>30</sup> The NO<sub>3</sub> radical will act as a VOC oxidant, with addition to double bonds

forming a nitroxy RO<sub>2</sub> species.<sup>23</sup> It will also contribute to ozone levels as NO<sub>3</sub> formation will decrease night time ozone concentrations, whilst catalysing daytime ozone formation.<sup>31</sup> The NO<sub>3</sub> radical is expected to be particularly important with regards to formation of SOA. This can be shown by Hoyle et al. who developed a chemical transport model which found NO<sub>3</sub> to be responsible for ca. 21% of worldwide SOA.<sup>32</sup>

### **1.3. Current Methods of Atmospheric Radical Detection**

As described above, radicals form essential components of atmospheric chemistry. Due to this, their accurate measurement can provide a great asset to efforts focussed on understanding and predicting the chemistry of the atmosphere. There are several different techniques applied to radical detection, including a range of indirect or direct measurements, with some of the main techniques described below.

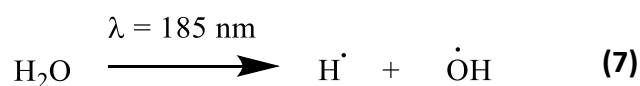
#### **1.3.1. Laser Induced Fluorescence/ Fluorescence Assay by Gas Expansion**

A widely used technique for the monitoring of atmospheric radicals HO<sub>x</sub> is the application of Laser Induced Fluorescence (LIF). Originally, this technique was conducted by excitation of hydroxyl radicals at 282 nm, with the resulting fluorescence then measured to provide a hydroxyl radical concentration.<sup>15</sup> However, a number of issues/interferences were persistent, such as self-generation of hydroxyl radicals at this wavelength, as has previously been shown in equations 2 and 3.<sup>33</sup>

Subsequent development of this technique involved Fluorescence Assay by Gas Expansion (FAGE), developed by Hard et al.<sup>34</sup> Here, the use of lower pressure extends the lifetime of the fluorescent OH radical, as well as decreasing the amount of ·OH that is artificially generated by interaction between moisture and ozone within the spectrometer. This process also incorporated a shift in excitation wavelength to 308 nm giving off resonance detection. While some self-generation will still occur, this can be pre-calculated in the calibration procedure from measurements.<sup>35</sup>

HO<sub>2</sub> radicals can also be monitored by this technique, however this requires conversion by reaction with NO, in order for the resulting OH radicals to be monitored.<sup>36</sup> This technique is also applicable to measurements of total RO<sub>2</sub> concentrations. For example, Fuchs et al. utilised conversion of RO<sub>2</sub> to HO<sub>2</sub>, and subsequent reaction to form ·OH, in order to measure RO<sub>2</sub> concentrations with a limit of detection of ca. 0.1 pptv.<sup>37</sup> This reaction process is shown in equations 13-15.

An important consideration for this technique is efficient calibration. The most widely used method for this is the photolysis of water vapour, as shown in equations 7-9.<sup>38,39</sup> Here,  $\mathfrak{S}_{185}$  = actinic flux of 185 nm light,  $\sigma_{H_2O}$  = photolysis cross section of water vapour at 185 nm,  $\varphi$  = photolysis quantum yield,  $\Delta t$  = water vapour exposure time to light.<sup>39</sup>



$$[OH] = [HO_2] = \mathfrak{S}_{185} \sigma_{H_2O} [H_2O] \varphi \Delta t \quad (9)$$

In the absence of significant wall loss, the total [HO<sub>x</sub>] = [HO·] + [HO<sub>2</sub>] should be twice [·OH], with the addition of NO to this mixture used to confirm this. However, changes in pressure mean that full calibrations in aircraft are difficult, with separate procedures having to be developed for in flight calibration.<sup>8</sup> For example, Martinez et al. used a relative calibration method for in-flight calibration, with [OH] considerably lower for these measurements compared to those at ground level.<sup>40</sup>

### 1.3.2. Chemical Ionisation Mass Spectrometry

Mass spectrometric based detection methods can also be used for indirect measurements of atmospheric radicals, with Chemical Ionisation Mass Spectrometry (CIMS) a widely applied technique. For hydroxyl radical measurement, ·OH is first converted to isotopically labelled H<sub>2</sub><sup>34</sup>SO<sub>4</sub>, as shown in equations 10-12.<sup>41</sup> The H<sup>34</sup>SO<sub>4</sub> anion is then detected by the mass spectrometer.



The use of isotopically labelled  ${}^{34}\text{SO}_2$  is important, as it enables differentiation of naturally occurring  $\text{H}_2{}^{32}\text{SO}_4$ . This technique has been used by Aufmhoff et al. to simultaneously measure ambient  $\text{H}_2\text{SO}_4$ , as well as  $\cdot\text{OH}$ , achieving detection limits of  $1.9 \times 10^5$  molecules  $\text{cm}^{-3}$ .<sup>42</sup> Measurements of total  $\text{RO}_2 + \text{HO}_2$  radicals have also been accomplished, via a further developed methodology, often termed 'PER-CIMS' (Peroxy Radical-CIMS).<sup>43,44</sup> This utilises reaction with  $\text{NO}$  to form  $\cdot\text{OH}$  from peroxy radicals, as is shown in equations 13-15.<sup>43</sup>



The  $\cdot\text{OH}$  from this process is then reacted as described in equations 10-12 for detection. Owing to this conversion process, no information is gathered regarding the identity of the 'R' group from the  $\text{RO}_2$  radical, thus meaning that the many different  $\text{RO}_2$  radicals cannot be differentiated at all by this technique. Conversely, modification of  $\text{NO}$  concentrations can be used to provide differentiation between  $\text{RO}_2$  and  $\text{HO}_2$  radical concentrations. In the presence of high  $\text{NO}$  concentrations, the reaction in equation 16 will preclude conversion of  $\text{RO}$  to  $\text{HO}_2$ , thus  $\text{HO}_2$  is not formed from  $\text{RO}_2$ , and that all  $\text{HO}_2$  being converted to  $\text{OH}$  comes from sampled  $\text{HO}_2$ .<sup>43</sup> This technique has been built on, for example Hornbrook et al. have utilised variation in the  $\text{NO}:\text{O}_2$  ratio in order to facilitate measurements of  $\Sigma \text{RO}_2$  or just  $\text{HO}_2$ .<sup>45</sup>



However,  $\text{RO}_2$  radical detection by CIMS will often have a higher limit of detection than  $\text{OH}$  detection, with limits of  $2 \times 10^6$  and  $5 \times 10^5$  molecules  $\text{cm}^{-3}$  recorded by Kukui et al.<sup>46</sup> They

suggest that this difference is partially due to the potential structural variations of the peroxy radicals being measured. Studies conducted comparing this technique to other indirect measurements, Ren et al. compared CIMS and LIF measurements, with good levels of agreement observed between the two techniques.<sup>47</sup>

A recent development of the CIMS methodology has been the use of Br<sup>-</sup> as a reagent anion for radical detection.<sup>48</sup> This technique utilised the detection of HO<sub>2</sub>Br<sup>-</sup> clusters – thus representing a more direct measurement of HO<sub>2</sub> radicals, unlike the above CIMS methods which convert HO<sub>2</sub> to hydroxyl radicals. The preliminary experiments conducted so far by Sanchez et al. have suggested a detection limit of 7 ppt for this technique.<sup>48</sup>

### 1.3.3. Chemiluminescence and Cavity Ring Down Spectroscopy

The conversion of atmospheric HO<sub>x</sub> or RO<sub>2</sub> radical species for measurements can be applied differently, focussing on the detection of NO<sub>2</sub> following a Peroxy Radical Chemical Amplification (PERCA) technique. This can be formed from both RO<sub>2</sub> or HO<sub>2</sub> radical reactions with NO and CO, as shown in equations 17-19.<sup>49</sup> Wall losses for these species are such that over 1000 NO<sub>2</sub> compounds can be formed per starting RO<sub>2</sub> radical, giving detection limits of ca. 10<sup>6</sup> molecules cm<sup>-3</sup>.<sup>10</sup>



Chemiluminescence has been used for these experiments, via the reaction between alkaline luminol (Figure 4) and NO<sub>2</sub>.<sup>10,50</sup> However, this was found to be subject to interferences, for example by reactions of luminol with O<sub>3</sub> (especially in urban environments), although application of dual channel instruments has reduced this problem.<sup>51</sup> This method also suffers from the inherent problem of a wet chemistry method being difficult and complex to use in field/aircraft measurements.

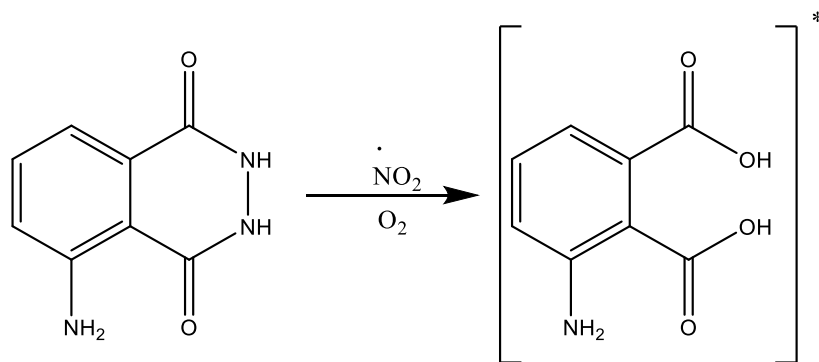


Figure 4: Reaction of luminol with NO<sub>2</sub>, to form an excited species. Fluorescence from relaxation of this species is then monitored for NO<sub>2</sub> measurement.

Another method involves the use of cavity ring down spectroscopy, a method that does not suffer the same degree of O<sub>3</sub> interference. This technique functions by measuring light intensity time decay from within an optical cavity, which will be able to produce a concentration, [A], for the substance being studied, according to the relationship given in equation 20.<sup>52</sup> Here  $\alpha$  = absorption coefficient,  $\sigma$  = absorption cross section,  $R_L$  = ratio of cavity length to length absorber is present,  $c$  = speed of light,  $1/\tau$  = decay rate constant from absorber containing cavity,  $1/\tau_0$  = decay rate constant from empty cavity.<sup>52</sup> Through this method, direct measurements of radical species such as NO<sub>3</sub> can be employed.<sup>53</sup>

$$\alpha = [A]\sigma = \frac{R_L}{c} \left( \frac{1}{\tau} - \frac{1}{\tau_0} \right) \quad (20)$$

Depending on the reflectance of mirrors used in this set-up, measurements with a 1 m cavity can match those of DOAS measurements with a 10 km path length, making this a very sensitive technique with detection limits less than  $1 \times 10^6$  molecules cm<sup>-3</sup>.<sup>54</sup> The most widely used version of this technique utilises 'pulsed' lasers, and is durable enough for use in aircraft based studies.<sup>55</sup> Other developments on this technique include utilisation of continuous wave light input, a much more power efficient technique.<sup>53,56</sup> Other variations of this technique include 'Dual Channel' techniques, for example that by Liu et al.<sup>49</sup> Here,

background and sample air flows were continuously monitored, resulting in a much lower impact from background variations.

#### 1.3.4. Differential Optical Absorption Spectroscopy

A less widely used technique to monitor atmospheric radical species is Differential Optical Absorption Spectroscopy (DOAS). Here, absorption of hydroxyl radicals is monitored, which can be related to  $[\cdot\text{OH}]$  by the Beer-Lambert law, as shown in equation 21 where  $I_0$  = light intensity before transmission,  $I$  = light intensity after transmission,  $\sigma_{\text{OH}}$  = OH absorption cross section,  $L$  = path length.<sup>57</sup> This detection technique can also be used for other species, such as  $\text{NO}_x$ , IO or BrO.<sup>58</sup> A long path length will be important for detection at low concentrations – for example, path lengths of 5 km have been used in order to obtain detection limits of  $10^5$  molecule  $\text{cm}^{-3}$ .<sup>59</sup>

$$[\text{OH}] = \ln \frac{(I_0/I)}{(\sigma_{\text{OH}}L)} \quad (21)$$

The key advantage of this technique is that it does not require external calibration, as LIF instruments do. Therefore, this technique has been used in several experiments alongside another radical detection techniques.<sup>60,61</sup> For example, LIF and DOAS were employed by Fuchs et al. in a chamber study of hydroxyl radicals from VOC (e.g. isoprene) decay under low  $\text{NO}_x$  conditions.<sup>61</sup> Here, the two instruments were found to agree well, with the two systems displaying accuracies of 6.5 and 10% for DOAS and LIF respectively. A wider study by Schlosser et al., using DOAS, CIMS and LIF instruments, also demonstrated good agreement between these techniques in both chamber and ambient air studies.<sup>54</sup>

This technique has been applied to the field measurement of several different species, beyond just  $\cdot\text{OH}$ . For example, Wagner et al. measured arctic  $\text{NO}_3$ , while Liao et al. monitored BrO levels in Greenland and Saiz-Lopez et al. measured Antarctic IO and BrO.<sup>58,62,63</sup> There have also been various adaptations to the basic DOAS technique, beyond just variations of path length. For example, Multi-Axis-DOAS (MAX-DOAS) has been used by Hendrick et al. in the measurement of  $\text{NO}_2$ .<sup>64</sup> This technique provides a ‘column’ of

measurements at different altitudes, using readings taken at different angles to the horizon, with a total uncertainty for NO<sub>2</sub> measurements found to be 12%.

### **1.3.5. Matrix Isolation EPR**

EPR has also been previously used as a method of atmospheric radical detection, with radicals trapped within a matrix of D<sub>2</sub>O at 77 K, hence termed 'Matrix Isolation EPR' (MI-EPR).<sup>19,65</sup> This method can provide a direct measurement of atmospheric radicals such as HO<sub>2</sub>, RO<sub>2</sub> or NO<sub>2</sub>, with detection limits of ca. 1 x 10<sup>8</sup> molecules cm<sup>-3</sup>. Indeed, this is the only current direct method of measuring atmospheric peroxy radicals.<sup>37</sup> The trapped radicals have been found to be stable for several weeks prior to the offline EPR analysis.<sup>65</sup>

Different radicals can be distinguished with this technique, for example Mihelcic et al. describe that HO<sub>2</sub> and RO<sub>2</sub> radicals can be differentiated from their splitting patterns.<sup>65</sup> However, this is difficult under atmospheric concentrations, hence these species are grouped together for ambient air measurements. As with DOAS, this technique does not require difficult calibration, unlike the LIF/FAGE technique, with MI-EPR having been used to provide evidence for the validity of water photolysis calibration for other instruments.<sup>66</sup>

This technique has also been compared to other techniques. A good agreement to DOAS measurements of NO<sub>3</sub> was found by Geyer et al., albeit with some deviation due to error regarding the NO<sub>3</sub> absorption cross-section.<sup>67</sup> The drawback with this technique is the time required to analyse each sample. While samples can be collected at temporal resolution of ca. 30 minutes, each sample takes ca. 5 hours to analyse, resulting in a significant amount of laboratory time to acquire experimental data.<sup>68</sup> This is considerably longer than the above techniques, where samples are analysed within minutes or less.

### **1.3.6. Other Methods for Radical Detection**

A different technique that has been applied to radical capture from the gas phase has been the use of salicylic acid.<sup>69</sup> In the presence of ·OH, this can form a fluorescent species as is

shown in Figure 5. This technique has been found to have detection limits of ca.  $7 \times 10^5$  molecules  $\text{cm}^{-3}$ .<sup>15</sup>

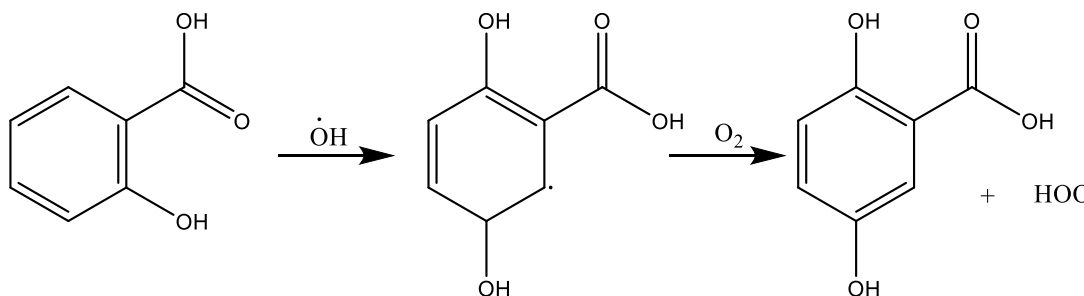


Figure 5: Capture of  $\cdot\text{OH}$  by salicylic acid

However, there are several limitations to this technique. Firstly, reactions with trace metals, bacteria or ozone can all contribute to formation of the same 2,5-dihydroxybenzoic acid. As such, this is not a technique that is selective to radical capture, with higher than expected radical concentrations given by this technique.<sup>70</sup> Also, more than just the 2,5 isomer will be formed, with products in Figure 6 also detected from this reaction.<sup>69</sup>

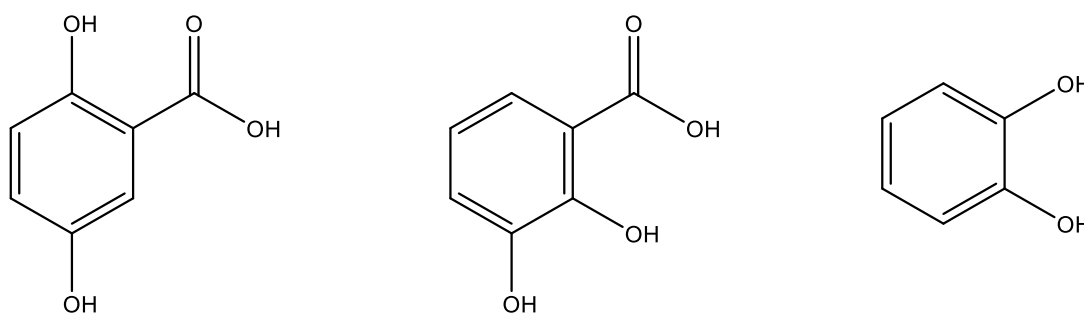


Figure 6: Dominant compounds formed from salicylic acid reactions with  $\cdot\text{OH}$

Salmon et al. describe that the 2,3 acid shown in Figure 6 would actually be a more preferable target for analysis – unlike the 2,5 isomer it is not formed by microbial metabolism of salicylic acid, as was found by Halliwell et al.<sup>69,71</sup> However, fluorescence of this species is much lower than the 2,5 isomer, hence making detection difficult and resulting in the continued use of the 2,5 isomer.

There are several more examples of  $\cdot\text{OH}$  detection via reaction with a 'probe' molecule, although with the exception of salicylic acid these have generally only been utilised in liquid phase reactions. Fang et al. have described the use of the terephthalate anion, with radical addition to the aromatic ring producing a fluorescent product.<sup>72</sup> Conversion of a fluorescent starting material to a non-fluorescent product by reaction with  $\cdot\text{OH}$  has also been applied. Ou et al. used fluorescein for this method of  $\cdot\text{OH}$  detection, in monitoring the antioxidant capacity of different foodstuffs.<sup>73</sup>

There are many examples of fluorescent probes that are specific for certain radicals, with these widely used within biological systems.<sup>74</sup> One such example is a study by Kim et al. discussing a fluorescent probe selective to reaction with  $\cdot\text{OH}$ .<sup>75</sup> This probe, based on a rhodamine dye, undergoes an  $\cdot\text{OH}$  hydrogen abstraction reaction, with the resulting compound being strongly fluorescent. However, while this is useful for establishing the presence of  $\cdot\text{OH}$ , it is difficult to apply this probe to other radical species. Indeed, no differentiation of different species can be accomplished, as there is no retention of the radical structure. In addition to this, a lack of specificity is shown by other reactive species also producing some of the fluorescent compound.

Other similar work has developed fluorescent probes with a much wider range of applicability, for example the detection of peroxy species from solution.<sup>76</sup> This made use of a fluorescamine based trap, which upon radical addition allowed significantly enhanced fluorescence to be detected. However, this method still suffers from non-specific reactions, as well as instability of reaction products, leading to difficulties in establishing the structures of peroxy species within the reaction mixtures.

### **1.3.7. Capture of Criegee Intermediates from Alkene Ozonolysis Systems**

A recent technique has been reported by Giorio et al. which describes the capture of Criegee intermediates and subsequent on-line analysis of the cycloaddition product.<sup>77</sup> The capture of these species is accomplished via reaction with the spin trap DMPO, to form

species of the structure given in Figure 7. The trapped species can then be analysed by MS, or even by NMR if sufficiently high concentrations are used.

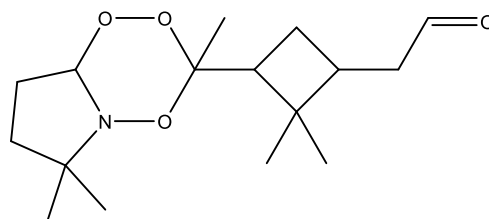


Figure 7: Structure of a captured Criegee intermediate from Giorio et al.<sup>77</sup>

In addition to this, Berndt et al. have also captured Criegee intermediates.<sup>78</sup> Their technique utilises stabilisation of the intermediate with protonated ethers and subsequent detection by CIMS. This has been successfully applied to CH<sub>2</sub>OO, the simplest Criegee intermediate, with a detection limit of ca.  $1 \times 10^5$  molecules cm<sup>-3</sup>.

As Criegee intermediates are important species in the non-photolytic formation of atmospheric radicals from ozonolysis, the study of these species will be very interesting within atmospheric chemistry, and a useful addition to studies on atmospheric radicals.<sup>79</sup> However, no information can be gathered from this technique regarding the speciation of peroxy or alkoxy radicals that will subsequently be formed from the Criegee intermediate during atmospheric reaction channels.

### 1.3.8. General Disadvantages of Current Techniques

The methodologies described above have been very successful in the measurements of radical species within the atmosphere. However, there are several key areas of potential improvement that can be targeted. The technologically complex, relatively large size, and running costs (from electrical equipment to manpower) of these techniques makes field measurements a far from trivial undertaking.<sup>80</sup> This serves to highlight the need for a technique that is easily portable and low cost, with sufficient detection limits for atmospheric radical detection.

Another important disadvantage is the lack of speciation provided by these techniques. While OH and HO<sub>2</sub> can relatively easily be distinguished, the 'radical amplification' techniques such as PER-CIMS used for this mean that no structural information can be gathered from RO<sub>2</sub> radicals.<sup>43</sup> As such, identifying the source of these radicals by these measurements is not possible. Successful speciation of atmospheric peroxy radicals would be greatly important as a method of validating current chemical models and establishing radical reaction processes within the atmosphere.

As such, there appears to be a need for the development of a radical detection technique that is sensitive to a range of atmospheric radical species such as HO·, RO· or RO<sub>2</sub>·, which is easily *portable, accurate, cost effective*, and can provide *speciation* of trapped radicals. It would also be useful for the sensors to be miniaturised, enabling greater special resolution than is currently obtainable.

## **1.4. Spin Trapping**

### **1.4.1. Common Spin Traps and Their Use**

Spin trap species are defined as compounds that will react with a radical species to form a new and more stable radical species. There are several different types of spin traps, often based around nitrones. 5,5-Dimethyl-pyrroline-N-oxide (DMPO) is a well-established example,<sup>81</sup> with many structurally similar compounds such as 5-Diethoxyphosphoryl-5-methyl-1-pyrroline (DEPMPO) also frequently utilised.<sup>82</sup> N-tert-Butyl- $\alpha$ -phenylnitronone (PBN) is another widely used nitronone spin trap, which again has several similar derivatives utilised for spin trapping, such as  $\alpha$ -(4-pyridyl N-oxide)-N-tert-Butylnitronone (POBN).<sup>83,84</sup> These species are shown in Figure 8.

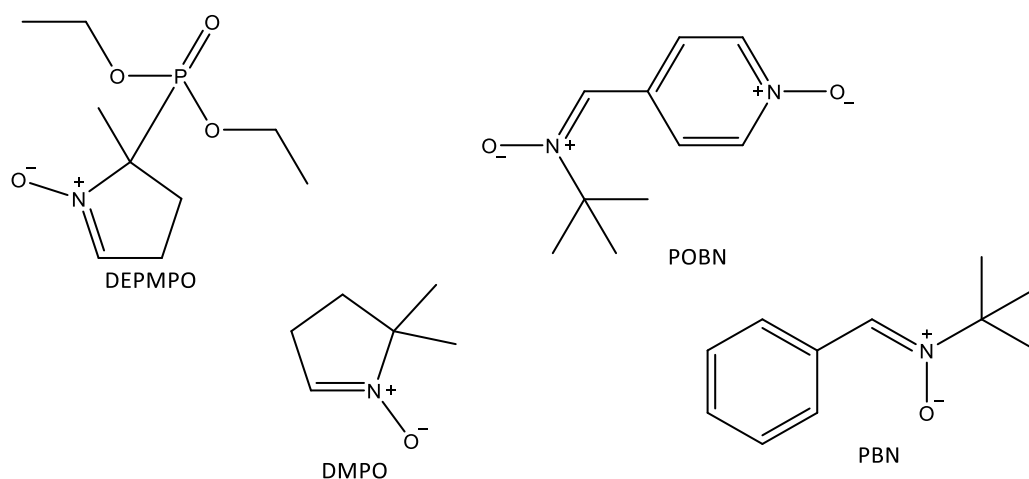


Figure 8: Structures of common spin traps

Spin trapping occurs by radical addition to the double bond of the spin trap, as is shown in Figure 9. This results in the formation of a persistent radical adduct which is typically then analysed by EPR, although methods such as mass spectrometry have also been applied.<sup>85</sup> In nitron spin traps, this radical adduct will be a nitroxide, with Janzen et al. providing one of the first examples of this with DMPO.<sup>86</sup>

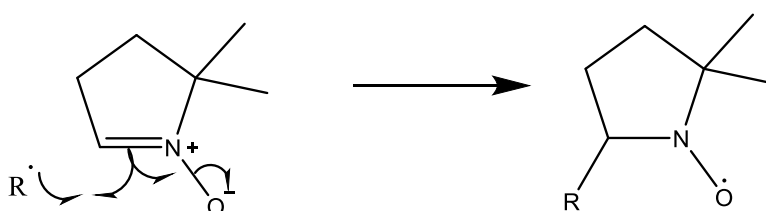


Figure 9: Traditional spin trapping of a radical species using DMPO

The stabilities of these spin adducts vary, with lifetimes in the region of several minutes being not uncommon. This means that the analysis of short lived radical species can be aided by the spin trap extending the lifetime of the radical, enabling species such as aqueous ·OH to be detected.<sup>87</sup> While this is useful, it does mean that off-line analysis is severely limited. Meanwhile, the sensitivity of EPR is such that concentrations of nM can be detected (e.g. 50 nM for TEMPO), however recent techniques such as rapid scan EPR are currently working towards lowering this detection limit.<sup>88,89</sup> While this is very useful, it is still significantly less sensitive than techniques such as mass spectrometry, with mass spectrometers able to detect picograms of material.<sup>90</sup>

Mass spectrometry has also been applied to the study of spin trapped radicals. In one such example, Guo et al. applied this to DMPO radical adducts, formed from capturing organic alkoxy radicals.<sup>91</sup> This serves as an interesting study, as mass spectrometric evidence here can provide structural information on the captured adducts. However, while the lifetime of these adducts are sufficiently stable to survive purification by High Pressure Liquid Chromatography (HPLC), there are limitations in applications of this technique: carbon centred DMPO adducts were not stable enough to survive this process, while other radicals are unlikely to survive beyond a few hours. As such, the inherent instability of this measurement technique means it is unlikely to be suitable for 'real world' analyses.

#### **1.4.2. Spin Trapping Radicals from the Gas Phase**

Spin trapping has been applied to gas phase sampling, with many examples found with the study of cigarette smoke. Furusawa et al. passed the smoke through a PBN solution, with the resulting spectra indicating a series of oxygen centred radicals.<sup>92</sup> The changes induced by the addition of a radical scavenger for parts of these experiments also provided evidence towards the presence of a range of organic peroxides being produced over several hours of the experiment.

Radicals have also been found to be present in smoke that is several minutes old: Pryor et al. studied this and proposed a mechanism to explain this phenomenon.<sup>93</sup> They proposed that NO within the smoke is slowly converted to NO<sub>2</sub>, which then reacts with non-radical species to produce the oxygen centred radicals that are still evident after several minutes within the smoke. Baum et al. attempted to develop a quantification methodology for measuring radicals within cigarette smoke.<sup>94</sup> They found that PBN to be the most useful spin trap for this process, with these measurements more reproducible and suffering less interference than those made with DMPO or POBN spin traps.

### **1.4.3. Limitations of Spin Trapping**

Besides the above mentioned lifetimes of spin adducts, there are several other limitations to the process of spin trapping. Several traps show poor stability in the presence of metal ions, for example, the oxidation of DMPO to a nitroxide radical will be catalysed in the presence of transition metals such as copper.<sup>95</sup> 'False positives' have also been observed from spin trapping experiments. As an example, in the Forrester-Hepburn mechanism nucleophilic attack, and subsequent oxidation, can produce the same products as would be expected from a radical spin trapping process.<sup>96</sup> Thus, spin trapping does show several areas where improvement can be made, predominantly regarding short lifetimes of spin adducts, their stability and the presence of artefacts. As such, the development of a new technique for the capture and analysis of radicals would be of great use.

### **1.5. Project Aims**

The aim of this project will be to develop a novel type of radical trap, suitable for application to the measurement of atmospheric radicals. This trap will need to provide radical speciation, as well as measurements at atmospherically relevant concentrations. It will also be important that the trapped adduct is sufficiently stable for off-line analysis to take place. These requirements can be tested in a range of atmospherically relevant model systems (e.g. monoterpene ozonolysis), in addition to 'real world' sampling experiments.

## 2. Trap Synthesis

### 2.1. Introduction

#### 2.1.1. Design Principles for a Trapping Molecule

First, the structure and key features of the target radical trapping molecule need to be determined – in essence how are we going to trap the radical into this new, stable molecule? The first factor to consider is how the molecule will react with a radical – fundamentally, determining the reactivity of the target molecule. The simplest answer that presents itself is to react the target radical ( $R\cdot$ ) with an alkene, shown in Figure 10. This takes advantage of the fact that radicals are known to add well to alkene functionality.<sup>97,98</sup> For example, pentyl radicals will react with methyl acrylate at an absolute rate of  $6.2 \times 10^5 \text{ M}^{-1} \text{ s}^{-1}$ , or styrene at  $1.3 \times 10^5 \text{ M}^{-1} \text{ s}^{-1}$ .<sup>98,99</sup> Utilisation of a terminal alkene will reduce the steric barrier to radical attack compared to that which would be present for a non-terminal alkene.

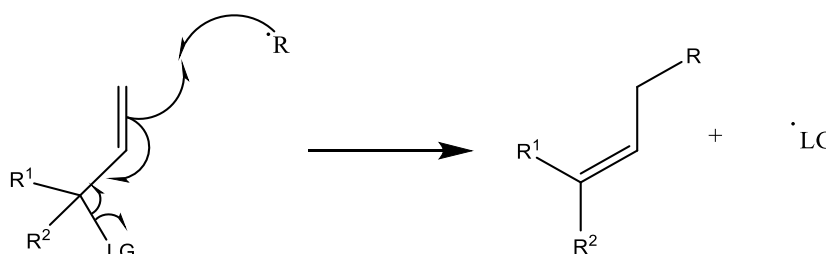


Figure 10: Target mechanism for trapping reaction (LG = leaving group)

The second step is to consider what happens after the initial radical attack. In order to form a stable closed shell species after reaction between the trap and a radical, the trap will need to be an alkene with a good radical leaving group ('LG'). This would be the biggest difference when compared to 'traditional' radical trapping techniques: as is shown previously, the product of the spin trapping reaction is still a radical species.

TEMPO, a highly stable radical, is chosen as the radical leaving group. The stability of this molecule arises from both steric hindrance and delocalisation of the unpaired electron, shown below in Figure 11. Steric shielding is provided by the four methyl groups near to the radical centre, hindering reactions of the radical. These also preclude the formation of a nitronium by oxidation, as there are no alpha hydrogen atoms present. Evidence for the stability of the TEMPO free radical can be demonstrated from the low bond dissociation energy ( $291 \text{ kJ mol}^{-1}$ ) of the O-H bond in the corresponding hydroxylamine.<sup>100-102</sup> This is much weaker than the equivalent bond in N-hydroxypiperidine ( $322 \text{ kJ mol}^{-1}$ ), or cyclohexanol (ca.  $450 \text{ kJ mol}^{-1}$ ).<sup>103</sup>

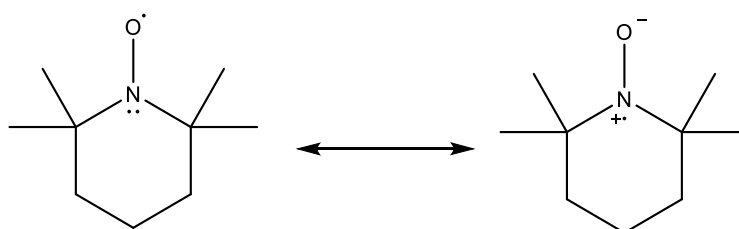


Figure 11: Resonance stabilisation of the TEMPO radical

The presence of hydrogen atoms available on the trapping molecule for abstraction, which could potentially compete with trapping, must be considered. In order to prevent hydrogen abstraction at the allylic position, this should be a quaternary centre. Within the remaining structure care should also be taken to ensure that there are no strongly labile hydrogen atoms. Therefore, a structure based around an alkyl chain would appear to be promising. With this in mind, a synthesis was designed whereby TEMPO would be added to an alkene containing molecule, to form a compound conforming to the template shown below in Figure 12.

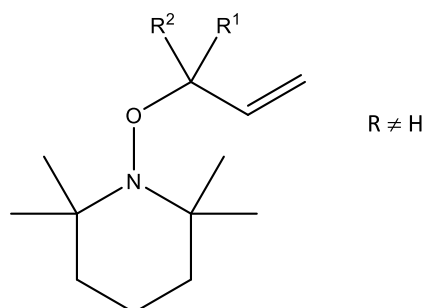


Figure 12: Structural template for a radical trapping molecule

### 2.1.2. Alkoxyamine Synthesis

Therefore, in order to develop a new type of radical trap, compounds based on alkoxyamines are likely to be of use. Alkoxyamines have been largely developed with a view to use as initiators for nitroxides in radical polymerisation reactions – i.e. living polymerisation.<sup>104–106</sup> However, they also have a number of different applications: for example within natural product synthesis, microwave assisted isomerisations, or polymer light stabilisation.<sup>107–109</sup> Examples of alkoxyamines used in these applications are shown in Figure 13.

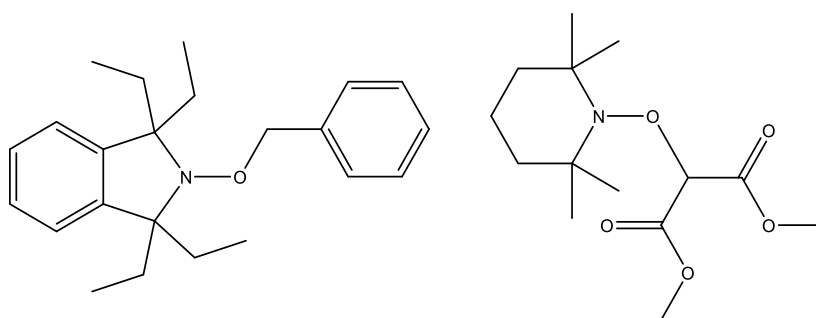


Figure 13: Literature examples of alkoxyamines<sup>106,108</sup>

There have been several methods developed for their synthesis, most of which utilise radical chemistry. A common example would be the use of copper systems, as was initially shown by Matyjaszewski et al.<sup>110</sup> Here the copper complex undergoes halogen transfer from an organic halide, forming a carbon centred radical which is trapped by a nitroxide (i.e. TEMPO), forming an alkoxyamine. This is shown in Figure 14.

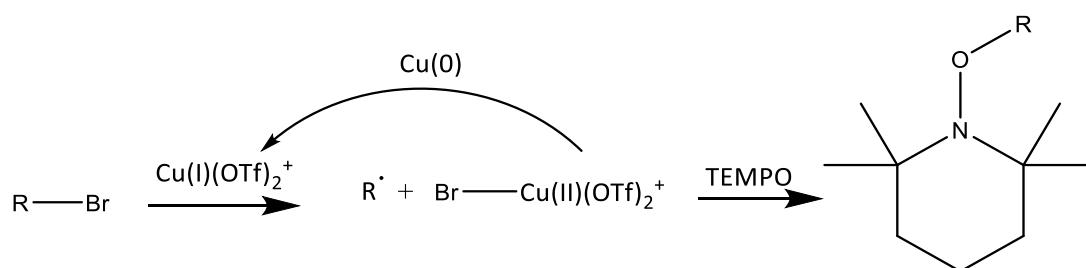


Figure 14: Formation of alkoxyamines using Cu(I), as suggested by Matyjaszewski<sup>110</sup>

This technique was originally utilised with alkyl bromides for atom transfer radical polymerization reactions, however this technique has been expanded on for alkoxyamine synthesis. For instance, Li et al. developed this method to utilise copper catalysed reactions with an assortment of hydrocarbons, as opposed to alkyl bromides.<sup>111</sup> A mild route for alkoxyamine formation using copper is also shown by Schoening et al., who describe copper catalysed reactions between nitroxides and aldehydes to produce alkoxyamines in good yields.<sup>112</sup>

There has also been a significant amount of work utilising non copper based systems. Van Humbeck et al. described an enamine based system, which can be used to induce enantioselective  $\alpha$ -oxidation of aldehydes, with a reaction employing either copper or iron based catalysts, as well as a chiral pyrrolidine based catalyst.<sup>113</sup> Another such example, by Kano et al., features the use of a binaphthyl chiral amine to form the desired alkoxyamines with a good enantioselectivity.<sup>114</sup> Again this reaction utilises an enamine intermediate, however rather than involving a catalytic metal the mechanism utilises the oxoammonium salt of TEMPO to act as the single electron oxidant. Other work to form alkoxyamines has been to utilise simple hydrogen abstraction reactions, with the reaction between a nitroxide and the resulting carbon radical forming the alkoxyamine. This is a very common procedure, and frequently involves generation of a radical from a peroxide species.<sup>115</sup> The simplest such example of this would be the formation of hydroxyl radicals from hydrogen peroxide, with an example given in Figure 15.

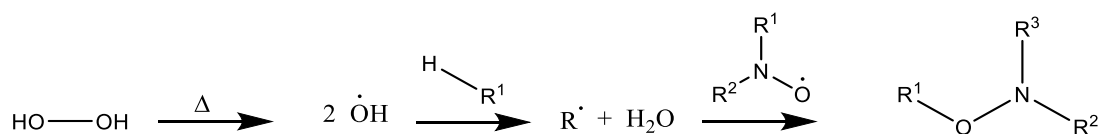


Figure 15: Example scheme showing peroxide decay, and subsequent hydrogen abstraction by the hydroxyl radical.

For example, Braslau et al. used photolysis of di-tert-butyl peroxide to generate an alkoxy radical which would then abstract a hydrogen atom from the substrate molecule, with

TEMPO trapping the ensuing carbon radical.<sup>116</sup> Thermolysis of peroxides is another procedure that can produce alkoxy radicals for hydrogen abstraction, with trapping of ensuing carbon centred radicals by nitroxides demonstrated by Cuthbertson et al.<sup>117</sup> Nitroxides can also be used in order to initiate this type of reaction with peroxides, as was shown by Moad et al.<sup>118</sup> In some instances, nitroxides are also able to directly abstract a hydrogen atom from a C-H bond, although this will vary noticeably with the C-H bond strength, and the nitroxide may in some cases easily be oxidised back to a radical.<sup>119</sup>

### **2.1.3. Aims**

The reactions described above are a useful starting point in determining a synthetic procedure for the formation a radical trapping molecule based on an alkoxyamine. Initially, the desired functionality of the trapping molecule will be determined: which types of functional groups are required, or which leaving groups will be utilised in order to trap radicals in a manner different to that employed in conventional spin trapping. A variety of methods for synthesising molecules of this type will then be explored. Once a trapping molecule has been synthesised, the stability of the trap will also need to be evaluated.

## **2.2. Initial Synthetic Plan**

In order to synthesise a radical trap according to the constraints described above, a retrosynthetic analysis (RSA) was conducted on the template molecule described above. This is shown below in Figure 16.

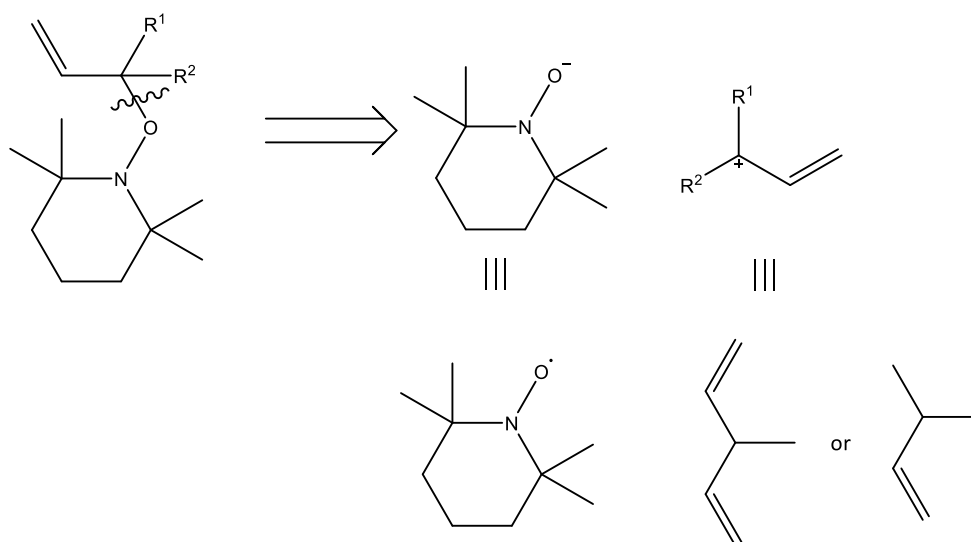


Figure 16: RSA for the formation of a radical trapping compound

The simplest route would be to perform a hydrogen abstraction on the alkene containing molecule, with TEMPO trapping the resultant radical. The alkenes 3-methylbut-1-ene and 3-methyl-1,4-pentadiene were used (Figure 17), two compounds with accessible alkene groups, which would be expected to have labile hydrogen atoms that enable the addition of TEMPO in a tertiary position. Indeed, the C-H bond dissociation energy for pentadiene is  $318 \text{ kJ mol}^{-1}$ , ca.  $80 \text{ kJ mol}^{-1}$  weaker than C-H bonds in the corresponding alkanes.<sup>120</sup> 3-Methyl-but-1-ene also has a low C-H bond dissociation energy of ca.  $326 \text{ kJ mol}^{-1}$ .<sup>120</sup> This compares to a typical value of ca.  $400 \text{ kJ mol}^{-1}$  for an alkane C-H bond.<sup>121</sup>

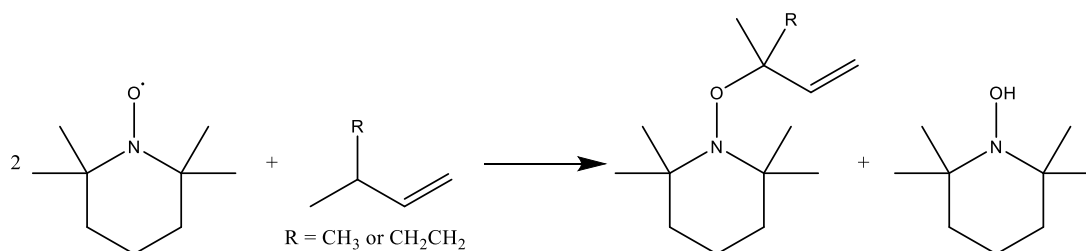


Figure 17: Target reaction between TEMPO and 3-methylbut-1-ene or 3-methyl-1,4-pentadiene

There are several potential methods that can be exploited in order to perform the hydrogen abstraction to generate the radical that is needed to react with TEMPO to form the alkoxyamine product. Numerous different radical generation methods can be applied, including use of a Fenton system, reaction with oxygen and a cobalt catalyst, and even reaction with just TEMPO itself. Reactions via a bromo-substituted alkene are also known to be a method of introducing TEMPO functionality into a molecule, which will also be explored.<sup>110,122</sup> Attempts to form the target molecule using these methodologies are discussed below.

### 2.2.1. Reaction Between TEMPO and 3-Methyl-1,4-pentadiene, Using a Cobalt Catalyst Under Oxygen.

Initially a diene was used as the starting alkene for these reactions to form **2.01**, as is shown in Figure 18. The substrate with two alkene groups was chosen to promote radical capture – the chances of a radical attacking a double bond are twice that of the single alkene substrate. The bis allylic hydrogen of this structure would be expected to be the most labile within this structure. The abstraction process will use TEMPO to abstract the proton, with the reaction itself catalysed by a cobalt catalyst to activate molecular oxygen,<sup>123,124</sup> as has been utilised elsewhere in literature.<sup>125</sup>

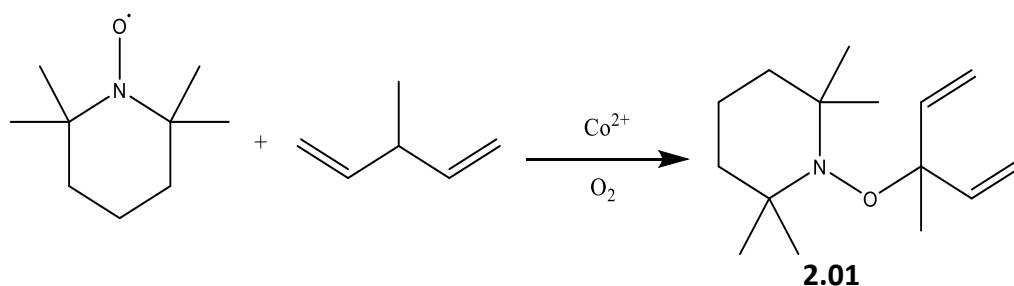


Figure 18: Hydrogen abstraction with a cobalt catalyst to form **2.01**

A hydrogen abstraction reaction, with subsequent trapping by TEMPO shown above in Figure 18 does appear to take place, with mass spectrometry of the reaction product at an  $m/z$  of 238.2 fragmented by MSMS to show TEMPO at  $m/z$  158.1. However  $^1\text{H}$  NMR analysis of the reaction product indicated the presence of two different isomers: the target

molecule **2.01**, and a rearranged product, **2.01'**. These can be clearly differentiated by different chemical shifts of the alkene protons, shown here in Figure 19.

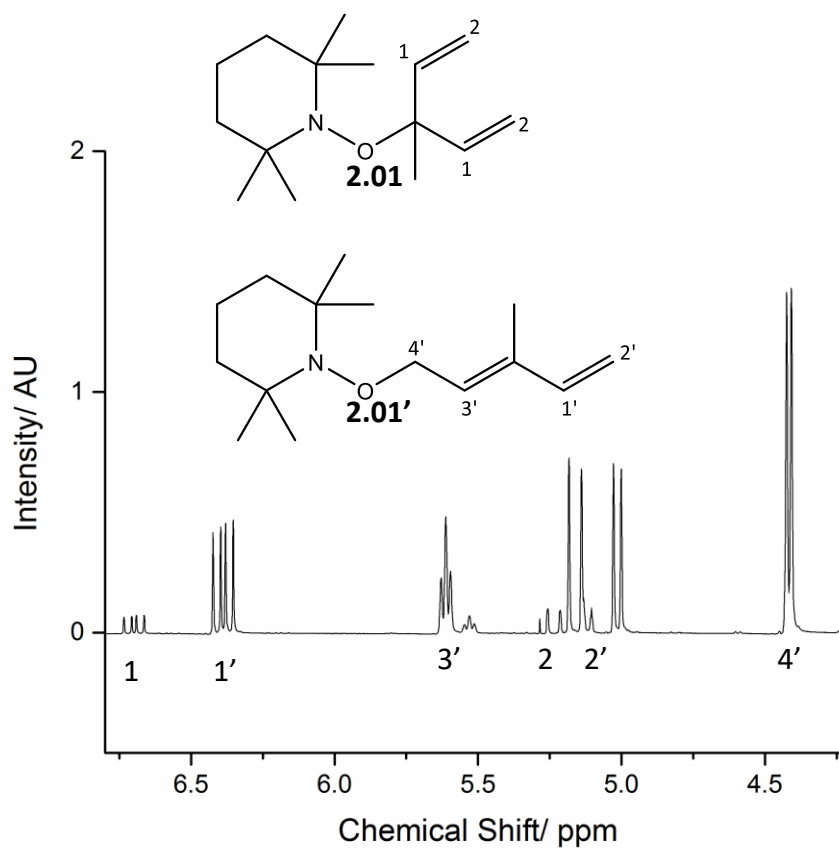


Figure 19: Alkene region of a  $^1\text{H}$  NMR of a mixture of **2.01** and **2.01'**

The dominant signals here are those corresponding to **2.01'**, however signals from **2.01** can also be observed – while both isomers have terminal alkene groups, they are distinguishable due to the differences in chemical shift induced by proximity to the oxygen atom from the TEMPO group. Comparison of the integration values suggest that **2.01'** is present in a 14:1 ratio to **2.01**.

Conducting the reaction without the cobalt, but under an atmosphere of pure oxygen (to provide a more oxidising environment) resulted in a similar ratio of tertiary:primary compound, albeit in with a lower overall yield (8%, compared to 44% in the presence of cobalt). Use of TEMPO under a standard atmosphere failed to produce any of target compound, illustrating the importance of molecular oxygen in this system.

The reason for the preferential formation of **2.01'** over **2.01** appears likely to be linked to steric effects. When only electronic effects are considered, it would be thought that the dominant product would be **2.01**, owing to the stabilisation of the radical centre from the presence of inductive effects of a tertiary system, as opposed to the primary system of **2.01'**. The relative stability trend of tertiary radicals being more stable than secondary, which are more stable than primary is well known. This effect can be demonstrated by the increasing C-H bond dissociation energy from tertiary to primary, with the formation of a more stable tertiary radical requiring less energy than a primary species.<sup>126</sup>

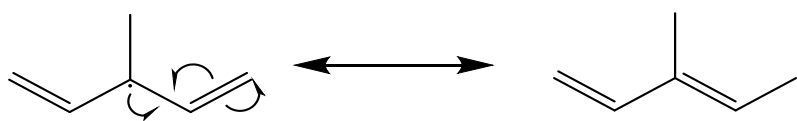


Figure 20: Resonance forms of the 3-methyl-1,4-pentadiene radical

However, formation of the 'primary' radical (shown in the resonance scheme in Figure 20) will be favoured by the increased stability caused by the more substituted alkene. This is because of hyperconjugation from the alkene pi bond, with each alkyl substituent stabilising the more substituted alkene by approximately 25 kJ mol<sup>-1</sup>.<sup>127</sup> In addition to this, the 'primary' product will be stabilised by conjugation between the two alkenes, which is not present within the desired tertiary product. This result is akin to the specificity that has been found in autoxidation of methyl linoleate.<sup>128</sup>

The prevailing reaction compound **2.01'** will unfortunately not be useful for application as a radical trap. Instead of the desired trapping process, it is likely that hydrogen abstraction by radicals present will occur instead. This unwanted reaction scheme is shown below in Figure 21. With only 6% of the product being identifiable as the desired compound, other reactions will need to be explored in order to facilitate the formation of the desired isomer.

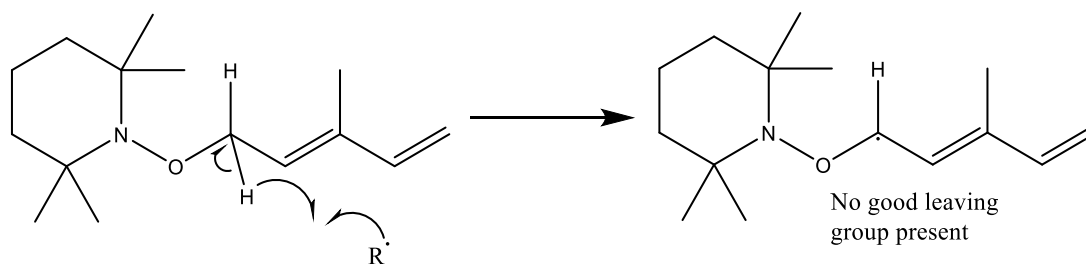


Figure 21: Unwanted trapping reaction by primary TEMPO compound **2.01'**

### 2.2.2. Other Methods of Forming **2.01** Through Hydrogen Abstraction Reactions.

Other methodologies for hydrogen abstraction were also examined. TEMPO complexes with Lewis acids are able to abstract labile hydrogen atoms, as has been shown by in the reaction of 9,10-dihydroanthracene to anthracene, given in Figure 22.<sup>129</sup>

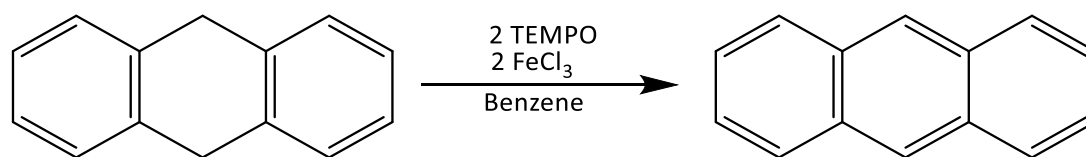


Figure 22: Formation of anthracene from 9,10-dihydroanthracene<sup>129</sup>

As such, reactions with both  $\text{AlCl}_3$  or  $\text{FeCl}_3$  as the Lewis acid were trialed with TEMPO and methyl pentadiene to form **2.01**. However, these reactions showed only starting material after reacting for 22 hours. This suggests that the hydrogen targeted for abstraction in the anthracene system is more labile than that in 3-methyl-1,4-pentadiene, and so this method was abandoned as a route to the target molecule **2.01**.

Another common method for radical generation is the utilisation of Fenton chemistry.<sup>130</sup> Fenton chemistry is a term used to describe the reaction of peroxide with metal salts, with the classic reaction being  $\text{Fe}^{2+}$  and hydrogen peroxide resulting in the formation of hydroxyl radicals, as in Figure 23.<sup>131</sup> However, the reaction itself has since expanded to a

series of 'Fenton like' systems, with use of different metals (i.e. Cu(I)) or other organic peroxides).<sup>132</sup>



Figure 23: Fenton Reaction to generate hydroxyl radicals

There are indeed examples of Fenton chemistry being used in conjunction with TEMPO in order to generate alkoxyamines, commonly through living polymerisation reactions.<sup>133,134</sup> A reaction of TEMPO with 3-methyl-1,4-pentadiene in the presence of  $\text{Fe}^{2+}$  and  $^t\text{BuOOH}$  yielded several TEMPO containing products, (including a methyl-TEMPO compound formed via  $\beta$ -scission of the  $^t$ butoxy group given in Figure 24).<sup>117</sup> Unfortunately, the same primary:tertiary problem was observed.

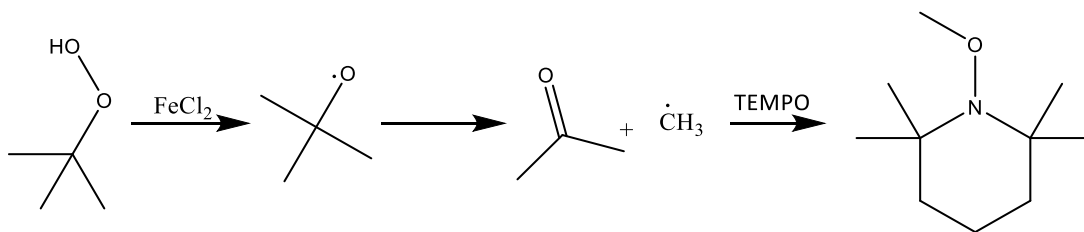


Figure 24: Formation of  $\beta$ -scission product

### 2.2.3. Reactions in the Presence of an Antioxidant.

Examination of the literature shows that this tertiary to primary rearrangement has been observed in other systems. For example, Brash attempted to facilitate the formation of 11-hydroperoxylinoleate from linoleic acid autoxidation (as opposed to the readily detectable 9 and 13-hydroperoxylinoleates).<sup>135,136</sup> It was found here that application of an antioxidant,  $\alpha$ -tocopherol, results in partial formation of the 11-hydroperoxylinoleate isomer, where before none was evident. It is suggested that this due to the  $\alpha$ -tocopherol acting as a hydrogen donor to trap the peroxy radicals formed in the linoleic acid system,

resulting in reduced isomerization and facilitating formation of the bis-allylic product. Without the antioxidant, Brash proposes that the 11-peroxy radical will fragment to lose  $O_2$ , with the carbon radical then rearranging to form the more thermodynamically stable, conjugated, 9 or 13 peroxy radical species upon reaction with oxygen. The addition of oxygen appears to be reversible, with the addition of the antioxidant is shifting the equilibrium such that some of the 11 peroxy species is observed. This proposed reaction route is shown below in Figure 25.

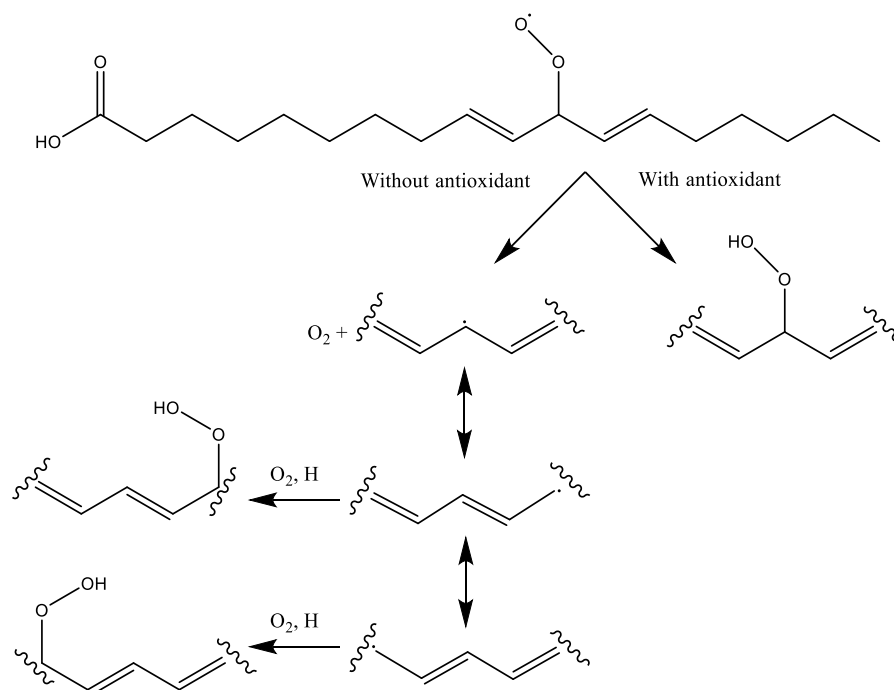


Figure 25: Route to formation of 9,11 or 13 hydroperoxy linoleic acid predicted by Brash<sup>135</sup>

In order to test this, the antioxidant butylated hydroxytoluene (BHT) is added to a reaction with 3-methyl-1,3-pentadiene. This resulted in very little difference in the overall ratio of **2.01'** to **2.01** (again ca. 14:1 when both 10 mol % and 2 equivalents of BHT were used), while the overall yields of the reactions appeared to decrease to 16%. This is for two reasons. Firstly, adding an antioxidant would be expected to decrease reaction yields from oxidation reactions. Secondly, the linoleic acid system is effectively relying on addition of tocopherol to shift the equilibrium of oxygen addition to the carbon radical towards the

peroxy radical. Obviously this is not desirable for formation of **2.01**, as the carbon radical needs to react with TEMPO, not O<sub>2</sub>.

### 2.3. Hydrogen Abstraction Reactions with 3-Methyl-but-1-ene

As described above, it appears that the problem with these hydrogen abstraction reactions is linked to regioselectivity, resulting in favourable trapping of a primary carbon radical by TEMPO. Therefore, in order to reduce this while retaining the desired quaternary carbon atom for the C-O-N fragment, the reaction of the less sterically bulky 3-methyl-but-1-ene was attempted, shown in Figure 26. While there are now fewer alkene groups present for radical trapping with this design, this system should still be able to sufficiently trap radicals in the event it can be synthesised.

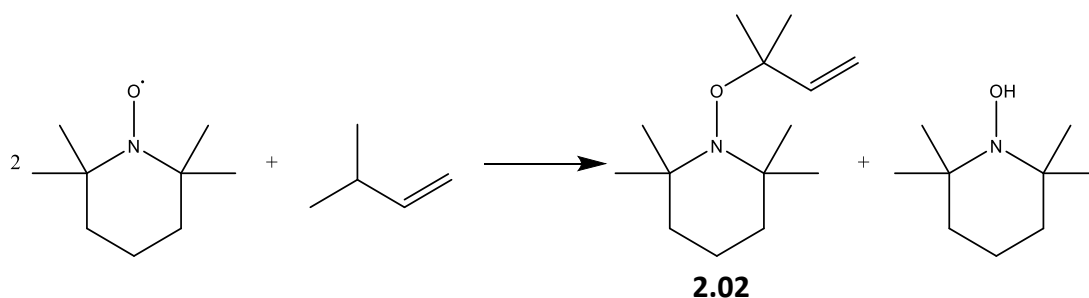


Figure 26: Formation of new target compound **2.02**

This reaction was trialed using the reaction under Fenton conditions. Nonetheless, it appears that the change to 3-methylbut-1-ene was not sufficient, as formation of the rearranged primary alkene **2.02'** still appears dominant, with the tertiary compound not visible by <sup>1</sup>H NMR in Figure 27. The tertiary compound would be expected to feature doublets of doublets at ca. 6.5 and 5 ppm, as was the case for this functionality in **2.01**.

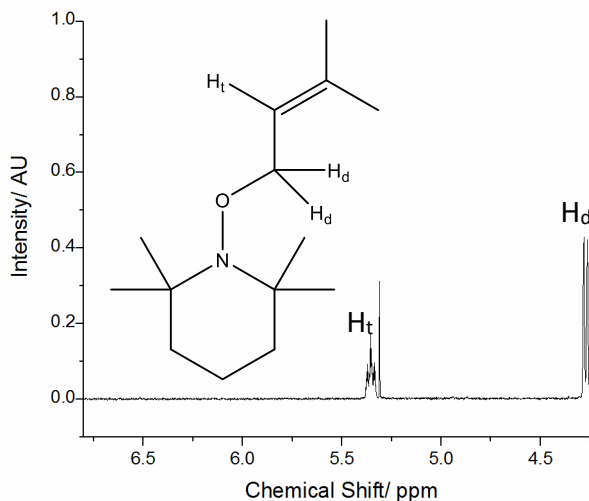


Figure 27: Alkene region of a  $^1\text{H}$  NMR of **2.02'**

It appears that of the two resonance structures possible for the radical intermediate, the primary molecule is still the most favourable for reaction with TEMPO. The change in steric environment, consisting of a methyl group present in the place of a  $-\text{CH}_2=\text{CH}_2$  group, appears to be creating no benefit towards the trapping of the tertiary species. As a relatively small change, this is not a surprising result, but is nonetheless disappointing. Indeed, Bergbreiter et al. observed only a small amount of a tertiary product when attempting to form a primary version, with no tertiary product at all present when larger groups, such as a phenyl ring, were added to the system.<sup>137</sup> Therefore, it appears that a different method will need to be considered in order to synthesise the target molecule.

## 2.4. Substitution Reactions to form a Halogen Containing Alkene

Another method known within the literature of introducing TEMPO into a system is via reaction with a radical formed by redox initiation of alkyl bromides with copper.<sup>110</sup> To synthesise the required bromide substrate 3-methyl-3-bromo-but-1-ene, **2.03**, the parent alcohol was reacted with HBr (Figure 28). While substitution of the alcohol for the bromine is observed, the compound again appears to rearrange with the primary isomer, **2.03'**, in a significant excess over the tertiary isomer, with an NMR ratio of 76:1. A significant excess of primary product is also observed when  $\text{PBr}_3$  is used as the bromine source.

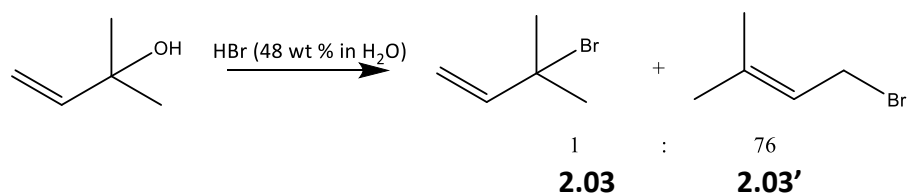


Figure 28: Bromination of 3-methyl-but-1-en-3-ol forming **2.03** and **2.03'**.

Bromination with HBr will proceed via an  $S_N1$  mechanism, hence a tertiary carbocation intermediate will be formed.<sup>138</sup> The reaction with  $PBr_3$  normally proceeds  $S_N2$ , however with the tertiary structure, and highly stable carbocation, an  $S_N1$  mechanism would be expected again. Electronic stabilisation from the inductive effect of nearby methyl alkyl groups would normally stabilise a tertiary carbocation more than the primary carbocation, therefore one would expect the tertiary compound to dominate. However, the primary compound is significantly favoured experimentally. This is likely because this primary compound features a more substituted alkene than the tertiary, with the more substituted alkene being the more stable intermediate.<sup>127</sup> This is confirmed by conducting the reaction with a less bulky halogen – chlorine. Indeed, reaction between 3-methyl-but-1-en-3-ol and HCl predominantly gave primary product **2.04'**, albeit in a ratio of 7:1 to tertiary product **2.04**, a result matched with thionyl chloride as the chlorine source.

These compounds will always react by an  $S_N1$  route, and the reactivity of the key carbocation intermediate cannot be modified. Therefore, there is no benefit to continuing with this method for synthesis of a radical trap. As such, a different synthetic route will need to be employed in the formation of the radical trapping compound.

## 2.5. Reactions via Aldehyde Functionality

The above synthetic methods have all shown that, while TEMPO can certainly be incorporated into 3-methyl-but-1-ene or 3-methyl-1,4-pentadiene, rearrangement around the alkene to form a more sterically favourable, and more substituted, alkene product is

preventing formation of the desired compounds. Ideally, the alkene group would be 'protected' in order to prevent rearrangement of the radical intermediate. An RSA of the target compound conducted with this in mind (Figure 29) suggests that the simplest method of implementing this would be by introducing the alkene functionality after that of the TEMPO group, therefore preventing the rearrangement process.

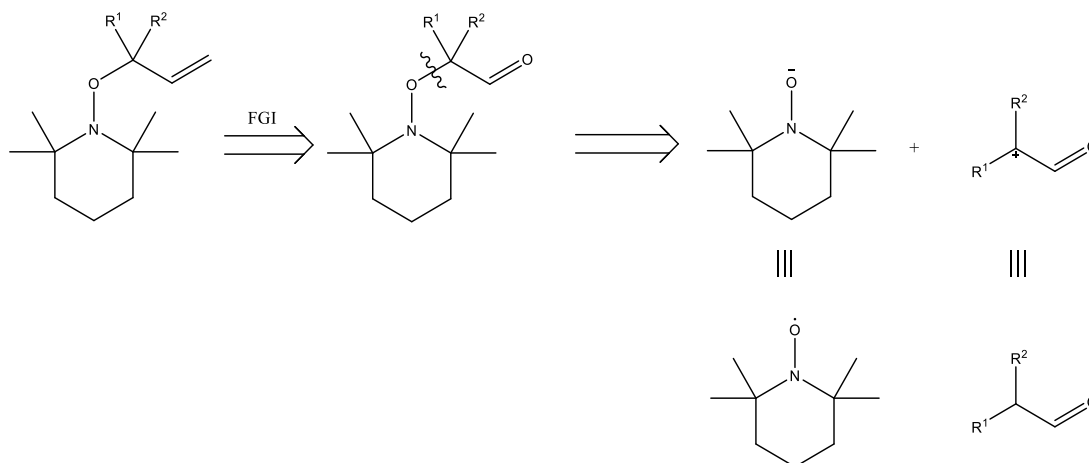


Figure 29: RSA for protecting the alkene prior to TEMPO addition

The addition of TEMPO into this system was attempted using hydrogen abstraction reactions again, now that there is no facility for undesired rearrangement to primary species. Once TEMPO has been incorporated, the aldehyde can be converted into an alkene via a Wittig reaction. Use of a phenyl group as part of this system will facilitate hydrogen abstraction, leading to a resonance stabilised benzylic radical. The structure of the new target precursor compound **2.05** is given in Figure 30.

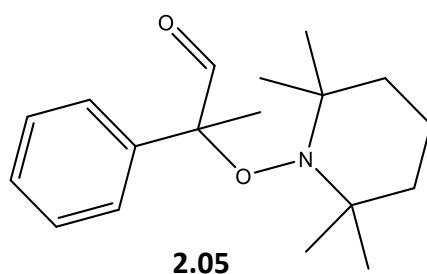


Figure 30: New target molecule **2.05**

### 2.5.1. Reaction Between TEMPO and 2-Phenyl propanal, Using a Cobalt Catalyst Under Oxygen.

The aldehyde 2-phenylpropanal was reacted with a  $\text{Co}^{2+}$  catalyst and oxygen, and the resulting radical trapped with TEMPO in order to form target precursor molecule **2.05**. This is shown below in Figure 31.

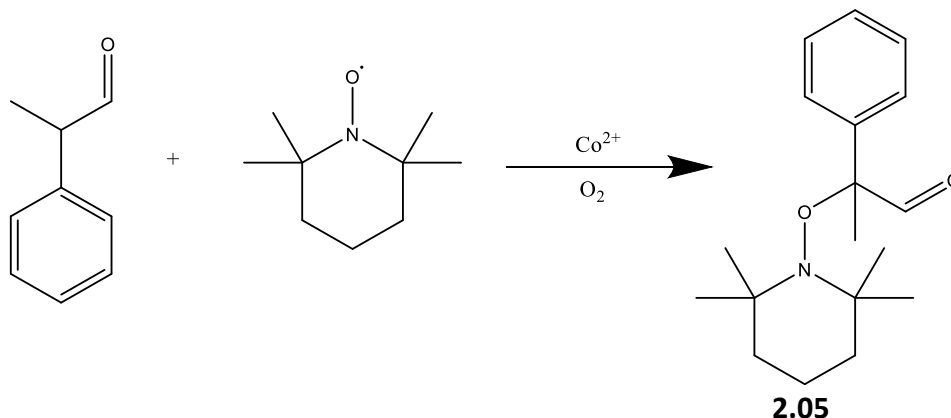


Figure 31: Proposed reaction to form **2.05**

However, the reaction failed to yield the target product, with starting material clearly detectable at the end of the synthesis. The failure of this reaction could be due to two reasons: steric hindrance or C-H bond strength. Regarding sterics, the trapping of TEMPO in this position is not made easier by the bulk around the carbon radical, however there are (admittedly few) examples of tertiary TEMPO functionality within the literature, so it is unlikely that sterics alone cause the failure of this reaction.<sup>139</sup> The C-H bond targeted for abstraction may be too strong for the reaction to easily occur: an observation supported by the lack of any indication of 'other' hydrogen abstraction products within the reaction mixture. Indeed, at approximately  $353 \text{ kJ mol}^{-1}$ , this is stronger than the C-H bonds targeted previously with the diene chemistry.<sup>120</sup> Supporting this is the observation in a literature system, again based around a cobalt activating oxygen, of radical reaction with aromatic toluene being ca. a sixth of non-aromatic equivalents.<sup>140</sup> Attempting to form **2.05** through hydrogen abstraction of 2-phenylpropanal also proved unsuccessful when Fenton chemistry was applied. As such, a different approach is instead required in order to synthesise a TEMPO functionalised aldehyde.

### 2.5.2. Oxidation of a TEMPO Functionalised Alcohol

Given the lack of success towards synthesising **2.05**, formation of the corresponding TEMPO functionalised alcohol **2.06**, and subsequent oxidation to **2.05** would be a potentially viable route. The formation of **2.06** has been described previously within the literature by Prechter et al.<sup>141</sup> This reaction, in Figure 32, proceeds in two key steps. The first is based on Fenton chemistry, and involves the formation of a hydroxyl radical, which will subsequently react with the double bond of  $\alpha$ -methylstyrene to form a carbon centred radical. The second step has the carbon radical trapped out by the excess TEMPO present within the reaction mixture, giving the tertiary functionalised alkoxyamine product **2.06**.

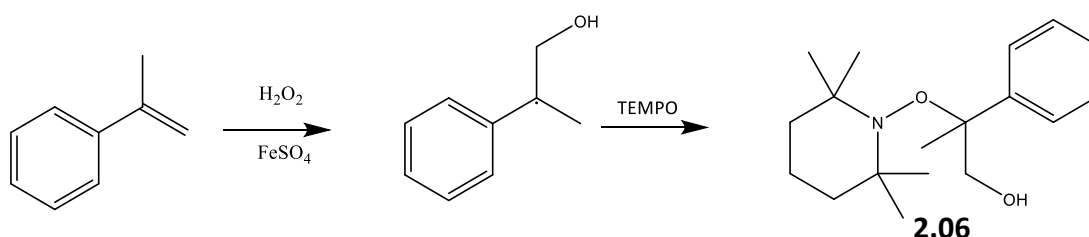


Figure 32: Formation of **2.06** via methodology from Prechter et al.<sup>141</sup>

Using this synthesis, a 24% yield of **2.06** was obtained, almost identical to that recorded by Prechter et al.<sup>141</sup> The next step, conversion of an alcohol to an aldehyde, is a common procedure within the literature: there are a variety of oxidation methodologies that can be applied in order to form the corresponding aldehyde **2.05** from alcohol **2.06** (Figure 33).

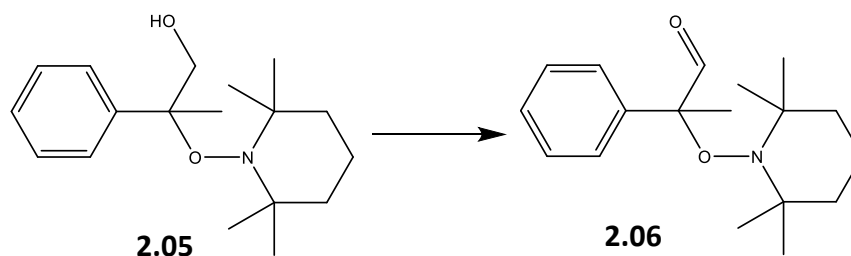


Figure 33: Oxidation of **2.06** to form **2.05**

The first method of oxidation trialled was reaction of **2.06** with pyridinium chlorochromate (PCC). This method, developed by Corey et al.,<sup>142</sup> is known to be an effective single oxidant, with the chromium being reduced from Cr(VI) to Cr(IV) during this process. However, the product obtained from this reaction was not the target aldehyde, indeed NMR suggests that the major product of the reaction was instead acetophenone, with no indication of the target aldehyde at all by NMR.

Formation of acetophenone from PCC oxidations has been observed in the past from other benzylic alcohols by Fernandes et al.<sup>143</sup> They suggested that the acetophenone is formed via a C-C bond cleavage, along with a degradative oxidation, and also provided evidence of similar reactions occurring with allylic alcohols. However in some instances the target oxidation products were also observed, although in a significantly lower yield than the product that has undergone C-C cleavage. Unfortunately there does not appear to be any of this non cleaved product in the system studied here.

Other methodologies for oxidation were also trialled, using the Dess-Martin procedure,<sup>144</sup> and also Swern oxidation.<sup>145</sup> The Dess-Martin procedure requires coordination of the alcohol to an iodine complex, Dess-Martin Periodinane (DMP), which will gradually decompose to release the oxidised aldehyde product.<sup>146</sup> The Swern oxidation meanwhile is based on 'activated' DMSO reacting with the starting alcohol, to form an alkoxyulfonium species which can subsequently be deprotonated before fragmentation to produce the aldehyde.<sup>147</sup> Both species are known to be effective single oxidants.

Both oxidation methods do however fail to oxidise alcohol **2.06**. In each case, starting material can clearly be observed, both by NMR and mass spectrometry. The failures of these reactions could be attributable to undesired interactions, for example between the oxygen of the TEMPO group with the periodinane. Also, oxidation around the nitrogen of TEMPO may be hindering formation of the desired compounds. DMP can be found within the literature to have oxidised an alkoxyamine,<sup>148</sup> however in doing so the rate constant for C-O bond cleavage increased, giving the suggestion that any small amount of oxidised compound is lost due to ensuing C-O homolysis. Given the failure of these oxidation

methods, it appears that changing focus to a different method of introducing TEMPO into a molecule already functionalised with an aldehyde may be prudent.

## 2.6. McMillan Chemistry: Use of a Single Electron Transfer Agent

A different method of introducing TEMPO into an aldehyde containing system is to utilise enamine chemistry. Once formed, the enamine could be oxidised by a single electron transfer (SET) agent, trapped by TEMPO, and then hydrolysed to give the TEMPO functionalised compound, as is shown in Figure 34 below.

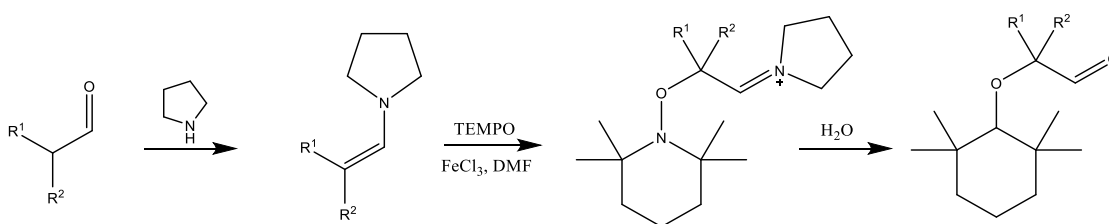


Figure 34: Addition of TEMPO via an enamine intermediate

Sibi et al. originally proposed that this reaction would proceed via singly occupied molecular orbital activation, however this was later proved to be incorrect by van Humbeck et al., who showed that the reaction instead proceeds via enamine catalysis with a TEMPO-metal complex.<sup>149,150</sup> Formation of **2.05** was attempted by application of this methodology to 2-phenylpropanal, as in Figure 35. However only starting material was evident at the end of the reaction.

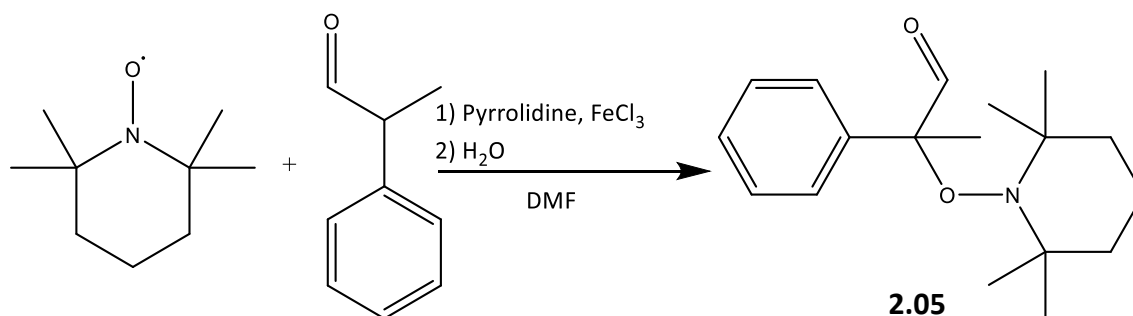


Figure 35: Attempted formation of **2.05** by McMillan Chemistry

The reaction is known to proceed with the less-substituted phenylacetaldehyde, (introducing TEMPO functionality at a secondary site) suggesting that the desired tertiary site for TEMPO may be sterically hindering the reaction.<sup>149</sup> Indeed, Simonovich et al. detail a range of different products that can be formed via this methodology, yet fail to give any examples of TEMPO in the tertiary position that is being targeted from this reaction.<sup>113</sup>

In an effort to modify the sterics of this reaction system, a cyclic molecule was instead utilised. The reaction scheme for this reaction to form **2.07** shown in Figure 36.

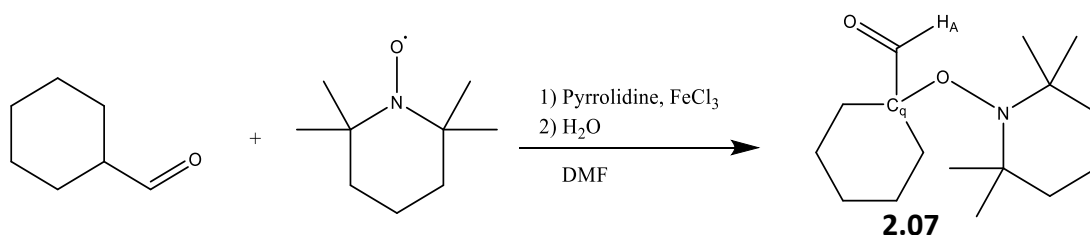


Figure 36: Formation of **2.07**, showing the aldehyde proton H<sub>A</sub>

This reaction formed **2.07** in an 84% yield. Initial evidence for the reaction is provided by a change in multiplicity of the aldehyde <sup>1</sup>H NMR signal, as **2.07** is expected to only produce a singlet for the aldehyde proton H<sub>A</sub>, which is indeed observed and shown in Figure 37.

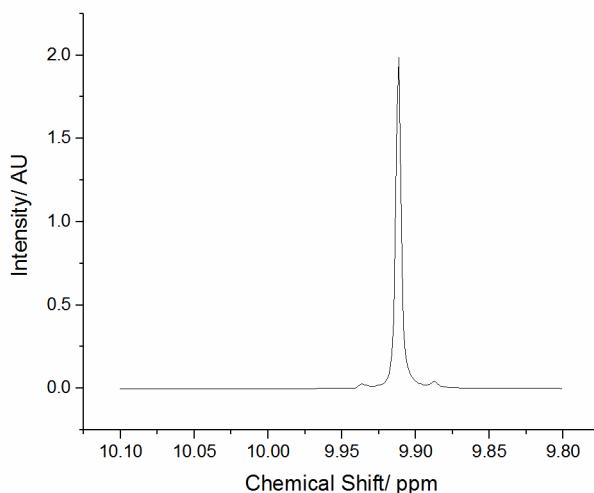


Figure 37: Zoomed in section of <sup>1</sup>H NMR for **2.07** showing singlet aldehyde signal

DEPT-135 and HMBC confirm that  $C_q$  is a quaternary carbon, with weak J coupling to aldehyde proton 'H<sub>A</sub>', this is shown in Figure 38. The HMBC NMR experiment is used to show the interactions between hydrogen and carbon atoms (although interactions between hydrogen and other heteroatoms, such as nitrogen, can also be shown) that are 2-3 bonds apart (typically 2-20 Hz), while suppressing interactions from atoms only one bond apart (typically much higher frequencies, e.g. 150 Hz).<sup>151</sup> Therefore, the signal produced for the highlighted atoms suggests that they are indeed coupled 2-3 bonds apart, thus providing further confirmation regarding the structure of **2.07**.

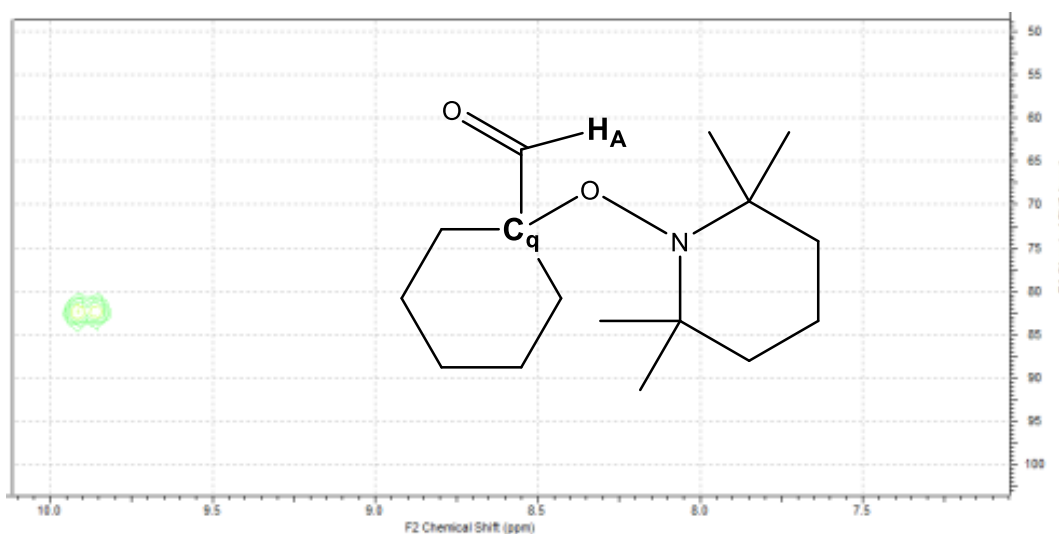


Figure 38: HMBC of **2.07**, showing interaction between the highlighted atoms in **2.07**

As this reaction was successful in a tertiary system with a moderately more sterically restricted system, attempts were made in order to use a significantly smaller acyclic molecule. In this instance, the starting material utilised was isobutyraldehyde – successful reaction would result in formation of the target compound **2.08**, containing a TEMPO group near minimal steric bulk from the aldehyde, shown in Figure 39.

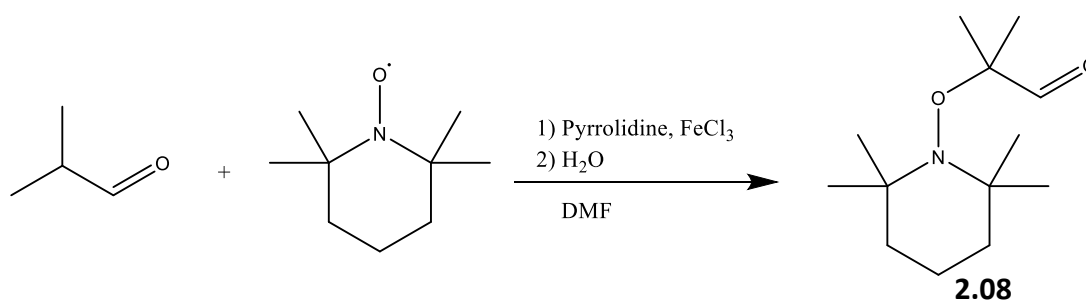


Figure 39: Target reaction for the formation of **2.08**

Unfortunately, this reaction once again showed no indication of a successful reaction. Therefore, the presence of cyclic functionality appears to be critical in enabling this reaction to occur, with steric bulk likely an interlinked factor. For that reason, the use of different cyclic aldehydes will be explored later in this chapter.

## 2.7. Wittig reaction of 2.08

Conversion of an aldehyde into an alkene via a Wittig reaction is a very common technique. Since its inception in 1953, the reaction has been applied to a wide range of substrates, in a very robust procedure.<sup>152,153</sup> It has also been expanded upon, with further derivations including the Horner-Wadsworth-Emmons reaction.<sup>154</sup> As such, this methodology is applied here in order to form **2.09**, from compound **2.07** as shown in Figure 40.

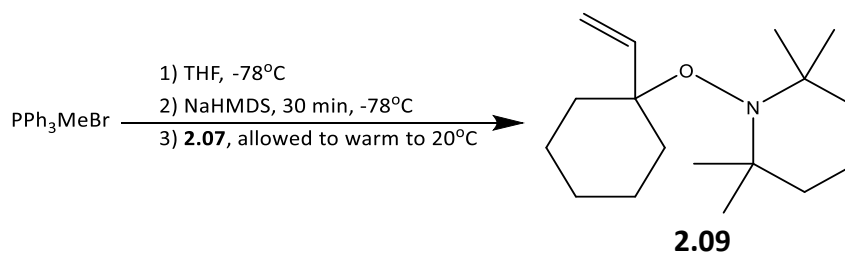


Figure 40: Formation of **2.09** through a Wittig reaction of **2.07**

The reaction was successful, with **2.09** obtained in a 48% yield.  $^1\text{H}$  NMR (Figure 41) confirms the disappearance of the aldehyde proton, as well as the formation of a new series of peaks in the alkene region, each of which can be assigned to one of the three alkene protons. Data from MS and  $^{13}\text{C}$  NMR experiments also confirm the presence of **2.09**.

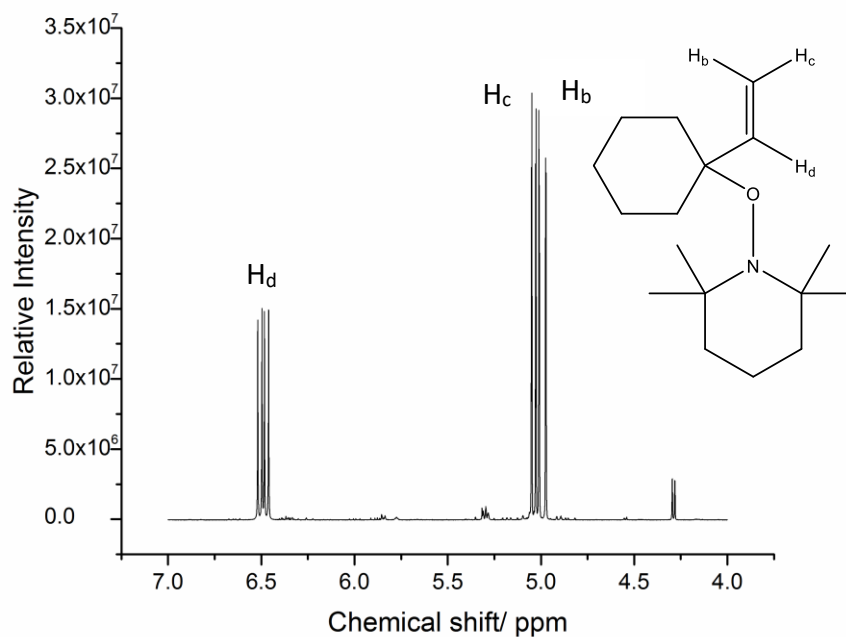


Figure 41: <sup>1</sup>H NMR Alkene region of **2.09**

## 2.8. Stability of **2.09**: Rearrangement to **2.09'**

Upon storage and subsequent re-analysis of a solution of **2.09**, it became evident that isomerisation was occurring within this molecule: originally pure compound by TLC developed a second spot over several hours. <sup>1</sup>H NMR experiments, conducted several hours apart also showed the formation of new signals within the alkene region, at approximately 5.3 and 4.3 ppm. This is shown in Figure 42.

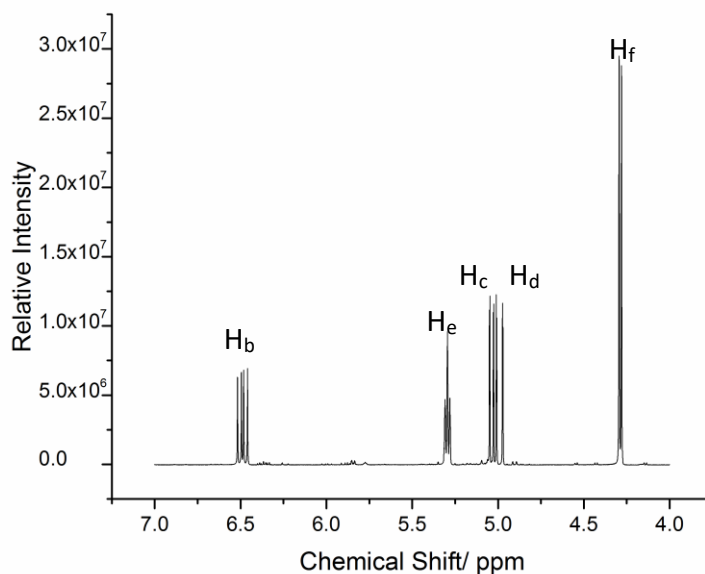


Figure 42: Alkene region of a solution of **2.09** after several hours. New signals are present at 5.3 and 4.3 ppm.

Examination of these new signals suggested the formation of **2.09'**, with the alkene having undergone rearrangement to now have the TEMPO molecule present in a primary arrangement. The triplet and doublet observed, at 5.3 and 4.3 ppm respectively, suggest the presence of CH-CH<sub>2</sub> functionality by the alkene, which would be expected in a compound with TEMPO in the primary position. The proposed structure of the degradation compound is shown in Figure 43.

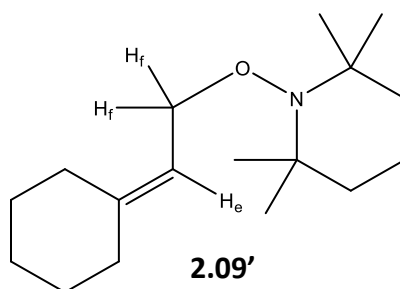


Figure 43: Structure of rearrangement product, **2.09'**

Carbon and DEPT-135 experiments give evidence to support this view. While there will be a slight shift in the position of the alkene signals, owing to the different environments now present, a more significant change can be observed with DEPT-135.

The alkene carbon atoms in **2.09** will produce two signals with a DEPT-135 experiment (the =CH<sub>2</sub> down and the =CH up), in **2.09'** the same experiment would only show evidence for one alkene carbon (the =CH up) as the quaternary carbon will not produce a signal. This change can be seen below in Figure 44.

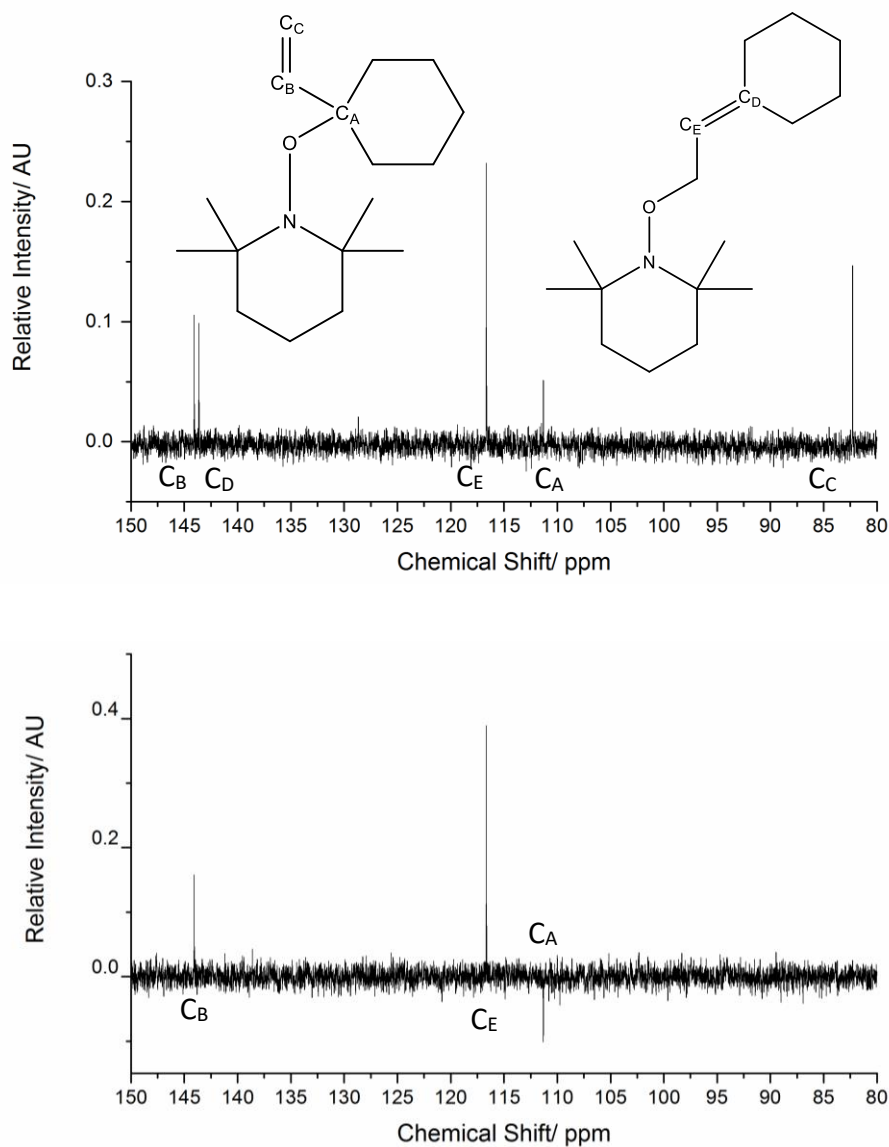


Figure 44: Signals from **2.09** and **2.09'** in <sup>13</sup>C and DEPT-135 experiments

The decay of **2.09** (to **2.09'**) can be monitored by <sup>1</sup>H NMR in order to calculate a lifetime for this compound, which in turn will indicate whether this compound is stable enough for use in trapping experiments, or whether it will decay too quickly. A decay plot for this species is shown in Figure 45.

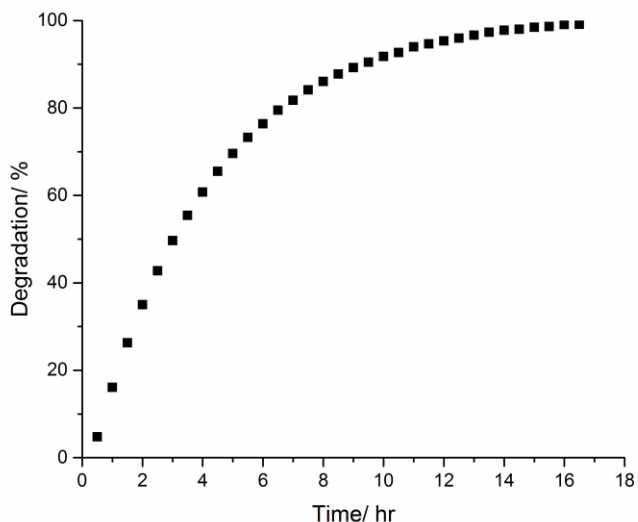


Figure 45: Degradation of **2.09** to form **2.09'**

This plot suggests that **2.09** has a half-life of ca. 3 hours in solution, with almost full conversion to **2.09'** over 17 hours. The half-life can be used to identify the rate constant for this reaction, found using equation 22 to be  $7 \times 10^{-5} \text{ s}^{-1}$  at 24.9°C.

$$[A] = [A]_0 e^{-kt} \quad (22)$$

$$\frac{[A]_0}{2} = [A]_0 e^{-kt_{1/2}}$$

$$\ln(0.5) = -kt_{1/2}$$

$$\frac{\ln 2}{t_{1/2}} = k$$

Despite this, the trapping molecule may be suitable for trapping experiments: the compound appears to be significantly more stable when not in solution, with minimal decay (< 5%) when **2.09** is deposited on a surface for ca. 3 hours prior to comparison with freshly isolated **2.09**. In addition to this, minimal degradation (< 5 %) is evident when examining **2.09** that has been stored in a freezer for several months, compared to freshly isolated **2.09**. Therefore, this compound can be applied in future trapping experiments.

This rearrangement could be explained by: the presence of unreacted TEMPO within the sample that has not been removed by purification, homolysis of the C-O bond and

subsequent rearrangement of the molecule, or 1,3 sigmatropic rearrangement of this system. The first argument is based on the addition of excess TEMPO to the double bond with the loss of the TEMPO leaving group, as is shown in Figure 46.

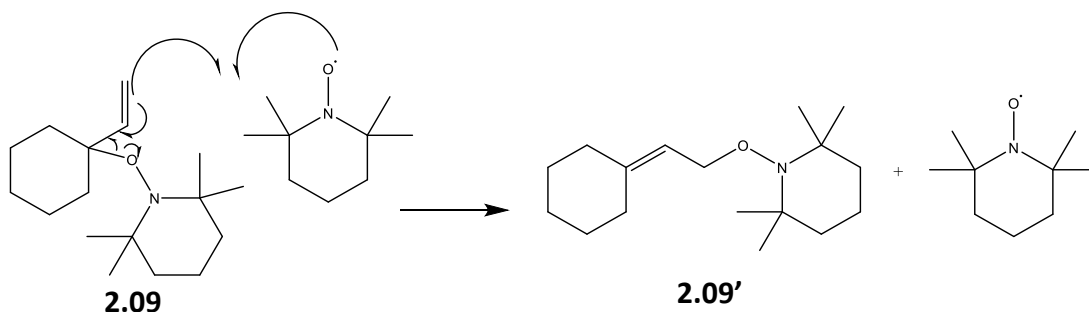


Figure 46: **2.09** trapping TEMPO to form **2.09'**

However, this would appear to be unlikely: the rate of rearrangement has been observed not to increase with the addition of excess TEMPO, which would not be the case were unreacted TEMPO to already be present. Also, TEMPO is very easy to observe by TLC, and elutes by flash chromatography with a significantly longer retention time than **2.07** or **2.09**, hence is unlikely to be carried through several purification stages.

Homolysis of the C-O bond appears, theoretically, to be a likely option. This bond is expected to be weak – indeed, given that reactions with very similar non cyclic tertiary compounds do not yield the target aldehyde, it suggests this is sterically a difficult bond to form, which in turn implies that breakage of this bond would be a sterically favourable event. Coupled with this is the fact that homolysis of this bond will release a stable radical leaving group (as is key to the original design of this species), further aiding the possibility of bond cleavage. Once cleaved, the carbon radical would be able to rearrange as was observed in earlier radical rearrangement sections, with subsequent radical trapping by TEMPO to form a significantly more stable bond to a ‘primary’ TEMPO group (Figure 47).

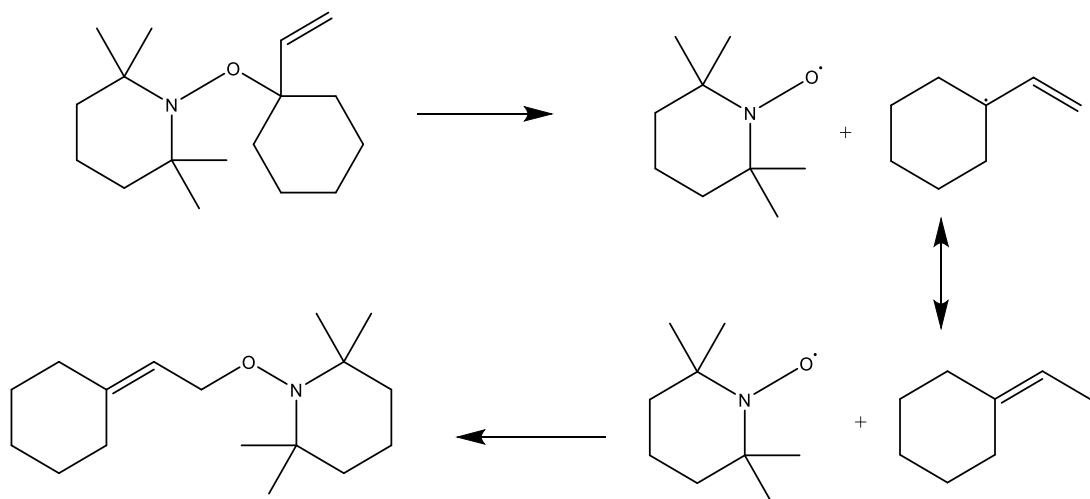


Figure 47: Homolysis of **2.09**, rearrangement and subsequent trapping to form **2.09'**

The stability of this type of C-O bond has been probed by a variety of groups within the literature, mainly due to the applications to living polymerisation reactions.<sup>104,155</sup> During this type of process, radicals produced from alkoxyamine homolysis are used in order to create polymers of very low polydispersity, making use of 'the persistent radical effect'.<sup>156</sup> As such, there is a large body of literature involving alkoxyamine C-O bond homolysis.

Marque et al. found that steric strain will indeed have a significant impact on the C-O stability, with notable changes in the BDE between tertiary and secondary/primary systems.<sup>157</sup> Indeed, Moad et al. recorded how a species that releases a tertiary radical (such as the case in this system) will typically have a half-life an order of magnitude smaller than that which releases a similar secondary radical.<sup>155</sup> This trend is likely owing to the varying stability of the radical leaving group, with the more stable radical having a correspondingly lower bond dissociation energy. Half-lives of alkoxyamines are typically measured at elevated temperatures, however half-lives of 10 min to an hour for some TEMPO based nitroxides at 60°C have been observed.<sup>155</sup> Analysis of different nitroxides has proved that steric hindrance has a large impact on half-life of these species.<sup>158</sup>

In addition to this, later work by Bertin et al. provided insight into the impact of electronic groups on the stability of this bond.<sup>159</sup> Electron withdrawing groups (on either the

nitroxide or alkyl moiety) were found to decrease the BDE of the C-O bond, therefore it would appear prudent to avoid the incorporation of these groups in future iterations of **2.09**. This destabilisation has been attributed to the polar ground state effect (PGSE),<sup>160</sup> whereby the C-ON bond can be considered as  $C^{\delta+} - \delta^-ON$ , and electron withdrawing groups will destabilise the ground state of this bond, thus promoting homolysis.<sup>161</sup> From this, it follows that electron donating groups would thus help to stabilise the ground state of these bonds.

The structure of the nitroxide would also provide steric influence, which will have some impact on the bond stability, with more sterically hindered systems expected to have weaker C-O bonds, and hence be more prone to homolysis.<sup>162</sup> Examples of some alkoxyamine structures are shown in Figure 48. Of these species, Alkoxyamines incorporating cyclic nitroxides, such as TEMPO, appear to have weaker CO-N bonds than acyclic 'open' nitroxides, for example di-tert-butyl-nitroxide (DBNO), indicating a weaker C-O bond in the 'open' nitroxides. In turn, the ring size of the closed nitroxides will also impact on C-O bond strength. A nitroxide present as a 5 membered heterocycle such as 1,1,3,3-tetramethylisindolin-2-yloxy, (TMIO) would be expected to have a stronger C-O bond than 6 membered heterocycles such as TEMPO.

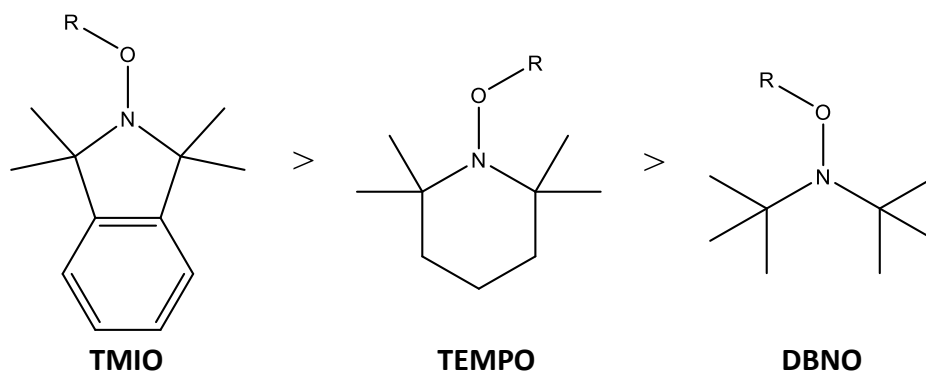


Figure 48: Trend in alkoxyamine C-O bond strength for different nitroxides

An indication into the steric hindrance of these systems can also be gained by examination of the C-N distance within the C-O-N segment of the nitroxide. Moad et al. found that this factor, which takes into account variation in C-O bond length as well as the C-O-N bond angle, correlates with bond dissociation energy.<sup>155</sup> As such, the larger the C-N distance,

the more steric hindrance is acting on this system, and hence as the distance increases, bond dissociation energy will decrease. This is shown in Figure 49. Studies by Grand et al. on the C-N-C bond angle drawn similar conclusions to these results.<sup>163</sup>

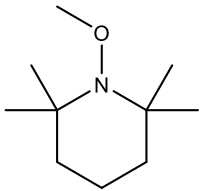
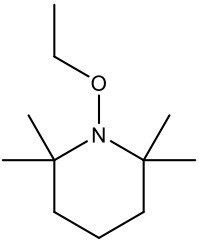
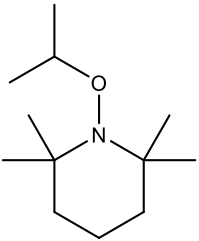
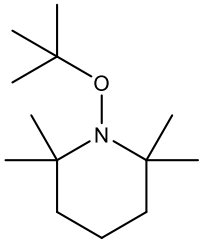
				
C-N distance/ Å	2.332	2.338	2.354	2.394
D <sub>C-O</sub> / kJ mol <sup>-1</sup>	165.8	130.1	101.0	75.9

Figure 49: Variation in C-N distance causing changes to C-O BDE, from Moad et al.<sup>155</sup>

In order to study the mechanism in Figure 47, the reaction was conducted with the use of a different nitroxide, oxo-TEMPO. In the event of the homolysis mechanism taking place a mixture of oxo-TEMPO and TEMPO based products would be observed. However, this was not observed: suggesting that bond homolysis is not the route of this rearrangement.

The final potential route for the observed rearrangement of this compound is through a [1,3]-sigmatropic rearrangement. Symmetry would suggest that this process must take place antarafacially, as suprafacial rearrangement is symmetry forbidden (Figure 50).

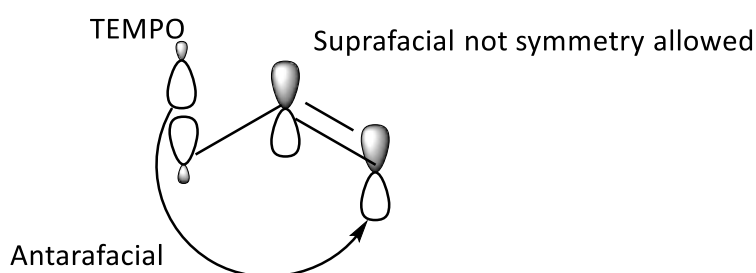


Figure 50: Suprafacial and antarafacial comparison for [1,3] rearrangement

All of the factors discussed above in the context of C-O bond cleavage are still relevant here (as the bond still breaks), however the mechanism of cleavage and rearrangement may be different. [1,3] carbon shifts, while uncommon, would be expected to take place as a concerted process between two radical intermediates.<sup>164</sup> It is possible that this route is going through a solvent caged radical pair, as suggested by Rautenstrauch for another

system exhibiting this type of rearrangement.<sup>165</sup> Here, the cage would be expected to quickly collapse, preventing other intramolecular reactions, with the argument that without a caged system, cyclisation reactions would be expected. These are not observed for this system. The activation energy of this rearrangement is likely to be very close to the C-O bond dissociation energy, hence a radical based pathway is likely.<sup>166</sup>

However, Majumdar investigated the [1,3] shift in nitroxide containing systems,<sup>167</sup> shown in Figure 51, and found that conducting the reaction in the presence of a radical initiator (or inhibitor) has no effect on the reaction, making a purely radical pathway unlikely.

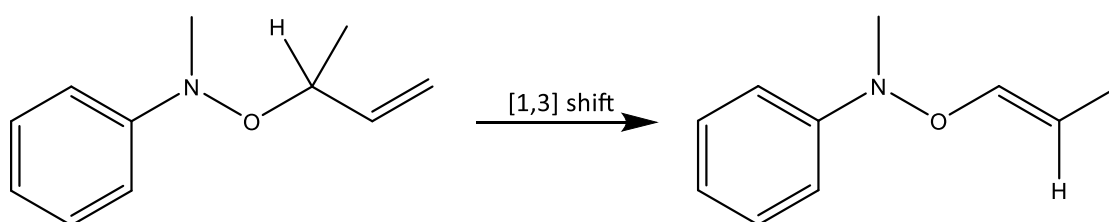


Figure 51: [1,3] shift from Majumdar et al.<sup>167</sup>

Therefore, it appears from this that the reaction is likely to take place through a concerted mechanism, such as that suggested by Bergbreiter et al.,<sup>137</sup> albeit one with a significant radical character. The sterics of the system also appear likely to impact on the concerted or radical based reaction mechanism. Berson et al. monitored the impact of an exo-methyl group compared to an endo-methyl group (which is more sterically unfavourable here) in a 1,3 rearrangement.<sup>168</sup> They concluded that the exo-methyl system was likely to take place in a concerted mechanism, while the endo-methyl system would be expected to utilise a di-radical based mechanism, shown in Figure 52. Therefore, a sterically hindered reaction would appear more likely to rearrange via a process of a more radical nature.

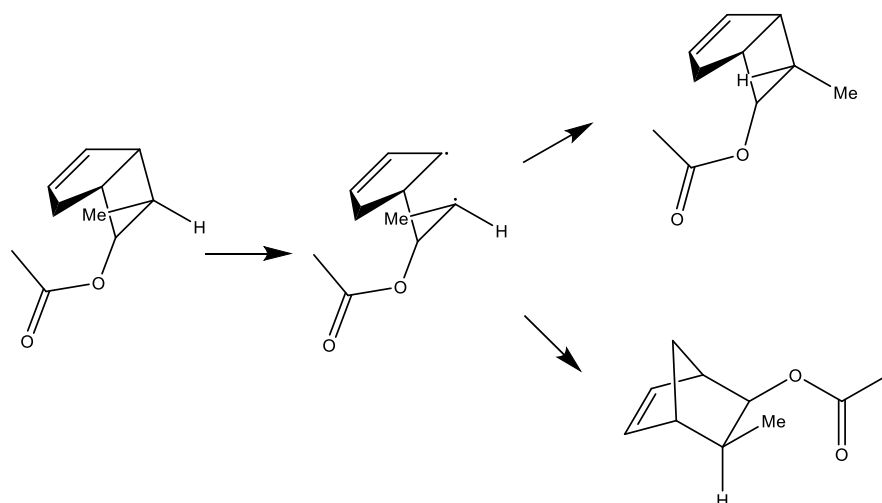


Figure 52: Di-radical rearrangement from Berson et al.<sup>168</sup>

## 2.9. Synthesis of Trapping Molecule Derivatives

While **2.09** has potential for use as a radical trapping compound, there are areas for improvements: primarily in improving the stability of the C-O bond to prevent degradation to the non-effective primary TEMPO system. It would also be useful for a range of trapping molecules to be synthesised, as trapping compounds with different masses will be very useful with regards to establishing reproducible self-consistency of the trapping process.

Based on the above work, retaining a cyclic starting aldehyde appears essential. Therefore, synthesis of **2.11** was attempted (Figure 53) in the same manner as for **2.09**, using a smaller cyclic aldehyde as a starting material, and proceeding via the TEMPO-aldehyde intermediate **2.10**. Further simple modification is possible by no longer using a purely alkyl group as the cyclic element to the compound. Therefore, synthesis of **2.13** was also attempted (Figure 54) with the introduction of a heteroatom into the ring, using tetrahydrofuran-3-carboxaldehyde as the starting aldehyde, via the intermediate **2.12**. The purpose of using these molecules was to evaluate whether a smaller ring size or the presence of a heteroatom can significantly alter the stability of the trap being developed.

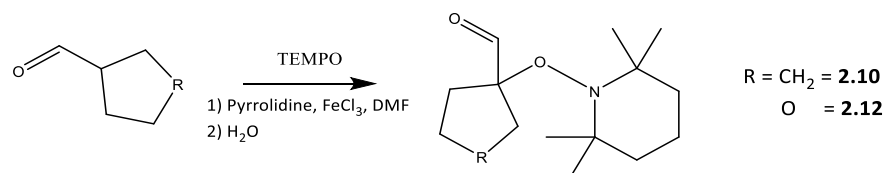


Figure 53: Formation of **2.10** and **2.12**

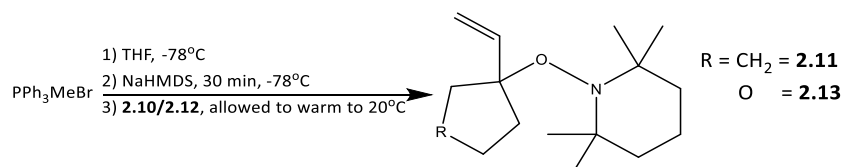


Figure 54: Formation of **2.11** and **2.13**

These syntheses were successful, with **2.10** and **2.11** produced in yields of 61 % and 24 % respectively, with the corresponding tetrahydrofuran analogues **2.12** and **2.13** formed in yields of 38 % and 40 %. However, in each case, rearrangement to form **2.11'** and **2.13'** (Figure 55) appears to be identifiable after the samples are aged overnight (ca. 18 hours).

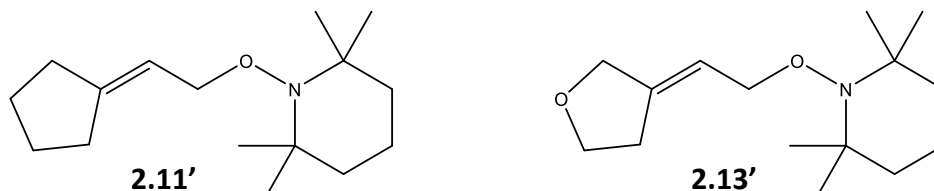


Figure 55: Structure of decay compounds **2.11'** and **2.13'**

While the C-O bond in **2.11** still appears to be sufficiently weak for rearrangement to occur, there does indeed appear to have been improvements following modification of the steric environment of this carbon centre. This can be observed in the changed rate of decay to form **2.11'** and **2.13'**, with rate constants of  $3.2 \times 10^{-5} \text{ s}^{-1}$  and  $1.75 \times 10^{-5} \text{ s}^{-1}$  and half-lives of 6 and 11 hours respectively.

A small change, by removing one CH<sub>2</sub> group from a cycle, has resulted in the lifetime of this radical trap almost doubling, with a half-life of just under 6 hours observed from this

system. Interestingly, **2.13** appears to have the longest lifetime of those studied thus far, with a half-life of approximately 11 hours. Part of this increase is expected due to the decreased size of the cyclic group, as was observed in **2.11**, however the incorporation of the oxygen heteroatom appears to have had a further impact. The O-alkyl group itself will act as an electron withdrawing group, although one would have expected this too be too far from the C-O bond to have a significant impact. Distortion of the ring structure caused by the replacement of a CH<sub>2</sub> group with an oxygen atom may provide a partial explanation for the enhanced lifetime of **2.13** relative to **2.11**.

### 2.9.1. A Less Volatile Trapping Agent

From the trapping materials **2.09**, **2.11** and **2.13** described above, there appears to be one potential flaw with all three species, their boiling points. Each small cycle species formed with only a hydrogen radical trapped, would be expected to have a relatively low boiling point, shown in Figure 56 for **2.14** and **2.15**. Therefore, this could present a problem when the capture of small radical species (e.g. ·H, ·CH<sub>3</sub>) is being attempted. This is because trapping is likely to utilise high air flow (ca. 5 L min<sup>-1</sup>) over a layer of deposited trap – products with a high volatility will thus be at risk of evaporation during the sampling process.

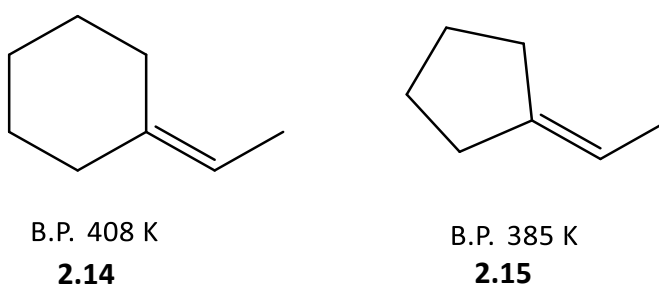


Figure 56: Anticipated boiling points of the expected adducts from H radical capture by **2.09** and **2.11**<sup>169,170</sup>

As such, modification of the cyclic section of the molecule would be useful, although care must be taken to avoid groups that could potentially interfere with the radical trapping system itself. One suitable group for structural incorporation would be a dimethylamide fragment: this would be expected to significantly raise the boiling point of the cyclic section

(a simple dimethylformamide molecule has a boiling point of 426 K), whilst not interrupting any radical trapping processes.<sup>171</sup> The target molecule, **2.16**, is shown below in Figure 57.

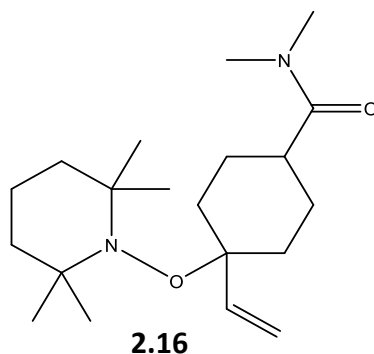


Figure 57: Structure of new target molecule

The functionalised aldehyde required for the synthesis of **2.16** is not commercially available, however it can easily be prepared by reduction of the corresponding acid chloride. This is shown below in Figure 58.

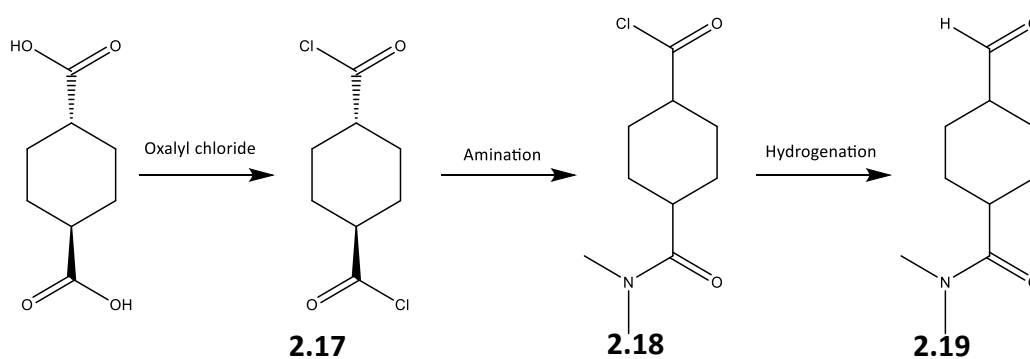


Figure 58: Reaction route to form **2.19**, precursor to **2.16**

The initial step for this reaction, formation of the di-acid chloride **2.17**, is a simple step, with several literature examples, utilising thionyl or oxalyl chloride as the chlorinating reagents.<sup>172,173</sup> In this instance oxalyl chloride was used, in order to form **2.17**. The subsequent formation of the amide **2.18** will produce an unwanted reaction product the di-amide **2.18'**, due to the presence of two equivalent acid chlorides. These are both shown in Figure 59. Although this can be limited, by slow addition of the amine and the use of only half an equivalent of amine, this will inevitably impact on the yield of this step.

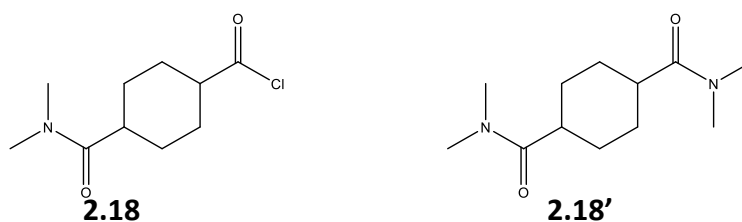


Figure 59: Structures of mono and di amides **2.18** and **2.18'**

Hydrogenation, utilising Pd/C and H<sub>2</sub>, on the remaining acid chloride was conducted in order to produce the aldehyde functionality required for the addition of the TEMPO group. With this step completed to isolate a product in a yield 19%, the next part of the synthesis utilising precursor **2.19** was carried out.

The latter part of the synthesis of **2.16** requires the incorporation of TEMPO to form **2.20** and subsequent formation of an alkene group giving **2.16**. This is expected to be simple, given that chemistry already applied to **2.09**, **2.11** and **2.13** is being applied. This was achieved in a yield of 20%, with a reaction scheme shown below in Figure 60.

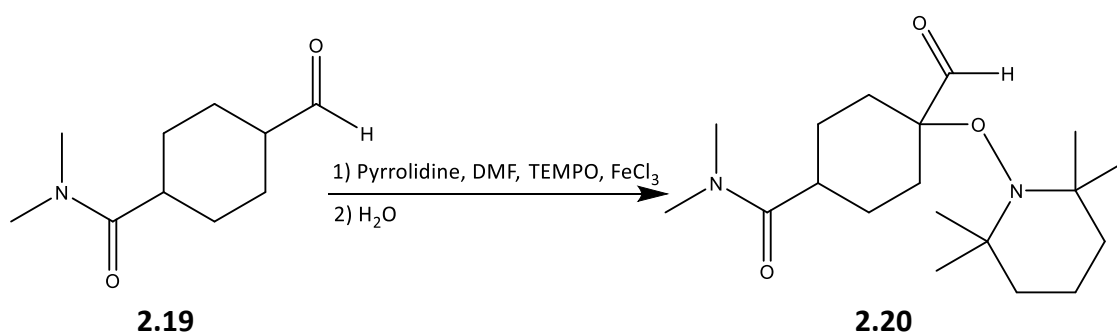


Figure 60: Formation of **2.20**.

It is important to note that the stereochemistry originally inherent within the molecule has been lost. The non stereoselective pyrrolidine based enamine intermediate will be able to react with TEMPO to give the TEMPO group either cis or trans relative to the amide functionality: there are two faces available for the TEMPO to attack.<sup>149</sup> While the

formation of the more sterically favourable TEMPO trans to the amide group would be expected to dominate, some cis product is still likely. However, precise stereochemical arrangement of **2.20** is not required for **2.16**. If control of this area were to be desired, then the enamine step would require an enantiospecific amine catalyst, such as those employed by Beeson et al. or Sibi et al. in their synthesis of TEMPO functionalised aldehydes.<sup>149,174</sup>

Aldehyde **2.20** was converted to **2.16**, again via a Wittig reaction. This is shown in Figure 61, and was achieved in a yield of 24%.

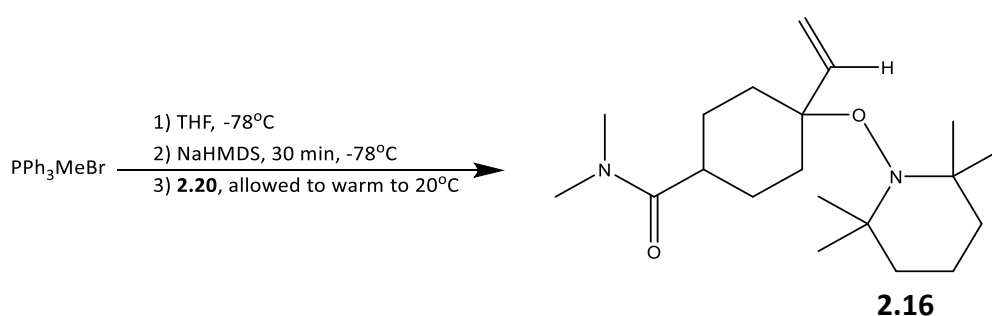


Figure 61: Formation of **2.16** from **2.20**

In addition to the removal of aldehyde signal present at 10.2 ppm in the  $^1\text{H}$  NMR of **2.16**, alkene proton signals provide evidence of a new terminal alkene. Correct relative integrations of the most distinguishable groups within **2.16**: the alkene protons, the methyl groups from the amide, and the methyl groups from TEMPO is also observed in Figure 62.

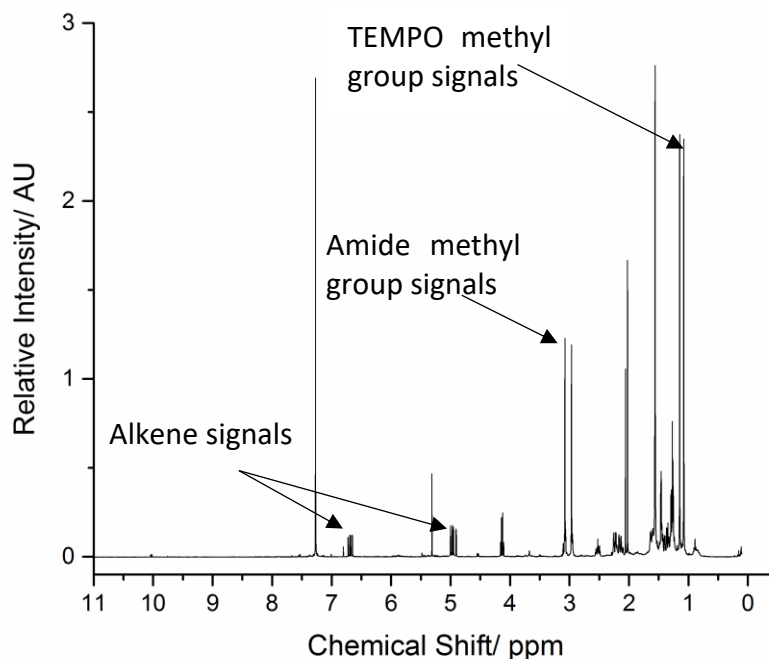


Figure 62:  $^1\text{H}$  NMR of **2.16**

The assignment was confirmed by a COSY NMR experiment (**Chapter 9**) showing signals corresponding to coupling from neighbouring hydrogens (e.g. 2-4 bonds distance).<sup>175,176</sup>

As with previous trapping compounds, re-examination of the  $^1\text{H}$  NMR spectrum after a few hours revealed that compound **2.16** also undergoes a rearrangement reaction shown in Figure 63 to form **2.16'**. The half-life established for this species was found to be 5 hours, very much in line with that for compounds previously discussed. Again the compound appears to be stable for long time periods (> 6 months) when kept below 263 K, and so will also be useable for radical trapping investigations.

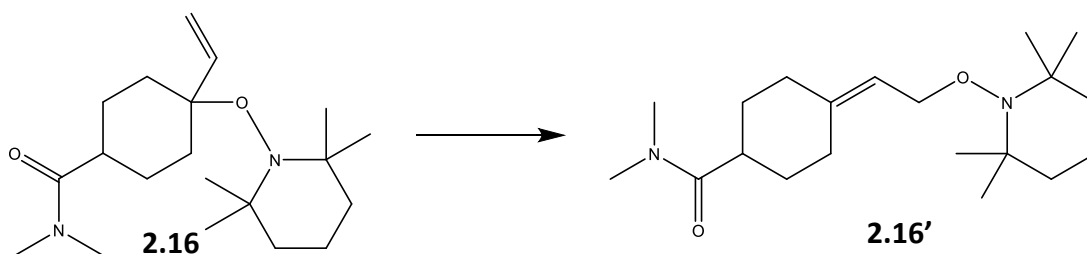


Figure 63: Rearrangement of **2.16** to form **2.16'**

## 2.10. Future Work

Synthesis of further trapping molecule derivatives would be useful. One method for this would be the modification of substrates used for the reaction with TEMPO. Given the success of **2.13**, aldehydes with other heterocyclic rings, such as those in Figure 64, would be useful starting compounds for the potential variation of the C-O bond stability.

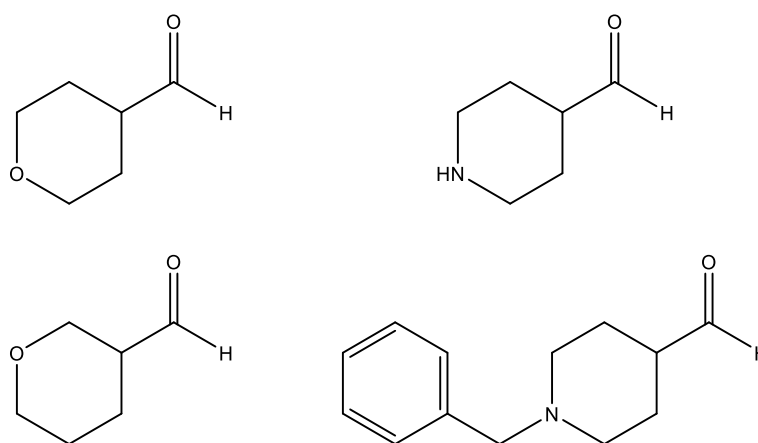


Figure 64: Different aldehydes that may be suitable precursors for trapping compounds

Alternatively, different nitroxide leaving groups may also be of use in the search for more stable systems, for example a smaller nitroxide ring structure (e.g. TMIO). Care should however be taken with the strengthening of this C-O bond: as it will be required to break during the radical trapping process, a bond of a sufficiently high BDE may preclude the trapping process altogether.

Another area of attention would be the ability to capture radicals from within biological systems, where, as with atmospheric chemistry, radical based reactions are of great interest.<sup>95,177</sup> In order for this to be accomplished, it would be necessary to synthesise a water soluble trapping molecule (i.e. with hydrophilic functionality). However, it is also important that the groups incorporated do not interfere with the functionality required for the trapping process – for example, avoiding groups with hydrogen atoms that are

highly available for abstraction by radicals. One simple idea, **2.21**, in Figure 65, utilises an amino group added to the cyclohexane ring, which would be expected to significantly enhance water solubility of this compound.

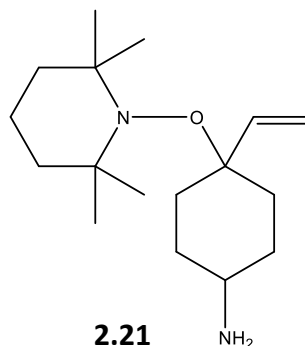


Figure 65: An example of a potentially water soluble trapping compound

## 2.11. Conclusion

Here we have highlighted a new radical trapping strategy for creating novel new radical trapping molecules (trapping radicals by radical attack on an alkene, with the loss of a leaving group to create a new stable non radical species). Several synthetic strategies were employed in order to synthesise a suitable species for radical trapping. A series of reactions focussed on allylic hydrogen abstraction reactions of alkenes were thwarted by regioselectivity to form compounds with the TEMPO functionality present in the primary position, which will not be suitable for the desired radical trapping methodology.

This led to modification of the synthetic process to incorporate the TEMPO functionality before the alkene functionality, by means of reactions with aldehydes. Oxidation reactions of the readily synthesisable TEMPO functionalised alcohol **2.06** proved unsuccessful, with unwanted reaction products or non-reaction observed. Utilisation of enamine chemistry failed to produce the target compound when applied to acyclic aldehydes, however the target functionality was achieved with cyclic aldehydes. These aldehydes proved readily convertible to alkenes, thus resulting in the synthesis of three different radical trapping

molecules, **2.09**, **2.11** and **2.13**. In addition to this, an amide functionalised trapping compound, **2.16**, is also synthesised, with the aim of being utilised in the detection of small radical species such as H $\cdot$ . These four traps are given in Figure 66.

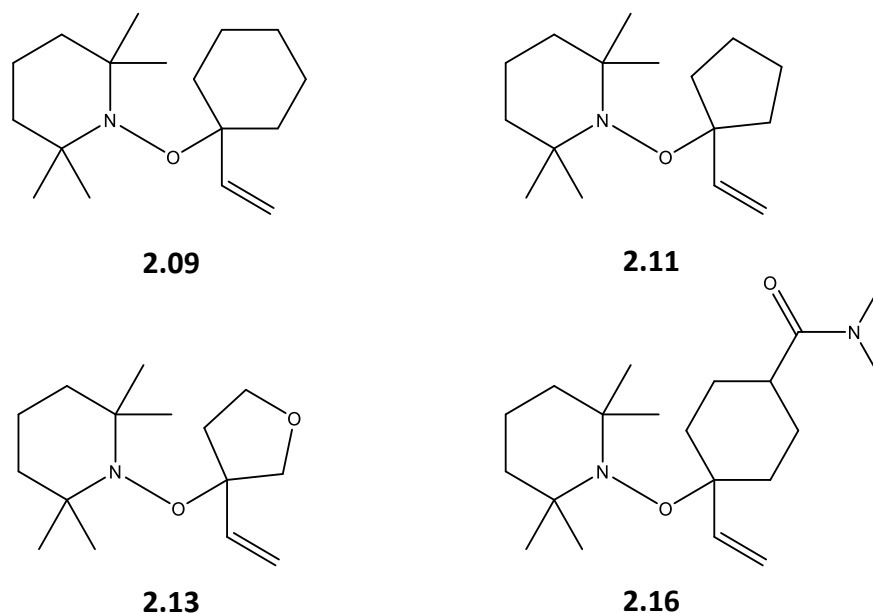


Figure 66: Structures of synthesised trapping molecules

An inherent problem with these compounds was also observed, in the form of a rearrangement from a tertiary to primary TEMPO position on the trapping compound. Variation of the cyclic system adjacent to this C-O bond induced notable variation in the rate of rearrangement, for example decreasing the ring size and adding in an electron donating group. However, this rearrangement appears not to be a problem, with compounds stable for several months when stored at -20 °C, suggesting that **2.09**, **2.11**, **2.13** or **2.16** are still likely to be effective radical trapping agents, while the timescale of rearrangement in solution appears slow enough (i.e. half-lives of several hours) not to completely remove the opportunity for radical trapping experiments to be conducted.

## 3. Solution Phase Radical Trapping

### 3.1. Introduction

#### 3.1.1. Solution Phase Spin Trapping

Initial testing of traps from **Chapter 2** would be experimentally simpler in the liquid phase. Radical spin trapping is often conducted within the liquid phase, with spin traps such as PBN routinely used here.<sup>178</sup> Radical products from spin trapping have also been analysed beyond just EPR studies. For example, Guo et al. used HPLC to separate spin adducts from the spin trapping of oxygen centred radicals with DMPO, with detection by both EPR and MS.<sup>91</sup> While this technique is limited by spin adduct stability, separation of reaction components allows EPR signals to be assigned to a specific mass, a very useful tool.

Other examples include the use of Ultra Performance Convergence Chromatography – Quadrupole Time of Flight – Mass Spectrometry (UPCC-QTOF-MS) by Wang et al.<sup>179</sup> This technique utilises supercritical CO<sub>2</sub> as the mobile phase for separation, resulting in a considerably improved separation process than is achievable using conventional HPLC. This is a particularly useful feature when analysing short lived spin adducts, such as the PBN spin trapped radicals from cigarette smoke examined by Wang et al.<sup>179</sup>

Another example of solution phase trapping can be found with biological systems. Halpern et al. used POBN to spin trap the hydroxyl radical within a mouse, which was positioned within an EPR cavity for analysis.<sup>180</sup> However, the potential toxicity of spin traps within biological systems is still an issue for these studies.<sup>181</sup>

#### 3.1.2. Methods of Radical Generation

In order to trap radicals in the liquid phase, they will first need to be generated. There are many different methods for the generation of radicals in the liquid phase, either by

homolysis of weak bonds (by heating or irradiation), or by electron transfer. A common example is that of photolysis, which is regularly used in order to photolyse peroxides such as  $\text{H}_2\text{O}_2$  to produce oxygen centred radicals.<sup>178</sup> Generation of radicals via thermal degradation of radical initiators is also a widely used technique. A commonly found example of this would be the use of azo compounds, such as azobisisobutyronitrile (AIBN).<sup>105,182</sup> This method of radical generation can be applied to many systems, with radical polymerization reactions being one such area.<sup>105,183</sup> Indeed, this is an area where alkoxyamines can also be used as radical initiators, with the radical being formed on homolysis of the C-O bond.<sup>184</sup>

Fenton based systems are also highly common methods of radical generation by electron transfer, with reaction between  $\text{Fe}^{2+}$  and  $\text{H}_2\text{O}_2$  to form hydroxyl radicals being the most common use of this system.<sup>91,185,186</sup> However, other peroxides, such as di-*t*-Butyl peroxide can also readily be used in the same manner of radical formation.<sup>187</sup> Alternatively, there are several examples of iron free 'Fenton like' reactions, which can result in radical formation from peroxides. These will again utilise single electron transfer and has been applied in  $\text{Cu}^+/\text{Cu}^{2+}$  or  $\text{Co}^{2+}/\text{Co}^{3+}$  systems.<sup>188</sup> Systems involving the use of lead dioxide have also been used for the generation of radicals from peroxides.<sup>189</sup> A final example of radical formation can be found with the formation of ketyl radicals. These can be formed through reactions between a ketone and a reducing metal, for example Gansäuer used titanocenes for this method of radical generation.<sup>190</sup>

### 3.1.3. Aims

The target for this chapter is to gather proof of concept evidence for for the successful trapping of radicals using traps from **Chapter 2**. There are two aspects to this. The first is to determine whether radicals can be captured by the desired trapping mechanism, and thus form expected products. The second is to test this scope of this trapping process by reacting different types of radicals with the trap.

### 3.2. Trapping the <sup>t</sup>BuOO radical

As an initial test into the ability of **2.09** to trap radicals, the trapping molecule was tested in a liquid phase system. This type of system is considerably easier experimentally as an initial test than a gas phase system, and so was a useful preliminary experiment. Here, the reaction between lead dioxide and <sup>t</sup>BuOOH was utilised in order to generate peroxy radicals for trapping, as shown in Figure 67.<sup>191</sup>

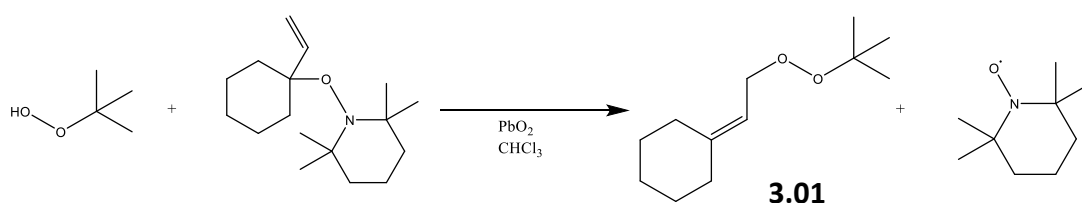


Figure 67: Trapping of <sup>t</sup>BuOO radical by **2.09** to form **3.01**

Analysis by mass spectrometry indicated the formation of **3.01**, the expected product from trapping the <sup>t</sup>BuOO· radical. This was detected as a sodiated species, with a mass of 221.1511 observed in Figure 68, which correlates well with the predicted mass of 221.1512 Da. Therefore it appears that radical trapping is indeed occurring within this system.

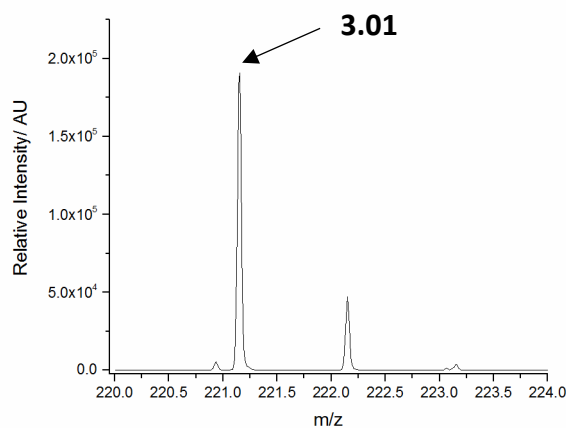


Figure 68: Signal corresponding to **3.01**

To confirm the identity of **3.01**, this species was subjected to LC-MSMS. The major ion detected from fragmentation (Figure 69) corresponds to the hydroperoxide formed from

loss of the <sup>t</sup>butyl group, in a typical alkyl peroxide fragmentation (Figure 70).<sup>192</sup> This, with the accurate mass of the detected species, is a good indication that **3.01** is being observed.

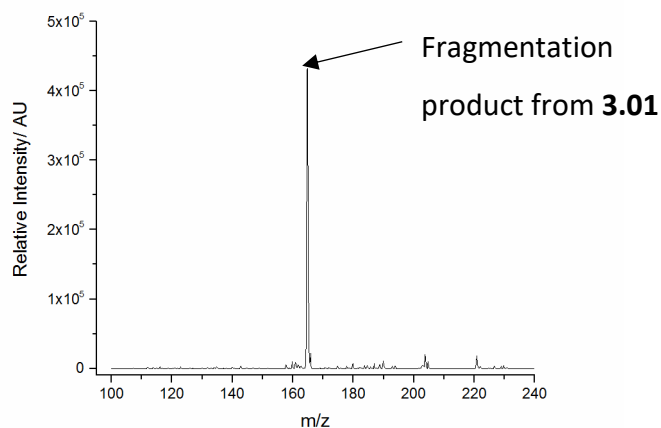


Figure 69: MS produced by fragmentation of **3.01**

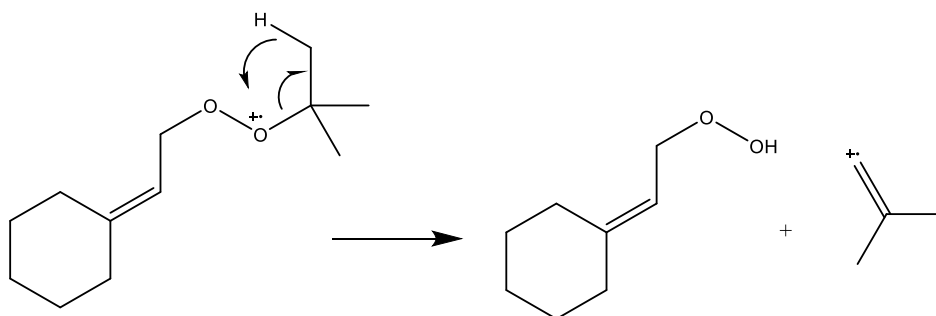


Figure 70: Fragmentation of **3.01**<sup>192</sup>

### 3.3. Trapping a Methyl Radical

As a further test of the trapping system, generation of different radicals in solution phase reactions, and exposure to trapping material, will be useful. This can be used to provide evidence regarding the versatility of the trapping material. While some traditional spin traps are not suitable for different radical centres (oxygen centred, carbon centred etc), this will probe the ability of these radical trapping molecules to capture different radical centres, as opposed to just the oxygen centred species that has currently been probed.

The detection of a carbon centred radical was targeted towards detection of the simplest carbon radical, the methyl radical. This can be generated in several ways, including reactions of DMSO with NaOH (with oxygen from air acting as the oxidant), or DMSO in a Fenton style system.<sup>84,193</sup> Here, the former method is utilised, as shown in Figure 71.

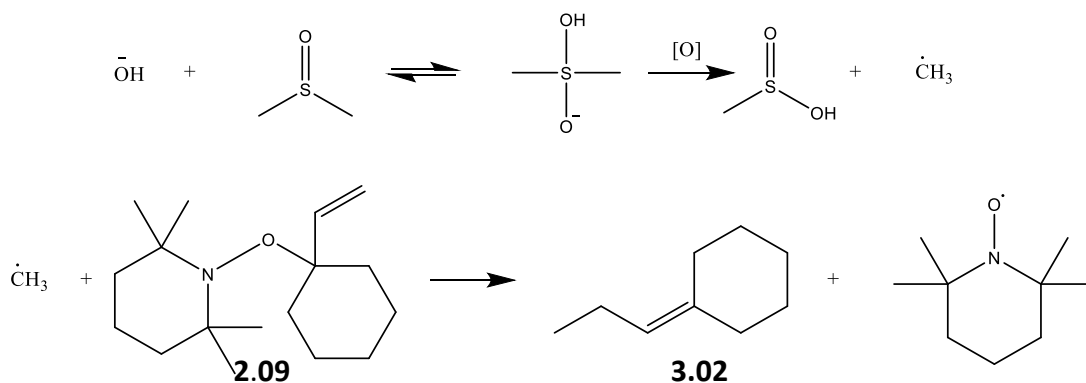


Figure 71: Generation and capture of the methyl radical to form **3.02**

Mass spectrometry of the reaction mixture (Figure 72) features a signal at 125.1332 m/z, suggesting that trapping of the methyl radical has occurred (theoretical accurate mass of 125.1325 for  $[\text{M}+\text{H}]^+$ ). The trapping of this species is a pleasing result, suggesting that the radical trapping design is not specific to just oxygen centred radicals, but can also be applied to carbon centred radicals.

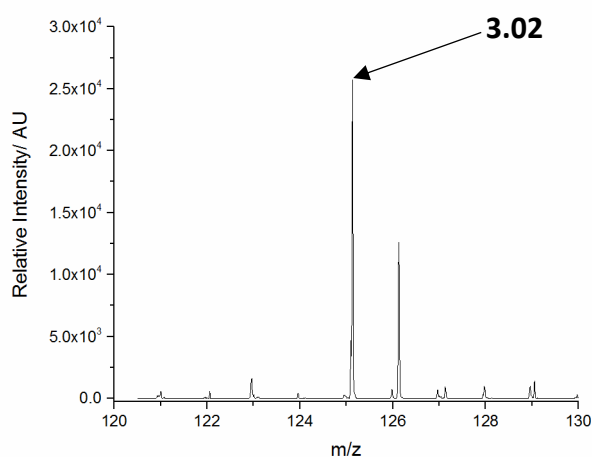


Figure 72: Mass Spectrum showing the formation of **3.02**

## 3.4. Experiments with a Nitrogen Centred Radical

### 3.4.1. Trapping a Nitrogen Centred Radical

Another radical species of interest to be studied was a nitrogen based radical. Examples of these such as NO are common within the atmosphere, while amine radical cations are widely applied in polymerisation chemistry, as well as within biological systems.<sup>194,195</sup> Generation of an aminyl radical is much easier than breaking a C-H bond to form a carbon centred radical. Instead of homolytic C-H bond cleavage, the amine can be oxidised to a radical cation, which can then form a radical upon deprotonation.<sup>196,197</sup> Here, radical formation was attempted using PbO<sub>2</sub> and n-butylamine, shown in Figure 73.

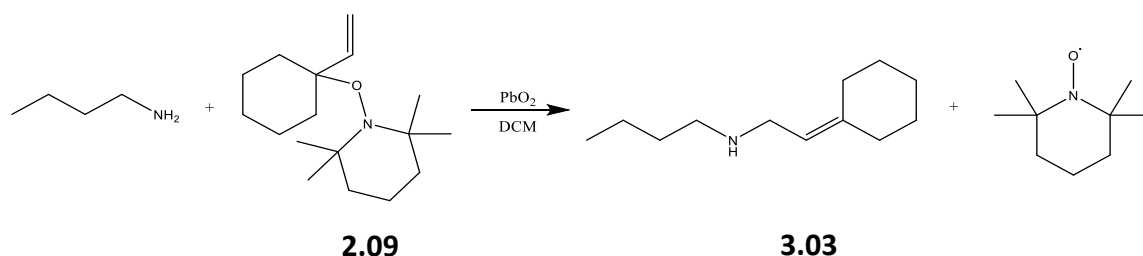


Figure 73: Formation of **3.03** by capture of a nitrogen centred radical

However, the reaction in Figure 73 does not appear to proceed as would have been anticipated. Rather than the expected [M+H]<sup>+</sup> ion being detected at 182 m/z, a signal was instead observed at 180 m/z. This is shown in the mass spectrum within Figure 74.

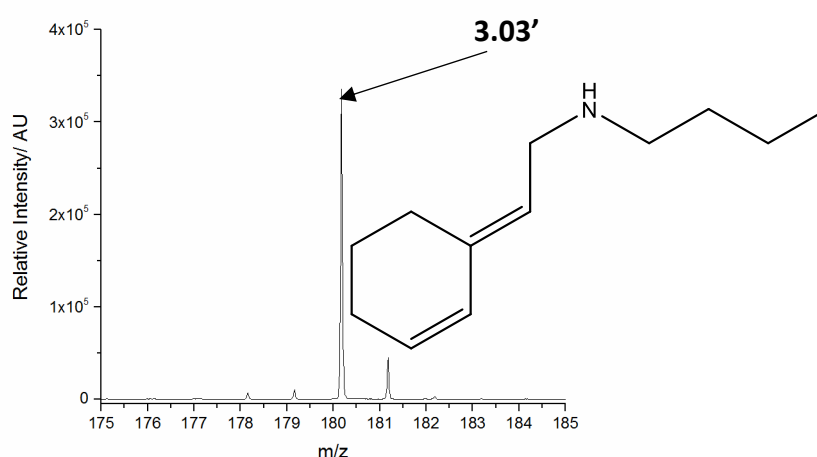


Figure 74: MS from **3.03'**, with a possible structure matching an [M+H-2]<sup>+</sup> ion of **3.03**

This suggests that further oxidation processes are occurring within this system, with the formation of another double bond within this system likely, forming **3.03'**. Use of a different amine, isopropylamine (Figure 75), maintained this difference of two mass units between expected and detected signals, shown in Figure 76.

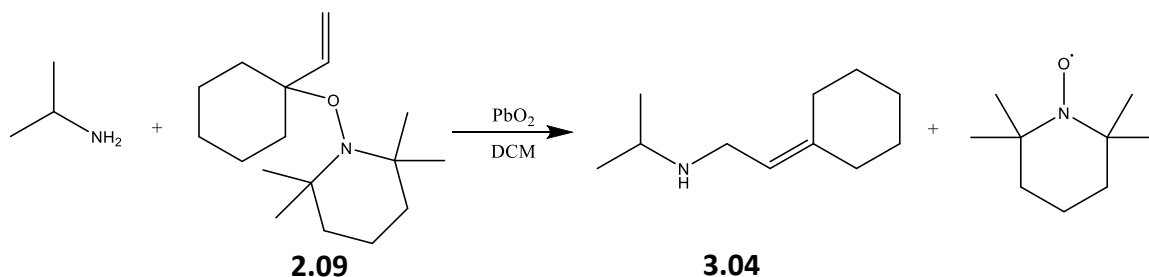


Figure 75: Expected capture of a nitrogen centred radical from isopropylamine

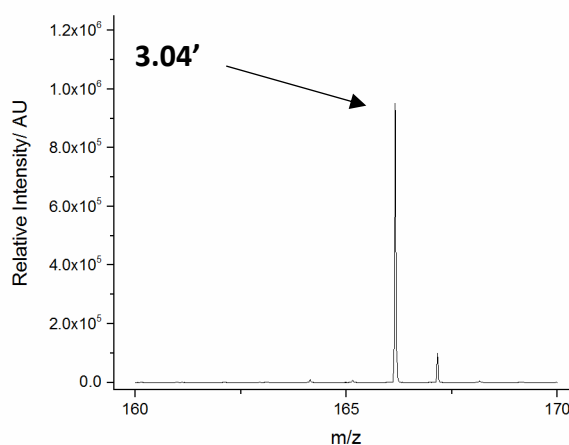


Figure 76:  $[\text{M}+\text{H}-2]^+$  product **3.04'**

A potential explanation for this observation is that the desired product, once formed, is reacting again with the  $\text{PbO}_2$  in the system. This could lead to the formation of an imine product two mass units different from the desired species. In order to test this, the reaction was conducted using  $t$ -butylamine (Figure 78). As shown in Figure 77, this cannot form an imine, hence would be expected to prevent this unwanted reaction and form **3.05**.

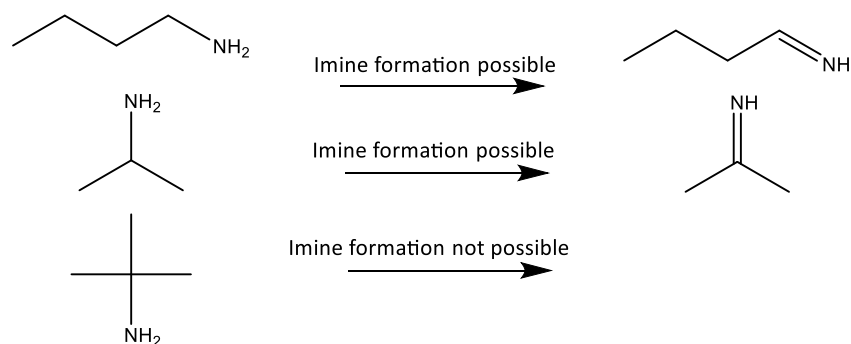


Figure 77: Possible imine formation from amines

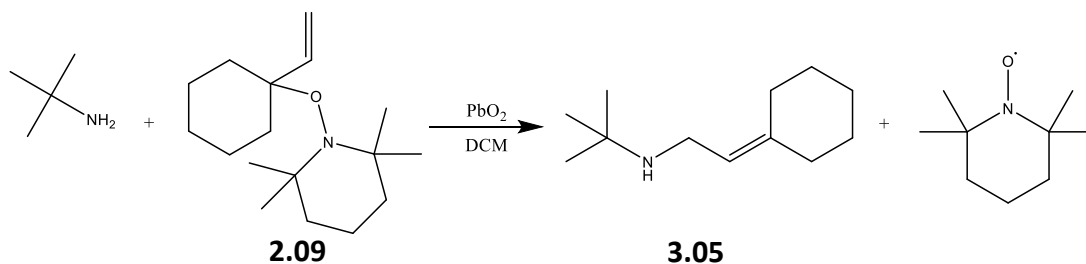


Figure 78: Reaction to form **3.05**

However, Figure 79 shows that the  $[M+H-2]^+$  product **3.05'** was still observed in this system in place of the expected  $[M+H]^+$  ion, therefore suggesting that imine formation is not the origin of this reaction. This implies that the oxidative dehydrogenation is taking place on the 'trap' side of the compound – as here it cannot occur on the amine side.

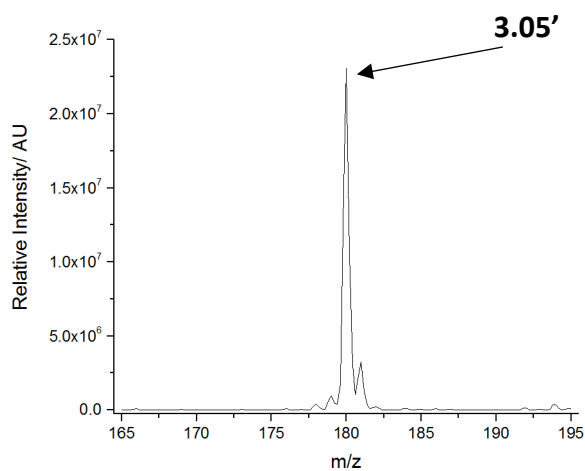


Figure 79: MS for **3.05'**

### 3.4.2. Utilisation of Isotopic Labelling

Oxidative dehydrogenation taking place on the 'trap' portion of the resulting compound would be surprising, given the successful reactions previously described. In order to rule out some form of rearrangement of the amine, and provide definitive confirmation of this, a trapping experiment was conducted using deuterated species **3.06**, shown in Figure 80.

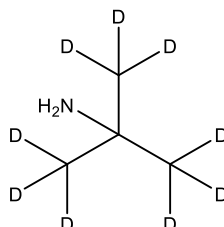


Figure 80: Structure of the deuterated species **3.06**

If oxidative dehydrogenation occurs on the amine portion of the compound, a mass shift of 4 Da would be observed with use of **3.06**, as opposed to shift of 2 Da detected with non-deuterated butylamine. However, as indicated by Figure 81, a mass shift of 2 Da was observed with **3.06** forming **3.07**. This confirms that, following reaction with <sup>t</sup>butylamine, oxidative dehydrogenation appears to be present on the trap segment of the product.

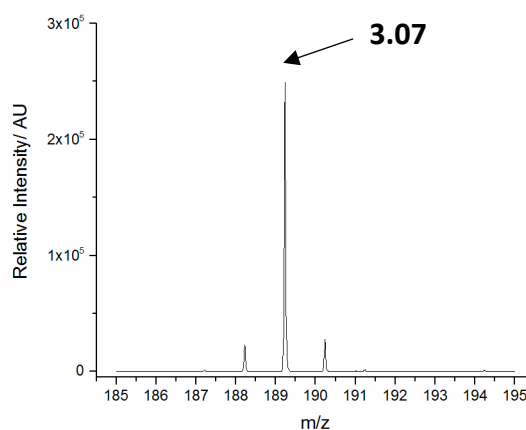


Figure 81: MS of **3.07**

### 3.4.3. Fragmentation Experiments on Captured Nitrogen Radicals

In order to gain some information on the location of the unexpected double bond in this system, MSMS was conducted on two examples of these species. The resulting

fragmentation patterns produced by the n-butylamine and t-butylamine based products **3.03** and **3.05** are compared in Figure 82 and Figure 83 respectively. As the extra double bond can only be on the 'trap' side from the t-butylamine product, this will provide a potentially useful comparison regarding whether the double bond is on the trap or trapped part of the compound following reaction with n-butylamine.

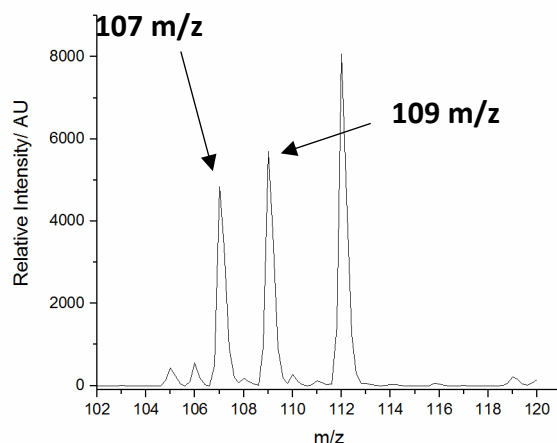


Figure 82: Fragmentation of m/z 180 from **3.03'**, with key fragmentations indicated

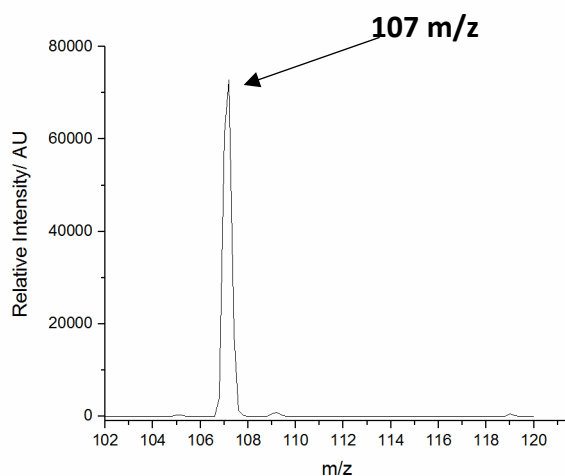


Figure 83: Fragmentation of m/z 180 from **3.05'**, with key fragmentation indicated

Both compounds exhibit a fragmentation to form a species of mass 107 Da. However, in the n-butyl system, this is observed in conjunction with a nearby signal at 109 Da, which is not present in the t-butyl system. Based on this mass, and possible fragmentations of the trapped compound, it appears likely that this is a cleavage of the C-N bond, with the resulting fragments shown in Figure 84. In the event of two protons being lost on the

'trap' section of the molecule, this would produce a signal at 107 Da, which is what is observed when the structure of the amine prevents oxidative dehydrogenation on the other side of the molecule.

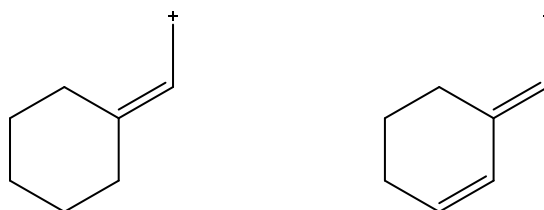


Figure 84: Anticipated structures corresponding to ions 109 and 107 m/z respectively

In order to provide some further evidence for this idea, a different trapping molecule (**2.11**) was employed (Figure 85). The different mass of **2.11** would be expected to produce different masses for the corresponding fragmentations to those shown in Figure 73 and Figure 78, hence providing validity regarding the suggested identity of the above fragments.

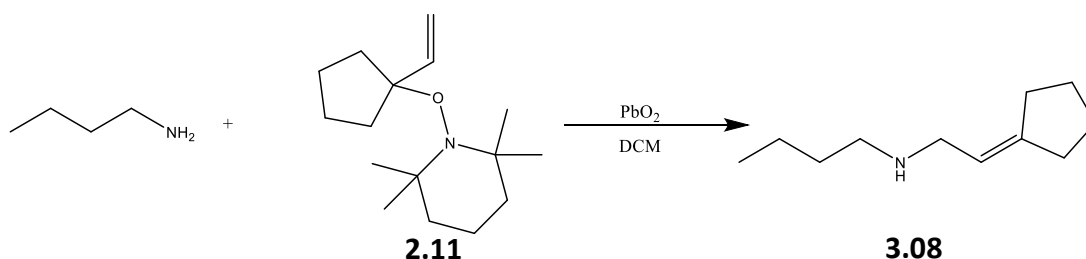


Figure 85: n-Butylamine trapping with **2.11** to form **3.08**

Indeed, upon application of **2.11**, the '[M+H-2]<sup>+</sup>' product, **3.08**, was again formed. Fragmentation of this species to form an ion with a m/z of 95 was observed, alongside an ion of similar intensity at 93 m/z, as shown in Figure 86. These correspond to the same fragmentations as described above in Figure 84, but 14 mass units smaller, owing to **2.11** being a CH<sub>2</sub> group smaller than **2.09**. The structure for these fragmentations are given in Figure 87. As such, these fragmentation experiments show that double bond formation does appear to be possible on both the trap and the 'trapped' side of the compound.

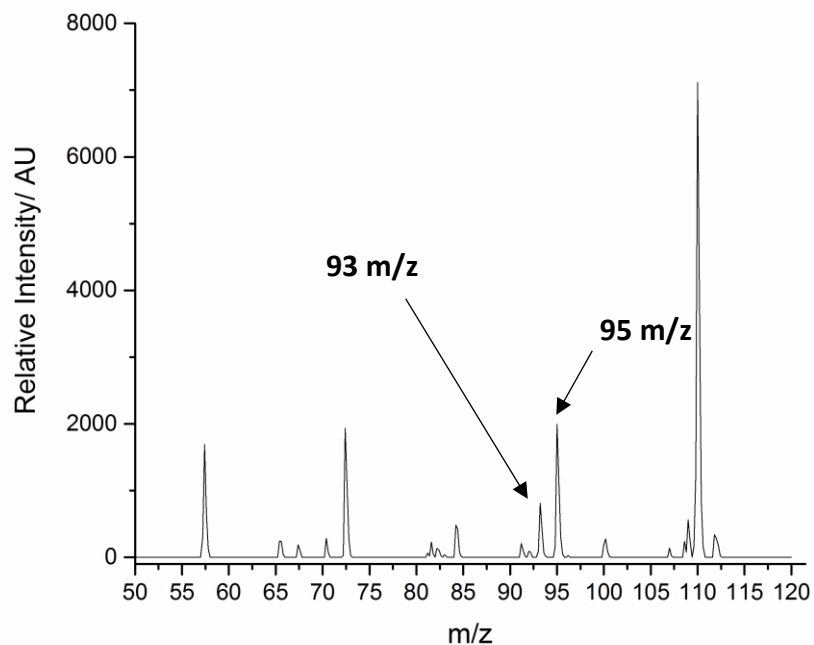


Figure 86: Fragmentation of  $m/z$  166 from **3.08'**, showing fragments at 95 and 93  $m/z$ .



Figure 87: Anticipated structures for fragments at 95 and 93  $m/z$  respectively

#### 3.4.4. Reactions with 2-Naphthylamine

An amine radical that contains aromatic functionality within the molecule was also studied. The use of 2-naphthylamine, shown in Figure 88, means that the aromatic amine cannot be dehydrogenated on the amine side of the product, as was the case for *t*-butylamine, thus it will be interesting whether the  $[M+H-2]^+$  ion is again observed. In addition to this, the scope of the reaction is also being further examined, with aromatic amines expected to have different reactivity compared to aliphatic amines.<sup>198</sup>

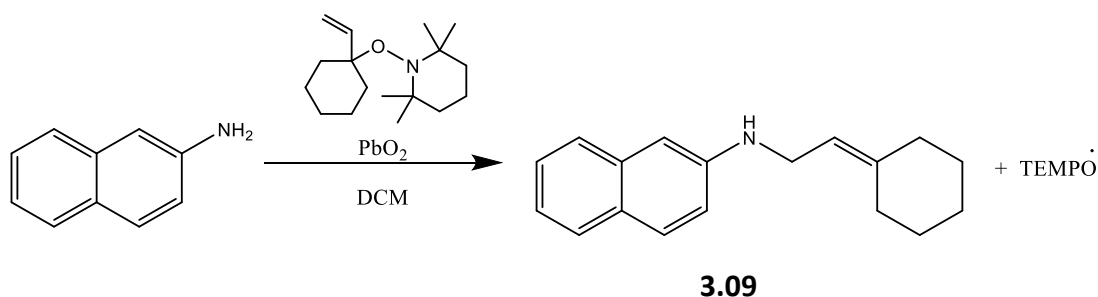


Figure 88: Reaction to form **3.09** from 2-naphthylamine

The MS of this reaction, shown in Figure 89, does also exhibit the same type of 'M+H-2' signal to form **3.09'** that has been described above, with again no observation of the expected  $[M+H]^+$  species **3.09**. As with the t-butylamine, it is likely that this **3.09'** signal at 250.1592 Da is due to reaction on the trap segment of the molecule, given that alkyne formation within the aromatic system would be very unlikely to occur.

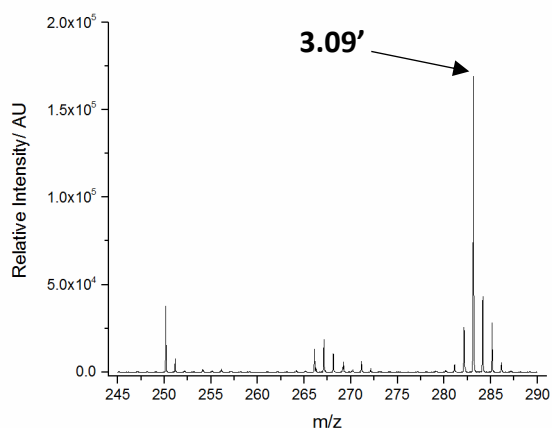


Figure 89: MS of **3.09'** from naphthylamine radical capture

#### 3.4.5. Test Reaction with a Surrogate Trapping Molecule

At this stage, it is not known whether the dehydrogenation is occurring during the radical generation step, after radical trapping, or within the MS machine. In order to probe the feasibility of adduct formation, a model compound (allylcyclohexylamine) resembling the expected adduct was reacted with lead dioxide, without addition of a trapping compound. This proposed scheme is shown in Figure 90. If this occurred, it would suggest that the

target product itself is being re-oxidised once formed, (either within the solution or the MS machine) hence preventing its detection.

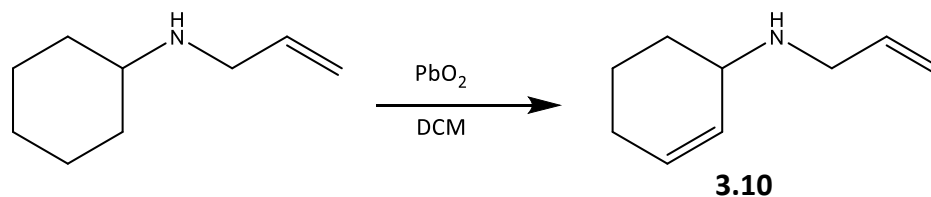


Figure 90: Possible scheme for formation of **3.10** through allylcyclohexylamine

It appears that exposure to  $\text{PbO}_2$  does not result in reaction with this compound, with starting material clearly identifiable by mass spectrometry after the reaction (Figure 91). The absence of any reaction here suggests that the reason for the previously described  $[\text{M}+\text{H}-2]^+$  compounds is unlikely to be due to a 'double oxidation' reaction. Instead the most likely explanation appears to be that a compound 2 mass units lower than the target species is being formed on exposure to lead dioxide, with the formation of **3.01'** not going via the formation of **3.01**, as it appears unlikely that the trapped species is reacting further after trapping.

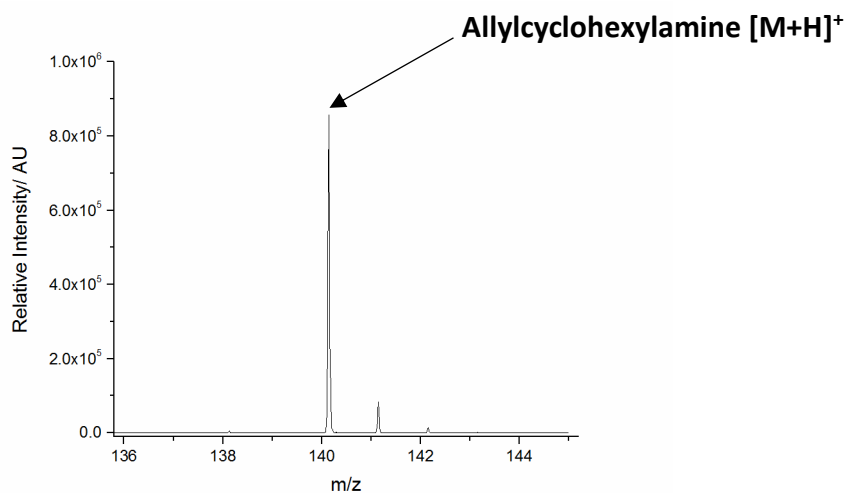


Figure 91: Post reaction allylcyclohexylamine with no indication of **3.10**

### 3.4.6. Fenton Based Amine Radical Generation

A different initiator was also applied to the reaction: Fenton based initiation.<sup>191</sup> This, as shown in Figure 92, would also be expected to form **3.01**.

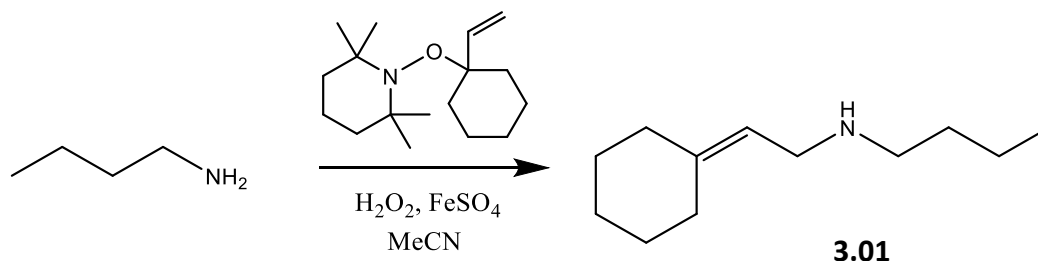


Figure 92: Expected formation of **3.01** via Fenton Reaction

However, once again the reaction produces no indication of **3.01**, with **3.01'** readily identifiable from the reaction mixture. Therefore, it appears that the formation of this **3.01'** species is not simply due to the choice of  $\text{PbO}_2$  as a means of radical generation.

## 3.5. Experiments with a Sulfur Centred Radical

### 3.5.1. Capture of a Sulfur Centred Radical

Lead dioxide was also employed in the generation of sulfur based radicals. Reaction with dodecanethiol, shown in Figure 93, would be expected to produce a sulfur centred radical, which can then be trapped by **2.09** to form **3.11**.

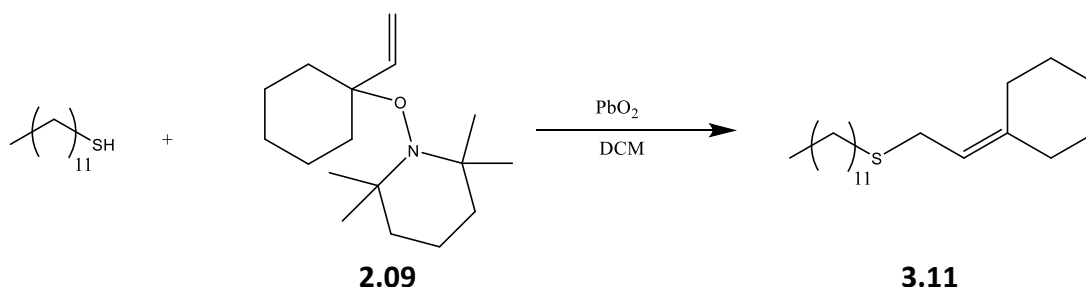


Figure 93: Expected trapping of a thiyl radical

As with the amine system, a signal was observed 2 Da lower than expected when the sample is examined by mass spectrometry: at 309 m/z (**3.11'**) as opposed to the expected 311 m/z. This, along with a number of other signals, is shown in Figure 94.

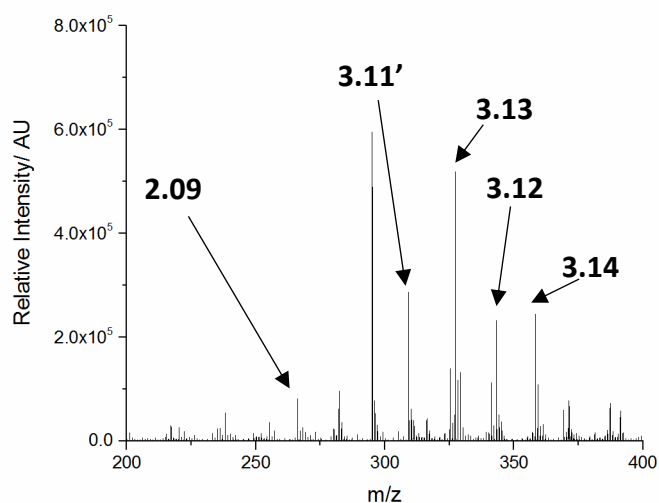


Figure 94: MS of thiol reaction products including **3.11'**

### 3.5.2. Detection of Other Radicals from the Sulfur System

Beyond **3.11'**, several other species appear to be present within Figure 94. Some of these signals can be attributed to **2.09** (266 m/z), or the TEMPO group (157m/z) that will have been lost during the trapping reaction. Yet, there are a number of other significant signals yet to be accounted for, suggesting the possibility that other radical species may be detected within this system. Indeed, signals at 327 m/z and 343 m/z appear likely to correspond to two trapped radical species that will have originated from the dodecanethiol reaction: the sulfinyl and sulfonyl radicals. These are species that would be expected to form via the initial sulfur radical reacting with oxygen, with a subsequent product formed as a result of this radical losing an oxygen atom. This reaction scheme is shown below in Figure 95. Alternatively, these products could be formed from oxidation of the sulfide adducts by PbO<sub>2</sub>. However, this is unlikely given that they are also detected in an AIBN system described in **3.5.3**.

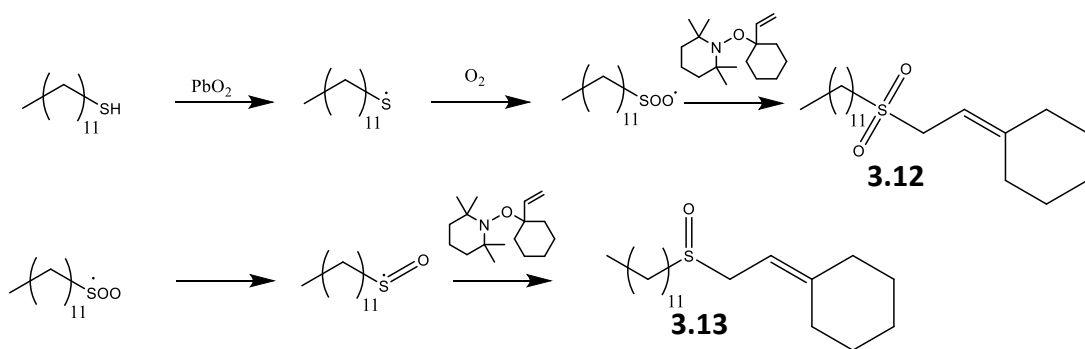


Figure 95: **3.12** and **3.13**, formed following thiyl radicals reacting with oxygen

The formation of these oxygenated sulfur radicals has previously been studied within the literature. Miller et al. shows that these species can be formed through reactions with superoxide or oxygen, while the source of oxygen in reaction products is indeed likely to be from molecular oxygen, not exchange with any water present in the system.<sup>199</sup> Karoui et al. describe how sulfur radicals will react with oxygen at diffusion controlled rates (ca.  $10^{10} \text{ M}^{-1} \text{ s}^{-1}$ ).<sup>200,201</sup> Therefore, the capture of these radicals is not unsurprising.

The detection of these species gives several pieces of interesting information. Firstly, it appears that the trapping reaction is not taking place faster than the time required for sulfinyl/sulfonyl formation from reactions between sulfur centred radicals and oxygen.<sup>200,201</sup> Secondly, **3.12** and **3.13** are detected as the expected 'M+H' ions, not the M+H-2 type that has been observed for the non-oxygenated sulfur radicals. This implies that, whatever the route to the formation of the M+H-2 species is, it does not occur to all species within the same reaction mixture. Finally, several different radical species are being detected from one reaction mixture. This is highly promising for future studies whereby the trapping molecule will be used to study very complex gas phase mixtures, suggesting that it will indeed be possible to capture a wide range of radicals from one trap.

Another interesting species here has a signal at 358 m/z. The accurate mass of this species (358.3136 m/z) suggests a structural formula of  $\text{C}_{21}\text{H}_{44}\text{NOS}$  for the  $[\text{M}+\text{H}]^+$  species (theoretical mass 358.3138 m/z). This suggests that a compound such as **3.14** may have formed (Figure 96). The formation of this species is surprising, given that this species

would be expected to fragment easily. Indeed, Goldestein et al studied similar systems,<sup>202</sup> finding that O-N cleavage is likely in these systems, with the reaction facilitated by reaction with water or H<sup>+</sup>. This would lead to an oxygenated sulfur species, akin to those that can be formed by reaction of a thio radical in the presence of oxygen.<sup>199</sup> An alternative structure, with TEMPO having added to the alkyl chain, is possible based purely on the mass of this species, however would in reality be highly unlikely, owing to the significant difference in strengths of alkane S-H (ca. 380 kJ mol<sup>-1</sup>) and C-H bonds (ca. 435 kJ mol<sup>-1</sup>).<sup>120</sup>

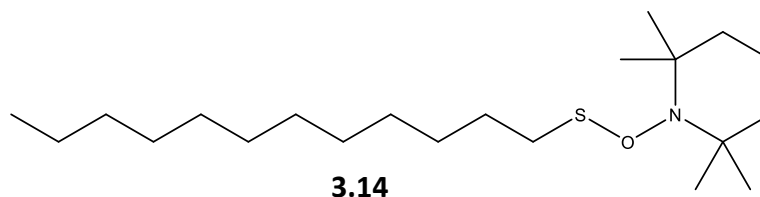


Figure 96: Species **3.14**, giving signal at 358 m/z.

### 3.5.3. AIBN Based Thiyl Radical Generation

In an attempt to further probe the identity of the [M+H-2]<sup>+</sup> phenomenon, a trapping reaction was conducted utilising a different initiator – AIBN. This will provide some indication regarding whether this observation is linked to the substance being trapped, or is instead caused by the use of lead dioxide as a reaction initiator. These initiators are expected to form induce radical formation by different routes: AIBN reactions will be expected to form radicals via a hydrogen abstraction process, PbO<sub>2</sub> reactions take place via electron transfer.<sup>203,204</sup>

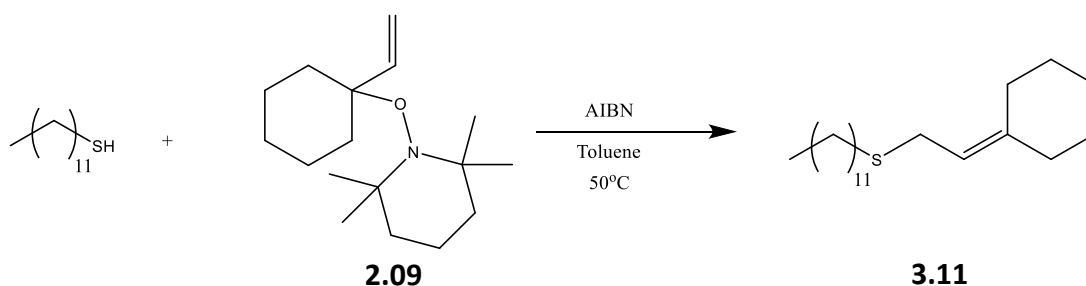


Figure 97: Capture of a thiyl radical, using AIBN as an initiator

Interestingly, in a reaction conducted under nitrogen the target compound from Figure 97, **3.11**, could now be observed with the correct mass (311.2759 m/z observed, 311.2767 m/z theoretical) from this reaction system (Figure 98). This suggests that an aspect of the reaction conditions, for example the activity of the lead dioxide or the presence of oxygen, was key to the 'M+H-2' observation. The previously described products (**3.12** and **3.13** based) can also be observed from this reaction system, as can **3.14**.

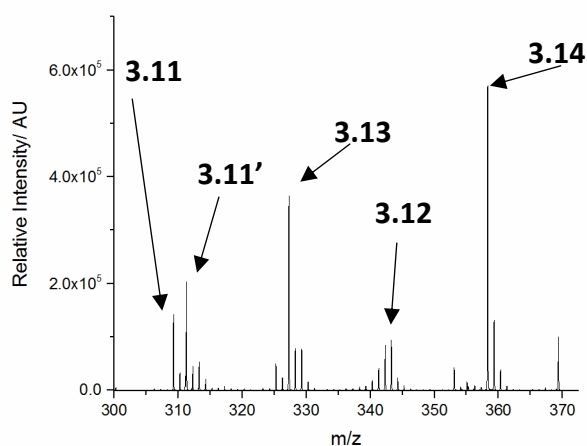


Figure 98: Partial MS of AIBN initiated thiyl radical capture

The presence of the captured sulfinyl and sulfonyl radicals suggests that significant quantities of oxygen were still present. Here, this can be attributed to the presence of residual oxygen within the system. It is also important to note that, while the target compound **3.11** can now be observed, **3.11'** is still present within the reaction mixture. This indicates that the use of lead dioxide as an oxidant is not likely to be the key reason for formation of **3.11'**, given that an AIBN initiated reaction has now been shown to produce the same product, as well as the Fenton based system previously applied to the amine reactions.

Intriguingly, conducting the same AIBN initiated reaction under air instead of an atmosphere of nitrogen failed to produce **3.11**. Instead, the M+H-2 product **3.11'** was again formed. Therefore, it appears likely that the presence of an oxidising species is key to the formation of this undesired reaction product. It gives the impression that the

presence of a more oxidative atmosphere can, in the presence of radical reactions with heteroatoms, lead to oxidative dehydrogenation, resulting in the formation of **3.11'**. It is notable that, for trapped species **3.01**, as well as **3.02** or **3.12** this oxidative dehydrogenation does not appear to occur, suggesting that the type of radical captured is key to whether the oxidative dehydrogenation will occur.

#### 3.5.4. Trapping a Deuterated Sulfur Species

In order to further examine this system, with regards to identifying which part of the molecule is undergoing oxidative dehydrogenation, a reaction with deuterated thiol **3.15** was conducted with **2.09**. This is shown in Figure 99.

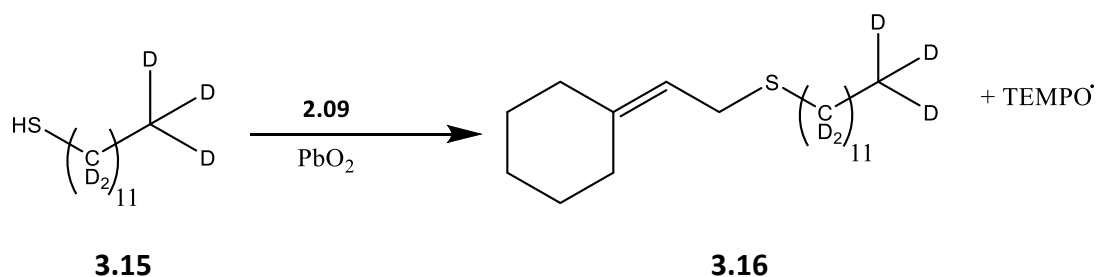


Figure 99: Formation of **3.17** from **3.15**

The observation in Figure 100 of signal at 334.4171 m/z shows a mass loss of two from the expected mass. This suggests that the oxidative dehydrogenation has occurred on the 'trap' side to form **3.16'**. The lack of a clear signal for a loss of four mass units suggests that this process is not taking place on the deuterated side of the compound, which implies that reaction on the 'trap' side is the favoured process here.

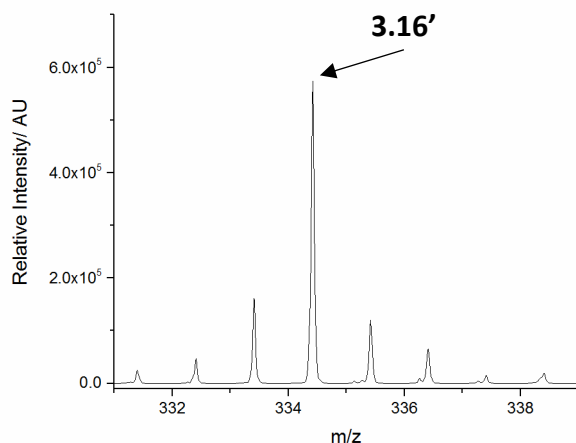


Figure 100: Signal from captured deuterated dodecanethiol radical

In order to confirm this oxidative dehydrogenation on the trap side of the compound, MSMS was used to study the above signal, with the resulting fragmentation shown in Figure 101. The key peak of interest from 334 m/z is that at 226 m/z, which appears to be from fragmentation of the C-S bond as in Figure 102.

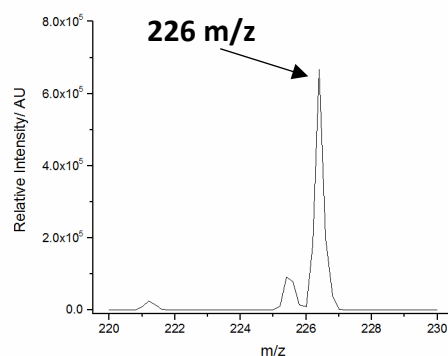


Figure 101: Fragmentation of signal at 334 m/z

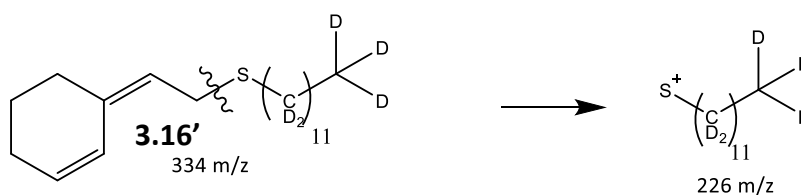


Figure 102: Fragmentations to form 226 m/z. The double bond is arbitrarily positioned on the trap segment of the starting species.

In addition to this, deuterated species **3.17** and **3.18** can still be observed corresponding to oxygenated sulfur radicals. These are present at 352.4285 and 368.4244 m/z in Figure 103, corresponding to deuterated analogues of **3.12** and **3.13** respectively. The reproducibility of the detection of this type of species provides further confirmation regarding the identification of these captured radical species. As with **3.12** and **3.13** there is still no indication of oxidative dehydrogenation occurring with these species.

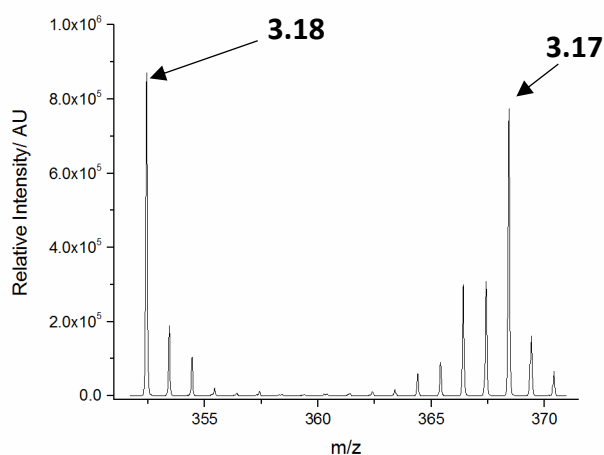


Figure 103: Signals from **3.18** and **3.19**

### 3.6. Future Work

While the aim of these experiments has simply been to capture radicals from the liquid phase, it would also be useful in future studies to conduct experiments targeted towards establishing a reason for the formation of the M+H-2 species in the nitrogen and sulfur radical systems. Following on from this, the study of other radical centred systems (e.g. halogen centred radicals) would be of interest regarding whether they also exhibit this phenomenon.

In order to build on this liquid phase trapping, it would also be interesting to conduct liquid phase trapping on a further series of amine/thio compounds, containing a wide variety of functionality (e.g. aromatic sulfur containing systems). This would be focussed towards

attempted detection of the M+H compounds, as opposed to the M+H-2 species that have generally been detected.

### 3.7. Conclusions

Overall, these experiments have shown that the concept of radical trapping is possible via the radical traps developed in **Chapter 2**. The detection of a number of different radical species (oxygen, carbon, sulfur etc) serve to indicate the applicability of this methodology to a range of different systems. Simultaneous detection of more than one species from a single reaction system (e.g. **3.11**, **3.12** and **3.13** from a dodecanethiol system) also serves to demonstrate the versatility of this trap for radical capture in the presence of several different radical species.

Radical generation when using nitrogen/ sulfur based radicals results in the unexpected observation of 'M+H-2' when analysed with this system. The consistency of this observation in both sulfur and amine reactions is interesting, as is the observation of this species when reacted with a <sup>t</sup>Butyl functionalised species (which would prevent imine formation). Conducting reactions in the presence of a different initiator, such as AIBN or Fenton chemistry, still results in the formation of this species. However, when the reaction is conducted in a low oxygen environment, some of the expected trapped radical can be detected. MSMS and deuteration experiments suggest that the oxidative dehydrogenation process appears to be possible on the trapping molecule, as indicated by the ions produced following MSMS experiments on **3.01** and **3.05**.

## 4. Gas Phase Trapping: Alkene Ozonolysis

### 4.1. Introduction:

#### 4.1.1. Ozonolysis: Criegee Intermediates Chemistry and Atmospherically Relevant Species

Reactions with ozone are important regarding the reactivity of atmospheric unsaturated species. OH radicals formed following alkene ozonolysis are a key source of non-photolytic ·OH (particularly relevant overnight), whilst this process is also an important source of non-photolytic hydroperoxyl and organic peroxy (RO<sub>2</sub>) radicals.<sup>23,205</sup> This will lead to the formation of carbonyl species, and non-volatile oxygenates, which will result in the creation of SOA.<sup>206</sup> In the gas phase, the primary ozonide formed following [3+2] cycloaddition of ozone to the alkene double bond will result in the formation of (excited) Criegee intermediates, a class of highly unstable compounds.<sup>207</sup> This process is shown in Figure 104. The solution phase process differs, with these intermediates quickly recombining to form a trioxolane intermediate (secondary ozonide).<sup>205,207</sup>

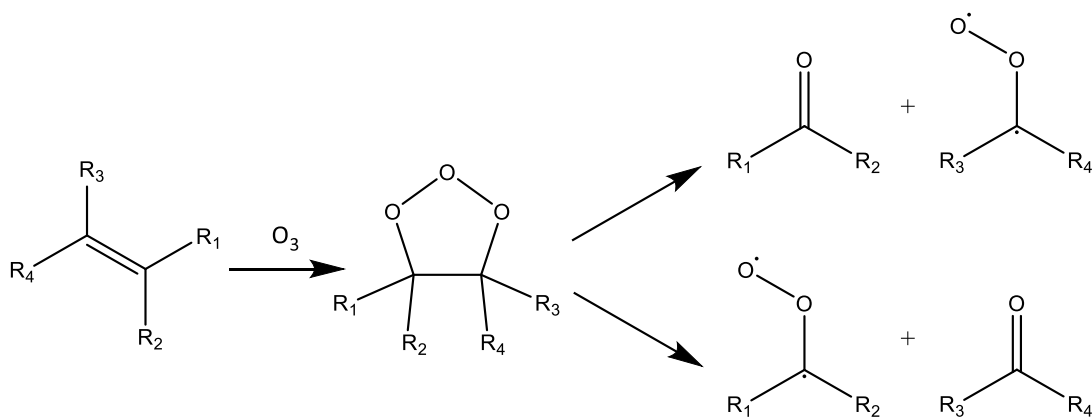


Figure 104: General gas phase ozonolysis mechanism

The simplest possible Criegee intermediate CH<sub>2</sub>OO, shown in Figure 105, was detected for the first time in 2008 by Taatjes et al., while direct measurement of this species by IR was achieved by Su et al. in 2013.<sup>208,209</sup> This species is shown as both a biradical and a zwitterion within the literature (Figure 105).<sup>210</sup> However, a 2013 study by Nakajima et al.

found that the C-O bond length is close to that of a typical double bond, as well as being shorter than the O-O bond, suggesting a zwitterion with a carbon-oxygen double bond is the more appropriate representation for this species.<sup>211</sup>

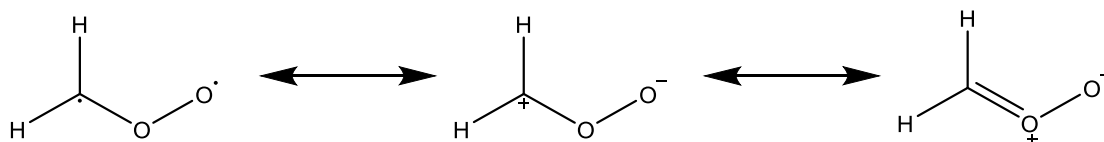


Figure 105: Resonance forms of a simple Criegee intermediate

Once formed, Criegee intermediates will, in the presence of oxygen, proceed to form a series of peroxy radicals. A mechanism showing the formation of this process through the vinyl hydroperoxide channel is given in Figure 106, with the radical version of a Criegee intermediate used in order to illustrate this mechanism.<sup>212,213</sup> The peroxy radical compounds from this mechanism have been shown by Ehn et al. to be precursors to the nucleation of SOA species over forested regions, therefore this mechanism is highly important with regard to accurate predictions of SOA.<sup>206</sup>

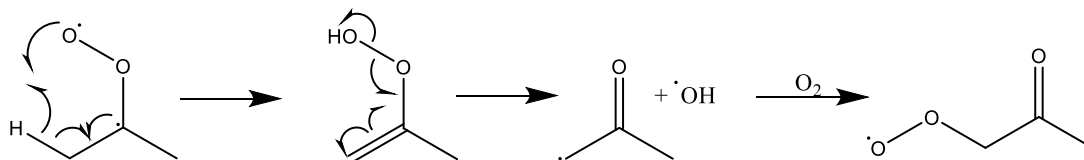


Figure 106: Mechanism for the formation of peroxy radicals from a Criegee intermediate

Considerable work has gone into confirming expected products formed from Criegee intermediates in the atmosphere. For example, Nguyen et al. have predicted a series of routes to explain the products detected from ozonolysis of isoprene.<sup>214</sup> Here, a range of compounds, such as formaldehyde or methanoic acid are detected in chamber experiments, with several different radical intermediates predicted to be formed from the Criegee intermediates. These reactions are important regarding the non-photolytic formation of hydroxyl radicals. As discussed in the introduction,  $\cdot\text{OH}$  is a highly important species which effectively controls the oxidative capacity of the atmosphere. In particular,

formation of hydroxyl radicals from ozonolysis is believed to be a dominant source of  $\cdot\text{OH}$  during the evening/night.<sup>20</sup> An example route for this formation from  $\alpha$ -pinene is shown in Figure 107.

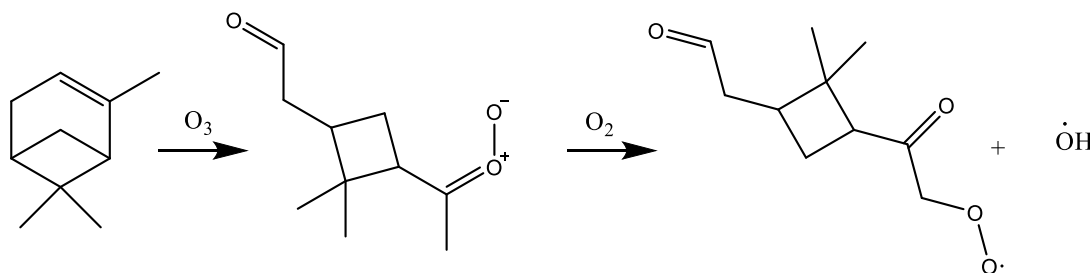


Figure 107: Route showing  $\cdot\text{OH}$  and a peroxy radical formation from  $\alpha$ -pinene ozonolysis

There have been several studies regarding the hydroxyl radicals that are produced from these ozonolysis reactions – with the primary example of this being evaluation of the hydroxyl radical yield from this reaction. Terpenes of particular atmospheric relevance have been found to have significant  $\cdot\text{OH}$  yields from ozonolysis, e.g. 25-35% for  $\beta$ -pinene, to  $> 80\%$  for  $\alpha$ -pinene.<sup>17,215</sup> Therefore, hydroxyl radical production via ozonolysis of alkenes is expected to be a significant source of hydroxyl radicals, especially during the night and into early morning.<sup>216</sup> As such, chamber studies of this system will commonly be used in combination with a suitable  $\cdot\text{OH}$  scavenger, in order to investigate the ozonolysis mechanism free from the interference of the  $\text{OH}$  radical and also to measure its ozonolysis yield. The importance of this reactivity can be shown by a study by Fick et al.<sup>217</sup> They conducted a chamber study on the  $\alpha$ -pinene ozonolysis reaction, showing that of all the  $\alpha$ -pinene reacted during an experiment, approximately 37% is removed by reaction with the hydroxyl radical. The  $\cdot\text{OH}$  scavenger 2-butanol was utilised in order to show this.

Ozonolysis reactions within the atmosphere are strongly linked with the formation of secondary organic aerosol (SOA).<sup>218</sup> As compounds become more functionalised within the atmosphere (i.e. they are oxidised) they become less volatile and hence are increasingly likely to be present in the condensed phase, leading to the formation of aerosol. The formation of SOA is unquestionably important within the atmosphere, with potential impacts on climate (radiative forcing, cloud formation), air quality and health.<sup>219–221</sup> While examples discussed here are biogenic in nature, anthropogenic SOA is also

increasingly important, as indicated by smog episodes that are often observed in and around large cities.<sup>222</sup>

As a highly important atmospheric species, the ozonolysis of C10 biogenic monoterpenes has been extensively studied in the literature, the products of which can lead to SOA formation and growth. As an example, a study by Hoffmann et al. identified pinonic acid as a major component of SOA formed from  $\alpha$ -pinene, a species that is indeed anticipated from mechanisms for  $\alpha$ -pinene ozonolysis, and has been found in several different studies (Figure 108).<sup>223,224</sup>

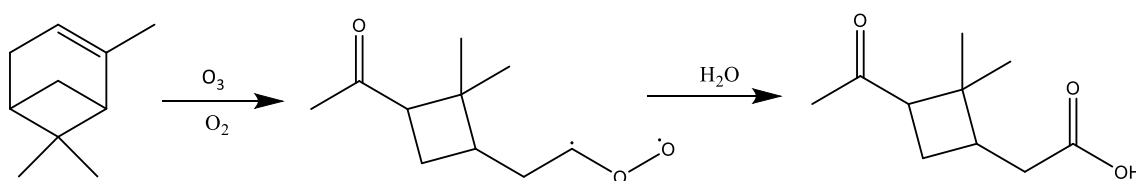


Figure 108: Formation of pinonic acid from  $\alpha$ -pinene ozonolysis<sup>224</sup>

However, there have been recent studies which have resulted in more information regarding  $\alpha$ -pinene SOA products. Ma et al. detected a series of low volatility acids (e.g. norpinonic acid) within  $\alpha$ -pinene SOA.<sup>225</sup> Detection of these species, via GC-MS, enabled further mechanistic evidence to be gathered regarding  $\alpha$ -pinene ozonolysis, with a series of postulated reaction steps given, which can subsequently be incorporated into atmospheric models. The proposed formation for norpinonic acid is shown in Figure 109.

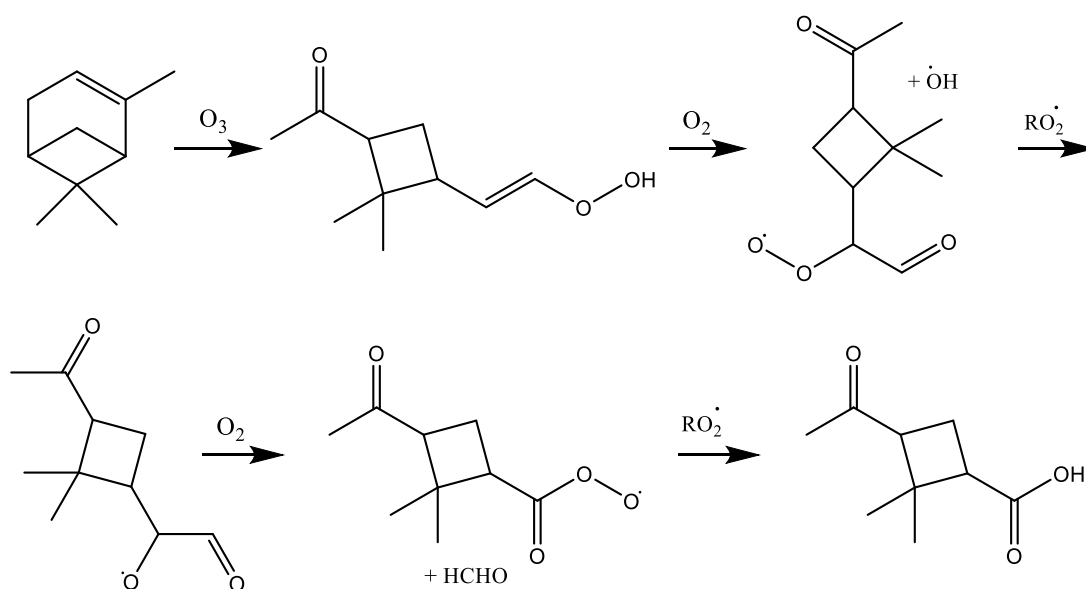


Figure 109: Proposed mechanism for norpinonic acid formation from Ma et al.<sup>225</sup>

In another study, Amin et al. scrutinised SOA formed from mixtures of  $\alpha$ -pinene with other important biogenic VOCs, such as 3-carene, or bornyl acetate.<sup>226</sup> From this, they found evidence that reaction pathways change when mixtures of VOCs are utilised. This leads to changes in the product composition of the SOA itself, with VOCs not expected to react with ozone also being incorporated into the SOA, which in turn is likely to lead in varying toxicities and physical properties of the SOA mixture.

Experiments examining the influence of different factors, such as humidity or  $\cdot OH$  radical concentration on products from  $\alpha$ -pinene ozonolysis in the gas phase have also been conducted. Kristensen et al. studied the formation of ester dimers from this reaction, using LC-MS techniques to identify assorted products formed with and without a hydroxyl radical scavenger being present.<sup>227</sup> Intriguingly, they found that noticeably higher yields of these species are produced in higher humidity, with most, although not all, ester dimers increasing in the presence of an  $\cdot OH$  scavenger. This shows that certain reaction products important for SOA formation can, in several cases, also be formed by reactions based upon hydroxyl radical attack, thus suggesting further reactions to be incorporated into the overall mechanism for  $\alpha$ -pinene reactions. The impact of humidity on product yields is something that also must be considered.

An effective summary of the products predicted to be formed from monoterpene ozonolysis, and the predicted radical intermediates within these processes, can be found in the Master Chemical Mechanism (MCM).<sup>228–230</sup> This is a source detailing expected reaction products and their rates of reaction for a range of atmospherically relevant species with reactive species such as NO<sub>3</sub>, O<sub>3</sub> and/or the hydroxyl radical. For example, predictions regarding products of  $\alpha$ -pinene ozonolysis can be obtained from this model. Rate constants throughout this mechanism are based either on experimental results, or on theoretical calculations based on structure-activity relationships.<sup>25</sup>

While many different studies have been conducted on ozonolysis of atmospherically relevant compounds, there is still a lack of definitive experimental mechanistic information regarding the speciation of radical products vital to the chemistry of forming the assorted non radical stable compounds that have been detected. In order to solve this, it would be useful to study the gas phase organic radicals formed from the initial Criegee intermediate.

#### **4.1.2. Aims**

The study of a (atmospherically relevant) gas phase radical generating system is key to the development of the trapping methodology being developed, in order to provide evidence for the capture of gas phase radicals under realistic conditions. The application of a well-known atmospheric process, gas phase ozonolysis of alkenes, will be utilised for this, with atmospherically relevant monoterpenes used as the alkenes. The study of this system is also useful with regard to providing experimental confirmation of radical intermediates predicted in various mechanisms, with captured radicals identified by mass spectrometry. Different experimental set-ups and timescales can also be trialled, with an aerosol chamber or a small quartz flow-tube as reaction systems applicable for radical generation.

## **4.2. Trapping System and Experimental Design**

As discussed in **Chapter 3**, radical capture from liquid phase systems has been successful. Thus, work can begin on the detection of radicals from the gas phase. The optimisation of gas phase sampling techniques is discussed separately in **Chapter 5**.

For trapping experiments, **2.09** was positioned on a support within a sampling tube, through which the reaction mixture was blown, at a rate of  $2.3 \text{ L min}^{-1}$ . Radicals were generated by exposure of  $\alpha$ -pinene to ozone, within a bag initially designed for the study of  $\alpha$ -pinene SOA. The bag shown in Figure 110 and Figure 111 has a maximum volume of 300 L, with ozone generated by a UV lamp (254 nm) positioned in the centre of the bag. Total residence time can vary significantly within this system, with a range of ca. 0.1 seconds to 130 minutes. After 90 minutes, the trap was removed by washing the glass wool with DCM, with the resultant products analysed by MS to establish the presence of trapped radical adducts.

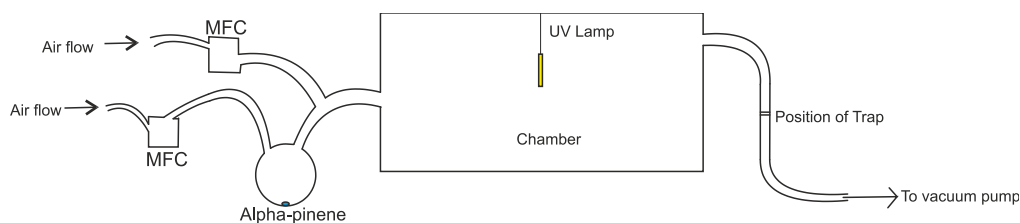


Figure 110: Schematic for trapping system utilising an aerosol chamber

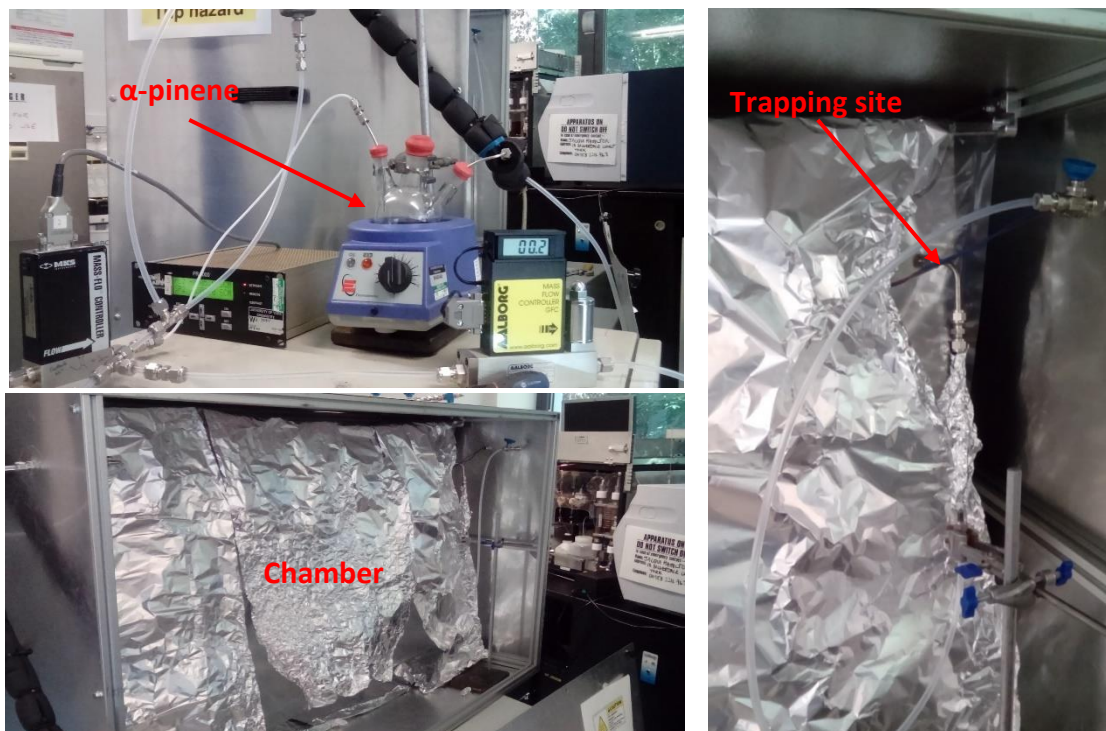


Figure 111: Trapping system utilising an aerosol chamber

The main benefit of this system is that it has already been utilised for  $\alpha$ -pinene ozonolysis study, by collecting the SOA from this reaction. There is expected to be a large range in chamber residence times within this system, due to the size of the bag and a relatively low flow rate. This may result in radical generation from further oxidation products, not just initial radicals from the  $\alpha$ -pinene + O<sub>3</sub> reaction (however these initial species are expected to be present in a significantly higher concentration than any subsequent species).

During the experiments, some trapping material was blown off the support. This was found by detection of **2.09** on filters down-stream of the main sampling site. While these quantities are small (ca. 2.5 mg material was found on the filters after the experiment, which was not entirely **2.09**), it is important to be aware of. If small amounts of **2.09** can be removed, it would not be unexpected for small amounts of trapped compounds (particularly low volatility species) to be removed, hindering detection and quantification.

Examination of an initial experimental result from the trapping system shows dominant signals corresponding to **2.09**. The [M+H]<sup>+</sup> signal for **2.09** at 266 m/z, as well as fragmentations of the TEMPO group at 158 and 142 m/z, are clearly visible from the collected mass spectrum in Figure 112. The fragmentations of TEMPO shown in Figure 113 have previously been observed in the literature.<sup>231</sup>

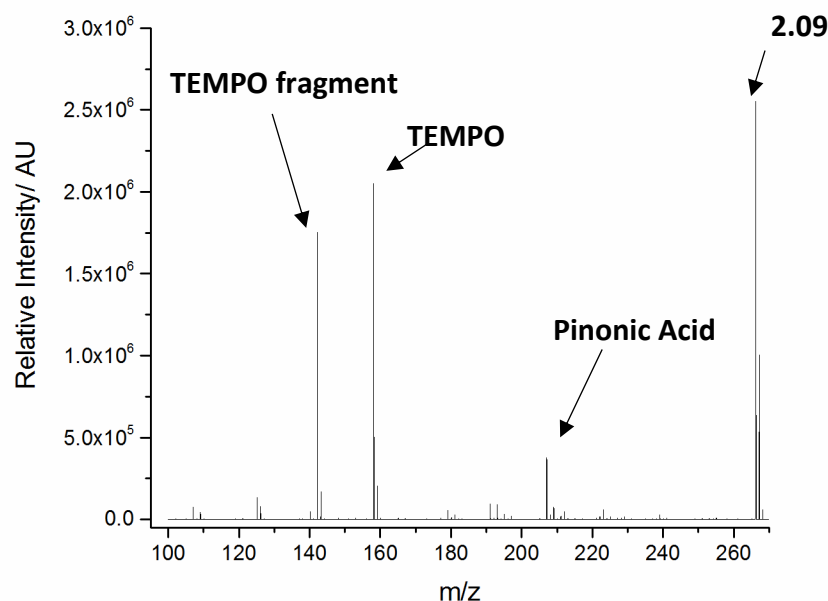


Figure 112: Overall MS from  $\alpha$ -pinene ozonolysis in an aerosol bag

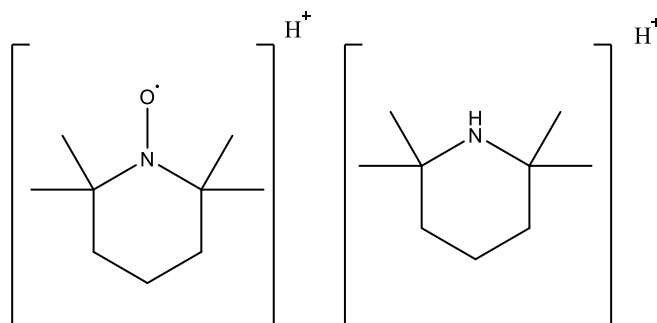


Figure 113: Structures of TEMPO based fragments at 158 m/z and 142 m/z

This is not an unexpected result. There are expected to be significantly lower concentrations of radicals in the gas phase, compared to the previous liquid phase experiments (**Chapter 3**). Indeed, there are lower concentrations of starting material – 2.2 mmol of  $\alpha$ -pinene was loaded at the start of the experiment (of which most remains by the end), while 14.4 mmol of peroxide was utilised for liquid phase experiments to form **3.01** in **Chapter 3**. Given the easily identifiable signal from **2.09** in the liquid phase experiments, it is expected to observe strong signals from **2.09** in gas phase systems.

There are also signals that appear to be present from SOA formed during the reaction, which is indeed visible as a green/yellow oily deposit at the sampling site and in the sample tube. The signals at 193 and 195 m/z correspond to  $[M+Na]^+$  ions of norpinonic acid and norpinic acid respectively, while those at 191 and 207 m/z, can be identified as the  $[M+Na]^+$  ions of pinonaldehyde and pinonic acid. These species in Figure 114 have all been observed previously in  $\alpha$ -pinene SOA.<sup>232</sup>

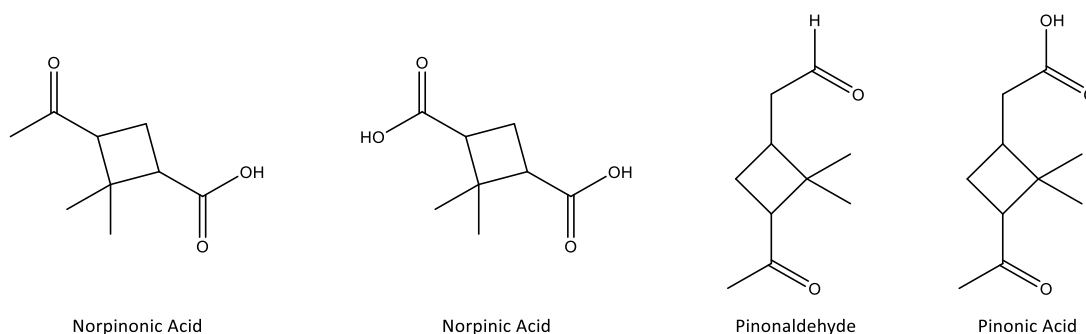


Figure 114: Detected non-radical products of  $\alpha$ -pinene ozonolysis

However, there are also a number of new signals (at a lower intensity) that correspond to assorted  $\alpha$ -pinene originating captured radical products. The detection of these species and their expected routes of formation are discussed in the sections below.

### 4.3. Detection of Radical Intermediates from Ozonolysis Reactions

As discussed earlier, ozonolysis of  $\alpha$ -pinene is the major reaction for the removal of  $\alpha$ -pinene from the atmosphere.<sup>233,234</sup> Upon reaction between  $\alpha$ -pinene and ozone, it would be expected for Criegee intermediates to form, which can then decay to form an array of carbon centred radical species. These will rapidly react with oxygen in the air to form peroxy radicals.<sup>223</sup> In the MCM the two isomeric initial peroxy radicals from  $\alpha$ -pinene ozonolysis are shown below in Figure 115.<sup>229,230</sup> These two isomers are expected to be formed in a relative ratio of ca. 55 to 45, **4.01a** to **4.01b** respectively.<sup>229,235</sup> Another peroxy radical species from  $\alpha$ -pinene ozonolysis is discussed later in Figure 119.

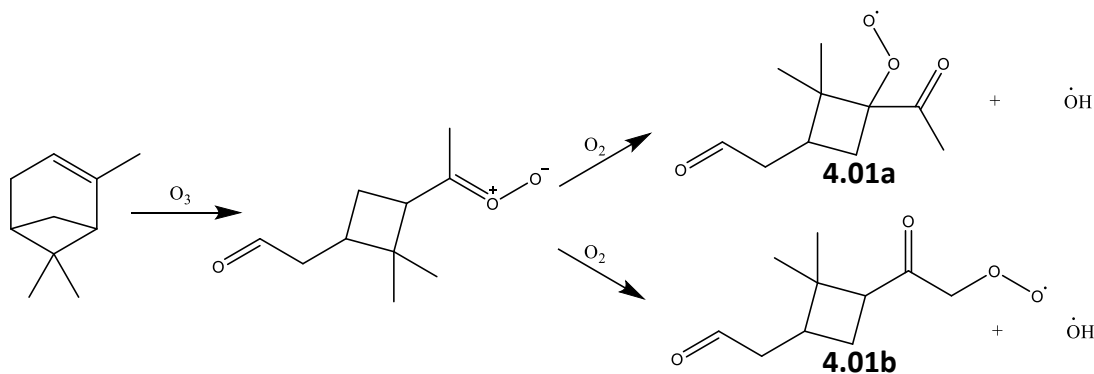


Figure 115: Formation of peroxy radicals **4.01a** and **4.01b** following  $\alpha$ -pinene ozonolysis<sup>229,230</sup>

Analysis of the reaction mixture showed a signal present at 331.187 m/z (Figure 117). This corresponds to trapped **4.01**, with these species sodiated during detection and matching well the theoretical mass of 331.1880 for the ion of **4.02a** and **4.02b**. Comparison to 'blank' measurements of the reaction system (run without ozone generation) indicated that these are genuine product signals, not just background noise. The structures for these compounds are given in Figure 116, with both isomers of the peroxy species shown. The successful observation of these species is a good indication that gas phase radical trapping is indeed occurring within these systems. Owing to the low intensity of product signals,

3D chromatograms are presented, showing different times in the MS measurement in order to provide evidence for these signals being above background levels.

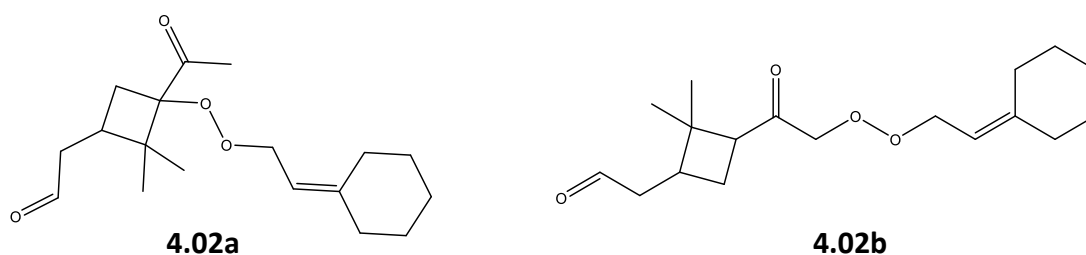


Figure 116: **4.02a** and **4.02b**, products formed upon trapping **4.01a** and **4.01b** with **2.09**.

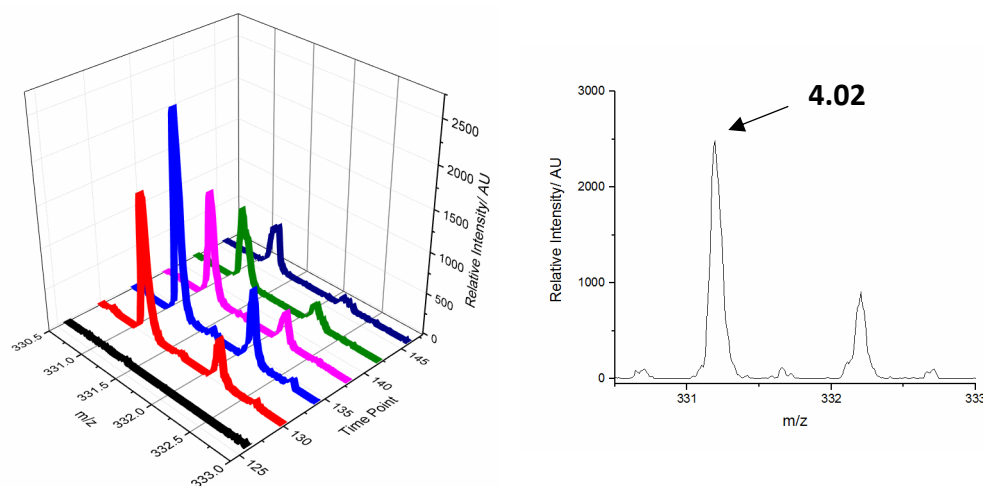


Figure 117: Signal observed for **4.02**

Identification of this signal can be assisted by the use of blank experiments. Here, the UV lamp was not ignited, hence no  $O_3$  is expected to be present in the system, thus ozonolysis reactions will not occur. MS analysis from this experiment in Figure 118 suggested that, as would be expected, **4.02** is not present in the blank system.

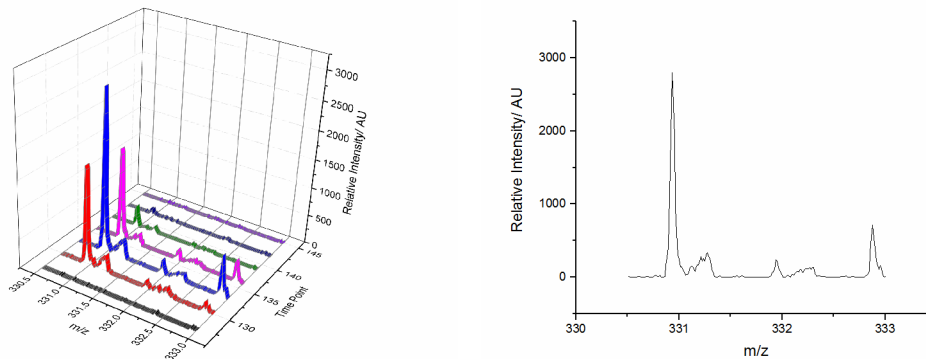


Figure 118: MS showing lack of signal for **2.02** in blank experiment

Information regarding the types of products anticipated to be detected can be found by use of the MCM. The successful trapping of these species also functions as a useful experimental confirmation regarding the validity of these predictions.<sup>229,230</sup> In addition to the formation of peroxy radicals **4.01a** and **4.01b**, the MCM suggests that the preceding Criegee intermediate can also decay to lose a CH<sub>2</sub> group, subsequently forming a different peroxy radical: **4.03** (Figure 119).<sup>229,230</sup>

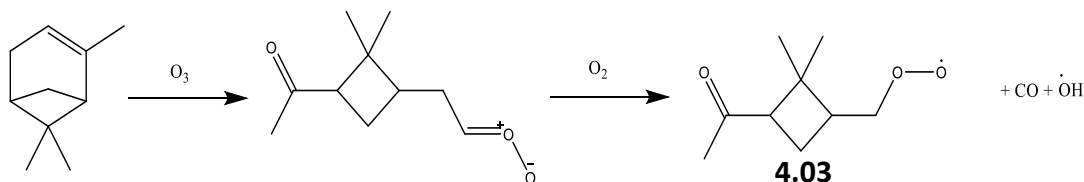


Figure 119: Formation of **4.03** through  $\alpha$ -pinene ozonolysis and loss of  $\text{CO} + \text{OH}$ .<sup>229,230</sup>

As with **4.01**, the radical species **4.03** can also be detected by the radical trap, forming **4.04** (Figure 120) as a result of the trapping reaction, with a detected mass of 303.1940  $m/z$  (Figure 121) corresponding to a predicted mass of 303.1931 for the  $[\text{M}+\text{Na}]^+$  ion. Detection of these species provides important experimental evidence for the different ozonolysis routes predicted within the MCM to be available to  $\alpha$ -pinene, and that the hydroperoxide mechanism is a route to non-photolytic production of  $\cdot\text{OH}$ .<sup>229,230</sup> It also suggests that the  $\text{RO}_2$  co-products are formed in significant amounts and that they are available precursors for SOA formation.<sup>206</sup> These radicals have been used in mechanisms to justify the formation of experimentally detected non radical species (e.g. pinonaldehyde), however identification of these radicals (i.e. **4.01**) has previously been elusive.<sup>236</sup>

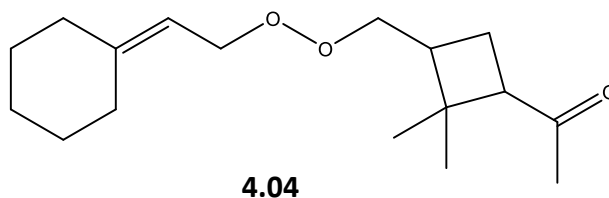


Figure 120: **4.04**, formed by capture of **4.03** with **2.09**

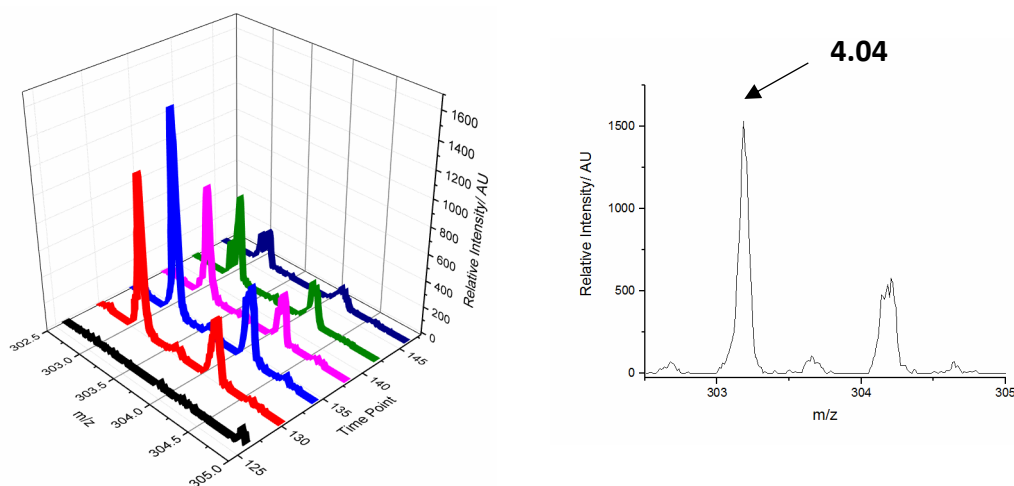


Figure 121: Signal observed corresponding to **4.04**

This result is backed up again by control experiments conducted without the addition of ozone. As can be seen in Figure 122, there is no clear indication of **4.04** from this experiment, thus justifying identification of the signal in Figure 121 as being from captured radicals to form **4.04**.

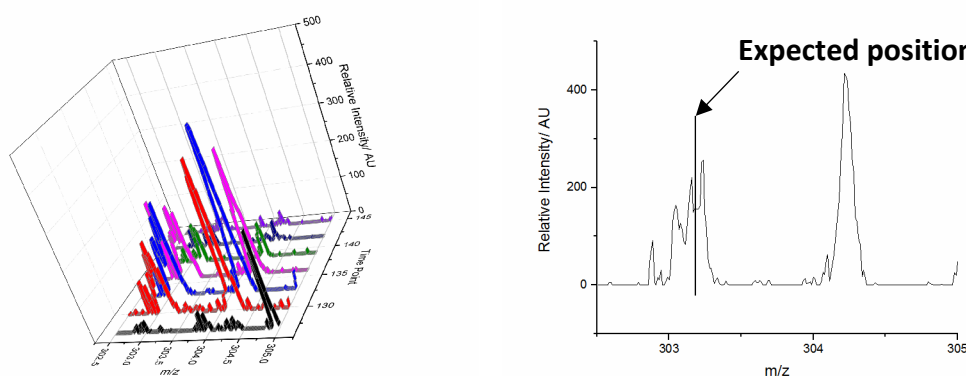


Figure 122: MS showing lack of signal for **4.04** from blank experiment

To gain further evidence confirming capture of radicals **4.01** and **4.03**, experiments were undertaken where trapping molecules **2.11** and **2.13** were employed. Trapping of the same radicals would be expected to produce trapped products with a mass difference of 14 and 12 Da respectively relative to **2.09**, in a similar way to the use of isotopically labelled traps. Indeed, the expected non radical adducts from trapping **4.01** and **4.03** do appear to be detected, with MS figures for the compounds in Figure 123 given in **Chapter 9**. The observation of different traps trapping radicals **4.01** and **4.03** provides useful evidence of reproducible self-consistency for the trapping process.

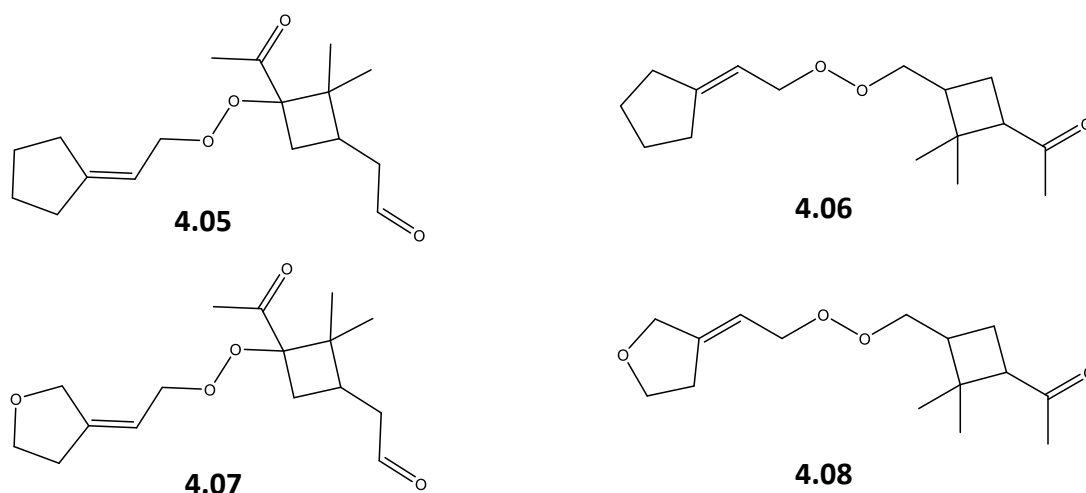


Figure 123: Compounds formed by capture of **4.01** and **4.03** with **2.11** and **2.13**

These radicals from ozonolysis reactions are believed to be important precursors to aerosol formation, because as the ozonolysis process proceeds, compounds will be formed that are increasingly oxidised.<sup>206,237</sup> As such, in the atmosphere they will become less volatile, and so eventually become incorporated within SOA. Indeed, evidence of this has been demonstrated by Ehn et al., with the use of isotopically labelled reactants which are increasingly oxidised following reactions with oxygen in the wake of hydrogen abstraction reactions under atmospheric conditions.<sup>206</sup> The routes to these compounds are frequently shown to be proceeding via radicals **4.01** or **4.03**, however typically only the non-radical reaction products are characterised.<sup>238,239</sup>

For example, Camredon et al. studied SOA formed from chamber experiments, evaluating the species present by MS.<sup>238</sup> The detected species were compared to those from MCM predictions, however these predictions go via a number of postulated uncharacterised radical intermediates. Other studies, such as Pavlovic et al., have spin trapped radicals produced from these reactions, proving the existence of radical species.<sup>240</sup> However, structural information beyond the type of radical (i.e. peroxy, alkoxy or alkyl) was not obtained, while the lack of hydroxyl radical scavengers means that products will also have been present from the  $\alpha$ -pinene +  $\cdot\text{OH}$  reaction. As such, detection here of adducts **4.02** and **4.04** provide some important confirmation regarding the structure of postulated radical species arising from  $\alpha$ -pinene ozonolysis via the vinyl hydroperoxide mechanism.

#### 4.4. Detection of Products from $\cdot\text{OH}$ Attack

The ozonolysis of terpenes is known to produce hydroxyl radicals in good yields under atmospheric conditions, with a yield of ca. 80% reported within the literature for  $\alpha$ -pinene ozonolysis.<sup>17,241</sup> As such, it would not be unexpected for some of this  $\cdot\text{OH}$  to react with  $\alpha$ -pinene present at a high concentration within the experimental system. Indeed, reaction of  $\cdot\text{OH}$  with terpenes in general is a very important mechanism for their removal from the atmosphere, and can also contribute to aerosol formation.<sup>6,206,242</sup> This reaction produces a series of isomeric peroxy species, depending on the site of  $\cdot\text{OH}$  attack, with radicals **4.09a-c** from this reaction shown in Figure 124.<sup>28,242,243</sup> The relative amounts of each reaction pathway are predicted to be 57%, 35% and 8% respectively in the MCM.<sup>229,230,236</sup> There are also expected to be very small amounts of compounds formed by hydrogen abstraction on different carbon centres, however these are very minor relative to the other available pathways, so are not discussed here.<sup>244</sup> As these are all isomers they are not distinguishable by the simple MS conducted here.

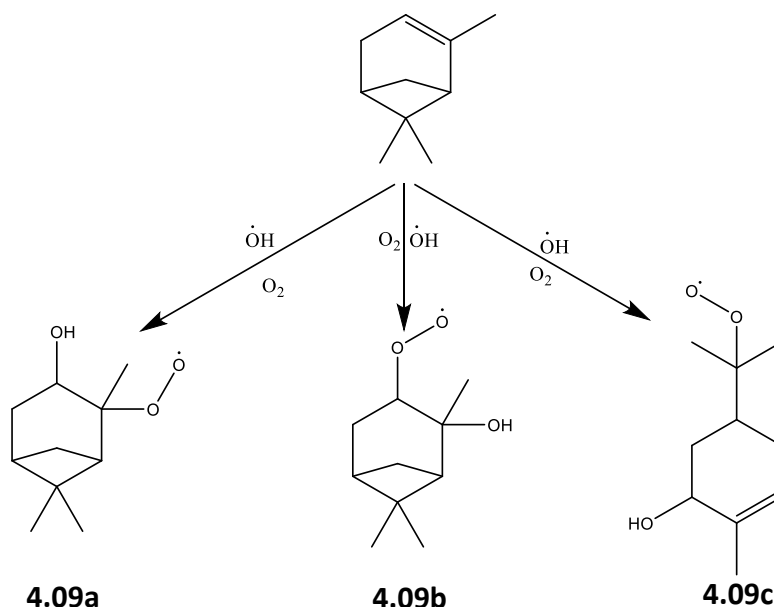


Figure 124: Radicals formed from  $\cdot\text{OH}$  attack on  $\alpha$ -pinene, in the presence of oxygen<sup>229,230</sup>

Therefore, these species also have the potential to be trapped. Indeed, this signal was detected (Figure 126), with the captured products **4.10a-c** having structures given below in Figure 125. As with detection of species **4.01** or **4.03**, there was no indication of this

signal from background experiments, while self-consistency was provided by successful trapping of **4.09** by different radical traps **2.11** and **2.13**.

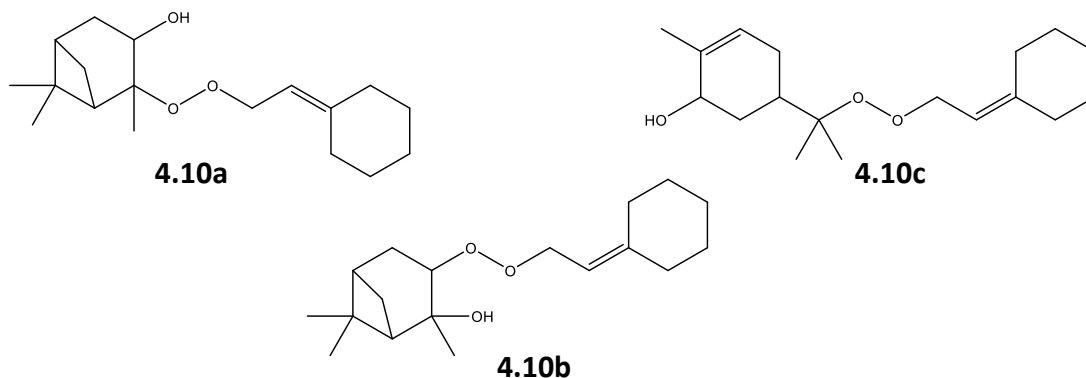


Figure 125: **4.10** formed by capture of **4.09** by **2.09**

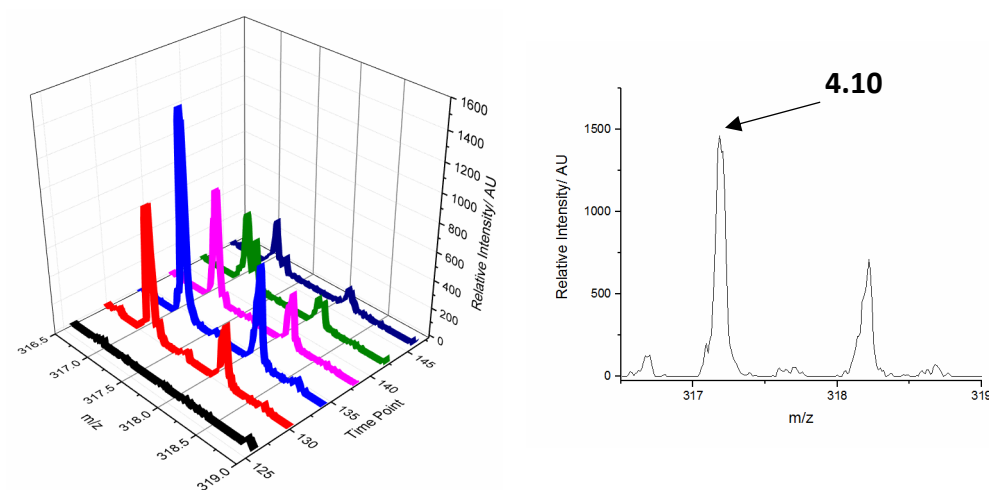


Figure 126: Signal corresponding to **4.10**

The observation of **4.09** from this system is particularly useful in terms of evaluating the trapping methodology being tested. When considered in addition to **4.01** and **4.03**, it shows that a range of different RO<sub>2</sub> species, from different reactions, can be detected from this gas phase system. This is a highly useful feature when beginning to consider this trapping system for ‘real world’ applications, owing to the large number of radical compounds expected to be present within the atmosphere. As with the RO<sub>2</sub> species arising from ozonolysis, observation of these species helps to provide experimental evidence of different radicals formed in the ozonolysis mechanism for  $\alpha$ -pinene and helps to explain the observation of non-radical products.<sup>229,236</sup> However, there are still a number of species detected from the  $\alpha$ -pinene ozonolysis reaction that have not yet been discussed.

## 4.5. Detection of Further Radical Species

### 4.5.1. Hydroperoxyl Radical Capture

Given the potential for a long residence time within this experimental set-up, it would indeed be anticipated for further radical species to be detected beyond the initial peroxy species. One of the most obvious of these species is the hydroperoxyl radical. This would be expected to be formed at various stages during reactions of  $\alpha$ -pinene with ozone or  $\cdot\text{OH}$ , with an example of one of these routes shown in Figure 127. However, given the potential for ambient  $\text{HO}_2\cdot$  formation from ozonolysis, observation of this species is not definitive proof of the below mechanism occurring.

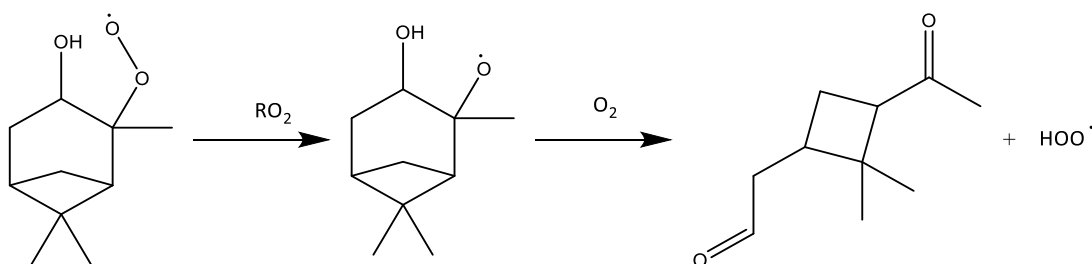


Figure 127: A route to formation of  $\text{HO}_2\cdot$  and pinonaldehyde from  $\alpha$ -pinene<sup>229,230</sup>

This species was however detected, with the presence of a clear signal at 165.0881 m/z when trap **2.09** was employed, suggesting the formation of **4.11** (Figure 129). Application of traps **2.11** and **2.13** (Figure 128) again clearly showed the capture of the same radical, with mass spectra indicating the formation of **4.12** and **4.13** given in **Chapter 9**. As such, capture of the hydroperoxy radical by this method appears to have been successful.

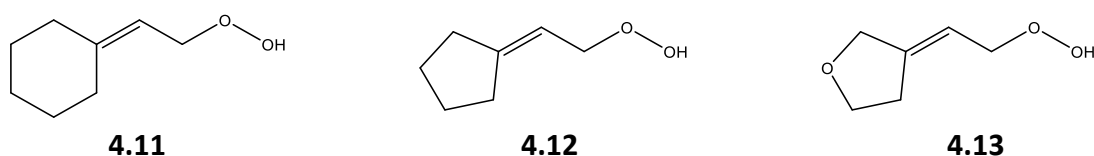


Figure 128: Compounds formed by capture of the hydroperoxyl radical by **2.09**, **2.11** and **2.13** respectively.

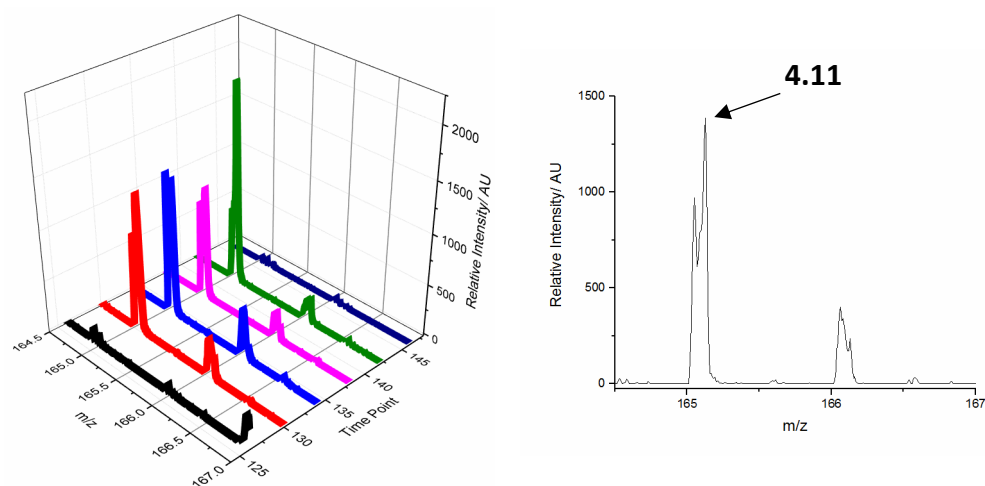


Figure 129: Signal corresponding to **4.11**

#### 4.5.2. Capture of Further Oxidation Products

There are several other radical compounds predicted within the literature to be formed from reactions of  $\alpha$ -pinene, of structures more complex than the  $\cdot\text{OOH}$  radical. One example of this is given by Zhang et al., who suggest the formation of species **4.14**, formed via a 1,7 hydrogen shift reaction (Figure 130).<sup>245</sup> This species is part of a route they postulate to justify the detection of pinic acid within their reactions, with models based on this system matching the experimental results. The proposed reaction proceeds via radical **4.01b**, which has already been established as captured during this reaction (Section 4.3.).

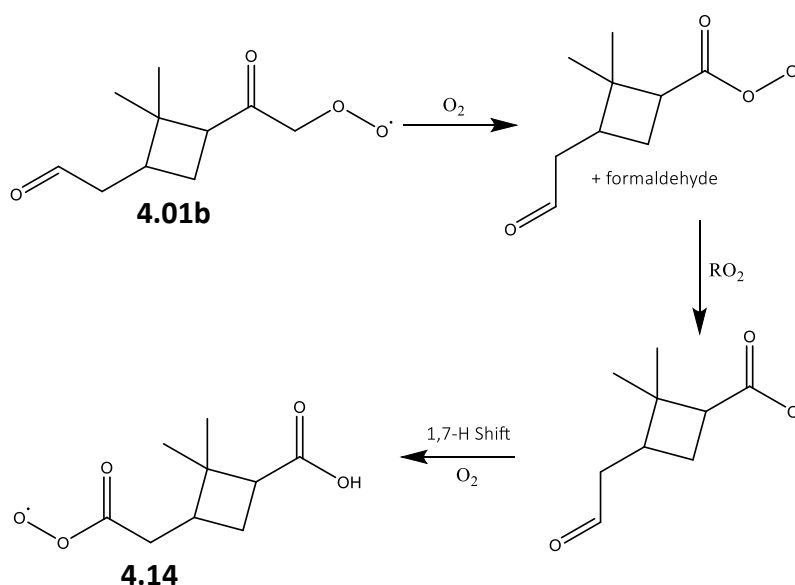


Figure 130: Formation of **4.14** via **4.01b**.<sup>245</sup>

However, analysis of the data in Figure 131 does not show any indication of **4.14** having been captured. One explanation for this observation could be that the reaction is occurring, but at very low levels – thus preventing any signal from this species being differentiated from background signal. Modelling this reaction, using rate constants for the formation of **4.14** from Zhang et al. (under the conditions utilised within the bag) supports this theory, with concentrations of **4.14** ca. five orders of magnitude lower than detected species such as **4.01**.<sup>245</sup> The results of this model are shown in **Chapter 9.3**.

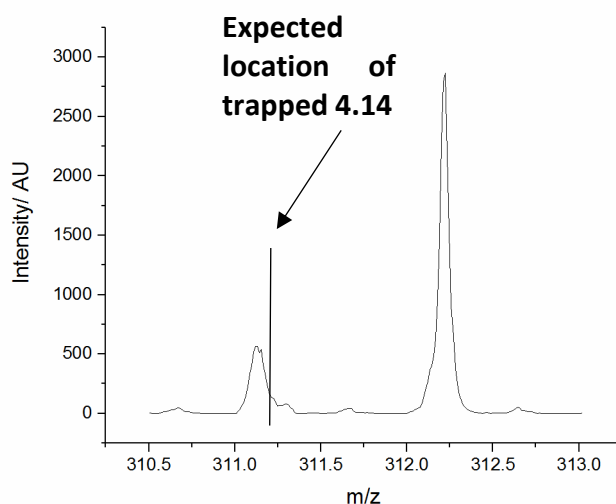


Figure 131: Lack of signal corresponding to trapped **4.14**

Another interesting group of compounds have been proposed by Berndt et al.<sup>242</sup> They propose the formation of a series of peroxy bridged species, which are expected to form following the attack of  $\cdot\text{OH}$  on  $\alpha$ -pinene. This highly oxygenated species would be of great interest to atmospheric chemists, owing to a very low volatility, hence providing potential to act as nucleators for secondary aerosol formation.<sup>206</sup> Such species may be helping to contribute to the 'missing' aerosol source in most models.<sup>246</sup> The proposed route to the formation of this species is given in Figure 132.

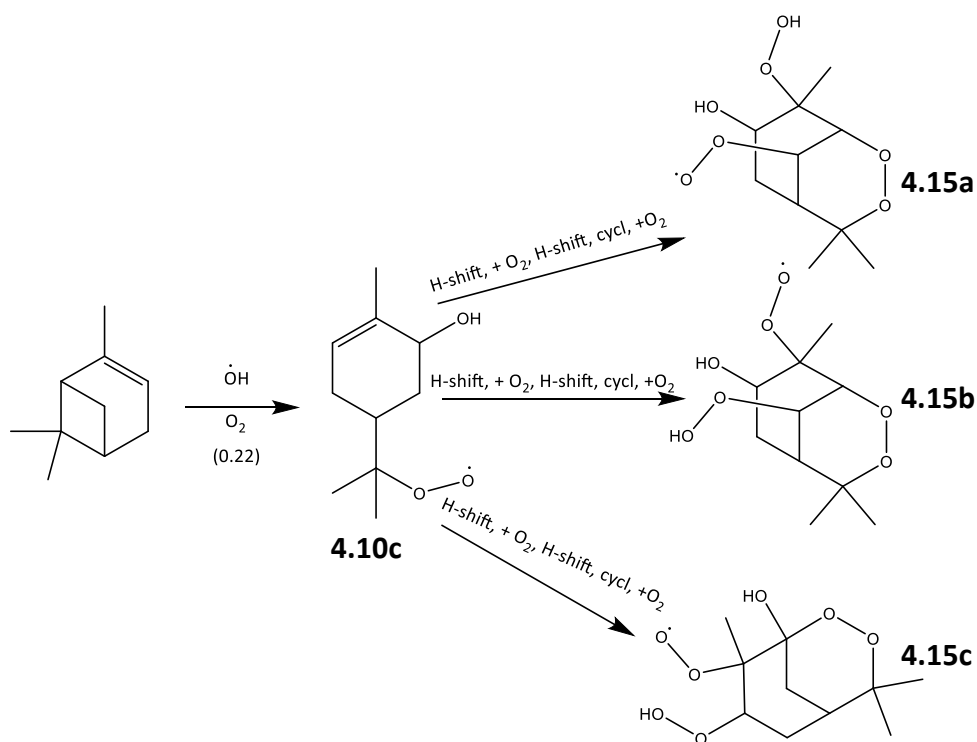


Figure 132: Formation of bridged peroxides **4.15**, as suggested by Berndt et al.<sup>242</sup>

Again, the initial radical species from this system, **4.10c**, has already been detected within this system. Pleasingly, a signal corresponding to **4.16**, the resulting trapped compound **4.15** (Figure 133), was detectable in Figure 134. The assorted compounds shown above resulting from the cyclisation of this species are again all isomers of one another, hence the three species are not differentiated here, with structures for **4.15a-c** in Figure 133 all likely to be present to some degree.

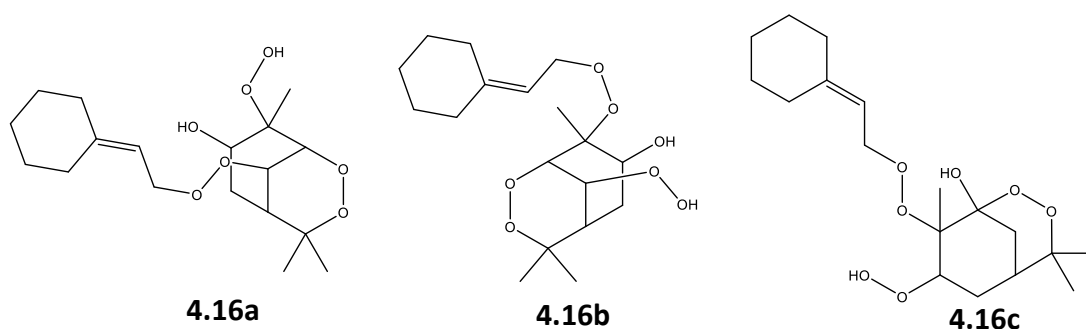


Figure 133: **4.16** formed by capture of **4.15** by **2.09**

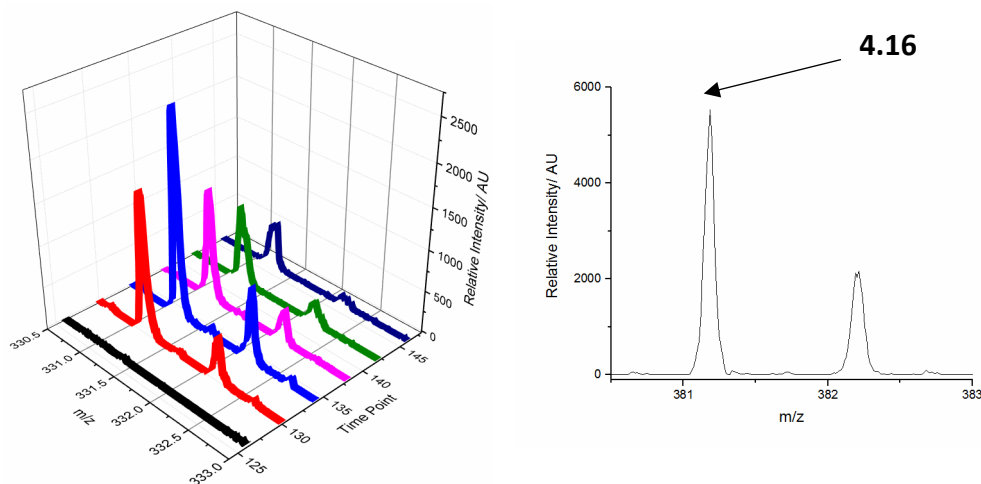


Figure 134: Signal corresponding to **4.16**

The formation of this species (and hence observation) is likely to be facilitated by the long residence times inherent within this experimental set-up, as there are several reactions required prior to the formation of this species, which also helps to show that further oxygenated RO<sub>2</sub> species are present. If the reaction were to be conducted in a considerably smaller reaction system, with correspondingly lower residence times, it would thus be expected that the concentration of this species would noticeably decrease, therefore resulting in the species dropping below the limit of detection for this system. Shorter reaction time experiments are examined later in **Section 4.6**.

#### 4.6. Experiments in a Quartz Tube Flow System

Despite the successful capture of radicals from the ozonolysis bag experiments, there are several problems with the experimental system itself. Firstly, this equipment can only be used for  $\alpha$ -pinene, as the aerosol bag will retain considerable amounts of  $\alpha$ -pinene and SOA residue, as indeed it was designed to do. Therefore, different reaction systems will need to be studied using a different experimental system set up. As well as this, the residence time for species within the bag is not controllable, hence it is difficult to establish the timescales involved in the formation of the different detected RO<sub>2</sub> species. The potentially large residence time may also be allowing radical generation from oxidation of non-radical products formed from the ozonolysis reactions. Finally, the generation of SOA

(as this system was initially designed for) results in a light green/yellow oily residue being collected at the trapping site, causing interference by the detection of SOA components. Whilst it is pleasing that trapped species can still be detected, despite SOA sampling, it is nevertheless far from ideal.

Therefore, a 'cleaner' reaction system was designed which can easily be applied to different radical systems, with controllable residence times and without the formation of large quantities of SOA. In this system the aerosol bag was replaced by a quartz tube, with ozone generated by a UV lamp adjacent to the quartz tube. The trapping site can be moved to different distances along the tube, hence we can utilise time resolved sampling. However maximum residence time is expected to be <1 second at the flow rate used ( $3 \text{ L min}^{-1}$ ). The flow will also be more laminar than the turbulent flow expected in the bag. This will result in considerably shorter and more controlled residence times than those possible with the aerosol chamber previously applied. Unlike the aerosol bag, it is simple to clean the quartz tube and thus use the system for ozonolysis reactions of species other than  $\alpha$ -pinene. The system is shown in Figure 135 and Figure 136. This new system was initially applied to  $\alpha$ -pinene ozonolysis, with the aim of reproducing observation of captured radicals from the bag system, achieving cleaner results than the bag, as well as generating data for a known residence time. These initial experiments were conducted with 90 minute exposures, at a  $3 \text{ L min}^{-1}$  flow rate.

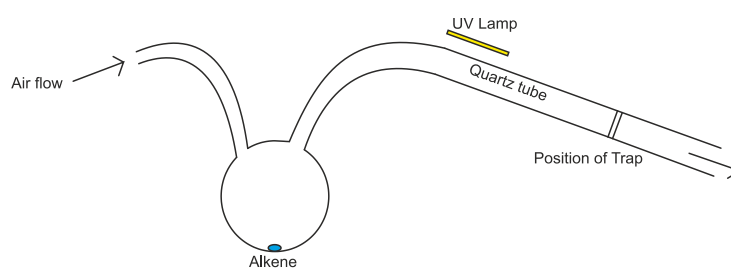


Figure 135: Schematic of quartz tube sampling system

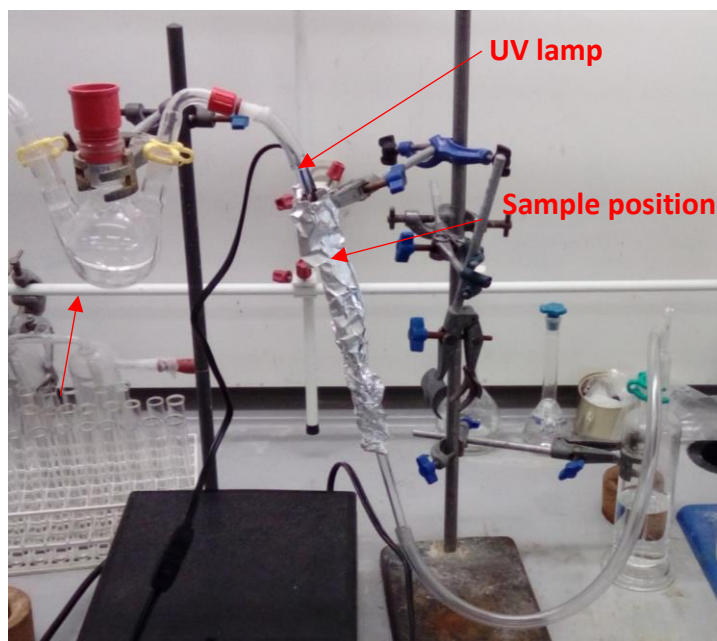


Figure 136: Quartz tube sampling system

#### 4.6.1. Confirmation of Radicals: Traditional Spin Trapping

The generation of radicals from this ozonolysis reaction can be confirmed by EPR. Exposing a 0.22 M solution of DMPO (a commonly used spin trap) in toluene (1 mL) to the gas flow from this experiment for 90 minutes and flow rate of  $3 \text{ L min}^{-1}$  results in the spin trapping of assorted radicals, generating the EPR spectrum below in Figure 137. Flow rate and exposure time are the same as for other experiments with this tube, thus similar quantities of radicals were expected to be produced.

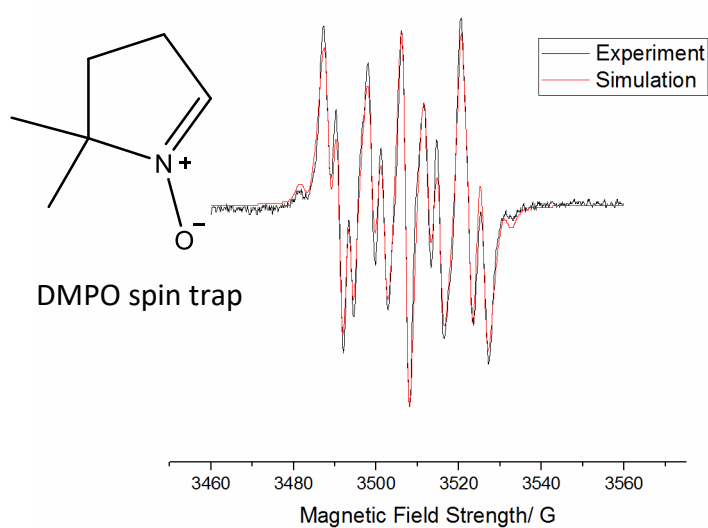


Figure 137: EPR from spin trapping of products from the  $\alpha$ -pinene ozonolysis gas flow

Whilst little structural information can be gathered via this methodology, it is nonetheless useful in providing evidence for the types of radicals being detected. The spectrum appears to contain several components, which are difficult to unambiguously assign to specific radical structures. However, some information can be gathered: the dominant central signals are indicative of oxygen centred peroxy radicals, while the small peaks towards the sides of the spectra are suggestive of a small amount of carbon centred radicals being detected. This assignment is supported by similarity to a simulated spectrum (shown in Figure 137), utilising peroxy and carbon centred radicals, as well as known products from DMPO decomposition. Therefore, it appears that this simpler, lower residence time ozonolysis system is still successfully producing radicals.

#### 4.6.2. Trapping Products from $\alpha$ -Pinene Ozonolysis Using Adapted Apparatus

Compound **2.09** was again applied to this new system in order to study the radicals present. After conducting these reactions with an  $\alpha$ -pinene system, it was clear from Figure 138 that there is significantly less SOA being collected, with no visible indication of the previously identified SOA residue at the trapping site. As shorter reaction times are being examined, only the early stages of the  $\alpha$ -pinene +  $O_3$  system are being probed, hence little SOA would be expected to form. It is likely due to this absence of significant SOA quantities that the overall MS for these reactions were considerably cleaner in appearance, for example norpinic acid can no longer be observed from this system.

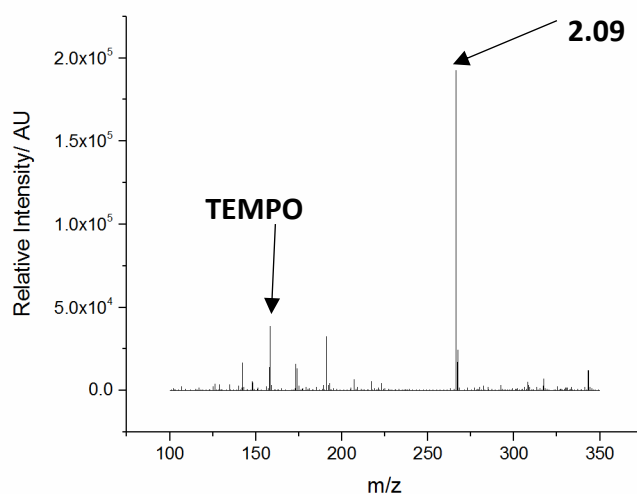


Figure 138: Overall MS of products from  $\alpha$ -pinene quartz tube ozonolysis

The key radicals, including **4.01**, **4.09** and the hydroperoxyl radical can still easily be detected in this lower residence time system, as shown in Figure 139. Therefore, the application of this new system suggests that residence times are not too low as to prevent formation of adducts **4.02**, **4.10** and **4.11** discussed previously.

Nevertheless, not all products identified from the bag system can be observed here, for example the bridged peroxy species **4.15** predicted by Berndt et al.<sup>242</sup> The key difference here was that the predicted maximum residence time in the new quartz tube system is likely to be ca.  $\leq 1$  second: considerably lower than that for the chamber experiments. This suggests that the large residence time within the aerosol bag was important to the detection of **4.15**, which would be expected to be formed with longer reaction times than those in the quartz tube. Indeed the residence times used by Berndt et al. were ca. 10 times those used in this quartz tube flow system.<sup>242</sup>

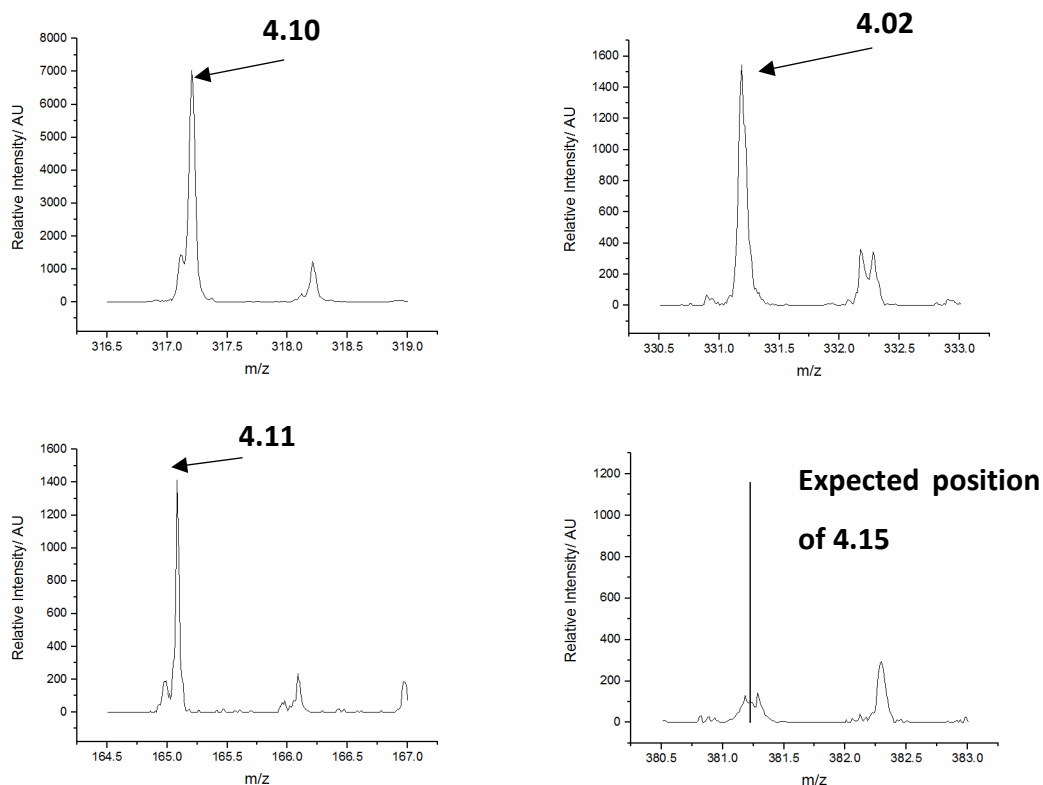


Figure 139: Signals detected in quartz tube system, corresponding to **4.02**, **4.10**, **4.11** and lack of signal for **4.15**.

There are further species that would be anticipated to be present in the reaction systems from  $\alpha$ -pinene ozonolysis. For example, there are several compounds that can be formed

following the formation of peroxy species **4.01** or **4.09**, with many of these compounds being radicals and therefore trappable.<sup>229</sup> As an example, alkoxy radicals **4.17** and **4.18** would be expected to be formed from **4.01** and **4.09** respectively, albeit with short lifetimes (Figure 140).<sup>236</sup>

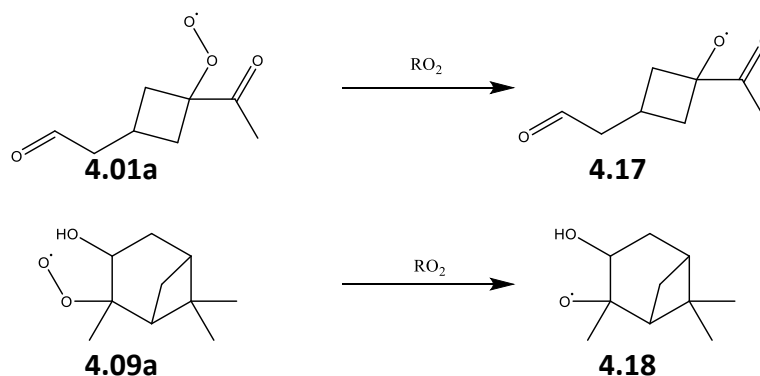


Figure 140: Formation of **4.17** and **4.18**<sup>229,230</sup>

Within these shorter, cleaner experiments, there does appear to be evidence for the formation of **4.19** and **4.20** radical adducts (Figure 141), trapped alkoxy radicals **4.17** and **4.18**. This is shown in Figure 142. Given that these alkoxy radicals are expected to have considerably shorter lifetimes than the preceding peroxy species, it is unsurprising that signals are noticeably weaker for these species. These species were not clearly observed in experiments with the aerosol bag: they will likely only be present in a significantly lower concentration than other radical species upon reaching the trapping site in that system, which can have a range of times between irradiation and detection.

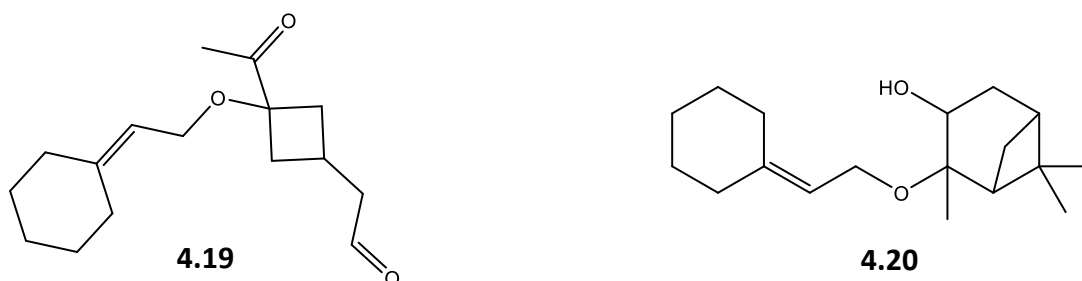


Figure 141: Compounds from trapped alkoxy radicals

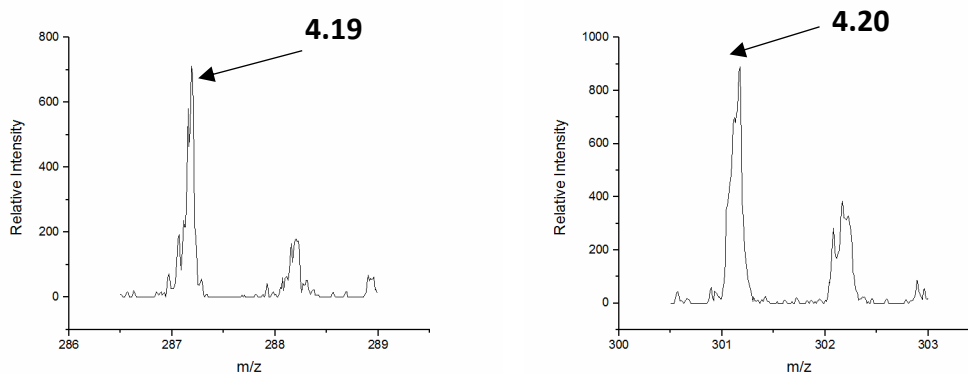


Figure 142: MS signals corresponding to **4.19** and **4.20**

### 4.6.3. Reactions to Assist Product Identification

The application of the quartz tube reaction system was also conducive to experiments designed to further probe this reaction. One aspect is to prove that **4.01** originates from  $\alpha$ -pinene reacting with ozone, while **4.09** is produced by the reaction of  $\alpha$ -pinene with  $\cdot\text{OH}$ , as is suggested by the MCM.<sup>229,230,236,247</sup> If this is correct then running the experiment in the presence of an  $\cdot\text{OH}$  scavenger, 2-butanol, will result in formation of **4.01** without formation of **4.09**, thus detection of radical adduct **4.02** but not **4.10**. The scavenger was introduced by the addition of 0.1 mL 2-butanol to the monoterpene flask at the start of the system, as has been used by Saha et al.<sup>248</sup>

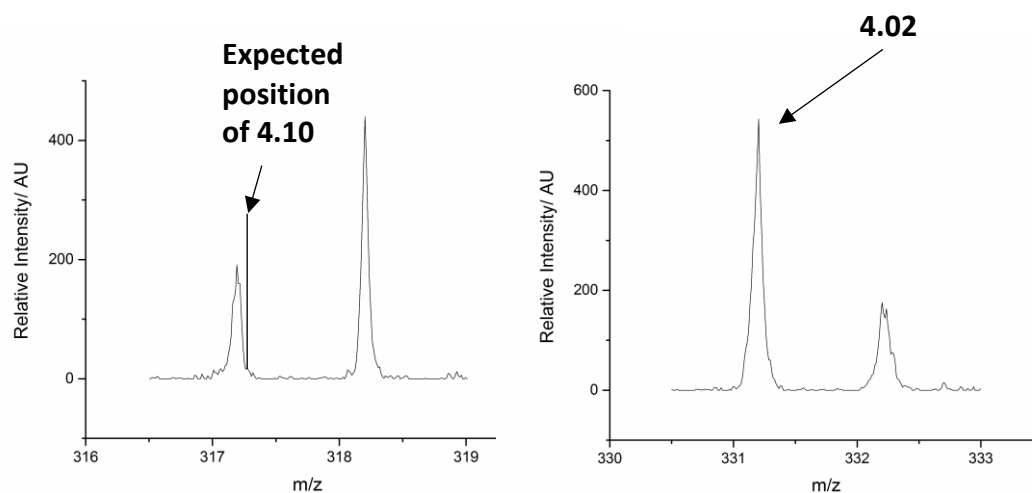


Figure 143: Lack of signal for **4.10** in the presence of an  $\cdot\text{OH}$  scavenger, while **4.02** can still be observed.

The results of this experiment (Figure 143) support this theory, with **4.10** not identified in the presence of a hydroxyl radical scavenger, while **4.02** is still observable. This simple

experiment illustrates the importance of this trapping technique, with speciation of different radicals from different reaction routes being confirmed for  $\alpha$ -pinene ozonolysis.

A D<sub>2</sub>O shake experiment provided further evidence of the structure of **4.10**. This is a common experiment used in NMR studies, where the deuterium signal will not be present in the <sup>1</sup>H region of the spectrum (spin = 1 for deuterium), hence the <sup>1</sup>H NMR signal from a hydroxyl group will disappear upon conversion to OD.<sup>249</sup> As **4.10** incorporates a hydroxyl group, exchange to form OD (Figure 145) would be expected during this reaction, with the resultant product shifted by one m/z unit during the subsequent analysis. This observation is shown in Figure 144. Compounds such as **4.02**, which do not contain easily exchangeable protons, show no change in m/z after this experiment.

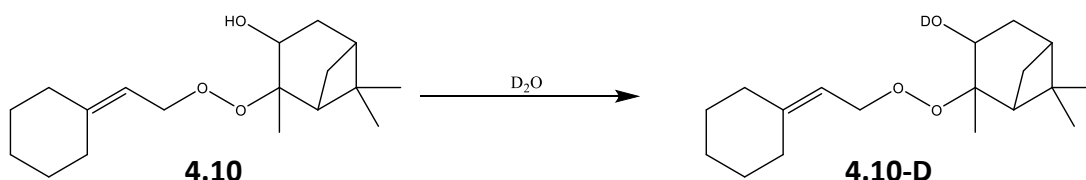


Figure 145: OH-OD exchange with **4.10**

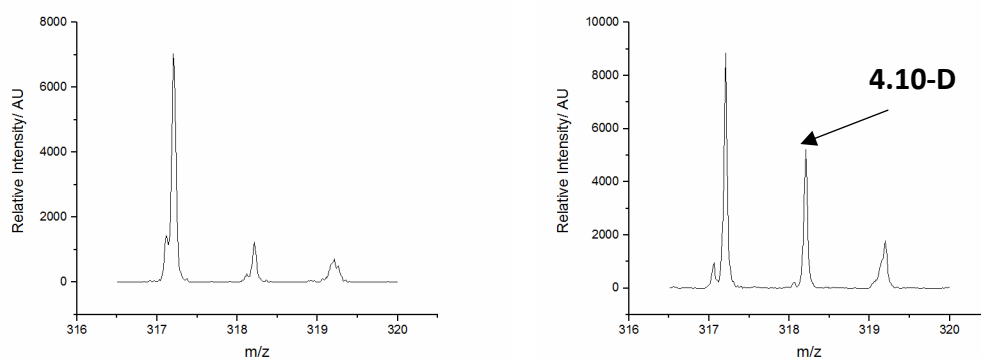


Figure 144: Change in signal upon D<sub>2</sub>O shake

#### 4.6.4. Reactions Investigating the Trapping Process

The quartz trapping system can also be used to gather information regarding the performance of different trapping molecules for the trapping process. Concurrent

trapping was conducted by running an experiment in the presence of **2.09** and **2.13**, mixed together on the sample support. This experiment, Figure 146, successfully showed both species trapping the same radicals from within the same reaction. This shows that the different trapping compounds are able to capture the same radical, under the same conditions, whilst the rates of capture by the traps are not sufficiently different to preclude trapping by one of the traps.

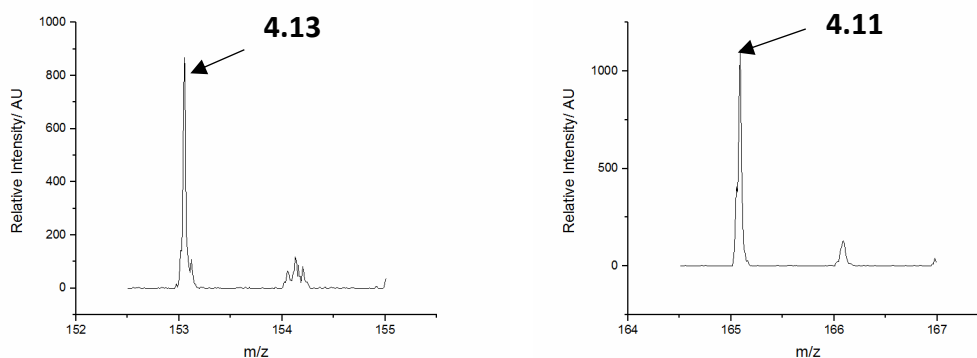


Figure 146: Signal from **4.13** and **4.11** detected with a mix of **2.13** and **2.09**

The trapping process can be further examined by the application of **2.09'** to the system as in Figure 147. This material is one that is expected not to capture radicals, however experimental confirmation of this would be useful. Therefore, **2.09'** was applied to this system, as the system is known to produce trappable gas phase radicals.

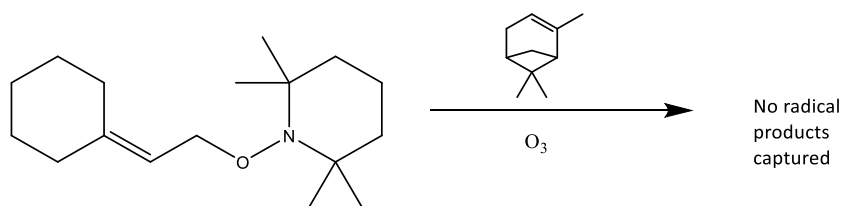


Figure 147: Application of **2.09'** to trapping system

The results from this experiment clearly demonstrate that this compound does not trap radicals, with no indication of captured species such as **4.01**, **4.09**, or the hydroperoxyl radical. This serves as a useful confirmation that the mechanism of radical trapping is indeed occurring via attack of the double bond being employed, as different trapping mechanisms (such as homolysis of the C-O bond to TEMPO and subsequent radical

combination) would still have the potential to form trapped products from the degraded compound **2.09**.

## 4.7. Application of Trapping System to Other Alkenes

### 4.7.1. Limonene Ozonolysis

Limonene is another monoterpene of atmospheric interest, where radicals are predicted to explain the formation of assorted observed reaction products and SOA.<sup>229,237,250,251</sup> This compound is also of importance regarding indoor air quality, as it is a common additive to many household products (e.g. air fresheners, scented cleaning agents).<sup>252</sup> As such, the ozonolysis of this system was conducted, using the same methodology as has already been applied to  $\alpha$ -pinene, to establish whether initial peroxy radical species predicted from the MCM can indeed be detected from this system.<sup>229,230</sup> This will thus demonstrate further the applicability of the trapping species **2.09** to different reaction systems in the gas phase. These experiments will also serve as useful proof of principle for the trapping of limonene ozonolysis products in an indoor air system, described in **Chapter 7**.

Several peroxy radical species were captured during these experiments. Again, these species come from two different reaction channels – ozonolysis, and the reaction of  $\cdot\text{OH}$  with limonene.<sup>229,230</sup> The ozonolysis channel shown in Figure 148 is expected to mainly produce two initial radical species, **4.21a-b**, of identical molecular mass. Therefore, adducts **4.22a-b** in Figure 149 will appear as the same signal when examined by MS.

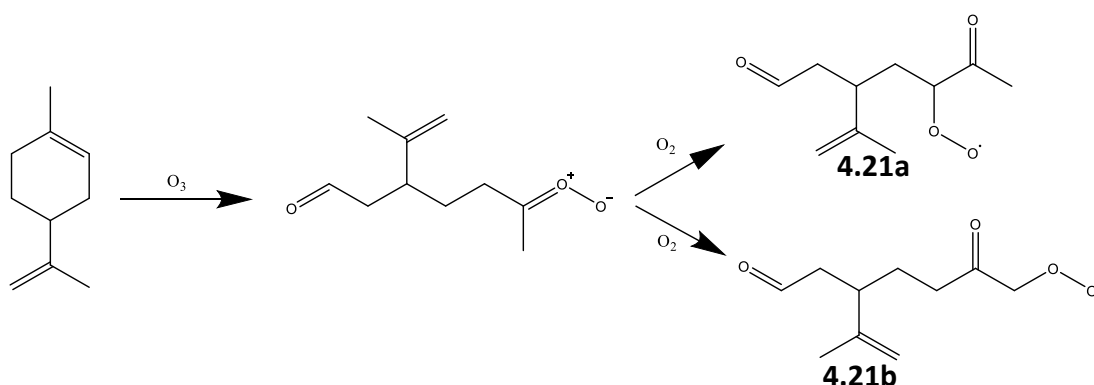


Figure 148: Formation of peroxy radicals **4.21a** and **4.21b** from limonene ozonolysis<sup>229,230</sup>

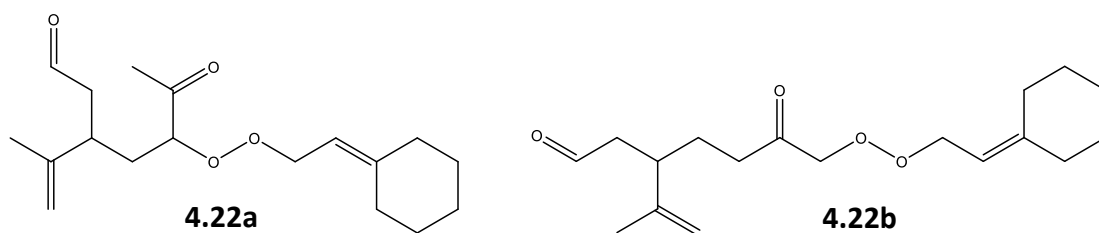


Figure 149: Expected structures of captured ozonolysis products

**4.22** can be observed via MS analysis, with a relevant portion of the mass spectrum given below in Figure 150. This is obviously not the only radical product that would be expected from the ozonolysis of limonene, however it is useful to know that initial peroxy products originating from ozonolysis reaction mechanisms can be captured. Again, trapping these species provides evidence to confirm the hydroperoxide mechanism for  $\cdot\text{OH}$  production is occurring through the detection of the  $\text{RO}_2$  co-product that can subsequently go on to form SOA, as shown within the MCM.<sup>229,230</sup> Detection of these species also provides species to search for in subsequent indoor air experiments (**Chapter 7**).

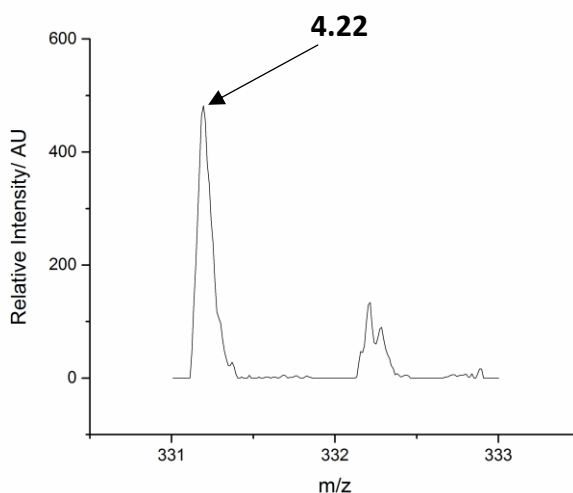


Figure 150: Product **4.22**, detected from ozonolysis of limonene

Products from the  $\cdot\text{OH}$  reaction channel are also anticipated to be formed in this experiment, as ozonolysis of limonene produces  $\cdot\text{OH}$  in a good yield (ca. 86%).<sup>17</sup> However, as with the ozonolysis process described above, there are expected to be several isomeric initial  $\text{RO}_2$  species, **4.23a-c**, from this reaction (Figure 151).

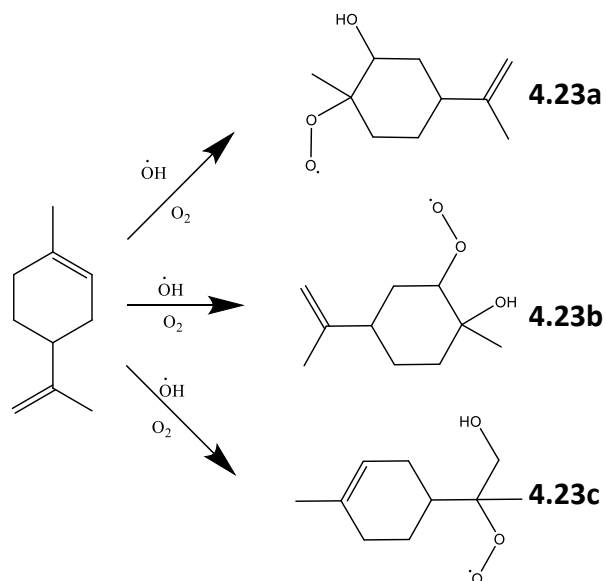


Figure 151: Formation of  $\text{RO}_2$  radicals from  $\cdot\text{OH}$  attack on limonene<sup>229,230</sup>

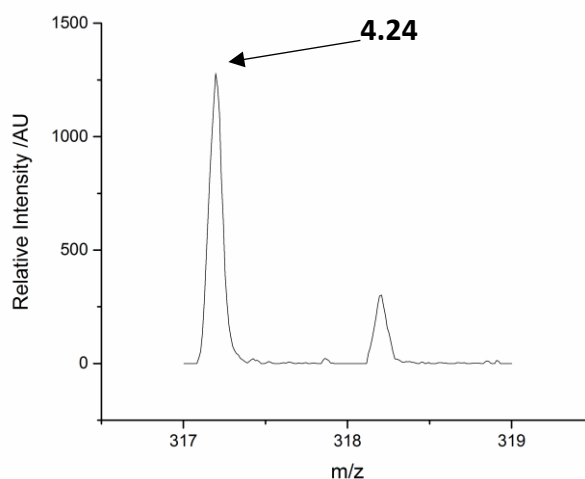


Figure 152: MS of **4.24**, captured from  $\cdot\text{OH}$  attack on limonene.

As expected, these products can be observed in Figure 152 as trapped to form **4.24a-c** (Figure 153) in the preliminary limonene experiments. However, these isomers have not been separated, thus the observed signal is likely to be comprised of signal from all three of the isomers in Figure 153. If trapping were to be based on expected relative formation of these species, they would be present in yields of 41, 22 and 37% from **4.24a-c** respectively, based on MCM predictions.<sup>229,230</sup> Despite this, the trapping experiments have

been successful with regard to detecting peroxy radicals predicted from hydroxyl radical attack on limonene using the trapping methodology based around trapping species **2.09**.<sup>229,230</sup>

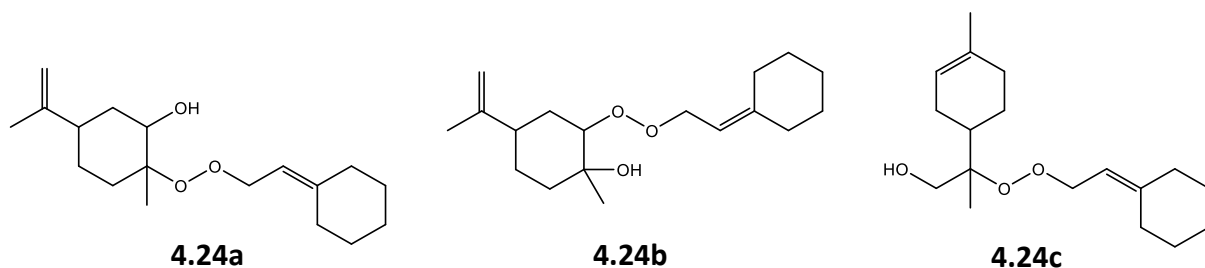


Figure 153: Expected structure of  $\cdot\text{OH}$  attack products from limonene

#### 4.7.2. $\beta$ -Pinene Ozonolysis

Another example of an atmospherically relevant monoterpene is  $\beta$ -pinene. The alkene group in  $\beta$ -pinene is terminal, and not part of the ring structure (as it is in  $\alpha$ -pinene) – hence  $\beta$ -pinene will fragment differently upon reaction with ozone. The type of products from this process are expected to be similar to  $\alpha$ -pinene, with a variety of  $\text{RO}_2$  radical products expected to form upon ozonolysis or reactions with the hydroxyl radical.<sup>229,230,247</sup> This will serve as continuation of the testing of consistency of the trapping method as a way to probe for radical products of gas phase reactions, as very similar species to those originating from  $\alpha$ -pinene or limonene ozonolysis will be generated from this reaction. Reaction with ozone is predicted by the MCM to result in the formation of the hydroperoxyl radical and **4.25**, again via a Criegee intermediate, as shown in Figure 154.<sup>229,230</sup>

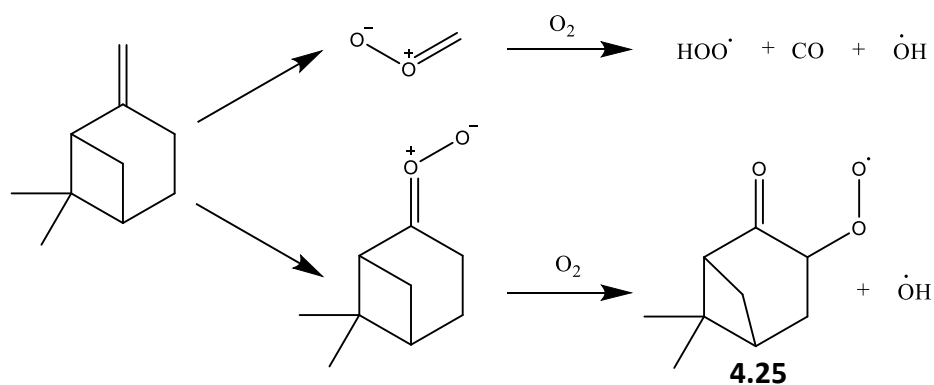


Figure 154: Formation of radicals via Criegee intermediates from  $\beta$ -pinene ozonolysis<sup>229,230</sup>

Unlike previous species, this process does not produce two isomeric species, owing to a terminal alkene being ozonolysed here, as opposed to one that is part of a cyclic structure in  $\alpha$ -pinene or limonene. The radical **4.25** would be expected to be trapped as **4.26** (Figure 156), this was indeed observed in Figure 155, hence providing evidence towards this predicted mechanism.<sup>229,230</sup> However, the hydroperoxyl radical produced by the alternative ozonolysis route can be formed by a variety of different routes and so is not in itself suggestive of the ozonolysis of  $\beta$ -pinene occurring. Therefore, despite the observation of the hydroperoxyl radical adduct **4.11**, this is not definitive evidence of the other ozonolysis reaction pathway.

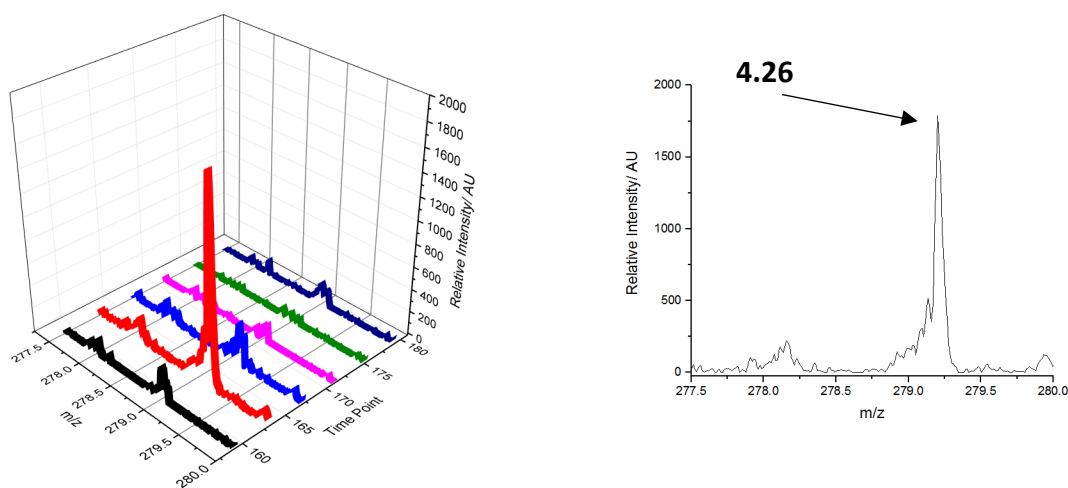


Figure 155: MS of **4.26**

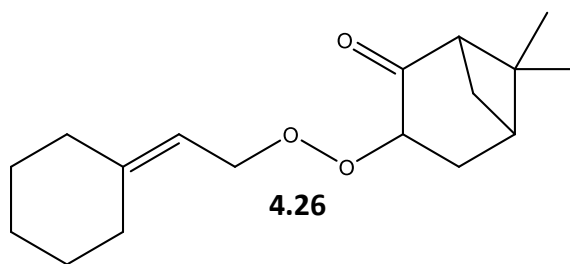


Figure 156: Compound formed by the trapping of **4.25**

As with  $\alpha$ -pinene, ozonolysis of  $\beta$ -pinene is known to produce hydroxyl radicals, albeit in a yield of ca. 24%, a noticeably lower yield than that of  $\alpha$ -pinene or limonene.<sup>17</sup> This is because the  $\text{CH}_2\text{OO}$  Criegee intermediate cannot form  $\cdot\text{OH}$  via a vinyl hydroperoxide intermediate.<sup>205</sup> However, hydroxyl radicals would still be anticipated to react with  $\beta$ -pinene within the system. A series of radicals are expected to form from this process, which **2.09** can be used to detect. Unlike the ozonolysis reactions, a series of isomers are again anticipated, **4.27a-c**, (Figure 157) and with the same mass as **4.10** from  $\alpha$ -pinene reactions.

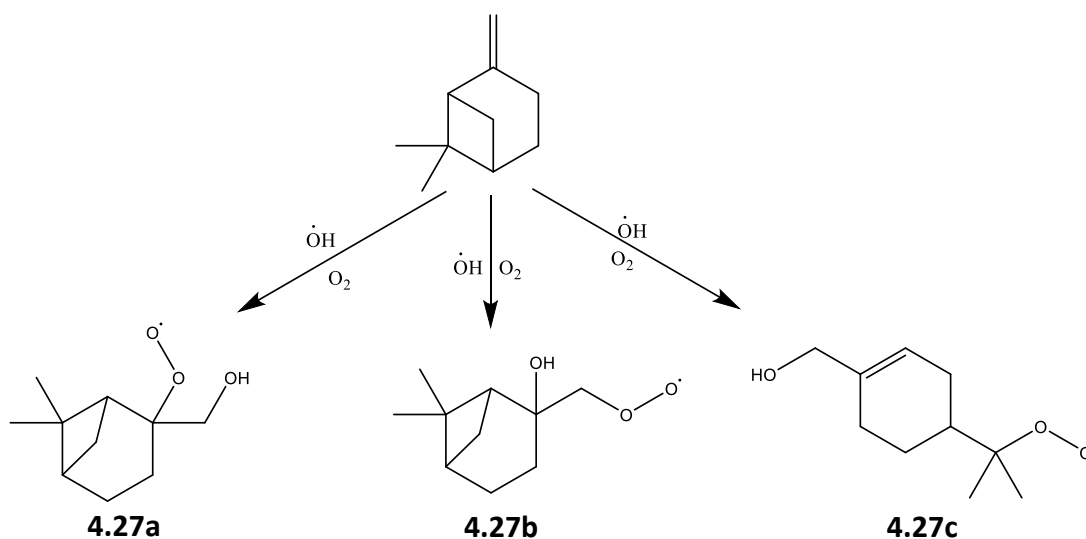


Figure 157: Isomers **4.27** formed from  $\cdot\text{OH}$  attack on  $\beta$ -pinene in the presence of oxygen<sup>229,230</sup>

The trapping of these species, to form **4.28** (Figure 158), was confirmed by detection of the expected mass by mass spectrometry in Figure 159. Therefore, a series of peroxy radical from ozonolysis of three different monoterpenes have now been observed. Again,

this provides good evidence regarding the applicability of this methodology to capturing radical products that are previously only predicted in models.<sup>229,230</sup>

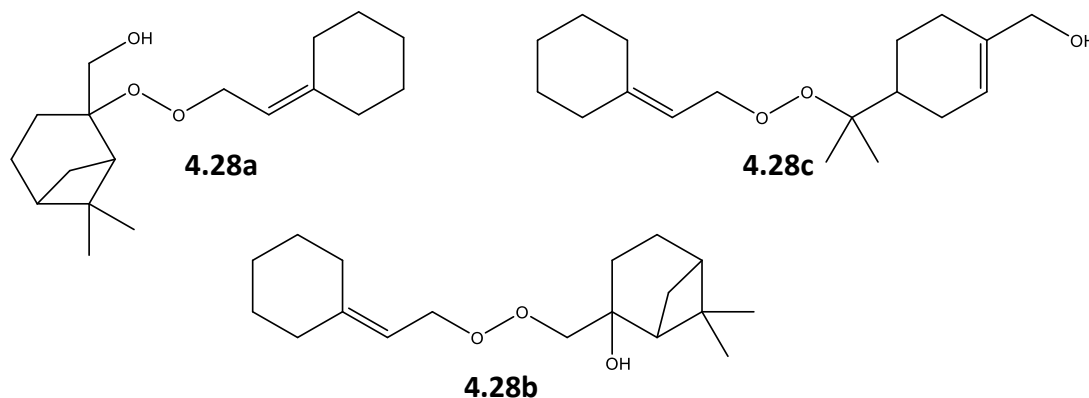


Figure 158: Compounds formed on trapping 4.27

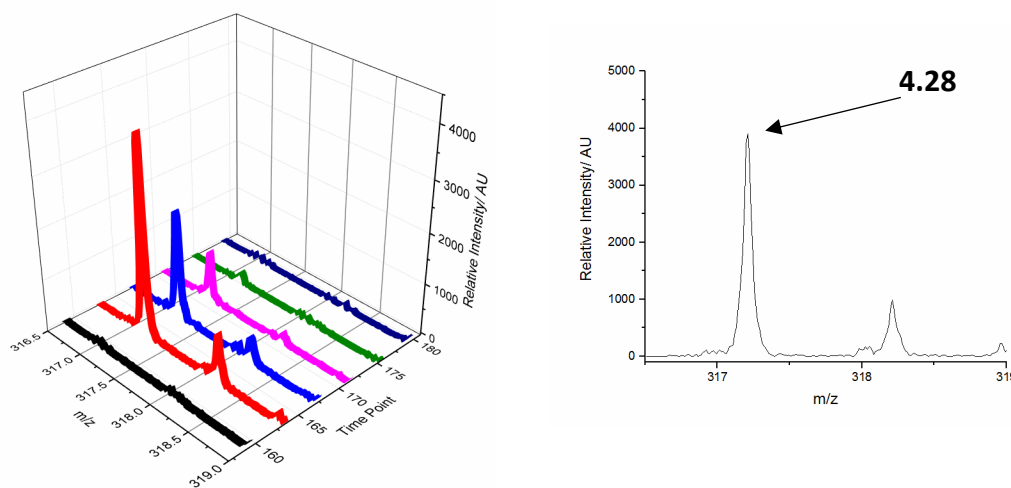


Figure 159: MS for 4.28

#### 4.7.3. 2,3-Dimethylbut-2-ene Ozonolysis

Ozonolysis reactions and products are all very similar for the above monoterpene systems, with a complex array of radical species products, many of which are isomers. Therefore it is useful to test the radical trapping system on the ozonolysis of a simple, non terpenoid compound and establish whether predicted products can indeed be easily detected. In this instance, 2,3-dimethylbut-2-ene (TME) is utilised (Figure 160). This is an important anthropogenic alkene, which can provide a clean system to investigate (as it is a

symmetrical compound), with an  $\cdot\text{OH}$  yield of ca. 90% (formed via vinyl hydroperoxide mechanisms).<sup>253</sup> This simple alkene system is a species that has been used by several groups in order to study the ozonolysis of alkenes.<sup>212,253,254</sup>

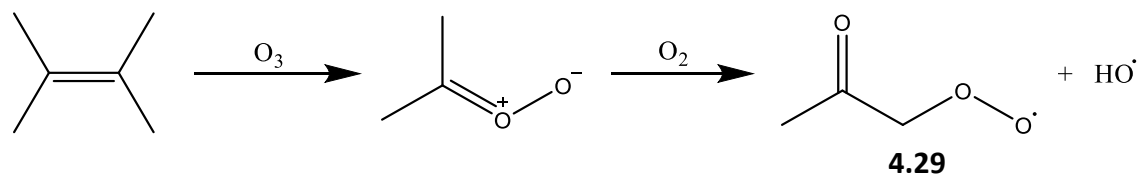


Figure 160: Formation of **4.29** from TME ozonolysis<sup>229,230</sup>

As with the terpenoid systems, a peroxy radical predicted to be originating from the hydroperoxide ozonolysis channel was observed (**4.29**).<sup>253</sup> The capture of this species, forming **4.30**, again provides evidence supporting that the VHP mechanism for the formation of **4.29** and  $\cdot\text{OH}$  is indeed occurring. This system was probed with **2.09**, with the expected adduct (**4.30**, Figure 161) from capture of **4.29** observed in Figure 162.

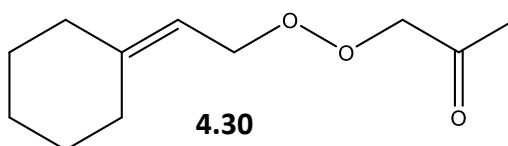


Figure 161: Compound from trapped **4.29**

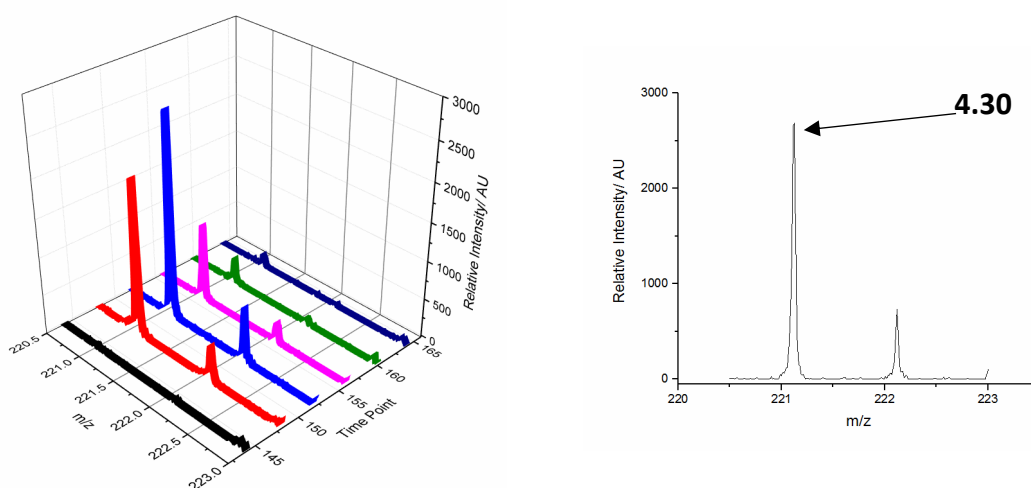


Figure 162: MS signal from **4.30**

Reaction products were also observed from reaction between the hydroxyl radical and TME, **4.31** in Figure 163. This is unsurprising given that the  $\cdot\text{OH}$  yield of TME is again high, having previously been found to be ca. 90% under dry conditions.<sup>255</sup> This species is trapped with **2.09** to form **4.32**, as shown in Figure 164.

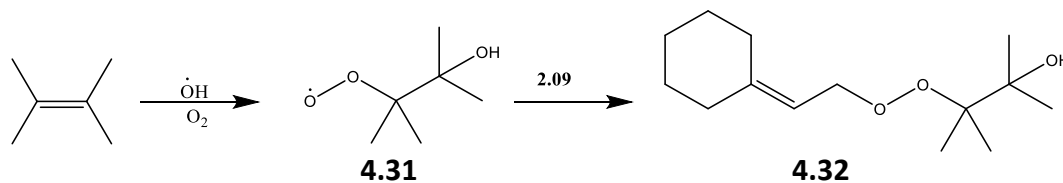


Figure 163: Formation and trapping of **4.31** from  $\cdot\text{OH}$  attack on TME<sup>229,230</sup>

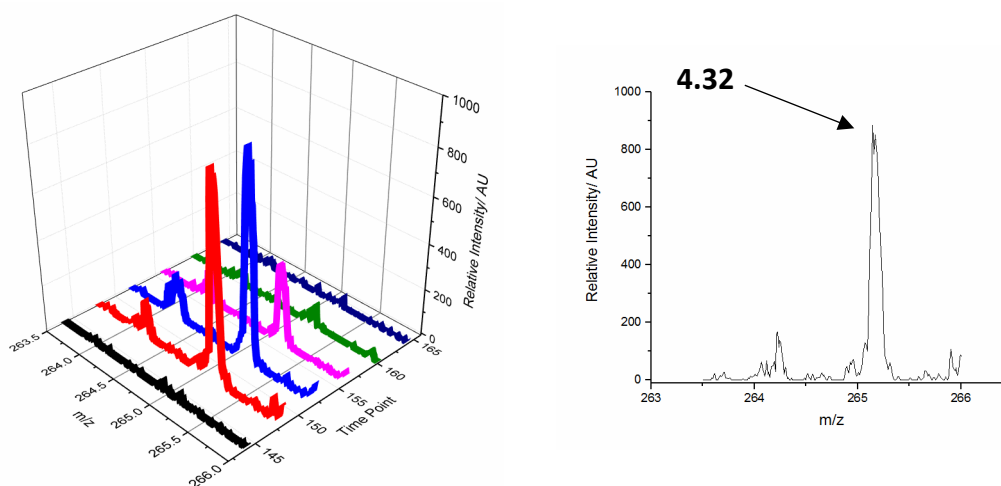


Figure 164: MS signal from **4.32**

## 4.8. Future Work

The proof of concept experiments demonstrated above indicate that this radical trapping methodology appears to have worked well and show promise towards the overall aim of observing and quantifying speciated radical intermediates from atmospheric process such as ozonolysis. There are several areas available for future work on the application of this trapping methodology to alkene ozonolysis systems. The first of these areas would be to incorporate some chromatography into the system. Conducting LCMS on these reactions will be useful in terms of isolating the trapped products, in particular separation of isomeric species such as **4.02a** and **4.02b** would be very interesting. If successful, this could then lead to relative amounts of these compounds being determined, which would then

provide experimental evidence to confirm ratios predicted in models such as the MCM.<sup>229,230</sup> This can also be combined with more detailed MS studies on these species, utilising HPLC-MS-MS.

Another area of work would be to conduct studies regarding the kinetics of the radicals being captured from this system. Flow tube experiments, with variation in the position of the radical capture site, would be expected to capture different quantities of different radicals along the tube, as is discussed in **Chapter 6** in the context of the nonane + ·OH reaction. The analysis of these captured species could then be used to generate kinetic profiles, which can again be compared and contrasted to modelled predictions.

Finally, it would be of interest to use this system in conjunction with other atmospheric radical detection techniques – i.e. in an atmospheric simulation chamber with a FAGE instrument, to provide high resolution, quantified HO· and HO<sub>2</sub>· (and some RO<sub>2</sub>) measurements.<sup>256</sup> This would enable overall radical concentration, as well as speciation of these radicals, to be easily conducted within the same experiment. Having two different instrumental techniques providing complementary information would be highly useful in examining not just the α-pinene ozonolysis reaction, but also as a method of evaluating experiments conducted within different chambers, leading towards chamber calibration of the trapping methodology.

## 4.9. Conclusions

Overall, the application and evaluation of **2.09** to the trapping of gas phase radicals produced via ozonolysis reactions has been established. By application to the α-pinene ozonolysis system, two gas phase detection systems have been utilised, with the main difference between systems being a significantly longer residence time in the aerosol bag experiments as opposed to the quartz tube experiments. This allows the probing of radical production over a range of reaction timescales. Initially, EPR trapping experiments have been utilised in order to confirm the presence of radicals in the quartz tube experimental system.

Both of these experimental systems have shown good evidence of radical trapping. Initial peroxy species, **4.01** and **4.03** formed via  $\alpha$ -pinene's reaction with ozone following the hydroperoxide channel have been detected. This provides mechanistic evidence for this channel and indicates that it is an efficient channel for the production of a range of radical species in the ozonolysis of alkenes. The hydroperoxide channel is also important in non-photolytic production of  $\cdot\text{OH}$ . Indeed, the trapping methodology has resulted in the detection of peroxy compounds such as **4.09** formed via  $\alpha$ -pinene reacting with  $\cdot\text{OH}$  produced from the ozonolysis reaction. These oxygenated species are expected to be precursors to ELVOC, which can lead to aerosol nucleation. Other species formed from this system have also been detected, including the hydroperoxyl radical (which will also be formed following ambient formation of  $\text{HO}_2\cdot$  from ozonolysis) and, in the aerosol bag system, there is also evidence of the presence of bridged peroxy species, **4.15**, as suggested by Berndt et al.<sup>242</sup> Products from both ozonolysis and hydroxyl radical routes have also been successfully detected for other atmospherically important alkenes such as limonene,  $\beta$ -pinene and TME when tested with the quartz tube methodology.

A number of experiments have also been conducted with the aim of providing some confirmation of the detected species. Experiments with a hydroxyl radical scavenger have confirmed the source of **4.10** as via  $\alpha$ -pinene's reaction with  $\cdot\text{OH}$ , while mass shifts caused by a  $\text{D}_2\text{O}$  shake to form **4.10-D** have provided evidence of a hydroxyl group functionality within trapped compound **4.10**. Finally, trapping experiments have confirmed the inability of **2.09** rearrangement species such as **2.09'** to capture radicals from the gas phase.

## 5. Gas Phase Trapping Development and Scoping

### 5.1. Introduction

#### 5.1.1. Gas Phase Trapping: Radicals and Aerosol Composition

Unlike the simple liquid phase experiments conducted in **Chapter 3**, the bi-phasic nature of trapping gaseous radicals with a non-gaseous trap as employed in **Chapter 4** requires thought on optimising the trapping process for gas phase species. There are a variety of methods that have already been developed to conduct gas phase sampling experiments. These types include direct on-line analyses, for example DOAS, or off-line methods, where samples are collected prior to future analysis experiments (for example when examining SOA).<sup>64,257</sup> As this trapping technique is targeted towards an off-line analysis, other literature off-line systems may provide influences regarding optimising this sampling process.

Techniques utilised within atmospheric chemistry are likely to provide inspiration for this radical trapping system. The trapping system itself is likely to be similar in terms of requirements to methodologies employed in the collection of SOA. In these systems, the air being studied is blown through a filter, constructed of an inert material such as quartz fibres, with the products then washed off and analysed. This can be used in order to collect sufficient material for offline compositional analysis of the SOA. For example, Tofful et al. used this system to conduct elemental analysis on the SOA, providing useful insights regarding the source of this material.<sup>258</sup> Other researchers have used these techniques in order to collect SOA to examine the impact of SOA on different systems. For example Niu et al. used such a method to collect SOA generated from D-limonene ozonolysis, with the collected material used to give evidence for the pulmonary impact of these species.<sup>259</sup> As such, a technique where air is blown over a sample of trapping material, which is then extracted for analysis, would seem easily feasible.

Alternatively, an analogy with gas chromatographic systems can be considered during the development of this methodology. The stationary phase of a GC column functions to separate the gasses being probed, with different interactions resulting in different elution times, thus separation is facilitated. As such, the stationary phase will need to have a high surface area available for interaction with the gas phase, as is the case for the trapping methodology being developed here. Capillary columns are widely used, with thin (< 50  $\mu\text{m}$ ) layers of stationary phase.<sup>260</sup> In many cases, GC columns can utilise a liquid stationary phase (for example with cyclodextrins, which can facilitate chiral separation).<sup>261</sup> This will be deposited onto a solid support within the column, as would be required for deposition of trapping material during this radical trapping methodology development.

A similar technique has been used for the spin trapping of gas phase radicals. Watanabe et al. deposited a spin trap (4-POBN) onto filter paper, with air blown through the paper during atmospheric sampling.<sup>262</sup> The spin adduct is then washed off, and the solution analysed by EPR. However, other radical adducts are not measured here, for example  $\text{HO}_2\cdot$ , as the lifetime of this species (ca. 10 hr) is not sufficiently long.<sup>262</sup> Nevertheless, this method does demonstrate the feasibility of trapping radicals from the gas phase, with  $\cdot\text{OH}$  concentrations of  $10^5$  molecules  $\text{cm}^{-3}$  observed. Other techniques, for example the trapping of carbon centred radicals from cigarette smoke by Flicker et al. have involved deposition of a spin trap on a high surface area support such as glass beads.<sup>263</sup> Alternatively, Conte et al. described a system where radicals are generated within a catalytic reactor, then blown into spin trap solution.<sup>125</sup> The resulting solution can then be removed and analysed offline by conventional EPR spectroscopy.

### 5.1.2. Aims

The general approach towards the design of this system is to deposit the liquid trap compounds (e.g. **2.09**) on an inert support. This support must be of a high surface area, for example utilising a porous material. This will help to spread the trapping material in a thin layer over the support, increasing the quantity of reactive material on the surface.

The support was packed into a column, through which a radical containing gas flow was passed for the duration of the sampling period.

There are several elements that are important to consider when building and optimising the methodology for trapping reactive species from the gas phase. The trapping molecule will need to be deposited on a support, the material required for which will need to be established, as will the amount of material used in each trapping experiment. Sample packing techniques will need to be determined, alongside both minimum and optimal sampling times for the trapping system. The aim of this will be to produce a sampling methodology that enables efficient radical capture, whilst also being both reproducible and consistent. This optimised methodology can then be applied to the trapping of radicals from a low temperature plasma based system. This will be useful in terms of attempting to validate the spin trapping based detection of radical species that has previously been conducted with low temperature plasma.<sup>264</sup>

## 5.2. Gas Phase Trapping Method Development

### 5.2.1. Scoping a Sample Support

The simplest way for the radical trapping process to occur is to pass a radical containing gas flow over a sample of trap. This is analogous to the trapping of SOA on filters.<sup>259</sup> For this, the trap will need to be deposited on a sample support, with a general scheme for the trapping process given below in Figure 165.

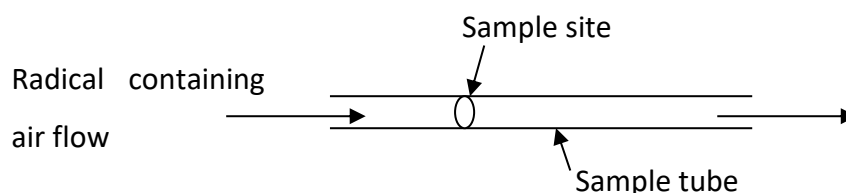


Figure 165: Simple trapping scheme

The use of a high surface area sample support will provide significant gains in signal, as opposed to directly coating the trapping material onto a sampling tube. Trapping could

also be accomplished by simply bubbling the radical containing air flow through a solution of radical trap. This was not pursued because, while some trapping would be expected, the high gas flow rates need large volumes of solution, thus resulting in large quantities of wasted trapping material (with solvent evaporation adding a further problem).

An initial system was developed using glass wool as a sample support. For sample loading, 20 mg of **2.09** was dissolved in DCM (2 mL) and added to glass wool (100 mg). The solvent was then evaporated, leaving the **2.09** deposited on the wool. This was loaded into the sample tube as in Figure 166. Extraction of products can be accomplished by re-addition of solvent to the wool, and offline analysis of the material dissolved in the solvent.

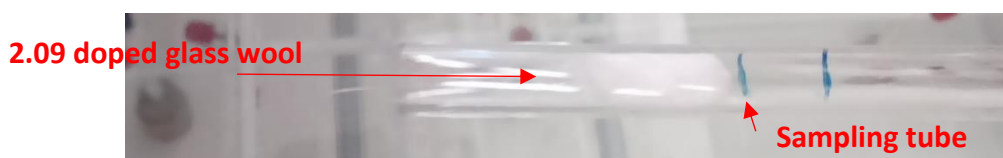


Figure 166: Glass wool loaded inside a sample tube

Trapping experiments using this glass wool system proved successful, with an assortment of products (e.g. **4.02**, **4.09** and **4.11**) detected from a gas phase  $\alpha$ -pinene ozonolysis experiment using the quartz flow tube. For the optimisation experiments discussed below, the signal corresponding to the hydroperoxyl radical adduct, **4.11**, is used for comparisons.

Surface area modification has the potential to enable substantial improvement on the signal intensities obtained from these experiments. Calculations of the glass wool surface area suggested a surface area of ca.  $0.02\text{m}^2\text{g}^{-1}$ , similar to literature values.<sup>265</sup> Meanwhile, a monolayer of a 10 mg sample of **2.09** would be expected to have a maximum surface area of ca.  $9\text{m}^2$ , based on typical bond lengths within **2.09**. Therefore, it is likely that a large proportion of **2.09** was within bulk layers, hence not exposed to gaseous radicals.

Glass beads have previously been used by Flicher et al. as a support for spin trapping of gas phase radicals.<sup>266</sup> Therefore, glass beads (100 mg,  $75\ \mu\text{m}$  diameter) were used as an alternative surface for these experiments, with a surface area of  $0.03\text{m}^2\text{g}^{-1}$ . The trap was deposited in the same way as that described above for the glass wool. Surprisingly, the

signal obtained from this system was clearly lower than that acquired from the glass wool system. This decrease in signal was attributed to the material forming clumps on addition of solvent, hence the trapping compound **2.09** was not evenly dispersed. A poor signal was still evident when the material has been vacuum dried overnight before application.

An octadecyl functionalised silica support was also trialed. This type of material is a common stationary phase in chromatography, due in part to the high surface area.<sup>267</sup> This silica is commercially available, and sold as having a surface area of ca.  $550 \text{ m}^2 \text{ g}^{-1}$ , significantly greater than the surface areas of the previous systems. 20 mg of **2.09** was deposited on this support by dissolution in 2 mL of DCM, which was added to 100 mg of silica, and the solvent evaporated. A significantly improved signal was identified with this support, as can be seen in Figure 167. The observed signal has not increased by the orders of magnitude that surface area has changed: this is likely because a theoretical 'perfect' monolayer has not formed (with an estimated a surface area of ca.  $900 \text{ m}^2 \text{ g}^{-1}$  for **2.09**, this monolayer would cover 33% of the silica). However, with 100 mg of glass wool or beads, there is expected to be sufficient material for several hundred layers of trap, thus more of the trap will certainly be expected to be exposed to radicals with the silica support.

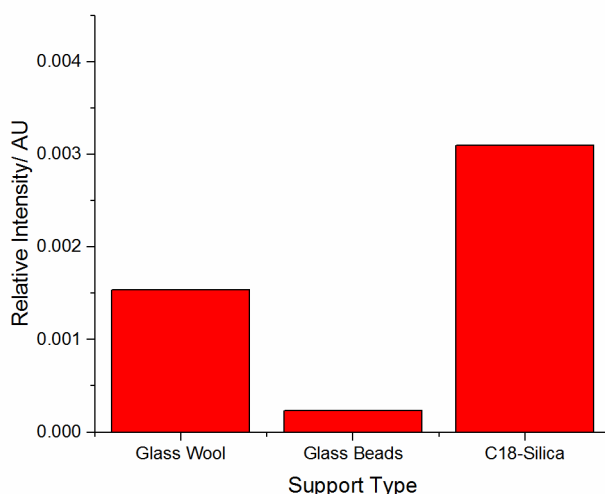


Figure 167: Signal change on variation of sample support

An interesting observation can also be made regarding the silica colour. While initially a white powder, by the end the colour appears to darken, to a beige hue. This is attributable

to the strongly coloured TEMPO species released during the trapping process. However, this was only a subtle change, and is not indicative in itself of a successful trapping reaction. Overall, for future experiments, ocadecyl functionalised silica was utilised as the sample support, owing to the noticeable improvement of signal obtained within these systems.

### 5.2.2. Scoping the Impact of Sample Loading

The quantities of trap required, and the ideal ratio of trapping material to support, also requires determination. For previous experiments, 20 mg of **2.09** was applied per experiment. While good signals were obtained, it is likely that large amounts of trap were wasted by being well below the initially reactive monolayer. Therefore it was desirable to use little trapping material as possible, whilst maintaining a reasonable product signal.

A series of experiments were conducted whereby the trapping material is systematically decreased (while deposited on 100 mg of silica) testing the mass of **2.09** required for product observation. This is shown in Figure 168. While signal can clearly be observed with 0.91 mg trap (covering a maximum of ca. 1.5% of the silica), experiments with 0.05 mg trap (a maximum silica coverage of ca. 0.08%) have no observable product signal.

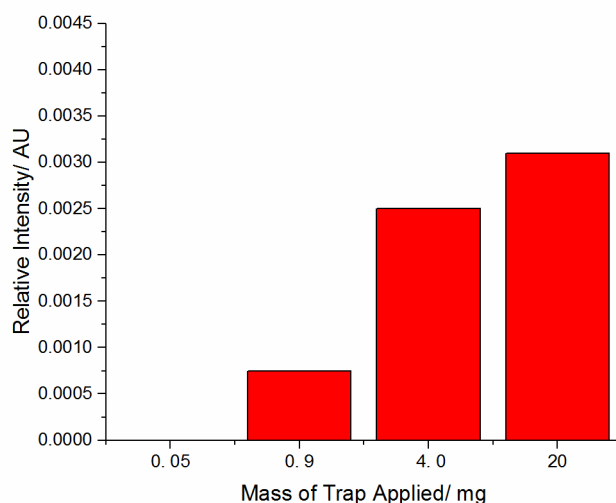


Figure 168: Change of signal for **4.11** with mass of trap applied

There are several possible reasons for this. The most obvious would be that the trapped products are simply below the limit of detection. However, this is unlikely to be the case. Throughout experiments, the dominant signal was the trapping material itself. Yet, with the 0.05 mg experiment there was no indication of this signal. The most likely explanation is that trapping material (and products) was evaporating from the support, thus making low sample mass experiments impractical. The sample evaporation hypothesis was confirmed by detection of **2.09** on filters at the end of the sampling system (well beyond the sampling location). Therefore it would be prudent to use at least 4 mg of trapping agents, to minimise the impact of sample being blown away during the experiment.

The trapping process can also be optimised with regard to the ratio of trap to silica. Again, this would be expected to have a noticeable impact on results, with increased ratios likely to result in more trap being available on the surface of the support. Therefore, various ratios of trapping material to silica were employed, with a constant amount of trapping material (4 mg) utilised. The resulting different signal intensities are shown in Figure 169.

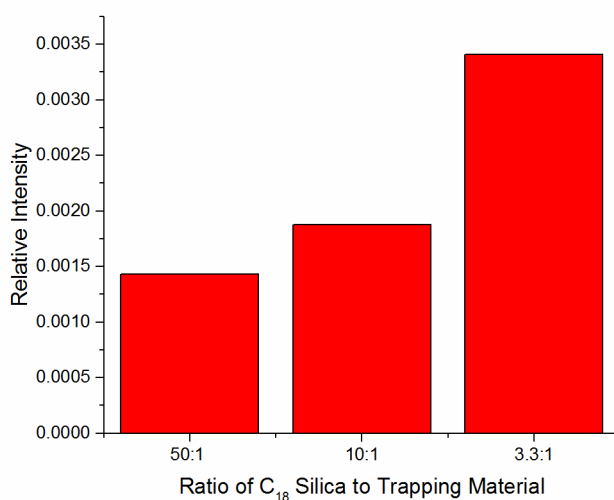


Figure 169: Comparison of different ratios of silica to trapping material for **4.11**

The use of increased trap to silica ratios will lead to less uncoated support, with coverage expected to increase from 3% to 51% as this ratio changes as in Figure 169. The increase in the percentage of support covered by **2.09** will lead to enhanced radical trapping. As

expected, this produced a noticeable improvement in signal. It is however unlikely that significant gains can be made beyond this ratio, as increased sample loading made the silica sticky and difficult to handle, with sample loading and removal problematic. Hence experiments were not conducted with trapping ratios of less than 3.3:1.

### 5.2.3. Optimising Sample Packing

The packing of the sample was another area where sample optimisation was required. This will also impact upon the reproducibility of samples, as the packing needs to be consistent from one experiment to another. Therefore, three different types of packing were trialled, in each case using 4 mg **2.09** on 20 mg silica, in a tube of 0.6 cm internal diameter. The first of these was simply tapping the sample tube after addition of the silica, in order to level out the silica on the glass wool bung. The second option was creating a silica 'sandwich' with glass wool either side of the silica. Finally, a 'squashing' method was tested, whereby the silica was loaded and pressed down into a narrow layer on top of the glass wool bung. These different methods are shown in Figure 170. The signal variation from these otherwise identical experiments can be seen in Figure 171.

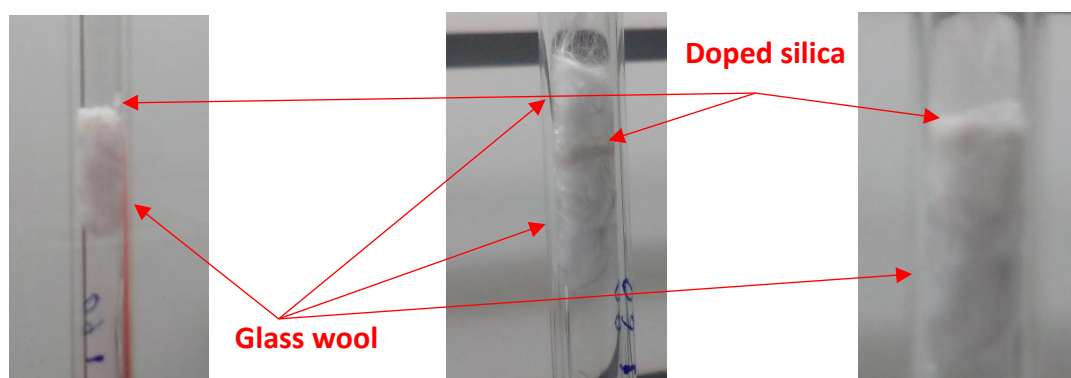


Figure 170: Different methods of silica loading, 'tapped', 'sandwiched' and 'squashed' respectively

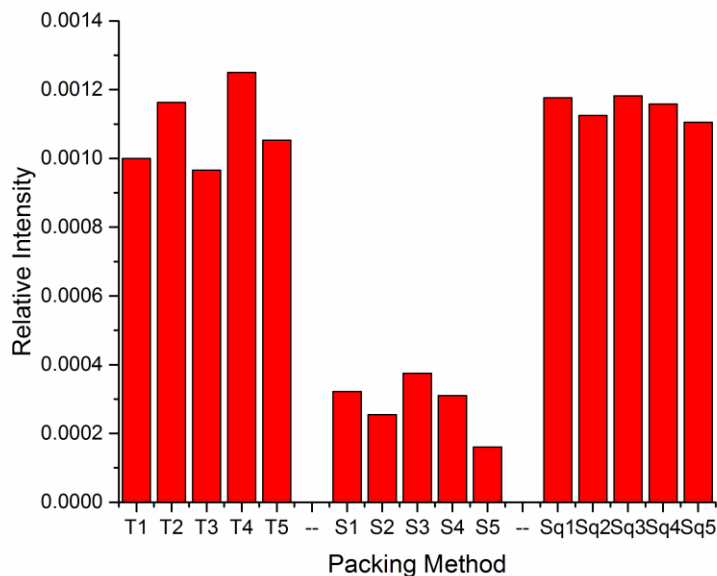


Figure 171: Variation in **4.11** signal with different packing method. T = Tapped, S = Sandwiched, Sq= Squashed

The consistently lower signal from the ‘sandwich’ packing experiments is clear. While this can be justified by radical decay from losses to the glass wool, it is surprising that a small layer of glass wool provides such a large impact. The reproducibility for these sandwiched signals is also rather noticeable, differing by up to 18%. This may be partially justifiable by differences in the packing of the top glass wool layer, and comparable to the error of 8.5% observed for the ‘tapping’ methodology. However, this is much larger than the error of 2.2% recorded for the ‘squashed’ samples. Literature methods of radical detection also feature significant errors, with CIMS measurements reported by Berresheim et al. with instrumental precision and accuracy errors of 19% and 28% respectively.<sup>268</sup> PERCA based measurements by Monks et al. meanwhile featured measurements of up to 30%.<sup>269</sup> Holland et al. have reported lower errors for LIF measurements of radicals, up to 16%.<sup>35</sup> As such, the errors recorded from this radical trapping technique are comparable to those obtained from field measurements with more established radical monitoring techniques.

The penetration of radicals into the silica was also probed. While the sandwich experiments showed a significant drop in silica from the addition of a layer of glass wool

before the trap, EPR spin trapping experiments previously discussed (**Chapter 2**) have shown that radicals can still be detected at the end of the process. In order to align these two results, a trapping experiment was conducted using a significantly deeper silica trap layer, shown in Figure 172, with different segments analysed to examine for different signal intensities down the tube.



Figure 172: Image of tube with a larger silica trap layer

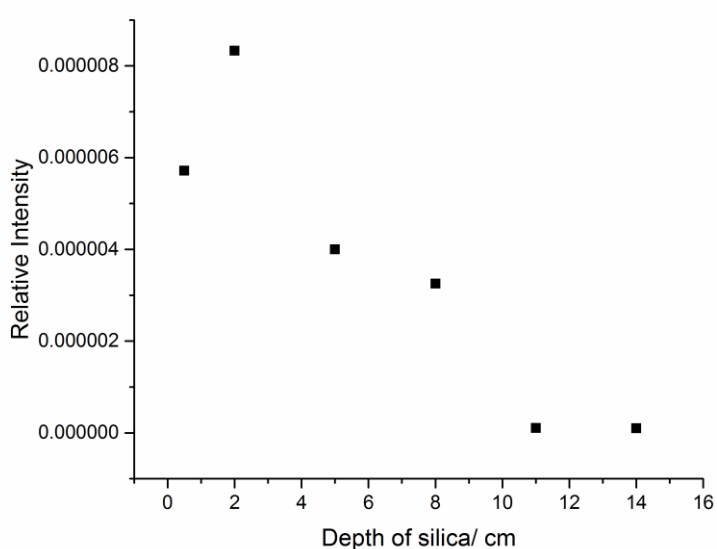


Figure 173: Variation in signal for **4.11** with silica depth

A notable decrease in radical signal was observed in Figure 173 as the different silica segments of silica analysed. While radicals can be detected down to ca. 8 cm there is a significant drop off during this range. Thus it appears that radicals can penetrate into the bulk sample support, however with significant signal loss from this process. This provides some justification for the signal decreases observed in the 'sandwich' experiments, as well as the observation of radicals beyond the initial sampling distance, by spin trapping in **Chapter 4**. Therefore, in future experiments, total sample depth will not exceed 1 cm.

### 5.3. Variation of Sampling Time

Sampling time modification provided another source of optimisation for this technique. There are two targets to these experiments. Firstly, an optimal sample time needs to be established. While a longer experiment would be expected to generate a greater signal, there are limitations to this approach, with a balance between sampling time and limit of detection required to make best use of sampling time. However, with this sampling technique, the impact of products being blown away from the support will also need to be considered. Secondly, the minimum time required for sample to be detected was essential to establish. This is key with regards to establishing limits of temporal resolution for this trapping technique under the conditions currently being tested.

#### 5.3.1. Optimisation of Sampling Time

Experiments have shown that longer sampling times provide an increased opportunity for the radical trap to be blown away from the sampling site – for example overnight experiments (ca. 16 hours) detected almost no compound after the experiment. While sample being blown away will still be a feature of experiments run at low exposure times, the overall percentage of sample blown away will reduce as exposure decreases. Therefore, as different exposure times were tested, an initial increase in signal intensity was expected, which will peak and begin to decrease as exposures get longer.

A second issue with longer sampling times is the potential for all of **2.09** to have reacted, hence resulting in no further trapped products beyond this point. However, unless the trapping molecule forms a perfect monolayer on the silica (which is highly unlikely), the material will effectively be saturated once surface material has reacted – bringing the time at which no new products will be caught considerably earlier. Radical diffusion into the bulk trapping material is unlikely: studies on radical rates of diffusion have found that these are generally lower than those of the equivalent closed shell species.<sup>270</sup> This is believed to be due to increased polarizability of radical species, leading to increased intermolecular

interactions, and as such lower diffusion rates. However, relative radical concentrations are likely to be such that sample saturation from gas phase sampling is highly unlikely.

The optimal length of sampling experiments was probed by a series of experiments at exposure times from 4 to 90 minutes. The trend from these experiments, in Figure 174, shows an increase in signal with exposure time, suggesting that the trapping material is not fully saturated over these time periods, or suffering from excessive loss due to being blown away. Therefore, experimental exposures of up to 90 minutes would be suitable for trapping. Signals from 90 minute experiments are on the same order of magnitude as experiments with a 5 minute sampling time, suggesting that 5 minute exposures can be utilised. However, as these experiments were conducted in a very simple system (i.e. only one source of peroxy radicals) it is likely that sample times greater than 5 min will be required when this methodology is applied to more diverse systems.

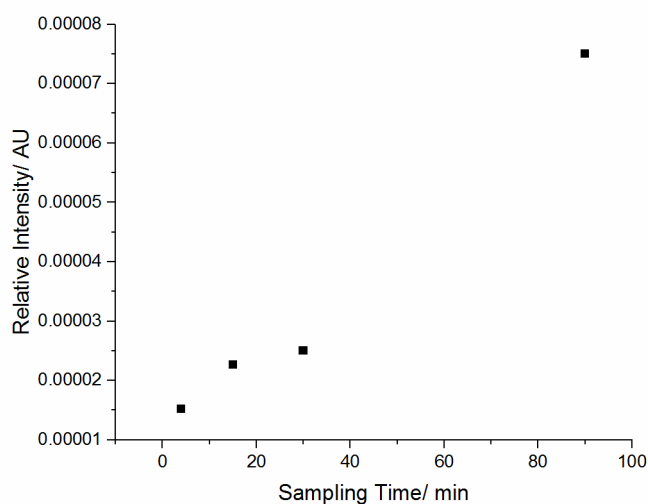


Figure 174: Change in signal for **4.11** as sampling time is modified from 4-90 minutes

### 5.3.2. Minimum Sampling Time

The minimum time required for signal detection within this system was probed in the same manner. If this methodology were to be applied to 'real world' scenarios, the ability to detect radicals with a temporal resolution of minutes, or below, would be of great use,

hence it was useful to test whether this is possible within this system prior to ‘real world’ tests (**Chapter 7**). As an example this would enable the variation in radicals present from reactions of emissions from rush hour traffic to be easily monitored. Results from short exposure times are presented below in Figure 175.

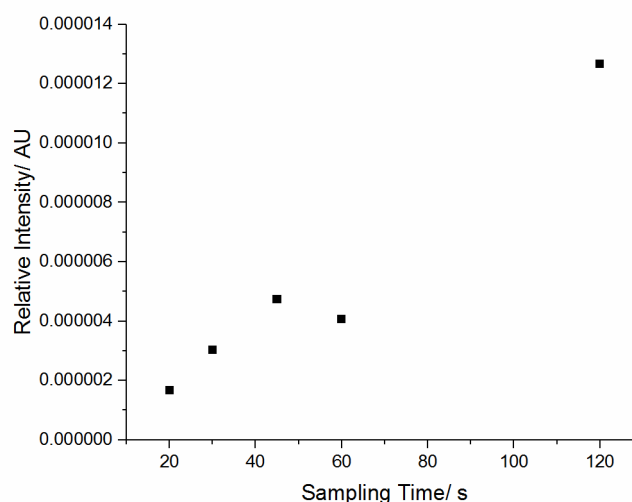


Figure 175: Change in signal for **4.11** as sampling time is modified between 20-120 seconds

It appears that signal can be detected with sampling times as low as 20 s. This is a promising result, suggesting that detection limits (for **4.11**) are reasonably low, and that temporal resolutions of under a minute are possible within this system. This compares well to literature methods of radical detection. LIF based techniques have typical temporal resolutions up to 100 s, while resolutions of up to 500 s have been recorded for DOAS experiments.<sup>271</sup> Meanwhile, MI-ESR based measurements have significantly higher temporal resolutions of ca. 30 min, but CIMS based techniques are capable of resolutions of a few seconds, significantly better than that achieved here.<sup>19,272</sup> However, the difference in signal between exposures of 1 and 90 minutes is considerable between Figure 174 and Figure 175, so at this stage in the research longer sampling times up to 90 minutes will be much more useful to pursue during future experiments.

It should however be mentioned that the low detection times of this system are unlikely to be reproducible in sampling of real outdoor/indoor sampling systems. This system

utilises a single reaction in order to trap a range of radicals – while several radicals are indeed detected, the concentrations of these species are significantly higher than predicted at atmospheric levels. The nature of this trapping technique means that in a mixture of radicals, the amount of each radical captured is likely to decrease as the total number of different radical species increases. Hence it is unlikely that temporal resolutions from the radical trapping technique will be able to reach levels of detection from field measurements via LIF, DOAS or CIMS.<sup>19,271,272</sup>

A final area of note for these experiments regards the stability of the non-radical species formed upon reaction of **2.09** with a radical. One of the key aspects of this technique is for the reaction products to be analysed offline, which requires the trapped species to survive for an extended period of time. Here, products of radical reactions with **2.09** (e.g. **4.11**, **4.02**) can be identified from reaction mixtures that have been stored at 253 K for up to four weeks. Therefore, it appears that the trapping technique fulfils the key requirement of products being sufficiently stable for off-line analysis.

## **5.4. Radical Capture from a Low Temperature Plasma**

### **5.4.1. Plasma Overview**

Gas phase radicals from plasma are being increasingly studied. Plasma is commonly termed ‘the fourth state of matter’, however this is not technically true. This was proven by Burm, by examining the phase transitions from gas to plasma, which are different to those between the traditional three states.<sup>273</sup> Meanwhile plasma can be described as a gas consisting of ions and electrons. Other species, such as excited oxygen or radicals will also often present within the plasma, depending on the composition of the feed gas.<sup>274</sup>

There are two main types of plasma: high and low temperature. High temperature plasmas are often regarded as plasma in which fusion reactions occur, with the sun being a classic example.<sup>275</sup> The constituents of this type of plasma will all be in thermal equilibrium.<sup>276</sup> However, this is not the case for low temperature plasma, which will have

electrons at a significantly greater temperature than the remaining constituents.<sup>276</sup> As such, low temperature plasma will also often be described as 'room temperature' plasma.<sup>277</sup> These low temperature plasmas are a mild source of highly reactive radicals, which are generated at approximately room temperature and atmospheric pressure.

Low temperature plasmas are often ignited with a helium feed gas, with various admixtures to generate the reactive species.<sup>278</sup> In the presence of an oxygen admixture, species including ozone or superoxide can be formed, while the addition of water can result in the formation of  $\cdot\text{OH}$  or  $\cdot\text{H}$ .<sup>279</sup> With an air admixture  $\text{NO}$  and  $\text{NO}_2$  are also expected to form.<sup>280</sup> Some work has already been done regarding the identification of species from a low temperature plasma. Cavity enhanced absorption has been utilised by Gianella et al. to prove the presence of the  $\text{HO}_2$  radical.<sup>281</sup> Meanwhile Gorbanev et al. used spin trapping (with DMPO) to characterise some of the radicals from a low temperature plasma system, with  $\cdot\text{H}$ ,  $\cdot\text{OH}$ , and  $\text{HO}_2\cdot$  identified from plasma formed with a water-saturated gas flow.<sup>264</sup> Similar spin trapping experiments with the PTIO spin trap have found that the addition of air enabled the detection of species such as  $\text{NO}\cdot$ .<sup>282</sup>

There are many proposed low temperature plasma applications. Sugiyama et al. described the use of plasmas for catalyst preparation, using thermal plasma to replace the standard calcination process.<sup>283</sup> Here, the plasma treated catalyst was found to be more selective, owing to surface layers of catalyst having been reduced during the treatment. Biomedical applications of plasma are also being explored. Plasma can be used to kill bacteria, as shown by Laroussi et al., with hydroxyl or  $\text{NO}_2$  radicals believed to be responsible for this.<sup>284</sup> However, some influence from UV irradiation from the plasma is also likely.<sup>285</sup> Laroussi et al. have also developed a device suitable for handheld application of low temperature plasma, with no heating observed from the skin contact with the plume.<sup>277</sup>

#### **5.4.2. System Design for Capture of Radicals from Plasma**

Radical trap **2.09** can be applied to detect radicals from a low temperature plasma. Detection was conducted using the octadecyl silica support at a ratio of 3.3:1, as discussed

above. The **2.09** doped silica was placed in a small cartridge, positioned 2 cm from the lower electrode, as illustrated in Figure 176. After the experiment, this is extracted with DCM and analysed by MS, in the same manner as the experiments described previously.

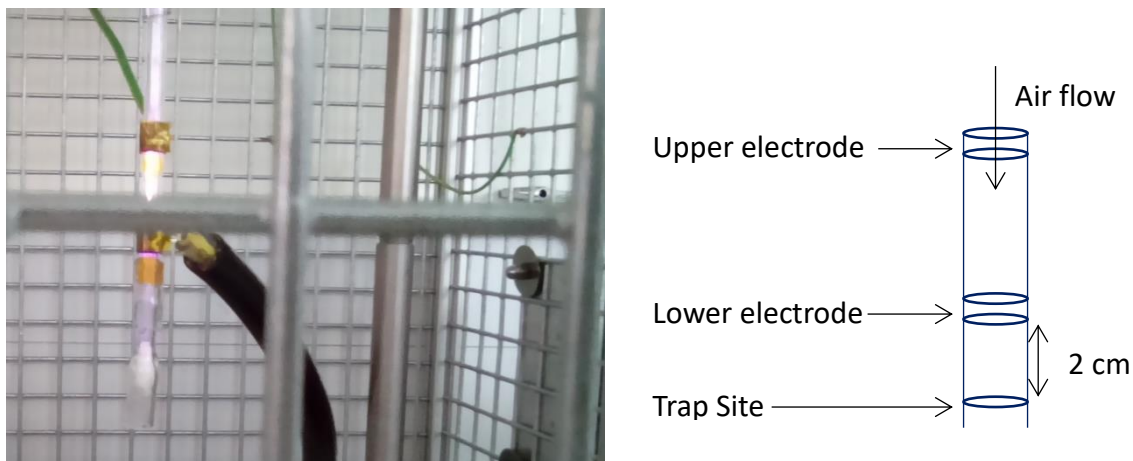


Figure 176: Scheme for radical trapping from plasma

#### 5.4.3. Detection of NO<sub>x</sub> Adducts

Sampling experiments were conducted at 20 kV, 10 mA, 24.8 kHz and 2 L min<sup>-1</sup> helium gas flow. The feed gas composition can be changed to generate different radical species. Experiments using 1% air will contain nitrogen, and so would be expected to produce NO<sub>x</sub> species. Therefore, radical adducts **5.01** and **5.02** (Figure 177) are expected to be detected from the plasma system, from the capture of the nitrogen centred NO and NO<sub>2</sub> radicals.<sup>286</sup>

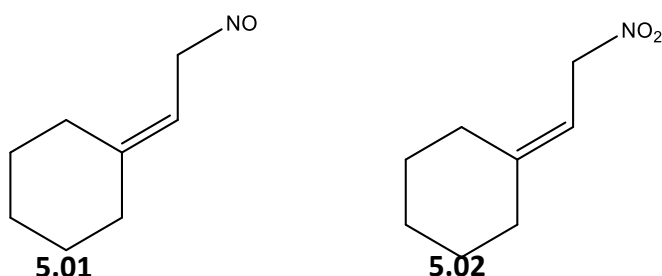


Figure 177: **5.01** and **5.02**, from **2.09** capturing NO and NO<sub>2</sub> respectively

These species are of interest regarding future atmospheric measurements, for example NO<sub>x</sub> is known to play a key role in the formation of photochemical smog – reducing air

quality severely in urban environments, with NO<sub>x</sub> emissions from diesel vehicles significantly impacting on human health.<sup>287</sup> Indeed, NO was detected in plasmas containing air, while the species is not detected in nitrogen free reactions. However, there is no indication of the NO<sub>2</sub> species **5.02** being detected. These are shown in Figure 178.

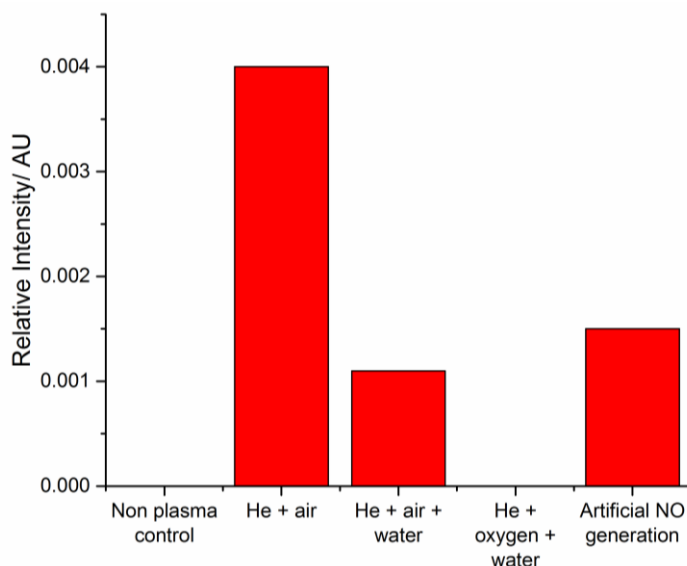


Figure 178: Detection of **5.01** from various plasma experiments

In order to confirm the origin of **5.01**, a control reaction was conducted whereby NO was generated through the reaction between dilute nitric acid and copper (equation 23), with the gas produced blown over a sample of **2.09**.<sup>288</sup> This resulted in the detection of **5.01**. Increasing the concentration of nitric acid would produce NO<sub>2</sub>, as shown in equation 24. However, again NO<sub>2</sub> was not trapped by **2.09**, suggesting that this trapping technique is not sensitive to NO<sub>2</sub>. While detection of NO<sub>2</sub> would be useful, this is not too detrimental to future applications of the trapping system, as other methods (e.g. conversion of NO<sub>2</sub> to NO and detection by chemiluminescence) are applied to atmospheric NO<sub>2</sub> measurement.



The detection of the NO radical has the potential to be very important for atmospheric reactions. Concentrations of NO are expected to be noticeably greater than RO<sub>2</sub> radical species, which could potentially swamp the detection technique with **5.01**. However, it should be remembered that NO concentrations in the plasma system are likely to be very high, compared to atmospheric concentrations (low ppt to hundreds of ppb) so the affinity for NO trapping may be such that detection is unlikely to be dominated by **5.01**. Indeed, Chauvin et al. detected NO<sub>x</sub> species at over 100 μM within a low temperature plasma by spin trapping species formed from plasma.<sup>279</sup> The failure to detect NO<sub>2</sub>, a species known to be present in this type of low temperature plasma, is also interesting.<sup>284</sup> An explanation is that while this species is present, concentrations relevant to the other detected radical species, are significantly lower. Alternatively, it may be an indication that relative rates of reaction between **2.09** and the NO or NO<sub>2</sub> radicals are significantly different.

In order to provide evidence of reproducible self-consistency within these plasma experiments, another trapping molecule, **2.11**, was exposed to the plasma system (Figure 179). This molecule exhibited the same reactivity as **2.09** with regards to capture of NO and lack of NO<sub>2</sub> capture.

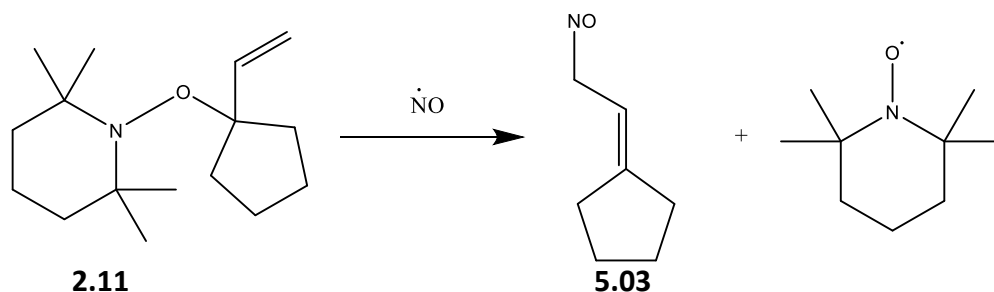


Figure 179: Formation of **5.03** through trapping of NO with **2.11**

Detection of **5.03** featured a considerably diminished signal, relative to **5.01**, as shown in Figure 180. This would not be expected on the basis of radical reactivity – both species are expected to react in a similar manner with radicals. One explanation relates to bond strength. The C-O bond in **2.11** is expected to be stronger than that in **2.09**, hence creating the potential for **2.11** to be less reactive. This is suggested by the longer lifetime of **2.11** prior to rearrangement to **2.11'**, compared to that for **2.09** and **2.09'**, as discussed in

**Chapter 2.** However, given that such a phenomenon was not obvious within reproducible self-consistency experiments for the  $\alpha$ -pinene systems, this seems an unlikely explanation.

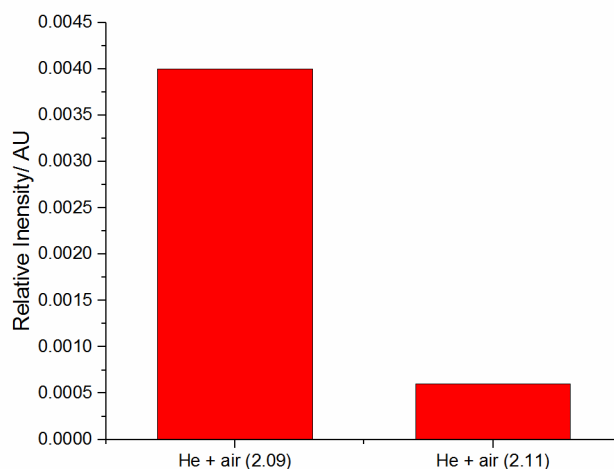


Figure 180: Comparison of signal for captured NO from **2.09** and **2.11**

Alternatively, this may be due to the increased volatility of **2.11** relative to **2.09**. This could result in more trap, and trapped products, being removed by the gas flow during the experiment, thus resulting in a diminished signal for these species. Unlike the ozonolysis system, the plasma trapping site warms considerably during plasma exposure. As such, this has the potential to result in more volatile product removal during the experiment.

Plasma experiments were also conducted over a range of sample times. While this has already been evaluated above, this is a very different system, likely to feature significantly different radical concentrations, leading to different trends to those observed previously. Figure 181 suggests that over 0.5 – 10 minute exposure times, the signal for **5.01** does still increase. However, the maximum sampling time is considerably lower than those utilised previously. This is due to the experimental set up used – as the experiment continues, plastic tubing attaching the sample tube to the plasma apparatus warms considerably, and eventually deforms to the extent that the sample tube detaches from the apparatus.

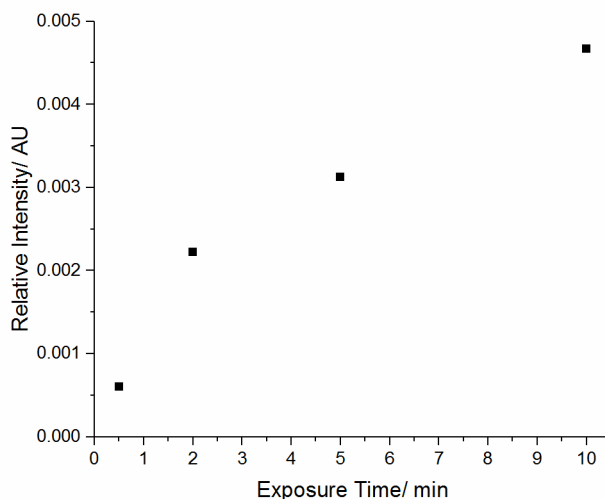


Figure 181: Variation in signal for **5.01** with exposure time

#### 5.4.4. Detection of HO<sub>2</sub><sup>·</sup> and H<sup>·</sup> Radicals from a Room Temperature Plasma

Within the plasma, the addition of water vapour enables the creation of hydroperoxyl radicals.<sup>264,281</sup> This species, **4.11**, has been observed in other atmospheric systems (**Chapter 4**), and was again observed here. Variation in signal for **4.11** with experimental duration exhibits a general increase (Figure 182) as was the case for NO adduct **5.01**. Reproducible self-consistency experiments conducted with **2.11** also detected the HO<sub>2</sub> adduct, although again this species was present at a noticeably lower intensity.

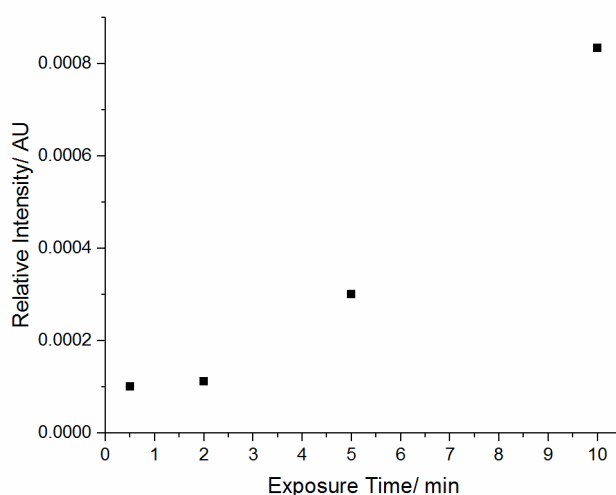


Figure 182: Variation in signal for **4.11** as exposure time changes

Another species that would be expected from these systems would be the hydrogen radical.<sup>264,289</sup> However, the adduct expected from capture of this species, **2.14** (Figure 183, was not observed. The most likely reason for this lies with the volatility of the product compound – evaporation during plasma exposure, or even during the extraction process from silica, would not be unexpected for this species, with a boiling point of ca. 135°C.<sup>169</sup>

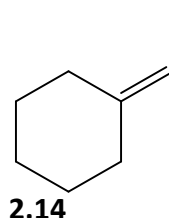


Figure 183: Expected product from hydrogen radical capture with **2.09**

A less volatile trap, **2.16**, was employed in order to attempt the detection of this species. Application of this trap was successful in capturing the hydrogen radical, with a species corresponding to the same mass as **5.04** observed by mass spectrometry. Fragmentation of this species would be expected to produce the ions shown in Figure 184. MSMS analysis of the  $[M+H]^+$  signal for **5.04** indeed provided evidence of this fragmentation, with signals from both possible ions (109 m/z and 72 m/z) observed in Figure 185. This is a good indication that **5.04** is indeed being observed, thus confirming capture of the hydrogen radical from this reaction.

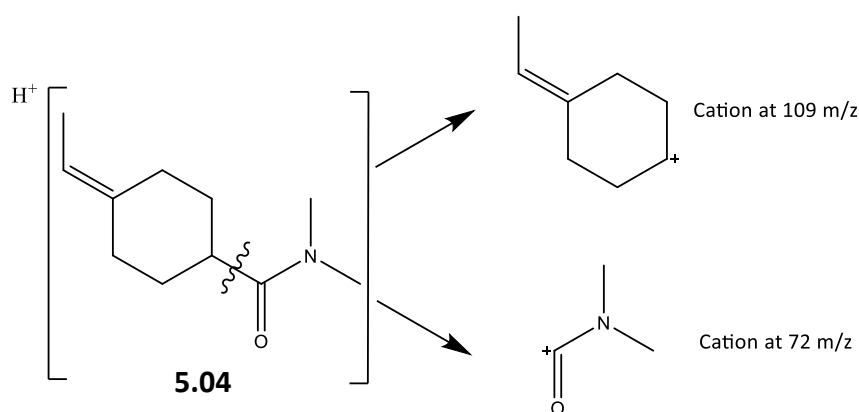


Figure 184: Possible cations from fragmentations of **5.04**

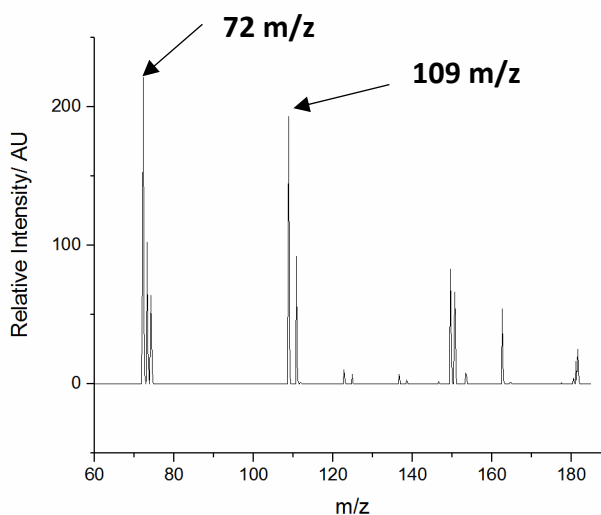


Figure 185: Fragmentation of **5.04**

## 5.5. Conclusions

Overall, optimised conditions for gas phase radical trapping experiments were established. Of a range of materials, octadecyl functionalised silica was found to be an effective trap support. The optimal packing was determined to be a flattened layer of trap, with an error of ca. 2.2 % with this arrangement. The loading of the sample should be at least 4 mg, with a high ratio of trap to support to ensure sufficient monolayer formation. Trapped products were detected at exposures down to 20 s, however there were noticeably improved signals at exposures of up to 90 min. This is very promising for future applications where a high degree of temporal resolution will be required, given the reactivity and short lifetimes of radicals. The trapped reaction products also appear to be sufficiently stable that they can be stored for several weeks prior to offline analysis.

The optimised gas phase trapping methodology was applied to a low temperature plasma system. This showed evidence for the capture of the NO radical, although the NO<sub>2</sub> radical could not be observed. Other species such as the HO<sub>2</sub> radical were also detected from this plasma system. A less volatile trapping compound (**2.16**) was also successfully deployed for the capture of the hydrogen radical from a plasma system.

## 6. Detecting Products from Reaction between Alkanes and the Hydroxyl Radical

### 6.1. Introduction

#### 6.1.1. Atmospheric Hydrocarbons

There are a wide range of non-methane hydrocarbons emitted into the atmosphere, from both biogenic and anthropogenic sources. As discussed in **Chapter 1**, radical reactions (i.e. with  $\cdot\text{OH}$  or  $\text{NO}_x$ ) will be the dominant method of atmospheric degradation for these species.<sup>290,291</sup> Reactions of VOCs with  $\text{NO}_x$  will lead to ozone formation, as well as SOA and species such as PAN, key components of photochemical smog.<sup>291–293</sup> Alkanes will predominantly react with  $\cdot\text{OH}$ , leading to the formation of peroxy radicals under atmospheric conditions. Indeed, the lifetime of propane with respect to  $\cdot\text{OH}$  reactions is ca. 11 days, while it is expected to be several years for reactions with  $\text{NO}_3$ .<sup>18</sup> As oxidation of the alkane proceeds, the products will often become less volatile, leading to SOA formation, particularly in the presence of  $\text{NO}_x$ .<sup>294</sup> For example, Lim et al. found SOA yields up to ca. 53% for  $\text{C}_{15}$  alkanes following reaction with  $\cdot\text{OH}$  in the presence of  $\text{NO}_x$ .

The wide ranging emissions of hydrocarbons to the atmosphere are under a large degree of scrutiny, with many studies being conducted into the environmental impact of anthropogenic sources, such as fuels and solvents. For example, the impact of different fuel blends (e.g. biodiesel compared to diesel) will have an impact on the types, amounts and reactivity of hydrocarbons emitted into the atmosphere. This was studied by Payri et al., showing how  $\text{C}_2$ - $\text{C}_{12}$  emission concentrations and relative amounts varied with the percentage biodiesel employed.<sup>295</sup> An example of the importance of fuel emissions can be found in Dunmore et al.<sup>296</sup> They found that diesel originating hydrocarbons can, in winter, dominate the reactivity of hydroxyl radicals in London, as well as making a significant contribution to ozone and SOA production. Other important sources of anthropogenic

hydrocarbons within the atmosphere include industrial emissions, for example oil refining or biomass burning.<sup>297</sup>

Biogenic hydrocarbons, emitted from a range of natural sources such as vegetation, are also prevalent throughout the atmosphere.<sup>298</sup> Globally, these emissions are estimated to be an order of magnitude greater (by mass) than anthropogenic emissions.<sup>299</sup> Monoterpenes such as  $\alpha$ -pinene, the chemistry of which is described in more detail in **Chapter 4**, and isoprene, the most abundant non – methane biogenic hydrocarbon in the natural atmosphere, have been found to be the most prevalent examples.<sup>300</sup> These biogenic species, when mixed with anthropogenic NO<sub>x</sub> emissions, have also been found to play an important role in the formation of photochemical smog, as shown by Chameides et al.<sup>301</sup> Field experiments by Hamilton et al. have also found a contribution from biogenic species (isoprene) to the composition of SOA, supporting evidence from smog chambers by Hoffmann et al.<sup>224,302</sup>

Reactions of hydrocarbons in the atmosphere can lead to a wide range of oxidised radical and non-radical products. Yu et al. conducted studies providing evidence for the formation of carbonyl groups from reactions of  $\Delta$ -3-carene by derivatisations with *o*-(2,3,4,5,6-pentafluorobenzyl)hydroxylamine (PFBHA), and carboxylic acid or alcohol groups by functionalisation with *n,o*-bis(trimethylsilyl)-trifluoroacetamine (BSTFA), shown in Figure 186.<sup>303</sup> These derivatisations enabled simple detection of these species by GC, with subsequent MS analysis indicating the presence of several previously undetected compounds (e.g. 2,2-dimethyl-3-(formylmethyl)cyclobutane-formic acid). The expected change in carbon to oxygen ratio within aerosol, caused by the oxidation process, has been examined for compounds such as *n*-decane by Lambe et al., finding a steady increase with exposure to  $\cdot$ OH for flow reactor studies.<sup>304</sup>

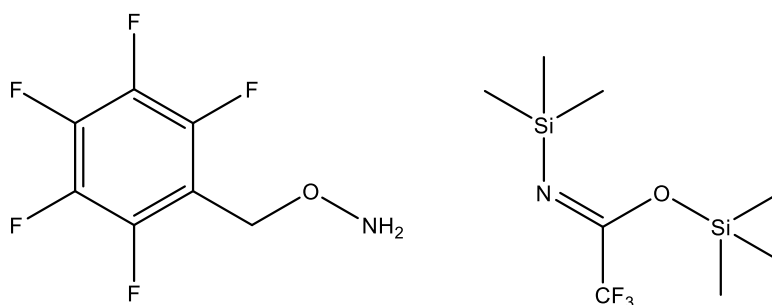


Figure 186: Structures of PFBHA and BSTFA used by Yu et al. for carbonyl and alcohol functionalisation respectively.<sup>303</sup>

Reaction with the hydroxyl radical is one of the dominant methods for the removal of alkanes from the atmosphere, with other reactions including that between hydrocarbons and chlorine radicals.<sup>305</sup> For example, Altshuller suggests  $\cdot\text{OH}$  reactivity is responsible for a lifetime of 14 hours for *n*-nonane within the atmosphere, under summer daylight conditions.<sup>306</sup> This is much longer than that of alkene containing species, such as  $\alpha$ -pinene which would be expected to have an atmospheric lifetime of ca. 6 hours.<sup>307</sup> Under urban atmospheric conditions (i.e. high concentrations of VOC and  $\text{NO}_x$ ), long chain alkane degradation will also likely lead to the formation of SOA, contributing to photochemical smog formation, hence significantly impacting on air quality and health.<sup>294,296</sup> However, the rate of reaction between hydroxyl radicals and atmospheric hydrocarbons will vary, according to species structure and composition. For example, Nishino et al. studied the reaction between  $\cdot\text{OH}$  and a range of anthropogenic alkenes, finding that the rate of this reaction appears to increase with carbon number, due to both hydrogen abstraction and alkene addition reactions.<sup>308</sup>

### 6.1.2. Aims

The primary goal of the experiments outlined in this chapter is to test radical trapping methodology using the radical trapping molecules designed and synthesised in **Chapter 2**. Quantitative time resolved measurements of gas phase radical species, in a simpler system than that employed for  $\alpha$ -pinene ozonolysis, will be performed. Application of this

trapping system to reactions of n-alkanes with hydroxyl radicals can be used to provide experimental confirmation of radical species predicted to be present via the MCM.<sup>229,230</sup>

An attempt will also be made to calibrate this trapping system, using the same calibration technique as is used for calibration of FAGE for methyl peroxy radicals and applied to alkane +  $\cdot\text{OH}$  reactions.<sup>309</sup> In addition to this, the reaction will be modelled using simple flow tube box model simulations, with the model used to compare the variation in the kinetic profiles of radical products detected within flow tube experiments with modelled profiles.

## 6.2. Reactions with Long Chain Alkanes

The degradation chemistry of almost all atmospheric hydrocarbons occurs through radical intermediates, and so **2.09**, **2.11** and **2.13** can be used to study and understand these chemical mechanisms: hence their impact on the chemistry of the atmosphere. In addition to ozonolysis based radical systems discussed in **Chapter 4**, there are other systems of interest to study using trapping molecules. One such important chemical system is the reactions of alkanes with the hydroxyl radical, in the presence of oxygen.<sup>310</sup> Alkanes are utilised because, whilst atmospherically important, their chemistry is considerably simpler than the previously studied monoterpene systems (**Chapter 4**). The MCM shows that  $\cdot\text{OH}$  will initially abstract a hydrogen (from a range of C-H sites), with the carbon centred radical originally formed rapidly reacting with oxygen present in the system, to form a range of peroxy radicals as is shown below in Figure 187.<sup>229,230</sup>

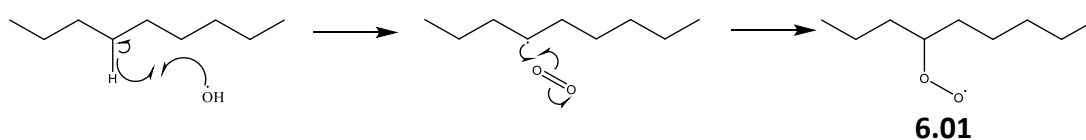
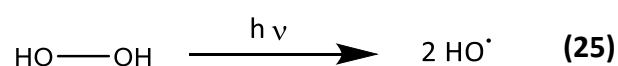


Figure 187: Expected mechanism for the formation of a peroxy radical via hydrogen abstraction from n-nonane (most likely  $\text{RO}_2$  species is shown)<sup>229,230</sup>

Once formed, it would be expected that the peroxy radicals can undergo further reactions, including fragmentation and hydrogen shift reactions, followed by subsequent reactions with oxygen producing further oxidation products.<sup>228</sup> These radicals would be expected to be trappable with the developed trapping family from **Chapter 2**: thus a range of different radical adducts are anticipated to be detected.

### 6.2.1. Radical Generation system

A system was designed to conduct the reaction between hydroxyl radicals and alkanes. Hydrogen peroxide was introduced into the system by a 3 L min<sup>-1</sup> air flow being bubbled through a 30% hydrogen peroxide solution. From this, hydroxyl radicals were generated via photolysis with a 100 W UV lamp at 405 nm, as in equation 25.



The alkane was introduced into the system by an air flow being passed over the liquid alkane within a flask. This hydrogen peroxide-alkane mixture was irradiated by a 100 W UV lamp, and blown along a flow tube, in the presence of oxygen, towards a layer of radical trap deposited on an octadecyl silica support, in the same manner as has already been accomplished for ozonolysis reactions. Subsequent extraction of this trapping layer then yielded the captured radical species from this reaction. The sampling time point can be varied by moving the trapping site closer/further from the point of irradiation, therefore facilitating temporal sampling of the chemical evolution of the reaction system. An image of the reaction set-up is given in Figure 188 and Figure 189.

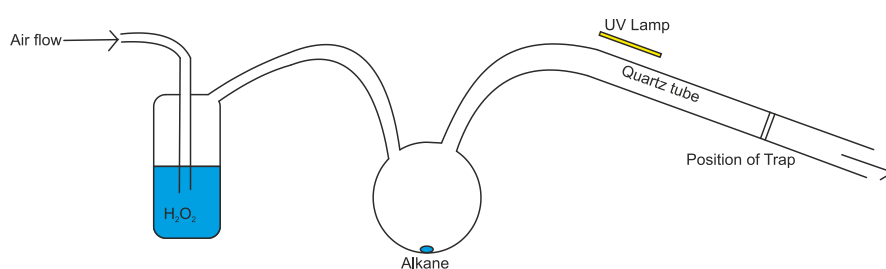


Figure 188: Scheme of the alkane reaction and trapping system

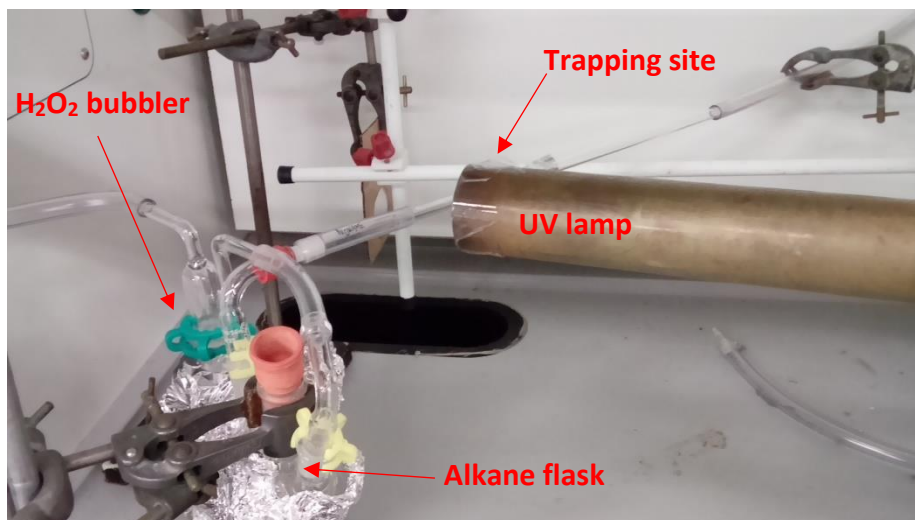


Figure 189: Photo of alkane reaction and trapping system

### 6.2.2. Initial Peroxyl Radical Detection

Initial studies were conducted using n-dodecane and n-decane. However, signals produced from analysis of these experiments were very weak (Figure 190), with the initial trapped peroxy species from n-decane only just detectable (Figure 191). This was attributable to the vapour pressures of these systems as opposed to poor radical trapping. The vapour pressure of n-dodecane is calculated as approximately 27 Pa ( $1.09 \times 10^{-5}$  mol  $\text{dm}^{-3}$ ) at room temperature, using the Antoine equation (equation 26) with parameters taken from Maia de Oliveira et al.<sup>311</sup> This is noticeably lower than the 650 Pa ( $2.62 \times 10^{-4}$  mol  $\text{dm}^{-3}$ ) for  $\alpha$ -pinene.<sup>312</sup>

$$\log P = A - \frac{B}{T + C} \quad (26)$$

Where P = Vapour Pressure/ KPa, T = Temperature/ K, A B and C = Antoine parameters for the compound being examined.

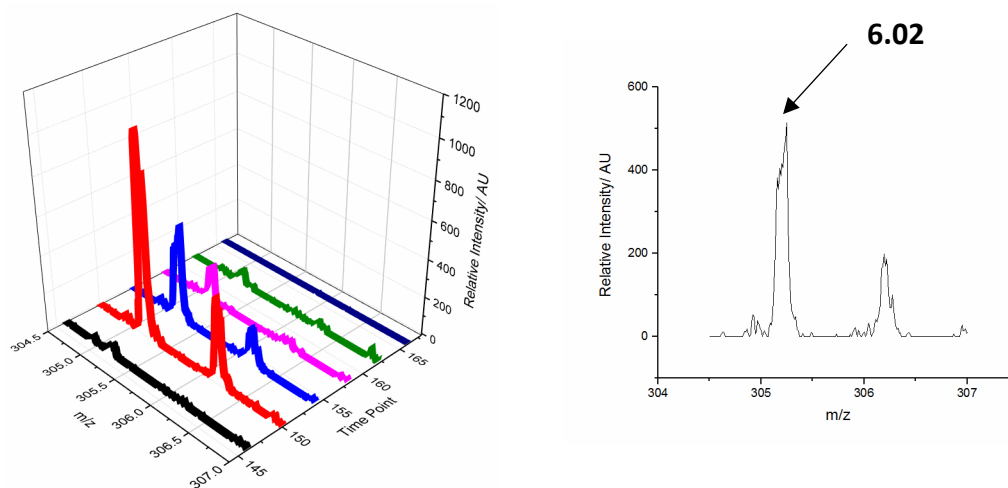


Figure 190: MS for **6.02** from n-decane

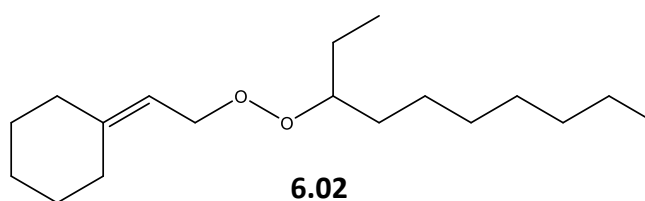


Figure 191: Structure of **6.02**

As such, experiments with n-nonane as the starting alkane were studied. As would be expected from a higher vapour pressure of 450 Pa ( $1.82 \times 10^{-4}$  mol dm<sup>-3</sup>) at room temperature (experimentally determined by Carruth et al.), signals could be easily detected from these n-nonane based reactions.<sup>313</sup> The first signal identified (Figure 192) is that attributable to **6.03**, the captured initial peroxy radical formed after hydroxyl attack in air (Figure 193), the formation of which is shown above in Figure 187.

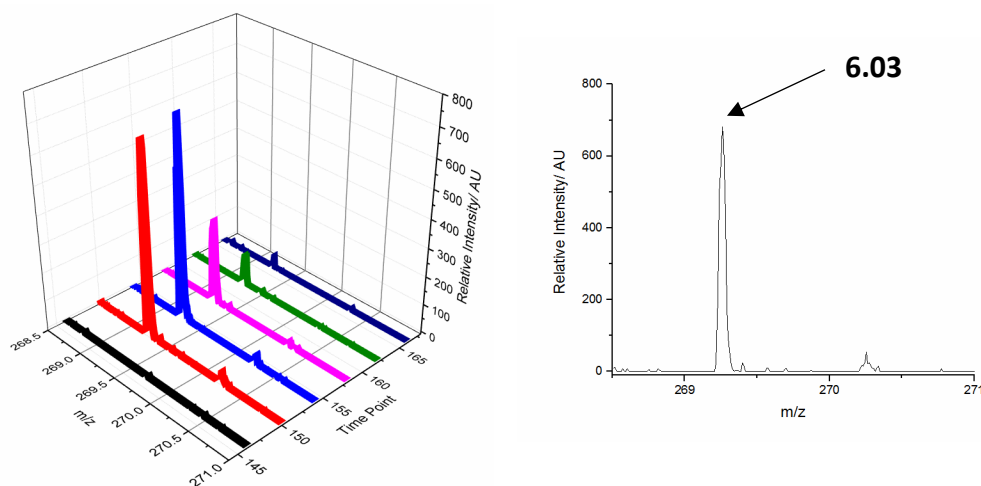


Figure 192: MS signal for **6.03**, captured **6.01**

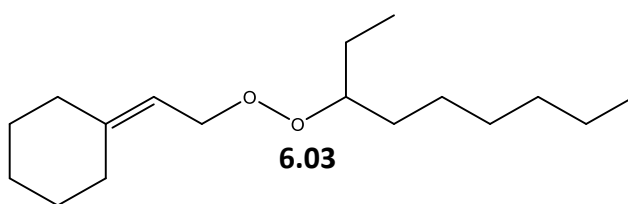


Figure 193: Structure of adduct **6.03**

The detection of this initial peroxy species is very useful, as it provides evidence that hydrogen abstraction and subsequent peroxy radical formation are indeed occurring, as is predicted by the MCM.<sup>229,230</sup> The carbon radical preceding this species does not appear to be detected, likely because of the fast reaction between oxygen and the carbon radical.<sup>314</sup> This agrees with the suggestion made in previous gas phase experiments (**Chapter 4**) that the rate of trapping of carbon centred radicals is slower than the rate of reaction between oxygen and a carbon radical. Given this is a fast reaction, with literature suggesting rates of at least  $10^9 \text{ M}^{-1} \text{ s}^{-1}$  at room temperature, this does not appear to be an unreasonable assumption.<sup>314</sup> The lowest residence time studied is 0.017 s, and a rate constant of  $10^9 \text{ M}^{-1} \text{ s}^{-1}$  suggests that all carbon centred radicals present here will have reacted with oxygen by this time. It is important to note that the location of the radical on nonane is simplified in these schemes. In reality, hydrogen can be abstracted at any point along the carbon chain, hence a range of structural isomers are likely to be present for this, and other radicals, with these for **6.03** shown in Figure 194.

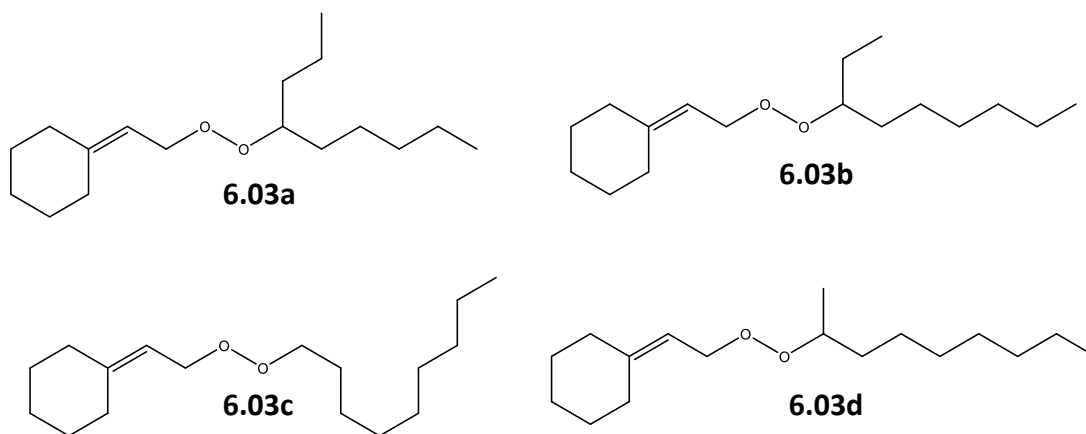


Figure 194: Different possible isomers of **6.03**

Structure-activity relationships suggest that the radical is most likely to be formed on carbons 3,4,5,6 and 7 on the chain, with reaction at terminal carbons highly unlikely.<sup>310,315</sup> The three different environments for n-nonane hydrogen abstraction are shown in Figure 195. However, the target of this methodology is currently simply the detection of these species, therefore elucidation of the exact experimental ratios of each isomer is not pursued. As such, figures throughout will treat the reaction as if it has occurred on C3 (or C7), which is consistent with the presentation of reactions given within the MCM.<sup>229,230</sup> As such any figures showing, for example, **6.03**, in reality show a mixture of isomers **6.03a-d**.

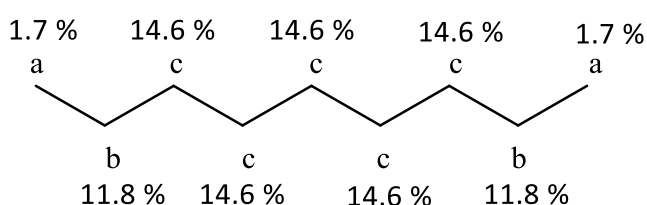


Figure 195: Percentage of attack at each carbon environment for hydrogen abstraction from n-nonane using structure activity relationships from Kwok et al.<sup>315</sup>

### 6.2.3. Detection of Further Peroxyl Radicals

After the formation of the initial peroxy radical, there are a number of radicals that would be expected to form. One such species is an RO<sub>2</sub> species formed via a 1,5 hydrogen shift

in the isomerisation of the alkoxy radical (Figure 196), a reaction that is predicted by the MCM to occur within this system.<sup>228</sup> This reaction occurs via an  $RO_2 + RO_2$  reaction which, owing to the amount of  $RO_2$  radicals expected to be in this experimental system, was expected to be a common reaction type observed. Indeed, it has been noted in the literature that this reaction type is often over represented in lab studies compared to field studies, due to the high relative concentrations of alkane in laboratory systems compared to those in the real atmosphere.<sup>316</sup> However, in the real atmosphere,  $RO_2 + NO$  reactions which will be dominant loss routes for  $RO_2$  would also result in formation of **6.05**.<sup>229,230</sup>

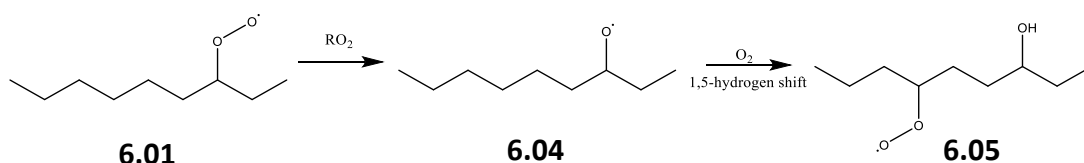


Figure 196: 1,5- hydrogen shift to form  $RO_2$  radical **6.05**

As with **6.01**, it would be expected that **6.05** would be formed via an alkyl radical. Once again there appears to be no capture of this carbon centred radical intermediate, furthering the suggestion that the rate of trapping is slower than the rate of reaction between oxygen and the carbon radical. However, there was detection of the subsequent peroxy species adduct, **6.06**, shown below in Figure 197 and Figure 198.

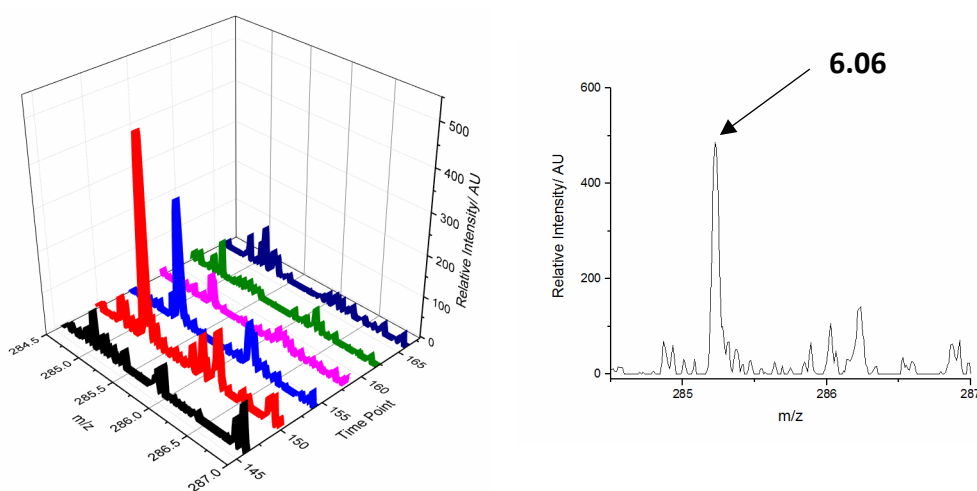


Figure 197: MS of **6.06**, trapped **6.05**

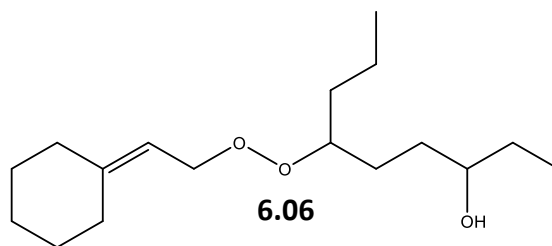


Figure 198: Structure of **6.06**, captured **6.05**.

This type of intramolecular hydrogen shift is expected from alkane systems: there are literature examples of products observed following this type of process.<sup>317</sup> For example, alkoxy radicals from hypochlorites have been found to undergo a hydrogen shift isomerisation, as shown in Figure 199.<sup>318</sup> Therefore detection of **6.06**, from this type of arrangement, is highly useful mechanistic information: confirmation that this process occurs under atmospherically relevant conditions. In particular it serves to validate the predicted mechanisms utilised within the MCM for the formation of this species.<sup>229,230</sup>

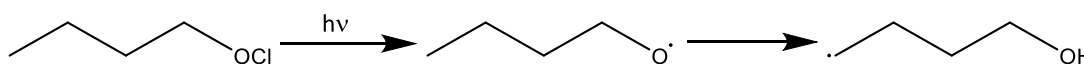


Figure 199: Example of intramolecular hydrogen abstraction from Jenner et al.<sup>318</sup>

Once formed, **6.05** was expected to form **6.09**. This reaction can proceed by three routes, shown in Figure 200: via alkoxy species **6.07**, diol **6.08**, or directly to the stable compound.

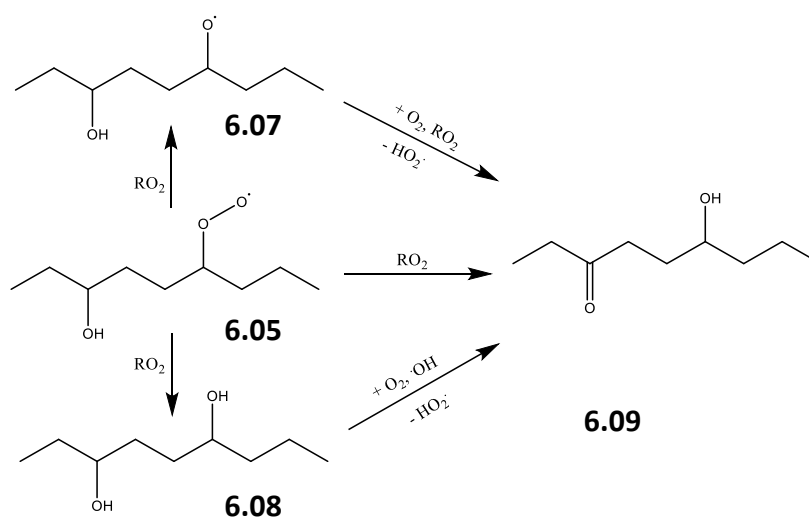


Figure 200: Routes to form **6.09** from **6.05**<sup>229,230</sup>

Of these, the route via **6.07** is the more likely, based on the MCM.<sup>229,230</sup> The rate of reaction for this step is predicted to be three times that of formation of **6.08** or direct formation of **6.09**.<sup>229,230</sup> This process also has the potential to release the hydroperoxy radical from several different routes, a species that has been identified as trapped in previous radical trapping reactions, and can indeed be observed again in these experiments (Figure 201). Within the atmosphere (i.e. at high NO<sub>x</sub> concentrations) a different route to **6.09**, via reaction of NO,<sup>29,228</sup> is also likely, but this is not relevant under the conditions applied here.

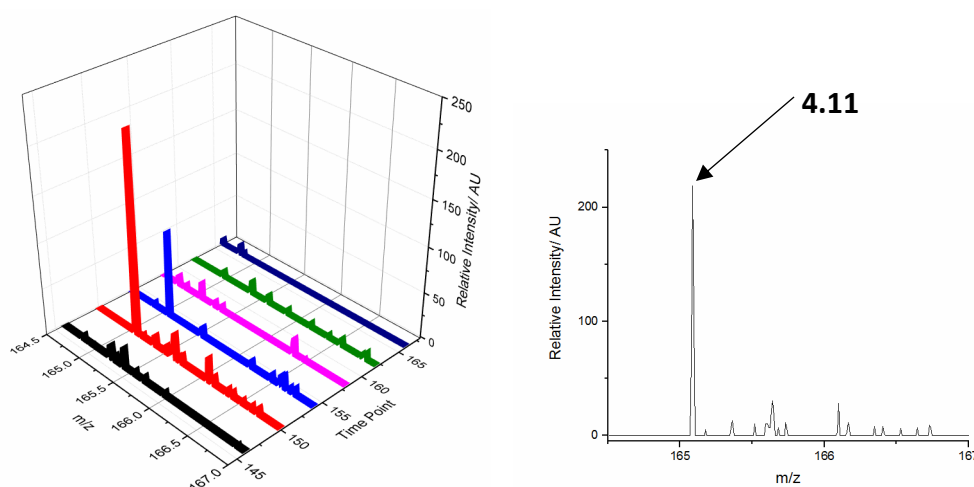


Figure 201: MS for **4.11**, captured hydroperoxy radical

The reactions that proceed via RO<sub>2</sub> + RO<sub>2</sub> reactions are likely to proceed via a tetra-oxide intermediate, as is shown in Figure 202, in the low NO<sub>x</sub> conditions studied here.<sup>319</sup>

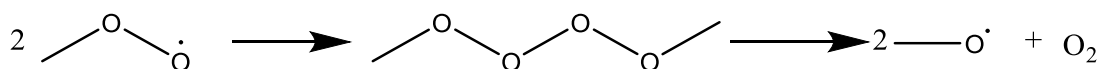


Figure 202: Formation of methyl alkoxy radicals via a tetraoxide intermediate

This type of reaction has been studied by several groups, for example Bohr et al. show that the C-O bond lengths are sensitive to the group this carbon is part of.<sup>320</sup> Shallcross et al. provided some rationalisation for the variation in reaction rates for peroxy radical self-reactions leading to tetraoxide intermediates.<sup>319</sup> The bond dissociation energies for the simplest tetraoxide, dimethyltetraoxide, were calculated by da Silva et al. to be 192, 84

and  $59 \text{ kJ mol}^{-1}$  for the  $\text{H}_3\text{C-O}$ ,  $\text{H}_3\text{CO-O}$  and  $\text{H}_3\text{COO-O}$  bonds respectively.<sup>321</sup> As such, it is clear that re-formation of the methyl peroxy radical, or forming a methyl alkoxy radical, are the most likely outcomes from this intermediate under these low  $\text{NO}_x$  conditions.

While reaction product **6.09** is not a radical, evidence for its formation can be elucidated by radical products of this compound formed following reaction with  $\cdot\text{OH}$ . Given the high concentrations of hydroxyl radical present, it is not unexpected that reactions of this type will occur, as shown in Figure 203. The compound **6.09** cannot be detected, with this region of the MS obscured by an  $\text{M}+1$  signal from TEMPO, shown in Figure 204.

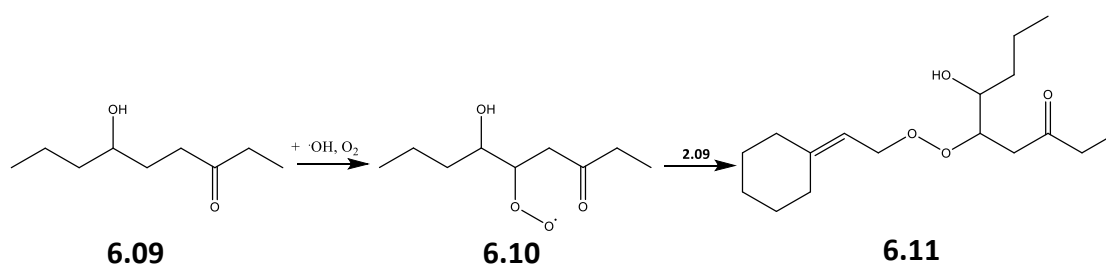


Figure 203: Formation of **6.10** and **6.11** from **6.09**<sup>229,230</sup>

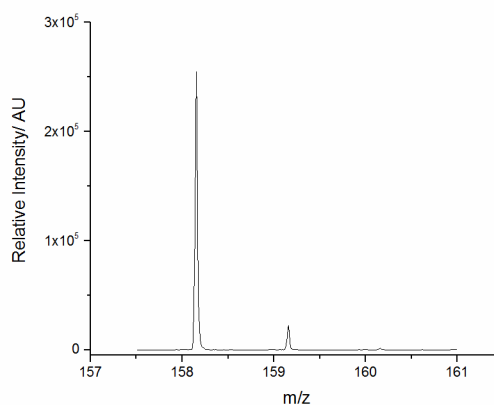


Figure 204: TEMPO  $\text{M}+1$  signal obscuring any signal for **6.09**

Formation of **6.10** was confirmed by the detection of the radical adduct species **6.11**, with the signal from the  $[\text{M}+\text{H}]^+$  ion shown in Figure 205. As such, this provides us with evidence not only for the predicted formation of **6.09** by the MCM, but also a species from its subsequent reactions.<sup>229,230</sup>

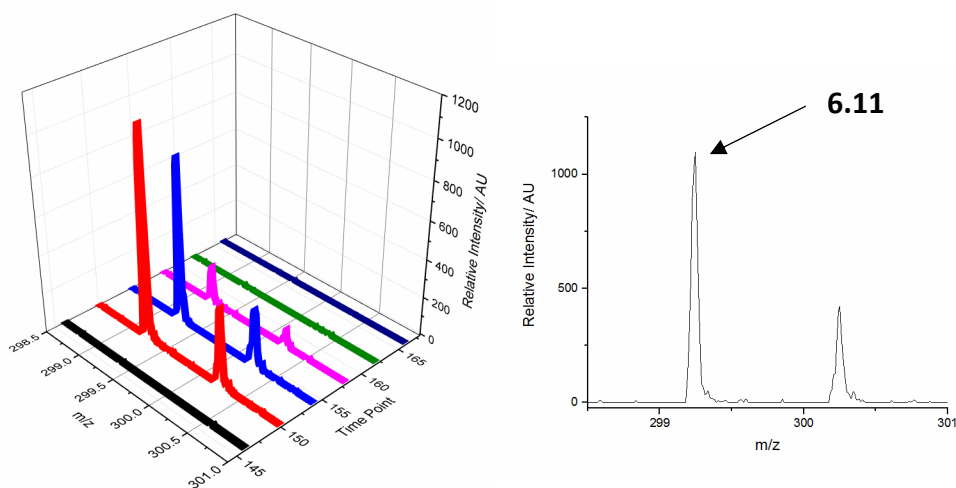


Figure 205: MS for **6.11**, captured **6.10**

Another example of this type of chemistry can be illustrated by the detection of radical species **6.12**. This compound was anticipated from the MCM to be formed via a subsequent oxidation of the earlier detected **6.01**, as shown in Figure 206.<sup>229,230</sup> Once more, this is an example of a peroxy radical expected to be formed relatively early within the n-nonane oxidation process.

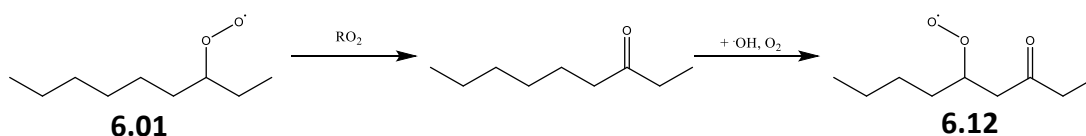


Figure 206: Formation of **6.12**, from **6.01**<sup>229,230</sup>

This compound, again, can be detected using the radical trapping methodology. As with the previous species, this signal was relatively well visible, with the  $[M+Na]^+$  ion of resulting adduct species **6.13** (Figure 208) observed here in Figure 207. Therefore, a range of several different peroxy species have now been detected from this system, proving that **2.09** is indeed successful with regards to capturing a wide range of radical chemistry from  $\cdot OH$  oxidation of n-nonane. These species also fit with the expected radicals predicted to be formed by the MCM, thus providing some confirmation regarding the modelled mechanisms.<sup>229,230</sup>

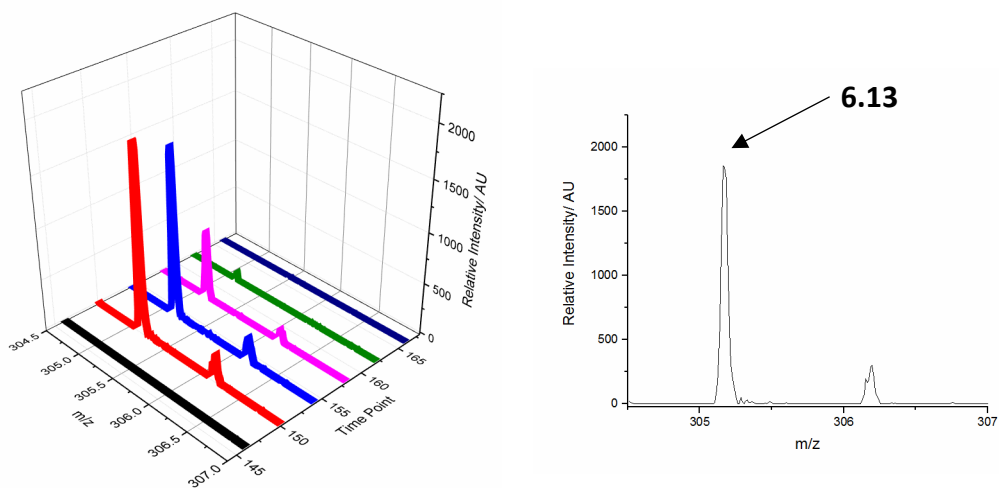


Figure 207: MS for **6.13**, captured **6.12**

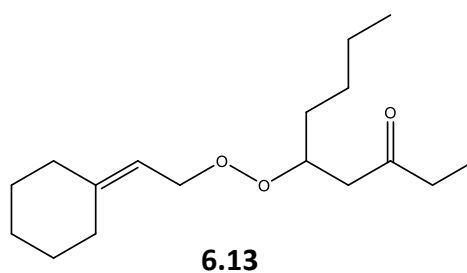


Figure 208: Structure of **6.13**

As a method of checking these results for evidence of reproducible self-consistency, the same trapping experiment was conducted with a different trapping molecule - **2.13**. As would be expected, the equivalent compounds to **6.03** and **6.06** (shown in Figure 209) were detected, with mass shifts of 12 m/z observed in Figure 211 and Figure 210 relative to compounds trapped with **2.09**.

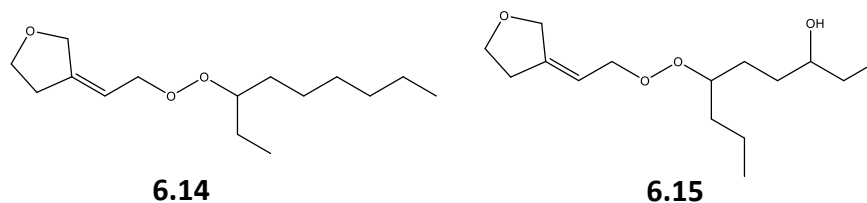


Figure 209: Structures of **6.14** and **6.15**, trapped **6.01** and **6.05** respectively

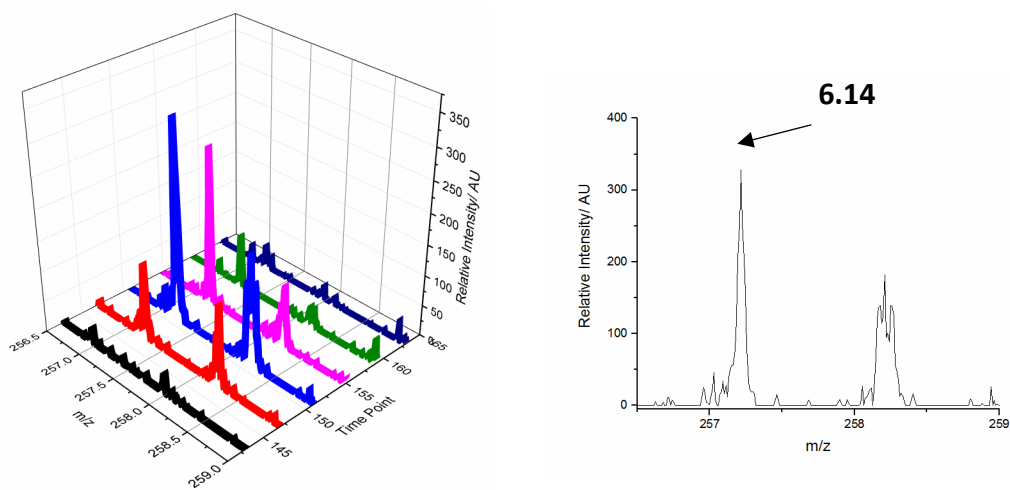


Figure 210: MS signal for **6.14**

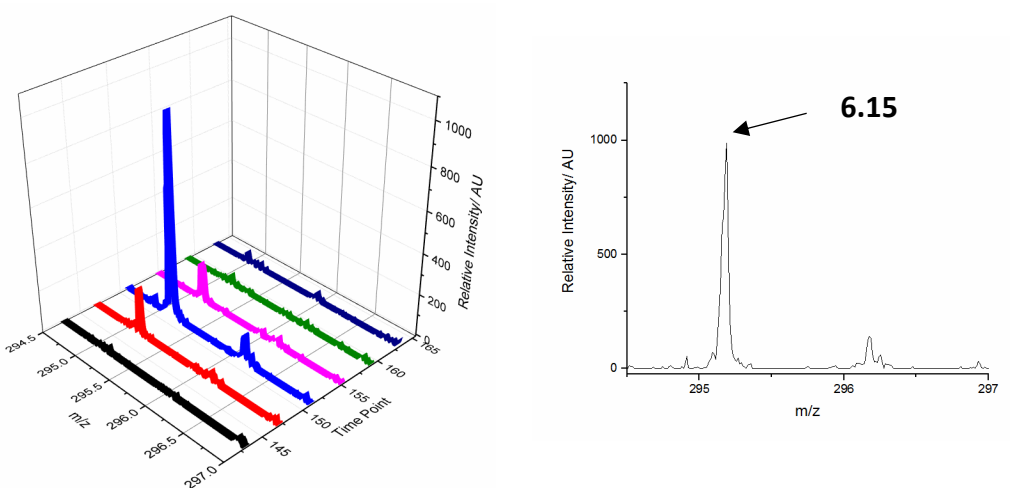


Figure 211: MS signal for **6.15**

#### 6.2.4. Attempted Detection of Alkoxy Radicals

Throughout the above schemes there are several instances where radicals are predicted to be formed via alkoxy radical species, such as those in Figure 213. As was the case with the  $\alpha$ -pinene system, these signals are expected to be in a very low concentration relative to the peroxy species. Examination of experimental results supports this, as there was no clear indication of the detection of these species shown in Figure 212.

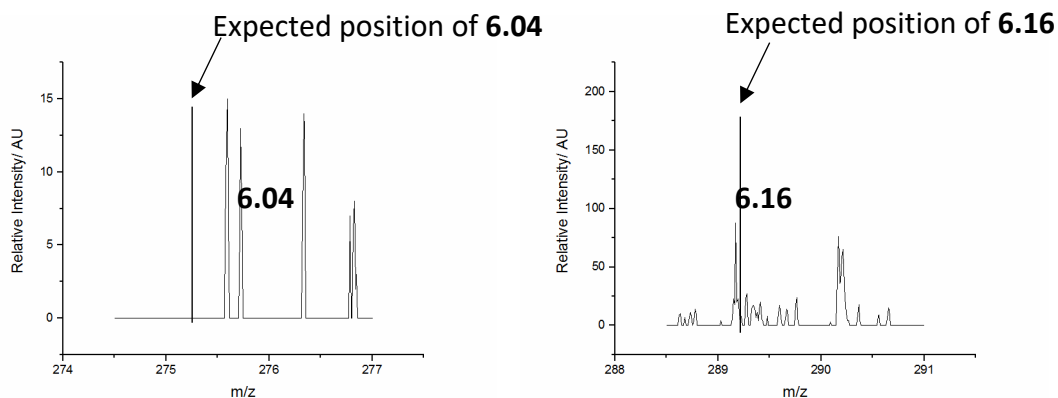


Figure 212: Lack of signal for trapped **6.04** or **6.16**

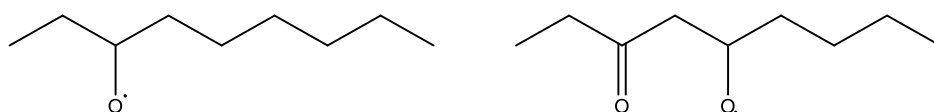


Figure 213: Structures of alkoxy radicals predicted to be present but not clearly identifiable as captured.

Overall, it appears that products from various steps of nonane oxidation are detectable through this system. Again, the ability of the trapping molecule to detect several different species of peroxy radicals from the same reaction mixture is useful with regard to future applications. Importantly, the key aim of detecting a range of radicals from alkane oxidation has been achieved, enabling experimental confirmation of predicted radical products. The kinetics of these various products would be interesting to attempt to probe with this methodology, this is discussed below. In addition to this, it would also be useful to gain further information regarding quantification of these radical species.

### 6.2.5. Time Profiles of Captured Radical Species

The sampling system can be utilised to generate time profiles of the radicals described above, which will be useful for comparison with a model of this system (see section 6.3.). In order to produce this data, the sampling site was moved to different distances from the

point of irradiation in the flow tube (as detailed in **Chapter 9**), enabling product change with reaction time to be monitored. The resulting variation is shown in Figure 214.

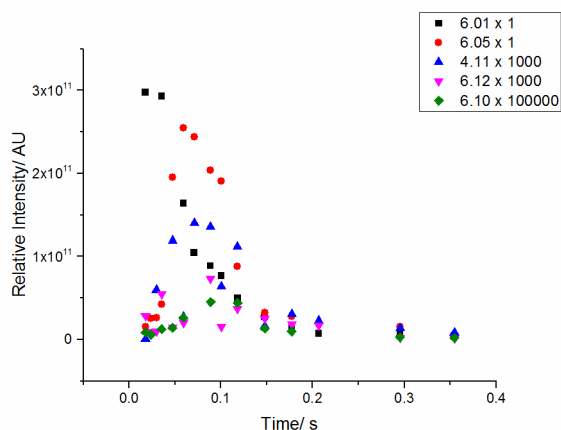


Figure 214: Variation in signal with experimental time for radicals from by the n-nonane +  $\cdot\text{OH}$  reaction

As such, it appears that variation in signal can be detected for the radical species discussed above over the time period measured. While the formation and decay of several species appears to be evident, it is noticeable that only decay of **6.01** can be found upon sampling at this timescale. This is likely due to formation of this species occurring on a fast timescale, something that can be confirmed upon subsequent comparison with modelled data for this species.

### 6.3. Comparison between Modelled and Experimental Kinetics

#### 6.3.1. Use of Chemical Models

In order to gain kinetic and mechanistic insight/understanding of a given chemical system, model simulations are frequently utilised. If it is fully understood, then experimental and theoretical results should correlate together perfectly. Models rely on accurate data regarding rates of reaction and product branching ratios. Key sources of this data for atmospheric systems are the Master Chemical Mechanism and chemical kinetic databases such as the IUPAC Atmospheric Chemical Kinetic Data Evaluation Database.<sup>229,230,322</sup> Rate

constant data and branching ratios can also be estimated using structure-activity relationships, as many species do not have experimentally determined rates of reaction.<sup>25</sup>

These models can gain particular use in examining data from atmospheric chambers, where a highly controlled environment is present, in which specific mixtures of different species can easily be prepared and their reactions monitored. Comparison between model and experimentally measured species formation and decay profiles can also be a useful method of probing reaction kinetics within chambers. The experimental data can be used to evaluate the MCM, improve its accuracy, and determine new reaction pathways. For example, Alam et al. used the MCM when examining radical yields from ozonolysis within the EUPHORE chamber.<sup>255</sup> Here  $\cdot\text{OH}$  yields were found to be in good agreement with the model, while humidity was shown to have a significant impact on  $\text{HO}_x$  yields.

An interesting aspect of this radical trapping process was the detection of several different compounds formed at various stages throughout the oxidative degradation of n-nonane. While assorted compounds were also detected from  $\alpha$ -pinene ozonolysis systems, the  $\cdot\text{OH}$  + n-nonane system was considerably simpler to study (there are no competing routes of oxidation, compared to the ozonolysis or hydroxyl radical based routes for terpenes) and should be better understood. As such, the evaluation of kinetics for this system would be interesting. This will be able to provide validation for the MCM chemistry, as well as establishing whether this method can be used for time resolved quantitative measurements of several radicals simultaneously within a fairly complex system.

### **6.3.2. Model Simulations Using the Master Chemical Mechanism**

Using a subset of chemistry from the MCM, an experimental specific chemical box model of the n-nonane +  $\cdot\text{OH}$  system was set up, using Kintecus software.<sup>229,230,323</sup> This includes reactions of the peroxy and alkoxy radicals, as well as closed shell species (e.g. hydroxyl ketone species **6.09**) formed within this series of reactions in the presence of oxygen. The model was constructed to closely match the parameters of the gas phase flow tube experiments described above, and was run with an experimental duration of 0.4 s. Initial

n-nonane and  $\cdot\text{OH}$  concentrations were  $4.8 \times 10^{14}$  and  $8.6 \times 10^{11}$  molecules  $\text{cm}^{-3}$  respectively, matching experimental conditions. Further model details are given in **Chapter 9**. To confirm the validity of model parameters, a series of modifications were made, with the resulting model sensitivities compared to experimental data.

Initial modifications were conducted to investigate the impact of varying model parameters which are not well established in the MCM, i.e. the rate of  $\text{RO}_2 + \text{RO}_2$  reactions.<sup>25</sup> As described above, the rates for these reactions are expected to be similar, but with some variation.<sup>324</sup> The MCM however groups  $\text{RO}_2$  reactions by type of  $\text{RO}_2$  (e.g. secondary alkyl peroxy or secondary peroxy radicals with oxygen or chlorine in an  $\alpha$  or  $\beta$  position), with  $\text{RO}_2$  within the same group all proceeding with the same rate constant.<sup>25</sup> The impact of changing these rates is shown in Figure 215 for the  $\text{RO}_2$  radical **6.05**.

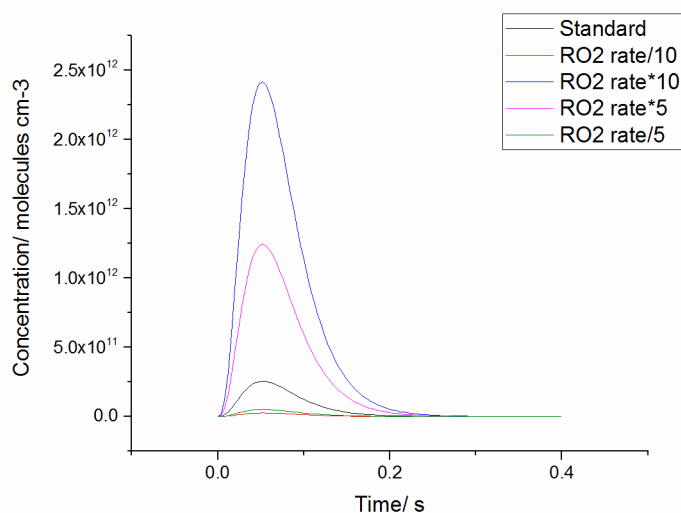


Figure 215: Impact on **6.05** concentration by varying  $\text{RO}_2 + \text{RO}_2$  reaction rates

Here the overall shape of the signal stays the same, despite the modification of this parameter, with the peak position also not being strongly influenced by the change. However, the overall concentration of this species appears to be the most impacted, as would be expected with slower rates of reaction enabling a larger concentration of this species to accumulate before it begins to react, and vice versa.

Concentration of hydroxyl radicals is another important factor in this model. Within the experimental system, this will be influenced by factors such as the extent of gas phase saturation by hydrogen peroxide and the duration and intensity of UV exposure. Therefore, the result of varying hydroxyl radical concentration was also studied, shown in Figure 216, again using the species **6.05**.

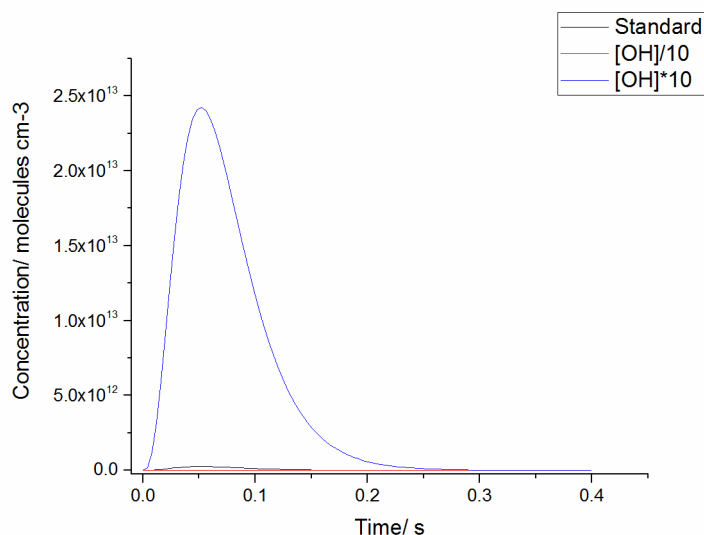


Figure 216: Impact on **6.05** of increasing/decreasing  $[\cdot\text{OH}]$  in the model

The model suggests that this variation would result in significant changes with regard to the concentration of species detected, as would be expected. Also, the peak position appears to feature a small shift to the right as  $[\cdot\text{OH}]$  increases. Given that the model and experiment for this signal fit well with the initial concentration applied, further changes to  $[\cdot\text{OH}]$  do not appear likely to be beneficial to improving the model-experimental fit.

The requirement for flow tube wall loss reactions to be taken into account within the model is also probed. In many gas phase reactions, losses to the walls within experiments are a known problem, in particular for the hydroxyl radical, and is expected to be a first order loss process.<sup>69,325</sup> Figure 217 shows the sensitivity of radical loss to the walls for the amount of **6.05** formed.

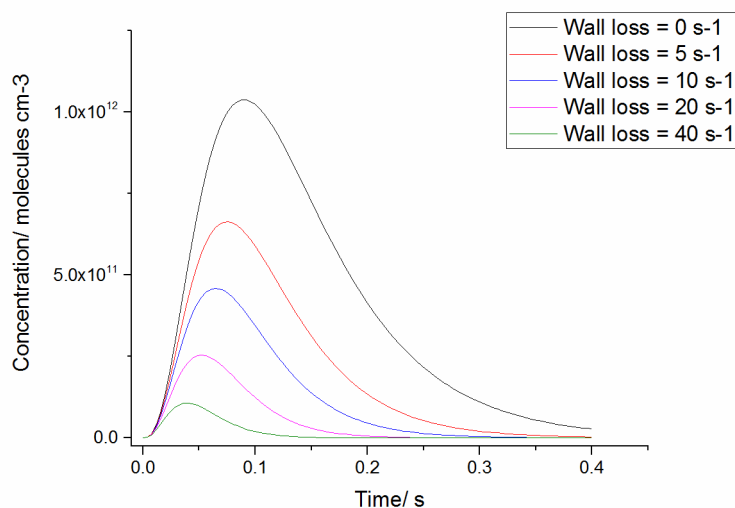


Figure 217: Variation for **6.05** with changing wall loss

Examination of the model without wall loss reactions shows significantly changed concentrations of radical species, particularly towards longer exposure times. As the modelled wall loss increases, signals become less broad, with the peak shifting towards shorter exposure times. This is expected – without wall loss reactions, each radical would have a longer lifetime, hence a broader peak. Given that in the experimental results there is very little signal detected by 0.4 s, wall loss reactions will certainly need to be accounted for within the model. Within the literature, wall losses for tubes of a similar length have been found as ca. 2.5 - 5.5 s<sup>-1</sup>.<sup>37,325</sup> However, wall losses to Teflon coated tubes, as used by Fuchs et al., are expected to be lower than those to quartz, which is used here.<sup>37</sup> In addition to this, significant ‘wall’ loss to uncovered areas of the silica support would also be expected, with a perfect monolayer of **2.09** leaving 66% of the silica uncoated under sample loadings used here. As such, the 20 s<sup>-1</sup> found here does not appear to be unreasonable.

The modelling of this system suggests that we would expect to observe several peroxy radical species within a flow experiment of 0.4 s duration. However, the slow reactions leading to the formation of later products (e.g. **6.05**) indicates that experiments at low residence times would be unlikely to observe all of these species. Throughout the model,

the concentrations of alkoxy radicals modelled to be present, e.g. **6.04**, appear to be considerably lower than peroxy radicals, e.g. **6.01**. The modelled relative concentrations of these species are shown in Figure 218.

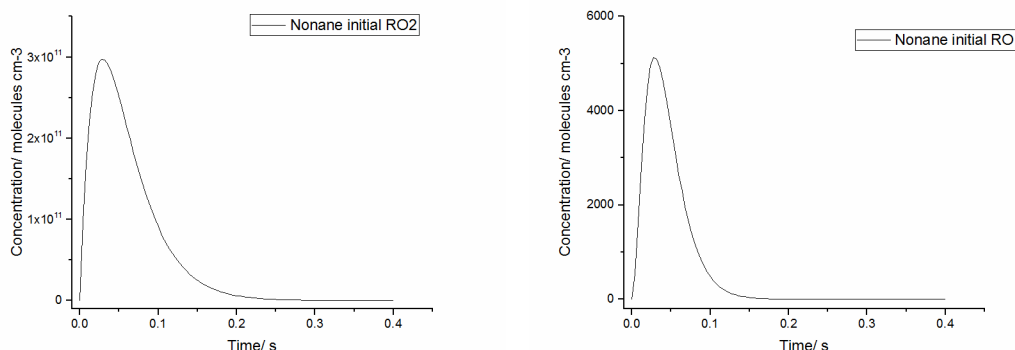


Figure 218: Modelled concentrations for initial species RO<sub>2</sub> **6.01** and RO **6.04**

The significantly lower levels for the alkoxy species suggests that it would not be unexpected that the detection of these species would be more difficult during the experimental studies. While reaction between trapping molecule and an alkoxy radical may occur, a difference of approximately eight orders of magnitude between predicted concentrations of these species means that it is less likely that alkoxy based adducts will be observable in this system compared to the peroxy adducts. This fits well with the lack of clear signal obtained experimentally for these species described in the nonane based experiments above in section **6.2.2**.

The experimentally optimised model parameters were used to model the time profiles of the five peroxy species described above (**6.2.2.**) (Figure 219). Of the modifications described above, wall loss rates of 20 s<sup>-1</sup> appeared to fit best to the RO<sub>x</sub> radicals profile within the experimental data, which are not unreasonable relative to wall loss rates observed within the literature.<sup>326</sup> Rates of RO<sub>2</sub> + RO<sub>2</sub> reactions are kept as given in the MCM. Model concentration profiles for several species are shown increased in order to be visible on one plot.

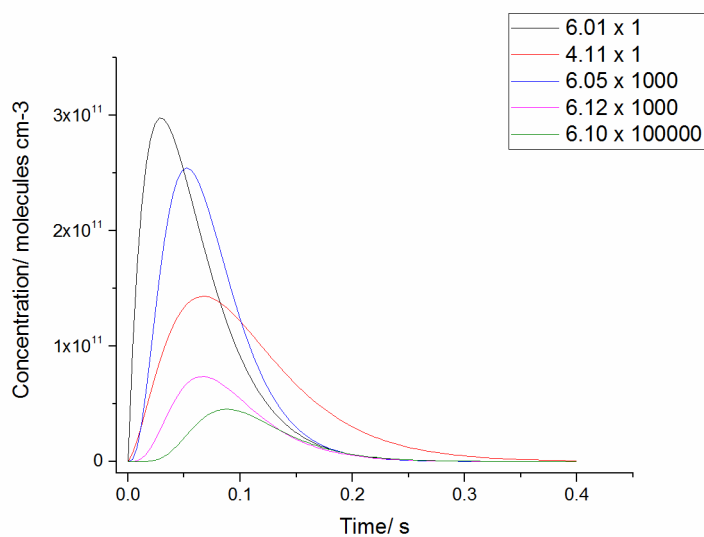


Figure 219: Results of modelling the kinetics of **6.01**, **6.05**, **6.10**, **6.12** and the hydroperoxy radical from the nonane +  $\cdot\text{OH}$  reaction

### 6.3.3. Evaluation Relative to Experimental Results

The modelled data was compared to experimental data in order to gather information regarding whether the trapping reaction products are following the MCM model predicted time profiles.<sup>228</sup> The results for this comparison are shown for each species in Figure 220.

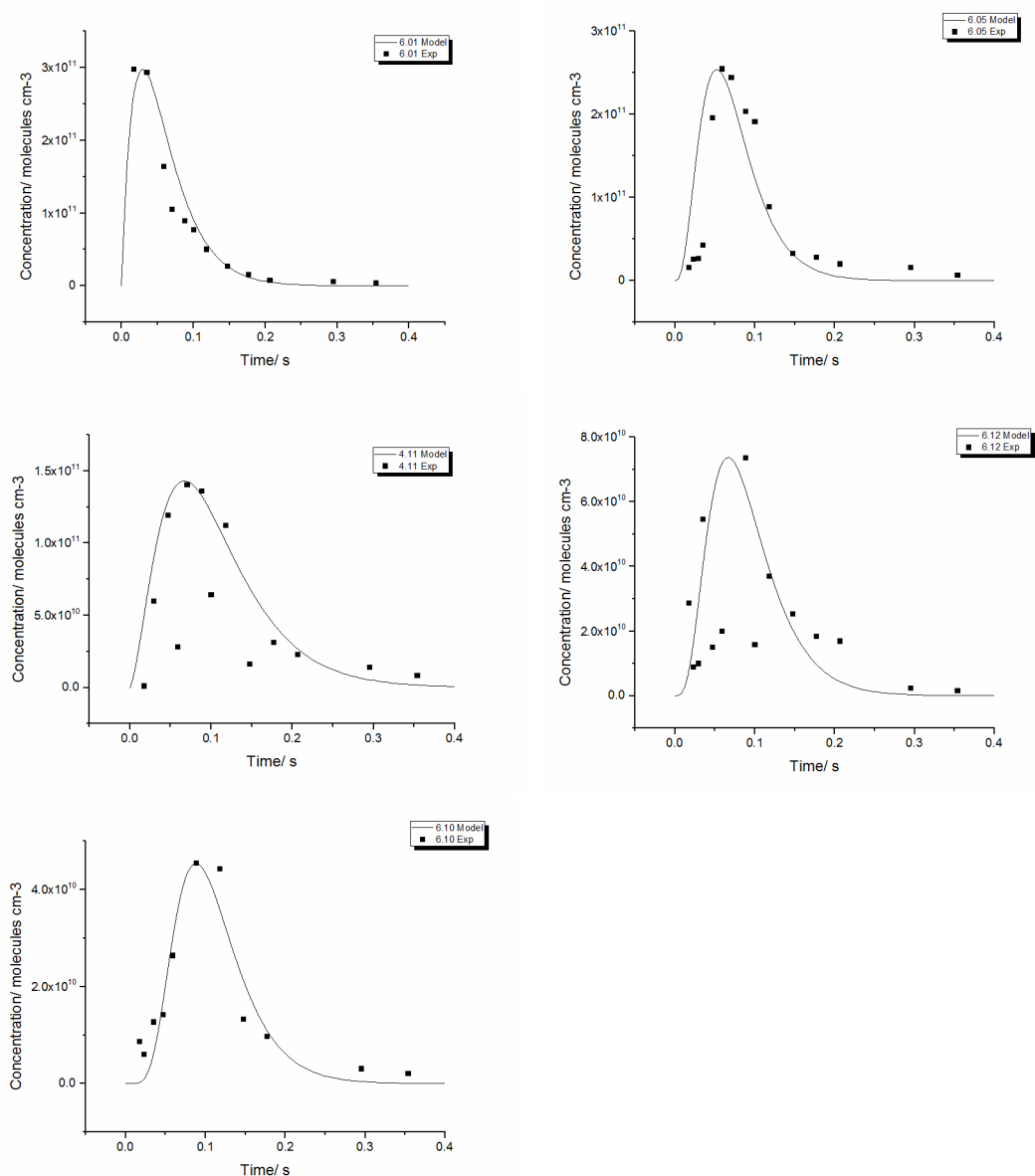


Figure 220: Experimental results compared to modelled kinetics for **6.01**, **6.05**, the hydroperoxy radical, **6.10** and **6.12**

The results appear to indicate that the products trapped are being formed in a manner generally consistent with the modelled kinetics. The initial species, **6.01**, decays well in relation to the model, however the formation is not followed experimentally. Upon comparison with the model this is indeed expected, as modelled formation of **6.01** appears to have peaked before the first experimental data point can be recorded. The lack of experimental data points tracking the formation of **6.01** is due to the problems associated with collecting very low time data points with the irradiation system – it is difficult to avoid

irradiation of the trap for low residence time systems, owing to the proximity of the point of irradiation and the trapping site. Irradiation is being avoided here, as it is likely to encourage the cleavage of peroxy bonds within trapped products, which would in turn preclude the detection of these species.

In contrast to the signal from **6.01**, a signal can be obtained for **6.05** formation. Short exposure time experiments, show very low initial concentrations of this species, which then increase to peak at ca. 0.06 s. This agrees well with the modelled results for this species, which also appears to peak at approximately this time. It is also of note that the formation of this species does not appear to fit the modelled predictions as well as the decay, which does appear to correlate well. This may be partially due to the error from MCM predictions of reaction formation rates here. Also, decay in this system appears to be dominated by wall loss, based on the model variations, this appears to have been modelled reasonably well.

It is notable in both the experimental and modelled data that the signal for the hydroperoxyl radical is broad, and the least well fit of all the species shown here. Regarding the model, this is likely attributable to there being several steps for the formation of HO<sub>2</sub>. However, experimentally, it is also possible that this is due to hydroperoxyl radical formation from reactions between hydroxyl radicals and water. Given that the modelled and experimental results do appear to follow the same trend reasonably well, this is clearly not a major process in this system, although there does appear to be some detectable impact.

The signal for species **6.12** also appears to show noticeable variation from the modelled kinetics. This is likely to be attributable to the relatively low intensity of this signal – the modelling shows it to be the lowest concentrated of the modelled peroxy radicals, while experimental results generally show weak signals for this species. The peroxy species, **6.10**, formed earlier in the chemical system, does not appear to show as low an intensity, both in modelled and experimental data, hence it is unsurprising that this signal shows considerably less fluctuation than that for **6.12**.

As was predicted by relative model concentrations, there appears to be no clearly identifiable signal for initial alkoxy radical adducts such as **6.04** from this reaction. Therefore, time profiles for this species cannot be plotted against experimental results. This would have been particularly useful in the full study of this system, as the current species shown are not from consecutive reaction steps (i.e. **6.05** is formed from **6.04**, which is in turn formed from **6.01**, with only **6.05** and **6.01** examined here).

#### 6.4. Calibration of Trapping Methodology

Calibration is an important aspect of all measurement techniques, and there are a variety of methods that have been applied for the measurement of gaseous radicals. This is a very difficult process – calibration standards of short lived radicals cannot be made. A common method for instrumentation using the laser induces fluorescence (LIF) technique for ·OH detection is that based on the photolysis of water at 185 nm.<sup>327,328</sup> During this process, ·OH is produced in a quantum yield of 1 from H<sub>2</sub>O, while O<sub>3</sub> is formed in a quantum yield of 2 from O<sub>2</sub>. Thus measurement of H<sub>2</sub>O, O<sub>2</sub> and O<sub>3</sub> concentrations, combined with the absorption cross sections of H<sub>2</sub>O and O<sub>2</sub> at 185 nm, enable the resultant hydroxyl radical concentration to be calculated using equation 27, where  $\sigma_{H_2O}$  and  $\sigma_{O_2}$  are the absorption cross sections of H<sub>2</sub>O and O<sub>2</sub> at 185 nm.<sup>329</sup>

$$\frac{[OH]}{[O_3]} = \frac{1}{2} \times \frac{\sigma_{H_2O}}{\sigma_{O_2}} \times \frac{[H_2O]}{[O_2]} \quad (27)$$

Different instruments/techniques themselves can also be inter-compared against each other. For example, Schlosser et al. tested DOAS and LIF instruments against one another within the SAPHIR chamber.<sup>60</sup> The use of a large chamber enables the sample environment to be maintained throughout the experiment, with results indicating that, while LIF measurements appeared to be more precise, DOAS instrumentation appeared to be the more accurate technique. Indeed, DOAS instrumentation has been used in several experiments in order to provide a reference to results obtained with LIF.<sup>61</sup>

A highly beneficial use of the radical trapping methodology would be its application to calculate concentrations, as well as speciation, of the radicals being captured. In order to accomplish this, the trapping technique will need to be calibrated using another radical measurement technique. A series of experiments were conducted in the School of Chemistry, University of Leeds, utilising the same calibration technique as is used for the FAGE instrument.<sup>36</sup>

During this process, radicals were generated using water photolysis. The concentration of the resulting HO<sub>x</sub> species was then calculated using a hygrometer to measure the water concentration. This is converted to [OH] by equation 28, as described by Onel et al. for calibration of methyl peroxy radicals.<sup>309</sup> Here,  $\sigma_{H_2O, 184.9 \text{ nm}}$  is the absorption cross section of water vapour at 184.9 nm,  $\Phi_{H_2O, 184.9 \text{ nm}}$  is the photodissociation quantum yield of ·OH,  $F_{184.9 \text{ nm}}$  is the photon flux of 184.9 nm light and  $\Delta t$  is the irradiation time.<sup>309,330</sup>

$$[OH] = [H_2O] \sigma_{H_2O, 184.9 \text{ nm}} \Phi_{H_2O, 184.9 \text{ nm}} F_{184.9 \text{ nm}} \Delta t \quad (28)$$

The HO· was then reacted with an alkane, in order to form organic peroxy radicals. During these experiments, the [alkane] was kept significantly higher than [HO<sub>x</sub>]. This acts to ensure that [HO·] = [RO<sub>x</sub>]. As such, a calibration plot can be created of signal vs ·OH, which is proportional to RO<sub>2</sub>.

The limitations of this calibration procedure need to be appreciated. Owing to the method behind measurements (i.e. making known amounts of oxidant and reaction with another molecule to produce the calibrant RO<sub>2</sub> radical), flow rate and sample loading will be very important to reproduce in these experiments. As the trapping is effectively cumulative (i.e. the more radicals that **2.09** is exposed to, the more intense the resulting trapped adduct signal), any change in these conditions will significantly affect the calibration.

In addition to this, the calibrations will be unique to every species – i.e. a calibration for the methyl radical would not be expected to function as a calibration for the n-nonane

derived peroxy radicals. This will be partially attributable to the fact that relative rates of reaction for each species with radical trap have not been studied. While different RO<sub>2</sub> radicals would be expected to have similar rates of reaction, they will not behave the same within the trapping system, hence application within a different system (with different radicals competing to be trapped) would also potentially result in a change to the calibrated system. For example, rates of reaction for C-H abstraction would be expected to increase with carbon number, which could result in larger RO<sub>2</sub> species out-competing smaller RO<sub>2</sub> radicals.<sup>308</sup> The variation in relative rates of reaction in the liquid phase for different alkyl peroxy radicals is shown by Morgan et al. and Osborne et al., with t-butyl peroxy and methyl peroxy radicals recorded as reacting with rate constants of ca. 3.6 and 167 dm<sup>3</sup> mol<sup>-1</sup> s<sup>-1</sup> respectively with 2-methylbut-1-ene.<sup>327,331</sup>

First, the calibration system was tested with radical trap **2.09** in order to confirm that radicals can indeed be detected from this system. Radical generation is subtly different here, compared to that in Figure 188, as water photolysis is instead employed as the source of ·OH radicals, with irradiation at 184.9 nm. This would result to much higher water concentrations than in the experiments described previously, potentially leading to higher amounts of hydroperoxy radicals being formed from water + ·OH reactions. However, given the prior use of 30% H<sub>2</sub>O<sub>2</sub> solution in water, this would not be expected to prevent the detection of alkane peroxy species. Indeed, species detected do match those detected previously in n-nonane experiments, therefore calibration experiments were conducted. The experimental set-up for these experiments is shown in Figure 221.

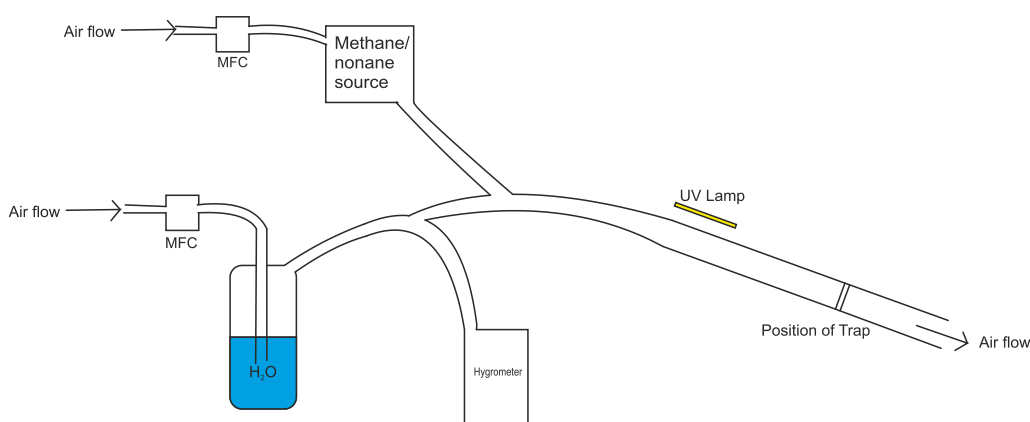


Figure 221: Set-up for calibration of trapping procedure

### 6.4.1. Methyl Peroxyl Calibration

Ideally, calibration experiments would be done on the simplest system possible – with only a single peroxy radical being present. As such, initial experiments were conducted using methane, as the alkane. This calibration methodology has been developed by Onel et al. in order to calibrate the FAGE for  $\text{MeO}_2$ .<sup>309</sup> Unlike n-nonane, total [peroxy radical] will be expected to be entirely one species: the methyl peroxide radical, as shown in Figure 222.

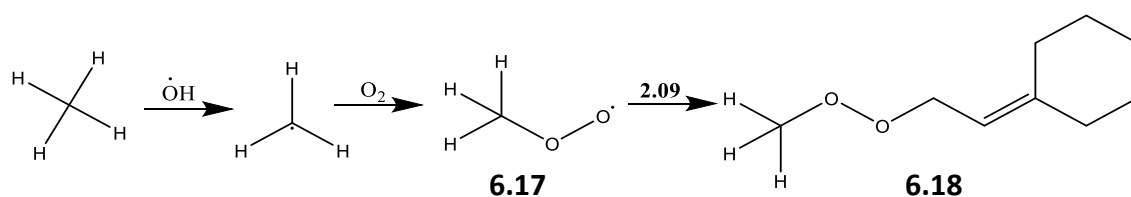


Figure 222: Capture of the methyl peroxide radical, **6.17**

It should be noted that water photolysis may also result in some hydroperoxide radical formation, so the methyl peroxide radical will not be exclusively the only peroxy species present. This is shown below in equations 29 and 30.



As expected given the success of the trapping procedure in the n-nonane system, the methyl peroxy radical does appear to be successfully trapped from this system. The resulting  $[\text{M}+\text{Na}]^+$  ion is shown here in Figure 223, with the structure of the captured species (**6.18**). The hydroperoxyl radical expected to form here was also observed.

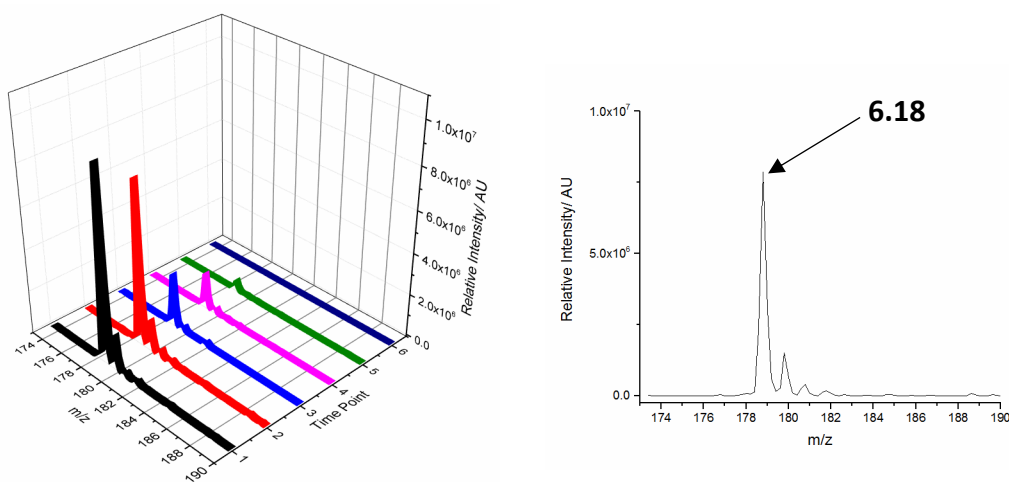


Figure 223: MS signal from **6.18**, captured **6.17**

Compound **6.18** is likely to be much more volatile than species such as **6.02**: a difference of eight CH<sub>2</sub> groups will make a significant difference to volatility. As such, it would not be unexpected for some of this species to be lost during the extraction steps, or if excessively high flow rates are used during trapping. However, sufficient signal can be detected for calibration experiments to be initiated. A series of radical concentrations were generated with variation of current supplied to the UV light used for photolysis.<sup>309</sup> The resulting calibration plot is shown in Figure 224. Intensity from MS is plotted against [HO], which as mentioned earlier, will fully convert to [RO<sub>2</sub>] under these excess alkane conditions.

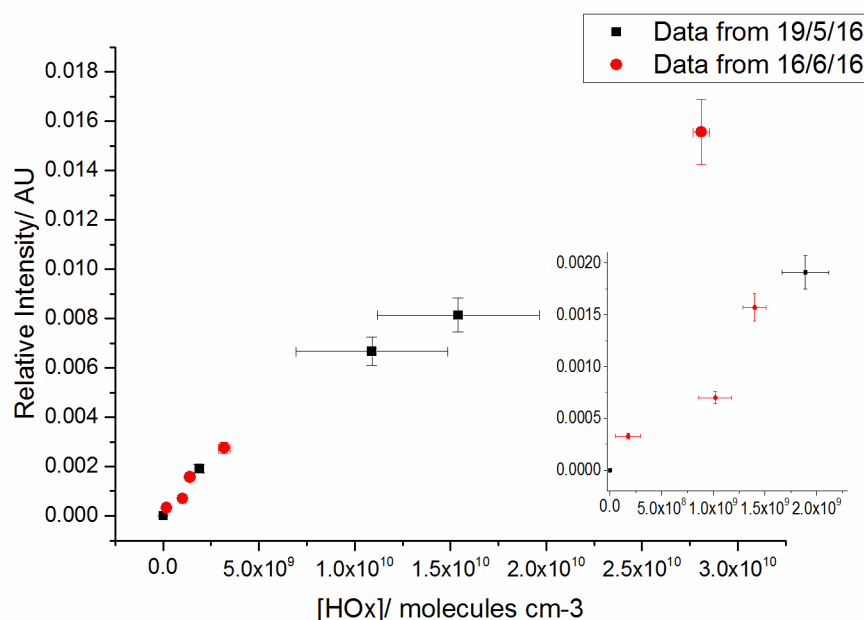


Figure 224: Calibration results for radical **6.17**

It appears that the radical trapping shows a good signal correlation relative to the concentrations of radicals being produced. Signals are measured from  $10^8 - 10^{10}$  molecule  $\text{cm}^{-3}$ , so the lower range is on the edge of what can be considered atmospherically relevant.<sup>332</sup> Lower measurements are not obtainable here as the UV lamp current cannot be decreased further. That signals can be detected over this range is very useful for future use of this trapping methodology. The errors within this plot are generally low, except for two central data points, which show considerable variation in  $[\text{HO}_x]$ . This was due to a large fluctuation of the lamp current towards the start of these measurements.

#### 6.4.2. Nonane Peroxyl Calibration

Establishing a calibration in a more complex system will also be useful: real world experiments will inevitably involve considerably more than just methyl peroxide radicals. Therefore, calibration experiments were conducted for  $\text{RO}_2$  species derived from n-nonane. As has already been shown, there are a number of different radicals that can be produced from the  $\cdot\text{OH} + \text{n-nonane}$  reaction, thus resulting in a more complex reaction system. Hence, there will be a considerable difference between  $[\text{RO}_x]$  and **[6.01]**, which may limit the sensitivity of this technique. A calibration for **6.01** is shown in Figure 225.

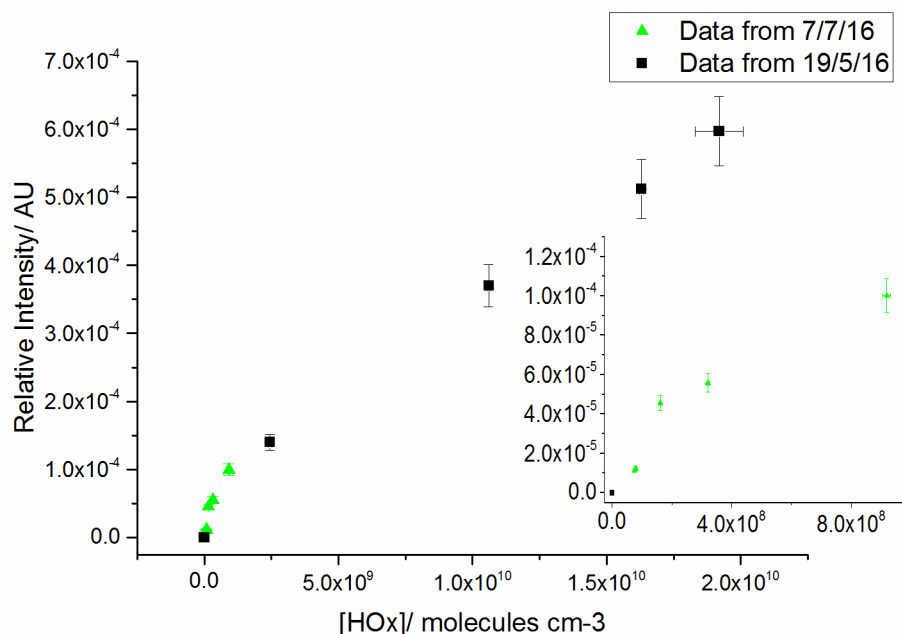


Figure 225: Calibration results for radical **6.01**

This again appears to imply a good correlation between measured  $[\text{HO}_x]$  and the detected adduct **6.03**. The spread of concentrations approaches expected atmospheric concentrations of organic radicals, therefore it again appears that this methodology has the potential for real world trapping experiments.<sup>332</sup> However, each of these experimental calibrations appears to feature a not fully linear trend. This is may be due to increasing concentrations getting closer to saturating the detector, thus resulting in a curve being observed. However, this is more pronounced in the nonane system, potentially due to the added complexity of this species relative to the less complex  $\text{MeO}_2\cdot$  system. Indeed, plots do appear linear if the low concentration range is examined in Figure 224 and Figure 225.

#### 6.4.3. Calibrating to Lower Concentrations

While detection of signal at concentrations of  $10^8 - 10^{10}$  molecule  $\text{cm}^{-3}$  is useful, it would be advantageous for 'real world' measurements to calibrate for the detection of concentrations of n-nonane derived  $\text{RO}_2$  (**6.01**) and methyl peroxy (**6.17**) approaching  $10^6$  molecules  $\text{cm}^{-3}$  or lower. These concentrations were difficult to achieve using the above calibration system, (i.e. UV lamp current cannot be further decreased) hence dilution experiments were conducted on samples collected at higher concentrations. For this, higher concentration experiments were diluted with methanol and re-analysed in order to test whether signal for the lower concentration captured species could still be observed.

To test the validity of this method, a sample of a starting concentration ca.  $10^{10}$  molecules  $\text{cm}^{-3}$  was used. This was twice diluted with methanol by a factor of 100 and then analysed by MS. The first of these data points falls very close to the experimentally determined concentration equivalent, and serves as confirmation regarding the suitability of these experiments. The second dilution appears to continue to follow the overall trend from these experiments, suggesting that detection of species down to  $10^6$  molecule  $\text{cm}^{-3}$  should indeed be possible. The incorporation of these dilutions for **6.17** are shown in Figure 226. In order to easily show the full range of samples collected, the data is shown on a logarithmic scale (hence the data point for the '0' measurement is not included).

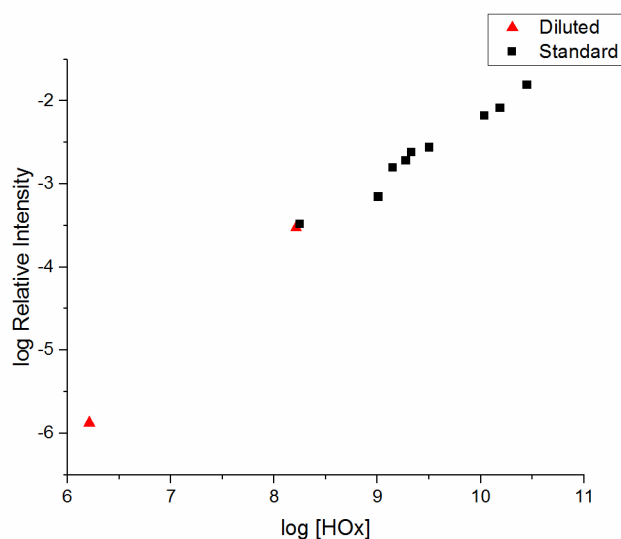


Figure 226: Applying dilutions to the methyl peroxy (6.17) calibration

Dilutions were then applied to the nonane system, in order to examine whether the detection of species at  $10^6$  molecule  $\text{cm}^{-3}$  is also true for this system. The resulting plot showing dilutions for 6.01 is given in Figure 227.

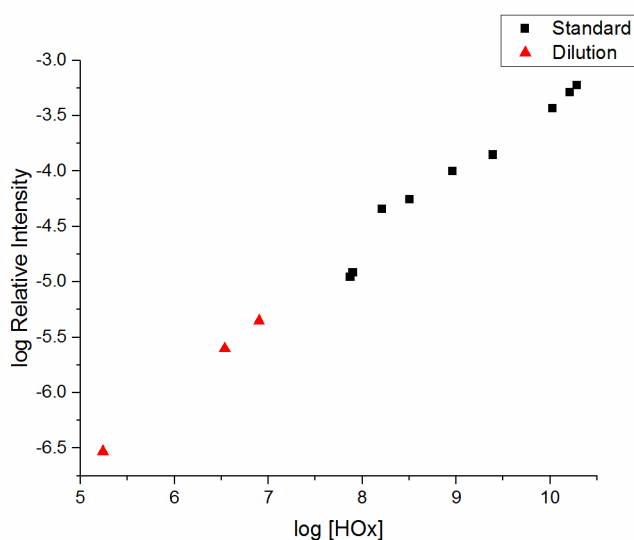


Figure 227: Applying dilutions to 6.01 calibration

Again, the dilutions from this system appear to follow the trend anticipated based on the standard measurements. As such, it appears to be likely that compounds present at the low concentrations reached in these dilutions will be detectable by this trapping technique. Indeed, the lowest dilution within this nonane system corresponds to an

anticipated concentration within the range of  $10^5$ - $10^6$  molecules  $\text{cm}^{-3}$ , which is certainly at levels relevant for atmospheric species.

Consequently it appears that the limit of detection for the current trapping system is down to concentrations of  $10^5$  molecules  $\text{cm}^{-3}$ . Literature techniques display a wide range of detection limits. Methods such as cavity enhanced absorption spectroscopy has been able to detect OH radicals at  $3.8 \times 10^9$  molecules  $\text{cm}^{-3}$ , however improvements to background conditions are predicted to allow concentrations of  $10^6$  molecules  $\text{cm}^{-3}$  to be detected, which is as expected under ambient atmospheric conditions.<sup>333</sup> Fuchs et al. describe a detection limit from FAGE measurements of  $1.5 \times 10^7$   $\text{cm}^{-3}$  for total RO<sub>2</sub> radical concentration, with the limit of detection for ·OH from the same instrument found to be  $3 \times 10^5$   $\text{cm}^{-3}$ .<sup>334</sup> Among the best detection limits is that of the CIMS technique, with OH detection recorded by Hens et al. to reach  $5 \times 10^4$  molecules  $\text{cm}^{-3}$ .<sup>216</sup> Detection by EPR techniques such as MI-EPR has achieved detection limits of  $4.9 \times 10^7$  molecules  $\text{cm}^{-3}$  for peroxy radicals.<sup>68</sup> This compares to detection limits of nM that have been achieved by ‘traditional’ EPR techniques for various spin trapped radical species.<sup>89</sup>

However, it should be noted that many of these detection limits are for relatively short exposure times – indeed, DOAS exposures of ca. 100 s to achieve detection of ·OH at  $10^6$  molecules  $\text{cm}^{-3}$  were deemed by Ren et al. to be too long for field measurements (typical ·OH lifetime is  $\leq 1$  s).<sup>47</sup> The experiments here were conducted with much longer exposures of 15 minutes, hence potentially providing much less temporal resolution than can currently be achieved. The key benefit to the calibration of **6.01** and **6.17** is that they are species specific – unlike the other RO<sub>2</sub> detection techniques described.<sup>8</sup> As such, the detection limits obtained from the above dilution experiments do suggest that trapping atmospheric species with these compounds will not be deemed irrelevant because of their long exposure times, with future work to examine trapping on a lower timescale.

## 6.5. Future Work

There are a number of experiments that could be conducted in order to build on this work. One series of reactions would be to conduct the examination of a hydrogen abstraction reaction with a different alkane (e.g. octane), and test the correlation between kinetic models and experimental results. Alternatively, it would also be interesting to conduct radical trapping based kinetic analysis on a more complex system, such as the RO<sub>2</sub> species formed from an aromatic system (e.g. toluene + ·OH) as the atmospheric chemistry of aromatic species is still not fully understood.<sup>335</sup> However, the mechanistic chemistry of this system for species beyond the initial peroxy species is likely to be considerably more complex than this alkane system that has been studied here.

Regarding kinetic modelling work, it would be interesting to study this system at lower sampling times, in order to gain experimental data points showing the modelled increase in **6.01** signal. Attempting to minimise wall loss processes (e.g. by use of a Teflon coated tube) would also be worthwhile, as this may increase the resolution of the experiments. The result of attempting to gather this data in mixtures (i.e. in the presence of methane) would also be useful to study, as it would demonstrate the value in applying this system to more dilute experimental mixtures. Alternatively, attempting to evaluate the system in the presence of NO<sub>x</sub> would also be interesting, to establish the impact/potential interferences of NO<sub>x</sub> based reactions on the species already studied, and to test whether these changes can be successfully measured with this technique.

On the subject of calibration investigations, conducting methane and nonane experiments at longer exposure times would be of interest, owing to the potential for increasing the signal: noise ratio of peaks, and enabling detection of lower radical concentrations. Also, calibration experiments on a different system would also be of interest, to probe whether calibrations for other RO<sub>2</sub> species could be generated, and how similar they are to those already obtained for nonane and methane initial peroxy radicals. Calibrating for the same species, within a different system (i.e. more than one alkane present simultaneously),

would also help to establish the quantification of the potential interferences impact on the calibration of different radicals being present.

## 6.6. Conclusion

In conclusion, the radical trapping methodology outlined in **Chapter 2** has been successfully applied to detecting a range of radicals in relatively simple atmospherically relevant oxidation systems. A number of different peroxy radical based products formed via hydrogen abstraction from n-nonane are detected, which include an assortment of secondary reaction products. Alkoxy species from this system are expected in a considerably lower concentration, hence it is unsurprising that these are not as clearly detected. The detection of radicals from this system again provides experimental evidence to support mechanisms proposed within the MCM.

Calibration experiments have also been conducted on RO<sub>2</sub> species formed in methane and nonane based reactions. Data suggests that this technique can indeed be calibrated, with **6.17** and **6.01** used as examples, from the methane and nonane experiments respectively. Using dilutions, these experiments show that calibration down to levels of 10<sup>6</sup> molecules cm<sup>-3</sup> can be achieved, close to concentrations of RO<sub>2</sub> radicals anticipated to be present within the atmosphere. Therefore, this technique would have the potential for use in ambient atmospheric sampling experiments, as well as in environmental chambers.

The kinetics of the n-nonane + ·OH reaction are also examined by capturing some of the assorted radical products formed throughout this reaction in time resolved flow tube experiments. This reaction system is also modelled, using subset mechanisms extracted from the MCM, with the resulting flow tube optimised model results compared to the values obtained experimentally. The experimental and modelled results appear to show a good agreement for the species that have been studied here. As such, this technique appears to be promising for the application of studying the kinetics of gas phase radical reactions.

## 7. Real World Sampling - Indoor and Outdoor Air

### 7.1. Introduction

Thus far, the radical trapping process has been applied to a number of model systems, with promising results regarding the capture of radical species. However, current methods of examining atmospheric radicals are not just conducted in model environments, but are also applied to field studies of 'real' environments. Therefore, the application of this radical trapping technique to indoor and outdoor environments would be an essential requirement for the development of this sampling technique.

#### 7.1.1. Indoor Air

Recently, there has been a surge in interest in studying indoor air, an area that has received considerably less attention than outdoor air. This is surprising given that many of us will spend over 80% of our lifetime within an 'indoor' environment.<sup>336</sup> The range of chemistry within the indoor air is large, and can easily be impacted by a variety of factors, including air fresheners, cleaning products, cooking etc.<sup>337</sup> These will contain a range of compounds: a study by Steinemann found that common cleaning product components include limonene,  $\alpha$ -pinene, ethanol and, acetone.<sup>338</sup>

The building itself will be an important aspect of an indoor system. The transmittance of light from outside through windows will play a key role in any indoor photochemistry, transmittance of ca. 30% of UV has been recorded by Drakou et al.<sup>339</sup> However, this varies greatly – other measurements have recorded values as low as 0.15 %, or up to 75 % UVA transmittance.<sup>340,341</sup> Painted surfaces can also contribute to indoor chemistry, for example nonanal from paint oxidation has been predicted by Kruza et al. to be one of the most important indoor aldehydes.<sup>342</sup> The indoor environment will also be considerably affected by air circulation rates, which are often low in modern 'energy saving' buildings. This can enable the accumulation of organic species, which would otherwise be diluted by air

exchange with the outdoor environment.<sup>343</sup> Concentrations of ozone can also increase significantly indoors from use of printers: Barrese et al. found ozone increases from 20 to 50 ppb from printers.<sup>344</sup> Given the low indoor half-life of ozone (ca. 10 min) from this study, it is clear that this species is significantly involved in indoor air chemistry.

The limited studies that have been conducted on indoor air have given evidence of potential implications for human health due to indoor air quality. Indeed, indoor air pollution is likely to make a significant contribution to the current estimates of deaths attributable to outdoor air pollution of approximately 5.5 million per year.<sup>345</sup> While there are guidelines for maximum level of indoor air pollution, these are often exceeded, and are often not regulated (e.g. in Europe). For example, Tofful et al. found evidence on several occasions for unexpectedly high levels of PM<sub>2.5</sub> (> 60 µg m<sup>-3</sup>) within schools in Italy, which exceeded WHO guidelines of 25 µg m<sup>-3</sup>.<sup>258</sup> From this study, organics and combustion products appeared to be responsible for over 70% of the PM<sub>2.5</sub> collected during the winter sampling period. The potential for indoor formation of carcinogenic multifunctional (oxygenated and nitrogenated) compounds such as formaldehyde, a known carcinogen, also represents a significant long term exposure risk to health.<sup>346</sup>

Given that the dominant source of radicals in air is through photochemical reactions, the lower UV levels indoors is expected to result in significantly lower radical concentrations than is observed outdoors.<sup>347</sup> However, studies have also found unexpectedly high levels of radical species, such as the observations by Gomez et al. in 2013 of higher than anticipated levels of hydroxyl radicals inside a school.<sup>348</sup> This observation, explained due to previously unaccounted HONO photolysis (equations 31 and 32), raises the possibility of secondary reaction products being formed via reactions with ·OH, with these secondary (multifunctional) oxygenated products likely to impact on human health.



While the source of HONO in the Gomez et al. paper was predicted to be ambient NO<sub>2</sub>, there are other sources of HONO in indoor air, such as direct emittance via combustion (with the use of scented candles in particular becoming increasingly widespread).<sup>348,349</sup> This has been studied within a chamber by Bartolomei et al., who used candles as a source of HONO, and also observed NO<sub>x</sub> from the experiment.<sup>350</sup> The hydroxyl radical concentrations observed were found to reach levels of ca. 10<sup>7</sup> molecules cm<sup>-3</sup>, comparable to outdoor levels, and certainly sufficient for substantial ·OH reactivity to occur indoors.

There have also been studies that have sought to directly examine the health impacts of the compounds formed from indoor air reactions. Niu et al. studied the potential health impact of SOA formed from limonene ozonolysis, both with and without ammonia. The decrease in O<sub>3</sub> levels in the presence of ammonia observed within these experiments was attributed to ammonia catalysing the ozone uptake for limonene ozonolysis.<sup>259,351</sup> They found that the increased SOA yields can induce a pulmonary inflammatory effect, while the addition of ammonia would also lead to larger and increasingly toxic (organo-nitrogen containing) particulate matter. This acts to support the implications suggested by other researchers on indoor air quality. However, human health is not the only aspect affected by indoor air. Areas such as museums are also impacted by indoor air quality, with potentially damaging results for exhibits such as paintings etc. Schieweck et al. found that despite efforts to combat this, elevated levels of species including acetic acid are still being formed from exhibit enclosures, with low air circulation rates again hindering dilution of these species.<sup>352</sup>

There is a wide assortment of techniques utilised in the study of indoor air, which are also utilised for the study of outdoor air. While there is no 'standard' technique, there are many methods which provide useful data.<sup>343</sup> Particulate matter (such as PM<sub>2.5</sub>) can be captured on filters, and then analysed using a scanning mobility particle sizer (SMPS), as well as XRF and ion chromatography.<sup>258,259</sup> Chemical information of particulate matter can be acquired by techniques such as thermal desorption or PTR-MS.<sup>239</sup> VOCs can also be monitored using 2D chromatography in the form of GC-MS, while NO<sub>x</sub> levels can be measured photolytically.<sup>337,350,352</sup> Radical species in indoor air are expected to be

predominantly formed by ozonolysis, with radicals not often measured directly in indoor air: use of a LIF-FAGE instrument to monitor  $\cdot\text{OH}$  levels, by Alvarez et al. and Carslaw et al. are two of relatively few examples of this.<sup>347,348</sup> It is surprising, given the knowledge that a wide assortment of radical chemistry can occur in indoor air, that more instruments currently used in 'outdoor' experiments are not being employed within indoor studies.

### 7.1.2. Outdoor Air

The composition of outdoor air will vary according to many different factors, including local environment, climate, weather and time of day. There will be a great many non-radical species present, from a variety of biogenic and anthropogenic sources. For example, methane is emitted at ca  $530 \text{ Tg yr}^{-1}$ , and typically has a concentration of  $4 \times 10^{13}$  molecules  $\text{cm}^{-3}$  in dry air, and is by far the dominant atmospheric hydrocarbon.<sup>6</sup> Isoprene is an example of a VOC also present in large amounts, which will vary with seasonality – Kesselmeier et al. recorded isoprene concentrations of ca.  $7 \times 10^{11}$  molecules  $\text{cm}^{-3}$  and  $2 \times 10^{10}$  molecules  $\text{cm}^{-3}$  during the end of dry and wet seasons respectively.<sup>353</sup> Monoterpenes are an example of a predominantly biogenic atmospheric species, with rural concentrations previously found by Hakola et al. at ca.  $3.2 \times 10^8$  molecules  $\text{cm}^{-3}$  and  $2.7 \times 10^8$  molecules  $\text{cm}^{-3}$  for limonene and  $\alpha$ -pinene respectively.<sup>354</sup> The atmospheric degradation of these species will often result in the formation of radicals, as has been described in **Chapter 1**.

There have been many studies on these outdoor radical species. As described in **Chapter 1**, several studies have been conducted that make an attempt to measure the outdoor concentrations of peroxy radical species, which are expected to have considerably longer lifetimes in the atmosphere ( $\leq 1$  minute) compared to hydroxyl radicals lifetimes ( $\leq 1$  second).<sup>291,328</sup> For example, Salisbury et al. measured total peroxy radical (i.e.  $\text{HO}_2 + \Sigma\text{RO}_2$ ) concentrations of nearly  $5.4 \times 10^8$  molecule  $\text{cm}^{-3}$  during summer measurements at a 'clean' marine boundary layer.<sup>355</sup> The impact of seasonality on these rural measurements is illustrated by the fact that spring measurements at the same site reached lower concentrations of  $3.2 \times 10^8$  molecule  $\text{cm}^{-3}$ .

However, advances based around the PERCA methodology (described in **Chapter 1**) have enabled measurements of HO<sub>2</sub>· and ΣRO<sub>2</sub>· species to be separated. For example, Miyazaki et al. found peak total RO<sub>2</sub> concentrations of 1.2 x 10<sup>9</sup> molecules cm<sup>-3</sup> in Tokyo, a highly urban environment.<sup>326</sup> The HO<sub>2</sub>· measurements for the same area were found to be at concentrations of 6.2 x 10<sup>8</sup> molecules cm<sup>-3</sup>. Of the wide range of organic peroxy radicals present within the atmosphere, the methyl peroxy radical is expected to be among the most abundant.<sup>332</sup> However, as has been discussed in **Chapter 1**, speciation of peroxy radicals beyond that achieved by separation of signal from hydroperoxy radicals remains a challenging issue in measurements of the outdoor air.<sup>37</sup>

### 7.1.3. Aims

A series of experiments are conducted within an indoor environment, consisting of an academic office and a meeting room. These experiments are targeted towards the characterisation of reactive species present within indoor air, as well as establishing the sensitivity of this methodology to measurements in real world atmospheric environments. The impact on the observed compounds caused by perturbations with typical indoor air contaminants (e.g. limonene, O<sub>3</sub>, air freshener) will also be worthwhile to examine. It will also be beneficial to conduct experiments sampling outdoor air. These will be useful proof of principle experiments, to capture and identify specific radicals at realistic concentrations.

## 7.2. Indoor Sampling Site details

Full details of each site are provided within **Chapter 9**, however key information is provided here. Sampling sites consisted of an adjacent office and meeting room, within a new (< 5 years old) building, which is next to a small wooded area. Sites had relative volumes of ca. 50000 dm<sup>3</sup> and 123000 dm<sup>3</sup> respectively, while ventilation rates have previously been found to be ca. 0.1 dm<sup>3</sup> hr<sup>-1</sup> for this building. Radical capture was conducted as in **Chapters 4 and 6**, with an air flow passed over a layer of **2.09** deposited on a solid support, with

typical exposure times of 2 hours. The sampling inlet was positioned in the centre of each room. Full room layouts are shown in Figure 228 and Figure 229.

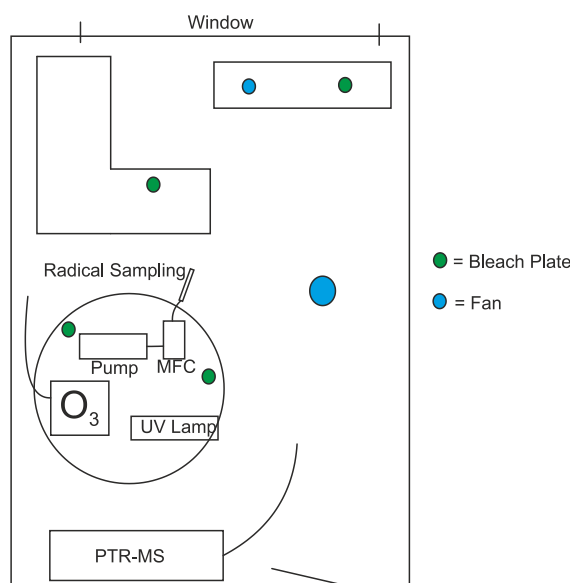


Figure 228: Room layout for office sampling, showing positions of  $O_3$  monitor, MS, and radical trapping equipment

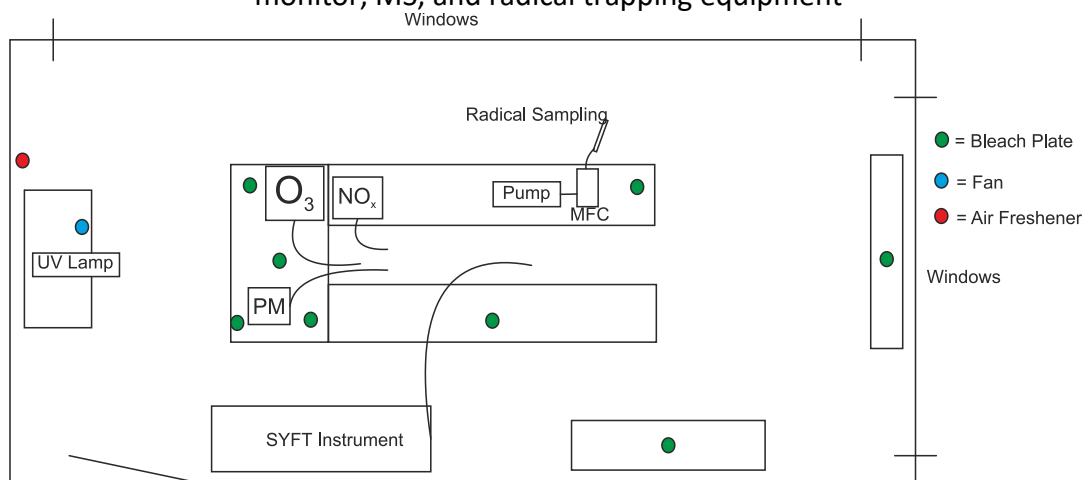


Figure 229: Room layout for meeting room sampling, showing positions of  $O_3$ ,  $NO$  and  $PM$  monitors, MS and the radical trapping equipment.

Ozone and VOC levels were artificially increased in several experiments, in order to boost the chemistry of interest within these rooms. Ozone levels were manipulated by the generation of  $O_3$  via a UV light, up to a maximum of ca. 30 ppb, while VOC levels are modified by the direct release of VOC into the rooms (limonene in office experiments, an

$\alpha$ -pinene-limonene mix for the meeting room). This ozone level is still below that which has been observed in many indoor environments: ozone concentrations within offices have been found to typically be ca. 20-40 ppb, at half that of outdoor concentrations.<sup>356</sup>

Experiment	Sampling Site	Time / hr	[O <sub>3</sub> ]/ ppb	[limonene]/ ppb	[ $\alpha$ -pinene]/ ppb	Other perturbations
1	O	2	3	Ambient	Ambient	OW
2	O	16	4	Ambient	Ambient	Night, CW
3	O	2	17	Ambient	Ambient	OW
4	O	2	19	50	Ambient	OW
5	O	2	24	50	Ambient	CW
6	O	2	28	Ambient	Ambient	SB, CW
7	M	2	7	Ambient	Ambient	
8	M	2	20	Ambient	Ambient	
9	M	2	15	30	60	
10	M	4 x 0.5	13	30	60	
11	M	2	15	Ambient	Ambient	SB
12	M	2	14	Ambient	Ambient	NSB
13	M	2 x 2	17	Ambient	Ambient	Air freshener

Table 1: Indoor air sampling. O = Office experiments, M = Meeting Room, OW = Open Window, CW = Closed Window, SB = Scented Bleach, NSB = Non Scented Bleach

During meeting room experiments, high levels of NO and NO<sub>2</sub> are reached, 33 and 16 ppb respectively. These are believed to be due to leakage from the SIFT-MS instrument, which produces NO in order for NO derived adducts to be detected.<sup>357</sup> While this cannot be compared to the office experiments, as no NO<sub>x</sub> detection methods were employed, it is notable that NO concentration decreased to ca. 2 ppb in the presence of O<sub>3</sub>, as would be expected according to equation 33. This results in lower O<sub>3</sub> levels (of up to 20 ppb) than were obtained in office experiments, but has the benefit of minimising NO concentrations in these experiments. It is possible that NO<sub>3</sub> is being formed from these reactions, however evaluation of these products was outside the scope of these initial experiments.



Other analytical instruments were also applied to these experiments, with the results of these experiments not discussed here. Samples of air were removed by canister sampling at assorted intervals, with these then analysed by GC-MS. On-line sampling with PTR-MS

and SIFT instruments was also applied to the office and meeting room sites respectively. Air freshener composition was also probed by GC-MS.

It is worthwhile to note that, in comparison to other radical techniques (e.g. FAGE) this is a considerably more portable sampling technique. Indeed, set-up can quickly be accomplished, with minimal difficulty in changing sampling location. This provides the opportunity for radical sampling to be conducted with considerably fewer experimental restrictions than are present with larger, more complex and power intensive methods such as DOAS or FAGE.

### **7.3. Indoor Air Sampling Results**

Prior to application within the indoor air system, the radical trapping methodology for ozonolysis reactions of both  $\alpha$ -pinene and limonene was tested in a smaller, more controlled laboratory system. This system, discussed in **Chapter 4**, provided evidence to suggest that radicals **4.21** and **4.23** from both the ozonolysis and hydroxyl radical attack channels of limonene respectively appear to be detectable by reaction with **2.09**. The radicals **4.01** and **4.09** from ozonolysis and hydroxyl radical attack of  $\alpha$ -pinene respectively have been detected in the same way. These species are focussed on throughout the discussion on indoor air experiments.

#### **7.3.1. A Peroxyl Radical Product from Ozonolysis: Office**

Relative concentrations of **4.22**, captured limonene ozonolysis product **4.21**, are shown below in Figure 230. The detection of **4.21** species is anticipated to be enhanced when ozone levels are artificially increased, as shown in Table 1, as indoor air chemistry is most likely to be initiated by ozonolysis reactions.<sup>358</sup> However, if ambient ozone and monoterpene levels are sufficiently high, these products may still be observed from samples taken without artificially increased ozone concentrations.

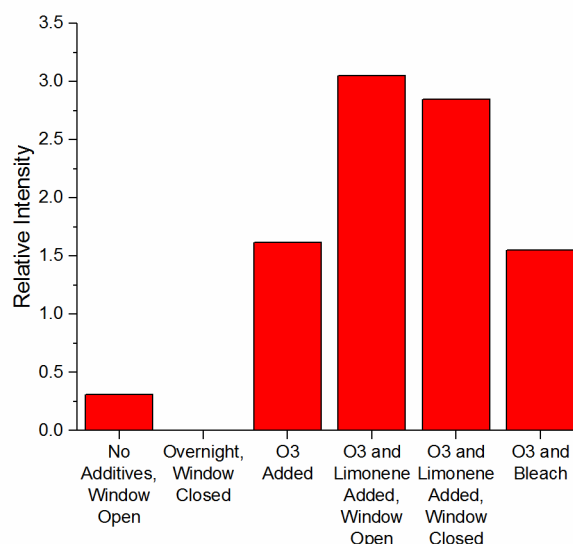


Figure 230: Plot showing changes in intensity of ozonolysis product **4.22** during indoor air office experiments

Firstly, it is clear that **4.21** is present in this system, with detection of adduct **4.22** from the non-perturbed experiment suggesting that ozonolysis of limonene is occurring within indoor air. Ambient concentrations of limonene will vary, however literature results from Girman et al. have recorded levels up to ca.  $6.2 \times 10^{12}$  molecules  $\text{cm}^{-3}$ .<sup>359</sup> The proximity of a small wooded area to this office will likely contribute to the ambient limonene concentrations. Recent modelling studies have suggested that, of the ozone loss from VOC reactions indoors, 68% can be attributed to reaction with limonene.<sup>360</sup> These results thus provide experimental evidence of this important reaction. The increased signal observed when both the limonene and ozone levels were artificially increased further suggests that these signals are indeed arising from the reaction between ozone and limonene.

The absence of signal in the overnight experiment is likely due to compounds of interest evaporating during the long sampling time (16 hours), as was also observed previously (**Chapter 4.2**). This is supported by the very low levels of **2.09** detected from analysis of this overnight experiment. An alternative explanation would be that no chemistry is occurring overnight. However, this is unlikely given that ozone levels within the room

stayed constant, at 4 ppbv (Table 1), and signal was successfully detected from the first 2 hr ‘ambient’ experiment, suggesting detectable levels of VOC.

Surprisingly **4.22** appeared strongest in an experiment with an open window and additional limonene VOC (Table 1). The open window, with a more localised dispersion of limonene, resulted in almost no detection of limonene from the PTR-MS instrumentation present for this experiment. Meanwhile, a closed window and a more even limonene dispersion resulted in the PTR-MS detecting elevated limonene levels (shown in Figure 231), therefore an increased signal would have been anticipated here. This may be due to an uneven distribution of limonene relative to the PTR and radical sampling sites. Alternatively, the difference could be attributable to experimental error – without running repeats of each experiment we cannot be certain of error associated with this system under ‘real’ conditions. However, repeats conducted as part of **Chapter 5** suggested errors of ca. 2% for this packing system, thus reproducibility is unlikely to be an issue for this technique. Other experiments have found increases in O<sub>3</sub> concentrations with an open window, but, with the low ambient ozone concentrations here this was not observed.<sup>361</sup>

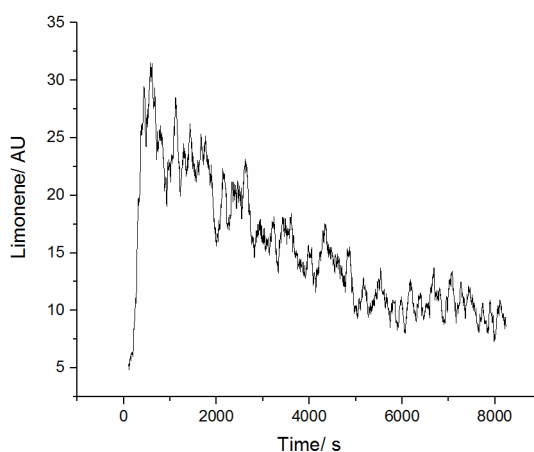


Figure 231: Limonene decay measured by PTR during experiment 5 (Table 1)

As a method of checking that a significant change in radical species’ relative concentrations would occur on increasing the limonene and ozone levels, a simple model of this system was constructed using Kintecus, with mechanistic data for limonene reactions with O<sub>3</sub> and ·OH taken from the MCM.<sup>229,230,323</sup> With starting conditions of 5 ppb ozone and 2 ppb

limonene (as an approximation of background concentration), the impact on **4.21** of increasing ozone levels to 25 ppb, and then limonene to 50 ppb, was modelled. The resulting increases shown in Figure 232 support the trends observed from the experimental work.

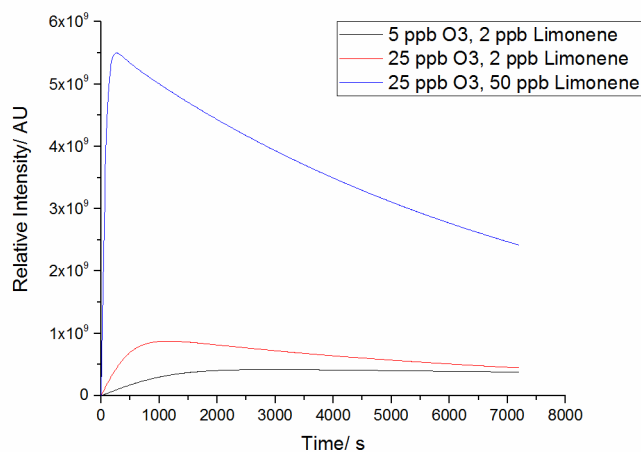


Figure 232: Kintecus plot on the effect of changing [limonene] and [O3] on **4.21** <sup>323</sup>

### 7.3.2. A Peroxyl Radical from $\cdot\text{OH} + \text{Limonene}$ Reaction: Office

As explained previously (**Chapter 4**), **4.23** would also be expected to form within the limonene ozonolysis system, being trapped as **4.24** following a limonene +  $\cdot\text{OH}$  reaction. The hydroxyl radical is expected to be formed from the ozonolysis of limonene in a yield of 86%.<sup>362</sup> Therefore, data for the detection of species **4.24**, given in Figure 233, can also be used to supplement the data already gathered regarding radical **4.21**, and further confirm the presence of radical reactivity within indoor air.

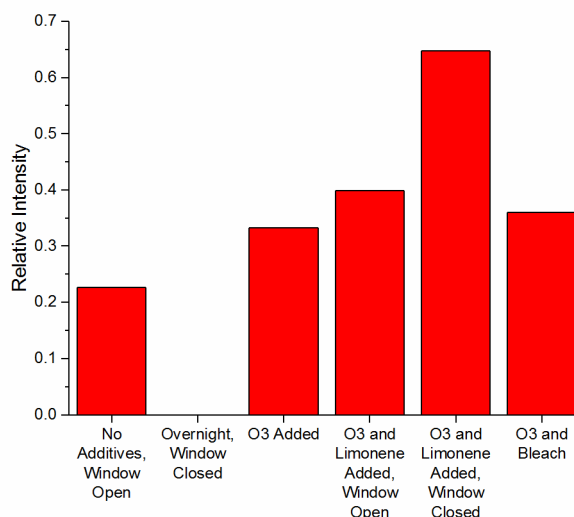


Figure 233: Plot showing changes in intensity of product **4.24** during office experiments

Species **4.23** also appears to be formed in most experiments, with adduct **4.24** present in both perturbed and non-perturbed systems. As was the case with ozone, reaction with limonene has been shown in the literature to also be a likely reaction process for indoor  $\cdot\text{OH}$  (responsible for 24% of  $\text{OH}$  loss).<sup>360</sup> Again, no signal was observed from the overnight experiment, while the largest signals were from experiments where the system was spiked with additional limonene and ozone. Once more this agrees with a prediction for these species modelled using Kintecus, shown in Figure 234.<sup>323</sup>

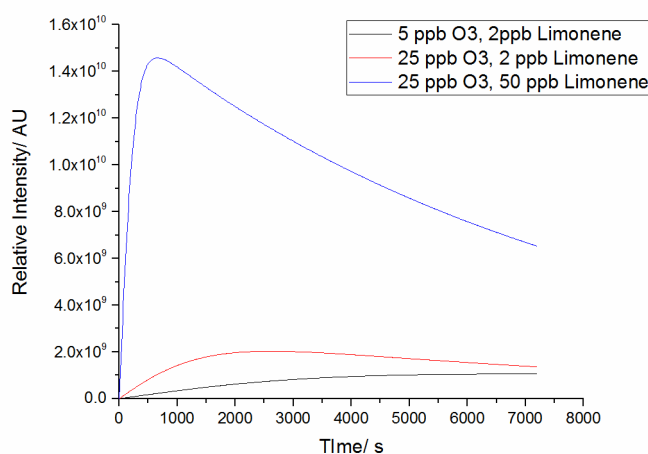


Figure 234: Kintecus plot showing the effect of changing [limonene] and  $[\text{O}_3]$  on **[4.23]**<sup>323</sup>

However, the signal for the VOC and  $\text{O}_3$  spiked system with a closed window now appears to be significantly higher than that for the open window. While this is the expected result

from a well-mixed closed system with a low ventilation rate, it nonetheless contradicts what is observed for the ozonolysis products. This is likely due to difficulty in fully resolving the signal for **4.24** within indoor experiment 4, thus resulting in a lower signal than that for the equivalent ozonolysis product **4.22**. Despite this, the observations of noticeably higher signals in VOC spiked experiments in both Figure 230 and Figure 233 were pronounced enough that it is clear the VOC spiking is responsible for increased formation of **4.24** and **4.22**. Signals from **4.24** also appear at a lower relative intensity than those from **4.22**, as is indicated by the modelled intensities of these species. This is expected, given literature predicted indoor hydroxyl radical concentrations in direct sunlight of  $1 \times 10^6$  molecules  $\text{cm}^{-3}$ ,<sup>348</sup> to as low as  $1 \times 10^4$  molecules  $\text{cm}^{-3}$ .<sup>363</sup>

### 7.3.3. Peroxyl Radical Products: Meeting Room

Experiments within the meeting room environment were conducted in order to attempt some replication of results from the office experiments, with the result of perturbation by additional  $\text{O}_3$ , and also a VOC (limonene/pinene) mixture (as shown in Table 1) given in Figure 235.

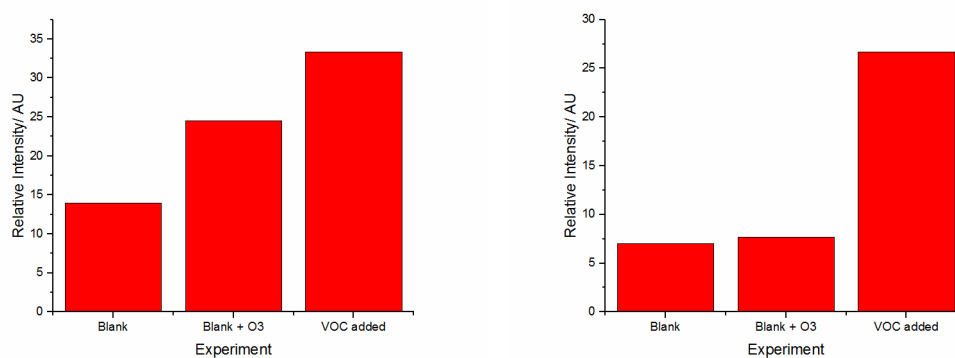


Figure 235: Signal variation for **4.24** and **4.22** respectively

The same general trend can be observed for **4.24** and **4.23** within Figure 235 as for the office experiments (Figure 230 and Figure 233): slight increases in signal upon the addition of  $\text{O}_3$ , and further increases with elevated  $\text{O}_3$  and spiking with VOC. This replication of experimental trends using different sampling sites is useful with regard to establishing the

effectiveness and reproducibility of radical trapping with **2.09** in ‘real’ chemical systems under ambient conditions. Background detection of radicals also provides evidence regarding the similarity of the two indoor environments, with ozone levels (Table 1) similar in each room. Literature studies on office environments have previously shown significant variability: Shair et al. found that loss rates of ozone can easily vary 30% from one office to another.<sup>364</sup> Therefore, these results are useful with respects to establishing that the indoor air chemistry is indeed proceeding in a similar manner in both environments.

As with the office experiments, this system was also modelled.<sup>323</sup> Both  $\alpha$ -pinene and limonene were now incorporated into this model, as an  $\alpha$ -pinene-limonene mixture was used for spiking meeting room experiments.<sup>229,230</sup> Species **4.01** and **4.22**, are used in the model, the outcome of which is given in Figure 236. Results follow the trend indicated by signal strength in Figure 235 as various system perturbations were applied.

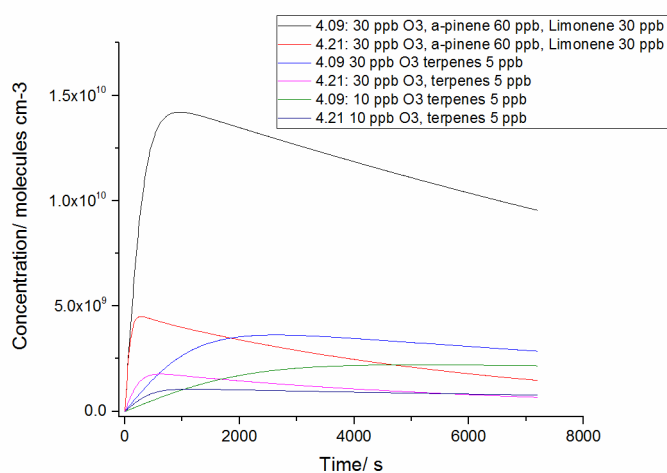


Figure 236: Model results for varying meeting room ozone and terpene concentrations<sup>323</sup>

Here, NO is also monitored, with levels up to 33 ppb detected (ambient NO measurements are expected to be within the 1-10 ppb range).<sup>348</sup> There is no indication of the NO radical being captured, despite the successful detection of **5.01** described in **Chapter 5**. However, it is likely that the NO radical concentrations were considerably higher in plasma experiments (which can reach up to 100  $\mu$ M) than those reached during the indoor air experiments.<sup>279</sup> Therefore, the lack of detection of this species is not concerning, as no studies have yet been conducted to establish a detection limit for **5.01**. This lack of

detection is also useful, as it prevents **2.09** from being swamped by NO. Also, NO can be removed by reaction with ozone, as can be seen in Figure 237. The beginning of ozone generation after ca. 170 min coincided with a significant decrease in NO concentration down to levels of ca. 1.5 ppb for the remainder of the experiment.

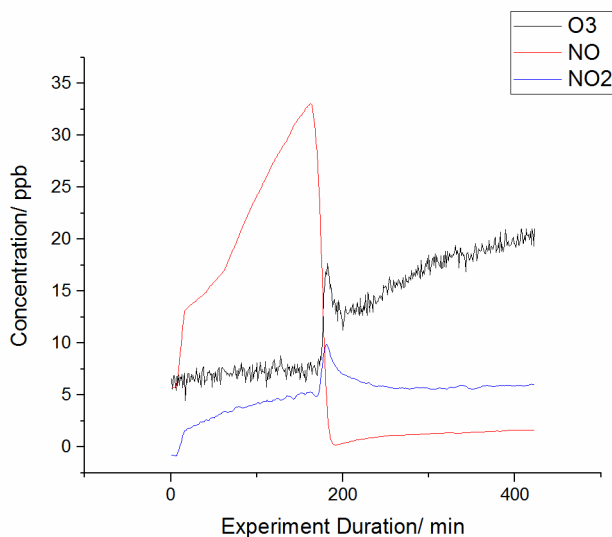


Figure 237: Change in NO and NO<sub>2</sub> levels upon ozone addition

NO and NO<sub>2</sub> were subsequently incorporated into the Kintecus model (in Figure 238), with changes of starting NO concentration modelled. These caused slight changes in concentrations of **4.21**, but no change to the overall trend of results described above.<sup>323</sup>

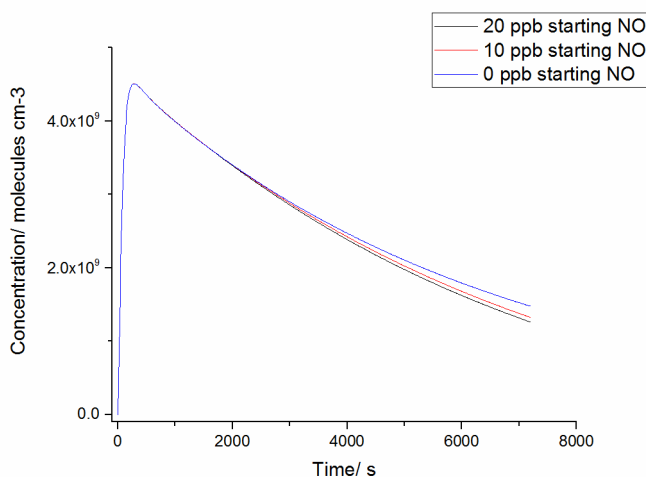


Figure 238: Impact on **4.21** from incorporating NO measurements into the model<sup>323</sup>

### 7.3.4. Alkoxy Radical Products

Many other different types of radical species can be formed in the experiments. The most obvious of these are produced by reactions with  $\text{RO}_2$  or  $\text{NO}$  to form the alkoxy radicals in Figure 239.<sup>229,230</sup>

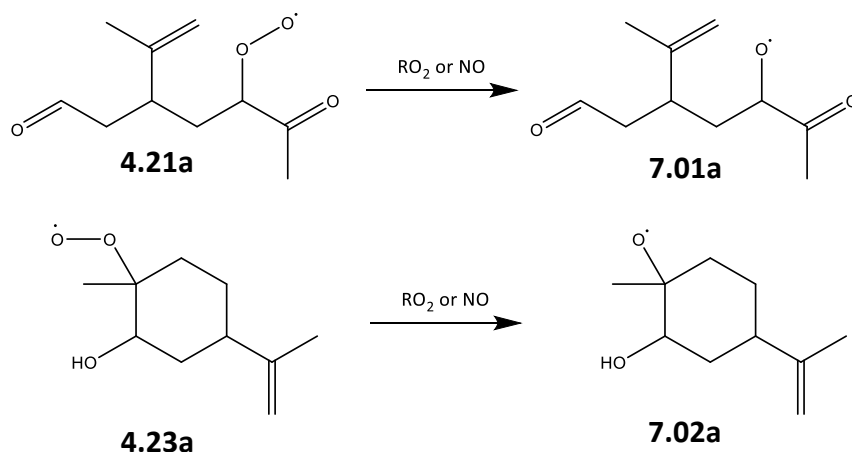


Figure 239: Alkoxy radicals **7.01a** and **7.02a** expected to form in oxidation of limonene

However, these species do not appear to be detected in any of the experiments conducted on indoor air. This is likely owing to the low concentration of these radicals, as they will quickly decompose, react with  $\text{O}_2$  or isomerise. When modelled (Figure 240), the concentration for these species was significantly below that of the previously detected **4.21** and **4.23**, with a difference of 9 orders of magnitude.<sup>323</sup> As such, the trapping methodology as currently applied in this system cannot provide direct evidence for the existence of these types of radical species within indoor air, although their presence could be inferred by the capture of subsequent product species (i.e. **7.05**).

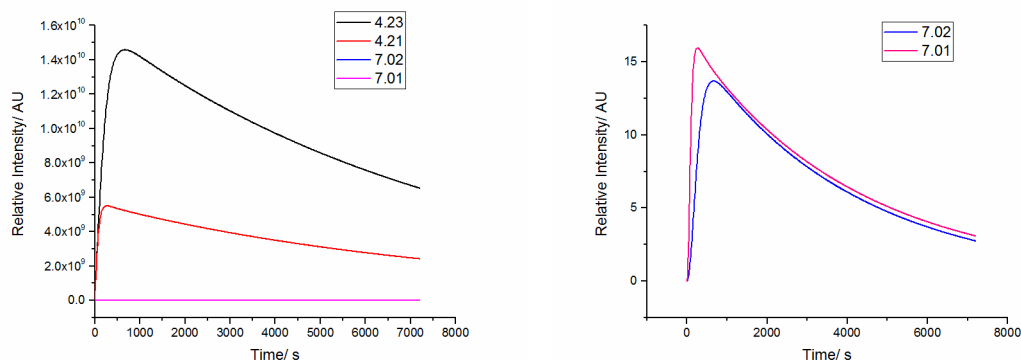


Figure 240: Modelled concentrations of peroxy species **4.21** and **4.23** and alkoxy species **7.01** and **7.02** from the indoor air system<sup>323</sup>

### 7.3.5. Results from Experiments with Bleach

Indoor experiments were also conducted with the addition of bleach to the room. Up to 8 bleach sample locations, with ca. 5 mL bleach each, were positioned around the room. It is well known that many commercial products contain terpenes, as fragrances etc,<sup>365,252</sup> and it would be of interest to observe radicals formed from these species. The overall emissions of VOC from cleaning products are an important source of indoor VOC, estimated to be 23% of total VOC coming from household products.<sup>366</sup> The concentration/types of terpenes from the scented bleach used in these experiments has not yet been studied, however monoterpenoid species are highly likely to be present, based on a study on an assortment of different bleaches by Odabasi et al..<sup>367</sup> A non-scented bleach was also studied in the same quantities as a comparison.

The scented bleach results in Figure 241 from meeting room experiments (Table 1) again showed that terpene based compounds **4.22** and **4.24** can be observed. For both adducts, scented bleach experiments gave increased signal relative to the non-scented bleach, suggesting that the species being captured are indeed from terpenes added to imbue fragrance in the bleach, not from any bleach activated chemistry of background terpenes.

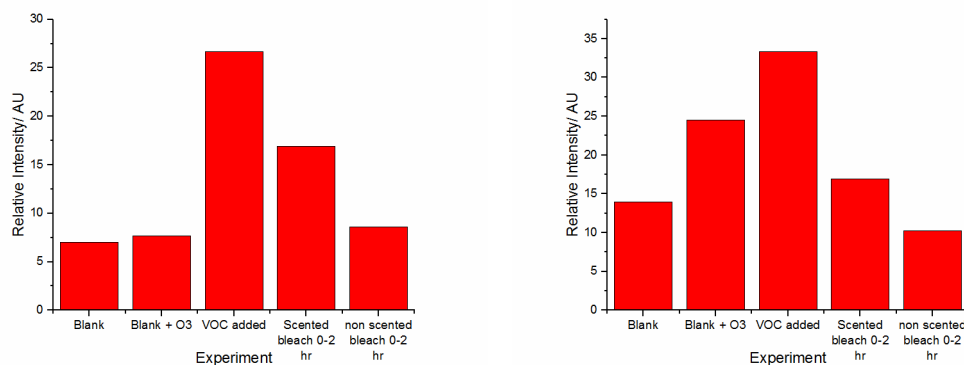


Figure 241: Signals for **4.22** and **4.24** respectively in meeting room experiments

However, measuring **4.24** in the meeting room and both **4.22** and **4.24** species in the office only show terpene originating species levels similar to those detected as background signals without additional VOC. This is shown above in Figure 230 and Figure 233, with the meeting room results in Figure 241. A potential explanation for this could be the terpenes from the bleach not being efficiently mixed around the room (for example, not evaporating substantially from the main bleach solution), compared to the meeting room. Nevertheless, the key result of increased signal for scented compared to non-scented bleach provides compelling evidence that there is some terpene release from scented bleach, although unlikely to be in such large quantities as used in VOC spiking experiments.

### 7.3.6. Other Radicals Captured from Indoor Air

A number of other radicals were detected in the indoor experiments. These are all species that can potentially be formed from limonene ozonolysis/ $\cdot\text{OH}$  attack, however many have other potential sources.<sup>229,230</sup> Their detection would play an important aspect in confirming the range of chemistry occurring within this indoor environment. The most obvious of these species is the  $\text{HO}_2$  radical, which will form **4.11** on trapping with **2.09**. This has previously been observed within indoor air at concentrations of  $2 \times 10^7$  molecules  $\text{cm}^{-3}$ .<sup>361</sup> There are a wide range of potential sources for this radical, which include the previously discussed  $\text{RO}_2 + \text{NO}$  reaction and terpene oxidation.<sup>347</sup>

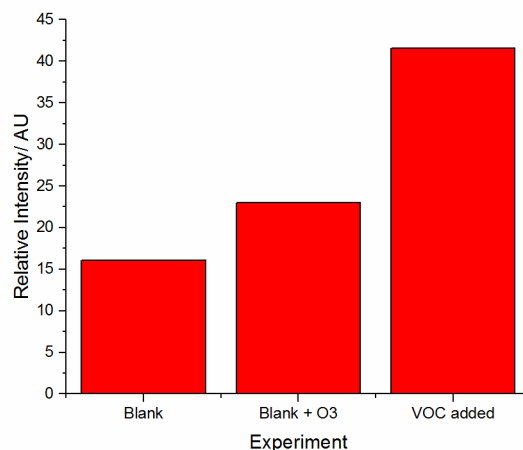


Figure 242: Variation in **4.11** during indoor air experiments

Indeed, this species can even be detected within the non-perturbed experiments, as shown in Figure 242. Examination of the MCM suggests that there are potential sources of this compound from both limonene ozonolysis and  $\cdot\text{OH}$  attack (as shown in **Chapter 4**), while it is also known to be present in ambient air.<sup>8,229,230</sup> Inspection of the data for this signal shows an increase in the experiments with spiked ozone/limonene levels, meaning that this signal can also be used to provide further indication of the extent of chemistry occurring within the indoor air system. As such, detection of this species is not definitively directly from monoterpene ozonolysis, yet this clearly becomes a more considerable factor in the experiments with additional limonene and ozone.

Another observable species is the  $\text{CH}_3\text{C}(\text{O})\text{O}_2$  acyl peroxy radical (**7.03**). This is an important species within atmospheric chemistry, as it can lead to the formation of peroxyacetyl nitrate (PAN) via reaction with  $\text{NO}_2$  as in Figure 243.<sup>310</sup> PAN is known to be a strong lachrymator, and also to be a feature of photochemical smog.<sup>292,368</sup>

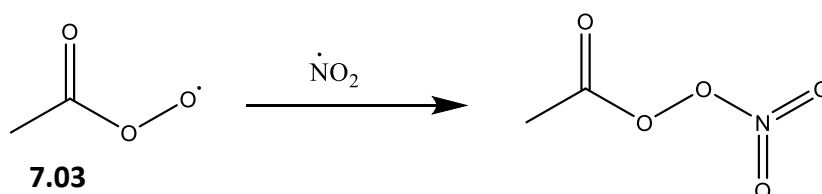


Figure 243: PAN formation from the  $\text{CH}_3\text{C}(\text{O})\text{O}_2$  radical

As with the HO<sub>2</sub> radical, the CH<sub>3</sub>C(O)O<sub>2</sub> radical can be formed via several different reaction paths, making isolation of the exact source difficult. Figure 244 shows an example reaction route from the MCM to form **7.03**, with the detected adduct (**7.04**) in Figure 245.<sup>229,230</sup>

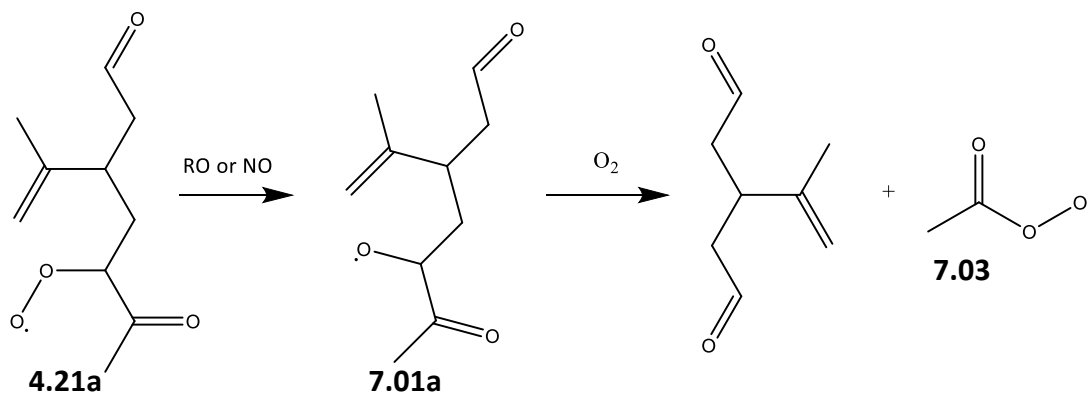


Figure 244: A route to form **7.03**<sup>229,230</sup>

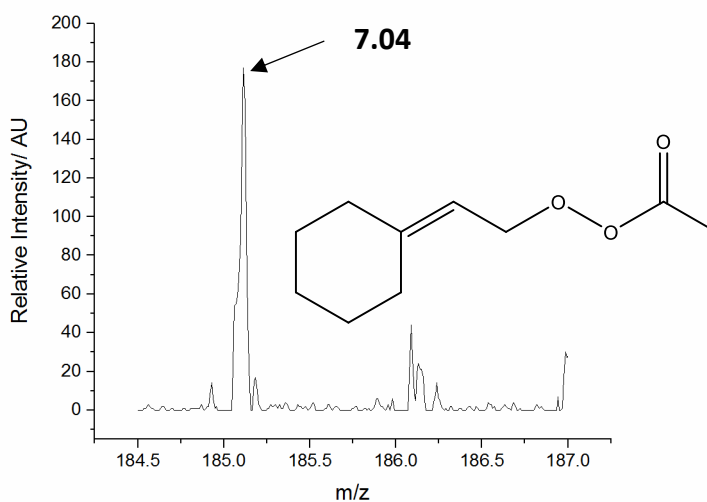


Figure 245: MS signal for **7.04**, the captured CH<sub>3</sub>C(O)O<sub>2</sub> radical

While there may be low undetected background levels of this species, they appear to be low enough that **7.04** is only detected with elevated VOC and O<sub>3</sub> levels, unlike the HO<sub>2</sub> radical described previously. As such, the presence of this species seems to be largely attributed to the perturbed indoor air chemistry.

Another signal that appears to be present is that for the CH<sub>3</sub>O<sub>2</sub> radical, **6.17**, a common atmospheric species with literature indoor concentrations of ca. 7.4 molecule cm<sup>-3</sup>

predicted.<sup>363</sup> However, this signal appears to be weak, only being distinguishable in the most perturbed experiment, the MS plot of which is shown in **Chapter 9.6**.

There are other signals which can also be directly linked to limonene chemistry, via their structure, as well as via variation in their concentrations.<sup>228</sup> Literature studies on limonene systems have found that limonaldehyde is one of the most abundant species formed via limonene ozonolysis, for example Waring et al. identify it as a major species for this reaction under indoor conditions.<sup>360</sup> Also, under ‘cleaning’ conditions, Carslaw estimated that 12% of species which accumulate following this process would be limonaldehyde.<sup>369</sup> One such mechanism for limonaldehyde’s formation is via  $\cdot\text{OH}$  attack, predicted within the MCM, is given in Figure 246.<sup>229,230</sup> Alternatively, limonaldehyde can be formed by ozonolysis reactions, given in Figure 247.<sup>229,230</sup> Indeed, the identification of **4.23** can be used as partial evidence for the existence of these mechanisms given in the MCM.

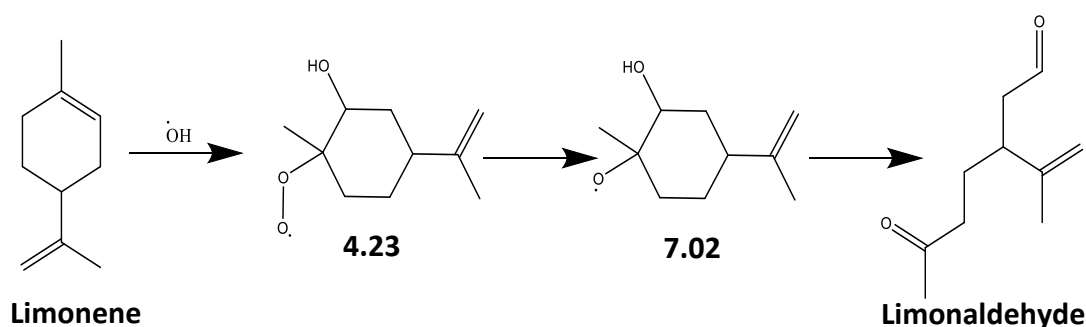


Figure 246: A mechanism for limonaldehyde formation via  $\cdot\text{OH}$  attack<sup>229,230</sup>

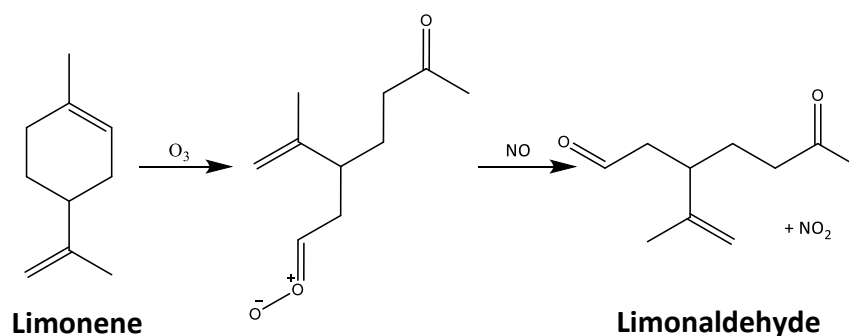


Figure 247: A mechanism for limonaldehyde formation via ozonolysis<sup>229,230</sup>

It appears that we can observe a product, **7.05**, linked to  $\cdot\text{OH}$  attack on limonaldehyde, with the radical products expected from this reaction shown in Figure 248.<sup>229,230</sup> Given the large amount of ozone and  $\cdot\text{OH}$  present in the system, (formed from the limonene ozonolysis reaction), this is not a surprising reaction to take place, an observation supported by modelling this system.<sup>17</sup> The simple model constructed previously was again utilised, with results for **4.06** also output here. The results, in Figure 249, indicate that **7.05** is expected to be formed in similar quantities to those of **4.21** and **4.23** described previously.<sup>229,230,323</sup>

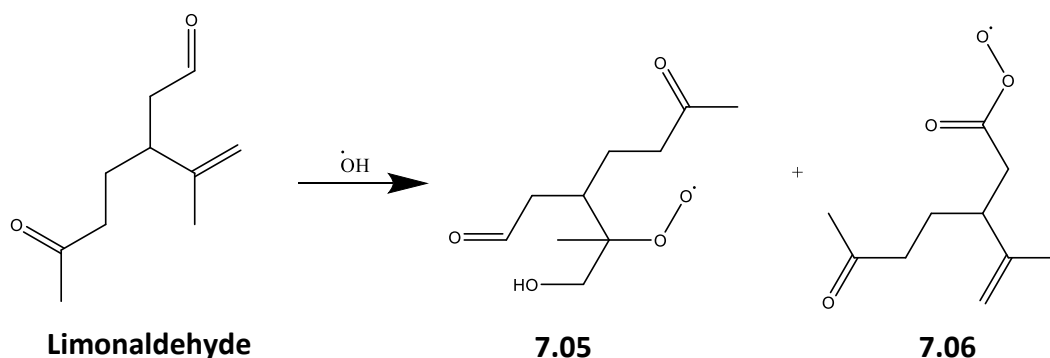


Figure 248: Formation of radical products from limonaldehyde<sup>229,230</sup>

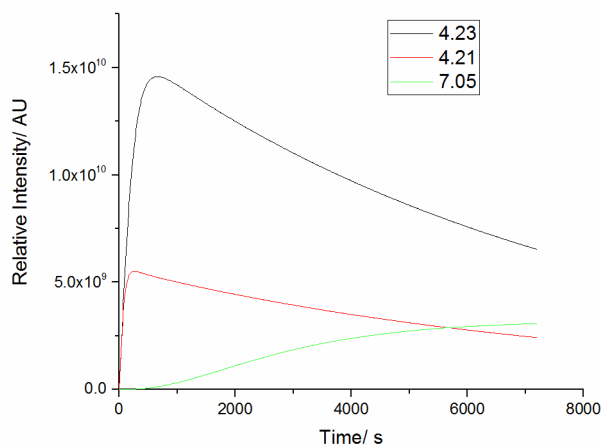


Figure 249: Model comparing expected formation of radicals **7.05** with **4.21** and **4.23** from ozonolysis and  $\cdot\text{OH}$  attack on limonene.<sup>323</sup>

**7.05** was clearly identified in experiments spiked with ozone, with the signal from experiments without VOC spiking noticeably less clear than that from experiments with

VOC spiked systems. This change can be seen in Figure 250, with captured species **7.07** shown in Figure 251.

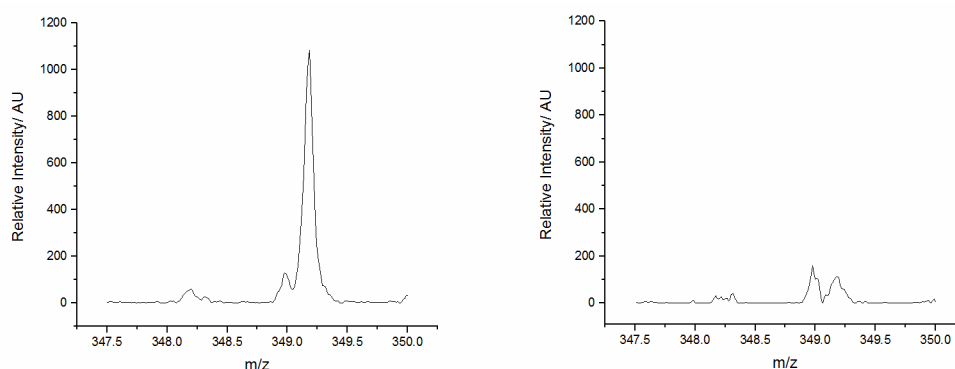


Figure 250: Variation in signal for adduct **7.07** in VOC+O<sub>3</sub> experiment, and elevated O<sub>3</sub> without VOC experiment respectively.

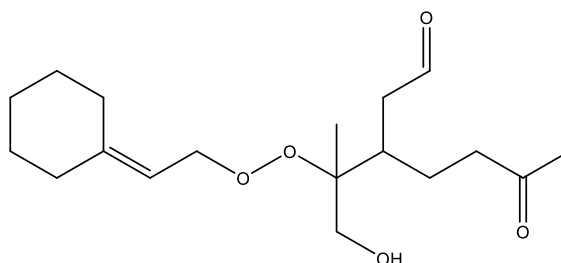


Figure 251: Structure for captured **7.07**

This signal for captured **7.05** variation matches the trend found previously from the limonene ozonolysis and ·OH attack initial RO<sub>2</sub> products, supporting the theory that this compound is originating from limonene. As such, it appears highly likely that this signal can be solely attributed to limonene reactions within the indoor experiment. The identification of this signal is also useful as evidence to prove that radical chemistry is occurring beyond just initial limonene products, and that the reaction products are not all being lost to deposition onto surfaces within the experiment (walls, carpet, tables etc). The process of identifying radicals from indoor air helps to provide some further background to literature measurements, providing evidence for the radical intermediates leading to oxidised species and SOA formation. For example, capture of species such as **7.05** provides evidence of gas phase precursor species that would be expected to lead to the limonene derived SOA described by Morawska et al. in a study on indoor air within classrooms.<sup>370</sup>

### 7.3.7. Experiments with Increased Temporal Resolution

An experiment was also conducted on a VOC spiked system with a higher time resolution, with samples taken with 30 minute exposures. This enabled variation in signal over the experiment to be examined in more detail, as opposed to longer duration measurements which just average the experimental period. A plot of this data, examining **4.22** (captured RO<sub>2</sub> from ozonolysis) is given in Figure 252, with O<sub>3</sub> variation given in **Chapter 9**.

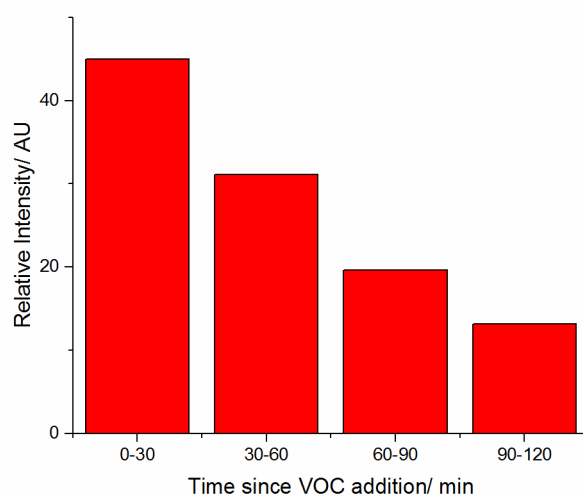


Figure 252: Variation in signal for adduct **4.22** during indoor air (meeting room) experiments

These results indicate a decay in levels of radical **4.21** as the experiment progresses. This is as expected – once VOC has been added, the amount of VOC will gradually decrease due to both ozonolysis and OH reactions. Data from GC-MS of canister samples taken during these experiments reinforces these results. This data (Figure 253) shows that the limonene concentration appears to be decreasing over a similar timescale to that observed for the peroxy species formed following limonene oxidation.

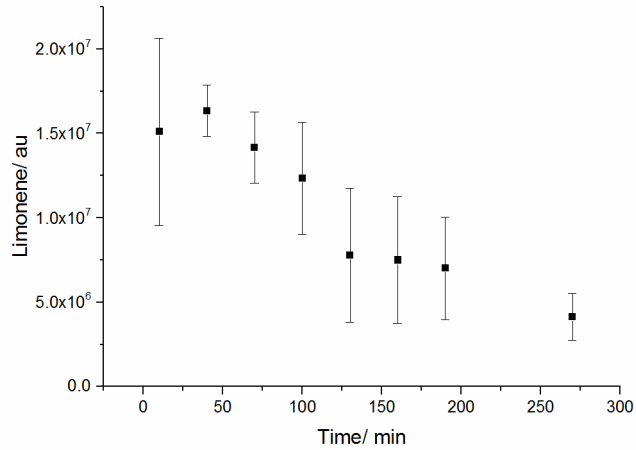


Figure 253: GC-MS data showing limonene decay

As a method of confirming these results, signals for different peroxy radical based products can be examined. As with **4.21**, these species are formed early in the oxidation of the VOC. Data for **4.24** and **4.02** are given below in Figure 254.

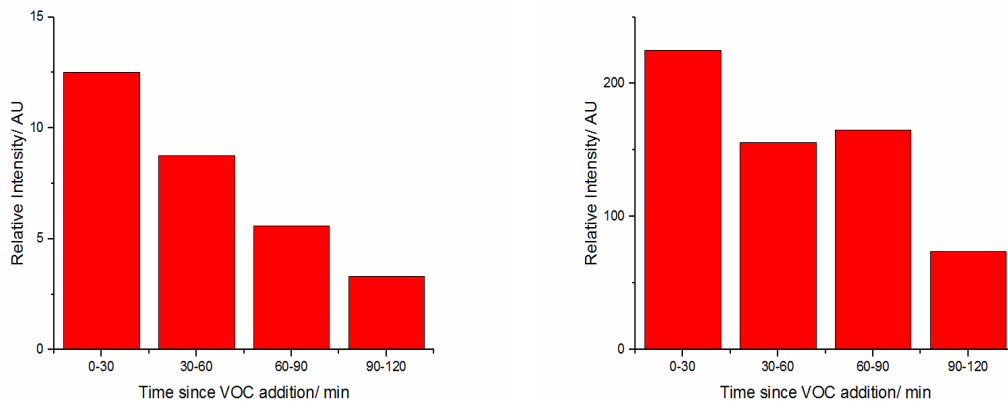


Figure 254: Variation in signal for **4.24** and **4.02** respectively during indoor air (meeting room) experiments

Both **4.24** and **4.02** exhibit an overall decay as the experiment continues. However, **4.02** does not appear as uniform – the signal for 60-90 minutes is slightly higher than 30-60, which does not fit with the rest of the observed data. This appears to be from an anomaly within the measurement – these are still single 30 minute measurements and, as has been

mentioned previously, repeats will be needed in order to remove errors such as this. Measurements of errors in **Chapter 5** suggested values of 2%: this is clearly larger than this. However, the sample area is not sealed as a simulation chamber would be, so external species may be entering the system and interfering with the measurement.

### 7.3.8. Air Fragrance Experiments

As a further set of experiments, a commercial fragrance system was deployed within the room. Compounds from air fresheners can be responsible for up to 23 % for indoor VOC emissions.<sup>366</sup> Studies on air fresheners have shown that most compounds contained are not listed in the product description.<sup>371</sup> However, the literature suggests that the majority of air fresheners contain monoterpenes such as limonene and other monoterpene derived species.<sup>338,372</sup> Subsequent GC-MS analysis of the air freshener indicated the presence of several terpenes, including  $\alpha$ -pinene and limonene. Measurements of **4.22** in experiments with an air freshener present are shown in Figure 255 below.

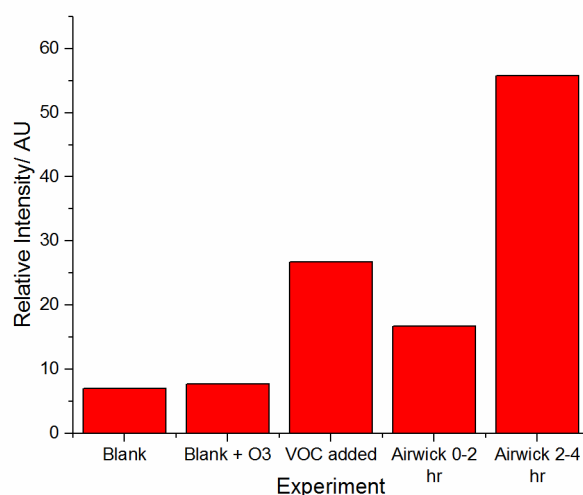


Figure 255: Comparison of signals for **4.22** from indoor air meeting room

There are clear signals for the formation of **4.22** (from ozonolysis derived limonene  $RO_2$  radical **4.21**) within these experiments, with significant differences in strength of signal observed from these experiments as the total exposure time increases. This is likely due

to a gradual increase in emitted product concentrations, until a steady state is reached. Indeed, GC-MS canister measurements (Figure 256) also showed an increase in limonene concentrations during these experiments.

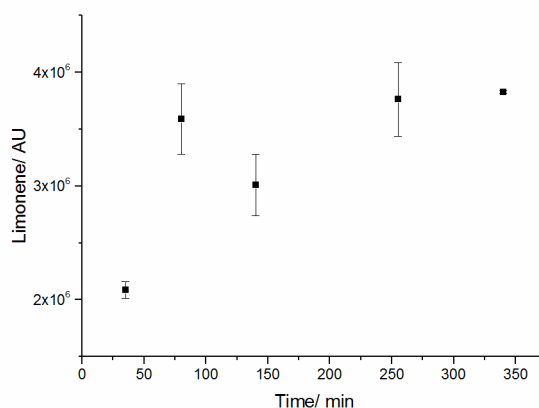


Figure 256: GC-MS data for limonene from canister samples of air freshener experiment

Signals from radical trapping after the initial 2 hours of operation are significantly strong – noticeably more intense than the signals generated from the VOC spiking experiments. The data here implies significantly high concentrations of limonene undergoing ozonolysis reactions, hence suggesting that significant levels of indoor chemistry is occurring from emission of the plug-in air freshener. This supports literature observations: Nørgaard et al. have found concentrations of over  $2.2 \times 10^{13}$  molecule  $\text{cm}^{-3}$  limonene from air freshener in a chamber experiment, with reaction products such as acetaldehyde reaching concentrations of  $2.7 \times 10^{12}$  molecule  $\text{cm}^{-3}$ .<sup>358</sup>

#### 7.4. Outdoor Air Sampling

The radical trapping methodology was also applied to outdoor systems. These proof of concept experiments are considerably more complex than the indoor systems, owing to a huge range of radicals and conditions potentially present. Despite considerably less control in these experiments (e.g. some control of the chemistry through controlling the ozone level or spiking with VOC), it would be interesting to investigate which species can be detected using 2.09 and the developed methodology.

During the outdoor ambient experiments (see Table 2 for conditions), two outdoor sampling sites were utilised. The first was at ground level, behind the atmospheric chemistry research building at the University of York, in close proximity to trees and leaf litter. The second was on the roof of the same building, which is two storeys high. It was hoped that the rooftop sampling experiments would be marginally cleaner, for example due to the absence of leaf litter, whilst also exposed to more processed air from a wider range of emission sources. The two sites are shown in Figure 257. The sampling technique itself is identical to that utilised for indoor air experiments (**Chapter 9**).

Experiment	Date	Time Range	Temperature/ K	Humidity/ %	O <sub>3</sub> / ppb
1	20/02/2017	13:30-16:40	284.4	80.2	20
2	22/02/2017	15:00-19:10	282	73.8	40
3	09/03/2017	14:30-16:20	282.1	64.3	40
4 (rooftop)	15/03/2017	11:30-15:30	283.5	66.1	35

Table 2: Outdoor Sampling Conditions. Temperature and humidity were measured from a weather station on the Physics building, ozone on the Atmospheric building roof



Figure 257: Images of indoor and outdoor sampling sites

#### 7.4.1. Products Detected from Ground Level Outdoor Sampling

As expected, several different radicals were observed from outdoor sampling with an exposure time of 15 minutes, shown in Figure 258. These include the hydroperoxyl radical

adduct **4.11** and the methyl peroxy species **6.18**, as well as signals corresponding to OH adduct **7.09** and terpenoid ozonolysis compound **4.04**. These are species that would indeed be anticipated to be present: atmospheric concentrations of methyl peroxy radicals are estimated at  $10^8$  molecules  $\text{cm}^{-3}$ , while hydroperoxy radicals have previously been detected outdoors at similar levels.<sup>38,328,373</sup> In addition to this, combined concentrations of these species have been measured at up to  $1.8 \times 10^9$  molecules  $\text{cm}^{-3}$  in urban areas.<sup>326</sup> As such, the formation and detection of **6.18** and **4.11** was a useful demonstration of successful application of this radical trapping methodology in the ‘real’ atmosphere.

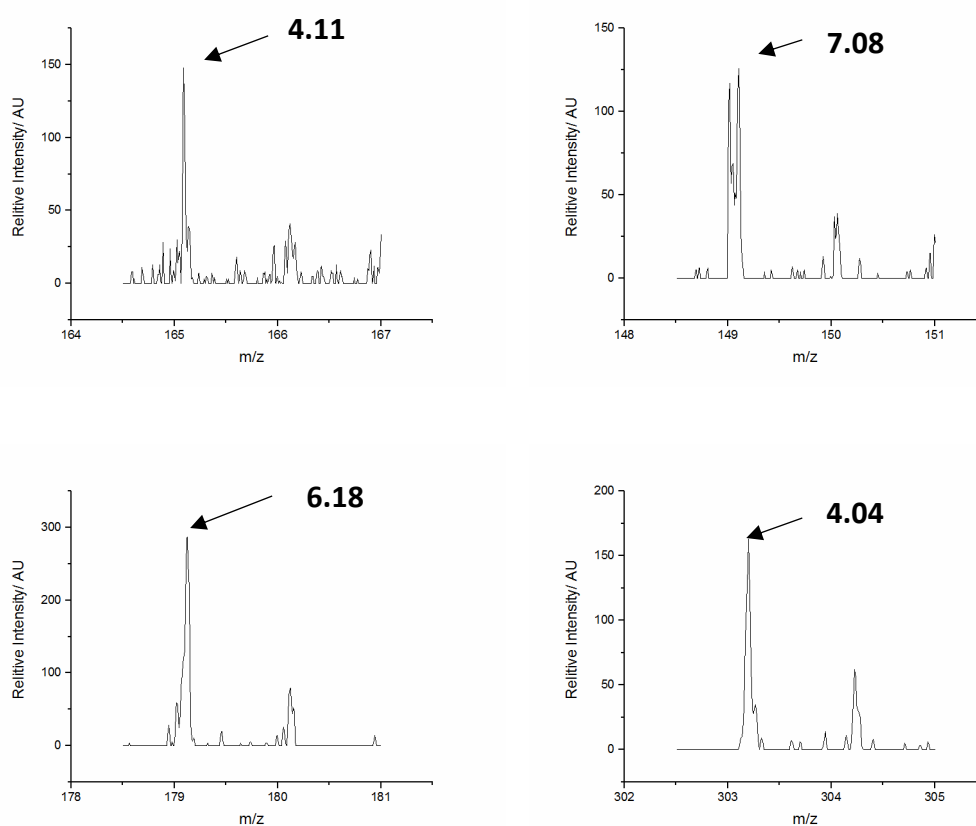


Figure 258: Signals detected from ground level outdoor sampling, corresponding **4.11**, **7.08**, **4.04** and **6.18** clockwise.

Compared to previous gas phase experiments, signals obtained from these experiments appear significantly weaker. This is unsurprising in a ‘real world’ ambient atmosphere application –experiments from **Chapter 4** and **6** are expected to be operating on very high concentrations with a considerably lower variety of species, while strong signals were only detected in indoor systems in the presence of additional ozone. Ozone levels during these

outdoor experiments were 15 ppb, which would be expected for an early spring suburban environment.<sup>374</sup> There is also some potential for humidity to influence this system, as a more humid environment could have a significant impact on radicals formed, as suggested by Kristensen et al.<sup>227</sup> Although both experiments were conducted on dry days, the ambient background was more humid than that from indoor experiments, or in previously described test systems.

#### 7.4.2. Products Detected from Rooftop Outdoor Sampling

Conducting rooftop sampling experiments at the same exposure times produced similar results to those in Figure 258, with rooftop sampling results shown in Figure 259. Once again, compounds **4.11**, **4.04**, **7.08** and **6.18** are identified, illustrating the similarity of the two different sampling environments, as well as the reproducibility of measurements.

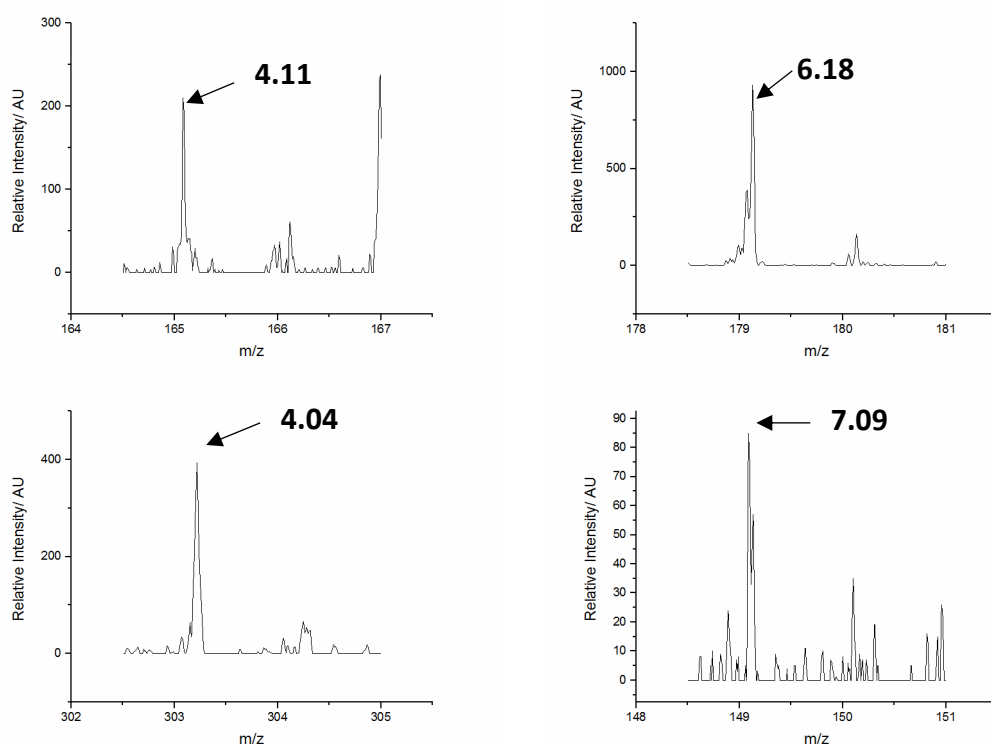


Figure 259: Results showing the capture of radicals from rooftop sampling

However, these samples appear to be noticeably stronger with regard to background levels than the equivalent samples taken at ground level. Given that sampling techniques were

identical, with the same loading of **2.09**, this change is attributed to different sampling conditions on the rooftop: being away from leaf litter likely decreased the overall variety of radical species to be sampled, thus enabling more of the trap to react with the radicals that were present, hence enhancing their signal to noise ratio compared to ground level experiments.

### 7.4.3. Sampling Time Variation for Outdoor Sampling

Sampling times were kept at  $\leq 30$  minutes for these experiments with a view to examining whether sufficient information can be gathered in 'real world' sampling at these exposure times. While signals have been detected with exposures of less than a minute in gas phase tests described in **Chapter 5**, those systems were considerably less complex than real atmospheric systems, with higher concentrations and a cleaner chemical system (i.e. formation of specific radical species). Hence it is far from certain that similarly low outdoor sampling times would prove effective. This short sampling time would be particularly useful for potential future applications of this air sampling technique where a high temporal resolution will be required.

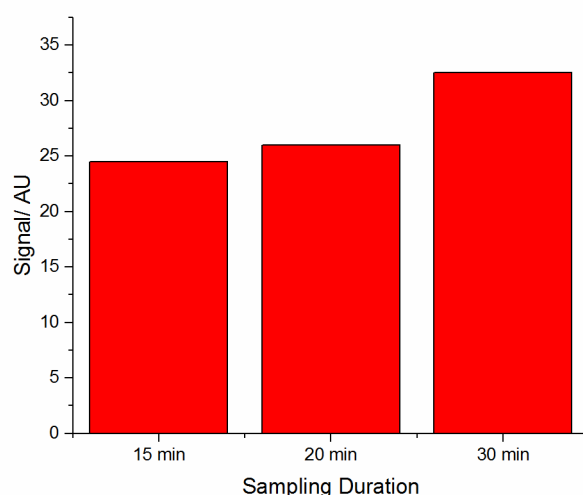


Figure 260: Change in **6.18** signal strength as sampling time changes in outdoor sampling.

The difference in signal between these experiments in Figure 260 demonstrated that, while sampling time does influence signal intensity, the overall change is not. For these

small sampling times, a lack of significant change between 15 and 30 minutes is not unexpected. Therefore, it appears that sampling times of 15 minutes are indeed feasible for sampling 'real' gas phase systems, as well as the model systems studied previously.

Finally, experiments were conducted under day (ca. 14:00) and night (ca. 19:00, sunset at ca. 17:00) conditions. Key oxidants such as  $\cdot\text{OH}$  are expected to have higher daytime concentrations, so overall radical concentrations should be lower at night.<sup>216</sup> Indeed, the previously observed **7.09** cannot be identified in night-time sampling, while **4.11** is difficult to identify from background noise, although is present at the correct mass in Figure 261.

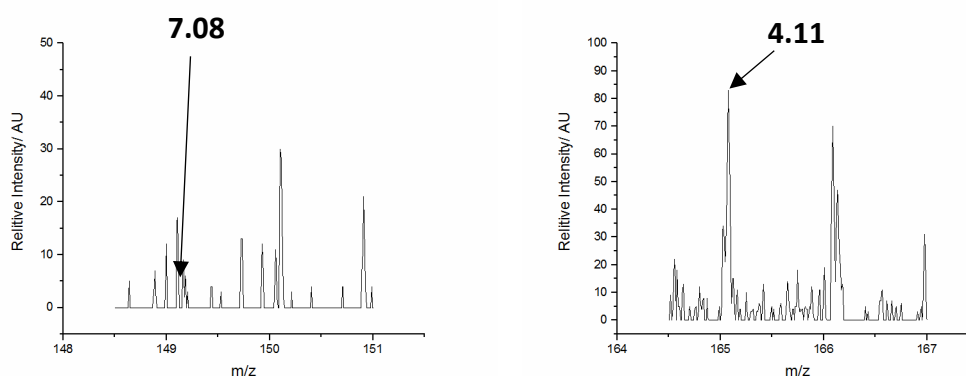


Figure 261: Lack of signal in night experiments for **7.08** and **4.11**

While this is disappointing, (capture of night-time radical species would be a very good indicator for use of this technique to monitor low concentration radicals) it must be noted that there is still plenty of scope to improve experimental detection limits. For example, extending sampling time would enhance the possibility of detecting the **7.08** or **4.11**, as temporal resolution at night-time for these experiments is clearly not currently sufficient.

## 7.5. Future work

There are many different avenues for future work based around these proof of concept 'real world' sampling experiments. Regarding indoor air experiments, one of the most obvious would be to conduct further repeats of these experiments, in an attempt to confirm the data already gathered. This would also ideally include use of a tracer

compound, which is suitably inert as to not interfere with radical chemistry, but can be monitored in order to better evaluate wall loss etc. in the indoor system. Conducting the same trapping experiment over a series of different days would also provide information regarding variation within the indoor air of this particular system. Another useful study would be to compare results to samples taken from a different indoor environment – for example a different building, or one with many indoor plants.<sup>375</sup> This would enable a comparison between ambient radicals detected within these different environments.

A similar series of experiments could also be designed which are more comprehensively instrumented. This will provide complementary data, enabling better understanding of sources and sinks of observed radicals. Using multiple radical trapping sites within the same system would be useful to study the homogeneity of the indoor chemical environment. For example, positioning the sampling sites by windows may give results showing different signals according to whether the area around the sample is in direct sunlight, or not. Bleach experiments can be expanded upon, with improved atmospheric mixing of bleach emissions around the room. Studying radical species present within indoor air from other commercial products (i.e. scented candles) or herbs etc used when cooking would also be very interesting. These will produce a wide assortment of species, with the detection of radicals linked to the formation of toxic products (i.e. formaldehyde or aromatic products) being of particular interest regarding human health.<sup>376,377</sup>

Regarding the outdoor systems, work is needed to build on the (very) preliminary work already completed. Studying the change in radicals detected, and their intensities, over a 24 hour period would be very interesting. Regular sampling would provide a high temporal resolution to this experiment, and enabling a 'diurnal radical profile' during a day to be generated. Conducting the experiment over different conditions/seasons (e.g. summer compared to winter, or high ozone levels compared to low) would also provide interesting data regarding the resultant changes in radicals present. This would also function towards further examining the applicability of the trapping molecule to different environmental conditions. It would be expected that correlations would be identifiable from factors such as wind direction, ozone concentration and UV intensity.

## 7.6. Conclusions

Overall, the indoor air experiments have produced some interesting results. Different types of radicals were captured from reactions within indoor air, both under 'ambient' conditions, and when the room has been spiked with ozone and/or a monoterpene(s). The detection of a wide variety of captured radicals, along with the origin of these species, can be adequately explained by examining the reaction routes postulated within the MCM.<sup>228</sup>

It is worth emphasising that the concentrations of terpene and ozone within the 'spiking' experiments are still within those that could be found in an inner-city office, which has some form of air freshener present.<sup>378</sup> There were also terpene originating signals detected in experiments where scented bleach is applied, with these signals not observed in the non-scented bleach equivalent. Analysis of indoor air in the presence of an air freshener also showed strong signals for terpenoid reaction products. The implications of this are important for future studies, particularly those surrounding indoor air quality.

Meanwhile, outdoor air experiments have shown that a range of radicals can also be detected and speciated in daytime experiments, including **4.11** and **7.08**, which are expected to be present from literature studies.<sup>326</sup> These were measured during early spring, hence in an environment with relatively low photochemical activity. Night-time experiments have thus far failed to detect **4.11** or **7.08**, with this likely due to the lower night-time concentrations of these species. Radicals **6.18** and **4.04** can also be observed in rooftop experiments in a similar location, providing evidence for the reproducibility of the measurements in a similar area. The signals produced from these experiments illustrate the potential for this radical trapping technique to be applied to 'real' ambient atmospheric sampling.

## 8. Conclusions and Future Work

A series of novel compounds (**2.09**, **2.11**, **2.13**, and **2.16**) have been synthesised in order to act as chemosensors for the trapping of short lived radicals. These are based upon the addition of a radical to a double bond, with subsequent loss of a stable radical leaving group. This leaves the original radical incorporated into a stable non radical compound suitable for off-line analysis. The synthesised traps are sufficiently stable for trapping experiments, however have half-lives  $\leq 15$  hours when in solution, owing to a 1,3-sigmatropic rearrangement. There is the opportunity for future work regarding these trapping species, namely the preparation of further traps that are more stable (with regard to 1,3-sigmatropic rearrangements such as **2.09** to **2.09'**). It would also be worthwhile to synthesise traps that are water soluble. This would enable sampling to take place within aqueous environments (i.e. biological systems). Traps which contain either bromine or chlorine atoms would also have a potential application, with the resulting isotopic ratios of molecular ion peaks enabling trapped products to be highly distinguishable upon MS analysis.

Initial tests of these compounds were conducted in liquid phase experiments. Here, the <sup>t</sup>butyl peroxy and methyl radicals were successfully captured, forming **3.01** and **3.02** respectively and providing evidence for radical trapping. However, attempts to capture nitrogen or sulfur centred radicals resulted in oxidative dehydrogenation of the trapped adduct, with the observation of species two mass units smaller than those expected. Utilisation of deuterated reagents suggests that the oxidative dehydrogenation occurs on the 'trap' side of the compound. Reactions under a nitrogen atmosphere appear to facilitate the formation of the originally expected reaction product.

The radical trapping system was subsequently applied to gas phase experiments, with the ozonolysis of atmospherically relevant alkenes ( $\alpha$ -pinene,  $\beta$ -pinene, limonene and TME) studied. This resulted in the capture of a series of peroxy radicals, which were able to be assigned structures based on their masses and comparison with radical species predicted

by the Master Chemical Mechanism (MCM).<sup>229,230</sup> The initial peroxy products detected (e.g. **4.01**, **4.29**) provide evidence for the vinyl hydroperoxide mechanism, a key night-time source of hydroxyl radicals. Conducting reactions with long residence times also appeared to facilitate the formation of oxygenated species such as **4.15**. Low volatility species such as this have the potential to be highly important as a source for atmospheric aerosol. Future work on this system should feature the development of HPLC separation of the trapped species. This would be particularly useful with regard to identifying relative amounts of trapped species (e.g. **4.02** and **4.04**), as well as separating isomers of various radicals (e.g. **4.02a-c**). Accomplishing this enables an important confirmation of predicted reaction pathways and branching ratios within the MCM. Another way towards evaluating relative pathways would be to utilise partially deuterated  $\alpha$ -pinene, with the relative intensities and mass shifts of product MS signals providing an indication regarding the comparative importance of different reaction pathways.<sup>379</sup> Conducting experiments in the presence of NO would again be useful, as this would provide the opportunity to evaluate the impact of NO on reaction routes/branching ratios, as well as to capture proposed nitro-peroxy radicals.<sup>380</sup>

Experiments probing the products from the reaction between n-nonane and hydroxyl radicals were also conducted. These were successful in capturing a series of peroxy radicals (e.g. **6.01**, **6.05**), which were again compared to predicted species from the MCM. Simple calibration experiments were also conducted with methane and n-nonane, which illustrated the potential for this methodology to be applied at low concentrations (i.e. atmospheric levels). In future work it would be useful to continue these calibration experiments in order to identify the impact on calibration of several types of RO<sub>2</sub> (e.g. both MeO<sub>2</sub> and **6.01**) being present within the system.

Measurements at different distances along a flow tube were utilised in order to vary reaction times, and enable the comparison of the experimental kinetics of radical species to those modelled by use of rate constants from the MCM. This showed good agreement between experimental and modelled predictions for these species. In order to expand upon these results, it would be beneficial to study the kinetics of another more complex

radical system, of which kinetics are not yet fully understood (e.g. oxidation of toluene under atmospheric conditions).

There is much scope for future studies of the radical trapping technique in conjunction with atmospheric chambers (e.g. HIRAC at The University of Leeds). Radicals, which will be produced in a steady state under controllable temperature, pressure and light, can be analysed by these chemosensors, as well as in situ spectroscopic methods. Systems such as formaldehyde photolysis, or the self-reaction of  $\text{MeO}_2$  would be simple systems suitable for these studies. More complex systems, i.e. the study of radical species involved in low temperature 'auto-ignition' chemistry of oxygenates, would also be worthwhile to study, which could lead to insights on the role of these species in SOA formation.

Finally, the trapping methodology was applied to real atmospheric conditions, sampling both indoor and outdoor air. Indoor experiments were successful in the detection of terpenoid  $\text{RO}_2$  species (e.g. **4.21**, **4.23**) under a variety of conditions, including upon addition of household fragrances. Experiments to expand upon this work could include the study of different indoor environments (e.g. kitchens) in order to evaluate the range of radical chemistry within those systems. Meanwhile, preliminary outdoor experiments detected  $\text{MeO}_2$ , an abundant atmospheric  $\text{RO}_2$  radical. These experiments also demonstrated the utility of this technique, with the sampling system being sufficiently portable to be readily usable in different locations. Future work in this area should focus on more detailed outdoor measurements, for example the measurement of a temporal radical profile under different conditions (e.g. summer/winter). Conducting experiments in the presence of another technique (e.g. a field FAGE instrument) would be useful to compare different measurement systems' sensitivities to ambient species such as  $\text{HO}_2$ .

Overall, a series of novel trapping compounds have been developed which trap radicals in a stable non-radical form for future offline analysis. These have been tested in liquid phase reactions, as well as gas phase reactions of atmospheric relevance and initial 'real world' sampling. The results of these tests suggest the utility of these compounds in future work regarding the identification of radicals under low concentrations.

## 9. Experimental

All reagents were used as purchased. When used, dry DCM, diethyl ether, THF and toluene were obtained from a Pure Solv solvent purification system.

NMR experiments were conducted on a Jeol ECS-400 spectrometer ( $^1\text{H}$  400 MHz,  $^{13}\text{C}$  100 MHz), however a Bruker AV500 was used for  $^1\text{H}$  500 MHz experiments.

TLC was conducted using Merck TLC silica gel 60 F254 Al backed plates. Flash chromatography used Sigma silica gel, 60 Å pore size, 35-75  $\mu\text{m}$  particle size.

MS experiments were run on a Bruker Daltronics microTOF system, with ESI ionisation. MSMS experiments used a Bruker HCTUltra ETD II spectrometer, with both EI and APCI ionisation utilised.

EPR experiments were conducted using a Bruker EMX<sub>micro</sub> spectrometer.

HPLC experiments were conducted with a Dionex Ultimate 3000 system with a reverse phase ODS column (Alphasil, 25 cm x 4.6 mm)

### 9.1. Experimental Details for Chapter 2:

**9.1.01. Cobalt catalysed reaction between 3-methyl-1,4-pentadiene and TEMPO under an oxygen atmosphere.**

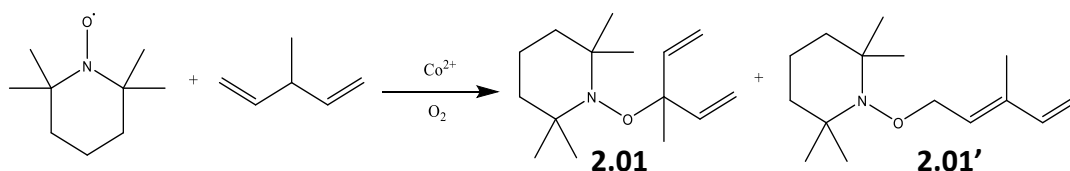


Figure 262: Formation of **2.01** by reaction with TEMPO and a Co catalyst

2,2,6,6-Tetramethylpiperidine 1-oxyl (TEMPO) (0.1583g, 1mmol), 3-methyl-1,4-pentadiene (0.08 mL, 0.66 mmol) and Co<sup>2+</sup> ethyl hexanoate (65 wt% in mineral spirits, 0.431 mL, 0.8 mmol) were added into a round bottom flask. The reaction was placed under an oxygen atmosphere and cooled to 0°C, before stirring for 24 hr. DCM (20 mL) was added to the reaction mixture, which was then washed with H<sub>2</sub>O (20 mL) (x3) and dried with MgSO<sub>4</sub> before solvent was removed by rotary evaporation. The remaining residue was purified by flash chromatography (49:1 PET ether: ethyl acetate, R<sub>f</sub> = 0.31) and the product collected and dried. Yield: 44 %, a mixture of **2.01'** (87%) and **2.01** (13%).

**2.01'** <sup>1</sup>H NMR: (400 MHz) 1.09 (s, 6H, C(CH<sub>3</sub>)<sub>2</sub>), 1.18 (s, 6H, C(CH<sub>3</sub>)<sub>2</sub>), 1.45 (m, 6H, CH<sub>2</sub>CH<sub>2</sub>CH<sub>2</sub>), 1.74 (s, 3H, CCH<sub>3</sub>), 4.42 (d, 2H, J=6.6 Hz, CHCH<sub>2</sub>), 5.01 (d, 1H, J=10.8 Hz, CCHH), 5.16 (d, 1H, J = 17.4 Hz, CCHH), 5.61 (t, 1H, J = 6.6 Hz, CHCH<sub>2</sub>), 6.39 (dd, 1H, J = 10.8, 17.4 Hz, CHCH<sub>2</sub>).

**2.01** <sup>1</sup>H NMR: (400 MHz) 1.09 (s, 6H, C(CH<sub>3</sub>)<sub>2</sub>), 1.18 (s, 6H, C(CH<sub>3</sub>)<sub>2</sub>), 1.45 (m, 6H, CH<sub>2</sub>CH<sub>2</sub>CH<sub>2</sub>), 1.74 (s, 3H, CCH<sub>3</sub>), 5.12 (d, 2H, J=10.6 Hz, CCHH), 5.24 (d, 2H, J=17.6 Hz, CCHH), 6.70 (dd, 2H, J= 10.6, 17.6 Hz, CHCH<sub>2</sub>).

MS (ESI): 238.2163, calculation for C<sub>15</sub>H<sub>28</sub>NO, [M+H]<sup>+</sup> = 238.2165

### 9.1.02. Reaction between 3-methyl-1,4-pentadiene and TEMPO under an oxygen atmosphere.

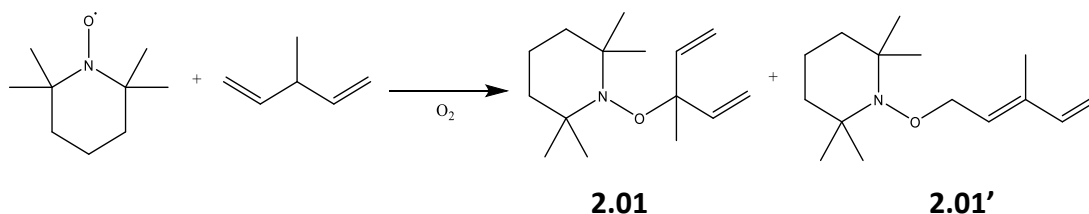


Figure 263: Formation of **2.01** and **2.01'** by reaction with TEMPO

2,2,6,6-Tetramethylpiperidine 1-oxyl (TEMPO) (0.1564 g, 1mmol) was added to 3-methyl-1,4-pentadiene (0.08 mL, 0.66 mmol). The reaction was placed under an oxygen atmosphere, cooled to 0 °C, and stirred for 24 hr, whilst warming to room temperature. DCM (20 mL) was added, and the solution washed with H<sub>2</sub>O (3x 20 mL) and dried with MgSO<sub>4</sub> before filtration and solvent removal by rotary evaporation. The remaining residue

was purified by flash chromatography (49:1 PET ether: ethyl acetate,  $R_f = 0.31$ ) to give a mixture of primary and tertiary TEMPO functionalised products. Yield = 8%, a mixture of **2.01'** (79.9%) and **2.01**, (20.1%) TEMPO functionalised product.

$^1\text{H}$  NMR: (400 MHz) 1.09 (s, 6H,  $\text{C}(\text{CH}_3)_2$ ), 1.18 (s, 6H,  $\text{C}(\text{CH}_3)_2$ ), 1.44 (m, 6H,  $\text{CH}_2\text{CH}_2\text{CH}_2$ ), 1.74 (s, 3H,  $\text{CCH}_3$ ), 4.42 (d, 2H,  $J=6.6$  Hz,  $\text{CHCH}_2$ ), 5.02 (d, 1H,  $J=10.6$  Hz,  $\text{CCHH}$ ), 5.16 (d, 1H,  $J = 17.2$  Hz,  $\text{CCHH}$ ), 5.61 (t, 1H,  $J = 6.6$  Hz,  $\text{CHCH}_2$ ), 6.39 (dd, 1H,  $J = 10.6, 17.2$  Hz,  $\text{CHCH}_2$ ).

**2.01**  $^1\text{H}$  NMR: (400 MHz) 1.09 (s, 6H,  $\text{C}(\text{CH}_3)_2$ ), 1.18 (s, 6H,  $\text{C}(\text{CH}_3)_2$ ), 1.44 (m, 6H,  $\text{CH}_2\text{CH}_2\text{CH}_2$ ), 1.74 (s, 3H,  $\text{CCH}_3$ ), 5.12 (d, 2H,  $J=10.6$  Hz,  $\text{CCHH}$ ), 5.24 (d, 2H,  $J=17.6$  Hz,  $\text{CCHH}$ ), 6.70 (dd, 2H,  $J= 10.6, 17.6$  Hz,  $\text{CHCH}_2$ ).

### 9.1.03. Reaction between 3-methyl-1,4-pentadiene and TEMPO under an oxygen atmosphere with an antioxidant

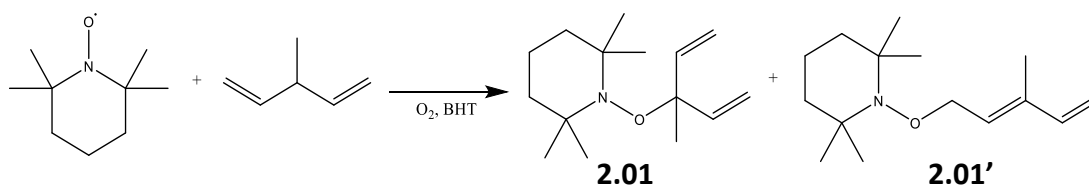


Figure 264: Formation of **2.01** and **2.01'** by reaction with TEMPO in the presence of BHT

2,2,6,6-Tetramethylpiperidine 1-oxyl (TEMPO) (80 mg, 0.5 mmol), butylated hydroxytoluene (9.2 mg, 0.05 mmol) and 3-methyl-1,4-pentadiene (0.04 mL, 0.33 mmol) were mixed together and stirred for 19 hr. DCM (20 mL) was added to the reaction, and the organic phase washed with  $\text{H}_2\text{O}$  (2 x 20 mL). After drying with  $\text{MgSO}_4$  and filtration, solvent was removed by rotary evaporation. The remaining residue was purified by flash chromatography (49:1 PET ether: ethyl acetate,  $R_f = 0.31$ ). Yield = 16%, a mixture of **2.01'** (82.9%) and **2.01** (17.9%) TEMPO functionalised products.

**2.01'**  $^1\text{H}$  NMR: (400 MHz) 1.09 (s, 6H,  $\text{C}(\text{CH}_3)_2$ ), 1.18 (s, 6H,  $\text{C}(\text{CH}_3)_2$ ), 1.44 (m, 6H,  $\text{CH}_2\text{CH}_2\text{CH}_2$ ), 1.74 (s, 3H,  $\text{CCH}_3$ ), 4.42 (d, 2H,  $J=6.9$  Hz,  $\text{CHCH}_2$ ), 5.02 (d, 1H,  $J=10.5$  Hz,  $\text{CCHH}$ ), 5.17 (d, 1H,  $J = 17.4$  Hz,  $\text{CCHH}$ ), 5.61 (t, 1H,  $J = 6.9$  Hz,  $\text{CHCH}_2$ ), 6.39 (dd, 1H,  $J = 10.5, 17.4$  Hz,  $\text{CHCH}_2$ ).

**2.01**  $^1\text{H}$  NMR (400 MHz) 1.09 (s, 6H,  $\text{C}(\text{CH}_3)_2$ ), 1.18 (s, 6H,  $\text{C}(\text{CH}_3)_2$ ), 1.44 (m, 6H,  $\text{CH}_2\text{CH}_2\text{CH}_2$ ), 1.74 (s, 3H,  $\text{CCH}_3$ ), 5.12 (d, 2H,  $J=11$  Hz,  $\text{CCHH}$ ), 5.24 (d, 2H,  $J=16.9$  Hz,  $\text{CCHH}$ ), 6.70 (dd, 2H,  $J=11, 16.9$  Hz,  $\text{CHCH}_2$ ).

**9.1.04. Reaction between 3-methyl-1,4-pentadiene and TEMPO using Fenton based radical generation.**

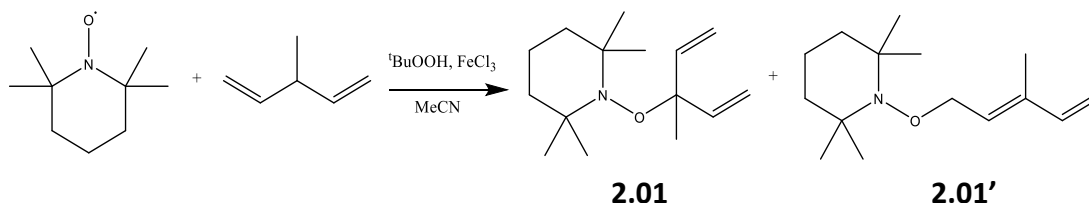


Figure 265: Formation of **2.01** and **2.01'** utilising Fenton chemistry

2,2,6,6-Tetramethylpiperidine 1-oxyl (TEMPO) (0.315 g, 2 mmol), 3-methyl-1,4-pentadiene (0.24 mL, 2 mmol) and tert-butoxy hydroperoxide (70% aq, 0.39 mL, 2.8 mmol) were mixed together in MeCN (0.1 mL).  $\text{FeCl}_3$  (3 mg, 0.02 mmol) was added, and the reaction stirred for 18 hr. DCM (20 mL) was added to the reaction mixture, and the solution washed with  $\text{H}_2\text{O}$  (2 x 20 mL). The organic layer was dried with  $\text{MgSO}_4$ , filtered, and solvent removed by rotary evaporation. The remaining residue was purified by flash chromatography (49:1 PET ether: ethyl acetate,  $R_f = 0.31$ ), and the product collected and dried. Yield = 8.4%, a mixture of **2.01'** (83.2%) and **2.01** (16.8%) TEMPO functionalised product.

**2.01'**  $^1\text{H}$  NMR: (400 MHz) 1.11 (s, 6H,  $\text{C}(\text{CH}_3)_2$ ), 1.20 (s, 6H,  $\text{C}(\text{CH}_3)_2$ ), 1.45 (m, 6H,  $\text{CH}_2\text{CH}_2\text{CH}_2$ ), 1.78 (s, 3H,  $\text{CCH}_3$ ), 4.44 (d, 2H,  $J=6.6$  Hz,  $\text{CHCH}_2$ ), 5.04 (d, 1H,  $J=10.6$  Hz,  $\text{CCHH}$ ), 5.19 (d, 1H,  $J = 17.6$  Hz,  $\text{CCHH}$ ), 5.64 (t, 1H,  $J = 6.6$  Hz,  $\text{CHCH}_2$ ), 6.41 (dd, 1H,  $J = 10.6, 17.6$  Hz,  $\text{CHCH}_2$ ).

**2.01**  $^1\text{H}$  NMR: (400 MHz) 1.11 (s, 6H,  $\text{C}(\text{CH}_3)_2$ ), 1.20 (s, 6H,  $\text{C}(\text{CH}_3)_2$ ), 1.45 (m, 6H,  $\text{CH}_2\text{CH}_2\text{CH}_2$ ), 1.77 (s, 3H,  $\text{CCH}_3$ ), 5.14 (d, 2H,  $J=10.2$  Hz,  $\text{CCHH}$ ), 5.26 (d, 2H,  $J=17.6$  Hz,  $\text{CCHH}$ ), 6.72 (dd, 2H,  $J=10.2, 17.6$  Hz,  $\text{CHCH}_2$ ).

### 9.1.05. Reaction of 3-methyl-1,4-pentadiene and TEMPO under air

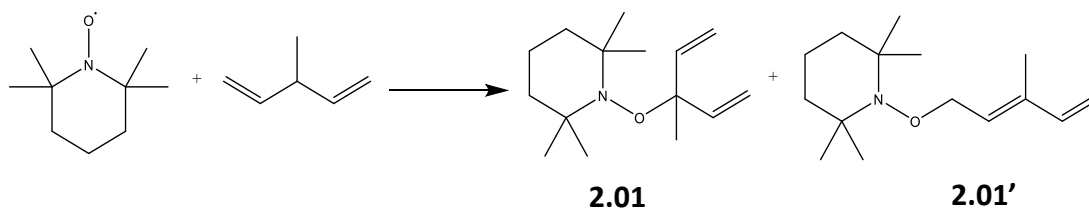


Figure 266: Formation of **2.01** and **2.01'**

2,2,6,6-Tetramethylpiperidine 1-oxyl (TEMPO) (0.1526 g, 1 mmol) was mixed with 3-methyl-1,4-pentadiene (0.06 mL, 0.5 mmol). After mixing for 16 hr, TLC indicated only the presence of starting materials.

### 9.1.06. Reaction of 3-methyl-1,4-pentadiene and TEMPO with $\text{AlCl}_3$

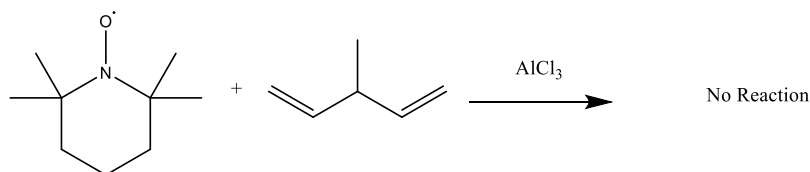


Figure 267: Attempted formation of **2.01** using  $\text{AlCl}_3$

2,2,6,6-Tetramethylpiperidine 1-oxyl (TEMPO) (0.1024 g, 0.7 mmol) was added to dry toluene (5 mL).  $\text{AlCl}_3$  (84.4 mg, 0.7 mmol) was then added, followed by 3-methyl-1,4-pentadiene (0.04 mL, 0.33 mmol). The mixture was stirred for 22 hr. Analysis of TLC and crude  $^1\text{H}$  NMR indicated only the presence of starting materials.

### 9.1.07. Reaction of 3-methyl-1,4-pentadiene and TEMPO with $\text{FeCl}_3$

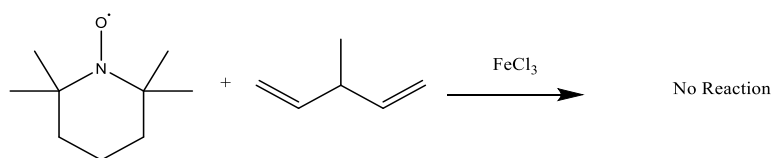


Figure 268: Attempted formation of **2.01** using  $\text{FeCl}_3$

2,2,6,6-Tetramethylpiperidine 1-oxyl (TEMPO) (0.1024 g, 0.7 mmol) was added to dry toluene (5 mL).  $\text{FeCl}_3$  (113 mg, 0.7 mmol) was then added, followed by 3-methyl-1,4-

pentadiene (0.04 mL, 0.33 mmol). The mixture was stirred for 22 hr. Analysis of TLC and crude  $^1\text{H}$  NMR indicated only the presence of starting materials.

#### 9.1.08. Reaction between 3-methyl-but-1-en-3-ol and HBr

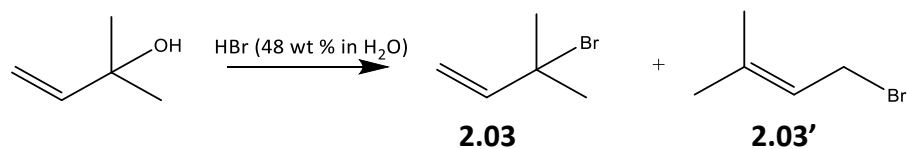


Figure 269: Formation of **2.03** and **2.03'** through reaction with HBr

HBr (48 wt % in H<sub>2</sub>O, 3.4 mL, 30 mmol) and 3-methyl-but-1-en-3-ol (1 mL, 9.5 mmol) were vigorously stirred together for 20 min. After the reaction was allowed to settle two layers formed, with the organic layer taken and sequentially washed with H<sub>2</sub>O (10 mL), NaHCO<sub>3</sub> (aq) (10 mL) and brine (10 mL). The solution was then dried with MgSO<sub>4</sub> and filtered. Yield = 56.4%. Examination by  $^1\text{H}$  NMR indicated a mixture of **2.03'** (98.7%) and **2.03** (1.3%) bromides.

**2.03'**  $^1\text{H}$  NMR: (400 MHz) 1.72 (s, 3H, CCH<sub>3</sub>), 1.78 (s, 3H, CCH<sub>3</sub>), 4.01 (d, 2H, J = 8.2 Hz, CH<sub>2</sub>Br), 5.52 (t, 1H, J = 8.2 Hz, CHCH<sub>2</sub>Br).

**2.03**  $^1\text{H}$  NMR: (400 MHz) 1.72 (s, 3H, CCH<sub>3</sub>), 1.78 (s, 3H, CCH<sub>3</sub>) 4.97 (d, 1H, J = 10.5 Hz, CHCHH), 5.17 (d, 1H, J=17.4 Hz, CHCHH), 6.25 (dd, 1H, J = 10.5, 17.4 Hz, CHCH<sub>2</sub>).

#### 9.1.09. Reaction between 3-methyl-but-1-en-3-ol and PBr<sub>3</sub>

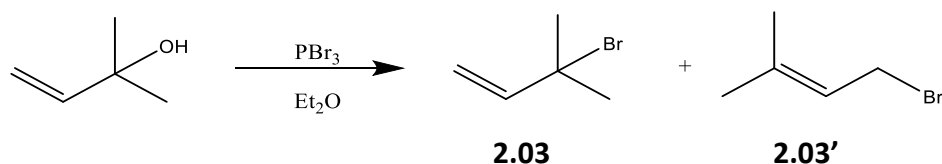


Figure 270: Formation of **2.03** and **2.03'** through reaction with PBr<sub>3</sub>

3-methyl-but-1-en-3-ol (1.21 mL, 11.6 mmol) was placed under a nitrogen atmosphere, mixed into dry Et<sub>2</sub>O (50 mL) and cooled in an ice bath. PBr<sub>3</sub> (3 mL, 31.9 mmol) was

separately mixed with dry Et<sub>2</sub>O (15 mL) and this solution then slowly added to the alcohol. The reaction mixture was stirred for 2.5 hr, whilst warming to room temperature. Ice cold water (60 mL) was added to the reaction mixture, and the organic phase extracted. This was then washed with NaHCO<sub>3</sub> (aq) (50 mL) and brine (50 mL), before drying with MgSO<sub>4</sub>, filtration, and solvent removal by rotary evaporation. Yield = 23.8%, in a mixture of **2.03'** (97%) and **2.03** (3%) bromides is obtained.

**2.03'** <sup>1</sup>H NMR: (400 MHz) 1.71 (s, 3H, CCH<sub>3</sub>), 1.78 (s, 3H, CCH<sub>3</sub>), 3.99 (d, 2H, J = 8.2 Hz, CH<sub>2</sub>Br), 5.50 (t, 1H, J = 8.2 Hz, CHCH<sub>2</sub>Br).

**2.03** <sup>1</sup>H NMR: (400 MHz) 1.71 (s, 3H, CCH<sub>3</sub>), 1.78 (s, 3H, CCH<sub>3</sub>) 4.95 (d, 1H, J = 10.5 Hz, CHCHH), 5.15 (d, 1H, J=17.4 Hz, CHCHH), 6.23 (dd, 1H, J = 10.5, 17.4 Hz, CHCH<sub>2</sub>).

#### 9.1.10. Reaction between 3-methyl-but-1-en-3-ol and HCl

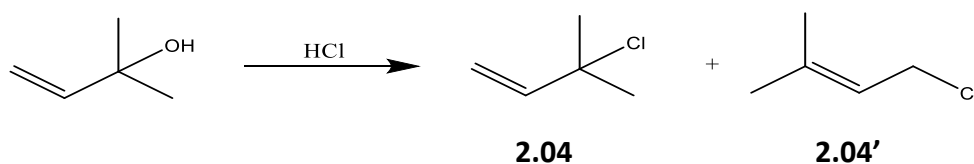


Figure 271: Formation of **2.04** and **2.04'** through reaction with HCl

This reaction was conducted as described above for HBr. Yield = 38.2%. Examination by <sup>1</sup>H NMR indicated a mixture of primary (88% and tertiary (12%) chlorides.

**2.04'** <sup>1</sup>H NMR: (400 MHz) 1.72 (s, 3H, CCH<sub>3</sub>), 1.75 (s, 3H, CCH<sub>3</sub>), 4.07 (d, 2H, J = 7.8 Hz, CH<sub>2</sub>Cl), 5.42 (t, 7.8 Hz, CHCH<sub>2</sub>Cl).

**2.04** <sup>1</sup>H NMR: (400 MHz) 1.72 (s, 3H, CCH<sub>3</sub>), 1.75 (s, 3H, CCH<sub>3</sub>), 5.02 (d, 1H, J= 10.5 Hz, CHCHH), 5.21 (d, 1H, J=17.4 Hz, CHCHH), 6.08 (dd, 1H, J= 10.5, 17.4 Hz, CHCH<sub>2</sub>).

#### 9.1.11. Reaction between 3-methyl-but-1-en-3-ol and thionyl chloride

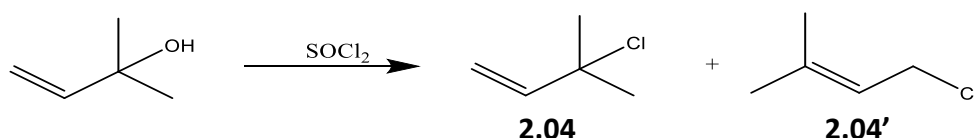


Figure 272: Formation of **2.04** and **2.04'** through reaction with thionyl chloride

Thionyl chloride (1.4 mL, 19 mmol) was added to 3-methyl-but-1-en-3-ol (1.05 mL, 10 mmol) in diethyl ether (15 mL). The reaction was stirred for 1 hr before a further addition of thionyl chloride (0.4 mL, 5.5 mmol), and stirred for 1 hr. The solution was then cautiously poured into ice cold water (100 mL), and the organic layer extracted with diethyl ether (20 mL). This organic phase was then washed with brine (2 x 20 mL), dried with MgSO<sub>4</sub>, filtered, and solvent removed by rotary evaporation. Yield = 43%, as a mixture of **2.04'** (87.5%) and **2.04** (12.5%).

**2.04'** <sup>1</sup>H NMR: (400 MHz) 1.74 (s, 3H, CCH<sub>3</sub>), 1.78 (s, 3H, CCH<sub>3</sub>), 4.10 (d, 2H, J = 8.2 Hz, CH<sub>2</sub>Cl), 5.45 (t, 1H, J = 8.2 Hz, CHCH<sub>2</sub>Cl).

**2.04** <sup>1</sup>H NMR: (400 MHz) 1.74 (s, 3H, CCH<sub>3</sub>), 1.78 (s, 3H, CCH<sub>3</sub>), 5.08 (d, 1H, J = 10.8 Hz, CHCHH), 5.16, 5.87 (d, 1H, J=17.6 Hz, CHCHH).

#### 9.1.12. Reaction of 3-methyl-but-1-ene and TEMPO under Fenton conditions

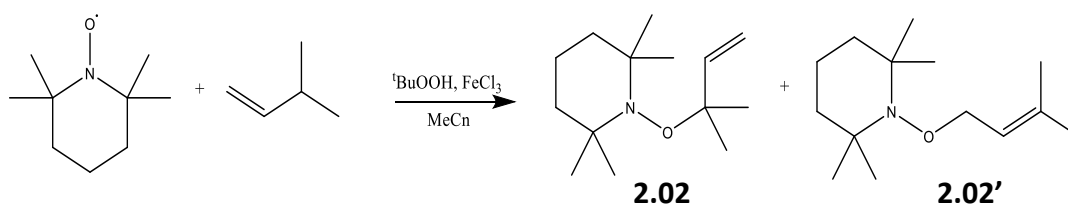


Figure 273: Attempted formation of **2.02** and **2.02'** through Fenton reaction

2,2,6,6-Tetramethylpiperidine 1-oxyl (TEMPO) (0.1531 g, 1 mmol), 3-methyl-but-1-ene (0.09 mL, 0.8mmol) and tert-butoxy hydroperoxide (70% in H<sub>2</sub>O, 0.19 mL, 1.4 mmol) were mixed together in MeCN (0.1 mL). FeCl<sub>3</sub> (3 mg, 0.02 mmol) was added, and the reaction stirred for 18 hr. The reaction mixture was added to DCM (10 mL) and the organic layer washed with H<sub>2</sub>O (2x 10 mL). The mixture was then dried with MgSO<sub>4</sub>, filtered, and solvent removed by rotary evaporation. The remaining residue was purified by flash chromatography (49:1 PET ether: ethyl acetate, R<sub>f</sub> = 0.36). **2.02'** Yield = 4.2%. <sup>1</sup>H NMR: (400MHz) 1.11 (s, 6H, C(CH<sub>3</sub>)<sub>2</sub>), 1.20 (s, 6H, C(CH<sub>3</sub>)<sub>2</sub>), 1.57 (m, 6H, CH<sub>2</sub>CH<sub>2</sub>CH<sub>2</sub>), 1.75 (s, 3H, CCH<sub>3</sub>), 4.27 (d, 2H, J = 6.9 Hz, CHCH<sub>2</sub>), 5.36 (t, 1H, J = 6.9 Hz, CHCH<sub>2</sub>).

### 9.1.13. Reaction between $\alpha$ -methylstyrene and TEMPO<sup>141</sup>

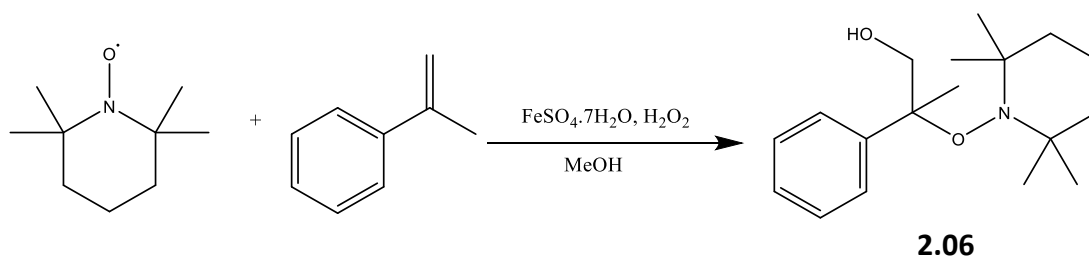


Figure 274: Formation of **2.06**, following method of Prechter et al.<sup>141</sup>

2,2,6,6-Tetramethylpiperidine 1-oxyl (TEMPO) (0.3113 g, 1.99 mmol) and  $\text{FeSO}_4 \cdot 7\text{H}_2\text{O}$  (0.6292 g, 2.26 mmol) were mixed together in degassed MeOH (5 mL).  $\alpha$ -methylstyrene (2.6 mL, 20 mmol) was mixed with degassed MeOH (6 mL) and added to the reaction flask. The mixture was heated to 40°C, and a mixture of  $\text{H}_2\text{O}_2$  (30% aq, 0.6 mL, 5.87 mmol) in degassed MeOH (0.8 mL) was added over 5 minutes. The mixture was then stirred at 40°C for a further 30 min before ascorbic acid (0.6 g, 3.41 mmol) was added and the solution stirred for 10 min at room temperature. After the addition of  $\text{H}_2\text{O}$  (20 mL) the mixture was extracted using DCM (3 x 8 mL). The mixture was then dried with  $\text{MgSO}_4$ , and filtered prior to solvent removal by rotary evaporation. The residue was purified by flash chromatography (95:5 PET ether: ethyl acetate,  $R_f = 0.42$ ) to give product **2.06**. Yield = 23.6%. Experiments doubling the amount of peroxide added (1.2 mL, 11.75 mmol), or leaving the reaction for a longer time period (3 h, monitored by TLC) resulted in no improvement of the yield.

**2.06** <sup>1</sup>H NMR: (400 MHz) 0.77 (s, 3H,  $\text{NCCH}_3$ ), 1.06 (s, 3H,  $\text{NCCH}_3$ ), 1.11 (s, 3H,  $\text{NCCH}_3$ ), 1.16 (s, 3H,  $\text{NCCH}_3$ ), 1.31 (m, 6H,  $\text{C}(\text{CH}_2)_3$ ), 1.53 (s, 3H,  $\text{OCCH}_3$ ), 4.08 (m, 1H,  $\text{CHHOH}$ ), 4.16 (d, 1H,  $J = 11.2$  Hz,  $\text{CHHOH}$ ), 4.50 (s, 1H,  $\text{CH}_2\text{OH}$ ) 7.25 (t, 1H,  $\text{CCHCHCH}$ ), 7.33 (t, 2H,  $\text{CCHCH}$ ), 7.56 (d, 2H,  $\text{CCH}$ ).

#### 9.1.14. Reaction of **2.06** with pyridinium chlorochromate

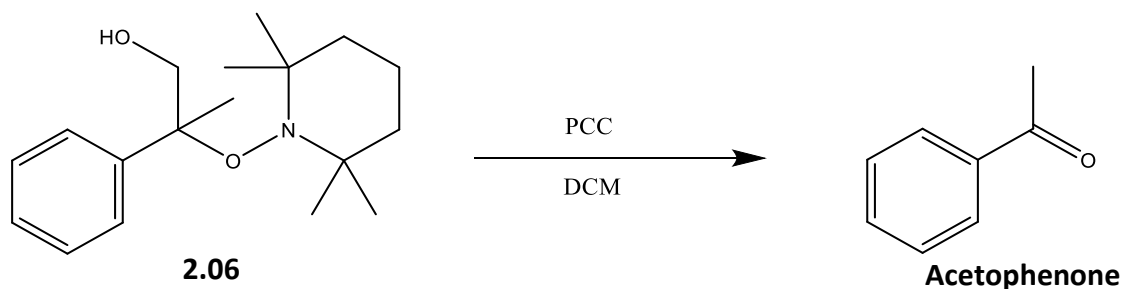


Figure 275: Formation of acetophenone through PCC oxidation

**2.06** (0.0147 g, 0.05 mmol) was dissolved in DCM (1 mL). Pyridinium chlorochromate (0.0173 g, 0.08 mmol) in DCM (1 mL) was added, and the solution stirred for 2 hours, during which time the solution turned from orange to blue. Product was extracted with Et<sub>2</sub>O, filtered, then dried with MgSO<sub>4</sub>. After filtration, solvent was removed by rotary evaporation. The remaining residue was purified by flash chromatography (9:1 Pet ether: ethyl acetate, R<sub>f</sub> = 0.41). Acetophenone yield = 83.2%. <sup>1</sup>H NMR: (400MHz) 2.65 (s, 3H, COCH<sub>3</sub>), 7.51 (t, 2H, J = 7.3 Hz, CCH), 7.61 (t, 1H, J = 7.3 Hz, CCHCHCH), 8.00 (d, 2H, J = 7.3 Hz, CCHCH).

#### 9.1.15. Reaction of **2.06** with Dess-Martin Periodinane

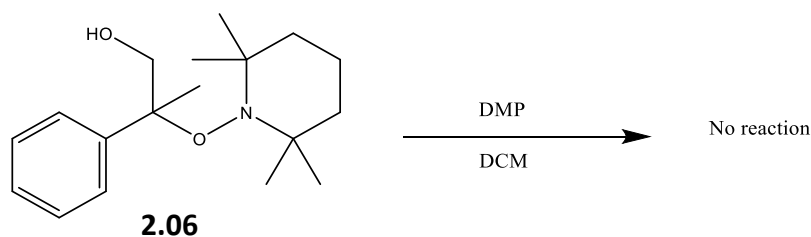


Figure 276: Attempted oxidation of **2.06** with DMP

**2.06** (0.019 g, 0.065 mmol) was placed under an atmosphere of argon, dissolved in dry DCM (1 mL) and cooled to 0 °C. Dess-Martin Periodinane (0.0342 g, 0.081 mmol) was added with stirring, and the solution allowed to warm to room temperature. After 24 hr, a 1:1 mixture of saturated aqueous Na<sub>2</sub>S<sub>2</sub>O<sub>3</sub> and NaHCO<sub>3</sub> (5 mL) was added, and the organic layer extracted with DCM. The solution was dried with MgSO<sub>4</sub>, filtered, and solvent

removed by rotary evaporation. TLC and NMR showed only starting materials and no indication of a successful reaction.

#### 9.1.16. Reaction of **2.06** using the Swern oxidation procedure.

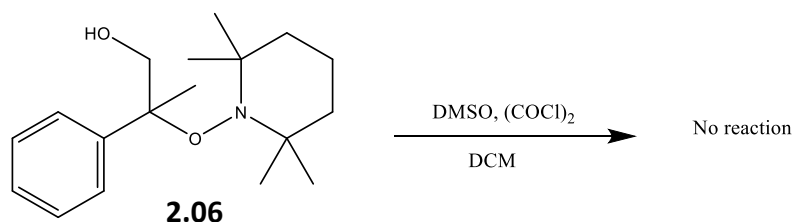


Figure 277: Attempted Swern oxidation of **2.06**

**2.06** (28.6 mg, 0.0981 mmol) was dissolved in DCM (0.5 mL). DMSO (17  $\mu$ L, 0.24 mmol) was added, cooled to  $-78$   $^{\circ}$ C, then oxalyl chloride (10  $\mu$ L, 1.2 mmol) was added and mixed for 5 min. Solution of **2.06** was then added and the reaction stirred for 15 minutes.  $\text{Et}_3\text{N}$  (70  $\mu$ L, 5 mmol) was added, stirred for a further 30 min, warmed to  $0$   $^{\circ}$ C and stirred for 1 hr.  $\text{H}_2\text{O}$  (1 mL) was subsequently added to quench the reaction. The organic layer was extracted with DCM (2 x 2 mL), dried with  $\text{MgSO}_4$ , and filtered prior to solvent removal by rotary evaporation. TLC and NMR showed only starting materials and no indication of a successful reaction.

#### 9.1.17. Reaction between 2-phenylpropanal and TEMPO

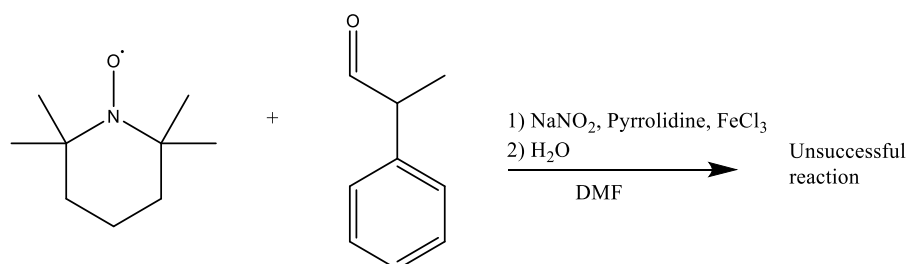


Figure 278: Attempted formation of **2.05**

2,2,6,6-Tetramethylpiperidine 1-oxyl (0.1566 g, 1 mmol) was dissolved in DMF (0.5 mL) and the solution stirred. 2-phenylpropanal (0.07 mL, 0.52 mmol) was then added, followed

by  $\text{NaNO}_2$  (0.011 g, 0.16 mmol). The solution was then stirred and cooled to  $-10\text{ }^\circ\text{C}$ . Pyrrolidine (0.008 mL, 0.1 mmol) and  $\text{FeCl}_3$  (0.015 g, 0.09 mmol) were added, and the reaction stirred for 19 hr. The reaction mixture was then quenched with  $\text{NH}_4\text{Cl}_{(\text{aq})}$  and the organic later extracted with DCM. After drying with  $\text{MgSO}_4$  and subsequent filtration, solvent was removed by rotary evaporation. The remaining residue was purified by flash chromatography (9:1 PET ether: ethyl acetate), however none of the target compound was identified from the products.

#### 9.1.18. Attempted preparation of 2.08

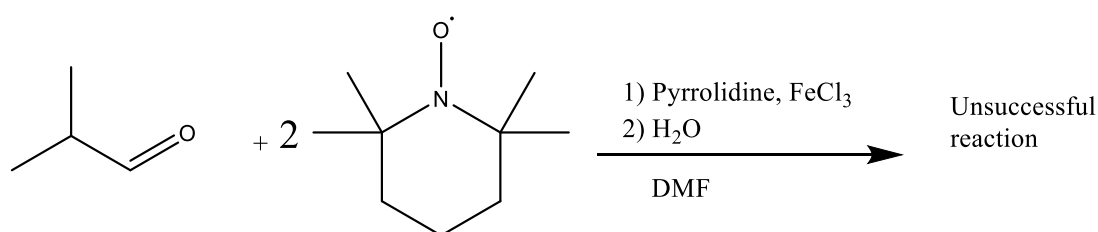


Figure 279: Attempted formation of **2.08**

2,2,6,6-Tetramethylpiperidine 1-oxyl (TEMPO) (80 mg, 0.51 mmol) was dissolved in dimethylformamide (DMF) (2.5 mL). Isobutyraldehyde (23  $\mu\text{L}$ , 0.25 mmol), pyrrolidine (4.2  $\mu\text{L}$ , 0.5 mmol) and iron (iii) chloride (8 mg, 0.049 mmol) were added, and stirred for 20 hr. A solution of sodium ascorbate (0.2 g) in water (7.5 mL) and diethyl ether (15 mL) was then added, shaken, and allowed to settle. The organic layer was extracted from the dark aqueous layer with diethyl ether (3 x 15 mL). The solution was dried with  $\text{MgSO}_4$ , filtered, and solvent removed by rotary evaporation. No **2.08** was identified following this process.

#### 9.1.19. Preparation of 2.07:

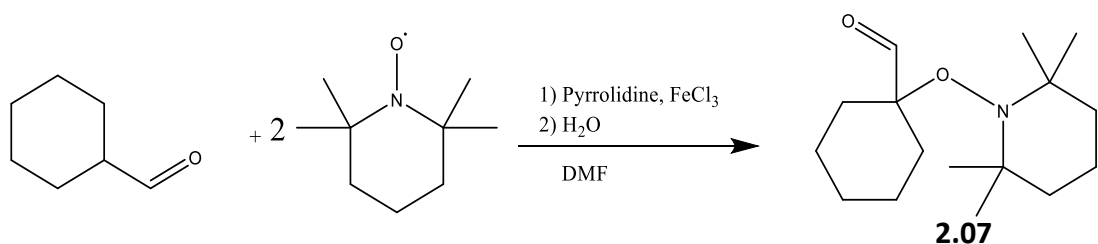


Figure 280: Formation of **2.07**

2,2,6,6-Tetramethylpiperidine 1-oxyl (0.781 g, 5 mmol) was dissolved in dimethylformamide (2.5 mL). Cyclohexanecarboxaldehyde (0.3 mL, 2.5 mmol), pyrrolidine (42  $\mu$ L, 0.5 mmol) and iron (iii) chloride (81.1 mg, 0.5 mmol) were added, and stirred for 20 hr. A solution of sodium ascorbate (1.98 g) in water (7.5 mL) and diethyl ether (15 mL) was then added, shaken, and allowed to settle. The organic layer was extracted from the dark aqueous layer with diethyl ether (3 x 15 mL). The solution was dried with  $MgSO_4$ , filtered, and solvent removed by rotary evaporation. The remaining residue was purified by flash chromatography (9:1 PET ether:DCM,  $R_f$  = 0.42) to give **2.07** as a pink oil. Yield = 84.0%.

$^1H$  NMR: (400 MHz) 1.13 (s, 6H,  $N(C(CH_3)_2)$ ), 1.14 (s, 6H,  $N(C(CH_3)_2)$ ), 1.49 (m, 10H,  $C(CH_2)_5$ ), 1.73 (m, 4H,  $CCH_2CH_2CH_2C$ ), 1.91 (m, 2H,  $CCH_2CH_2CH_2C$ ), 9.91 (s, 1H, COH).  $^{13}C$  NMR (100 MHz) 16.43, 19.96, 21.55, 24.75, 31.07, 33.62, 40.02, 59.48 ( $C_q$ ), 81.99 ( $C_q$ ), 203.46 (HC=O). DEPT 135 (100MHz) 16.41 ( $CH_2$ ), 19.95 ( $CH_3$ ), 21.54 ( $CH_2$ ), 24.74 ( $CH_2$ ), 31.05 ( $CH_2$ ), 33.61 ( $CH_3$ ), 40.01, 203.46 (HC=O). MS (ESI) 268.2274, calculation for  $C_{16}H_{29}NO_2$ ,  $[M+H]^+$  = 268.2271

#### 9.1.20. Preparation of **2.10**:

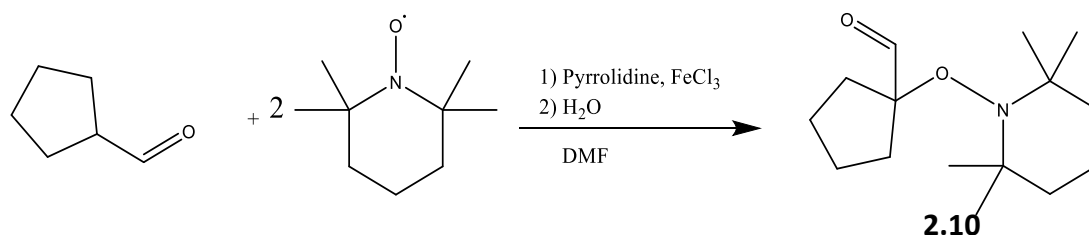


Figure 281: Formation of **2.10**

2,2,6,6-Tetramethylpiperidine 1-oxyl (0.781 g, 5 mmol) was dissolved in dimethylformamide (DMF) (2.5 mL). Cyclopentanecarboxaldehyde (0.27 mL, 2.5 mmol), pyrrolidine (42  $\mu$ L, 0.5 mmol) and iron (iii) chloride (81.1 mg, 0.5 mmol) were added, and stirred for 20 hr. A solution of sodium ascorbate (1.98 g) in water (7.5 mL) and diethyl

ether (15 mL) was then added, shaken, and allowed to settle. The organic layer was extracted from the dark aqueous layer with diethyl ether (3 x 15 mL). The solution was dried with MgSO<sub>4</sub>, filtered, and solvent removed by rotary evaporation. The remaining residue was purified by flash chromatography (19:1 PET ether:DCM, R<sub>f</sub> = 0.36) to give **2.10** as a pale oil. Yield = 61.1%. <sup>1</sup>H NMR (400 MHz) 1.09 (s, 6H, N(C(CH<sub>3</sub>)<sub>2</sub>)), 1.12 (s, 6H, N(C(CH<sub>3</sub>)<sub>2</sub>)), 1.48 (m, 8H, (CH<sub>2</sub>)<sub>4</sub>), 1.71 (m, 2H, CH<sub>2</sub>CH<sub>2</sub>CH<sub>2</sub>), 1.97 (m, 2H, CCH<sub>2</sub>), 2.18 (m, 2H, CCH<sub>2</sub>), 10.01 (s, 1H, OCH). <sup>13</sup>C NMR (100 MHz) 16.84, 20.21, 24.71, 33.01, 34.34, 40.11, 59.79 (C<sub>q</sub>), 94.61 (C<sub>q</sub>), 201.99. DEPT 135 (100 MHz) 16.84 (CH<sub>2</sub>), 20.21 (CH<sub>3</sub>), 24.71 (CH<sub>2</sub>), 33.01 (CH<sub>3</sub>), 34.34 (CH<sub>2</sub>), 40.11 (CH<sub>2</sub>), 201.99 (CH). MS (ESI) 254.2103, calculation for C<sub>15</sub>H<sub>27</sub>NO<sub>2</sub>, [M+H]<sup>+</sup> = 254.2114

#### 9.1.21. Preparation of **2.12**:

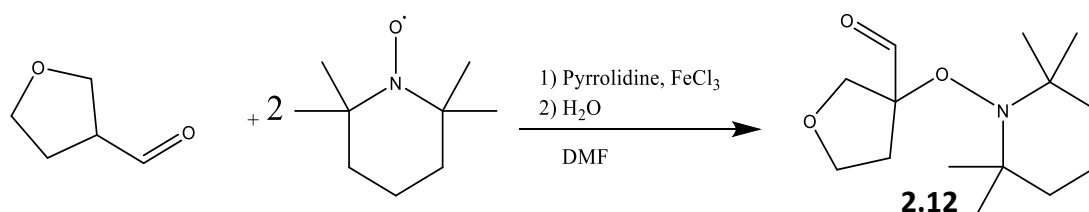


Figure 282: Formation of **2.12**

2,2,6,6-Tetramethylpiperidine 1-oxyl (0.781 g, 5 mmol) was dissolved in dimethylformamide (2.5 mL). Tetrahydrofuran-3-carboxaldehyde (0.45 mL, 2.5 mmol, 50 weight % in H<sub>2</sub>O) was extracted, dried, and added, followed by pyrrolidine (42 μL, 0.5 mmol) and iron (iii) chloride (81.1 mg, 0.5 mmol), and the solution stirred for 20 hr. A solution of sodium ascorbate (1.98 g) in water (7.5 mL) and diethyl ether (15 mL) was then added, shaken, and allowed to settle. The organic layer was extracted from the dark aqueous layer with diethyl ether (3 x 15 mL). The solution was dried with MgSO<sub>4</sub>, filtered, and solvent removed by rotary evaporation. The remaining residue was purified by flash chromatography (9:1 PET ether:EtOAc, R<sub>f</sub> = 0.42) to produce **2.12** as a pale oil. Yield = 38.2%. <sup>1</sup>H NMR: (400 MHz): 1.02 (s, 3H, CH<sub>3</sub>), 1.09 (s, 3H, CH<sub>3</sub>), 1.11 (s, 6H, (CH<sub>3</sub>)<sub>2</sub>), 1.47 (m, 6H), 2.37 (m, 2H, CH<sub>2</sub>), 3.73 (q, 1H, CHH, J = 7.8 Hz), 3.94 (m, 2H, CH<sub>2</sub>), 4.12 (d, 1H, CHH, J = 9.8 Hz), 10.06 s, 1H, OCH). <sup>13</sup>C NMR: (100 MHz) 17.16 (CH<sub>2</sub>), 20.67 (CH<sub>3</sub>), 32.80 (CH<sub>3</sub>),

35.32 (CH<sub>2</sub>), 40.41 (CH<sub>2</sub>), 60.572 (C<sub>q</sub>), 68.50 (CH<sub>2</sub>), 74.12 (CH<sub>2</sub>), 94.220 (C<sub>q</sub>), 200.31 (CH).  
DEPT (135): 17.16 (CH<sub>2</sub>), 20.67 (CH<sub>3</sub>), 32.80 (CH<sub>3</sub>), 35.32 (CH<sub>2</sub>), 40.41 (CH<sub>2</sub>), 68.50 (CH<sub>2</sub>),  
74.12 (CH<sub>2</sub>), 200.31 (CH). MS: (ESI) 256.1911, calculation for C<sub>14</sub>H<sub>25</sub>NO<sub>3</sub>, [M+H]<sup>+</sup> = 256.1907

### 9.1.22. Preparation of **2.09**:

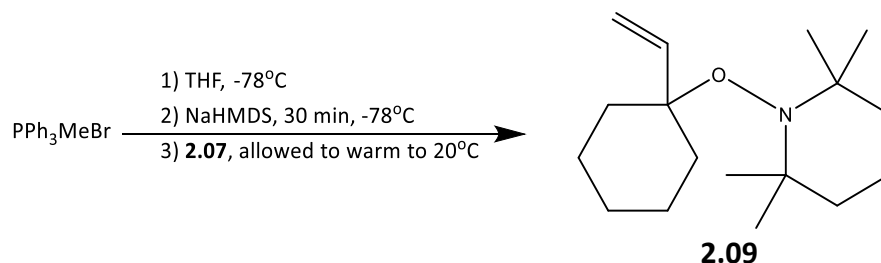


Figure 283: Formation of **2.09**

Methyltriphenylphosphonium bromide (1.25 g, 3.5 mmol) was placed under a nitrogen atmosphere and dry tetrahydrofuran (20mL) added. The mixture was cooled in a dry-ice - acetone bath prior to slow addition of sodium bis(trimethylsilyl)amide (1 M in tetrahydrofuran, 3.5 mL, 3.5 mmol) and the reaction stirred for 30 min. **2.07** (0.935 g, 3.5 mmol) was then slowly added and the mixture allowed to warm to room temperature with stirring for 3 hours. Saturated aqueous ammonium chloride (10 mL) was added to the beige reaction mixture, and the organic layer extracted with ethyl acetate (3 x 15 mL). The organic layer was washed with saturated aqueous sodium hydrogen carbonate (20 mL) then brine (20 mL). The solution was dried with MgSO<sub>4</sub>, filtered, and solvent removed by rotary evaporation. The remaining residue was purified by flash chromatography (9:1 PET ether: DCM, R<sub>f</sub> = 0.45) to give **2.09** as a peach coloured oil (48.4% yield).

<sup>1</sup>H NMR (400 MHz) 1.11 (s, 6H, N(C(CH<sub>3</sub>)<sub>2</sub>)), 1.130 (s, 6H, N(C(CH<sub>3</sub>)<sub>2</sub>)), 1.48 (m, 10H, C(CH<sub>2</sub>)<sub>5</sub>), 1.77 (m, 4H, CCH<sub>2</sub>CH<sub>2</sub>CH<sub>2</sub>C), 1.99 (m, 2H, CCH<sub>2</sub>CH<sub>2</sub>CH<sub>2</sub>C), 4.99 (dd, 1H, J = 17.9, 1.8 Hz, HC=CHH), 5.04 (dd, 1H, J = 11.4, 1.8 Hz, HC=CHH), 6.50 (dd, 1H, J = 11.4, 17.9, HC=CHH).  
<sup>13</sup>C NMR: (100 MHz) 16.72, 19.93, 22.19, 25.62, 31.37, 34.26, 40.47, 59.79 (C<sub>q</sub>), 82.28 (C<sub>q</sub>), 111.30, 144.06. DEPT 135: (100 MHz) 16.72 (CH<sub>2</sub>), 19.930 (CH<sub>3</sub>), 22.190 (CH<sub>2</sub>), 25.62 (CH<sub>2</sub>), 31.37 (CH<sub>2</sub>), 34.26 (CH<sub>3</sub>), 40.47 (CH<sub>2</sub>), 111.30, (CH<sub>2</sub>) 144.06 (CH). MS: (ESI) 266.2481, calculation for C<sub>17</sub>H<sub>31</sub>NO, [M+H]<sup>+</sup> = 266.2478 MSMS: (ESI, isolating fragment 266.2481) 266.25115, 158.15731

### 9.1.23. Preparation of 2.11:

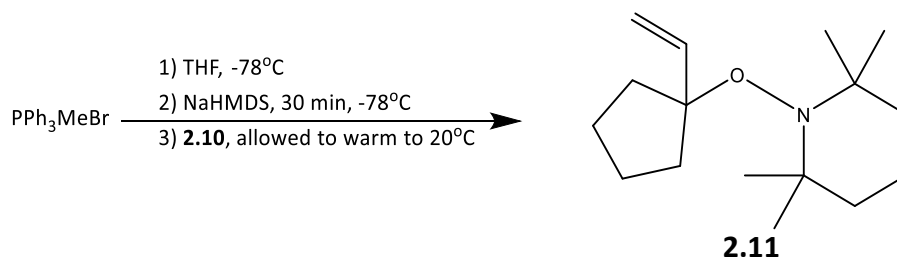


Figure 284: Formation of **2.11**

Methyltriphenylphosphonium bromide (1.25 g, 3.5 mmol) placed under a nitrogen atmosphere and dry tetrahydrofuran (20 mL) added. The mixture was cooled in a dry-ice - acetone bath prior to the slow addition of sodium bis(trimethylsilyl)amide (1 M in tetrahydrofuran, 3.5 mL, 3.5 mmol) and the reaction stirred for 30 min. **2.10** (0.886 g, 3.5 mmol) was then slowly added and the mixture allowed to warm to room temperature with stirring for 3 hours. Saturated aqueous ammonium chloride (10 mL) was added to the beige reaction mixture, and the organic layer extracted with ethyl acetate (3 x 15 mL). The organic layer was washed with saturated aqueous sodium hydrogen carbonate (20 mL) then brine (20 mL). The solution was dried with  $\text{MgSO}_4$ , filtered, and solvent removed by rotary evaporation. The remaining residue was purified by flash chromatography (9:1 PET ether:DCM,  $R_f = 0.43$ ) to produce **2.11** as a pale oil (23.9% yield).  $^1\text{H}$  NMR: (400 MHz) 1.08 (s, 6H,  $\text{N}(\text{C}(\text{CH}_3)_2)$ ), 1.09 (s, 6H,  $\text{N}(\text{C}(\text{CH}_3)_2)$ ), 1.49 (m, 8H,  $(\text{CH}_2)_4$ ), 1.71 (m, 2H,  $\text{CH}_2\text{CH}_2\text{CH}_2$ ), 1.95 (m, 4H,  $(\text{CCH}_2)_2$ ), 4.90 (dd, 1H,  $\text{CCHCHH}$ ,  $J = 17.2, 1.5$  Hz), 4.99 (dd, 1H,  $\text{CCHCHH}$ ,  $J = 11.2, 1.5$  Hz), 6.54 (dd, 1H,  $\text{CCHCH}_2$ ,  $J = 17.6, 11.2$  Hz).  $^{13}\text{C}$  NMR: (100 MHz) 17.09, 20.36, 23.32, 33.41, 38.24, 40.31, 59.13 ( $\text{C}_q$ ), 75.60, 90.96 ( $\text{C}_q$ ), 110.02, 115.62, 143.59. DEPT (135): 17.09 ( $\text{CH}_2$ ), 20.36 ( $\text{CH}_3$ ), 23.32 ( $\text{CH}_2$ ), 33.41 ( $\text{CH}_3$ ), 38.24 ( $\text{CH}_2$ ), 40.31 ( $\text{CH}_2$ ), 75.60 ( $\text{CH}_2$ ), 110.02 ( $\text{CH}_2$ ), 115.62 ( $\text{CH}$ ), 143.59 ( $\text{CH}$ ). MS (ESI) 252.2315, calculation for  $\text{C}_{16}\text{H}_{29}\text{NO}$ ,  $[\text{M}+\text{H}]^+ = 252.2322$

### 9.1.24. Preparation of **2.13**:

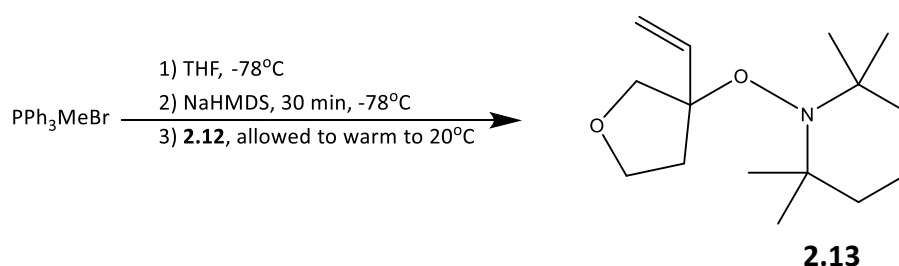


Figure 285: Formation of **2.13**

Methyltriphenylphosphonium bromide (1.25 g, 3.5 mmol) was placed under a nitrogen atmosphere and dry tetrahydrofuran (20mL) added. The mixture was cooled in a dry-ice - acetone bath prior to the slow addition of sodium bis(trimethylsilyl)amide (1 M in tetrahydrofuran, 3.5 mL, 3.5 mmol) and the reaction stirred for 30 min. **2.12** (0.886 g, 3.5 mmol) was then slowly added and the mixture allowed to warm to room temperature with stirring for 3 hours. Saturated aqueous ammonium chloride (10 mL) was added to the beige reaction mixture, and the organic layer extracted with ethyl acetate (3 x 15 mL). The organic layer was washed with saturated aqueous sodium hydrogen carbonate (20 mL) then brine (20 mL). The solution was dried with  $\text{MgSO}_4$ , filtered, and solvent removed by rotary evaporation. The remaining residue was purified by flash chromatography (9:1 PET ether:DCM,  $R_f = 0.37$ ) to produce the product **2.13** as a pale oil (40.0% yield).  $^1\text{H}$  NMR (500 MHz): 0.98 (s, 3H,  $\text{CH}_3$ ), 1.05 (s, 3H,  $\text{CH}_3$ ), 1.07 (s, 6H,  $(\text{CH}_3)_2$ ), 1.43 (m, 6H), 2.11 (1H, m), 2.39 (1H, m), 3.77 (q, 1H,  $\text{CHH}$ ,  $J = 7.5$  Hz), 3.87 (q, 2H,  $\text{CH}_2$ ,  $J = 8.8$  Hz), 3.99 (m, 1H,  $\text{CHH}$ ), 5.07 (dd, 1H,  $\text{CHCHH}$ ,  $J = 17.9, 0.5$  Hz), 5.08 (dd, 1H,  $\text{CHCHH}$ ,  $J = 10.9, 0.5$  Hz), 6.65 (dd, 1H,  $\text{CCHCH}_2$ ,  $J = 17.9, 11.2$  Hz).  $^{13}\text{C}$  NMR: (100 MHz) 17.10, 20.46, 32.85, 33.14, 39.06, 59.51 ( $\text{C}_q$ ), 67.76, 77.60, 89.16 ( $\text{C}_q$ ), 111.52, 141.49. DEPT 135 (100 MHz) 17.10 ( $\text{CH}_2$ ), 20.46 ( $\text{CH}_3$ ), 32.85 ( $\text{CH}_2$ ), 33.14 ( $\text{CH}_3$ ), 39.06 ( $\text{CH}_2$ ), 67.76 ( $\text{CH}_2$ ), 77.60 ( $\text{CH}_2$ ), 111.52 ( $\text{CH}_2$ ), 141.49 (CH). MS: (ESI) 254.2126, calculation for  $\text{C}_{15}\text{H}_{27}\text{NO}_2$ ,  $[\text{M}+\text{H}]^+ = 254.2114$

### 9.1.25. Rearrangement of **2.09** to form **2.09'**:

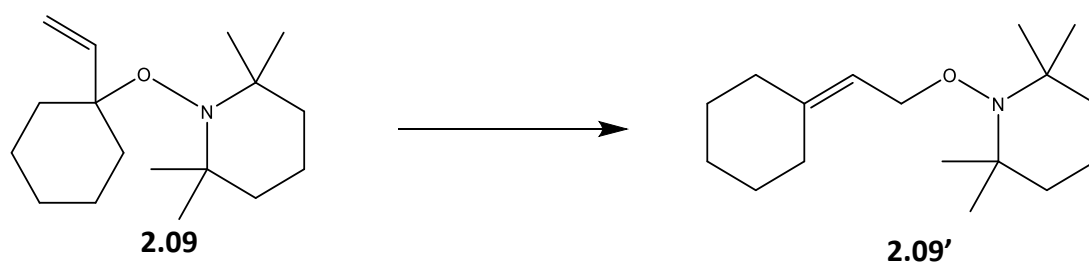


Figure 286: Formation of **2.09'**

Product formed by **2.09** rearranging whilst remaining in solution over several hours to form **2.09'**.  $^1\text{H}$  NMR: (400 MHz) 1.10 (s, 6H,  $\text{N}(\text{C}(\text{CH}_3)_2)$ ), 1.19 (s, 6H,  $\text{N}(\text{C}(\text{CH}_3)_2)$ ), 1.46 (m, 4H,  $\text{CCH}_2\text{CH}_2\text{CH}_2\text{C}$ ), 1.55 (m, 10H,  $\text{C}(\text{CH}_2)_5$ ), 2.12 (m, 2H,  $\text{CCH}_2\text{CH}_2\text{CH}_2\text{C}$ ), 4.28 (d, 2H,  $J = 7.3$  Hz,  $\text{CH}_2\text{CH}$ ), 5.28 (t, 1H,  $J = 7.3$  Hz,  $\text{CH}_2\text{CH}$ ).  $^{13}\text{C}$  NMR: (100 MHz) 17.19, 20.21, 22.61, 26.77, 29.35, 33.08, 39.67, 59.57 ( $\text{C}_q$ ), 73.39, 116.92, 143.93 ( $\text{C}_q$ ). DEPT 135: (100 MHz) 17.19 ( $\text{CH}_2$ ), 20.21 ( $\text{CH}_3$ ), 22.62 ( $\text{CH}_2$ ), 26.77 ( $\text{CH}_2$ ), 29.35 ( $\text{CH}_2$ ), 33.08 ( $\text{CH}_3$ ), 39.67 ( $\text{CH}_2$ ), 73.39 ( $\text{CH}_2$ ), 116.92 ( $\text{CH}$ ).

Plot indicates a half-life of approximately 3 hours.

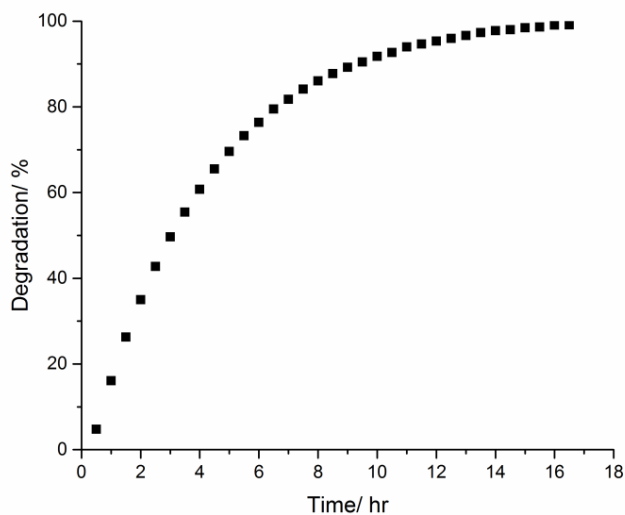


Figure 287: Degradation of **2.09**

### 9.1.26. Rearrangement of **2.11** to form **2.11'**

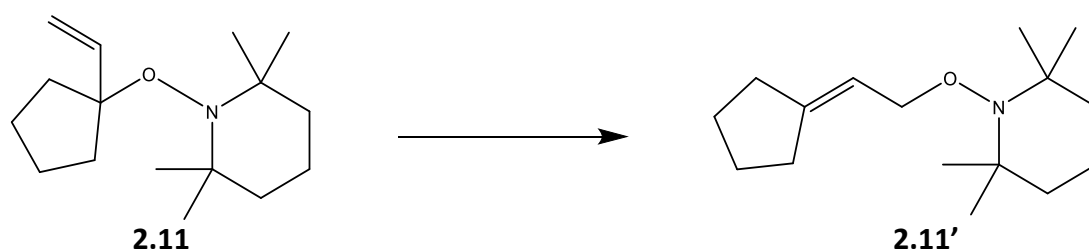


Figure 288: Formation of **2.11'**

Product formed by **2.11** rearranging whilst remaining in solution over several hours to form **2.11'**.  $^1\text{H}$  NMR: (500 MHz) 1.09 (s, 6H,  $\text{N}(\text{C}(\text{CH}_3)_2)$ ), 1.18 (s, 6H,  $\text{N}(\text{C}(\text{CH}_3)_2)$ ), 1.32, (m, 8H,  $(\text{CH}_2)_4$ ), 1.54 (m, 2H,  $\text{CH}_2\text{CH}_2\text{CH}_2$ ), 1.65 (m, 4H,  $(\text{CCH}_2)_2$ ), 4.25 (d, 2H,  $\text{CCHCH}_2$ ,  $J = 7.5$  Hz), 5.44 (t, 1H,  $\text{CCHCH}_2$ ,  $J = 7.5$  Hz).  $^{13}\text{C}$  NMR: (100 MHz) 16.92, 19.99, 26.07, 28.80, 32.780, 33.48, 39.44, 59.38 ( $\text{C}_q$ ), 75.84, 115.50, 147.33 ( $\text{C}_q$ ). DEPT 135: (100 MHz) 16.92 ( $\text{CH}_2$ ), 19.99 ( $\text{CH}_3$ ), 26.07 ( $\text{CH}_2$ ), 28.80 ( $\text{CH}_2$ ), 32.78 ( $\text{CH}_3$ ), 33.48 ( $\text{CH}_2$ ), 39.44 ( $\text{CH}_2$ ), 75.84 ( $\text{CH}_2$ ), 115.50 ( $\text{CH}$ ).

Plot indicates a half-life of approximately 6 hours.

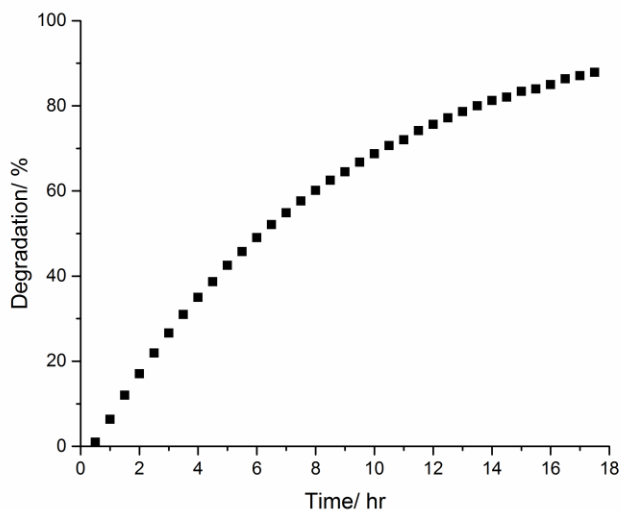


Figure 289: Degradation of **2.11**

### 9.1.27. Rearrangement of 2.13 to form 2.13'

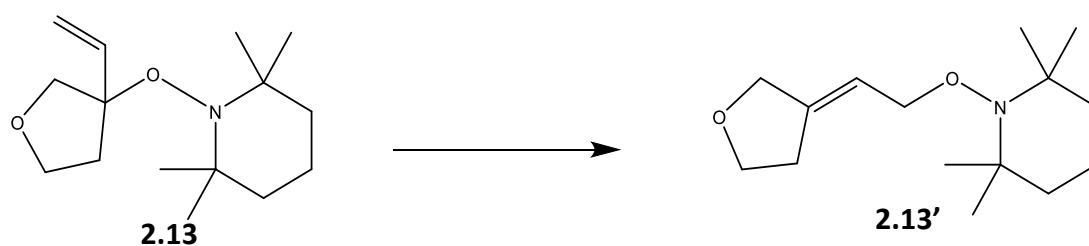


Figure 290: Formation of 2.13'

Product formed by 2.13 rearranging whilst remaining in solution over several hours to form 2.13'. <sup>1</sup>H NMR (500 MHz): 0.98 (s, 3H, CH<sub>3</sub>), 1.06 (s, 3H, CH<sub>3</sub>), 1.07 (s, 6H, (CH<sub>3</sub>)<sub>2</sub>), 1.44 (m, 6H), 2.53 (2H, m, CCH<sub>2</sub>CH<sub>2</sub>OCH<sub>2</sub>), 3.77 (q, 1H, CHH, J = 7.5 Hz), 3.84 (q, 2H, CCH<sub>2</sub>CH<sub>2</sub>OCH<sub>2</sub>, J = 8.8 Hz), 3.90 (m, 2H, CCH<sub>2</sub>CH<sub>2</sub>OCH<sub>2</sub>), 4.30 (m, 2H, CHCH<sub>2</sub>), 5.51 (m, 1H, CCH). <sup>13</sup>C NMR: (100 MHz) 16.12, 19.21, 32.00, 38.64, 58.73 (C<sub>q</sub>), 67.82, 70.24, 74.15, 74.61, 114.77, 140.93 (C<sub>q</sub>). DEPT 135: (100 MHz) 16.12 (CH<sub>2</sub>), 19.21 (CH<sub>3</sub>), 32.00 (CH<sub>3</sub>), 38.64 (CH<sub>2</sub>), 67.82 (CH<sub>2</sub>), 70.24 (CH<sub>2</sub>), 74.15 (CH<sub>2</sub>), 74.61 (CH<sub>2</sub>), 114.77 (CH).

Plot indicates a half-life of approximately 11 hours.

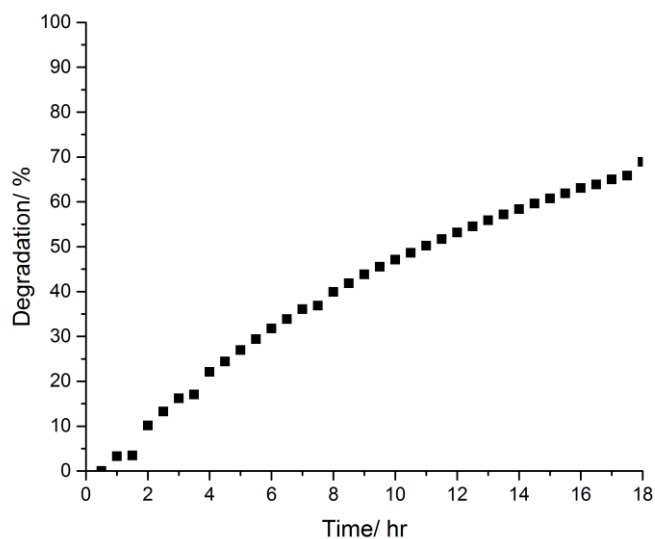


Figure 291: Degradation of 2.13

### 9.1.28. Probing rearrangement by addition of another nitroxide

**2.09** (10 mg, 0.0037 mmol) was dissolved in  $\text{CHCl}_3$  (2 mL). Oxo-TEMPO (6.4 mg, 0.0038 mmol) was added and the solution mixed for 12 hr. Reaction was then compared to mixture where TEMPO (5.9 mg, 0.0038 mmol) was added in place of Oxo-TEMPO. TLC (9:1 PET-ether:ethyl acetate) showed only indication of **2.09** ( $R_f = 0.88$ ), **2.09'** ( $R_f = 0.26$ ), TEMPO ( $R_f = 0.35$ ) or oxo-TEMPO ( $R_f = 0.1$ ) respectively, with no other spots present, thus no indication of an oxo-TEMPO product. Solvent was removed from each solution by rotary evaporation, and then analysed by  $^1\text{H}$  NMR. No difference indicative of Oxo-TEMPO substituting the TEMPO group could be clearly observed.

### 9.1.29. Reaction between trans-1,4-cyclohexanedicarboxylic acid and oxalyl chloride

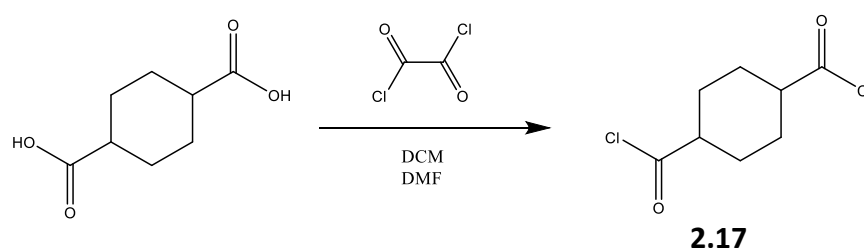


Figure 292: Formation of **2.17**

Trans 1,4-cyclohexanedicarboxylic acid (0.5 g, 2.9 mmol) was placed under a nitrogen atmosphere and dissolved in dry DCM (20 mL). DMF (3 drops) was added, and the solution cooled to  $0^\circ\text{C}$ . Oxalyl chloride (0.36 mL, 4.3 mmol) was added cautiously. After 1 hr the reaction flask was allowed to warm to temperature, with the reaction stirred for a further 3 hr. Solvent is removed by rotary evaporation to produce **2.17** as a white powder. Crude yield = 95%. This product is then used without further purification.  $^1\text{H}$  NMR: (400 MHz) 1.30 (m, 4H), 1.89 (m, 4H), 2.15 (m, 2H, *CHC*).

### 9.1.30. Reaction between 2.17 and dimethylamine.

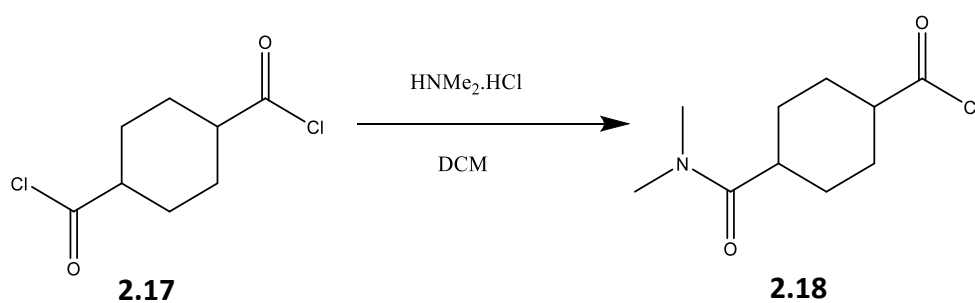


Figure 293: Formation of **2.18**

**2.17** (0.5156 g, 2.5 mmol) was placed under a nitrogen atmosphere and dissolved in dry  $\text{DCM}$  (20 mL). The solution was then cooled to  $0^\circ\text{C}$ .  $\text{HNMe}_2 \cdot \text{HCl}$  (0.1019 g, 1.25 mmol) was dissolved in dry  $\text{DCM}$  (5 mL) and added dropwise to the reaction mixture. The solution was then allowed to warm to room temperature and was stirred for 19 hr. The solution was then filtered, and solvent removed by rotary evaporation to produce **2.18** as a pale beige powder. This product is then used without any further purification to form **2.19** as described below.

### 9.1.31. Hydrogenation of 2.18

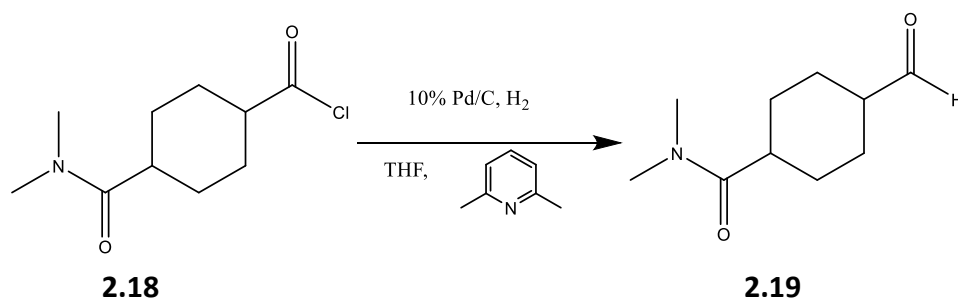
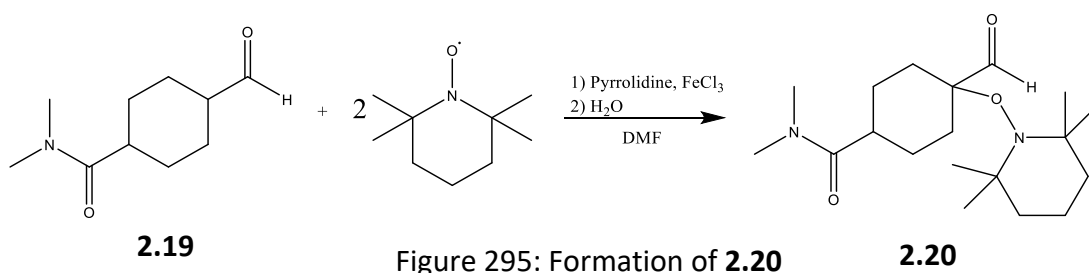


Figure 294: Formation of **2.19**

2,6-Lutidine (0.29 mL, 2.5 mmol) was placed under a nitrogen atmosphere and dissolved in dry  $\text{THF}$  (20 mL).  $10\% \text{Pd/C}$  (45 mg, 0.042 mmol) was added, and the flask then purged with  $\text{H}_2$ . **2.18** (0.5368 g, 2.5 mmol) was dissolved in dry  $\text{THF}$  (10 mL) and added dropwise to the reaction mixture. After again being purged with  $\text{H}_2$  the reaction is left to stir for 19 hr. The solution was then filtered over celite, and solvent removed by rotary evaporation

to give a pale beige powder. This was re-dissolved in Et<sub>2</sub>O (30 mL), and washed with HCl (1 M, 20 mL), NaHCO<sub>3(aq)</sub> (20 mL) and brine (20 mL). The solution was then dried with MgSO<sub>4</sub>, filtered, and solvent removed by rotary evaporation. The resulting residue was purified by flash chromatography (7:3 DCM: Ethyl acetate, R<sub>f</sub> = 0.33) to give **2.19**. Yield = 43.8%. <sup>1</sup>H NMR: (400 MHz) 1.30 (m, 4H), 1.60 (m, 4H), 2.10 (m, 2H), 2.93 (s, 3H, NCH<sub>3</sub>CH<sub>3</sub>), 3.04 (s, 3H, NCH<sub>3</sub>CH<sub>3</sub>), 9.63 (s, 1H, HCHO). MS (ESI) 184.1334, calculation for C<sub>10</sub>H<sub>17</sub>NO<sub>2</sub>, [M+H]<sup>+</sup> = 184.1332.

### 9.1.32. Reaction between **2.19** and TEMPO



**2.19** (20 mg, 0.11 mmol) was dissolved in DMF (1 mL). 2,2,6,6-Tetramethylpiperidine 1-oxyl (TEMPO) (34 mg, 0.22 mmol), pyrrolidine (2 μL, 0.025 mmol) and FeCl<sub>3</sub> (10 mg, 0.062 mmol) were added, and the solution stirred for 20 hr. Sodium ascorbate (0.66 g, 3.3 mmol) was dissolved in H<sub>2</sub>O (10 mL) and added to the reaction mixture with Et<sub>2</sub>O (20 mL). The organic phase was extracted with Et<sub>2</sub>O (3 x 20 mL) and dried with MgSO<sub>4</sub>. Product was then filtered, and solvent removed by rotary evaporation. The remaining residue was purified by flash chromatography (1:1 DCM: Ethyl acetate, R<sub>f</sub> = 0.39) to produce **2.20** as a pale orange oil. Yield = 20%. <sup>1</sup>H NMR: (400 MHz) 1.14 (s, 3H, C(CH<sub>3</sub>)<sub>2</sub>), 1.16 (s, 3H, C(CH<sub>3</sub>)<sub>2</sub>), 1.49 (m, 12H), 1.718 (m, 2H), 2.53 (m, 1H, HCCON), 2.95 (s, 3H, NCH<sub>3</sub>CH<sub>3</sub>), 3.06 (s, 3H, NCH<sub>3</sub>CH<sub>3</sub>), 10.22 (s, 1H, CCHO). MS (ESI) 339.2635, calculation for C<sub>19</sub>H<sub>34</sub>N<sub>2</sub>O<sub>3</sub>, [M+H]<sup>+</sup> = 339.2642.

### 9.1.33. Wittig reaction of **2.20**

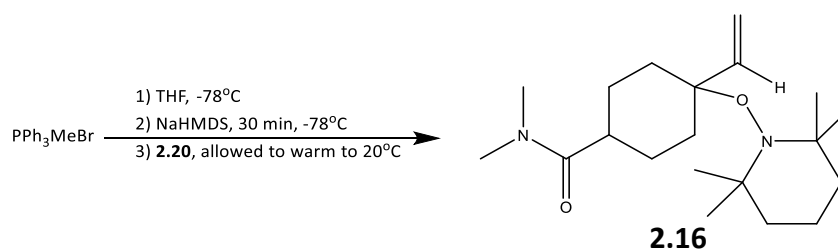


Figure 296: Formation of **2.16**

Dry THF (5 mL) was added to PPh<sub>3</sub>MeBr (21.2 mg, 0.059 mmol) under an atmosphere of nitrogen. The mixture was then cooled to -77 °C and NaHMDS (1 M in THF, 60 μL, 0.06 mmol) added. After stirring for 30 min **2.20** (20 mg, 0.059 mmol) was added, and the reaction is allowed to warm to room temperature with stirring over 2 hr. The solution was then extracted with ethyl acetate (3 x 5 mL), washed with NH<sub>4</sub>Cl<sub>(aq)</sub> (5 mL), NaHCO<sub>3</sub> (5 mL) and brine (5 mL), before being dried with MgSO<sub>4</sub>. The solution was then filtered, and solvent removed by rotary evaporation. The remaining residue was purified by flash chromatography (7:3 DCM: Ethyl acetate, R<sub>f</sub> = 0.42) to give product **2.16** as a pale peach oil. Yield = 24%. <sup>1</sup>H NMR: (400 MHz) 1.08 (s, 3H, C(CH<sub>3</sub>)<sub>2</sub>), 1.15 (s, 3H, C(CH<sub>3</sub>)<sub>2</sub>), 1.46 (m, 12H), 1.64 (m, 2H), 2.53 (m, 1H, HC CON), 2.97 (s, 3H, NCH<sub>3</sub>CH<sub>3</sub>), 3.08 (s, 3H, NCH<sub>3</sub>CH<sub>3</sub>), 4.93 (dd, 1H, J = 18.4, 1.6 Hz, HCCHH), 4.98 (dd, 1H, J = 11.6, 1.6 Hz, HCCHH), 6.69 (dd, 1H, J = 18.4, 11.6 Hz, HCCHH). <sup>13</sup>C NMR: (100 MHz) 17.25, 21.41, 24.58, 34.66, 36.30, 36.95, 40.40, 40.80, 59.30 (C<sub>q</sub>), 85.88 (C<sub>q</sub>), 110.38, 144.00, 192.20 (C<sub>q</sub>). DEPT 135: (100 MHz) 17.25 (CH<sub>2</sub>), 21.41 (CH<sub>3</sub>), 24.57 (CH<sub>2</sub>), 34.66 (CH<sub>3</sub>), 36.30 (CH<sub>2</sub>), 36.95 (CH), 40.40 (CH<sub>3</sub>), 40.80 (CH<sub>2</sub>), 110.38 (CH<sub>2</sub>), 144.00 (CH). MS (ESI) 337.2847, calculation for C<sub>20</sub>H<sub>36</sub>N<sub>2</sub>O<sub>2</sub>, [M+H]<sup>+</sup> = 337.2850.

COSY: Shown in Figure 297

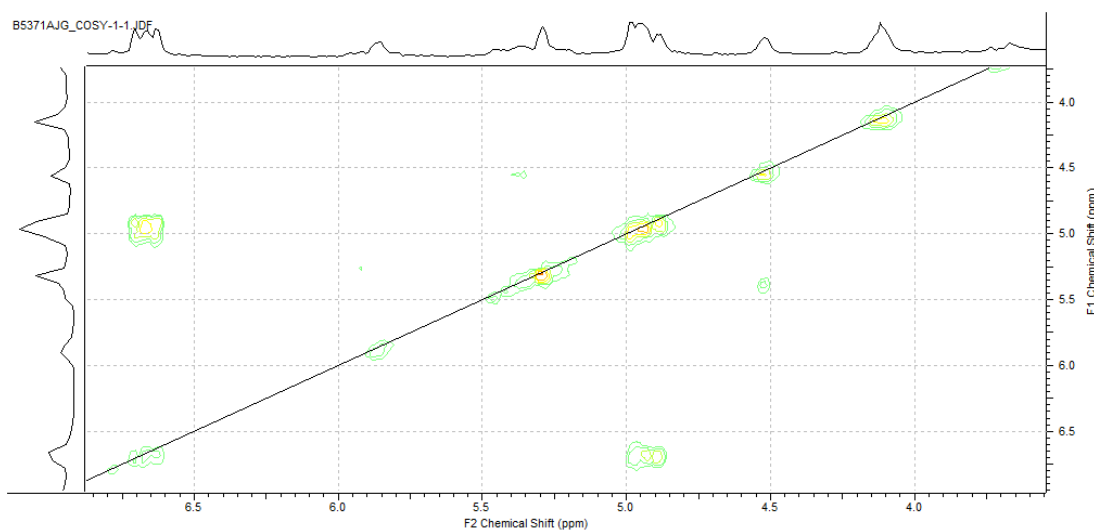


Figure 297: COSY of **2.16**

#### 9.1.34. Rearrangement of **2.16** to form **2.16'**

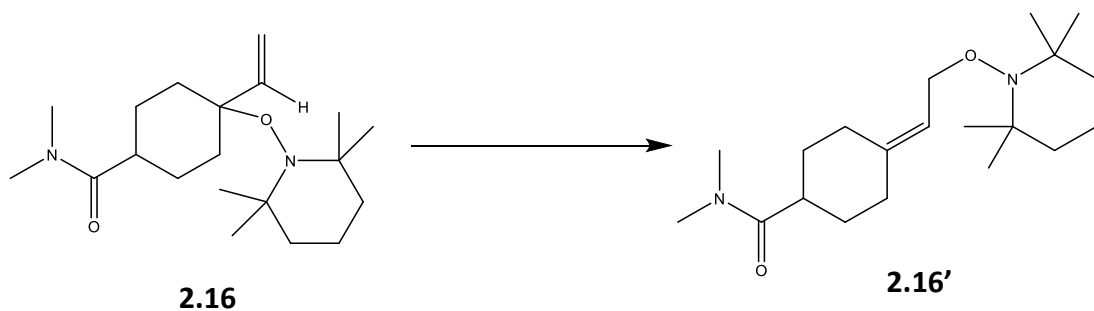


Figure 298: Formation of **2.16'**

Product formed by **2.16** rearranging whilst remaining in solution over several hours to form **2.16'**, with a half-life of 5 hr.  $^1\text{H}$  NMR (400 MHz): 1.09 (s, 3H,  $\text{C}(\text{CH}_3)_2$ ), 1.16 (s, 3H,  $\text{C}(\text{CH}_3)_2$ ), 1.47 (m, 12H), 1.65 (m, 2H), 2.53 (m, 1H,  $\text{HCCON}$ ), 2.98 (s, 3H,  $\text{NCH}_3\text{CH}_3$ ), 3.07 (s, 3H,  $\text{NCH}_3\text{CH}_3$ ), 4.55 (d, 2H,  $J = 7.6$  Hz,  $\text{CCHCH}_2$ ), 5.40 (t, 1H,  $J = 7.6$  Hz,  $\text{CCHCH}_2$ ).

## 9.2. Experimental Details for Chapter 3

### 9.2.01. Trapping a <sup>t</sup>BuOO· radical

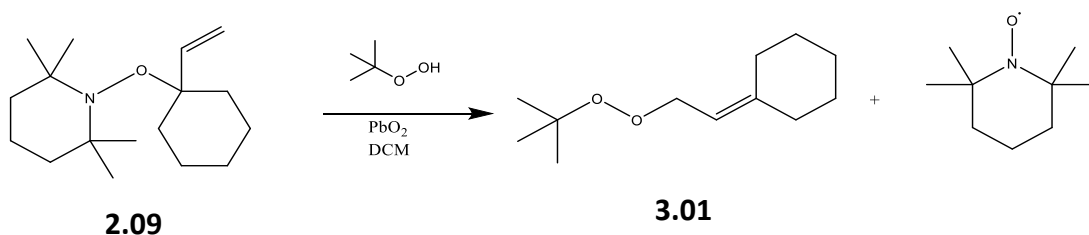


Figure 299: Trapping of the <sup>t</sup>BuOO· radical by **2.09**

**2.09** (100 mg, 0.377 mmol) was dissolved in CHCl<sub>3</sub> (10 ml). Tert-BuOOH (70% in H<sub>2</sub>O, 2 mL, 14.4 mmol) was added, followed by PbO<sub>2</sub> (500 mg, 2.1 mmol). The mixture was stirred overnight and filtered to produce an orange liquid. Solvent was removed by rotary evaporation. For flash column purification, the residue is passed through a silica column with a solution of THF: PET ether (5:95). R<sub>f</sub> = 0.29. After drying, compound, is re-purified by passing through a silica column with a solution of acetone: PET ether (5:95). R<sub>f</sub> = 0.33. LC-MSMS of the mixture was conducted with a reverse phase ODS column (Alphasil, 25 cm x 4.6 mm), flow rate = 1 ml min<sup>-1</sup>. Initial solvent conditions were 50:50 methanol:water, rising to 65:35 methanol:water over 30 min, and then to 85:15 over another 30 min. MS (22 min): (EI) 221.1505, calculation for C<sub>12</sub>H<sub>22</sub>O<sub>2</sub>, [M+Na]<sup>+</sup> = 221.1512 MSMS (221): 165.1.

### 9.2.02. Trapping a methyl radical

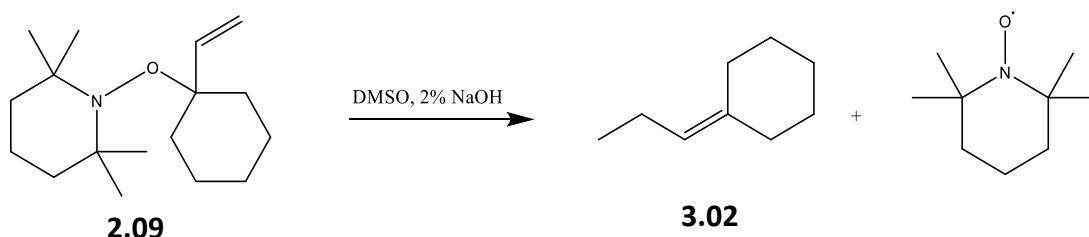


Figure 300: Capture of a methyl radical by **2.09**

**2.09** (2.9 mg, 0.011 mmol) was mixed with degassed DMSO (2 mL). An aqueous sample of 2% NaOH (w/v) (2 mL) was degassed and added to the main reaction mixture. This was

stirred for 15 min, before the organic layer was extracted with cyclohexane, dried and analysed. MS (ESI): 125.1316 calculation for  $C_9H_{16}$ ,  $[M+H]^+ = 125.1325$

### 9.2.03. Trapping an aminyl radical from n-butylamine with $PbO_2$ radical generation

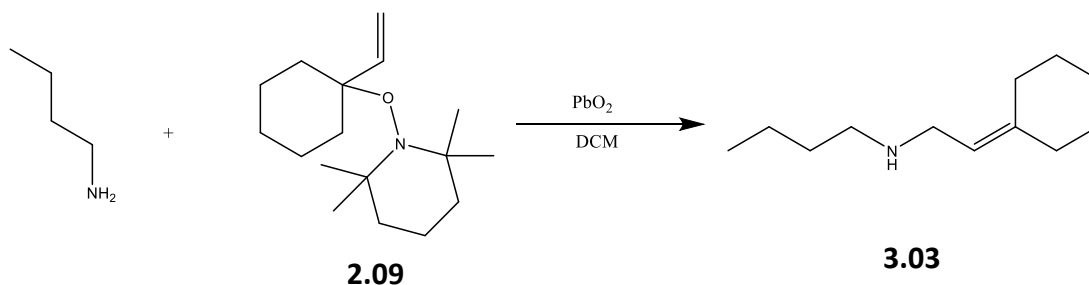


Figure 301: Anticipated reaction for the formation of **3.03**

**2.09** (20 mg, 0.075 mmol) was mixed in DCM (2 mL). n-Butylamine (57  $\mu$ L, 0.577 mmol) is added, followed by  $PbO_2$  (250 mg, 1.05 mmol) and the mixture stirred overnight. The reaction was filtered, producing an orange liquid, with solvent then removed by rotary evaporation. Product **3.03'** was observed. MS (ESI): 180.1740 calculation for  $C_{12}H_{21}N$ ,  $[M+H]^+ = 180.1747$

### 9.2.04. Trapping an aminyl radical from isopropylamine with $PbO_2$ radical generation

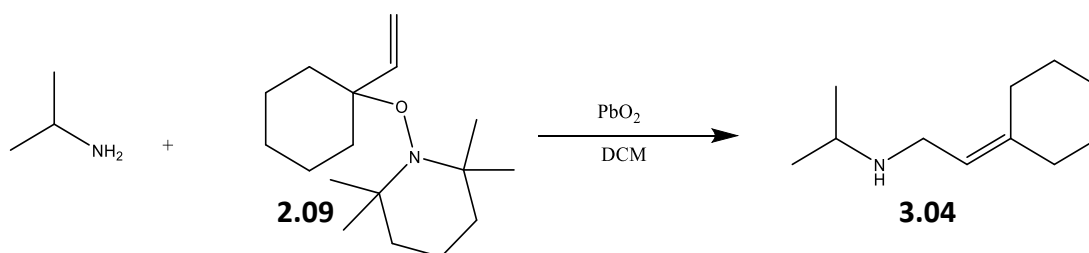


Figure 302: Anticipated reaction for the formation of **2.09**

**2.09** (20 mg, 0.075 mmol) was mixed in DCM (2 mL). Isopropylamine (49  $\mu$ L, 0.57 mmol) was added, followed by  $PbO_2$  (250 mg, 1.05 mmol) and the mixture stirred overnight. The reaction was filtered, producing an orange liquid, with solvent then removed by rotary evaporation. Product **3.04'** was observed. MS (ESI): 166.1592, calculation for  $C_{11}H_{19}N$ ,  $[M+H]^+ = 166.1590$

### 9.2.05. Trapping an aminyl radical from t-butylamine with PbO<sub>2</sub> radical generation

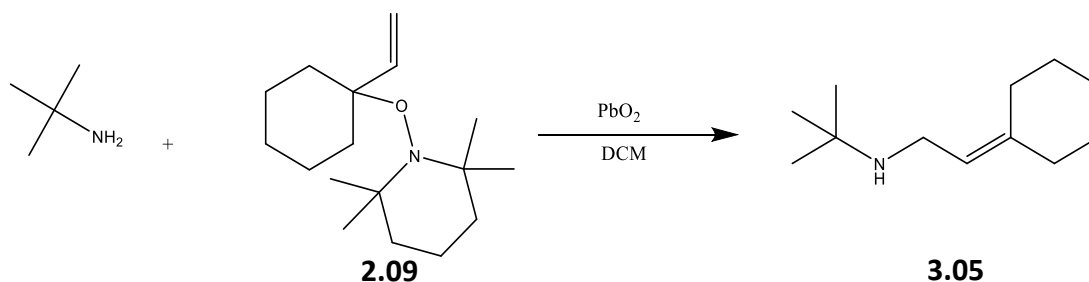


Figure 303: Anticipated reaction for the capture of a nitrogen based radical by **2.09**

**2.09** (19.3 mg, 0.073 mmol) was mixed in DCM (2 mL). t-butylamine (60  $\mu$ L, 0.57 mmol) was added, followed by PbO<sub>2</sub> (250 mg, 1.05 mmol) and the mixture stirred overnight. The reaction was filtered, producing a pale orange liquid, with solvent then removed by rotary evaporation. Product **3.05'** was observed. MS (ESI): 180.1740, calculation for C<sub>12</sub>H<sub>21</sub>N, [M+H]<sup>+</sup> = 180.1747

### 9.2.06. Trapping an aminyl radical with 2.11 and PbO<sub>2</sub> radical generation

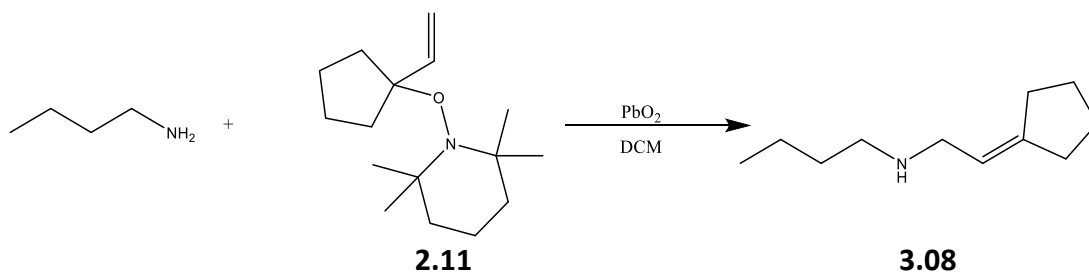


Figure 304: Anticipated reaction for trapping of an amine radical with **2.11**

**2.11** (20 mg, 0.080 mmol) was mixed in DCM (2 mL). n-Butylamine (57  $\mu$ L, 57 mmol) was added, followed by PbO<sub>2</sub> (250 mg, 1.05 mmol) and the mixture stirred overnight. The reaction was filtered, producing an orange liquid, with solvent then removed by rotary evaporation. Product **3.08'** was observed. MS (ESI): 166.1587 calculation for C<sub>11</sub>H<sub>19</sub>N, [M+H]<sup>+</sup> = 166.1590

### 9.2.07. MSMS Fragmentation experiments

MSMS (APCI) was conducted, with isolation and fragmentation of ions from **3.03'**, **3.05'** and **3.08'**.

**3.03'** (180): 112, 109, 107

**3.05'** (180): 107

**3.08'** (166): 110, 995, 93, 72

### 9.2.08. Trapping an aminyl radical from 2-naphthylamine with PbO<sub>2</sub> radical generation

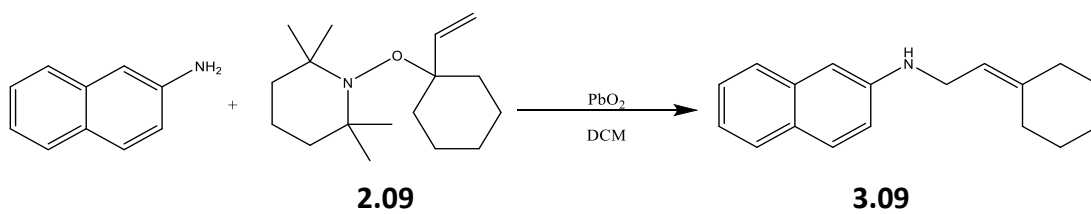


Figure 305: Anticipated reaction for trapping of an amine radical with **2.09**

**2.09** (20 mg, 0.075 mmol) was mixed in DCM (2 mL). 2-Naphthylamine (23 mg, 0.16 mmol) was added, followed by PbO<sub>2</sub> (50 mg, 0.21 mmol) and the mixture stirred overnight. After filtration, the red liquid had solvent removed by rotary evaporation. Product **3.09'** was observed. MS (ESI): 250.1043, calculation for C<sub>18</sub>H<sub>19</sub>N, [M+H]<sup>+</sup> = 250.1090

### 9.2.09. Trapping a Deuterated aminyl radical

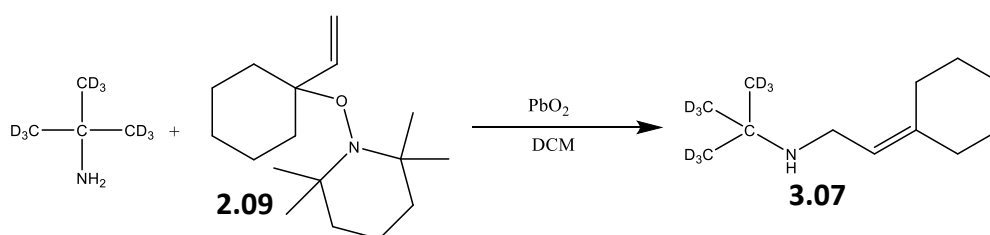


Figure 306: Capture of a deuterated amine radical

**2.09** (10 mg, 0.0375 mmol) was mixed in DCM (2 mL). n-Butylamine (57  $\mu$ L, 0.65 mmol) is added, followed by PbO<sub>2</sub> (50 mg, 0.21 mmol) and the mixture stirred overnight. The reaction was filtered, producing an orange liquid, with solvent then removed by rotary evaporation. Product **3.03'** was observed. MS (ESI): 189.2316 calculation for C<sub>12</sub>H<sub>12</sub>D<sub>9</sub>N, [M+H]<sup>+</sup> = 189.2312.

### 9.2.10. Trapping an aminyl radical with Fenton based radical generation

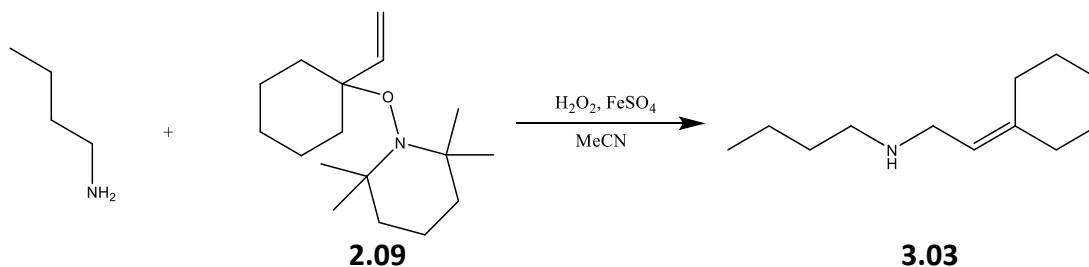


Figure 307: Anticipated reaction for amine radical trapping with **2.09** via Fenton chemistry

**2.09** (20 mg, 0.075 mmol) and H<sub>2</sub>O<sub>2</sub> (30 %, 0.1 mL, 0.1 mmol) were mixed into MeCN (4 mL). n-butylamine (10  $\mu$ L, 0.1 mmol) was added, followed by two drops of an iron sulphate solution (0.271 g FeSO<sub>4</sub> in 2 mL H<sub>2</sub>O). The reaction effervesced, with a burgundy precipitate forming. The reaction was then extracted with DCM (3 x 2 mL), and solvent then removed from the resulting pale yellow solution by rotary evaporation. **3.03'** was observed. MS (ESI): 180.1742, calculation for C<sub>12</sub>H<sub>21</sub>N, [M+H]<sup>+</sup> = 180.1747

### 9.2.11. Attempted Rearrangement of 3.10

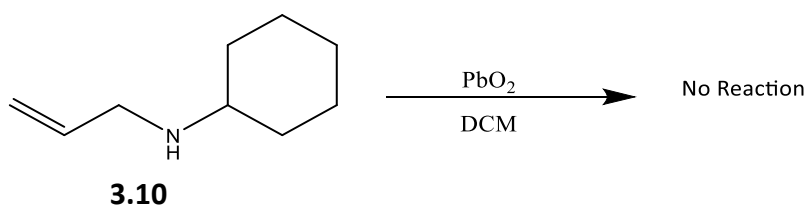


Figure 308: Reaction of surrogate trapping molecule **3.10**

**3.10** (10  $\mu$ L, 0.069 mmol) was added to DCM (2 mL). PbO<sub>2</sub> (95 mg, 0.40 mmol) was then added, and the reaction stirred for 21 hr. The reaction mixture was filtered, and the

resulting solvent removed by rotary evaporation.  $^1\text{H}$  NMR (400 MHz) 1.136 (m, 6H,  $\text{CHCH}_2(\text{CH}_2)_3\text{CH}_2$ ), 1.681 (m, 1H, NCH), 1.770 (m, 4H,  $\text{CHCH}_2(\text{CH}_2)_3\text{CH}_2$ ), 2.417 (m, 1H, NH), 3.239 (m, 2H,  $\text{NHCH}_2$ ), 5.033 (m, 1H,  $J = 10.4$  Hz,  $\text{HC}=\text{CHH}$ ), 5.126 (m, 1H,  $J = 17.2$  Hz,  $\text{HC}=\text{CHH}$ ), 5.877 (ddt, 1H,  $J = 6.5, 10.4, 17.2$  Hz).

### 9.2.12. Trapping a thio radical with $\text{PbO}_2$ radical generation

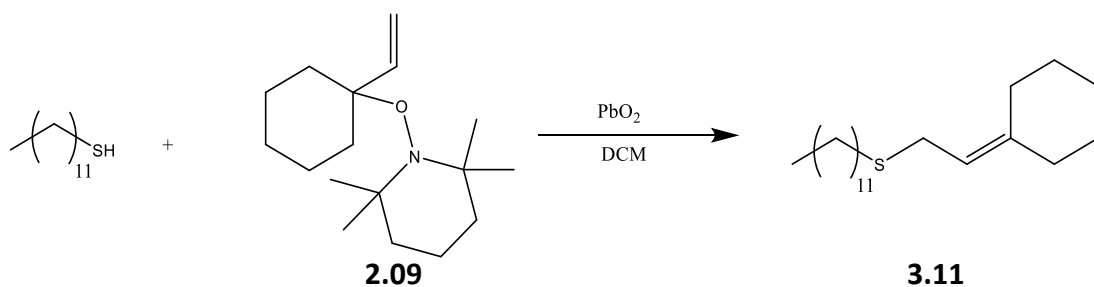


Figure 309: Anticipated reaction for the capture of a thio based radical by **2.09**

**2.09** (21.3 mg, 0.08 mmol) was dissolved in  $\text{CHCl}_3$  (2 mL). *n*-Dodanethiol (0.14 mL, 0.58 mmol) was added, followed by  $\text{PbO}_2$  (263 mg, 1.1 mmol). The solution was left to stir overnight. After filtration the pale yellow solution has solvent removed by rotary evaporation. **3.11'** was observed. MS of crude reaction mixture (APCI): 309.2608, calculation for  $\text{C}_{20}\text{H}_{36}\text{S}$ ,  $[\text{M}+\text{H}]^+ = 309.2610$

### 9.2.13. Generation and trapping a thio radical with AIBN radical generation

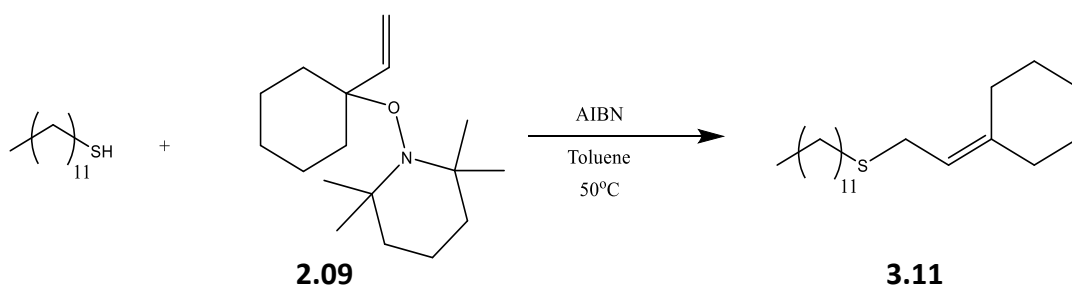


Figure 310: Generation and capture of a thio radical using AIBN initiator

**2.09** (20 mg, 0.075 mmol) was placed under nitrogen and dissolved in toluene (0.4 mL). *n*-dodecanethiol (27  $\mu\text{L}$ , 0.11 mmol) added, and the solution heated to  $50^\circ\text{C}$ .

Azobisisobutyronitrile (AIBN) (0.25 mg, 0.0015 mmol) was added to toluene (0.1 mL) and added into the main reaction mixture and stirred. After 2 hr the reaction was allowed to cool before extraction with DCM. Solvent was removed by rotary evaporation. **3.11** and **3.11'** were observed. MS (APCI): 311.2755, calculation for C<sub>20</sub>H<sub>38</sub>S, [M+H]<sup>+</sup> = 311.2767 and 309.2609, calculation for C<sub>20</sub>H<sub>36</sub>S, [M+H]<sup>+</sup> = 309.2610

When repeated under a standard atmosphere of air, no **3.11** was observed. MS (APCI): 309.2611, calculation for C<sub>20</sub>H<sub>36</sub>S, [M+H]<sup>+</sup> = 309.2610.

#### 9.2.14. Trapping radicals from deuterated thiol **3.16**

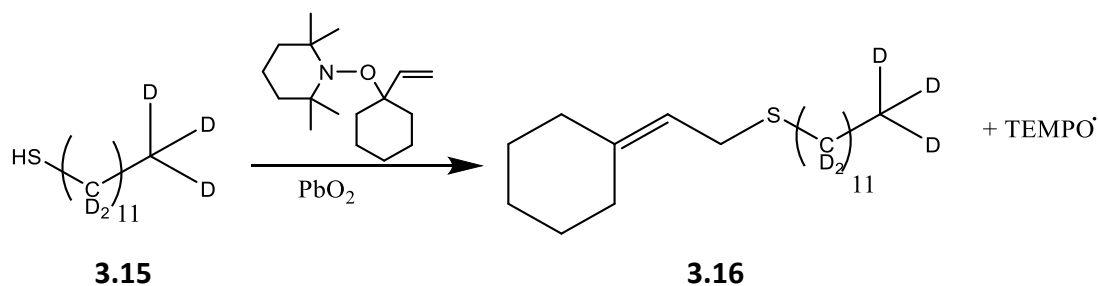


Figure 311: Trapping a thioyl radical from a deuterated thiol

**2.09** (10 mg, 0.0375 mmol) was dissolved in CHCl<sub>3</sub> (2 mL). **3.15** (15 μL, 0.053 mmol) was added, followed by PbO<sub>2</sub> (50 mg, 0.21 mmol). The solution was left to stir overnight. After filtration the pale yellow solution has solvent removed by rotary evaporation. **3.16'** and **3.16''** were observed. MS (ESI): 334.4171, calculation for C<sub>20</sub>H<sub>11</sub>D<sub>25</sub>S, [M+H]<sup>+</sup> = 334.4180 MSMS (APCI): (334) 226.2

### 9.3. Experimental details for Chapter 4

#### 9.3.01. Radical Trapping from an Aerosol Bag System

**2.09** (20 mg, 0.075 mmol) was dissolved in DCM, added to a sample of glass wool (160 mg) and solvent removed by rotary evaporation. The sample was then loaded into a glass tube, and attached to the outflow of an aerosol generation chamber. The chamber consists of

a regulated air flow ( $2.3 \text{ L min}^{-1}$ ) passed over an excess of  $\alpha$ -pinene ( $350 \mu\text{L}$ ,  $2.20 \text{ mmol}$ ) into the aerosol bag (maximum volume =  $300 \text{ L}$ ). A UV lamp ( $254 \text{ nm}$ ,  $230 \text{ W}$ ) within the bag was used to generate  $\text{O}_3$ . Air was pulled through the bag and sampling tube by a vacuum pump, with additional solid matter collected by a filter at the end of the system. After sampling for  $90 \text{ min}$ , glass wool was removed and the products extracted by washing the sample with DCM ( $5 \text{ mL}$ ). The sample was then dried and analysed by mass spectrometry.

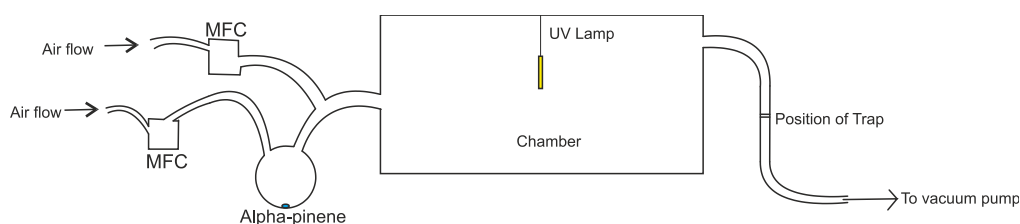


Figure 312: Schematic representation of aerosol bag system

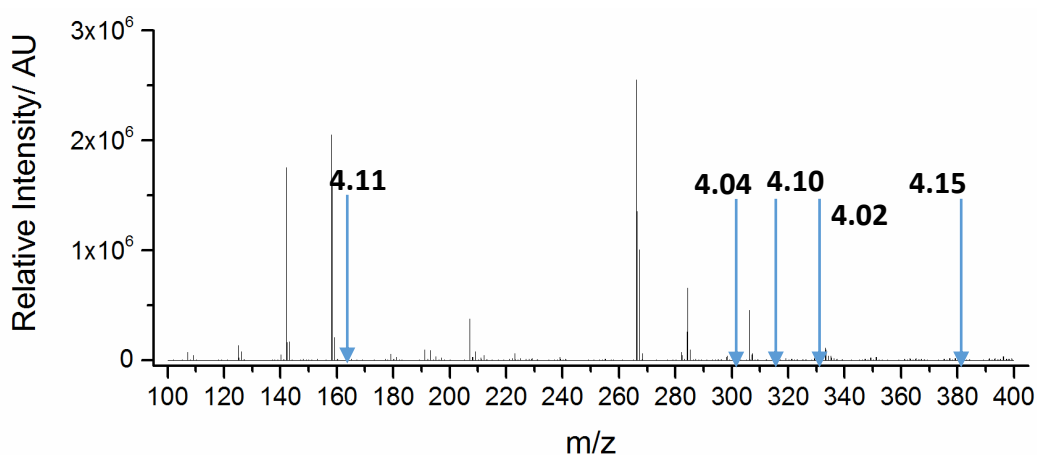


Figure 313: MS of products captured from aerosol bag experiment with **2.09**. The positions of key captured radicals discussed in **Chapter 4** are indicated

Products captured with application of **2.11** (20 mg, 0.080 mmol):

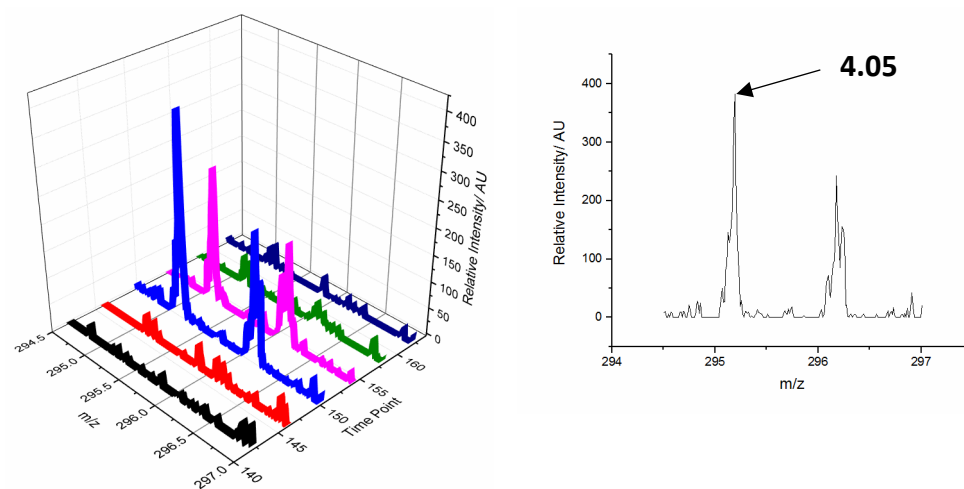


Figure 314: Capture of **4.01** to form **4.05**

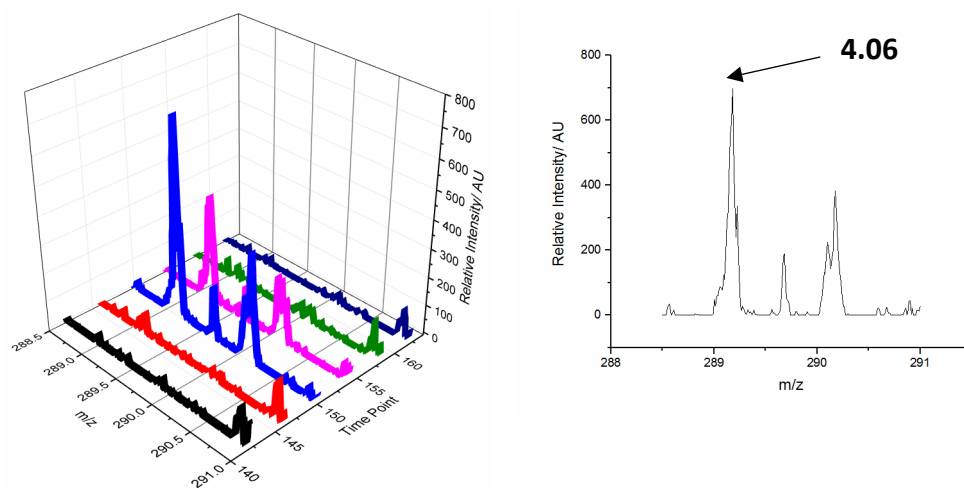


Figure 315: Capture of **4.03** to form **4.06**

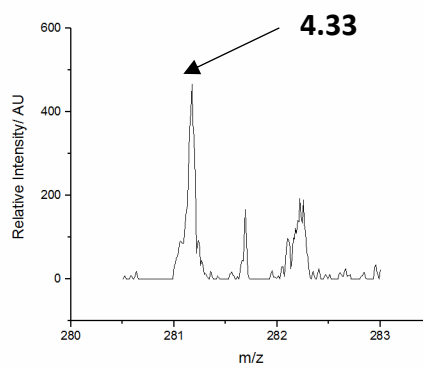
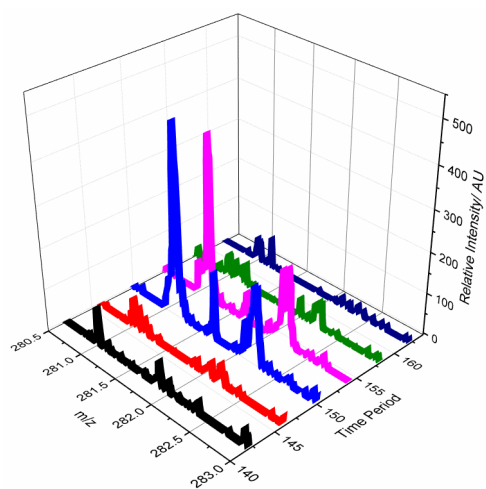


Figure 316: Capture of 4.09 to form 4.33

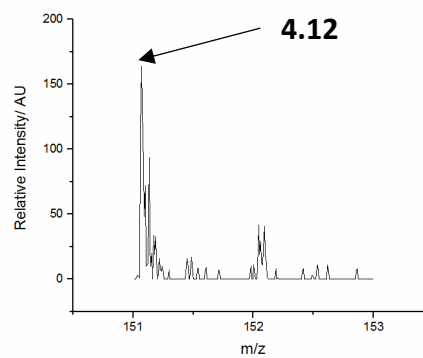
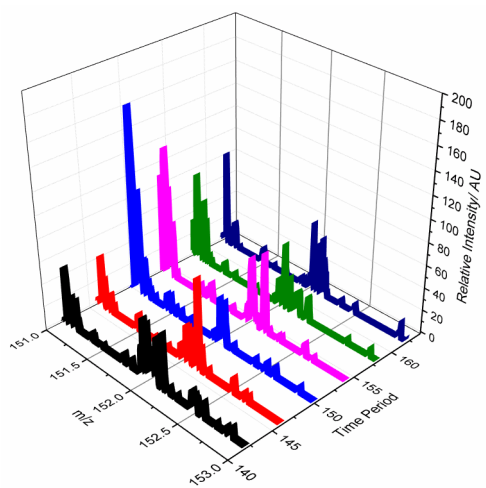


Figure 317: Capture of  $\text{HOO}\cdot$  to form 4.12

Products captured with application of **2.13** (20 mg, 0.079 mmol)

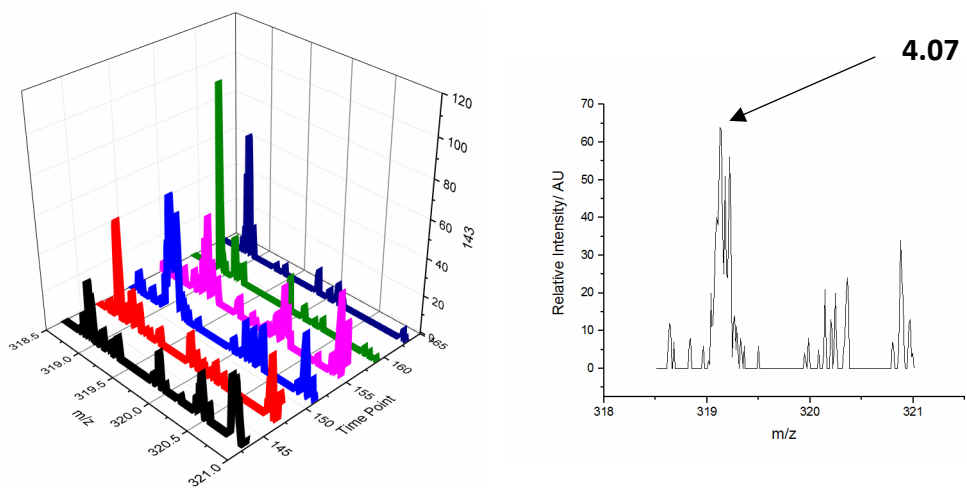


Figure 318: Capture of **4.01** to form **4.07**

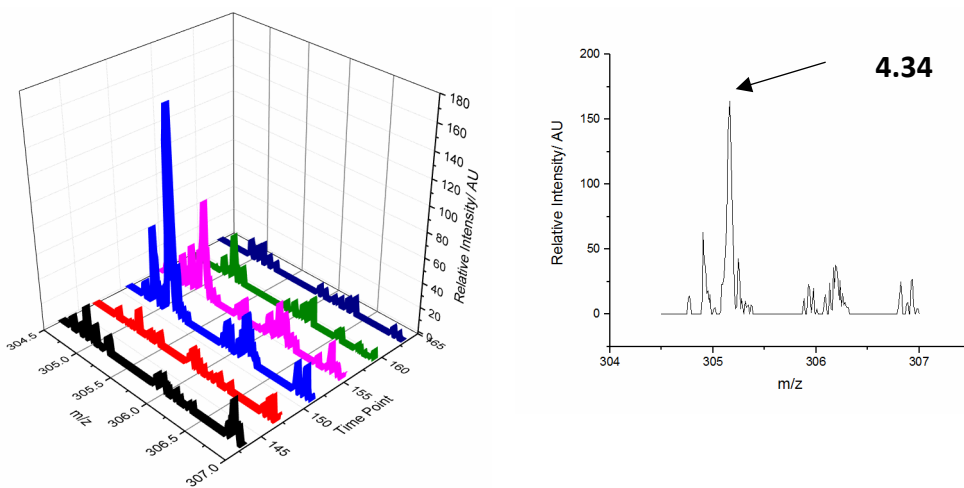


Figure 320: Capture of **4.09** to form **4.34**

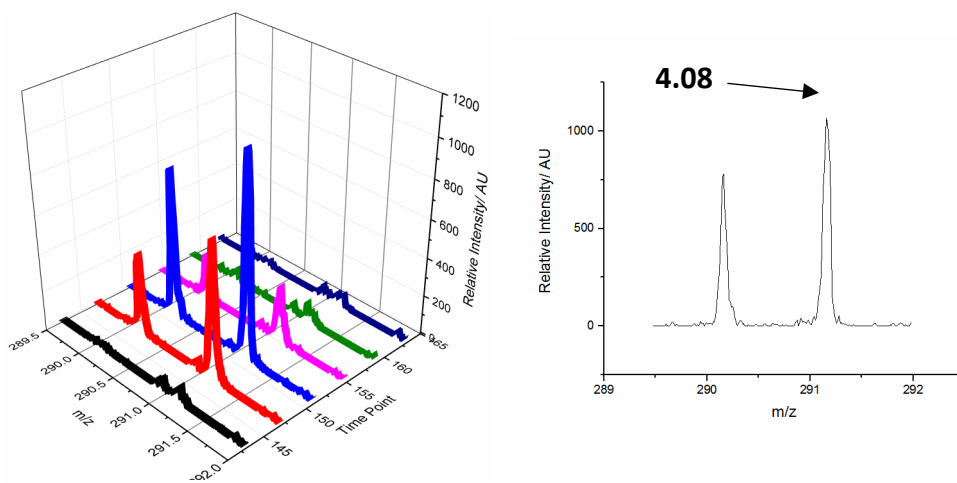


Figure 319: Capture of **4.03** to form **4.08**

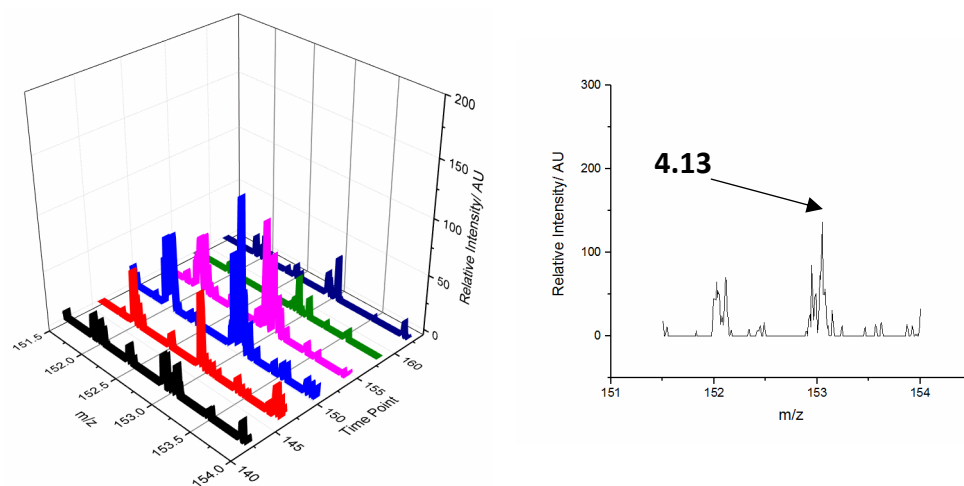


Figure 321: Capture of  $\text{HOO}\cdot$  to form **4.13**

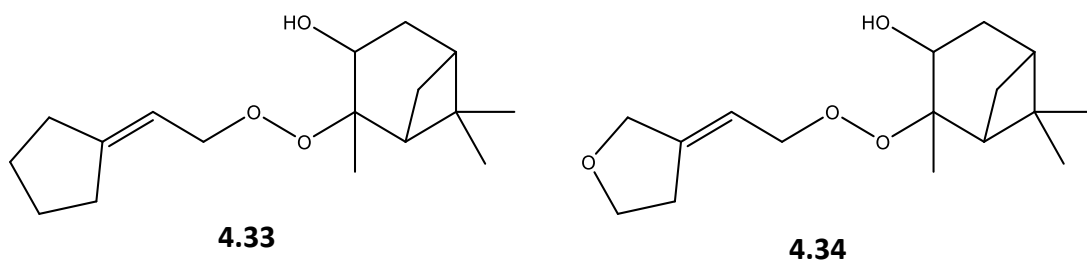


Figure 322: Structures of **4.33** and **4.34**

Blank experiments are also conducted as described above with **2.09**, however the UV lamp was not ignited for these experiments. Expected reaction products were not observed, as shown in Figure 323 and Figure 324.

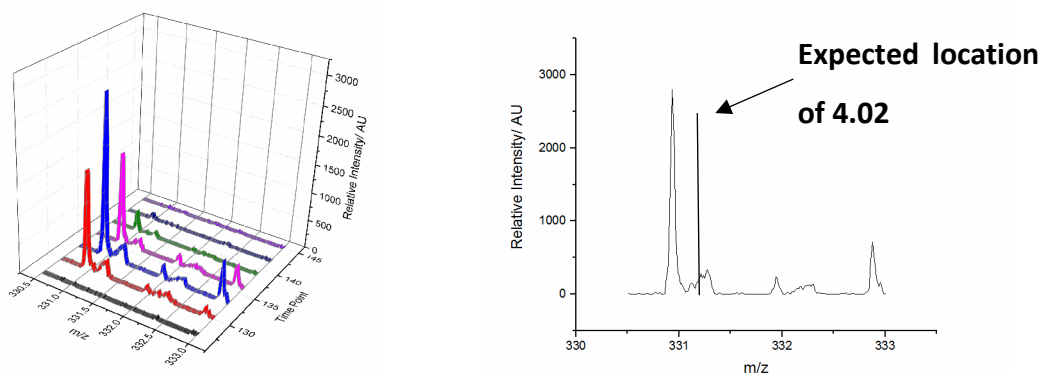


Figure 323: Lack of **4.02** from blank experiment

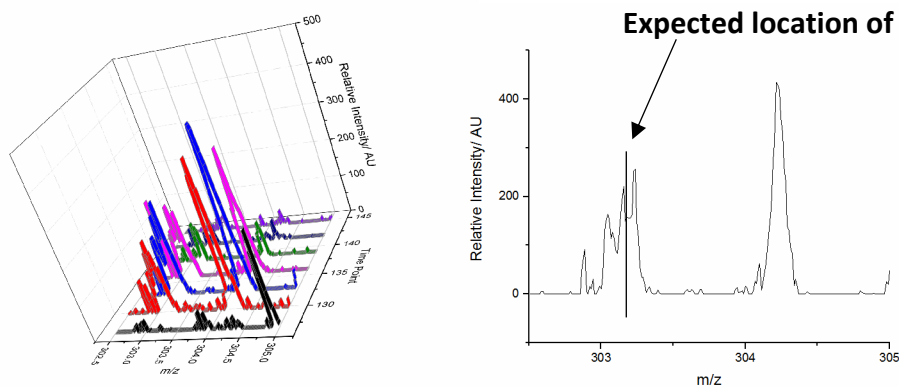


Figure 324: Lack of **4.04** from blank experiment

### 9.3.02. Model for Prediction of 4.14

The kinetics of this reaction are modelled using Kintecus software.<sup>323</sup> The chemical and mechanistic information is taken from the Master Chemical Mechanism.<sup>229,230</sup> Rate constants for the formation of **4.14** and related species are taken from Zhang et al.<sup>245</sup>

General model parameters include a starting Integration Time: 0.000001 s, maximum integration time: 10 s, Ea units: Kelvin, concentration units: molecules cm<sup>-3</sup>, temperature 298 K, simulation length: 120.4 s, accuracy: 0.00000001. Initial concentrations of all species are set to 0, with the exception of  $\alpha$ -pinene ( $1.25 \times 10^{12}$  molecules cm<sup>-3</sup> and ozone  $5 \times 10^{11}$  molecules cm<sup>-3</sup>).

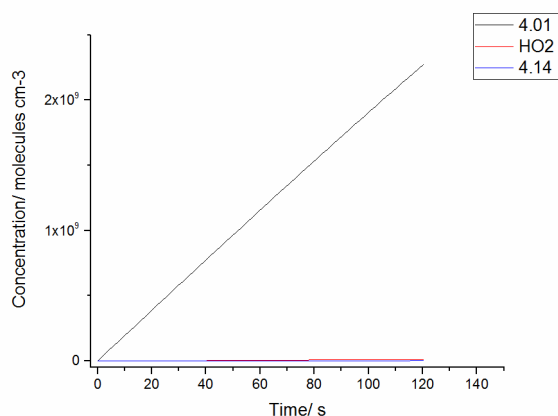


Figure 325: Modelled formation of **4.14** compared to **4.01**

### 9.3.03. General Procedure for Radical Trapping via an Quartz Flow Tube

**2.09** (20 mg, 0.075 mmol) was dissolved in DCM and added to a sample of glass wool (100 mg) and solvent removed by rotary evaporation. The sample was then loaded into a quartz tube, which was positioned after round bottom flask containing  $\alpha$ -pinene (0.4 mL, 2.5 mmol). A UV lamp (184.9 nm, 1.1 W) was positioned 10 cm prior to the trapping site, adjacent to the quartz tube in order to generate  $O_3$ , generating ca. 400 ppb. Air was pushed through this system for up to 90 min, after which the glass wool is removed and the products extracted by washing the sample with DCM (5 mL). The sample was then dried and analysed by mass spectrometry.

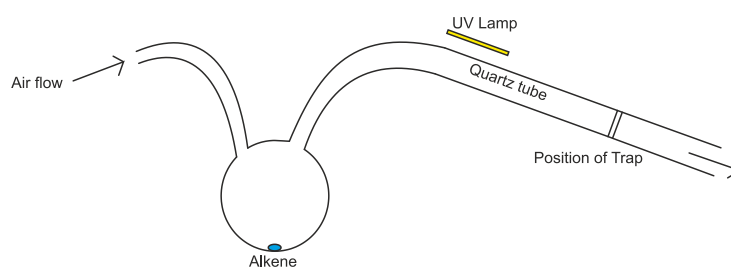


Figure 326: Schematic for trapping within a quartz flow tube

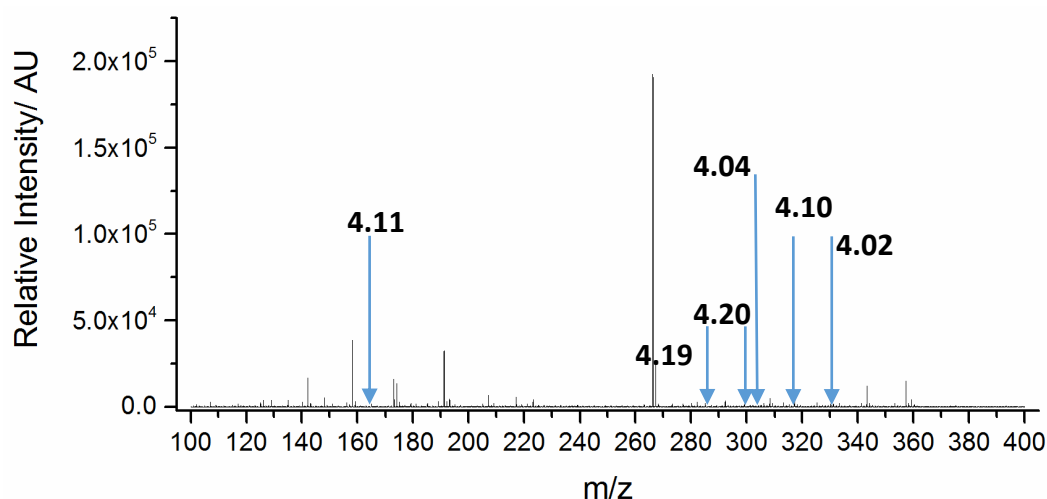


Figure 327: MS of products captured from quartz flow tube experiment with **2.09**. The positions of key captured radicals discussed in **Chapter 4** are indicated

#### 9.3.04. Trapping with both **2.09** and **2.13**

The reaction was conducted as for the general ozonolysis quartz procedure above, but with **2.09** (4.96 mg, 0.019 mmol) and **2.13** (4.72, 0.019 mmol) both deposited on the sample support. Products were observed from trapping with both types of trap.

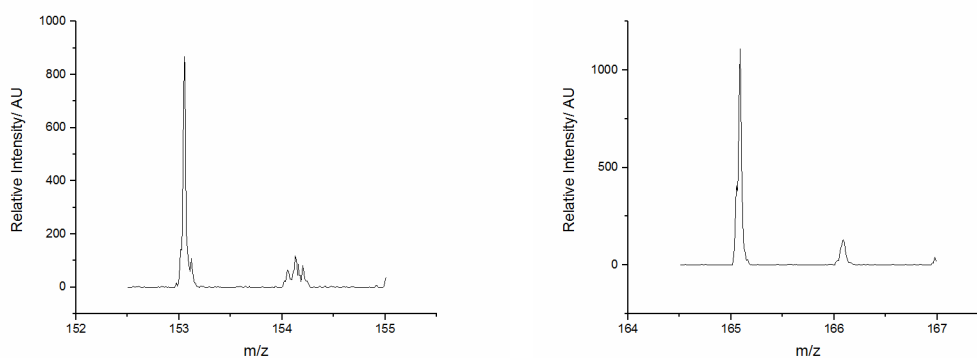


Figure 328: **4.13** and **4.11** produced from trapping with a mixture of **2.09** and **2.13**

#### 9.3.05. Reaction in the presence of an $\cdot\text{OH}$ scavenger

Reaction was conducted as for the general ozonolysis quartz tube procedure above, but with  $\alpha$ -pinene (0.1 mL, 0.63 mmol) and  $\cdot\text{OH}$  scavenger 2-butanol (0.1 mL, 1.1 mmol) deposited inside the round bottom flask.

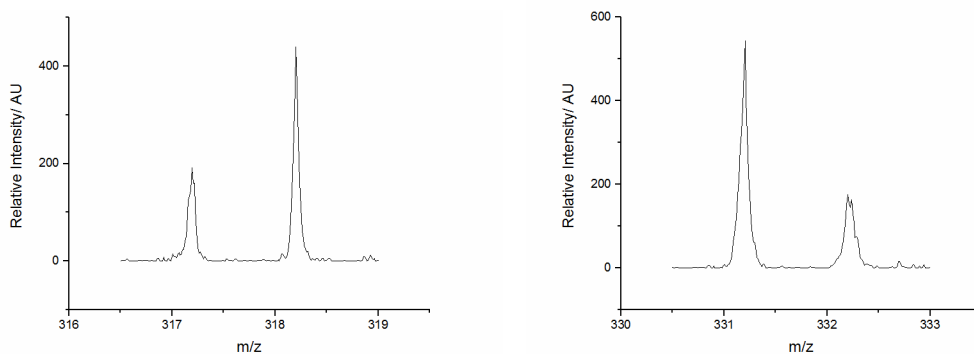


Figure 329: No **4.10**, but presence of **4.02** following reaction with an  $\cdot\text{OH}$  scavenger

### 9.3.06. A D<sub>2</sub>O Shake Reaction

Reaction was conducted as for the general ozonolysis quartz tube procedure above. After the sample is extracted by DCM, the sample is washed with D<sub>2</sub>O (2 mL), before being dried and analysed by mass spectrometry. The resultant signal change is given in Figure 330.

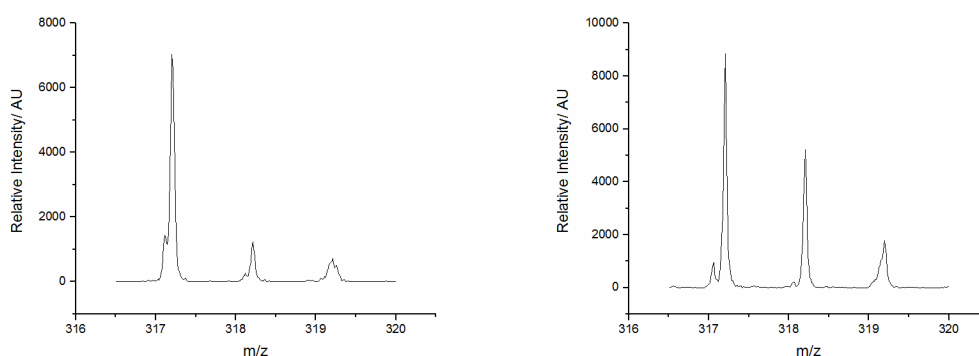


Figure 330: Change in signal for **3.10** upon D<sub>2</sub>O shake

### 9.3.07. Spin Trapping Radicals Produced from the Quartz Flow Tube

A solution of 5,5-Dimethyl-1-pyrroline *N*-oxide (25.28 mg, 0.22 mmol) was dissolved in toluene (1 mL) and positioned at the end of the  $\alpha$ -pinene quartz tube experimental set up described above, with a distance of 15 cm between the UV lamp and the trapping site, and a 3 L min<sup>-1</sup> flow rate. After 90 min, the solution is removed and analysed by EPR, generating the spectrum in Figure 331. EPR simulation uses RO<sub>2</sub> radical hyperfines of 13.59 and 10.5, carbon radical hyperfines of 13.8 and 21.4, and DMPO degradation products with hyperfines of 15.7 and 13.6. Relative contributions are 56, 2, 29 and 11 respectively.

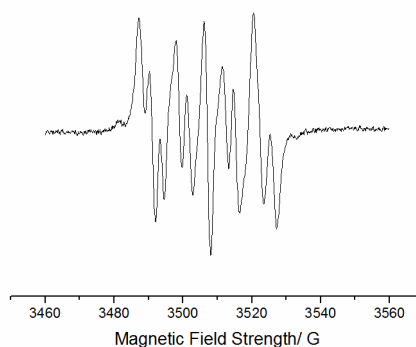


Figure 331: EPR from capture of radicals from  $\alpha$ -pinene ozonolysis

### 9.3.08. Application of **2.09'** to Radical Trapping

Reaction conducted as for the general ozonolysis quartz tube procedure, however **2.09'** (4.81 mg, 0.018 mmol) was utilised instead of **2.09**. No indication of radical trapping products was detected.

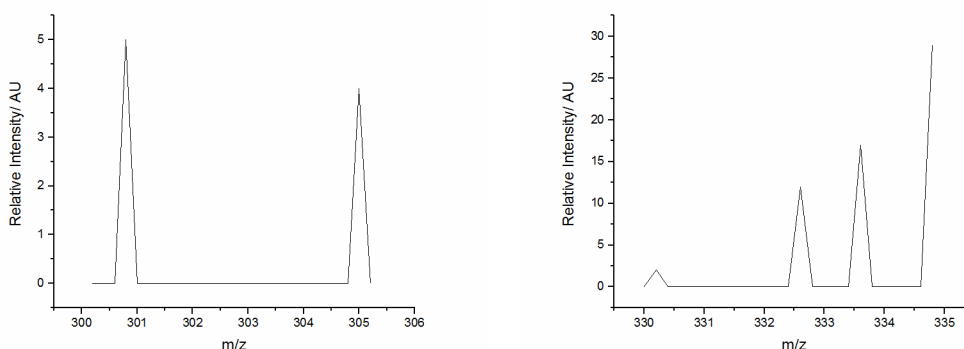


Figure 332: Lack for signal for trapping with **2.09'**

### 9.3.09. Trapping Radicals from Limonene Ozonolysis

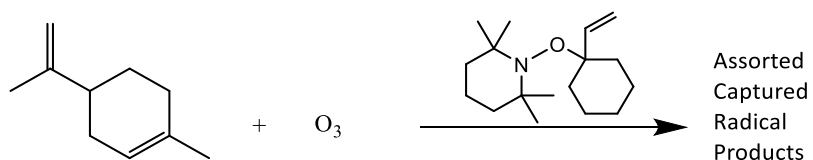


Figure 333: Capture of radical products from Limonene, using **2.09**

Reaction was conducted in the same manner as the general ozonolysis quartz tube procedure above. Limonene (0.1 mL, 0.62 mmol) was utilised in the place of  $\alpha$ -pinene.

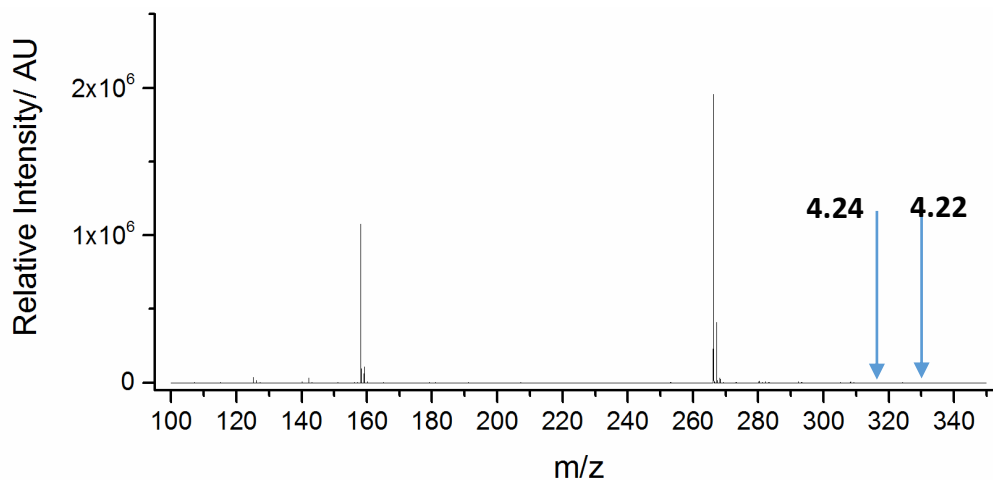


Figure 334: Overall MS from trapping of radicals from limonene

### 9.3.10. Trapping Radicals from the Ozonolysis of $\beta$ -pinene

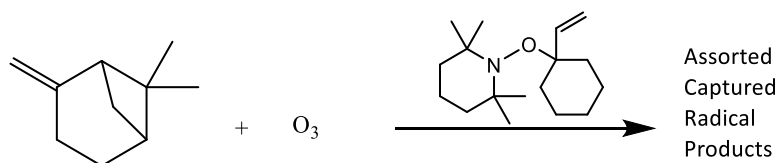


Figure 335: Capture of radical products from  $\beta$ -pinene, using **2.09**

Reaction was conducted in the same manner as the general ozonolysis quartz tube procedure above.  $\beta$ -pinene (0.1 mL, 0.64 mmol) was utilised in the place of  $\alpha$ -pinene.

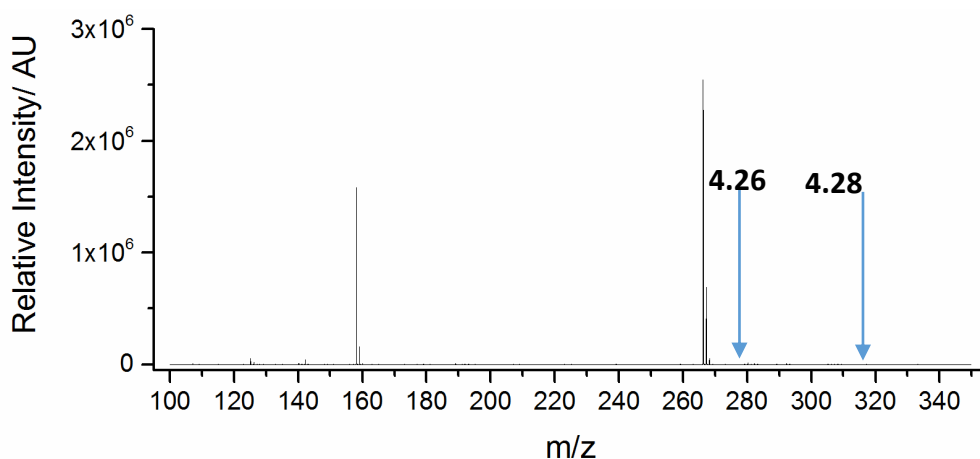


Figure 336: Overall MS from trapping products from  $\beta$ -pinene

### 9.3.11. Trapping Radicals From the Ozonolysis of Tetramethylethene

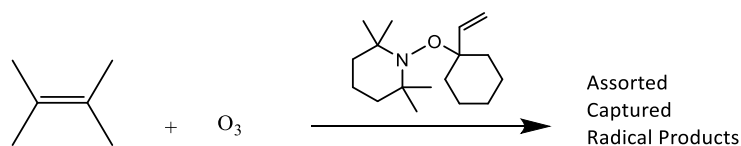


Figure 337: Capture of Radical Products from TME, using **2.09**

Reaction was conducted in the same manner as the general ozonolysis quartz tube procedure above. TME (0.1 mL, 0.84 mmol) was utilised in the place of  $\alpha$ -pinene.

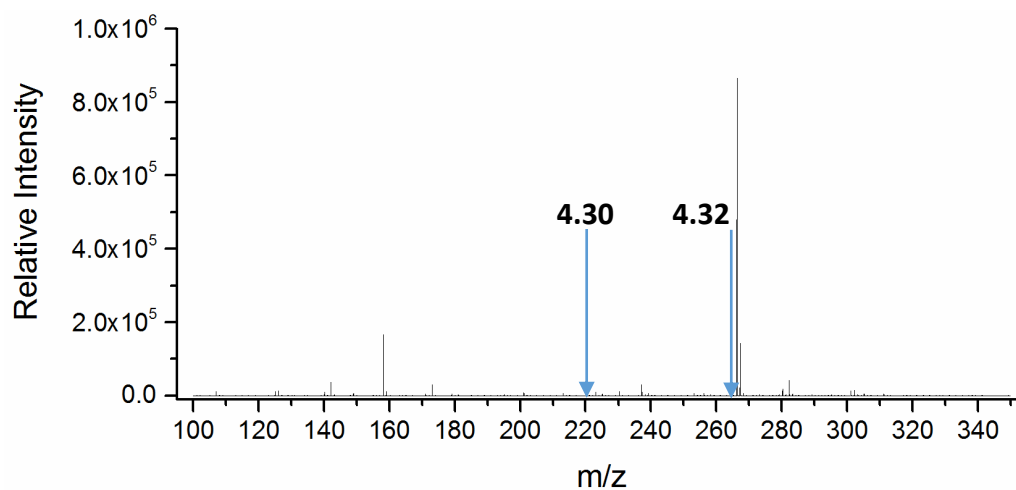


Figure 338: MS showing products captured from TME

## 9.4. Experimental details for Chapter 5

### 9.4.01. Optimisation of Sample Support

As a representative sample loading procedure, **2.09** (20 mg, 0.075 mmol) was dissolved in DCM (2 mL) and added to the sample support. Solvent was then removed by rotary evaporation. The doped support was then loaded into a quartz sampling tube. After the 90 minute trapping experiment the sample was removed, and extracted by washing with DCM (2 mL), with the products of the reaction then analysed by mass spectrometry.

Signals are compared between the samples by evaluation of the signal corresponding to the HO<sub>2</sub> adduct, **4.11**, an easily visible signal from these experiments.

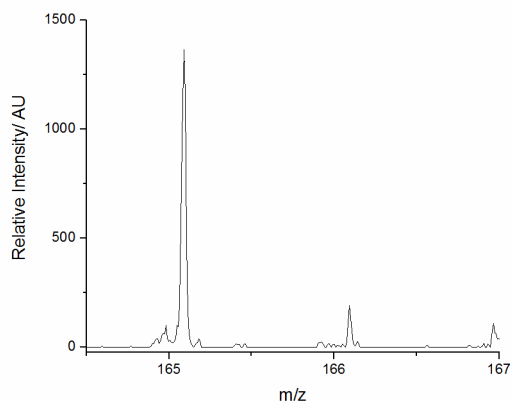


Figure 339: Signal for **4.11** from radical trapping

During the optimisation of sample support, mass of trap and sample support mass, experiments are conducted as shown in Table 3.

Mass of trap/ mg	Support	Support Mass/ mg
20	Glass wool	100
20	Glass Beads	100
20	C <sub>18</sub> Silica	100
0.05	C <sub>18</sub> Silica	100
0.9	C <sub>18</sub> Silica	100
4	C <sub>18</sub> Silica	100
4	C <sub>18</sub> Silica	200
4	C <sub>18</sub> Silica	40
4	C <sub>18</sub> Silica	12

Table 3: Experiments conducted during optimisation studies

#### 9.4.02. Optimisation of Sample Packing

Reactions were conducted according to the previously described general procedure. In each case, **2.09** (4 mg) was deposited on octadecyl silica (20 mg). Experiments with 'tapped' packing have the tube gently tapped to flatten out the **2.09** doped silica on top of

a glass wool support. Experiments with 'sandwich' packing have the **2.09** doped silica held between two layers of glass wool. Experiments with 'squashed' packing have the **2.09** doped silica squashed down on top of a layer of glass wool.

#### **9.4.03. Signal Variation with Sample Depth**

Reactions were conducted according to the previously described general procedure. However, the sample support here consisted of a 15 cm deep layer of **2.09** doped silica placed inside the quartz tube. After the experiment, samples are extracted from depths of 0.5, 2, 5, 8, 11 and 14 cm, which are subsequently analysed by mass spectrometry following extraction by DCM washing.

#### **9.4.04. Optimisation of Sampling Time**

Reactions were conducted according to the previously described general procedure. **2.09** (4 mg) was used with an octadecyl silica support (20 mg). Exposure times trialled: 90, 60, 30, 18 and 4 minutes, as well as shorter exposures of 120, 60, 45, 30 and 20 seconds.

#### **9.4.05. Representative Procedure for Trapping Radicals from a Low Temperature Plasma**

**2.09** (5 mg, 0.019 mmol) was dissolved in DCM (0.1 mL) and added to C<sub>18</sub> functionalised silica (20 mg). Solvent was removed by rotary evaporation to leave **2.09** deposited on the silica. The sample was positioned onto a glass wool bung within a sampling tube, and positioned with the sample 2 cm from the lower electrode, and 1 cm from the nozzle. Plasma was created using a gas flow of 2 L min<sup>-1</sup> helium, 20 kV and a frequency of 24.8 Hz, with a return current of 7 mA. Distance between electrodes was 2 cm. For experiments with air, 0.5 % air flow was added to the system prior to plasma generation. For experiments with oxygen, 10 mL min<sup>-1</sup> of oxygen was added prior to the plasma generation. For experiments with water, the helium flow was saturated by passing through a H<sub>2</sub>O bubbler. After the experiment, the sample was removed and stored in a freezer until analysis in the same manner as previous samples. An overall MS for an

experiment with air and water admixtures is given in Figure 340. Assorted experimental conditions are given in Table 4.

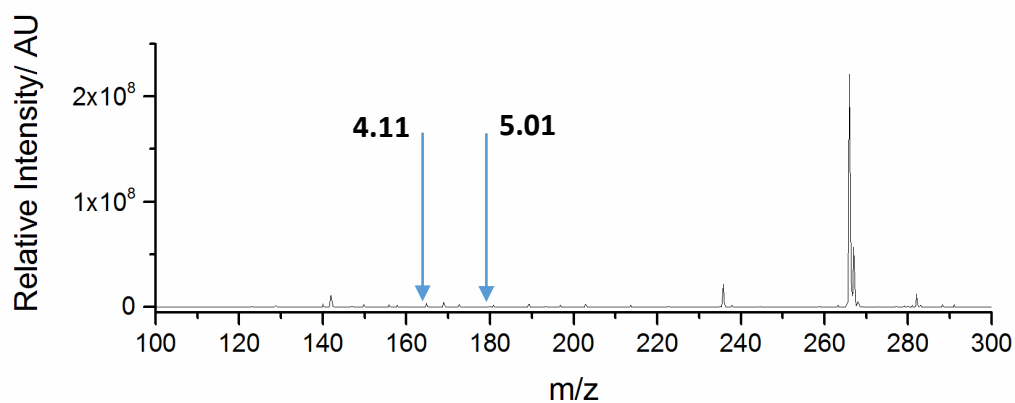


Figure 340: MS from exposure of **2.09** to plasma (with air and water)

Experiment	Duration/ min	Additives to Gas Flow	Trap
1	10	0.5 % air	<b>2.09</b>
2	5	0.5 % air	<b>2.09</b>
3	2	0.5 % air	<b>2.09</b>
4	0.5	0.5 % air	<b>2.09</b>
5	5	0.5 % air	<b>2.11</b>
6	5	0.5 % air, water saturation	<b>2.09</b>
7	10	0.5 % O <sub>2</sub> , water saturation	<b>2.09</b>
8	5	0.5 % O <sub>2</sub> , water saturation	<b>2.09</b>
9	2	0.5 % O <sub>2</sub> , water saturation	<b>2.09</b>
10	0.5	0.5 % O <sub>2</sub> , water saturation	<b>2.09</b>
11	5	0.5 % O <sub>2</sub> , water saturation	<b>2.11</b>
12	5	0.5 % O <sub>2</sub> , water saturation	<b>2.16</b>

Table 4: Variations for plasma experiments

For experiments with **2.11**, 5.4 mg, 0.0021 mmol, was used.

For experiments with **2.16**, 2.0 mg, 0.00059 mmol, was used

#### 9.4.06. Trapping of NO

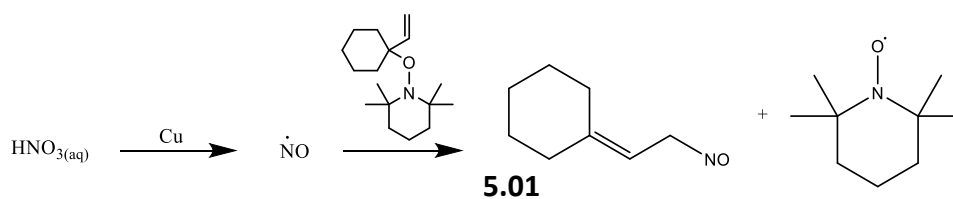
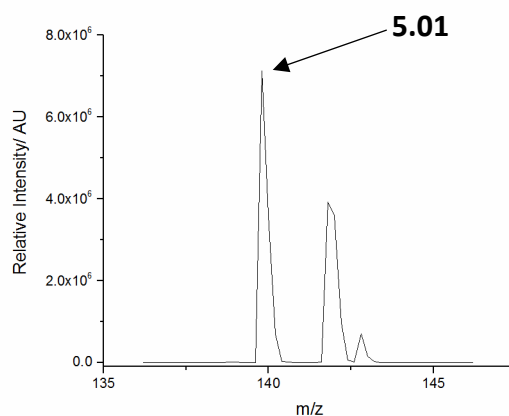


Figure 341: Capture of the NO radical

**2.09** (5 mg, 0.019 mmol) was dissolved in DCM and added to octadecyl-functionalised silica gel (30 mg), and solvent removed by rotary evaporation. The doped silica was then loaded into a sampling tube, bunged with glass wool. HNO<sub>3</sub> (70 %, 1 mL) was added to H<sub>2</sub>O (19 mL). Copper turnings (50 mg, 0.79 mmol) were added to the solution, initiating effervescence. Air was blown over this solution and through the radical trap containing tube. After 15 minutes the trapping molecule was removed from silica by a DCM wash, solvent removed by rotary evaporation, and product analysed by mass spectrometry.



#### 9.4.07. Attempted Trapping of NO<sub>2</sub>

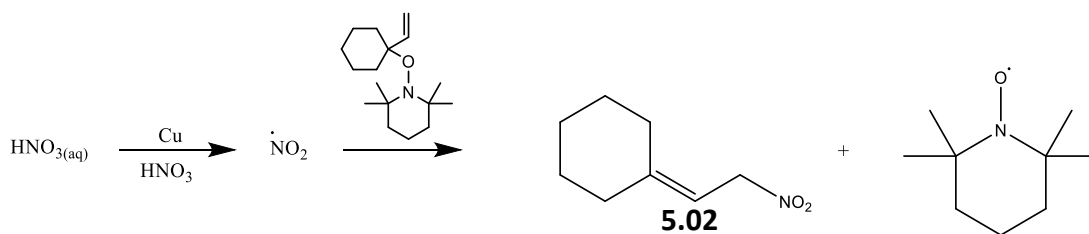


Figure 342: Target reaction for the capture of NO<sub>2</sub>

**2.09** (5 mg, 0.019 mmol) was dissolved in DCM and added to octadecyl-functionalised silica gel (30 mg), and solvent removed by rotary evaporation. The doped silica was then loaded into a sampling tube, bunged with glass wool. HNO<sub>3</sub> (70 %, 1 mL) was added to H<sub>2</sub>O (19 mL). Copper turnings (50 mg, 0.79 mmol) were added to the solution, initiating effervescence. Gradual addition of further HNO<sub>3</sub> (70 %, 10 mL) induced the formation of a brown gas. Air was blown over this solution and through the radical trap containing tube. After 15 minutes the trapping molecule was removed from silica by a DCM wash, solvent

removed by rotary evaporation, and product analysed by mass spectrometry. Target species **5.02** was not observed.

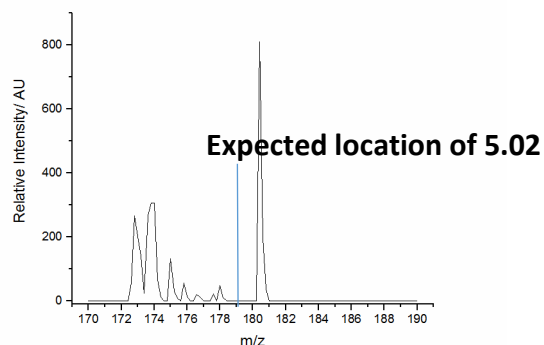


Figure 343: Lack of signal for **5.02**

## 9.5. Experimental Details for Chapter 6

### 9.5.01. Generation and Trapping of Radicals from dodecane + $\cdot\text{OH}$ reaction

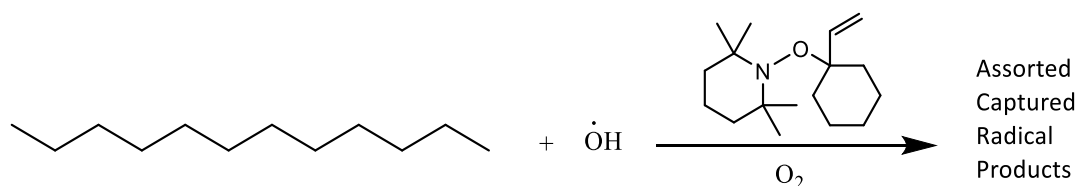


Figure 344: Capture of radical products from dodecane's reaction with  $\cdot\text{OH}$ , using **2.09**

As a representative procedure, **2.09** (5 mg, 0.019 mmol) was dissolved in DCM (1 mL) and added to octadecyl-functionalised silica gel (20 mg), with solvent then removed by rotary evaporation. The doped silica was then loaded into a quartz tube, supported on a layer of glass wool. Standard air was sequentially passed through a dreschel flask containing  $\text{H}_2\text{O}_2$  (30 %) and a round bottom flask containing dodecane (0.1 mL, 0.4 mmol) at a flow rate of ( $3 \text{ L min}^{-1}$ ). This was then fed into the quartz tube containing **2.09** doped silica. A UV lamp (Hg Arc, 100 W, 405 nm), with an Oriel 68805 power supply was used to form  $\cdot\text{OH}$  in the tube, with the point of irradiation 10 cm from the sampling site. After 90 min the doped silica was removed and products extracted by washing with DCM (2 x 2 mL) before analysis by mass spectrometry. No  $\text{RO}_2$  radical adducts were detected.

### 9.5.02. Generation and Trapping of Radicals from decane + $\cdot\text{OH}$ reaction

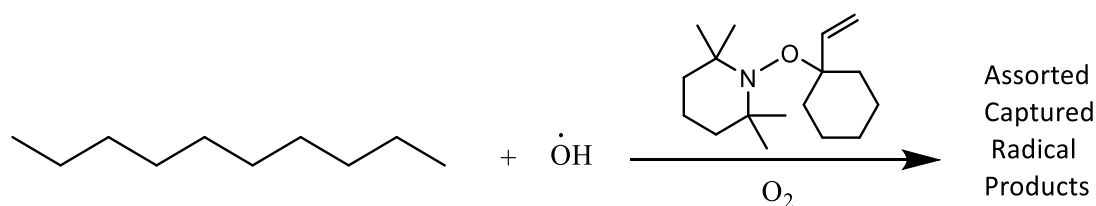


Figure 345: Capture of radical products from decane's reaction with  $\cdot\text{OH}$ , using **2.09**

Reaction was conducted according the above general procedure for alkane +  $\cdot\text{OH}$  reactions.

Decane (0.1 mL, 0.51 mmol) was used as the alkane for these experiments.

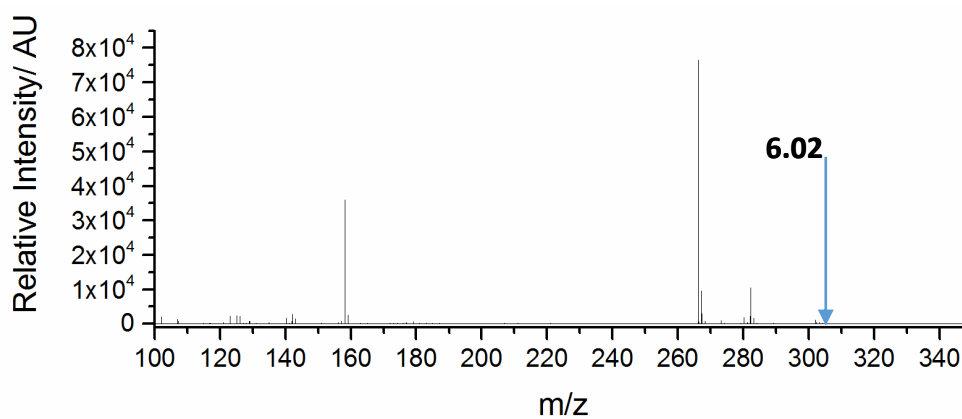


Figure 346: Overall MS for decane reaction

### 9.5.03. Generation and Trapping of Radicals from Nonane + $\cdot\text{OH}$ reaction

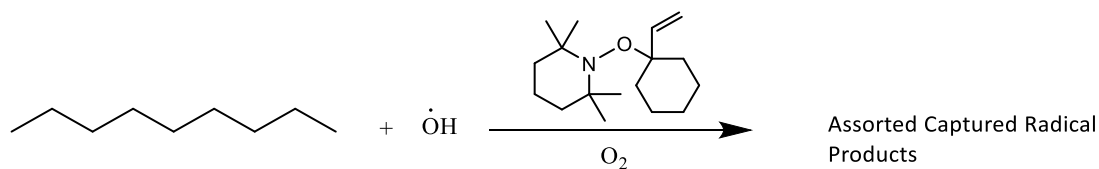


Figure 347: Capture of radical products from nonane's reaction with  $\cdot\text{OH}$ , using **2.09**

Reaction was conducted according the above general procedure for alkane +  $\cdot\text{OH}$  reactions. Nonane (0.1 mL, 0.56 mmol) was used as the alkane for these experiments.

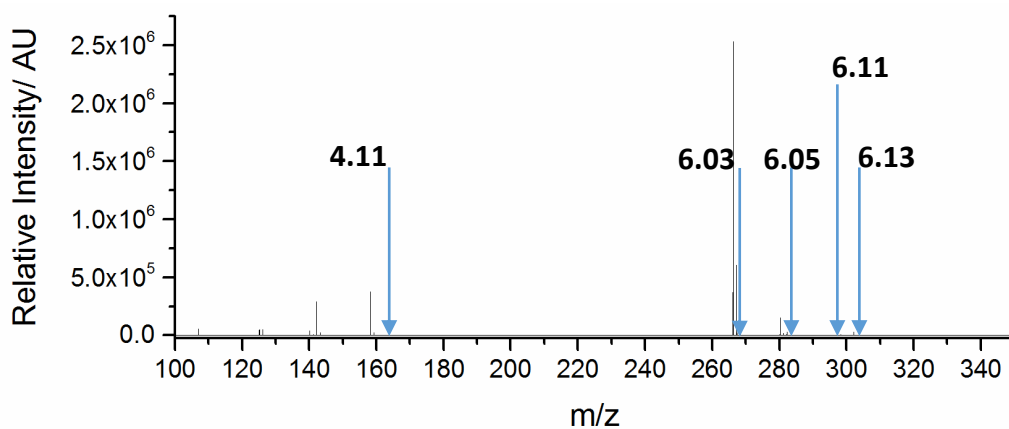


Figure 348: Overall MS for nonane experiments with **2.09**

#### 9.5.04. Application of **2.13** to the nonane + $\cdot\text{OH}$ reaction

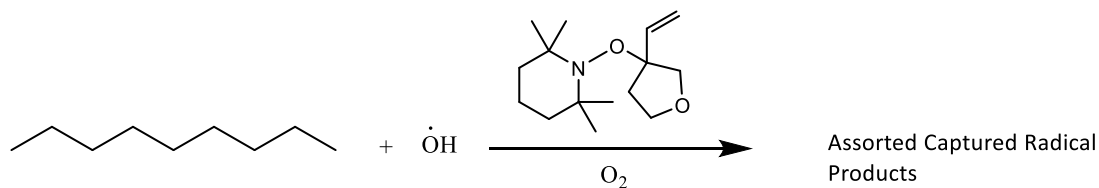


Figure 349: Capture of radical products from nonane's reaction with  $\cdot\text{OH}$ , using **2.13**

Reaction was conducted according the above general procedure for alkane +  $\cdot\text{OH}$  reactions. **2.13** (5 mg, 0.019 mmol) was used as the trapping material. Nonane (0.1 mL, 0.56 mmol) was used as the alkane for these experiments.

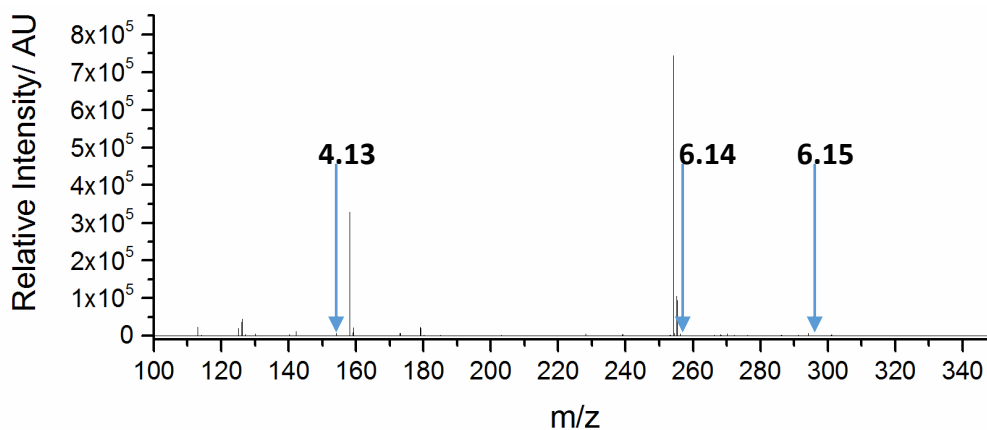


Figure 350: Overall MS for nonane experiments with **2.13**

#### 9.5.05. Modelling the Nonane + $\cdot\text{OH}$ reaction with Kintecus

The kinetics of this reaction were modelled using Kintecus.<sup>323</sup> The chemical and mechanistic information was taken from the Master Chemical Mechanism, MCM v3.3.<sup>229,230</sup> The 'nonane' subset was extracted, consisting of 1107 reactions and 354 organic species. General model parameters included a starting Integration Time: 0.0000001 s, maximum integration time: 0.004 s, Ea units: Kelvin, concentration units: molecules  $\text{cm}^{-3}$ , temperature 298 K, simulation length: 0.4 s, accuracy: 0.00000001. Initial concentrations of all species were set to 0, with the exception of nonane ( $4.8 \times 10^{14}$  molecules  $\text{cm}^{-3}$ ), Hydroxyl radicals ( $8.6 \times 10^{11}$  molecules  $\text{cm}^{-3}$ ) and  $\text{H}_2\text{O}_2$  ( $8.6 \times 10^{13}$  molecules  $\text{cm}^{-3}$ ). Wall loss rates of 20 were used for all radical species.

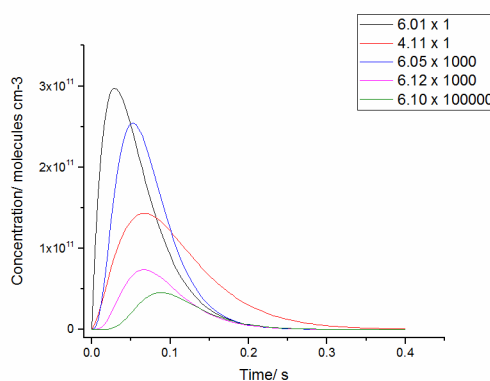


Figure 351: Model for investigated radical species formed in nonane +  $\cdot\text{OH}$  reaction.

### 9.5.06. Testing variations in the model

The impact on the model of variation in the rate of  $\text{RO}_2 + \text{RO}_2$  reactions was also modelled. These experiments were conducted at initial rates as given in the MCM, and subsequently varied as shown below, using the modelled signal for **6.05**.<sup>229,230</sup>

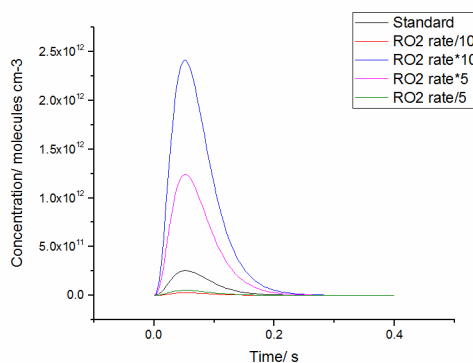


Figure 352: Variation in signal on changing  $\text{RO}_2$  reaction rate

Impact of changing the  $[\text{OH}]$  was calculated by running the model with  $[\text{OH}]$  at  $8.6 \times 10^{10}$  molecules  $\text{cm}^{-3}$ ,  $8.6 \times 10^{11}$  molecules  $\text{cm}^{-3}$  and  $8.6 \times 10^{12}$  molecules  $\text{cm}^{-3}$ . This was examined using the modelled signal for **6.05**.

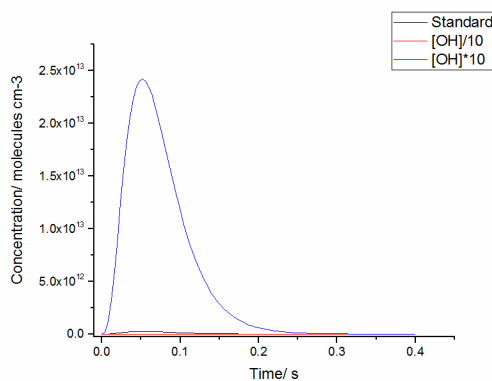


Figure 353: Variation in signal on changing  $[\text{OH}]$

The impact on the model of incorporating wall loss rates was calculated by running the model with a series of different wall losses. After an initial experiment where wall loss = 0, the model is also run with rates of 5, 10, 20 and  $40 \text{ s}^{-1}$ . This was again examined using the modelled signal for **6.05**.

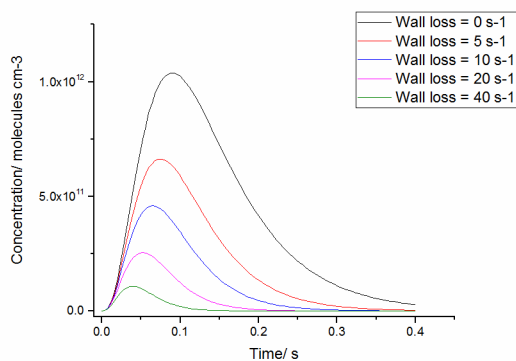


Figure 354: Variation in signal on changing wall loss rates

### 9.5.07. Experimental Kinetic Information for Nonane + $\cdot\text{OH}$ reaction

Experiments were conducted for nonane +  $\cdot\text{OH}$  as has been described above. Distances between sampling site and the point of irradiation were varied, in order to modify the total residence time prior to the detection site. The relationship between this and total reaction time is given in Table 5.

Distance/ cm	Residence Time/ s
3	0.017
4	0.023
5	0.029
6	0.035
8	0.047
10	0.059
12	0.070
15	0.088
17	0.100
20	0.118
25	0.147
30	0.177
35	0.206
50	0.295
60	0.354

Table 5: Table showing distances between point of irradiation and trapping site used for experimental nonane +  $\cdot\text{OH}$  kinetic measurements

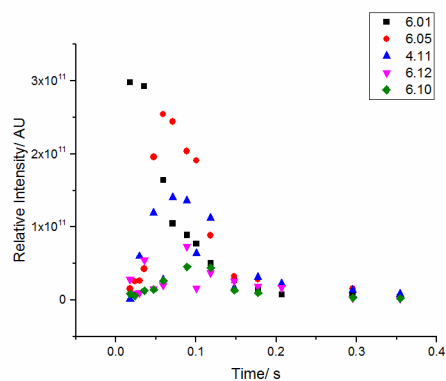


Figure 355: Experimental kinetic information for Nonane +  $\cdot\text{OH}$  reaction.

#### 9.5.08. Calibration of Methane + $\cdot\text{OH}$ reaction for the $\text{MeO}_2$ radical

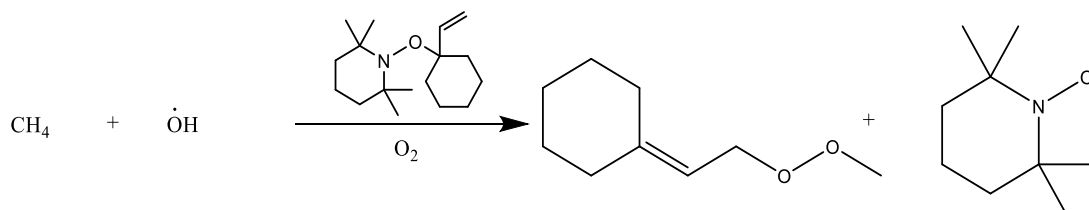


Figure 356: Trapping the  $\text{MeO}_2$  radical to form **6.17**

**2.09** (5 mg, 0.019 mmol) was dissolved in DCM (1 mL) and added to octadecyl-functionalised silica gel (20 mg). Solvent was removed by rotary evaporation, and the sample frozen overnight prior to being positioned on a layer of glass wool within a sampling tube. Air (20.5 %  $\text{O}_2$ ) was blown through the system, being bubbled through a solution of  $\text{H}_2\text{O}$  at  $8 \text{ L min}^{-1}$ , regulated by an MFC (Brooks). Of this flow,  $1.5 \text{ L min}^{-1}$  was diverted to a hygrometer (CR4 Buck Research Instruments). A flow of methane was added at  $0.15 \text{ L min}^{-1}$ , regulated by an MFC (Brooks). Methane flow was tested with FAGE to ensure 100 % conversion of  $\text{OH}$  to  $\text{RO}_x$ : increasing methane concentration does not result in increased  $\cdot\text{OH}$  signal. The combined mixture was irradiated by a preheated Hg Pen-Ray lamp (184.9 nm) incorporated into the system. Lamp current can be varied from 0-21 mA. Calibration between lamp and  $[\text{HO}_x]$  for this system is shown in Figure 358. Distance between sampling site and irradiation is 13 cm, resulting in a residence time of  $4.2 \times 10^{-2}$  s. Calibration experiments were conducted for 15 minutes. Sample was then removed and frozen prior to analysis by mass spectroscopy. Diluted samples are generated by two methanol dilutions of a sample of  $1.6 \times 10^{10} \text{ molecules cm}^{-3}$  by a factor of 100.

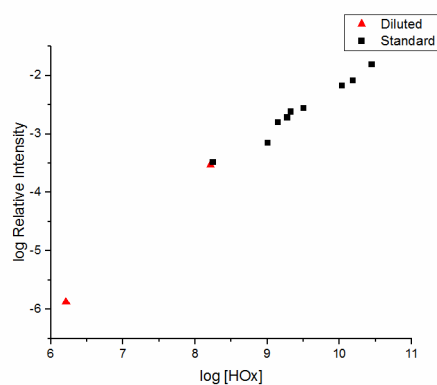


Figure 357: Calibration plot for **6.17**

Calibration for current to [HO<sub>x</sub>]

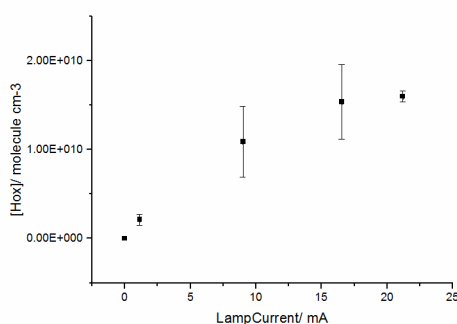


Figure 358: Calibration between lamp current and [HO<sub>x</sub>]

### 9.5.09. Calibration of Nonane + ·OH reaction for the nonane-O<sub>2</sub> radical

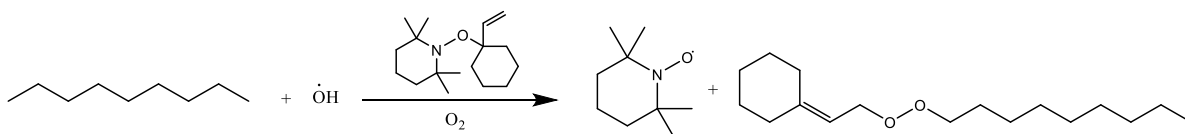


Figure 359: Trapping the nonane peroxy radical to form **6.03**

**2.09** (5 mg, 0.019 mmol) was dissolved in DCM (1 mL) and added to octadecyl-functionalised silica gel (20 mg). Solvent was removed by rotary evaporation, and the sample frozen prior to being positioned on a layer of glass wool within a sampling tube. Air (20.5 % O<sub>2</sub>) was blown through the system, being bubbled through a solution of H<sub>2</sub>O at

8 L min<sup>-1</sup>, regulated by an MFC (Brooks). Of this flow, 1.5 L min<sup>-1</sup> was diverted to a hygrometer (CR4 Buck Research Instrument). A flow of nonane vapour was achieved by diverting 2 L min<sup>-1</sup> of air flow from the water bubbler and instead bubbling through a solution of nonane (10 mL). The combined mixture was irradiated by a preheated Hg Pen-Ray lamp (184.9 nm) incorporated into the system. Lamp current can be varied from 0-21 mA. Calibration between lamp current and [HO<sub>x</sub>] for this system is shown in Figure 361. Distance between sampling site and irradiation was 13 cm, resulting in a residence time of 4.2 × 10<sup>-2</sup> s. Calibration experiments were conducted for 15 minutes. Sample was then removed and frozen prior to analysis by mass spectroscopy. Diluted samples were conducted with methanol, and generated at concentrations of ca. 1.7 × 10<sup>5</sup>, 3.4 × 10<sup>6</sup> and 8.0 × 10<sup>6</sup> molecules cm<sup>-3</sup>.

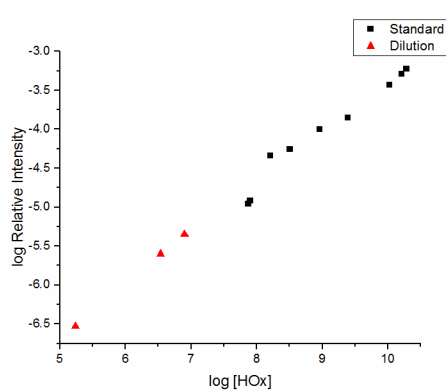


Figure 360: Calibration plot for 6.03

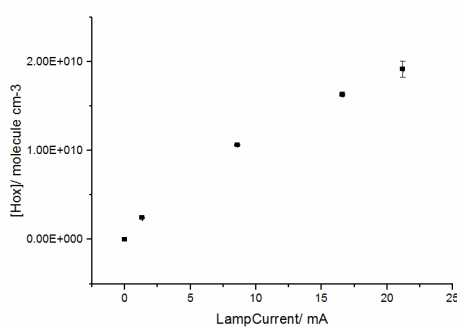


Figure 361: Relationship between current and [HO<sub>x</sub>]

## 9.6. Experimental Details for Chapter 7

### 9.6.01. Indoor Air Experiments

Indoor Air experiments are conducted as given in Table 6.

Experiment	Site	Time / hr	[O <sub>3</sub> ]/ ppb	[limonene]/ ppb	[α-pinene]/ ppb	Other perturbations
1	O	2	3	Ambient	Ambient	OW
2	O	16	4	Ambient	Ambient	Night, CW
3	O	2	17	Ambient	Ambient	OW
4	O	2	19	50	Ambient	OW
5	O	2	24	50	Ambient	CW
6	O	2	28	Ambient	Ambient	SB, CW
7	M	2	7	Ambient	Ambient	
8	M	2	20	Ambient	Ambient	
9	M	2	15	30	60	
10	M	4 x 0.5	13	30	60	
11	M	2	15	Ambient	Ambient	SB
12	M	2	14	Ambient	Ambient	NSB
13	M	2 x 2	17	Ambient	Ambient	Airfreshener

Table 6: Experiments conducted on indoor air. O = office, M = meeting room, OW = Open Window, CW = Closed Window, SB = Scented Bleach, NSB = Non Scented Bleach

### 9.6.02. Indoor Air Trapping: Small Office

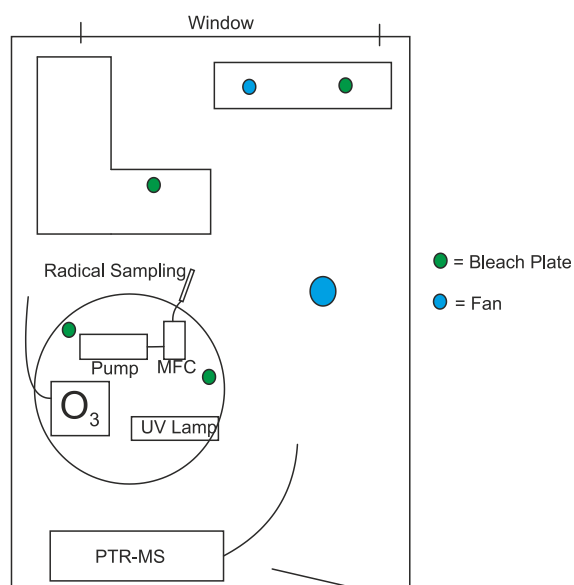


Figure 362: Room layout for office sampling, showing positions of O<sub>3</sub> monitor, MS, and radical trapping equipment

**2.09** (10 mg, 0.038 mmol) was dissolved in DCM, added to octadecyl-functionalised silica gel (20 mg), and solvent removed by rotary evaporation. The doped silica was then loaded into a sampling tube bunged with glass wool. Air to be sampled was pulled through this tube at a flow rate of 4.9 L min<sup>-1</sup> for the experimental duration. Sample can then be extracted by washing with DCM, with the products of the reaction then analysed by mass spectrometry. Temperature and ozone levels were monitored throughout the experiment, with the data for these given below.

### Indoor Air 25/01/17 to 27/01/17

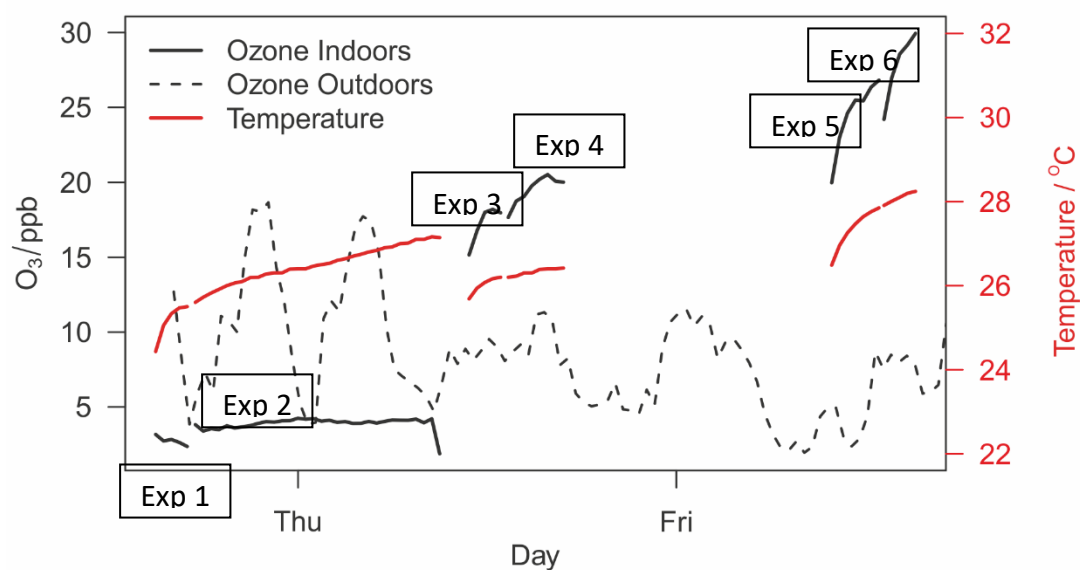


Figure 363: Temperature and O<sub>3</sub> Variation during office experiments

Limonene was introduced into the room by release of canisters containing an air-limonene mixture, set to create a 50 ppb limonene concentration within the room being studied. Bleach was introduced into the room by distribution of 4 plates (5 mL per plate), positioned around the room. Room windows were also varied between open and closed. O<sub>3</sub> was generated using a UV lamp (183 nm). The majority of captured radicals are shown in **Chapter 7**, however those that are not are shown here. Detection of captured MeO<sub>2</sub> radical, **6.17**.

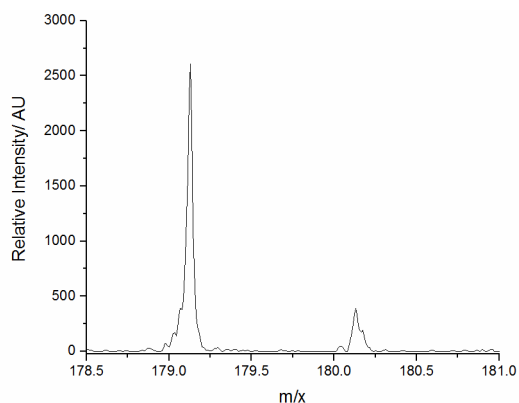


Figure 364: **6.17** from indoor air experiments

### 9.6.03. Modelling the Limonene Ozonolysis system

The kinetics of this reaction are modelled using Kintecus.<sup>323</sup> The chemical and mechanistic information was taken from the Master Chemical Mechanism, MCM v3.3.<sup>229,230</sup> The limonene subset was extracted, consisting of 2141 reactions and 701 species. Starting Integration Time: 0.000001 s, maximum integration time: 10 s, Ea units: Kcal, concentration units: molecules cm<sup>-3</sup>, temperature 298 K, simulation length: 2 hr, accuracy: 0.00000001. Initial concentrations of all species are set to 0, with the exception of limonene (up to  $1.25 \times 10^{11}$  molecules cm<sup>-3</sup>) and ozone (up to a constant concentration of  $6.25 \times 10^{11}$  molecules cm<sup>-3</sup>).

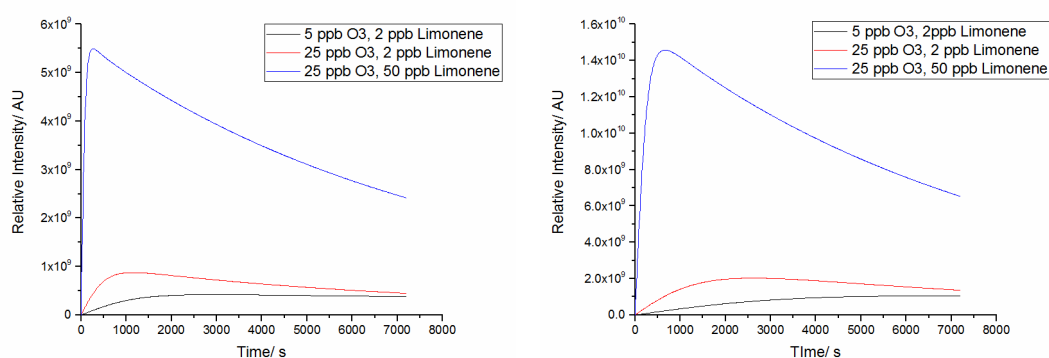


Figure 365: Modelled data for office experiments

### 9.6.04. Indoor Air Trapping: Meeting room

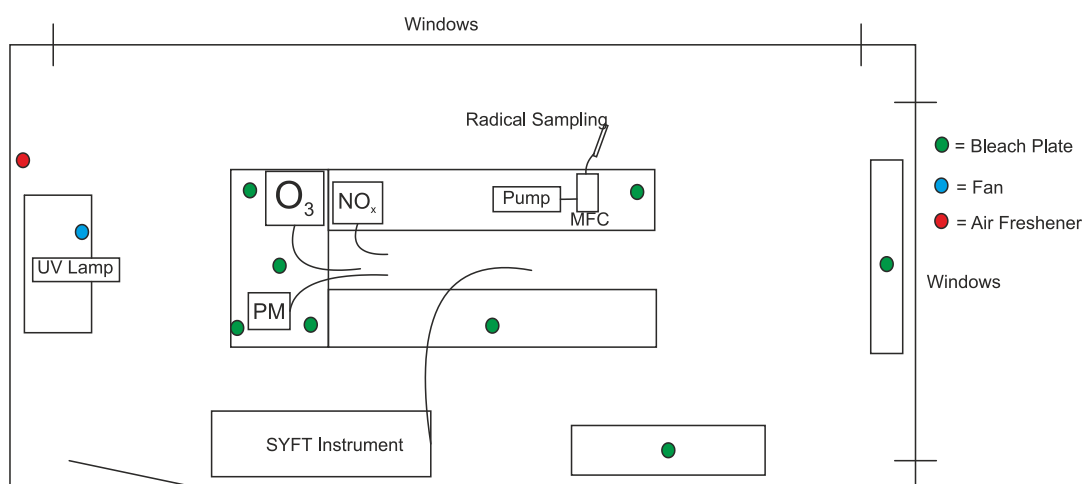


Figure 366: Meeting room layout

**2.09** (10 mg, 0.038 mmol) was dissolved in DCM, added to octadecyl-functionalised silica gel (20 mg), and solvent removed by rotary evaporation. The doped silica was then loaded into a sampling tube bunged with glass wool. Air to be sampled was pulled through this tube at a flow rate of 4.9 L min<sup>-1</sup> for the duration of the experiment. Sample can then be extracted by washing with DCM, with the products of the reaction then analysed by mass spectrometry. Temperature, NO, NO<sub>2</sub> and ozone levels were monitored throughout the experiment, with the data for these given below.

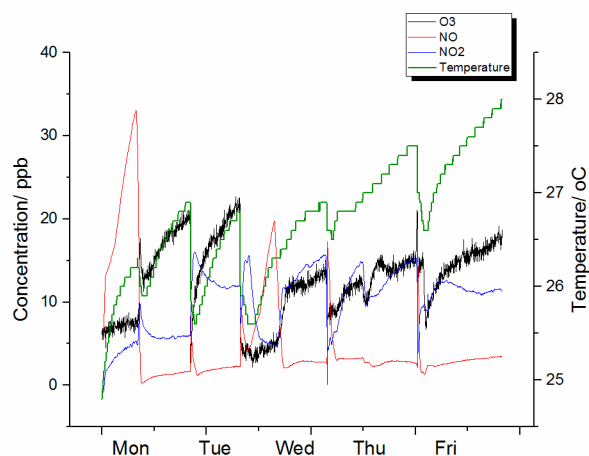


Figure 367: Conditions for Meeting room experiments

In several experiments,  $\alpha$ -pinene and limonene were introduced into the room by release of canisters containing an air-  $\alpha$ -pinene-limonene mixture, set to create a 60 and 30 ppb concentration of each terpene respectively within the room being studied. Bleach was introduced into the room by distribution of 8 plates (5 mL per plate), positioned around the room. Room windows were kept closed for the duration of the experiments. Air freshener (Airwick), was introduced into the room in a distribution system as sold, on a medium setting. Ozone was generated using a UV lamp (183 nm).

Canister Data from Airwick experiments is given in Figure 368.

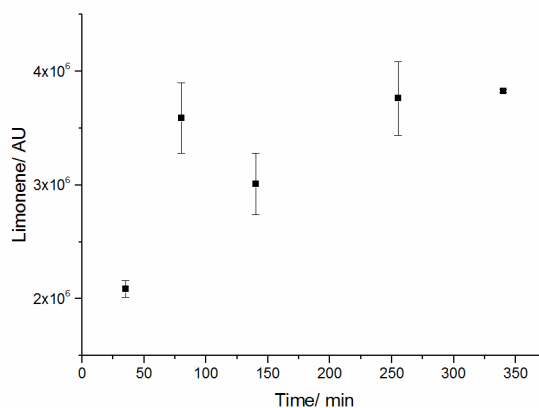


Figure 368: Canister data for Air Freshener experiments

#### 9.6.04. Modelling the $\alpha$ -pinene and limonene ozonolysis system

The kinetics of this reaction were modelled using Kintecus.<sup>323</sup> The chemical and mechanistic information was taken from the Master Chemical Mechanism, MCM v3.3.<sup>229,230</sup> The limonene and  $\alpha$ -pinene subsets were extracted, consisting of 2804 reactions and 925 species. Starting Integration Time: 0.000001 s, maximum integration time: 10 s, Ea units: Kcal, concentration units: molecules cm<sup>-3</sup>, temperature 298 K, simulation length: 2 hr, accuracy: 0.00000001. Initial concentrations of all species were set to 0, with the exception of  $\alpha$ -pinene ( $1.5 \times 10^{12}$  molecules cm<sup>-3</sup>), limonene ( $7.5 \times 10^{11}$  molecules cm<sup>-3</sup>) and ozone (a constant concentration of  $2.5 \times 10^{11}$  molecules cm<sup>-3</sup>).

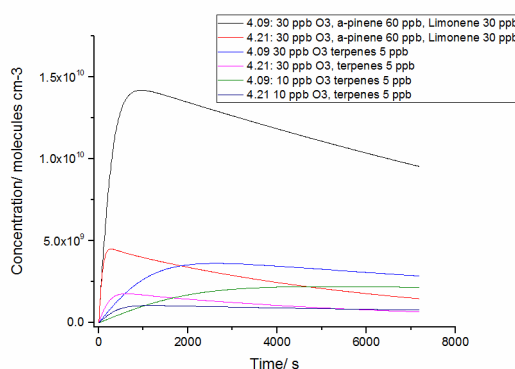


Figure 369: Model variation in meeting room experiments

### 9.6.05. Outdoor Air Sampling

**2.09** (10 mg, 0.038 mmol) was dissolved in DCM, added to octadecyl-functionalised silica gel (20 mg), and solvent removed by rotary evaporation. The doped silica was then loaded into a sampling tube bunged with glass wool. The sampling tube was positioned outside, either at ground level or on a rooftop. Air to be sampled was pulled through this tube at a flow rate of 4.9 L min<sup>-1</sup> for the duration of the experiment. Sample could then be extracted by washing with DCM, with the products of the reaction then analysed by mass spectrometry. Samples conducted at ground level were taken behind a building, in close proximity to a number of trees and leaf litter on the ground. Samples at roof level were conducted on the roof of the same building, which is two storeys high. Experiments are conducted as in Table 7.

Experiment	Date	Time Range	Temperature/ K	Humidity/ %	O <sub>3</sub> / ppb
1	20/02/2017	13:30-16:40	284.4	80.2	20
2	22/02/2017	15:00-19:10	282	73.8	40
3	09/03/2017	14:30-16:20	282.1	64.3	40
4 (rooftop)	15/03/2017	11:30-15:30	283.5	66.1	35

Table 7: Outdoor Air Experiments

## List of Abbreviations:

$\mu\text{s}$  = microsecond

TEMPO = 2,2,6,6-Tetramethylpiperidine 1-oxyl

<sup>t</sup>Bu = tertiary butyl

EPR = Electron Paramagnetic Resonance

$m_s$  = electron spin quantum number

NMR = Nuclear Magnetic Resonance

DMPO = 5,5-dimethyl-pyrroline-N-oxide

DEPMPO = 5-diethoxyphosphoryl-5-methyl-1-pyrroline-N-oxide

PBN = N-tert-butyl- $\alpha$ -phenylnitron

POBN =  $\alpha$ -(4-pyridyl N-oxide)-N-tert-butylnitron

nM = nanomolar

HPLC = High Pressure Liquid Chromatography

$\cdot\text{OH}$  = Hydroxyl radical

$\text{HO}_2\cdot$  = Hydroperoxyl radical

cm = Centimeter

s = second

NO<sub>x</sub> = Nitrogen Oxides

HO<sub>x</sub> = Hydroxyl/hydroperoxyl radical

SOA = Secondary Organic Aerosol

VOC = Volatile Organic Compound

ROS = Reactive Oxygen Species

LIF = Laser Induced Fluorescence

FAGE = Fluorescence Assay by Gaseous Expansion

nm = nanometer

RO<sub>2</sub> = Organic peroxy radical

pptv = Parts per trillion volume

CIMS = Chemical Ionisation Mass Spectrometry

PER-CIMS = Peroxy Radical CIMS

PERCA = Peroxy Radical Chemical Amplification

DOAS = Differential Optical Absorption Spectroscopy

km = Kilometer

MAX-DOAS = Multi Axis DOAS

MI-EPR = Matrix Isolation EPR

MS = Mass Spectroscopy

LG = Leaving Group

RSA = Retrosynthetic Analysis

kJ = kilojoule

mol = moles

MSMS = Mass Spectroscopy-Mass Spectroscopy

BHT = Butylated hydroxytoluene

ppm = parts per million

PCC = Pyridinium Chlorochromate

DMP = Dess-Martin Periodinane

DMSO = Dimethylsulfoxide

SET = Single Electron Transfer

DEPT = Distortionless Enhancement by Polarisation Transfer

HMBC = Heteronuclear Multiple Bond Correlation

DMF = Dimethylformamide

TLC = Thin Layer Chromatography

BDE = Bond Dissociation Enthalpy

PGSE = Polar Ground State Effect

Oxo-TEMPO = 4-oxo-2,2,6,6-tetramethyl-1-piperidinyloxy free radical

DBNO = di-tert-butyl nitroxide

TMIO = 1,1,3,3-tetramethylisoindolin-2-yloxy

COSY = Homonuclear Correlation NMR Spectroscopy

UPCC-QTOF-MS = Ultra Performance Convergence Chromatography – Quadrupole Time of Flight Mass Spectroscopy

AIBN = Azobisisobutyronitrile

Da = Daltons

LCMSMS = Liquid Chromatography MSMS

GC-MS = Gas Chromatography MS

MCM = Master Chemical Mechanism

UV = Ultraviolet

DCM = Dichloromethane

mg = milligram

mmol = millimole

TME = Tetramethylethene

kV = kilovolt

mA = milliamp

kHz = kilohertz

PAN = Peroxyacetyl nitrate

PFHBA = O-(2,3,4,5,6-pentafluorobenzyl) hydroxyl amine

BSTFA = N,O-bis(trimethylsilyl)-trifluoroacetamine

Pa = Pascal

IUPAC = International Union of Pure and Applied Chemistry

EUPHORE = European Photoreactor

WHO = World Health Organisation

PM = Particulate Matter

SMPS = Scanning Mobility Particle Sizer

PTR-MS = Proton Transfer MS

ppb = Parts per billion

SIFT = Selected Ion Flow Tube

mL = millilitre

SATP = Standard Ambient Temperature and Pressure

XRF = X-Ray Fluorescence

## **Key Structures Discussed Throughout this Thesis**

## References

- 1 E. G. Rozantsev and D. V. Loshadkin, *Des. Monomers Polym.*, 2001, **4**, 281–300.
- 2 E. Bothe, M. N. Schuchmann, D. Schulte-Frohlinde and C. Sonntag, *Photochem. Photobiol.*, 1978, **28**, 639–644.
- 3 M. Gomberg, *J. Am. Chem. Soc.*, 1900, **22**, 757–771.
- 4 G. M. Coppinger, *J. Am. Chem. Soc.*, 1957, **79**, 501–502.
- 5 D. F. Church, *Anal. Chem.*, 1994, **66**, 419–427.
- 6 R. G. Prinn, *Annu. Rev. Environ. Resour.*, 2003, **28**, 29–57.
- 7 D. H. Ehhalt, *Phys. Chem. Chem. Phys.*, 1999, **1**, 5401–5408.
- 8 D. Stone, L. K. Whalley and D. E. Heard, *Chem. Soc. Rev.*, 2012, **41**, 6348–6404.
- 9 U. Platt and M. Hausmann, *Res. Chem. Intermed.*, 1994, **20**, 557–578.
- 10 C. A. Cantrell, D. H. Stedman and G. J. Wendel, *Anal. Chem.*, 1984, **56**, 1496–1502.
- 11 V. Naik, A. Voulgarakis, A. M. Fiore, L. W. Horowitz, J.-F. Lamarque, M. Lin, M. J. Prather, P. J. Young, D. Bergmann, P. J. Cameron-Smith, I. Cionni, W. J. Collins, S. B. Dalsøren, R. Doherty, V. Eyring, G. Faluvegi, G. A. Folberth, B. Josse, Y. H. Lee, I. A. MacKenzie, T. Nagashima, T. P. C. van Noije, D. A. Plummer, M. Righi, S. T. Rumbold, R. Skeie, D. T. Shindell, D. S. Stevenson, S. Strode, K. Sudo, S. Szopa and G. Zeng, *Atmos. Chem. Phys.*, 2013, **13**, 5277–5298.
- 12 F. Rohrer, K. Lu, A. Hofzumahaus, B. Bohn, T. Brauers, C.-C. Chang, H. Fuchs, R. Häsel, F. Holland, M. Hu, K. Kita, Y. Kondo, X. Li, S. Lou, A. Oebel, M. Shao, L. Zeng, T. Zhu, Y. Zhang and A. Wahner, *Nat. Geosci.*, 2014, **7**, 559–563.
- 13 C. M. Spivakovsky, J. A. Logan, S. A. Montzka, Y. J. Balkanski, M. Foreman-Fowler, D. B. A. Jones, L. W. Horowitz, A. C. Fusco, C. A. M. Brenninkmeijer, M. J. Prather, S. C. Wofsy and M. B. McElroy, *J. Geophys. Res.*, 2000, **105**, 8931–8980.
- 14 S. N. Khan and E. Miliordos, *Phys. Chem. Chem. Phys.*, 2017, **19**, 18152–18155.
- 15 D. E. Heard and M. J. Pilling, *Chem. Rev.*, 2003, **103**, 5163–5198.
- 16 Y. F. Elshorbany, R. Kurtenbach, P. Wiesen, E. Lissi, M. Rubio, G. Villena, E. Gramsch, A. R. Rickard, M. J. Pilling and J. Kleffmann, *Atmos. Chem. Phys. Discuss.*, 2009, **9**, 2257–2273.
- 17 A. R. Rickard, D. Johnson, C. D. McGill and G. Marston, *J. Phys. Chem. A*, 1999, **103**, 7656–7664.

- 18 R. Atkinson and J. Arey, *Chem. Rev.*, 2003, **103**, 4605–4638.
- 19 D. Mihelcic, D. Klemp, P. Musgen, H. W. Patz and A. Volz-Thomas, *J. Atmos. Chem.*, 1993, **16**, 313–335.
- 20 K. M. Emmerson and N. Carslaw, *Atmos. Environ.*, 2009, **43**, 3220–3226.
- 21 J. J. Orlando and G. S. Tyndall, *Chem. Soc. Rev.*, 2012, **41**, 6294–6317.
- 22 S. S. Brown and J. Stutz, *Chem. Soc. Rev.*, 2012, **41**, 6405–6447.
- 23 G. Salisbury, A. R. Rickard, P. S. Monks, A. C. Lewis, D. J. Creasey and J. D. Lee, *J. Geophys. Res.*, 2001, **106**, 12669–12687.
- 24 D. E. Shallcross, K. E. Leather, A. Bacak, P. Xiao, E. P. F. Lee, M. Ng, D. K. W. Mok, J. M. Dyke, R. Hossaini, M. P. Chipper, M. A. H. Khan and C. J. Percival, *J. Phys. Chem. A*, 2015, **119**, 4618–4632.
- 25 M. E. Jenkin, S. M. Saunders and M. J. Pilling, *Atmos. Environ.*, 1997, **31**, 81–104.
- 26 J. W. Harder, A. Fried, S. Sewell and B. Henry, *J. Geophys. Res.*, 1997, **102**, 6267–6282.
- 27 S. Friedfeld, M. Fraser, K. Ensor, S. Tribble, D. Rehle, D. Leleux and F. Tittel, *Atmos. Environ.*, 2002, **36**, 4767–4775.
- 28 R. C. McVay, X. Zhang, B. Aumont, R. Valorso, M. Camredon, Y. S. La, P. O. Wennberg and J. H. Seinfeld, *Atmos. Chem. Phys.*, 2016, **16**, 2785–2802.
- 29 M. Hallquist, J. C. Wenger, U. Baltensperger, Y. Rudich, D. Simpson, M. Claeys, J. Dommen, N. M. Donahue, C. George, A. H. Goldstein, J. F. Hamilton, H. Herrmann, T. Hoffmann, Y. Iinuma, M. Jang, M. E. Jenkin, J. L. Jimenez, A. Kiendler-Scharr, W. Maenhaut, G. McFiggans, T. F. Mentel, A. Monod, A. S. H. Prévôt, J. H. Seinfeld, J. D. Surratt, R. Szmigielski and J. Wildt, *Atmos. Chem. Phys.*, 2009, **9**, 5155–5236.
- 30 S. A. Penkett, R. A. Burgess, H. Coe, I. Coll, Ø. Hov, A. Lindskog, N. Schmidbauer, S. Solberg, M. Roemer, T. Thijssen, J. Beck and C. E. Reeves, *Atmos. Environ.*, 2007, **41**, 3465–3478.
- 31 S. S. Brown, T. B. Ryerson, A. G. Wollny, C. A. Brock, R. Peltier, A. P. Sullivan, R. J. Weber, W. P. Dubé, M. Trainer, J. F. Meagher, F. C. Fehsenfeld and A. R. Ravishankara, *Science*, 2006, **311**, 67–70.
- 32 C. R. Hoyle, T. Berntsen, G. Myhre and I. S. A. Isaksen, *Atmos. Chem. Phys.*, 2007, **7**, 5675–5694.

- 33 C. C. Wang, L. I. Davis, C. H. Wu and S. Japar, *Appl. Phys. Lett.*, 1976, **28**, 14–16.
- 34 T. M. Hard, R. J. O’Brien, C. Y. Chan and A. A. Mehrabzadeh, *Environ. Sci. Technol.*, 1984, **18**, 768–777.
- 35 F. Holland, A. Hofzumahaus, J. Schäfer, A. Kraus and H.-W. Pätz, *J. Geophys. Res.*, 2003, **108**, 8246.
- 36 F. A. F. Winiberg, S. C. Smith, I. Bejan, C. A. Brumby, T. Ingham, T. L. Malkin, S. C. Orr, D. E. Heard and P. W. Seakins, *Atmos. Meas. Tech.*, 2015, **8**, 523–540.
- 37 H. Fuchs, F. Holland and A. Hofzumahaus, *Rev. Sci. Instrum.*, 2008, **79**, 84104.
- 38 D. Tan, I. Faloon, J. B. Simpas, W. Brune, P. B. Shepson, T. L. Couch, A. L. Sumner, M. A. Carroll, T. Thornberry, E. Apel, D. Riemer and W. Stockwell, *J. Geophys. Res. Atmos.*, 2001, **106**, 24407–24427.
- 39 I. C. Faloon, D. Tan, R. L. Lesher, N. L. Hazen, C. L. Frame, J. B. Simpas, H. Harder, M. Martinez, P. Di Carlo, X. Ren and W. H. Brune, *J. Atmos. Chem.*, 2004, **47**, 139–167.
- 40 M. Martinez, H. Harder, D. Kubistin, M. Rudolf, H. Bozem, G. Eerdeken, H. Fisher, T. Klupfel, C. Gurk, R. Königstedt, U. Parchatka, C. L. Schiller, A. Stickler, J. Williams and J. Lelieveld, *Atmos. Chem. Phys.*, 2010, **10**, 3759–3773.
- 41 D. J. Tanner, A. Jefferson and F. L. Eisele, *J. Geophys. Res.*, 1997, **102**, 6415–6425.
- 42 H. Aufmhoff, M. Hanke, J. Uecker, H. Schlager and F. Arnold, *Int. J. Mass Spectrom.*, 2011, **308**, 26–34.
- 43 G. D. Edwards, C. A. Cantrell, S. Stephens, B. Hill, O. Goyea, R. E. Shetter, R. L. Mauldin, E. Kosciuch, D. J. Tanner and F. L. Eisele, *Anal. Chem.*, 2003, **75**, 5317–5327.
- 44 M. Hanke, J. Uecker, T. Reiner and F. Arnold, *Int. J. Mass Spectrom.*, 2002, **213**, 91–99.
- 45 R. S. Hornbrook, J. H. Crawford, G. D. Edwards, O. Goyea, R. L. Mauldin III, J. S. Olson and C. A. Cantrell, *Atmos. Meas. Tech.*, 2011, **4**, 735–756.
- 46 A. Kukui, M. Legrand, S. Preunkert, M. M. Frey, R. Loisil, J. Gil Roca, B. Jourdain, M. D. King, J. L. France and G. Ancellet, *Atmos. Chem. Phys.*, 2014, **14**, 12373–12392.
- 47 X. Ren, J. Mao, W. H. Brune, C. A. Cantrell, R. L. Mauldin III, R. S. Hornbrook, E. Kosciuch, J. R. Olson, J. H. Crawford, G. Chen and H. B. Singh, *Atmos. Meas. Tech.*, 2012, **5**, 2025–2037.

- 48 J. Sanchez, D. J. Tanner, D. Chen, L. G. Huey and N. L. Ng, *Atmos. Meas. Tech.*, 2016, **9**, 3851–3861.
- 49 Y. Liu and J. Zhang, *Anal. Chem.*, 2014, **86**, 5391–5398.
- 50 Y. Maeda, K. Aoki and M. Munemori, *Anal. Chem.*, 1980, **52**, 307–311.
- 51 T. J. Green, C. E. Reeves, Z. L. Fleming, N. Brough, A. R. Rickard, B. J. Bandy, P. S. Monks and S. A. Penkett, *J. Environ. Monit.*, 2006, **8**, 530–536.
- 52 S. Brown, *Chem. Rev.*, 2003, **103**, 5219–5238.
- 53 W. R. Simpson, *Rev. Sci. Instrum.*, 2003, **74**, 3442–3452.
- 54 E. Schlosser, T. Brauers, H.-P. Dorn, H. Fuchs, R. Häsel, A. Hofzumahaus, F. Holland, A. Wahner, Y. Kanaya, Y. Kajii, K. Miyamoto, S. Nishida, K. Watanabe, A. Yoshino, D. Kubistin, M. Martinez, M. Rudolf, H. Harder, H. Berresheim, T. Elste, C. Plass-Dülmer, G. Stange and U. Schurath, *Atmos. Chem. Phys. Discuss.*, 2009, **9**, 14081–14139.
- 55 W. P. Dube, S. S. Brown, H. D. Osthoff, M. R. Nunley, S. J. Ciciora, M. W. Paris, R. J. McLaughlin and A. R. Ravishankara, *Rev. Sci. Instrum.*, 2006, **77**, 34101.
- 56 D. B. Atkinson and J. L. Spillman, *J. Phys. Chem. A*, 2002, **106**, 8891–8902.
- 57 G. Hubler, D. Perner, U. Platt, A. Tonnissen and D. H. Ehhalt, *J. Geophys. Res.*, 1984, **89**, 1309–1319.
- 58 A. Saiz-Lopez, A. S. Mahajan, R. A. Salmon, S. J.-B. Bauguitte, A. E. Jones, H. K. Roscoe and J. M. C. Plane, *Science*, 2007, **317**, 348–351.
- 59 K. Clemetshaw, *Crit. Rev. Environ. Sci. Technol.*, 2004, **34**, 1–108.
- 60 E. Schlosser, B. Bohn, T. Brauers, H. P. Dorn, H. Fuchs, R. Häsel, A. Hofzumahaus, F. Holland, F. Rohrer, L. O. Rupp, M. Siese, R. Tillmann and A. Wahner, *J. Atmos. Chem.*, 2007, **56**, 187–205.
- 61 H. Fuchs, H.-P. Dorn, M. Bachner, B. Bohn, T. Brauers, S. Gomm, A. Hofzumahaus, F. Holland, S. Nehr, F. Rohrer, R. Tillmann and A. Wahner, *Atmos. Meas. Tech.*, 2012, **5**, 1611–1626.
- 62 T. Wagner, C. Otten, K. Pfeilsticker, I. Pundt and U. Platt, *Geophys. Res. Lett.*, 2000, **27**, 3441–3444.
- 63 J. Liao, L. G. Huey, D. J. Tanner, N. Brough, S. Brooks, J. E. Dibb, J. Stutz, J. L. Thomas, B. Lefer, C. Haman and K. Gorham, *Atmos. Chem. Phys.*, 2011, **11**, 8577–8591.
- 64 F. Hendrick, J.-F. Müller, K. Clémer, P. Wang, M. De Mazière, C. Fayt, C. Gielen, C.

- Hermans, J. Z. Ma, G. Pinardi, T. Stavrakou, T. Vlemmix and M. Van Roozendaal, *Atmos. Chem. Phys.*, 2014, **14**, 765–781.
- 65 D. Mihelcic, P. Musgen and D. H. Ehhalt, *J. Atmos. Chem.*, 1985, **3**, 341–361.
- 66 H. Fuchs, T. Brauers, R. Hasler, F. Holland, D. Mihelcic, P. Musgen, F. Rohrer, R. Wegener and A. Hofzumahaus, *Atmos. Meas. Tech.*, 2009, **2**, 55–64.
- 67 A. Geyer, B. Alicke, D. Mihelcic, J. Stutz and U. Platt, *J. Geophys. Res.*, 1999, **104**, 26097–26105.
- 68 U. Platt, B. Alicke, R. Dubois, A. Geyer, A. Hofzumahaus, F. Holland, M. Martinez, D. Mihelcic, T. Klupfel, B. Lohrmann, D. Perner, F. Rohrer, J. Schafer and J. Stutz, *J. Atmos. Chem.*, 2002, **42**, 359–394.
- 69 R. A. Salmon, C. L. Schiller and G. W. Harris, *J. Atmos. Chem.*, 2004, **48**, 81–104.
- 70 X. Chen and K. Mopper, *J. Atmos. Chem.*, 2000, **36**, 81–105.
- 71 B. Halliwell, H. Kaur and M. Ingelman-Sundberg, *Free Radic. Biol. Med.*, 1991, **10**, 439–441.
- 72 X. Fang, G. Mark and C. von Sonntag, *Ultrason. Sonochem.*, 1996, **3**, 57–63.
- 73 B. Ou, M. Hampsch-Woodill, J. Flanagan, E. K. Deemer, R. L. Prior and D. Huang, *J. Agric. Food Chem.*, 2002, **50**, 2772–2777.
- 74 J. Chan, S. C. Dodani and C. J. Chang, *Nat. Chem.*, 2012, **4**, 973–984.
- 75 M. Kim, S.-K. Ko, H. Kim, I. Shin and J. Tae, *Chem. Commun.*, 2013, **49**, 7959–7961.
- 76 M. Jia, Y. Tang, Y.-F. Lam, S. A. Green and N. V Blough, *Anal. Chem.*, 2009, **81**, 8033–8040.
- 77 C. Giorio, S. J. Campbell, M. Bruschi, F. Tampieri, A. Barbon, A. Toffoletti, A. Tapparo, C. Paijens, A. J. Wedlake, P. Grice, D. J. Howe and M. Kalberer, *J. Am. Chem. Soc.*, 2017, **139**, 3999–4008.
- 78 T. Berndt, H. Herrmann and T. Kurtén, *J. Am. Chem. Soc.*, 2017, jacs.7b05849.
- 79 C. A. Taatjes, D. E. Shallcross and C. J. Percival, *Phys. Chem. Chem. Phys.*, 2014, **16**, 1704–1718.
- 80 D. E. Heard, *Annu. Rev. Phys. Chem.*, 2006, **57**, 191–216.
- 81 E. G. Janzen, R. V. Shetty and S. M. Kunanec, *Can. J. Chem.*, 1981, **59**, 756–758.
- 82 J. Maury, L. Feray, S. Bazin, J.-L. Clément, S. R. A. Marque, D. Siri and M. P. Bertrand, *Chem. A Eur. J.*, 2011, **17**, 1586–1595.

- 83 M. L. McCormick, G. R. Buettner and B. E. Britigan, *J. Biol. Chem.*, 1995, **270**, 29265–29269.
- 84 N. E. Polyakov, A. I. Kruppa, T. V. Leshina, T. A. Konovalova and L. D. Kispert, *Free Radic. Biol. Med.*, 2001, **31**, 43–52.
- 85 M. A. Rudat and C. N. McEwen, *J. Am. Chem. Soc.*, 1981, **103**, 4349–4354.
- 86 E. Janzen and J. I.-P. Liu, *J. Magn. Reson.*, 1973, **9**, 510–512.
- 87 G. R. Buettner and L. W. Oberley, *Biochem. Biophys. Res. Commun.*, 1978, **83**, 69–74.
- 88 J. Möser, K. Lips, M. Tseytlin, G. R. Eaton, S. S. Eaton and A. Schnegg, *J. Magn. Reson.*, 2017, **281**, 17–25.
- 89 P. K. Witting, D. J. Douglas and A. G. Mauk, *J. Biol. Chem.*, 2000, **275**, 20391–20398.
- 90 C. Zhu, K. Kawamura and B. Kunwar, *Atmos. Chem. Phys.*, 2015, **15**, 1959–1973.
- 91 Q. Guo, S. Y. Qian and R. P. Mason, *J. Am. Soc. Mass Spectrom.*, 2003, **14**, 862–871.
- 92 K. Furusawa, T. Kawamura, Y. Akutsu, M. Arai and M. Tamura, *Atmos. Environ.*, 1997, **31**, 3363–3367.
- 93 W. A. Pryor, M. Tamura and D. F. Church, *J. Am. Chem. Soc.*, 1984, **106**, 5073–5079.
- 94 S. L. Baum, I. G. M. Anderson, R. R. Baker, D. M. Murphy and C. C. Rowlands, *Anal. Chim. Acta*, 2003, **481**, 1–13.
- 95 S. Pou, D. J. Hassett, B. E. Britigan, M. S. Cohen and G. M. Rosen, *Anal. Biochem.*, 1989, **177**, 1–6.
- 96 F. Leinisch, J. Jiang, E. F. DeRose, V. V. Khramtsov and R. P. Mason, *Free Radic. Biol. Med.*, 2013, **65**, 1497–1505.
- 97 B. B. Giese and S. Lachheinl, *Angew. Chemie - Int. Ed.*, 1981, **20**, 967.
- 98 D. V. Avila, K. U. Ingold, J. Lusztyk, W. R. Dolbier and H. Q. Pan, *J. Org. Chem.*, 1996, **61**, 2027–2030.
- 99 A. L. J. Beckwith and J. S. Poole, *J. Am. Chem. Soc.*, 2002, **124**, 9489–9497.
- 100 S. J. Blanksby and G. B. Ellison, *Acc. Chem. Res.*, 2003, **36**, 255–263.
- 101 D. L. Marshall, G. Gryn'ova, M. L. Coote, P. J. Barker and S. J. Blanksby, *Int. J. Mass Spectrom.*, 2015, **378**, 38–47.
- 102 L. R. Mahoney, G. D. Mendenhall and K. U. Ingold, *J. Am. Chem. Soc.*, 1973, **95**, 8610–8614.

- 103 F. G. Bordwell and W.-Z. Liu, *J. Am. Chem. Soc.*, 1996, **118**, 8777–8781.
- 104 M. K. Georges, R. P. N. Veregin, P. M. Kazmaier and G. K. Hamer, *Macromolecules*, 1993, **26**, 2987–2988.
- 105 J. Chiefari, Y. K. B. Chong, F. Ercole, J. Krstina, J. Jeffery, T. P. T. Le, R. T. A. Mayadunne, G. F. Meijs, C. L. Moad, G. Moad, E. Rizzardo, S. H. Thang and C. South, *Macromolecules*, 1998, **9297**, 5559–5562.
- 106 S. P. Cresidio, F. Aldabbagh, W. K. Busfield, I. D. Jenkins, S. H. Thang, C. Zayas-Holdsworth and P. B. Zetterlund, *J. Polym. Sci. Part A Polym. Chem.*, 2001, **39**, 1232–1241.
- 107 R. V Todesco and N. Ergenc, *Chimia*, 2002, **56**, 225–238.
- 108 C. Wetter and A. Studer, *Chem. Commun.*, 2004, 174–175.
- 109 J. Xu, E. J. E. Caro-Diaz, L. Trzoss and E. A. Theodorakis, *J. Am. Chem. Soc.*, 2012, **134**, 5072–5075.
- 110 K. Matyjaszewski, B. E. Woodworth, X. Zhang, S. G. Gaynor and Z. Metzner, *Macromolecules*, 1998, **31**, 5955–5957.
- 111 L. Li, Z. Yu and Z. Shen, *Adv. Synth. Catal.*, 2015, **357**, 3495–3500.
- 112 K.-U. Schoening, W. Fischer, S. Hauck, A. Dichtl and M. Kuepfert, *J. Org. Chem.*, 2009, **74**, 1567–73.
- 113 S. P. Simonovich, J. F. Van Humbeck and D. W. C. Macmillan, *Chem. Sci.*, 2012, **3**, 58–61.
- 114 T. Kano, H. Mii and K. Maruoka, *Angew. Chem. Int. Ed. Engl.*, 2010, **49**, 6638–6641.
- 115 H. Paul, R. D. Small and J. C. Scaiano, *J. Am. Chem. Soc.*, 1978, **100**, 4520–4527.
- 116 R. Braslau, L. C. Burrill, M. Siano, N. Naik, R. K. Howden and L. K. Mahal, *Macromolecules*, 1997, **30**, 6445–6450.
- 117 M. J. Cuthbertson, E. Rizzardo and D. H. Solomon, *Aust. J. Chem.*, 1983, **36**, 1957–1973.
- 118 G. Moad, E. Rizzardo and D. H. Solomon, *Tetrahedron Lett.*, 1981, **22**, 1165–1168.
- 119 N. Koshino, Y. Cai and J. H. Espenson, *J. Phys. Chem. A*, 2003, **107**, 4262–4267.
- 120 D. F. McMillen and D. M. Golden, *Annu. Rev. Phys. Chem.*, 1982, **33**, 493–532.
- 121 J. M. Hudzik, J. W. Bozzelli and J. M. Simmie, *J. Phys. Chem. A*, 2014, **118**, 9364–9379.
- 122 B. Janza and A. Studer, *Org. Lett.*, 2006, **8**, 1875–1878.

- 123 C. Galli, P. Gentili and O. Lanzalunga, *Angew. Chemie - Int. Ed.*, 2008, **47**, 4790–4796.
- 124 W. Adam, C. R. Saha-Moller and P. A. Ganeshpure, *Chem. Rev.*, 2001, **101**, 3499–3548.
- 125 M. Conte, K. Wilson and V. Chechik, *Rev. Sci. Instrum.*, 2010, **81**, 104102.
- 126 J. J. Brocks, H.-D. Beckhaus, A. L. J. Beckwith and C. Rüchardt, *J. Org. Chem.*, 1998, **63**, 1935–1943.
- 127 B. Braid, V. Prana and P. C. Hiberty, *Angew. Chemie - Int. Ed.*, 2009, **48**, 5724–5728.
- 128 N. A. Porter, S. E. Caldwell and K. A. Mills, *Lipids*, 1995, **30**, 277–290.
- 129 J. J. Scepaniak, A. M. Wright, R. A. Lewis, G. Wu and T. W. Hayton, *J. Am. Chem. Soc.*, 2012, **134**, 19350–19353.
- 130 D. H. R. Barton and N. Le Gloahec, *Tetrahedron*, 1998, **54**, 15457–15468.
- 131 S. Goldstein, D. Meyerstein and G. Czapski, *Free Radic. Biol. Med.*, 1993, **15**, 435–445.
- 132 L. P. Candeias and P. Wardman, *Radiat. Res.*, 2013, **145**, 523–531.
- 133 T. J. Connolly, M. V. Baldovf, N. Mohtat and J. C. Scaiano, *Tetrahedron Lett.*, 1996, **37**, 4919–4922.
- 134 D. H. R. Barton, V. N. Le Gloahec and J. Smith, *Tetrahedron Lett.*, 1998, **39**, 7483–7486.
- 135 A. R. Brash, *Lipids*, 2000, **35**, 947–952.
- 136 S. Bergstrom, *Nature*, 1945, **156**, 717–718.
- 137 D. E. Bergbreiter and B. Walchuk, *Macromolecules*, 1998, **31**, 6380–6382.
- 138 H. Masada and Y. Murotani, *Bull. Chem. Soc. Jpn.*, 1980, **53**, 1181–1182.
- 139 M. Hartmann, Y. Li and A. Studer, *J. Am. Chem. Soc.*, 2012, **134**, 16516–16519.
- 140 A. Onopchenko and J. G. D. Schulz, *J. Org. Chem.*, 1866, **38**, 3729–3733.
- 141 A. Prechter and M. R. Heinrich, *European J. Org. Chem.*, 2013, **2013**, 5585–5589.
- 142 E. J. Corey and J. W. Suggs, *Tetrahedron Lett.*, 1975, **31**, 2647–2650.
- 143 R. A. Fernandes and P. Kumar, *Tetrahedron Lett.*, 2003, **44**, 1275–1278.
- 144 D. B. Dess and J. C. Martin, *J. Org. Chem.*, 1983, **48**, 4155–4156.
- 145 K. Omura and D. Swern, *Tetrahedron*, 1978, **34**, 1651–1660.
- 146 D. B. Dess and J. C. Martin, *J. Am. Chem. Soc.*, 1991, **113**, 7277–7287.
- 147 A. J. Mancuso, D. S. Brownfain and D. Swern, *J. Org. Chem.*, 1979, **44**, 4148–4150.

- 148 G. Audran, P. Brémond, S. R. A. Marque and T. Yamasaki, *J. Org. Chem.*, 2016, **81**, 1981–1988.
- 149 M. P. Sibi and M. Hasegawa, *J. Am. Chem. Soc.*, 2007, **129**, 4124–4125.
- 150 J. F. Van Humbeck, S. P. Simonovich, R. R. Knowles and D. W. C. Macmillan, *J. Am. Chem. Soc.*, 2010, **132**, 10012–10014.
- 151 A. Bax and M. F. Summers, *J. Am. Chem. Soc.*, 1986, **108**, 2093–2094.
- 152 P. A. Byrne and D. G. Gilheany, *Chem. Soc. Rev.*, 2013, **42**, 6670–6696.
- 153 G. Wittig and G. Geissler, *Justus Liebigs Ann. Chem.*, 1953, **580**, 44–57.
- 154 M. W. Rathke and M. Nowak, *J. Org. Chem.*, 1985, **50**, 2624–2626.
- 155 G. Moad and E. Rizzardo, *Macromolecules*, 1995, **28**, 8722–8728.
- 156 H. Fischer, *Chem. Rev.*, 2001, **101**, 3581–610.
- 157 S. Marque, H. Fischer, E. Baier and A. Studer, *J. Org. Chem.*, 2001, **66**, 1146–1156.
- 158 E. Rizzardo and D. H. Solomon, *Aust. J. Chem.*, 2012, **65**, 945–969.
- 159 D. Bertin, D. Gigmes, S. R. A. Marque and P. Tordo, *Chem. Soc. Rev.*, 2011, **40**, 2189–98.
- 160 W. M. Nau, *J. Phys. Org. Chem.*, 1997, **10**, 445–455.
- 161 D. Bertin, D. Gigmes, S. R. A. Marque and P. Tordo, *Macromolecules*, 2005, **38**, 2638–2650.
- 162 S. Marque, C. Le Mercier, P. Tordo and H. Fischer, *Macromolecules*, 2000, **33**, 4403–4410.
- 163 A. Grand and R. Rey, *Acta Crystallogr. Sect. B*, 1979, **35**, 2149–2153.
- 164 J. E. Baldwin and P. A. Leber, *Org. Biomol. Chem.*, 2008, **6**, 36–47.
- 165 V. Rautenstrauch, *Helv. Chim. Acta*, 1973, **56**, 2492–2508.
- 166 J. Y. Choi, C. K. Kim, C. K. Kim and I. Lee, *J. Phys. Chem. A*, 2002, **106**, 5709–5715.
- 167 K. C. Majumdar and G. H. Jana, *J. Org. Chem.*, 1997, **62**, 1506–1508.
- 168 J. A. Berson and G. L. Nelson, *J. Am. Chem. Soc.*, 1970, **92**, 1096–1097.
- 169 D. R. Kerur and D. G. M. Diaperm, *Can. J. Chem.*, 1973, **51**, 3110–3113.
- 170 M. I. Kanishev, A. A. Schegolev, M. J. Kelner, W. A. Smit and R. Caple, *J. Am. Chem. Soc.*, 1979, **101**, 5660–5671.
- 171 B. J. Deadman, C. Battilocchio, E. Sliwinski and S. V. Ley, *Green Chem.*, 2013, **15**, 2050–2055.

- 172 B. Zhang and S. R. Turner, *Polymer*, 2013, **54**, 4493–4500.
- 173 D. F. Taber, P. B. Decker and M. D. Gaul, *J. Am. Chem. Soc.*, 1987, **109**, 7488–7494.
- 174 T. D. Beeson, A. Mastracchio, J. Hong, K. Ashton and D. W. C. Macmillan, *Science*, 2007, **316**, 582–585.
- 175 M. Rance, O. W. Sørensen, G. Bodenhausen, G. Wagner, R. R. Ernst and K. Wüthrich, *Biochem. Biophys. Res. Commun.*, 1983, **117**, 479–485.
- 176 A. Bax and R. Freeman, *J. Magn. Reson.*, 1981, **44**, 542–561.
- 177 D. R. Blake, R. E. Allen and J. Lunec, *Br. Med. Bull.*, 1987, **43**, 371–385.
- 178 E. G. Janzen, D. E. Nutter Jr., E. R. Davis, B. J. Blackburn, J. L. Poyer and P. B. McCay, *Can. J. Chem.*, 1978, **56**, 2237–2242.
- 179 Y. Wang, M. Liu, Y. Zhu, K. Cheng, W. Da, B. Liu and F. Li, *Talanta*, 2016, **160**, 106–112.
- 180 H. J. Halpern, C. Yu, E. Barth, M. Peric and G. M. Rosen, *Proc. Natl. Acad. Sci. U. S. A.*, 1995, **92**, 796–800.
- 181 N. Khan, C. M. Wilmot, G. M. Rosen, E. Demidenko, J. Sun, J. Joseph, J. O’Hara, B. Kalyanaraman and H. M. Swartz, *Free Radic. Biol. Med.*, 2003, **34**, 1473–1481.
- 182 T. Ishikawa, M. Takagi, M. Kanou, S. Kawai and H. Ohashi, *Biosci. Biotechnol. Biochem.*, 1999, **63**, 173–177.
- 183 D. J. Gravert, A. Datta, P. Wentworth and K. D. Janda, *J. Am. Chem. Soc.*, 1998, **120**, 9481–9495.
- 184 G. Audran, E. G. Bagryanskaya, P. Brémond, M. V. Edeleva, S. R. A. Marque, D. A. Parkhomenko, O. Y. Rogozhnikova, V. M. Tormyshev, E. V. Tretyakov, D. V. Trukhin and S. I. Zhivetyeva, *Polym. Chem.*, 2016, **7**, 6490–6499.
- 185 V. V. Khramtsov, V. A. Reznikov, L. J. Berliner, A. K. Litkin, I. A. Grigorev and T. L. Clanton, *Free Radic. Biol. Med.*, 2001, **30**, 1099–1107.
- 186 G. Bacić, I. Spasojević, B. Sećerov and M. Mojović, *Spectrochim. Acta. A. Mol. Biomol. Spectrosc.*, 2008, **69**, 1354–1366.
- 187 Y. Zhang and C. J. Li, *European J. Org. Chem.*, 2007, 4654–4657.
- 188 A. D. Bokare and W. Choi, *J. Hazard. Mater.*, 2014, **275**, 121–135.
- 189 H. Hock and H. Kropf, *J. fur Prakt. Chemie*, 1958, **6**, 121–128.
- 190 A. Gansäuer, *Synlett*, 1998, **8**, 801–809.

- 191 P. Carloni, E. Damiani, M. Scattolini, P. Stipa and L. Greci, *J. Chem. Soc. Perkin Trans. 2*, 2000, 447–451.
- 192 R. T. M. Fraser, N. C. Paul and L. Phillips, *J. Chem. Soc. B*, 1970, 1278–1280.
- 193 I. Rosenthal, M. M. Mossoba and P. Riesz, *Can. J. Chem.*, 1982, **60**, 1486–1492.
- 194 I. Janovský, W. Knolle, S. Naumov and F. Williams, *Chem. A Eur. J.*, 2004, **10**, 5524–5534.
- 195 E. Praske, J. D. Crouse, K. H. Bates, T. Kurtén, H. G. Kjaergaard and P. O. Wennberg, *J. Phys. Chem. A*, 2015, **119**, 4562–4572.
- 196 O. Brede, D. Beckert, C. Windolph and H. A. Gottinger, *J. Phys. Chem. A*, 1998, **102**, 1457–1464.
- 197 A. Adenier, M. M. Chehimi, I. Gallardo, J. Pinson and N. Vilà, *Langmuir*, 2004, **20**, 8243–8253.
- 198 S. Laha and R. G. Luthy, *Environ. Sci. Technol.*, 1990, **24**, 363–373.
- 199 B. L. Miller, T. D. Williams, Christian and T. Schöneich, *J. Am. Chem. Soc.*, 1996, **118**, 11014–11025.
- 200 H. Karoui, N. Hogg, C. Frejaville, P. Tordo and B. Kalyanaraman, *J. Biol. Chem.*, 1996, **271**, 6000–6009.
- 201 G. Merényi, J. Lind and L. Engman, *J. Phys. Chem.*, 1996, **100**, 8875–8881.
- 202 S. Goldstein, A. Samuni and G. Merenyi, *J. Phys. Chem. A*, 2008, **112**, 8600–8605.
- 203 D. Melandri, P. C. Montevecchi and M. L. Navacchia, *Tetrahedron*, 1999, **55**, 12227–12236.
- 204 V. T. Kasumov, B. Karabulut, I. Kartal and F. Koksai, *Transit. Met. Chem.*, 2001, **26**, 64–70.
- 205 D. Johnson and G. Marston, *Chem. Soc. Rev.*, 2008, **37**, 699–716.
- 206 M. Ehn, J. A. Thornton, E. Kleist, M. Sipilä, H. Junninen, I. Pullinen, M. Springer, F. Rubach, R. Tillmann, B. Lee, F. Lopez-Hilfiker, S. Andres, I.-H. Acir, M. Rissanen, T. Jokinen, S. Schobesberger, J. Kangasluoma, J. Kontkanen, T. Nieminen, T. Kurtén, L. B. Nielsen, S. Jørgensen, H. G. Kjaergaard, M. Canagaratna, M. D. Maso, T. Berndt, T. Petäjä, A. Wahner, V.-M. Kerminen, M. Kulmala, D. R. Worsnop, J. Wildt and T. F. Mentel, *Nature*, 2014, **506**, 476–479.
- 207 R. Criegee, *Angew. Chem. Int. Ed.*, 1975, **14**, 745–752.

- 208 Y. Su, Y. Huang, H. A. Witek and Y. Lee, *Science*, 2013, **340**, 174–177.
- 209 C. A. Taatjes, G. Meloni, T. M. Selby, A. J. Trevitt, D. L. Osborn, C. J. Percival and D. E. Shallcross, *J. Am. Chem. Soc.*, 2008, **130**, 11883–11885.
- 210 W. Sander, *Angew. Chemie Int. Ed. English*, 1990, **29**, 344–354.
- 211 M. Nakajima and Y. Endo, *J. Chem. Phys.*, 2013, **139**, 101103.
- 212 G. T. Drozd, J. Kroll and N. M. Donahue, *J. Phys. Chem. A*, 2011, **115**, 161–166.
- 213 A. Novelli, L. Vereecken, J. Lelieveld and H. Harder, *Phys. Chem. Chem. Phys.*, 2014, **16**, 19941–19951.
- 214 T. B. Nguyen, G. S. Tyndall, J. D. Crouse, A. P. Teng, K. H. Bates, R. H. Schwantes, M. M. Coggon, L. Zhang, P. Feiner, D. O. Miller, K. M. Skog, J. C. Rivera-Rios, M. Dorris, K. F. Olson, A. Koss, R. J. Wild, S. S. Brown, A. H. Goldstein, J. A. de Gouw, W. H. Brune, F. N. Keutsch, J. H. Seinfeld and P. O. Wennberg, *Phys. Chem. Chem. Phys.*, 2016, **18**, 10241–10254.
- 215 T. L. Malkin, A. Goddard, D. E. Heard and P. W. Seakins, *Atmos. Chem. Phys.*, 2010, **10**, 1441–1459.
- 216 K. Hens, A. Novelli, M. Martinez, J. Auld, R. Axinte, B. Bohn, H. Fischer, P. Keronen, D. Kubistin, A. C. Nölscher, R. Oswald, P. Paasonen, T. Petäjä, E. Regelin, R. Sander, V. Sinha, M. Sipilä, D. Taraborrelli, C. Tatum Ernest, J. Williams, J. Lelieveld and H. Harder, *Atmos. Chem. Phys.*, 2014, **14**, 8723–8747.
- 217 J. Fick, L. Pommer, B. Andersson and C. Nilsson, *Atmos. Environ.*, 2002, **36**, 3299–3308.
- 218 R. J. Barthelmie and S. C. Pryor, *J. Geophys. Res.*, 1999, **104**, 23657–23699.
- 219 G. Lin, J. E. Penner, M. G. Flanner, S. Sillman, L. Xu and C. Zhou, *J. Geophys. Res. Atmos.*, 2014, **119**, 9567–9577.
- 220 D. F. Zhao, A. Buchholz, B. Kortner, P. Schlag, F. Rubach, H. Fuchs, A. Kiendler-Scharr, R. Tillmann, A. Wahner, K. Watne, M. Hallquist, J. M. Flores, Y. Rudich, K. Kristensen, A. M. K. Hansen, M. Glasius, I. Kourtchev, M. Kalberer and T. F. Mentel, *Atmos. Chem. Phys.*, 2016, **16**, 1105–1121.
- 221 J. L. Mauderly and J. C. Chow, *Inhal. Toxicol.*, 2008, **20**, 257–288.
- 222 R. Volkamer, J. L. Jimenez, F. San Martini, K. Dzepina, Q. Zhang, D. Salcedo, L. T. Molina, D. R. Worsnop and M. J. Molina, *Geophys. Res. Lett.*, 2006, **33**, 7–10.

- 223 S. Hatakeyama, K. Izumi, T. Fukuyama and H. Akimoto, *J. Geophys. Res.*, 1989, **94**, 13013–13024.
- 224 T. Hoffmann, J. R. Odum, F. Bowman, D. Collins, D. Klockow, R. C. Flagan and J. H. Seinfeld, *J. Atmos. Chem.*, 1997, **26**, 189–222.
- 225 Y. Ma, A. T. Russell and G. Marston, *Phys. Chem. Chem. Phys.*, 2008, **10**, 4294–4312.
- 226 H. S. Amin, M. L. Hatfield and K. E. Huff Hartz, *Atmos. Environ.*, 2013, **67**, 323–330.
- 227 K. Kristensen, Å. K. Watne, J. Hammes, A. Lutz, T. Petäjä, M. Hallquist, M. Bilde and M. Glasius, *Environ. Sci. Technol. Lett.*, 2016, **3**, 280–285.
- 228 S. M. Saunders, M. E. Jenkin, R. G. Derwent and M. J. Pilling, *Atmos. Chem. Phys.*, 2003, **3**, 161–180.
- 229 M. E. Jenkin, J. C. Young and A. R. Rickard, *Atmos. Chem. Phys.*, 2015, **15**, 11433–11459.
- 230 [Http://mcm.leeds.ac.uk/MCM](http://mcm.leeds.ac.uk/MCM), .
- 231 M. Ni, Y. Zhang, T. Gong and B. Feng, *Adv. Synth. Catal.*, 2017, **359**, 824–831.
- 232 C. N. Dalton, M. Jaoui, R. M. Kamens and G. L. Glish, *Anal. Chem.*, 2005, **77**, 3156–3163.
- 233 R. K. Pathak, C. O. Stanier, N. M. Donahue and S. N. Pandis, *J. Geophys. Res. Atmos.*, 2007, **112**, D03201.
- 234 R. Atkinson, *Atmos. Environ.*, 2000, **34**, 2063–2101.
- 235 D. Zhang and R. Zhang, *J. Chem. Phys.*, 2005, **122**, 114308.
- 236 P. G. Pinho, C. A. Pio, W. P. L. Carter and M. E. Jenkin, *J. Atmos. Chem.*, 2007, **57**, 171–202.
- 237 T. Jokinen, M. Sipilä, S. Richters, V.-M. Kerminen, P. Paasonen, F. Stratmann, D. Worsnop, M. Kulmala, M. Ehn, H. Herrmann and T. Berndt, *Angew. Chem. Int. Ed. Engl.*, 2014, **53**, 14596–600.
- 238 M. Camredon, J. F. Hamilton, M. S. Alam, K. P. Wyche, T. Carr, I. R. White, P. S. Monks, A. R. Rickard and W. J. Bloss, *Atmos. Chem. Phys.*, 2010, **10**, 2893–2917.
- 239 C. Meusinger, U. Dusek, S. M. King, R. Holzinger, T. Rosenørn, P. Sperlich, M. Julien, G. S. Remaud, M. Bilde, T. Röckmann and M. S. Johnson, *Atmos. Chem. Phys.*, 2017, **17**, 6373–6391.
- 240 J. Pavlovic and P. K. Hopke, *J. Atmos. Chem.*, 2010, **66**, 137–155.

- 241 M. Siese, K. H. Becker, K. J. Brockmann, H. Geiger, A. Hofzumahaus, F. Holland, D. Mihelcic and K. Wirtz, *Environ. Sci. Technol.*, 2001, **35**, 4660–4667.
- 242 T. Berndt, S. Richters, T. Jokinen, N. Hyttinen, T. Kurtén, R. V. Otkjær, H. G. Kjaergaard, F. Stratmann, H. Herrmann, M. Sipilä, M. Kulmala and M. Ehn, *Nat. Commun.*, 2016, **7**, 13677.
- 243 L. Vereecken, J.-F. Müller and J. Peeters, *Phys. Chem. Chem. Phys.*, 2007, **9**, 5241–5248.
- 244 J. Peeters, L. Vereecken and G. Fantechi, *Phys. Chem. Chem. Phys.*, 2001, **3**, 5489–5504.
- 245 X. Zhang, R. C. McVay, D. D. Huang, N. F. Dalleska, B. Aumont, R. C. Flagan and J. H. Seinfeld, *Proc. Natl. Acad. Sci. U. S. A.*, 2015, **112**, 14168–14173.
- 246 C. L. Heald, D. J. Jacob, R. J. Park, L. M. Russell, B. J. Huebert, J. H. Seinfeld, H. Liao and R. J. Weber, *Geophys. Res. Lett.*, 2005, **32**, L18809.
- 247 M. E. Jenkin, *Atmos. Chem. Phys. Discuss.*, 2004, **4**, 2905–2948.
- 248 P. K. Saha and A. P. Grieshop, *Environ. Sci. Technol.*, 2016, **50**, 5740–9.
- 249 P. K. Jauhari, A. Bhavani, S. Varalwar, K. Singhal and P. Raj, *Med. Chem. Res.*, 2008, **17**, 412–424.
- 250 L. Jiang, R. Lan, Y. S. Xu, W. J. Zhang and W. Yang, *Int. J. Mol. Sci.*, 2013, **14**, 5784–5805.
- 251 S. Kundu, R. Fisseha, A. L. Putman, T. A. Rahn and L. R. Mazzoleni, *Atmos. Chem. Phys.*, 2012, **12**, 5523–5536.
- 252 T. Wainman, J. Zhang, C. J. Weschler and P. J. Lioy, *Environ. Health Perspect.*, 2000, **108**, 1139–1145.
- 253 A. S. Hasson, G. Orzechowska, K. T. Kuwata and S. E. Paulson, *J. Geophys. Res.*, 2001, **106**, 131–143.
- 254 H. Niki, P. D. Maker, C. M. Savage, L. P. Breitenbach and M. D. Hurley, *J. Phys. Chem.*, 1987, **91**, 941–946.
- 255 M. S. Alam, A. R. Rickard, M. Camredon, K. P. Wyche, T. Carr, K. E. Hornsby, P. S. Monks and W. J. Bloss, *J. Phys. Chem. A*, 2013, **117**, 12468–12483.
- 256 D. R. Glowacki, A. Goddard, K. Hemavibool, T. L. Malkin, R. Commane, F. Anderson, W. J. Bloss, D. E. Heard, T. Ingham, M. J. Pilling and P. W. Seakins, *Atmos. Chem.*

- Phys.*, 2007, **7**, 5371–5390.
- 257 A. A. Presto, K. E. H. Hartz and N. M. Donahue, *Environ. Sci. Technol.*, 2005, **39**, 7036–7045.
- 258 L. Tofful and C. Perrino, *Atmosphere*, 2015, **6**, 1422–1443.
- 259 X. Niu, S. S. H. Ho, K. F. Ho, Y. Huang, J. Cao, Z. Shen, J. Sun, X. Wang, Y. Wang, S. Lee and R. Huang, *Sci. Total Environ.*, 2017, **579**, 212–220.
- 260 J. de Zeeuw and J. Luong, *Trends Anal. Chem.*, 2002, **21**, 594–607.
- 261 G. A. Eiceman, H. H. Hill and J. Gardea-Torresday, *Anal. Chem.*, 2000, **72**, 137–144.
- 262 T. Watanabe, M. Yoshida, A. Onoe, M. Hirota and S. Igarashi, *Anal. Chem.*, 1982, **54**, 2470–2474.
- 263 T. M. Flicker and S. A. Green, *Anal. Chem.*, 1998, **70**, 2008–2012.
- 264 Y. Gorbanev, D. O’Connell and V. Chechik, *Chem. A Eur. J.*, 2016, **22**, 3496–3505.
- 265 M. Ono-Ogasawara and N. Kohyama, *Ann. Occup. Hyg.*, 1999, **43**, 505–511.
- 266 T. M. Flicker and S. A. Green, *Environ. Health Perspect.*, 2001, **1091**, 765–771.
- 267 M. Bonose-Crosnier de Bellaistre, W. Nowik, A. Tchapla and S. Heron, *J. Chromatogr. A*, 2011, **1218**, 778–786.
- 268 H. Berresheim, T. Elste, C. Plass-Dülmer, F. L. Eisele and D. J. Tanner, *Int. J. Mass Spectrom.*, 2000, **202**, 91–109.
- 269 P. S. Monks, L. J. Carpenter, S. A. Penkett, G. P. Ayers, R. W. Gillett, I. E. Galbally and C. P. Meyer, *Atmos. Environ.*, 1998, **32**, 3647–3664.
- 270 M. Terazima, Y. Nogami and T. Tominaga, *Chem. Phys. Lett.*, 2000, **332**, 503–507.
- 271 A. Hofzumahaus, U. Aschmutat, U. Brandenburger, T. Brauers, H.-P. Dorn, M. Hausmann, M. Hessling, F. Holland, C. Plass-Dulmer and D. H. Ehhalt, *J. Atmos. Chem.*, 1998, **31**, 227–246.
- 272 P. Veres, J. M. Roberts, C. Warneke, D. Welsh-Bon, M. Zahniser, S. Herndon, R. Fall and J. de Gouw, *Int. J. Mass Spectrom.*, 2008, **274**, 48–55.
- 273 K. T. A. L. Burm, *Plasma Chem. Plasma Process.*, 2012, **32**, 401–407.
- 274 T. Murakami, K. Niemi, T. Gans, D. O’Connell and W. G. Graham, *Plasma Sources Sci. Technol.*, 2013, **22**, 15003.
- 275 C. Charles, *Front. Phys.*, 2014, **2**, 39.
- 276 R. Foest, M. Schmidt and K. Becker, *Int. J. Mass Spectrom.*, 2006, **248**, 87–102.

- 277 M. Laroussi and X. Lu, *Appl. Phys. Lett.*, 2005, **87**, 113902.
- 278 J. L. Walsh, F. Iza, N. B. Janson, V. J. Law and M. G. Kong, *J. Phys. D. Appl. Phys.*, 2010, **43**, 75201.
- 279 J. Chauvin, F. Judée, M. Yousfi, P. Vicendo and N. Merbahi, *Sci. Rep.*, 2017, **7**, 1–15.
- 280 D. Xu, D. Liu, B. Wang, C. Chen, Z. Chen, D. Li, Y. Yang, H. Chen and M. G. Kong, *PLoS One*, 2015, **10**, e0128205.
- 281 M. Gianella, S. Reuter, A. L. Aguila, G. A. D. Ritchie and J. P. H. Van Helden, *New J. Phys.*, 2016, **18**.
- 282 Y. Gorbanev, N. Stehling, D. O'Connell and V. Chechik, *Plasma Sources Sci. Technol.*, 2016, **25**, 55017.
- 283 K. Sugiyama, G. Anan, T. Shimada, T. Ohkoshi and T. Ushikubo, *Surf. Coat. Technol.*, 1999, **112**, 76–79.
- 284 M. Laroussi and F. Leipold, *Int. J. Mass Spectrom.*, 2004, **233**, 81–86.
- 285 M. Moisan, J. Barbeau, S. Moreau, J. Pelletier, M. Tabrizian and L. Yahia, *Int. J. Pharm.*, 2001, **226**, 1–21.
- 286 L. G. Forni, V. O. Mora-Arellano, J. E. Packer and R. L. Willson, *J. Chem. Soc. Perkin Trans. II*, 1986, **0**, 1–6.
- 287 A. A. Presto, K. E. Huff Hartz and N. M. Donahue, *Environ. Sci. Technol.*, 2005, **39**, 7046–7054.
- 288 R. G. de Lima, M. G. Sauaia, D. Bonaventura, A. C. Tedesco, L. M. Bendhack and R. S. da Silva, *Inorganica Chim. Acta*, 2006, **359**, 2543–2549.
- 289 H. Uchiyama, Q. L. Zhao, M. A. Hassan, G. Andocs, N. Nojima, K. Takeda, K. Ishikawa, M. Hori and T. Kondo, *PLoS One*, 2015, **10**, e0136956.
- 290 H. Levy, *Science*, 1971, **173**, 141–143.
- 291 P. S. Monks, *Chem. Soc. Rev.*, 2005, **34**, 376–395.
- 292 P. R. Veres, P. Faber, F. Drewnick, J. Lelieveld and J. Williams, *Atmos. Environ.*, 2013, **77**, 1052–1059.
- 293 L. Xue, R. Gu, T. Wang, X. Wang, S. Saunders, D. Blake, P. K. K. Louie, C. W. Y. Luk, I. Simpson, Z. Xu, Z. Wang, Y. Gao, S. Lee, A. Mellouki and W. Wang, *Atmos. Chem. Phys.*, 2016, **16**, 9891–9903.
- 294 Y. B. Lim and P. J. Ziemann, *Environ. Sci. Technol.*, 2005, **39**, 9229–9236.

- 295 F. Payri, V. R. Bermúdez, B. Tormos and W. G. Linares, *Atmos. Environ.*, 2009, **43**, 1273–1279.
- 296 R. E. Dunmore, J. R. Hopkins, R. T. Lidster, J. D. Lee, M. J. Evans, A. R. Rickard, A. C. Lewis and J. F. Hamilton, *Atmos. Chem. Phys.*, 2015, **15**, 9983–9996.
- 297 J. H. Tang, L. Y. Chan, C. C. Chang, S. Liu and Y. S. Li, *J. Geophys. Res. Atmos.*, 2009, **114**, D03304.
- 298 R. Atkinson, D. L. Baulch, R. A. Cox, J. N. Crowley, R. F. Hampson, R. G. Hynes, M. E. Jenkin, M. J. Rossi and J. Troe, *Atmos. Chem. Phys. Discuss.*, 2003, **3**, 6179–6699.
- 299 A. Guenther, C. N. Hewitt, D. Erickson, R. Fall, C. Geron, T. Graedel, P. Harley, L. Klinger, M. Lerdau, W. A. McKay, T. Pierce, B. Scholes, R. Steinbrecher, R. Tallamraju, J. Taylor and P. Zimmerman, *J. Geophys. Res.*, 1995, **100**, 8873–8892.
- 300 B. Lamb, A. Guenther, D. Gay and H. Westberg, *Atmos. Environ.*, 1987, **21**, 1695–1705.
- 301 W. L. Chameides, R. W. Lindsay, J. Richardson and C. S. Kiang, *Science*, 1988, **241**, 1473–1475.
- 302 J. F. Hamilton, M. R. Alfarra, N. Robinson, M. W. Ward, A. C. Lewis, G. B. McFiggans, H. Coe and J. D. Allan, *Atmos. Chem. Phys.*, 2013, **13**, 11295–11305.
- 303 J. Yu, R. C. Flagan and J. H. Seinfeld, *Environ. Sci. Technol.*, 1998, **32**, 2357–2370.
- 304 A. T. Lambe, T. B. Onasch, D. R. Croasdale, J. P. Wright, A. T. Martin, J. P. Franklin, P. Massoli, J. H. Kroll, M. R. Canagaratna, W. H. Brune, D. R. Worsnop and P. Davidovits, *Environ. Sci. Technol.*, 2012, **46**, 5430–5437.
- 305 W. R. Simpson, S. S. Brown, A. Saiz-Lopez, J. A. Thornton and R. Von Glasow, *Chem. Rev.*, 2015, **115**, 4035–4062.
- 306 A. P. Altshuller, *J. Atmos. Chem.*, 1991, **12**, 19–61.
- 307 A. Montenegro, J. S. A. Ishibashi, P. Lam and Z. Li, *J. Phys. Chem. A*, 2012, **116**, 12096–12103.
- 308 N. Nishino, J. Arey and R. Atkinson, *J. Phys. Chem. A*, 2009, **113**, 852–857.
- 309 L. Onel, A. Brennan, P. W. Seakins, L. Whalley and D. E. Heard, *Atmos. Meas. Tech. Discuss.*, 2017, 1–20.
- 310 W. R. Stockwell, C. V. Lawson, E. Saunders and W. S. Goliff, *Atmosphere*, 2012, **3**, 1–32.

- 311 H. N. Maia de Oliveira, F. W. Bezerra Lopes, A. A. Dantas Neto and O. Chiavone-Filho, *J. Chem. Eng. Data*, 2002, **47**, 1384–1387.
- 312 J. E. Hawkins and G. T. Armstrong, *J. Am. Chem. Soc.*, 1954, **76**, 3756–3758.
- 313 G. Carruth and R. Kobayashi, *J. Chem. Eng.*, 1973, **18**, 115–126.
- 314 B. Maillard, K. U. Ingold and J. C. Scaiano, *J. Am. Chem. Soc.*, 1983, **105**, 5095–5099.
- 315 E. S. C. Kwok and R. Atkinson, *Atmos. Environ.*, 1995, **29**, 1685–1695.
- 316 J. H. Kroll and J. H. Seinfeld, *Atmos. Environ.*, 2008, **42**, 3593–3624.
- 317 A. Fish, *Q. Rev. Chem. Soc.*, 1964, **18**, 243–269.
- 318 E. L. Jenner, *J. Org. Chem.*, 1962, **27**, 1031–1032.
- 319 D. E. Shallcross, M. T. Raventos-Duran, M. W. Bardwell, A. Bacak, Z. Solman and C. J. Percival, *Atmos. Environ.*, 2005, **39**, 763–771.
- 320 F. Bohr, E. Henon, I. Garcia and M. Castro, *Int. J. Quantum Chem.*, 1999, **75**, 671–682.
- 321 G. Da Silva and J. W. Bozzelli, *J. Phys. Chem. A*, 2007, **111**, 12026–12036.
- 322 R. Atkinson, D. L. Baulch, R. A. Cox, J. N. Crowley, R. F. Hampson, R. G. Hynes, M. E. Jenkin, M. J. Rossi and J. Troe, *Atmos. Chem. Phys. Discuss.*, 2006, **6**, 3625–4055.
- 323 J. C. Ianni, in *Computational and Fluid Solid Mechanics*, 2003, pp. 1368–1372.
- 324 M. D. King and K. C. Thompson, *Atmos. Environ.*, 2003, **37**, 4517–4527.
- 325 K. C. Clemitshaw, L. J. Carpenter, S. A. Penkett and M. E. Jenkin, *Environ. Technol.*, 1997, **102**, 25405–25416.
- 326 K. Miyazaki, A. E. Parker, C. Fittschen, P. S. Monks and Y. Kajii, *Atmos. Meas. Tech.*, 2010, **3**, 1547–1554.
- 327 M. E. Morgan, D. A. Osborne and D. J. Waddington, *J. Chem. Soc., Faraday Trans. 2*, 1984, **11**, 1869–1873.
- 328 D. E. Heard and M. J. Pilling, *Chem. Rev.*, 2003, **103**, 5163–5198.
- 329 Y. Kanaya, Y. Sadanaga, J. Hirokawa, Y. Kajii and H. Akimoto, *J. Atmos. Chem.*, 2001, **38**, 73–110.
- 330 C. A. Cantrell, A. Zimmer and G. S. Tyndall, *Geophys. Res. Lett.*, 1997, **24**, 2195–2198.
- 331 D. A. Osborne and D. J. Waddington, *J. Chem. Soc. Perkin Trans. 2*, 1980, **0**, 925–930.
- 332 F. Kirchner and W. R. Stockwell, *J. Geophys. Res.*, 1996, **101**, 21007–21022.
- 333 G. Hancock and V. L. Kasyutich, *Appl. Phys. B*, 2004, **79**, 383–388.

- 334 H. Fuchs, Z. Tan, A. Hofzumahaus, S. Broch, H. P. Dorn, F. Holland, C. Kunstler, S. Gomm, F. Rohrer, S. Schrade, R. Tillmann and A. Wahner, *Atmos. Meas. Tech.*, 2016, **9**, 1431–1447.
- 335 Y. Ji, J. Zhao, H. Terazono, K. Misawa, N. P. Levitt, Y. Li, Y. Lin, J. Peng, Y. Wang, L. Duan, B. Pan, F. Zhang, X. Feng, T. An, W. Marrero-Ortiz, J. Secrest, A. L. Zhang, K. Shibuya, M. J. Molina and R. Zhang, *Proc. Natl. Acad. Sci.*, 2017, **114**, 8169–8174.
- 336 W. Su, *Resour. Conserv. Recycl.*, 1996, **16**, 77–91.
- 337 B. C. Singer, H. Destailats, A. T. Hodgson and W. W. Nazaroff, *Indoor Air*, 2006, **16**, 179–191.
- 338 A. Steinemann, *Air Qual. Atmos. Heal.*, 2015, **8**, 273–281.
- 339 G. Drakou, C. Zerefos, I. Ziomas and M. Voyatzaki, *Atmos. Environ.*, 1998, **32**, 595–610.
- 340 W. W. Nazaroff and G. R. Cass, *Environ. Sci. Technol.*, 1986, **20**, 924–934.
- 341 F. Almutawa, R. Vandal, S. Q. Wang and H. W. Lim, *Photodermatol. Photoimmunol. Photomed.*, 2013, **29**, 65–72.
- 342 M. Kruza, A. C. Lewis, G. C. Morrison and N. Carslaw, *Indoor Air*, 2017, **27**, 1001–1011.
- 343 S. Nehr, E. Hosen and S. ichi Tanabe, *Environ. Int.*, 2017, **98**, 233–237.
- 344 E. Barrese, A. Giofrè, M. Scarpelli, D. Turbante, R. Trovato and S. Iavicoli, *Occup. Dis. Environ. Med.*, 2014, **2**, 49–55.
- 345 M. H. Forouzanfar, *Lancet*, 2015, **386**, 2287–2323.
- 346 M. Alavanja, J. A. Baron, R. C. Brownson, P. A. Buffler, D. M. DeMarini, M. V. Djordjevic, R. Doll, E. T. H. Fontham, Y. T. Gao, N. Gray, P. C. Gupta, A. Hackshaw, S. S. Hecht, K. Husgafvel-Pursiainen, E. Matos, R. Peto, D. H. Phillips, J. M. Samet, G. Stoner, M. J. Thun, J. Trédaniel, P. Vineis, H. E. Wichmann, A. H. Wu and D. Zaridze, *IARC Monogr. Eval. Carcinog. Risks to Humans*, 2004, **83**, 1–1473.
- 347 N. Carslaw, L. Fletcher, D. Heard, T. Ingham and H. Walker, *Indoor Air*, 2017, 1–10.
- 348 E. Gomez Alvarez, D. Amedro, C. Afif, S. Gligorovski, C. Schoemaeker, C. Fittschen, J. Doussin and H. Wortham, *Proc. Natl. Acad. Sci.*, 2013, **110**, 13294–13299.
- 349 M. Derudi, S. Gelosa, A. Sliepcevich, A. Cattaneo, R. Rota, D. Cavallo and G. Nano, *Atmos. Environ.*, 2012, **55**, 257–262.

- 350 V. Bartolomei, E. Gomez Alvarez, J. Wittmer, S. Tlili, R. S. Strekowski, B. Temime-Roussel, E. Quivet, H. Wortham, C. Zetzsch, J. Kleffmann and S. Gligorovski, *Environ. Sci. Technol.*, 2015, **49**, 6599–6607.
- 351 T. E. Graedel, *J. Geophys. Res.*, 1977, **82**, 5917–5922.
- 352 A. Schieweck and T. Salthammer, *J. Cult. Herit.*, 2011, **12**, 205–213.
- 353 J. Kesselmeier, U. Kuhn, S. Rottenberger, T. Biesenthal, A. Wolf, G. Schebeske, M. O. Andreae, P. Ciccioli, E. Brancaleoni, M. Frattoni, S. T. Oliva, M. L. Botelho, C. M. A. Silva and T. M. Tavares, *J. Geophys. Res. D Atmos.*, 2002, **107**, 1–13.
- 354 H. Hakola, V. Tarvainen, T. Laurila, V. Hiltunen, H. Hellén and P. Keronen, *Atmos. Environ.*, 2003, **37**, 1623–1634.
- 355 G. Salisbury, P. S. Monks, S. Bauguitte, B. J. Bandy and S. A. Penkett, *J. Atmos. Chem.*, 2002, **41**, 163–187.
- 356 C. J. Weschler, *Indoor Air*, 2000, **10**, 269–288.
- 357 D. Smith and P. Španěl, *Analyst*, 2015, **140**, 2573–2591.
- 358 A. W. Nørgaard, J. D. Kudal, V. Kofoed-Sørensen, I. K. Koponen and P. Wolkoff, *Environ. Int.*, 2014, **68**, 209–218.
- 359 J. R. Girman, G. E. Hadwen, L. E. Burton, S. E. Womble and J. F. McCarthy, in *Indoor Air 1999*, eds. G. Raw, C. Aizlewood and P. Warren, Construction Research Communications Ltd, London, 1999, pp. 460–465.
- 360 M. S. Waring and J. R. Wells, *Atmos. Environ.*, 2015, **106**, 382–391.
- 361 M. Mendez, D. Amedro, N. Blond, D. A. Hauglustaine, P. Blondeau, C. Afif, C. Fittschen and C. Schoemaeker, *Indoor Air*, 2017, **27**, 434–442.
- 362 A. R. Rickard, D. Johnson, C. D. McGill and G. Marston, *J. Phys. Chem. A*, 1999, **103**, 7656–7664.
- 363 G. Sarwar, R. Corsi, D. Allen and C. Weschler, in *Indoor Air 2002: Proceedings of the Ninth International Conference on Indoor Air Quality and Climate*, 2002, pp. 80–85.
- 364 F. H. Shair and K. L. Heitner, *Environ. Sci. Technol.*, 1974, **8**, 444–451.
- 365 S. Youssefi and M. S. Waring, *Environ. Sci. Technol.*, 2014, **48**, 7899–7908.
- 366 W. W. Nazaroff and C. J. Weschler, *Atmos. Environ.*, 2004, **38**, 2841–2865.
- 367 M. Odabasi, T. Elbir, Y. Dumanoglu and S. C. Sofuoglu, *Atmos. Environ.*, 2014, **92**, 376–383.

- 368 J. D. Lee, C. Helfter, R. M. Purvis, S. D. Beevers, D. C. Carslaw, A. C. Lewis, S. J. Møller, A. Tremper, A. Vaughan and E. G. Nemitz, *Environ. Sci. Technol.*, 2015, **49**, 1025–1034.
- 369 N. Carslaw, *Atmos. Environ.*, 2013, **80**, 507–513.
- 370 L. Morawska, C. He, G. Johnson, H. Guo, E. Uhde and G. Ayoko, *Environ. Sci. Technol.*, 2009, **43**, 9103–9.
- 371 A. Steinemann, *Build. Environ.*, 2017, **111**, 279–284.
- 372 E. Uhde and N. Schulz, *Atmos. Environ.*, 2015, **106**, 492–502.
- 373 Y. Kanaya, A. Hofzumahaus, H. P. Dorn, T. Brauers, H. Fuchs, F. Holland, F. Rohrer, B. Bohn, R. Tillmann, R. Wegener, A. Wahner, Y. Kajii, K. Miyamoto, S. Nishida, K. Watanabe, A. Yoshino, D. Kubistin, M. Martinez, M. Rudolf, H. Harder, H. Berresheim, T. Elste, C. Plass-Dulmer, G. Stange, J. Kleffmann, Y. Elshorbany and U. Schurath, *Atmos. Chem. Phys.*, 2012, **12**, 2567–2585.
- 374 S. I. Bohnenstengel, S. E. Belcher, A. Aiken, J. D. Allan, G. Allen, A. Bacak, T. J. Bannan, J. F. Barlow, D. C. S. Beddows, W. J. Bloss, A. M. Booth, C. Chemel, O. Coceal, C. F. Di Marco, M. K. Dubey, K. H. Faloon, Z. L. Fleming, M. Furger, J. K. Gietl, R. R. Graves, D. C. Green, C. S. B. Grimmond, C. H. Halios, J. F. Hamilton, R. M. Harrison, M. R. Heal, D. E. Heard, C. Helfter, S. C. Herndon, R. E. Holmes, J. R. Hopkins, A. M. Jones, F. J. Kelly, S. Kotthaus, B. Langford, J. D. Lee, R. J. Leigh, A. C. Lewis, R. T. Lidster, F. D. Lopez-Hilfiker, J. B. McQuaid, C. Mohr, P. S. Monks, E. Nemitz, N. L. Ng, C. J. Percival, A. S. H. Prévôt, H. M. A. Ricketts, R. Sokhi, D. Stone, J. A. Thornton, A. H. Tremper, A. C. Valach, S. Visser, L. K. Whalley, L. R. Williams, L. Xu, D. E. Young and P. Zotter, *Bull. Am. Meteorol. Soc.*, 2015, **96**, 779–804.
- 375 C. D. Forester and J. R. Wells, *Indoor Air*, 2011, **21**, 400–409.
- 376 X. B. Pang and A. C. Lewis, *Anal. Methods*, 2012, **4**, 2013–2020.
- 377 F. Klein, S. M. Platt, N. J. Farren, A. Detournay, E. A. Bruns, C. Bozzetti, K. R. Daellenbach, D. Kilic, N. K. Kumar, S. M. Pieber, J. G. Slowik, B. Temime-Roussel, N. Marchand, J. F. Hamilton, U. Baltensperger, A. S. H. Prévôt and I. El Haddad, *Environ. Sci. Technol.*, 2016, **50**, 1243–1250.
- 378 B. C. Singer, B. K. Coleman, H. Destailats, A. T. Hodgson, M. M. Lunden, C. J. Weschler and W. W. Nazaroff, *Atmos. Environ.*, 2006, **40**, 6696–6710.

- 379 X. Zhang, A. T. Lambe, M. A. Upshur, W. A. Brooks, A. Gray Bé, R. J. Thomson, F. M. Geiger, J. D. Surratt, Z. Zhang, A. Gold, S. Graf, M. J. Cubison, M. Groessl, J. T. Jayne, D. R. Worsnop and M. R. Canagaratna, *Environ. Sci. Technol.*, 2017, **51**, 5932–5940.
- 380 L. Vereecken and H. M. T. Nguyen, *Int. J. Chem. Kinet.*, 2017, **49**, 752–760.